Universidade de Lisboa

Faculdade de Motricidade Humana

Development and implementation of a new system for the production of custom ankle-foot orthoses for stroke patients

Rui Miguel Almeida Dias Silva

Orientador: Prof. Doutor António Prieto Veloso

Coorientadores: Prof. Doutor Pedro Gil Frade Morouço; Prof. Doutor Nuno Manuel Fernandes Alves

Tese especialmente elaborada para obtenção do grau de Doutor em Motricidade Humana, na especialidade de Biomecânica

2025

Universidade de Lisboa

Faculdade de Motricidade Humana

Development and implementation of a new system for the production of custom ankle-foot orthoses for stroke patients

Rui Miguel Almeida Dias Silva

Orientador: Prof. Doutor António Prieto Veloso

Coorientadores: Prof. Doutor Pedro Gil Frade Morouço; Prof. Doutor Nuno Manuel Fernandes Alves

Júri:
Presidente: Prof. Doutor Duarte Fernando da Rosa Belo Patronilho de Araújo
Vogais:
Prof. Doutor João Paulo Vilas Boas
Professor Catedrático da Faculdade de Desporto da Universidade do Porto

Prof. Doutor João Manuel Ribeiro da Silva Tavares
Professor Catedrático da Faculdade de Engenharia da Universidade do Porto

Prof. Doutor António Prieto Veloso
Professor Catedrático da Faculdade de Motricidade Humana da Universidade de Lisboa

Prof. Doutora Sandra Cristina Fernandes Amado
Professora Adjunta da Escola Superior de Saúde do Politécnico de Leiria

Prof. Doutora Filipa Oliveira da Silva João
Professora Auxiliar da Faculdade de Motricidade Humana da Universidade de Lisboa

2025

Dedication

Para os meus pais e namorada

que sempre acreditaram em mim

Acknowledgments

Personal Acknowledgments

This thesis is not just a reflection of my effort, but a testament to the invaluable support and guidance I've received from those around me.

First and foremost, I extend my sincere gratitude to my supervisor, Professor António Prieto Veloso. His encouragement was a pivotal factor in my decision to pursue a PhD in Human Motricity, a decision that was sparked at our meeting at CDRSP. His ongoing support and profound wisdom have not only guided me but also deepened my passion for Biomechanics.

To my co-supervisor, Professor Pedro Gil Frade Morouço, a long-standing friend and mentor, whose unwavering presence and guidance have been cornerstones throughout my academic and research journey. Much of my academic achievements can be attributed to your mentorship and support.

I am also thankful to my co-supervisor, Professor Nuno Manuel Fernandes Alves, for his steady support and assistance throughout this extensive journey.

My gratitude extends to my friend and colleague, Diogo Ricardo, for his consistent support and for imparting his extensive knowledge about ankle foot orthoses.

Heartfelt thanks to my friend Dr. Inês Campos from CMRRC – Rovisco Pais, for her tireless support and deep expertise in ankle foot orthoses and stroke patients.

To my colleague and friend Bruno Pedro. A companion since the first day I began my PhD.

To all my co-authors – Cristiana Fernandes, Bruna Silva, Artur Mateus, Dr. Jorge Lains, Dr. Paula Amorim, Filipe Perdigoto, Moisés Domingues, Rachel Habiba, Ana Amaro, Carla Moura, Daniela Trindade, André Antão, Rui Martins, Cândida Malça, and Ricardo Branco – collaborating with you has been an honor.

To every patient who participated in this study, your resilience and perseverance have been truly inspirational.

To all those involved in the ReinventO project – reinventing the way we build custom-made Orthosis. A special thanks to Diana Moreira, Miguel Santos, Moisés Domingues and Filipe Perdigoto.

To Dr. Célia Sousa (Portuguese Society of Rehabilitation Engineering / CRID), Dr. José Simões (University of Aveiro), Dr. Daniel Marinho (University of Beira Interior), and Dr. Rui Rúben (Polytechnic Institute of Leiria) for believing in the potential of this Doctorate project.
Finally, heartfelt thanks to my parents, António Silva and Vera Lopes, and my girlfriend, Tânia Leal, for their constant support and unwavering belief in me throughout my academic journey. Your faith and encouragement have been my constant source of strength.

Institutional Acknowledgments

I like to express my gratitude for the institutional support provided by the Portuguese Foundation for Science and Technology (FCT) through projects SFRH/BD/145292/2019, UIDB/04044/2020, UIDP/04044/2020, PAMI ROTEIRO/0328/2013 (CENTRO2020: N 22158), and PTDC/EMD-EMD/5804/2020 (Development of a simulation platform based on musculoskeletal models to predict recovery of gait following orthopaedic interventions in cerebral palsy children), as well as the National Innovation Agency (ANI) through the project ReinventO (POCI-01-0247-FEDER-040021) and the project INOV.AM — Innovation in Additive Manufacturing (02-C05-i01.01-2022.PC644865234-00000004), funded by the European Union — Next Generation EU, PRR — Recovery and Resilience Plan.

I am also deeply grateful to the Centre for Rapid and Sustainable Product Development (CDRSP) and the Interdisciplinary Center for the Study of Human Performance (CIPER) for providing an excellent academic and research environment that greatly contributed to the development of this work.

Furthermore, I wish to express my sincere thanks to the Centro de Medicina de Reabilitação da Região Centro – Rovisco Pais for their openness, collaboration, and support in enabling the clinical trials associated with this research.

Contents

RESUMO ..... **X**

ABSTRACT ..... **XI**

LIST OF FIGURES ..... **XII**

LIST OF TABLES ..... **XIV**

LIST OF ABBREVIATIONS ..... **XV**

THESIS STRUCTURE ..... **XVII**

I. GENERAL INTRODUCTION **1**

II. RELEVANCE OF THE STUDIES **7**

STUDY 1 8
STUDY 2 8
STUDY 3 8
STUDY 4 9
STUDY 5 9

III. STUDIES **11**

A REVIEW ON 3D SCANNERS STUDIES FOR PRODUCING CUSTOMIZED ORTHOSES 11
Abstract *12*
Introduction *13*
Materials and Methods *14*
Results *15*
Discussion *21*
Conclusion *27*
Acknowledgements *28*
Conflicts of Interest *28*
References *28*

A REVIEW OF ADDITIVE MANUFACTURING STUDIES FOR PRODUCING CUSTOMIZED ANKLE-FOOT ORTHOSES 33
Abstract *34*
Introduction *35*
Materials and Methods *36*
Results *37*
Discussion *44*
Conclusion *48*
Acknowledgments *48*
Conflicts of Interest *49*
References *49*

INNOVATIVE DESIGN AND DEVELOPMENT OF PERSONALIZED ANKLE-FOOT ORTHOSES FOR STROKE SURVIVORS WITH EQUINOVARUS FOOT: A FEASIBILITY AND COMPARATIVE TRIAL PROTOCOL 53
Abstract *54*

Introduction 56
Goal of this study 57
Methods 58
Results 61
Discussion 62
Acknowledgements 63
Conflicts of Interest 64
References 64
PHOTOGRAMMETRY IN ANKLE FOOT ORTHOSES: A REVOLUTIONARY SYSTEM FOR RAPID 3D SCANNING AND MODELLING 67
Abstract 68
Introduction 69
Methods 70
Results 75
Discussion 82
Conclusion 85
Acknowledgements 86
Conflicts of Interest 86
References 86
FROM SCANS TO STEPS: ELEVATING STROKE REHABILITATION WITH 3D-PRINTED ANKLE-FOOT ORTHOSES 89
Abstract 90
Introduction 91
Materials and Methods 95
Results 101
Discussion 111
Conclusion 120
Acknowledgements 120
Conflicts of Interest 121
References 121
IV. GENERAL DISCUSSION 127
V. GENERAL CONCLUSION 136
VI. METHODOLOGICAL CONSIDERATIONS 137
MOTION CAPTURE 137
MARKER SET 138
FILTER CUT-OFF FREQUENCY 139
VII. RECOMMENDATIONS FOR FUTURE RESEARCH 140
VIII. GENERAL REFERENCES 143
IX. OTHER PUBLICATIONS (CONFERENCE PAPERS AND SECONDARY PUBLICATIONS) 162
DEVELOPMENT OF A LOW-COST ONE-SHOT SYSTEM FOR ACQUIRING 3D MODELS 162
Abstract 163

Introduction *163*
Materials and Methods *164*
Results and Discussion *164*
References *166*
PHOTOGRAMMETRIC SCANNER FOR LOWER LIMBS 167
Abstract *168*
Introduction *168*
Description *169*
Conclusions *170*
References *170*
FLEXIBLE 3D SCANNING APPARATUS FOR ANATOMIC APPLICATIONS: CONCEPT AND PRELIMINARY RESULTS 171
Abstract *172*
Introduction *172*
Development of Photogrammetric 3D Scanners *173*
Conclusion *175*
References *175*
IMPACT RESISTANCE OF ADDITIVELY MANUFACTURED POLYMERIC MATERIALS FOR BIOMEDICAL APPLICATIONS 177
Abstract *178*
Introduction *178*
Materials and Methods *179*
Results and Discussion *180*
Conclusions *185*
References *185*
MATERIAL PERFORMANCE EVALUATION FOR CUSTOMIZED ORTHOSES: COMPRESSION, FLEXURAL, AND TENSILE TESTS COMBINED WITH FINITE ELEMENT ANALYSIS 187
Abstract *188*
Introduction *188*
Materials and Methods *189*
Discussion *200*
Conclusions *202*
References *203*
X. DATASETS 208
KINEMATICS, KINETICS AND SPATIOTEMPORAL 210
PATIENT 1 ..... *210*
PATIENT 2 ..... *232*
PATIENT 3 ..... *254*
PATIENT 4 ..... *276*
PATIENT 5 ..... *292*
PATIENT 6 ..... *314*

PATIENT 7 ..... *330*
PATIENT 8 ..... *352*
PATIENT 9 ..... *374*
PATIENT 10 ..... *396*
GLOBAL *418*
MATERIAL TESTING 442
Compression Tests *442*
Flexural Tests *448*
Tensile Tests *455*

Resumo

O Acidente Vascular Cerebral, continua a ser uma das principais causas de mortalidade e incapacidade a longo prazo no Mundo. Geralmente, os sobreviventes de um Acidente Vascular Cerebral apresentam uma série de défices motores, incluindo fraqueza muscular, espasticidade e coordenação reduzida, o que pode prejudicar significativamente a sua capacidade de realizar atividades diárias. Com foco em melhorar a mobilidade, estabilidade e, em última análise, a qualidade de vida, as ortóteses desempenham um papel fundamental na reabilitação e no suporte. Esta tese representa um avanço significativo no cuidado ortopédico para sobreviventes de Acidentes Vasculares Cerebrais, destacando o papel transformador do fabrico aditivo no design e produção de ortóteses tornozelo-pé. Centrado no desenvolvimento de um inovador scanner 3D baseado na tecnologia de fotogrametria, este estudo assinala uma mudança de paradigma na precisão e personalização ortótica. Fundamental para este sucesso é a ênfase na captura anatómica rápida e precisa, melhorando notavelmente o conforto do doente e acelerando a entrega de ortóteses sob medida. Ao longo da tese são abordados vários aspetos relacionados com o tema. Foram realizadas revisões detalhadas de tecnologias de scanner 3D, metodologias de fabrico aditivo, estudos empíricos que validam um novo sistema de obtenção da superfície do membro inferior do doente e a sua integração clínica. Também foi realizada uma análise comparativa abrangente de ortóteses tornozelo-pé personalizadas vs. pré-fabricadas em 10 doentes. Esta abordagem multifacetada, englobando avaliações biomecânicas, e de satisfação do doente, oferece uma visão holística do impacto das ortóteses na reabilitação pós Acidente Vascular Cerebral. Os estudos revelam que as ortóteses tornozelo-pé produzidas por fabrico aditivo são, no mínimo, equivalentes e, em alguns casos, superiores às ortóteses pré-fabricadas em termos de eficácia biomecânica com o feedback dos doentes indicando uma clara preferência pelas ortóteses personalizadas. Este estudo não fornece apenas evidências convincentes dos benefícios do fabrico aditivo na produção de ortóteses, mas também estabelece um precedente para futuras pesquisas e práticas clínicas destacando-se pela análise de dados biomecânicos nunca realizados em estudos anteriores. Serve também como uma base para a inovação centrada no doente, incentivando uma abordagem mais personalizada e baseada em evidências no design ortopédico para melhorar a qualidade de vida dos sobreviventes de Acidentes Vasculares Cerebrais.

Palavras-Chave: Cinemática, Cinética, Pontuação do Perfil de Marcha, Espaço temporal, Acidente Vascular Cerebral, Scanner 3D, Fabrico Aditivo, QUEST, Ortóteses Tornozelo-Pé, Fotogrametria

Abstract

Stroke continues to be one of the leading causes of mortality and long-term disability globally. Commonly, stroke survivors exhibit a range of motor deficits, including muscle weakness, spasticity, and reduced coordination, significantly impairing their ability to perform daily activities. Focused on improving mobility, stability, and ultimately quality of life, orthoses play a crucial role in rehabilitation and support. This thesis represents a significant advancement in orthotic care for stroke survivors, highlighting the transformative role of additive manufacturing in the design and production of ankle-foot orthoses. Centered on the development of an innovative 3D scanner based on photogrammetry technology, this study signals a paradigm shift in orthotic precision and customization. Central to this success is the emphasis on rapid and accurate anatomical capture, notably enhancing patient comfort and expediting the delivery of tailored orthoses. Throughout the thesis, various aspects related to the theme are addressed. Detailed reviews of 3D scanner technologies, additive manufacturing methodologies, empirical studies validating a new system for capturing the lower limb surface of patients, and its clinical integration were conducted. A comprehensive comparative analysis of custom vs. prefabricated ankle-foot orthoses in 10 patients was also carried out. This multifaceted approach, encompassing biomechanical assessments, and patient satisfaction, offers a holistic view of the impact of orthoses on post-stroke rehabilitation. The studies reveal that ankle-foot orthoses produced by additive manufacturing are, at minimum, equivalent, and in some cases superior to prefabricated orthoses in terms of biomechanical efficacy, with patient feedback indicating a clear preference for the custom variants. This study not only provides compelling evidence of the benefits of additive manufacturing in orthotic production but also establishes a precedent for future research and clinical practices, distinguished by the analysis of biomechanical data never conducted in previous studies. It also serves as a foundation for patient-centered innovation, encouraging a more personalized and evidence-based approach in orthotic design to improve the quality of life of stroke survivors.

Keywords: Kinematics, Kinetics, Gait Profile Score, Spatiotemporal, Stroke, 3D Scanner, Additive Manufacturing, QUEST, Ankle Foot Orthosis, Photogrammetry

List of Figures

FIGURE III.1 - FLOW DIAGRAM OF THE SEARCH HISTORY AND SELECTION PROCESS 15

FIGURE III.2 - FLOW DIAGRAM OF THE SEARCH HISTORY AND SELECTION PROCESS 38

FIGURE III.3 - DESIGN OF THE PRINTED CIRCUIT BOARD. THE UPPER RECTANGULAR AREA IS WHERE THE RASPBERRY PI COMPUTE MODULE 3+ IS INTEGRATED. THE LOWER AREA IS WHERE THE NETWORK AND POWER CABLES ARE CONNECTED. 71

FIGURE III.4 - DESIGN OF THE NEW SCANNER CREATED TO CAPTURE THE SURFACE OF THE PATIENT'S LEG AND FOOT USING PHOTOGRAMMETRY TECHNOLOGY. IT IS POSSIBLE TO SEE IN DETAIL THE CONNECTION BETWEEN THE ACRYLIC AND THE SCANNER'S STRUCTURE, WITH THE CAPABILITY TO ADJUST ITS POSITION HORIZONTALLY AND VERTICALLY FOR AN OPTIMAL FIT TO THE PATIENT'S LEG. 72

FIGURE III.5 - VIEW OF THE REAR OF THE SCANNER WITH ALL MODULES CONNECTED IN SERIES FOR DATA TRANSMISSION AND POWER SUPPLY. 75

FIGURE III.6 - ACCURACY TEST COMPARING THE NEW SCANNER WITH THE STEINBICHLER COMET 5 SCANNER. THE YELLOW AREAS REPRESENT IDENTICAL ZONES, THE RED AREAS INDICATE POSITIVE DEVIATIONS, AND THE BLUE AREAS INDICATE NEGATIVE DEVIATIONS. 76

FIGURE III.7 - MAIN PAGE OF THE WEB MODULE WITH OPTIONS TO SELECT EITHER THE SCANNER PAGE OR THE PATIENT MANAGEMENT PAGE. 76

FIGURE III.8 - MAIN SCANNER PAGE, WHERE IT IS POSSIBLE TO VIEW OR CHANGE THE ASSOCIATED SETTINGS. A LIVE PREVIEW FROM ALL 60 CAMERAS CAN ALSO BE ACCESSED. 77

FIGURE III.9 - WORKFLOW FROM THE SCANNER TO THE ORTHOTIC PRINTOUT. THE USER CAN VIEW ALL THE STEPS THAT HAVE BEEN COMPLETED OR ARE YET TO BE DONE. IT'S POSSIBLE TO PREVIEW THE 3D MODEL OF THE LEG OR THE ORTHOSIS. 77

FIGURE III.10 - BLENDER MODULE FOR LEG ALIGNMENT, MESH MODIFICATIONS, OR LEG MEASUREMENT. IN THIS 3D MODEL, THE PATIENT WAS WEARING A STOCKING FOR SMOOTHER SURFACE RENDERING, AVOIDING DEFECTS FROM VEINS OR LEG HAIR. 78

FIGURE III.11 - MODULE FOR CONSTRUCTING THE AFO IN RHINOCEROS. ALL FEATURES OF THE ORTHOSIS CAN BE ADJUSTED USING SLIDERS LOCATED ON THE RIGHT. 78

FIGURE III.12 - DESIGN OF THE FINAL ORTHOSIS OVERLAID ON THE PATIENT'S LEG MODEL, WITH INCORPORATION OF EYELETS FOR FUTURE PLACEMENT OF VELCRO STRAPS. 79

FIGURE III.13 - 3D PRINTED AFO IN NYLON 12 MATERIAL. 79

FIGURE III.14 - PATIENT WITH THE LEFT LOWER LIMB IN THE SCANNER TO CAPTURE THE 3D MODEL OF THE LEG AND FOOT SURFACE (INCLUDING THE SOLE). 79

FIGURE III.15 - REPRESENTATION OF THE ANGLES FROM THE AVERAGE OF THE 6 GAIT CYCLES FOR THE LEFT FOOT AND RIGHT FOOT. 82

FIGURE III.16 – ON THE LEFT SIDE – VIRTUAL IMAGE OF THE NOVEL PHOTOGRAMMETRIC 3D SCANNER. ON THE RIGHT SIDE – LEFT HEMIPARETIC LOWER LIMB OF THE PATIENT ON THE SCANNER 97

FIGURE III.17 - 3D PRINTED AFO IN NYLON 12 MATERIAL 98

FIGURE III.18 - TESTING ENVIRONMENT. REPRESENTATION OF TEST ENVIRONMENT WITH TWELVE INFRARED HIGHSPEED CAMERAS AND TWO FORCE PLATFORMS DURING THE GAIT CYCLE OF THE PATIENT IN THE QUALISYS TRACK MANAGER SOFTWARE 99

FIGURE III.19 – MEAN JOINT ANGLES OF ALL PATIENTS (LEFT) AND THE RESPECTIVE 1D-SPM ANALYSIS (RIGHT) DURING THE GAIT CYCLE, FOR THE PO AFO (RED LINE) AND THE CO AFO (BLACK LINE). GREY SHADED REGIONS ON THE LEFT SIDE SHOWS THE

NORMATIVE DATA FOR THE GAIT CYCLE OF HEALTHY PATIENTS AND GREY SHADED REGIONS ON THE RIGHT SIDE INDICATE WHERE DIFFERENCES WERE STATISTICALLY SIGNIFICANT.....104

FIGURE III.20 - MEAN MOMENTS OF ALL PATIENTS (LEFT) AND THE RESPECTIVE 1D-SPM ANALYSIS (RIGHT) DURING THE GAIT CYCLE, FOR THE PO AFO (RED LINE) AND THE CO AFO (BLACK LINE). GREY SHADED REGIONS ON THE LEFT SIDE SHOWS THE NORMATIVE DATA FOR THE GAIT CYCLE OF HEALTHY PATIENTS AND GREY SHADED REGIONS ON THE RIGHT SIDE INDICATE WHERE DIFFERENCES WERE STATISTICALLY SIGNIFICANT.....107

FIGURE III.21 – MEAN AND STANDARD DEVIATION OF SYMMETRY VS ASYMMETRY OF ALL PATIENTS FOR STEP LENGTH, SWING TIME AND STANCE TIME LOR AFFECTED LIMB (LIGHT GREY) AND UNAFFECTED LIMB (DARK GREY). *P VALUE* INDICATES IF DIFFERENCES WERE STATISTICALLY SIGNIFICANT.....108

FIGURE VII.22 – MODEL AND LOCATION OF THE RETROREFLECTIVE MARKERS 138

List of Tables

TABLE III.1 - INCLUDED STUDIES WITH 3D SCANNER DETAILS, ANATOMICAL ZONE, TYPE OF SOFTWARE, OUTCOMES, AND CONCLUSIONS. 16

TABLE III.2 - INCLUDED STUDIES WITH AFO DETAILS, PARTICIPANT/PATIENT CHARACTERISTICS, INTERVENTION AND CONTROL CONDITIONS, OUTCOMES, AND MAIN RESULTS 39

TABLE III.3 - GRADE EVIDENCE PROFILE 43

TABLE III.4 - COMPARISON BETWEEN THE DIFFERENT MAXIMUM ANGLES OBTAINED BY THE ANKLE AND KNEE OF THE LEG WITH THE AFO AT THE STANCE PHASE 44

TABLE III.5 - CLINICAL CHARACTERISTICS OF THE SUBJECT 73

TABLE III.6 - SPATIOTEMPORAL PARAMETERS FOR BOTH CONDITIONS 80

TABLE III.7 - DEMOGRAPHIC AND CLINICAL PROFILE OF STROKE PATIENTS: A DETAILED OVERVIEW OF GENDER, AGE, PHYSICAL CHARACTERISTICS, STROKE TYPE, AFFECTED SIDE, AND ORTHOTIC PREFERENCES 96

TABLE III.8 - COMPARATIVE ANALYSIS OF GAIT SYMMETRY INDICES: ASSESSING STEP LENGTH, SWING TIME, AND STANCE TIME FOR PO AND CO IN STROKE PATIENTS 108

TABLE III.9 - COMPARATIVE ANALYSIS OF GAIT PARAMETERS: PO AND CO IN STROKE PATIENTS 108

TABLE III.10 - DETAILED GAIT ANALYSIS COMPARING AFFECTED AND UNAFFECTED LIMBS FOR PO AND CO USE IN STROKE PATIENTS: STEP LENGTH, TIME, STRIDE, STANCE, SWING, CYCLE TIME, AND FREQUENCY 108

TABLE III.11 - COMPREHENSIVE GAIT PROFILE SCORE (GPS). ANALYSIS FOR STROKE PATIENTS: COMPARING AFFECTED AND UNAFFECTED LIMBS FOR PO AND CO WITH MEDIAN AND INTERQUARTILE RANGE WITH MEDIAN DIFFERENCES 110

TABLE III.12 - ASSESSMENT OF AFO SATISFACTION: COMPARISON OF USER EXPERIENCE WITH QUEST 111

List of Abbreviations

3D - Three-Dimensional

ABS - Acrylonitrile Butadiene Styrene

AFO - Ankle-Foot Orthoses

AM - Additive Manufacturing

API - Application Programming Interface

AR - Augmented Reality

CAD - Computer-Aided Design

CAST - Calibrated Anatomical System Protocol

CO - Custom (Additive Manufacturing) Orthosis

CT - Computed Tomography

DAFO - Dynamic Ankle-Foot Orthosis

EMG - Electromyography

FDM - Fused Deposition Modeling

FEM - Finite Element Method

FoV - Field of View

fps - Frames Per Second

GRADE - Grading of Recommendations Assessment, Development and Evaluation

GRF - Ground Reaction Force

HTTP - Hypertext Transfer Protocol

Hz - Hertz

LED - Light Emitting Diode

M - Male

MJF - Multi-Jet Fusion

MRI - Magnetic Resonance Imaging

Mpx - Megapixels

PAF – Project Automation Framework (Qualisys)

PA12 - Polyamide 12

PCB - Printed Circuit Board

PD-AFO - Passive Dynamic Ankle-Foot Orthosis

PLA - Poly-Lactic Acid

PLS - Posterior Leaf Spring

PO - Prefabricated Orthosis (off-the-shelf)

PP - Polypropylene

PRISMA - Preferred Reporting Items for Systematic Reviews and Meta-Analyses

QUEST - Quebec User Evaluation of Satisfaction with Assistive Technology

QTM - Qualisys Track Manager

SLA - Stereolithography

SLS - Selective Laser Sintering

SPIRIT - Standard Protocol Items: Recommendations for Interventional Trials

SQL - Structured Query Language

STL - Standard Triangle Language (File Format)

TTPP - Traditional Thermoformed Polypropylene

TPU - Thermoplastic Polyurethane

UV - Ultraviolet

VR - Virtual Reality

Thesis Structure

The PhD thesis structure is organized in **X chapters**, assembling information needed to understand the conducted research.

Chapter I – General Introduction

This introductory chapter establishes the foundation of the thesis, detailing the overarching research theme, its significance in the field, and the broader context within which the study is situated. It outlines the specific objectives and hypotheses of the research, providing a clear roadmap for the thesis. This chapter also sets the stage for the reader, explaining the relevance of the research in addressing current challenges in stroke rehabilitation and orthotic care, and how it aims to contribute to the existing body of knowledge.

Chapter II – Relevance of the studies

In this chapter, the relevance and rationale behind each of the conducted studies are explored. It demonstrates the significance of each paper within the thesis, explaining why each study was undertaken and what goals it aimed to achieve. This chapter elucidates the importance of each research paper in contributing to the overall understanding and advancement in the field of stroke rehabilitation and orthotic development. It provides a context for the research, highlighting how each study addresses specific gaps in the field and contributes to the broader scientific and medical community.

Chapter III – Research Studies

Presents the five scientific studies written during the PhD process. Each of them was organized following the structure of a scientific paper format: Introduction, Methods, Results, Discussion, Conclusions, and References; and each one was reformatted for consistency with the thesis.

Chapters IV and V – General Discussion and Conclusions

Synthesizes the main findings from Chapter III and provides overall conclusions, discussing the implications and significance of the research.

Chapter VI – Methodological Considerations

Examines the methodologies used in the research studies, discussing their rationale, strengths, and limitations.

Chapter VII – Recommendations for Future Research

Outlines potential areas for future study, based on the findings and limitations of the current research.

Chapter VIII – General References

Lists all references used throughout the thesis.

Chapter IX – Other Publications (Conference Papers and Secondary Publications)

Presents four papers that were showcased at specialty conferences, demonstrating the practical application and reception of the research in professional circles. This chapter illustrates the active engagement of the research with the wider academic and professional community, showcasing its relevance and impact.

Chapter X - Datasets

Provides a comprehensive compilation of all datasets used in the research, encompassing kinematic, kinetic, and spatiotemporal data from patients, as well as mechanical tests conducted on materials. This chapter underscores the thoroughness and rigor of data collection and analysis, essential for the validation and reliability of the research findings.

I. General Introduction

Stroke, an Acute Cerebrovascular Accident, remains a leading cause of both mortality and long-term disability (Feigin et al., 2018). This condition, which affects blood flow in the brain can be triggered by either ischemia (ischemic stroke) or haemorrhage (haemorrhagic stroke) posing significant challenges in the realms of medical research and healthcare (Krishnamurthi et al., 2013).

Comprehending the pathophysiology of stroke is an undertaking that involves various factors such as cerebral ischemia, neuroinflammation and neuronal death (Zhang et al., 2020). Ischemic strokes account for 87% of all cases and occur due to the blockage of blood flow in the brain often caused by thrombosis or embolism (Yan et al., 2015). On the other hand, haemorrhagic strokes are less common but tend to be more severe as they result from ruptures within blood vessels in the brain (Krishnamurthi et al., 2013).

Significant progress has been made in neuroimaging and biomarker studies greatly enhancing the understanding of strokes. These advancements have led to improved accuracy and increased potential for tailoring treatment strategies on an individual basis (Simpkins et al., 2019) however, the impact of stroke on a scale continues to be significant. There has been an increase in stroke cases observed in middle income countries, which can be attributed to changes in lifestyle and the aging populations (Feigin et al., 2015). Over the few decades there have been remarkable advancements in stroke management. The introduction of reperfusion therapies like thrombolysis and mechanical thrombectomy has completely revolutionized how strokes are treated (Lee et al., 2015). Additionally, rehabilitation strategies that focus on cognitive, physical, and emotional recovery have played a crucial role in enhancing the quality of life for individuals who have experienced a stroke (Lowry & Jin 2020). Despite these developments, there are still challenges that need to be addressed to ensure timely and adequate treatment for many patients (Saenger & Christenson 2010).

Commonly, stroke survivors experience a range of motor deficits, including muscle weakness, spasticity, and reduced coordination, which can significantly impair their ability to perform daily activities. Focusing on improving mobility, stability, and, ultimately, the quality of life, orthoses commonly referred to as orthotic devices, play a important role in the rehabilitation and support. They are designed to aid in the correction, support, or enhancement of the function of a limb or the torso. Upper limb orthoses, including wrist-hand orthoses, are

utilized to support weakened or paralyzed arms and hands. These devices assist in maintaining functional positioning, preventing contractures, and enabling the performance of tasks that require manual dexterity. Similarly, lower limb orthoses, such as ankle-foot orthoses (AFOs), are commonly prescribed for stroke survivors to address issues like foot drop, which results from the inability to raise the front part of the foot due to weakness or paralysis of the dorsiflexor muscles. By providing the necessary support and alignment, AFOs can enhance gait patterns, reduce the risk of falls, and promote greater independence in ambulation.

The variety of AFOs available caters to the diverse needs arising from stroke-induced mobility challenges. Solid AFOs, characterized by their rigid structure, are predominantly used for patients exhibiting significant ankle weakness or spasticity. Made typically from plastic and custom-fitted, these AFOs provide substantial support and stability, enhancing gait and preventing foot drop nonetheless, their rigidity can be a double-edged sword, potentially limiting ankle mobility and leading to muscle atrophy due to reduced muscle usage (Wada et al. 2021). Articulated AFOs, on the other hand, incorporate a hinged mechanism, offering a compromise between support and mobility (Kilmartin & Wallace, 1994). These hinges, adjustable for controlling the range of motion, make articulated AFOs suitable for patients who retain some control over their ankle movements. While they facilitate more natural gait patterns, their complexity necessitates careful adjustment and may not suffice for patients with severe muscle weakness (Pons et al., 2016). Dynamic AFOs represent a more flexible option, often crafted from a blend of materials like plastic and metal (Momosaki et al., 2015). Designed to support natural foot movement during walking, these AFOs are particularly beneficial for patients in the recovery phase who are regaining muscle function. They encourage active muscle usage, aiding in muscle strengthening. Conversely, their suitability is limited for patients with severe spasticity or instability, as they provide less rigid support compared to other types (Tyson & Kent, 2011). Additionally, Floor Reaction AFOs are tailored to control knee buckling by providing anterior support at the shin level (Adiputra et al., 2019). They are particularly effective for patients with quadriceps weakness, aiding in knee extension during the stance phase of gait. Despite their effectiveness, these AFOs can be somewhat bulky and may require fine-tuning for optimal knee control (Briko et al., 2021).

Lastly, Posterior Leaf Spring AFOs, made from thinner and more flexible materials, offer mild dorsiflexion assistance, and are primarily used for foot drop prevention (Rao et al., 2014). Their lightweight and slim profile provide a cosmetic advantage, but they offer limited support and control, making them less suitable for patients with significant spasticity or instability (Meadmore et al., 2018).

In selecting the appropriate AFO for a stroke patient, it is imperative to consider factors such as the degree of muscle weakness, range of motion, spasticity, and the patient's functional goals (Cui et al., 2023). Managing foot drop, PLS AFOs stands out for their specific application offering essential support for dorsiflexion impairment. Within this category, the distinction between off-the-shelf and custom-made PLS AFOs, particularly those crafted using the traditional plaster cast method, is significant.

Off-the-shelf PLS AFOs are widely available and provide a general level of support suitable for a broad range of patients. The primary advantage of these prefabricated orthoses lies in their immediate availability and cost-effectiveness. They are designed to fit a wide array of foot and ankle sizes, which makes them a convenient option for patients requiring immediate orthotic support yet, the one-size-fits-all approach of off-the-shelf PLS AFOs can also be a limitation. These devices may not offer the optimal fit for every individual, potentially leading to discomfort or inadequate support, especially in cases where the patient's anatomy deviates from the norm (Creylman et al., 2013).

In contrast, custom-made PLS AFOs, particularly those fabricated using the traditional plaster cast method, are tailored to the individual's specific anatomical and functional needs. The process involves creating a plaster mold of the patient's lower limb, ensuring that the orthosis conforms precisely to the contours of the limb. This personalized approach results in a higher level of comfort and better support, as the orthosis is designed to accommodate the unique characteristics of the patient's condition. Additionally, custom-made PLS AFOs can be adjusted to cater to specific requirements, such as varying degrees of rigidity and support, based on the patient's rehabilitation progress (Creylman et al., 2013; Banga et al., 2020). Still, the advantages of custom-made PLS AFOs come with certain drawbacks. The process of creating a plaster cast and fabricating the orthosis is time-consuming, which may not be ideal for patients requiring immediate intervention. Furthermore, these custom orthoses are typically more expensive than their off-the-shelf counterparts, a factor that can be a significant consideration for many patients (Creylman et al., 2013).

This is where the integration of advanced technologies like reverse engineering and additive manufacturing brings a transformative change. The integration of rapid prototyping technologies, 3D printing and 3D scanning is starting to revolutionize orthotic fabrication (Baghbanbashi et al., 2022). This fusion of technology and medicine is not just a step forward; it's a leap into a future where each orthotic device is as unique as the individual it is designed for (Konttila et al., 2018; Lu & Zhan, 2018; Spaulding et al., 2019; Netten et al., 2020). The intersection of biomedical engineering, materials science, physical therapy, and orthotic expertise is crucial for the successful development and application of these advanced devices (Netten et al., 2020; Spaulding et al., 2020). This interdisciplinary approach ensures that orthotic devices are not only technologically sophisticated but also clinically relevant and aligned with the specific therapeutic goals of patients. Nevertheless, integrating these advanced technologies into clinical practice presents significant challenges (Johnson et al., 2021; Navarro-Martínez et al., 2023). One of the primary hurdles is the need for specialized training for healthcare professionals, including prosthetist-orthotist and therapists, to effectively utilize and interpret the data from advanced scanning and manufacturing technologies (Netten et al., 2020; Spaulding et al., 2020). Furthermore, aligning these new technologies with existing healthcare workflows and protocols requires careful planning and adaptation (Anderson et al., 2021).

The journey of creating a custom AFO with these new technologies begins with the accurate capture of the patient's limb geometry. This is where advanced 3D scanning technologies come into play, each with its unique capabilities and nuances. Structured light scanners, for instance, project a specific light pattern onto the limb. Cameras then capture the distortions in this pattern, which are processed to create a detailed 3D model of the limb. The precision offered by this technology is remarkable, allowing for a nuanced capture of the limb's contours (Voisin et al., 2007). Although, its efficacy can be influenced by external lighting conditions, and it requires a controlled environment for optimal results (Adamczyk et al., 2020). Laser scanning, another sophisticated technology, employs a focused laser beam to map the limb's surface. This method is renowned for its high level of detail and accuracy, making it ideal for capturing the complex geometries of a patient's limb. While laser scanners provide exceptional precision, they are generally more expensive and can be slower in operation compared to structured light scanners (Goda et al., 2012). Photogrammetry presents a different approach. By taking a series of photographs from various angles and using

software algorithms to stitch these images together, a 3D model of the limb is created. This method's flexibility and lower equipment cost make it an attractive option, especially in settings where access to high-end scanners is limited. However, the accuracy and resolution of photogrammetry depend heavily on the skill of the operator and the quality of the photographs taken (Struck et al., 2019).

Once the digital model of the limb is obtained, the role of additive manufacturing becomes crucial. AM technologies, such as Fused Deposition Modelling (FDM), Selective Laser Sintering (SLS), and Stereolithography (SLA), each bring distinct advantages to the table (Banga et al., 2018). FDM, one of the more accessible forms of 3D printing, uses thermoplastic filaments that are heated and extruded layer by layer to construct the AFO (Alam et al., 2015). This method is particularly beneficial for its rapid prototyping capabilities and cost-effectiveness. Conversely, the resolution and strength of FDM-printed AFOs might not match the requirements for more demanding applications (Powers et al., 2021).

SLS, on the other hand, offers a more sophisticated approach. By using a laser to sinter powdered material, it creates AFOs that are both lightweight and strong. The design freedom afforded by SLS allows for the creation of complex, patient specific AFOs with tailored mechanical properties. The trade-off, however, comes in the form of higher costs and more complex post-processing requirements (Funes-Lora et al., 2021). SLA technology stands out for its ability to produce AFOs with fine details and high-quality finishes. Utilizing a laser to cure liquid resin, SLA can create orthoses with intricate designs and smooth surfaces. The limitation of SLA lies in the range of materials available and the long-term durability of the products, which may not be suitable for all AFO applications (Martín-Montal et al. 2021).

Also, the role of biomechanical analysis in this context cannot be overstated. By thoroughly understanding the mechanics of human movement, orthotists can design AFOs that not only fit the anatomical structure of the patient but also align with their specific movement patterns and functional requirements. This level of customization was challenging to achieve with traditional manufacturing methods.

Furthermore, the psychological benefits of a well-fitted, functional AFO cannot be overstated. A custom-made orthosis that comfortably supports the patient's limb and aids in their mobility can significantly boost their confidence and motivation. This psychological uplift is a critical component of the rehabilitation process, encouraging patients to engage more actively in their recovery exercises and daily activities (Pfeifer et al. 2011). Also, patient

feedback into the design and testing process is an essential component. Engaging with patients to gather feedback can lead to more intuitive and user-friendly designs, thereby increasing compliance and effectiveness (Mavroidis et al. 2011).

Another exciting prospect is the integration of biometric sensors into orthotic devices. These sensors could monitor a range of physiological parameters, such as muscle activity, joint movement, and gait patterns, providing valuable feedback for both patients and healthcare providers (Perlmutter et al. 2020). This data can be used to continuously adjust and improve the design and functionality of the orthoses, making them more responsive to the patient's changing needs. Furthermore, the combination of virtual reality (VR) and augmented reality (AR) technologies with orthotic care could revolutionize rehabilitation practices. These technologies could provide immersive and interactive environments for patients, making rehabilitation exercises more engaging and effective (Huang et al. 2022).

As the field of orthotics continues to evolve with these technological advancements, the potential for further innovation in AFO design and manufacturing is vast. The integration of new technologies is not just enhancing the current functionalities of AFOs but is also paving the way for future developments in orthotic care. Ongoing research and exploration in this field are essential, ensuring that stroke patients receive the most effective, personalized, and advanced care possible. The future of orthotic care, shaped by these technological advancements, holds promising prospects for improved patient outcomes and quality of life.

II. Relevance of the studies

The escalating prevalence of strokes, and their long-term ramifications underscore the imperative for significant advancements in rehabilitation and orthotic care. Strokes, precipitated by ischemic or haemorrhagic events, present a formidable challenge to both medical research and patient care. Rehabilitation of stroke survivors is a complex endeavour, encompassing multifaceted strategies aimed at recuperating mobility and independence. Within this scope, AFOs emerge as pivotal devices, assisting in correction, support, or enhancement of the function of affected limbs. Despite the substantial body of literature on AFOs, a glaring gap persists in developing an optimal solution for crafting AFOs through AM. Traditional methods, while somewhat effective, have not fully addressed the nuanced needs of stroke survivors. Also, off-the-shelf AFOs are far from being ideal. This thesis is situated at this crucial juncture, aiming to bridge this gap by introducing an innovative approach that leverages the latest in photogrammetry and AM. The significance of this thesis lies not only in its technological innovation but also in its potential to fundamentally transform patient care in orthotics. By proposing a method that surpasses the limitations of existing practices, this research endeavours to set a new standard in the fabrication of personalized orthoses, particularly for those affected by the debilitating consequences of strokes.

This thesis aimed to develop and validate an innovative 3D scanner system based on photogrammetry for the creation of personalized AFOs, surmounting the limitations of traditional approaches. The primary goal was to revolutionize the AFO fabrication process, making it faster, more accurate, and tailored to individual needs. The AFOs produced by the new system were expected to offer enhanced comfort and effectiveness, significantly improving the quality of life for stroke patients. This thesis also constitutes the most exhaustive analysis to date of gait cycle data from stroke patients using AM custom AFOs. This extensive data collection is pivotal, as it provides a comprehensive reference for understanding the specific movement patterns and functional needs of stroke survivors. In doing so, the research transcends mere physical measurements, delving into the nuanced interplay between biomechanics and individual experiences of mobility. Moreover, an important aspect, often overlooked by other studies, is the emphasis this research places on the patient's qualitative perspective, rather than relying solely on the quantitative aspects typically derived from biomechanical analyses.

Study 1

A Review on 3D Scanners for Custom Orthoses Production

This comprehensive review critically examines the evolution and applicability of various 3D scanning technologies in the production of custom orthoses. Emphasizing on photogrammetry, the study assesses its superiority in digitizing the human body for orthotic applications. The review highlights the technological progression that allows for reduced scanning times and the potential integration of these technologies in clinical settings, marking a significant leap in orthopaedic care and rehabilitation.

Study 2

A Review of Additive Manufacturing Studies for Producing Customized Ankle-Foot Orthoses

The study presents an exhaustive review of the state-of-the-art in using AM for producing customized AFOs. It delves into evaluating the various AM processes, customization steps, and the biomechanical properties imparted to the AFOs. By scrutinizing nineteen studies, this review provides a critical analysis of the methodologies, underscoring the advantages of AM over traditional manufacturing, and highlights the need for more rigorous research to further enhance this domain.

Study 3

Innovative Design and Development of Personalized Ankle-Foot Orthoses for Stroke Survivors with Equinovarus Foot: A Feasibility and Comparative Trial Protocol

Serving as a foundational methodology for the optimal development of subsequent investigations. The protocol introduces a novel system for AFO design specifically tailored to stroke patients. By leveraging the capabilities of 3D scanning and custom software solutions, this protocol outlines a systematic approach to produce orthoses that aim to surpass conventional designs in terms of biomechanical effectiveness and patient satisfaction.

Central to this protocol is the development of a distinctive 3D scanner, complemented by specialized software, intended to accurately capture the biomechanical data of leg movements during gait in stroke patients. This data collection is instrumental in guiding the creation of patient specific AFO designs. Furthermore, the protocol sets forth a comparative

framework wherein these personalized orthoses will be evaluated against traditional AFO models, using both quantitative and qualitative assessments.

The methodology delineated in this protocol employs advanced statistical tools such as paired t-tests and the Statistical Parametric Mapping (SPM) method to analyse spatial-temporal parameters and graphically compare kinematic and kinetic data across the entire gait cycle. Additionally, patient satisfaction is a crucial component, assessed through the QUEST evaluation tool, aiming to capture a holistic understanding of the patient experience.

Study 4

Photogrammetry in Ankle Foot Orthoses: A Revolutionary System for Rapid 3D Scanning and Modelling

Introducing a novel 3D photogrammetric scanner, this research evaluates its integration into the orthotic design process. The study tests the scanner's precision in capturing foot anatomy and assesses its usability in a clinical environment. A comparative case study further explores the differences between traditional and 3D printed AFOs, showcasing the scanner's capability in producing detailed anatomic models rapidly, thereby hinting at the future of efficient orthotic design.

Study 5

From Scans to Steps: Elevating Stroke Rehabilitation with 3D-Printed Ankle-Foot Orthoses

This study represents the most exhaustive research undertaken to date in terms of collecting and analysing a comprehensive array of data for AM AFOs vs Standard AFOs. It focuses on a critical validation of the newly proposed system, utilizing a sample of ten stroke patients. The research is distinguished by its extensive use of kinematic, kinetic, and spatiotemporal data, which collectively offer a multifaceted understanding of the orthoses' performance.

In addition, the study incorporates the Gait Profile Score (GPS) and assessments through the QUEST tool, providing a holistic evaluation of both the functional and qualitative aspects of the AFOs. This approach not only demonstrates the biomechanical superiority of AM-produced AFOs over traditional models but also captures the patient's experience and satisfaction with the orthoses. The thoroughness of this research, in terms of both the

breadth and depth of the data collected, sets a new benchmark in the field of orthotic development, particularly for stroke rehabilitation.

III. Studies

Study 1

A review on 3D scanners studies for producing customized orthoses

Authors: **Rui Silva**, Bruna Silva, Cristiana Fernandes, Pedro Morouço, Nuno Alves and António Veloso

Abstract

When a limb suffers a fracture, rupture, or dislocation, it is traditionally immobilized with plaster. This may induce discomfort in the patient, excessive itching and sweating, which creates the growth of bacteria, leading to an unhygienic and difficulty to keep clean from treatment. Furthermore, if the plaster remains for a long period, it may cause lesions in the joints and ligaments. To overcome all these disadvantages, orthoses have emerged as important medical devices to help patients in rehabilitation, as well as for self-care of deficiencies in clinics and daily life. Traditionally, these devices are produced manually, which becomes time-consuming and error prone. From another point-of-view, it is possible to use imageology (X-ray or computed tomography) to scan the human body; a process that may help orthoses manufacturing but induces radiation to the patient. To overcome this great disadvantage, several types of 3D scanners, without any kind of radiation have emerged. This article describes the use of various types of scanners capable of digitizing the human body, to produce custom orthoses. Studies have shown that photogrammetry is the most used and most suitable 3D scanner for the acquisition of the human body in 3D. With this evolution of technology, it is possible to decrease the scanning time and it will be possible to introduce this technology in clinical environment.

Keywords: 3D Scanner; Orthoses; Photogrammetry; Structured Light

Introduction

Orthoses are external medical devices designed to support users' biomechanical needs, significantly contributing to their quality of life (Mavroidis et al., 2011; Roberts et al., 2016). They serve as pivotal elements in controlling and restoring the functionality of the injured body part (Belokar et al., 2017; Dias Hensen et al., 2018). Customized orthoses, tailored to individual measurements, exhibit innovative attributes concerning device ventilation, thereby minimizing heat injuries, pressure wounds, and skin breakage (Brognara et al., 2022; Chudnofsky et al., 2004).

Traditionally, a custom-made orthosis has been manufactured using a plaster cast. This conventional practice has several downsides including high plaster consumption, time-intensive processes, being invasive for patients due to the contact of the plaster and prosthetist-orthotist with the patient's limb, and lacking data storage for future reference. To circumvent these medical challenges, reverse engineering techniques have been employed, necessitating three-dimensional (3D) geometric data acquisition. An important requirement for orthoses is comfort, which is attained through a high level of customization facilitated by an accurate capture of the patient's anatomy (Górski et al., 2020; Volonghi et al., 2018) Given that each patient possesses unique body geometry, custom-made orthoses have emerged as the "gold standard" since the orthosis geometry is individually adapted for each patient (Munhoz et al., 2016; Oud et al., 2023). The journey towards acquiring a custom-made orthosis entails several stages including scanning (digitization), importing the scanned data into a computer to create a computer-aided design (CAD) file, modelling, topological optimization, and 3D printing (Dal Maso & Cosmi, 2019; Geoffroy et al., 2018; Sansoni et al., 2009; Servi et al., 2018). The digitization phase is a critical component in this process. To generate a reliable CAD file of the limb, the patient is required to remain still for a certain duration during the acquisition process, hence, fast scanning systems are highly desirable (Dombroski et al., 2014a). Also, offers advantages in terms of non-invasiveness, ease of use, and low cost, making it appealing for reconstructing, measuring, and tracking the evolution of human anatomy for clinical applications (Neri et al., 2023).

In recent years, several types of 3D scanners have been introduced to expedite the manufacture of customized orthoses. Most digitization systems leverage laser scanners (e.g., HandyScan, Faro), structured light (e.g., Vorum, Artec, Sense 3D), photogrammetry software

with conventional cameras (e.g., PhotoModeler, 3DSOM, My3DScanner, PhotoScan, 123D Catch, Hypr3D, RhinoPhoto), or a mixture of diverse technologies. These technologies compute a cloud of three-dimensional points of the object employing the principle of optical triangulation to shape the natural geometry (Belokar et al., 2017; Eder et al., 2013; Geoffroy et al., 2018; Ho et al., 2021; Munhoz et al., 2016). The selection of the most suitable 3D scanner is contingent on the application and the requisite accuracy (Nam et al., 2018; Rogati et al., 2019).

This review aims to explore the use of 3D scanners on human limbs for creating CAD models used in orthosis construction. The study further investigates recent advancements in 3D scanning technology and examines how these developments are improving the custom fabrication of orthoses. This includes a focus on increasing accuracy in capturing the patient's anatomy, which contributes to enhanced patient outcomes.

Materials and Methods

To identify the articles that could be included in this review, the searches were carried out between August and September 2023 in the Web of Science and SCOPUS databases. Searches related to the 3D scanner (3d scanner, photogrammetry, reverse engineering, optical scan, laser scanning, structure light) combined with terms for Orthoses (ortho-sis, orthoses) and medical device were performed. No restrictions were applied to the year or type of publication.

Original articles written in English with 3D scanners used to acquire human limb to make custom orthotics were included. All narrative, systematic reviews and dissertations were excluded. Any articles not written in English were excluded. Any article with another scanner device (ex. computational tomography (CT) or X-ray) were excluded. Articles using 3D scanners other than for obtaining the human body and other than for orthoses were excluded. Articles whose purpose uses 3D scanners for prostheses were also excluded.

After the removal of excluded articles and deletion of duplicates based on PRISMA, data extraction was standardized. Titles and abstracts from the search results were screened using the eligibility criteria and reviewed by two authors (R.S. and B.S.) for inclusion. Data extraction and evaluation of the remaining articles were performed independently by the same authors. In case of disagreement, an additional reviewer (P.M.) was consulted. Data extraction

included first author and year, the aim of the study (reverse engineering, 3D scanner and different types, orthoses) among others.

Results

Figure 1 summarizes the results of the different steps to identify appropriate articles for the review, based on PRISMA guidelines (Page & Moher, 2017). The initial database search identified 4912 articles, and after duplicate removal, 4110 were considered potentially relevant and were screened for relevant content. No additional articles were identified following a hand search of reference lists. After reading the title and abstract of the 4110 articles, 338 were selected for possible inclusion in this systematic review and full-text articles were retrieved. In the last phase, articles that used CT/OCT/X-ray; that did not use humans in their methodology (ex. Moulds) and were not written in English were excluded. 30 of the 338 articles were included in this review organized by type of 3D Scanner (Table 1).

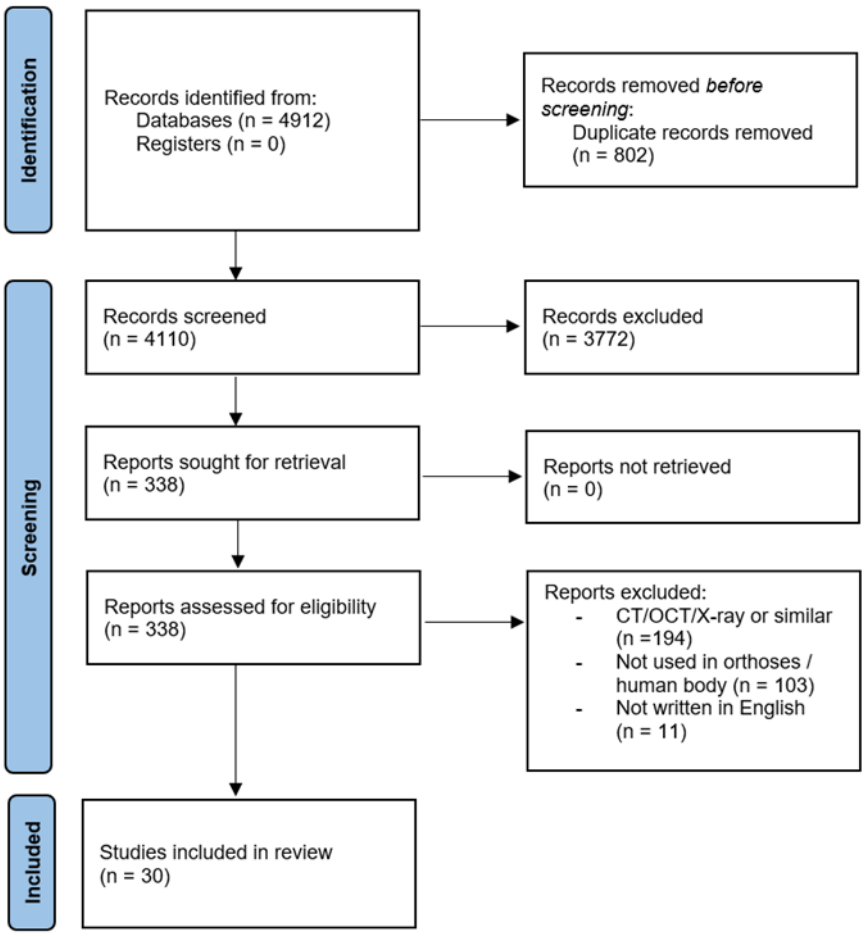

FIGURE III.1 - Flow diagram of the search history and selection process

TABLE III.1 - Included studies with 3D Scanner details, anatomical zone, type of software, outcomes, and conclusions.

Reference	Anatomical Zone	3D Scanner			Software Used to Process the Data Acquired		Outcomes	Conclusions
		Name	Type of 3D Scanner	Characteristics of 3D Scanner	Scanner	CAD		
PHOTOGRAMMETRY								
Dal Maso and Cosmi (2019)	Ankle-Foot	Default Camera	Photogrammetry	No data	Agisoft Photoscan Pro	SolidWorks	150 photos taken. 80% of calculation time was used for photo alignment, tie point cloud, sparse cloud cleaning and cleaning. Mesh exportation to STL format with ≈20000 faces.	Scanner can be used on other parts of the body. The printed orthosis had great geometrical correspondence and comfort. The method showed instability when converting STL into CAD which requires experience and ability.
Ciobanu et al. (2013)	Foot	Default Camera	Photogrammetry	No data	3DSOM	No data	20 to 40 leg shots were taken. The software automatically created a cloud of 3D points from photos and transformed the points into a 3D mesh.	Use of photogrammetry were feasible in the case of foot orthosis fabrication as a cost-effective 3D reconstruction technique. Some problems in surfaces with indentations and blind holes.
Ranaldo et al. (2022)	Forearm	Structure Sensor Mark II (Occipital)	Photogrammetry	Based on active stereo vision	Autodesk MeshMixer	Rhinoceros	The analysis was carried out on three cast meshes having different pattern distributions but an identical overall shape. All models show a perfectly elastic behaviour, with a maximum σv well below the tensile strength of the material (50 MPa) and a maximum displacement.	This study shows that a semi-automatic, programmable tool allows to design anatomical customized orthopaedic casts with optimized features for the treatment of forearm fractures. Its main advantages are: it does not require specific CAD skills to perform the design of the orthosis; it does not take significant time for the generation of the model; the designs can be subject to finite element analysis to foresee different load scenarios and validate the choice of geometry.
STRUCTURED LIGHT								
Baronio et al. (2016)	Hand (including fingers)	3D Scan-in-a-Box optical scanner	Structured light	Scans in about 4 seconds, with metric accuracy of 0.1% in relation to the size of the object size	No data	Rhinoceros	Anatomy was obtained with 8 acquisitions (2min each). Total scanning time was 1h30min for acquisition with data cleaning and rigid alignment with 1h for mesh creation, regularization, and repair.	The methodology was geometrically satisfactory with a favourable trade-off between high-accuracy (in the reproduction of the patient anatomy) and low-cost requirements.
Krajňáková et al. (2020)	Shoulder, neck and face	Artec EVA	Structured light	Resolution: 0.5 mm; accuracy: 0.1 mm; distance accuracy: 0.03% at 1000 mm; texture resolution: 1.3 Mpx;	Artec Studio	No data	The scanner captured all types of hair. Better results with tousled hair and wet hair. Beard is not advisable, as the neck area will be blurred. It is possible to scan complicated body shapes.	Scanner outputs can be used in medicine for the design and manufacture of orthoses and dental implants; simulation before and after plastic surgery, preservation of cultural heritage and virtual reality.
Dessery and Pallari (2018)	Knee brace	Artec EVA and iSense	Structured light	Artec Eva: Resolution: 0.5 mm; frame rate: 16Hz iSense: Resolution: 0.9 (at 0.5m) ± 30mm (at 3m); frame rate: 30 Hz	Artec Studio 9 (Artec Eva); 3DSizeMe (iSense)	Artec Studio 9 (Artec Eva); MSoft (iSense)	Three scans were performed on each participant with Artec (410s ± 118s) and iSense (507s ± 94s) from the malleolus to the upper thigh art. Processing time was 3588s ± 423s for Artec and 460s ± 169s for iSense. Mean circumferences were created to compare results.	Manual measurement is the accurate method to take lower limb measurements, but the inter- and intra-reliability is poor and information about leg shape is limited. 3D scanners can provide lower limb measurements with similar accuracy, but better repeatability ((intraclass correlation coefficient: 0.99 − 1.0) and 0.15% mean differences).
Rogati et al. (2019)	Foot	Microsoft Kinect Sensor and IQube	Structured light	Microsoft Kinect: Laser emitter an infrared and an RGB camera to obtain a 300.000 point-cloud Accuracy: 2.8 ± 0.6mm; IQube: No data	Skanect (Kinect); No data (IQube)	Geomagic	Acquisition time for the Kinetic was 25s. The comparison between 3D scans of the plantar surface resulted in error of 2.8±0.6mm (left feet) and 2.9±0.4mm (right feet). In the arch region were 1.4±0.4mm (left feet) and 1.6±0.5mm (right feet). Good repeatability of the Kinect scans was observed. The foot	The total cost of the prototype created with the Kinetic Sensor is about 200–300€, which is at least one order of magnitude lower than that of commercial laser-based foot scanners. While accuracy and repeatability results were largely consistent across subjects, and between left and

							dimensions were like the corresponding PodoBox (manual measurement).	right foot intra-subject, the sample of feet analysed was small.
Dombroski, Balsdon and Froats (2014)	Foot	Microsoft Kinect	Structured light	No data	No data	MeshLab	Two AFOs were created. One by AM with Kinect and one created by TPCM. The TPCM provided the most control over movement of the medial longitudinal arch. The arch height index (AHI) was 21.2mm (shod only), 21.4mm (AM AFO) orthosis and 22.0mm (TPCM).	The 3D printing AFO resulted in a higher AHI than the shod condition, however, the differences between the 3 conditions were minimal. Variability was similar with standard deviations within 0.13 mm. Sample size of only one subject was small. Kinect could be a low-cost method of custom foot orthotic manufacturing.
Cha et al. (2017a)	Ankle-Foot	Artec Eva	Structured light	Maximum snap rate: Up to 16 fps	No data	MediACE 3D	The study compared an AM AFO with conventional AFO. In QUEST, all items were ranked as "very satisfied" or "satisfied." The patient was more satisfied with the AM AFO regarding weight and ease of use and more effectiveness on conventional AFO.	The AM AFO focused on the weight, individualization, and comfort rather than the function. In addition, the printed AFO had the advantage of being easily wearable inside a shoe compared to the conventional AFO, which usually requires larger shoes to wear.
Kim et al. (2018)	Wrist and hand	Artec™ Eva	Structured light	No data	Artec™ Eva	Geomagic Touch and Geomagic Freeform software	The Patient-Rated Wrist Evaluation showed significant pain relief in both groups. Two items of the 28 Orthotics and Prosthetics Users' Survey (OPUS) questions, "Put toothpaste on brush and brush teeth" and "Dial a touch tone phone," showed high satisfaction scores, with statistically significant difference in the experimental group.	The 3D-printed wrist orthosis was superior to the cock-up orthosis in some items of the OPUS. Wrist pain was reduced in the 3D-printed wrist orthosis as well as the cock-up orthosis, so the 3D-printed wrist orthosis could possibly play the same role as the off-the shelf cock-up orthosis.
Powers et al. (2022)	Ankle-Foot	Occipital, Inc., San Francisco CA	Structured light	No data	Design Studio software (Standard Cyborg, Inc., San Francisco CA)	No data	Excellent interrater reliability was obtained for scan-based measures. Excellent intrarater test-retest reliability was established for the scanning process. MDC values for intrarater test-retest reliability were typically around or below 4mm for foot and ankle measures, and under 6mm for circumference and length	The results of this study demonstrate that low-cost 3D limb scanning can be used to obtain valid and reliable measurements of 3D limb geometry for the purpose of AFO fitting, when collected using the clinically relevant standardized conditions presented here.
Ambu et al. (2023)	Neck	Microsoft Azure Kinect DK	Structured light	1Mpx depth sensor, a 12Mpx RGB camera and two IR illuminators to obtain mappings of the object's depth with high accuracy in a very short time. The illuminator used in wide field of-view mode is tilted an additional 1.3 degrees downward relative to the depth camera	No data	No data	Topology Optimization (TO) model, structurally evaluated by means of FE analysis, also in comparison with an orthosis having a ventilation pattern configured as Voronoi cells, showed a satisfactory behaviour also considered that, voids are large for extension and flexion loading, stress distribution occurs in areas of limited size with reference to the extent of the upper parts where the load is applied. The highest values of maximum displacement and maximum Von Mises stress was obtained for extension loading; however, maximum displacement was lower than 2 mm, while maximum stress was under the limit value for HPB.	A scanning system made up of three synchronized low-cost sensors, suitably arranged, has been developed. This system allows a fast acquisition, about 5 s, with minimum discomfort for the patient. The scanning system is also potentially suitable to hospital setting, being low cost and provided with a GUI for semi-automatic management of the device. The manufacturing of prototypes was done with a new bio-based material, which also contribute to lightness and satisfies the aesthetic demands. Neck temperature measurements highlighted a better performance for the TO orthosis even with the insertion of a padding. TO orthosis is very promising as regards user's comfort, an automatized strategy for the procedure will be investigated.
Mo et al. (2019)	Foot	David SLS HD 3D scanner	Structured light	No data	No data	Geomagic Freeform	Results showed lower peak rearfoot eversion angles during running with TPM or 3D printed (3DP) orthoses than no-orthoses control condition (CON). No differences were observed in other biomechanical parameters among the three conditions. Running with TPM and 3DP orthoses resulted in better perceived comfort in "medial-lateral control" and "heel cushioning" than CON. There were no statistical differences in all parameters between TPM and 3DP orthoses.	The present findings indicate improved comfort during running with TPM or 3DP orthoses, which hinted 3DP orthoses could be a viable alternative to TPM orthoses for clinical practice.
Chu et al. (2020)	Hand	Occipital Inc.	Structure light	No data	Apple Corp., Cupertino	Digital Vernier Caliper	The QUEST revealed the highest score in the mean satisfaction level. The items evaluated	The new process saves time and is highly accurate in clinical practice. The short thumb orthosis

							were dimension, weight, adjustments, safety, durability, simplicity, comfort, and effectiveness.	prototype created by the proposed design procedure offers satisfactory functional quality in numerous aspects and high practicality in clinical practice.
Kuo et al. (2019)	Head and neck	Go! SCAN 50, Creaform	Structured light	Max Resolution: 0.5mm	No data	No data	Smartphone use increased the head and neck flexion angles in all postures, and sitting without back support showed the greatest head and neck flexion angles. The posture-correcting effect of the customized collar was better than the Aspen Vista and Sport-aid collars. In addition, the customized collar was more comfortable to wear than the other two collars in most contact areas.	Smartphone use increased both the head and neck flexion in different postures, and the proposed customized 3D-printed cervical collar significantly reduced the head and neck angles.
Lee et al. (2019)	Hand	Artec Eva, Artec	Structured light	No data	No data	Geomagic Freeform	The JHFT score improved after application 3D printed devices. In most QUEST items, 3D printed devices showed better results than ready-made assistive devices. The typing speed became faster in 3D printed devices than in ready-made assistive devices. The patient was satisfied with the orthosis in writing a pen, eating food and typing keyboard because of its fitness to his hand and easy-to-use.	The study designed and manufactured a patient-specific assistive device optimized for patient function after estimating the disability status of a patient with brain injury through 3D printing techniques.
LASER								
Roberts et al. (2016)	Ankle-Foot	FastSCAN	Laser	No data	No data	Rodin 4D	134 AFOs fabricated with CAD technology and traditional plaster method in a double-blind randomised (1:1) controlled trial design was compared. No difference in time taken to cast or scan the limbs. Rectification and moulding time for cast AFOs was 55.1±26.0min and for scanned AFOs was 26.9±12.2min.	70% of patients said they preferred to be scanned than to have their limbs cast in plaster. A significantly higher proportion of scan based AFOs failed to meet the specification stipulated by the orthotist increasing production time by 9 days.
Parry, Best and Banks (2020)	Grip for the Hand	ROMER Absolute Arm	Laser	No data	Geomagic Wrap	Fusion 360 with Nettfab	The data collection was approximately 10 min. Manufacturing time was 10h5min with a cost of €10.90 (with overheads and machine depreciation excluding labour).	The study demonstrated that AM and Scanners is a viable method of producing customised daily living aids, which is anticipated to improve quality of life for sufferers of arthritis at low-cost.
Liu et al. (2019)	Ankle-foot	EinScan—Pro, SHINING 3D	Laser	No data	No data	Geomagic Studio	With respect to the temporal-spatial parameters, the velocity and stride length in the gait with AFO increased significantly as compared to the gait without AFO. The cadence increased, double limb support phase decreased, and the step length difference decreased in the gait with AFO; however, the difference was not statistically significant.	This study confirmed the feasibility of patient specific AFO fabricated by AM techniques and demonstrated the process of modifying AFO models successfully. The specific ankle-foot orthoses fabricated by material PA12 have a significant effect on the improvement of velocity and stride length in people with stroke.
Telfer et al. (2013a)	Foot	No data	Laser	No data	No data	No data	Significant group effects were seen with customized FOs reducing above knee muscle activity in pronated foot types compared to normal foot types. Interaction effects were seen for gastrocnemius medialis and soleus. Significant linear effects of posting level were seen for plantar pressure at the lateral rearfoot, midfoot and lateral forefoot. A group effect was also seen for plantar pressure at the medial heel.	This study provides evidence that a customized FOs can provide a dose response effect for selected plantar pressure variables, but no such effect could be identified for muscle activity. Foot type may play an important role in the effect of customized orthoses on activity of muscles above the knee.

Telfer et al. (2013b)	Foot	No data	Laser	No data	No data	No data	Significant and linear effects of posting were seen for the peak and mean rearfoot eversions, peak and mean ankle eversion moments, and peak and mean knee adduction moment variables. Group effects were observed for the peak and mean forefoot abduction and for the peak knee adduction moment	These data indicate that a dose–response effect, with a linear trend for both the rearfoot and knee, exists for customized FOs used to treat pronated foot type.
OPTICAL								
Sabyrov et al. (2021)	Neck	Sense (2nd generation)	Optical scanner	No data	No data	Fusion 360	The extended support section, which is positioned on trapezius muscles, improved comfortability, and stability. The breathability of skin is achieved via well distributed elliptical holes. The convex shape at the front model gives convenient swallowing. Application of flexible TPE (flex) material adds flexible property, hence enhance the dressing process. Comparative to PLA material, it has a lower density, which defines low weight. The negligible deformation during numerical assessment emphasized the strength of design.	The fabricated orthosis model possesses high accuracy in terms of the neck shape of the patient. This was accomplished through 3D scanning and further processing of the CAD model. The advantage and applicability of new cervical orthosis design and the flexible filament were demonstrated.
Buonamici et al. (2021)	Arm	Oplà 2.0	Optical scanner	Depth technology: Active stereoscopic Operating range: ~0.16–10 m Resolution: 1280 × 720 Framerate: Up to 90fps Field of view FOV: H69°, V43°, D77° (±3°)	Oplà 2.0 GUI	No data	All errors measured in the reconstruction were in the range [−2.9, 1.5] mm, the mean error of the signed distance is −0.49 mm with a standard deviation of 0.64 mm. The composition of the panel group has allowed the validation of the acquisition system on significantly different hand-wrist-arm anatomies.	Except some local errors, Oplà 2.0 performed well within the limits imposed by the accuracy requirements.
Zheng et al. (2020)	Wrist-hand	HCP	Optical scanner	No data	No data	Unigraphics NX 8.0 Software	After six weeks: -A significant difference was found between the two groups (experimental group and control group) in the change of Modified Ashworth Scale scores -There was no statistically significant difference between the two groups in flexion and radial-deviation angles -There was a significant difference between the two groups in the change of Fugl-Meyer Assessment scores -No statistically significant difference was found in the change of visual analogue scale scores between the two groups -A statistically significant difference was found in the change of swelling scores between the two groups -No statistically significant difference was found in the change of subjective feeling scores between the two groups.	3D-printed orthosis showed greater changes than low-temperature thermoplastic plate orthosis in reducing spasticity and swelling, improving motor function of the wrist and passive range of wrist extension for stroke patients.
Fu et al. (2022)	Ankle-Foot	Sense (2nd generation)	Optical scanner	No data	No data	Rhinoceros	The study acquired data from 10 hemiplegic stroke participants. Gait performance and Plantar Pressure for AM AFO, standard AFO and Barefoot on 10-m walking. Plantar pressure of hemiplegic leg increased at in AM AFO compared with bare foot. Contact area and peak pressure increased with AM AFO vs standard AFO and barefoot. QUEST was made to evaluate participant satisfaction. Mixed	Dynamic plantar pressure measurement is feasible and useful for evaluation of ankle equinovarus deformity in hemiplegic stroke patients. AM AFO has at least the same ability to increased medial midfoot plantar pressures over affected leg compared with standard AFO. More medial weight bearing and more symmetric contact area over sole with AM AFO, which is more similar to physiological finding in normal subject.

							results for satisfaction obtained without statistical differences.	
COMBINATION OF DIFFERENT SCANNERS								
Grazioso et al. (2018)	Spinal	INBODY and Polhemus FastSCAN SCORPION	Photogrammetry and Laser	Photogrammetry: Circular structure, 17 pillars (7 cameras each with 5Mpx). Polhemus FastSCAN SCORPION: No data	No data	No data	Photogrammetry allowed instantaneous capture, but processing time was longer vs. laser scanner. Deviation between scanners was +0.90 mm and −1.11mm. The laser scan obtained 13,150 faces and the inbody scan obtained 68,750 faces.	The photogrammetric scanner showed good accuracy and high-fidelity colour. The availability in medical centres could help the patients, thanks to the minimally invasive procedure and medical practitioners, in having a system which results simple to use.
Belokar, Banga and Kumar (2017)	Ankle-Foot	No data	Laser with structured light	No data	No data	No data	The 3D scanner was rotated manually around patient's limb to create the template model in just one minute. Time-saving approach when digitizing.	3D scanning is suitable to produce custom orthotics.
Weigert et al. (2016)	Foot	Default Camera and Roland MDX-40	Photogrammetry and Mechanical 3D scanner (Touch Probe / Point-to-point scanner)	Photogrammetry: Sony Xperia SP C5303 smartphone Roland MDX-40: Head course: 305 x305x105mm; Accuracy variable and up to 0.04mm	Scanner: No data (Roland MDX-40); Memento (photogrammetry)	CATIA; Geomagic	62 photos taken for photogrammetry and reconstruction take 30min. MDX-40 took 26H to scan the plaster cast. Relative error between plaster model and photogrammetry was 2.85% and 0.72% between plaster model and MDX-40.	Both scans showed similar topography of the foot. Mechanical presented more irregularities; however, this mesh provided more details that the MDX-40 especially between the toes. The 2.85% relative error presented by photogrammetry could be compensated with the application of soft material on the surface.
Volonghi, Baronio and Signoroni (2018)	Hand	Cronos 3D Dual (static scanner) and Insight3 (real-time scanner)	Structured light and optical scanner	Cronos 3D Dual: 4s per frame; 2 Mpx. Accuracy: ±30–60 µm. Insight3: Real time; 1280 × 1024 Px Accuracy: ±0.25–0.5 mm.	Optical RevEng 2.4	No data	Scan processing time was 7.5min for volunteers and 9min for patients. Error inferior to 0.5mm between scanners. Cronos 3D with volunteers achieved a complete. Insight3 with patients did not have any motion artifacts.	For Cronos 3D, motion artefacts relating to involuntary movements were successfully corrected. The preservation of all fine textural information of the final aligned model was demonstrated. For Insight 3, motion artefacts were reduced or even avoided. Both scanners proved appropriate for hand anatomy acquisition.
NO SCANNER TYPE SPECIFIED								
Murzac et al. (2021)	Spine	No data	No data	No data	Meshmixer	Fusion 360	The scanning and processing of the obtained data can be done following the procedure described in this paper. This ensures a compliant geometry for virtual analysis of the product that will be produced for a certain user. At the same time, the generative design guarantees the choice of a geometry, manufacturing technologies and a material that leads to the choice of the optimal option from a technological and economic point of view. Also, with the help of the software filters it is possible to identify the optimal variant for the manufacturer according to the objectives set for each production cycle	The chosen option can vary from one production batch to another and from one stage of the product life cycle to another. The final concept of the spinal orthosis is designed for upper body posture correction of clinically healthy individuals, with no pre-existing congenital malformations of the spine.

TPCM – Traditional Plaster Casting Method; Mpx – Megapixels; Px – Pixels; fps – frames per second; Hz – Hertz; QUEST – Quebec User Evaluation of Assistive Technology; AM – Additive Manufacturing; AFO – Ankle Foot Orthosis; m – meters; h – hours; FO – Foot Orthosis; PA12 – Polyamide 12 (Nylon 12); TPM – Traditional Plaster Method; TPE – Thermoplastic Elastomer; TPU - Thermoplastic Polyurethane; PLA - Polylactic Acid; CAD – Computer-Aided Design.

Discussion

The production of customized orthotics has increasingly garnered attention, with projections indicating a significant surge in their utilization over the next decade. This growth is primarily attributed to advancements in 3D scanning technologies, which are becoming faster, simpler, and more effective (Parry et al., 2020). The clinical and research applications of 3D scanning systems, particularly in anthropometric measurement, have been well-documented. Considering growing concerns regarding the use of radiation in medical imaging, these systems offer a safer alternative by minimizing patient exposure to radiation, as seen with X-ray or computer tomography.

Despite their potential, the integration of new 3D technologies in the National Health Service remains limited. The main hurdles are the high costs involved, as well as the time and training required for prosthetist orthotist professionals to adapt to using 3D Scanners. Overcoming these challenges could revolutionize the process of supplying customized orthoses, making it more efficient and cost-effective (Roberts et al., 2016). Several studies have validated the feasibility of Additive Manufacturing (AM) and scanners in producing customized daily living aids. This approach is expected to significantly enhance the quality of life at a reduced cost (Belokar et al., 2017; Cha et al., 2017a; Dessery & Pallari, 2018; Dombroski et al., 2014a; Parry et al., 2020; Powers et al., 2022; Roberts et al., 2016; Rogati et al., 2019; Sabyrov et al., 2021). Patients have expressed a preference for scanning over traditional plaster casting methods (Roberts et al., 2016). The 3D-printed orthoses are noted for their accurate geometrical correspondence to patient anatomy and comfortable fit, striking a balance between precision and affordability (Baronio et al., 2016; Dal Maso & Cosmi, 2019).

Photogrammetric Scanners

Photogrammetry, as a 3D scanning technology, utilizes photographs to create detailed three-dimensional models. This method involves taking multiple photographs of an object from various angles and merging these images to construct a comprehensive 3D representation. Such an approach is particularly valuable in orthotic design, where the accurate replication of body parts is essential. Additionally, photogrammetry eliminates the issues of body movement during scanning and does not require markers on the patient (Grazioso et al., 2018).

Dal Maso and Cosmi (2019) and Ciobanu et al. (2013) have effectively demonstrated the utility of photogrammetry in creating detailed and accurate 3D models for orthotic applications. Their research, which focused on ankle-foot orthoses, illustrated the method's capability in generating high-fidelity scans. These scans were instrumental in producing orthoses that are both well-fitting and comfortable for the wearer. The study particularly highlighted photogrammetry's strength in capturing intricate details, a critical factor for areas needing precise support. Ciobanu et al. (2013) expanded the use of photogrammetry to the creation of foot orthoses. Their findings emphasized photogrammetry's potential in generating detailed mesh structures, crucial for designing orthoses that accurately match a patient's anatomical structure. They also identified challenges in scanning areas with deep depressions or occlusions, which can affect the precision of the final 3D model. A notable advantage of photogrammetry is its ability to quickly acquire data. This is a significant benefit over other scanning methods that might necessitate extended and static patient positioning. With photogrammetry, a complete scan can be obtained in a relatively short period, thereby reducing patient discomfort, and minimizing errors caused by movement (Ciobanu et al., 2013). The evolution of photogrammetry software has also played a key role in simplifying the transformation of raw images into usable 3D models. Improvements in image processing algorithms have enabled more accurate model reconstruction, even in suboptimal photographic conditions. This advancement is particularly important in clinical environments where time efficiency and resource optimization are crucial. However, photogrammetry does have its limitations. The need for precise alignment of images in photogrammetry and the possibility of inaccuracies in regions with complex geometry or poor contrast are challenges that need to be addressed (Struck et al., 2019). Moreover, converting STL models to CAD for orthotic design requires a certain level of expertise in both photogrammetry and CAD software (Mavroidis et al., 2011).

Structured Light Scanners

Structured light scanning, a critical technology in the field of orthotic design, is represented significantly in this review, comprising 13 out of the 30 studies analysed. This prevalence underscores its extensive utilization and importance in the development of orthotic devices. This technology works by projecting patterned light lines from a fixed source (like a projector), capturing detailed coordinates of the scanned model, including colours and textures

(Agudelo-Ardila et al., 2019; Pribanić et al., 2019; Salvi et al., 2010), providing high-resolution data crucial for creating detailed orthotic devices.

All the studies concluded that this technology is capable to accurately replicate complex body geometries including fine details, surface textures and minor anatomical variations, an important aspect in the creation of effective and comfortable orthoses. Furthermore, the authors addressed various challenges associated with structured light scanning. One of the primary limitations noted is the requirement for the subject to remain still during the scanning process. As structured light involves capturing multiple images from different angles in a constant flow, even slight movements can lead to inaccuracies in the final model (Shamata & Thompson, 2018). This aspect can be particularly challenging when working with certain patient groups, such as children or individuals with certain disabilities. Another consideration is the processing time and computational requirements (Zhang & Yilmaz, 2016). While this technology can capture highly detailed data, processing this data into a usable 3D model can be time-consuming and resource intensive. Advances in computing power and software optimization are gradually overcoming these limitations, making structured light scanning more accessible and efficient.

This technology has been tested and analysed on practically every part of the body, ranging from head and neck (Ambu et al., 2023; Krajňáková et al., 2020; Kuo et al., 2019); upper limb including the hand (Baronio et al., 2016; Chu et al., 2022; Kim et al., 2018; Krajňáková et al., 2020; K. H. Lee et al., 2019) to lower limb (Cha et al., 2017b; Dessery & Pallari, 2018; Dombroski et al., 2014b; Mo et al., 2019; Powers et al., 2022; Rogati et al., 2019).

Baronio et al. (2016) exemplify the potential of structured light scanning in orthotic fabrication. Their research focused on the creation of spinal orthoses. They highlighted the technology's ability to capture the complex curvature and nuances of the spine with remarkable precision, a critical factor in designing effective spinal orthoses. There was a particular focus in the cases of Krajňáková et al. (2020), Powers et al. (2022) and Rogati et al. (2019) on determining whether the obtained anatomical model was accurate both metrically and qualitatively. Krajňáková et al. (2020) study, especially, addresses the limitations in capturing hair and facial hair (beard), a common problem across all technologies. While it is possible to eliminate this interference in certain parts of the human body (for example, using a sock on a lower limb or gloves on upper limbs), in other body parts it may become complicated without some form of prior hair removal. The studies by Rogati et al. (2019),

Powers et al. (2022), and Ambu et al. (2023) were the only ones that directly addressed the monetary value comparison between scanners, but they never directly compared them with the traditional plaster casting method.

Laser Scanners

Laser technology is typically employed for scanning shapes and surfaces. It efficiently gathers anthropometric data, aiding in the production of customized orthoses based on digital scans (S. Y. Lee et al., 2013; Parry et al., 2020). Nonetheless, its limited range can be a disadvantage, particularly for larger body parts like legs and feet, as the process becomes time-consuming (Glock et al., 2017).

Roberts et al. (2016) study becomes relevant for the comparison between 3D scanners and the Traditional Method Plaster Caster. Theu tested a considerable sample of lower leg scans to construct 134 AFOs and conducted a double-blind randomized controlled trial. This trial demonstrated that the time for constructing an orthosis using 3D scanners is on average 28.2 minutes less, and that 70% of patients expressed a preference for being scanned rather than having their limbs cast in plaster. Nonetheless, a significantly higher proportion of scan based AFOs failed to meet the specifications stipulated by the orthotist, resulting in an increased production time of 9 days. The most recent study employing laser scanning technology dates to 2020, which may indicate a decline in the use of this type of technology for acquiring human models for subsequent orthosis construction via AM.

Optical Scanners

Optical scanners, which project light over the body and trace surface topography, collect data to form a "point cloud." This data is then processed through computer algorithms to generate a precise model (Wells, 2019). While these scanners are accurate, they require a balance between scanning speed and the resolution of their optical and electronic components to produce a clean CAD model (Del Corso et al., 2009).

Optical scanners tend to be more cost-effective and user-friendly compared to other types. However, they are more susceptible to errors during capture, as they do not emit their own light and are extremely dependent on the quality of ambient lighting where the acquisition is taking place. Notably, Buonamici et al. (2021) study constructed a new type of scanner,

achieving reconstruction errors in the range of [−2.9, 1.5] mm using Active Stereoscopic technology.

Comparing Technologies

When comparing different technologies, photogrammetry enables rapid capture, but its processing time can be lengthy (Grazioso et al., 2018). For example, Weigert et al. (2016) found that while capturing 62 photos through photogrammetry took only 30 minutes, the reconstruction process was time-consuming. Belokar, Banga, and Kumar (2017) combined laser and structured light technologies, completing a scan in just one minute by manually rotating the scanner around the patient's limb. Despite the processing times, these methods are still faster than traditional plaster casting. From a global perspective, photogrammetry stands out as one of the most promising options due to its accuracy, minimal acquisition time, high-fidelity colour (Grazioso et al., 2018) and shape reproduction (Sabyrov et al., 2021) although only 3 studies used this technology. Probably due to the expensive cost associated with photogrammetry equipment and can often be beyond the means of departments and healthcare professionals. The equipment also lacks accurate calibration. Despite this, low-cost photogrammetry has been increasingly recognized as a feasible and effective method. Particularly Structure-from-Motion photogrammetry has been highlighted as a low-cost and accurate technique for acquiring 3D models of human limbs (Westoby et al., 2012). The use of low-cost 3D limb scanning technology has been evaluated for its repeatability and validity in obtaining accurate representations of limb geometry at a reasonable cost (Ismail et al., 2020). Additionally, smartphone photogrammetry has been investigated, demonstrating the optimization of methods and quantitative evaluation of suitability for prosthetics and orthotics (Cullen et al., 2021). The integration of photogrammetry with smartphone technology has been explored to facilitate low-cost limb scanning, expanding the scope of orthotic telemedicine, and providing affordable scanned limbs to underserved areas (Cabrera et al., 2022). Moreover, the combination of photogrammetry and transfer learning with DeepLabv3 for image segmentation has been proposed to facilitate low-cost limb scanning using cell phones, further emphasizing the potential for cost-effective applications in orthotics (Cabrera et al., 2022).

Patient Centred Outcomes

From a biomechanical perspective, the study by Mo et al. (2019) compared standard and 3D printed orthoses created using 3D scanners and AM technologies. They found lower peak rearfoot eversion angles during running with both types of orthoses compared to running barefoot, although no statistical differences were observed between the orthoses. Similarly, Telfer et al. (2013), employing the same patient data acquisition methodology, demonstrated that customized foot orthoses could provide a dose-response effect for selected plantar pressure variables. However, they found no corresponding effect on muscle activity. They further noted a dose-response effect, with a linear trend for both the rearfoot and knee, in treating pronated foot type with customized foot orthoses.

In comparisons of AM Ankle-Foot Orthoses (AFO) with conventional ones, patients preferred the AM AFO for its lighter weight and ease of use, despite the conventional AFO being more effective in certain aspects (Cha et al., 2017a). Notably, four studies (Cha et al., 2017b; Chu et al., 2022; Fu et al., 2022; K. H. Lee et al., 2019) employed the Quebec User Evaluation of Satisfaction with Assistive Technology (QUEST) test to evaluate dimensions, weight, adjustments, safety, durability, simplicity, comfort, and effectiveness. Two of these studies involved orthoses designed using 3D structured light scanners, and their findings demonstrate that patients are more satisfied with 3D-printed orthoses than with conventional orthoses. These observations underscore the critical role of patient-centred design in orthotic development, where customization and material choice are pivotal in enhancing the user experience. The integration of evaluation tools like QUEST into clinical practice provides invaluable insights for healthcare professionals, facilitating a deeper understanding of patient needs and preferences. This comprehension is crucial in guiding the selection and design of more effective and comfortable orthotic solutions, particularly in rehabilitation contexts. Such patient-centric approaches in orthotic design not only cater to functional needs but also significantly improve the overall satisfaction and quality of life for the users.

Zheng et al. (2020) reported that AM orthoses resulted in better outcomes compared to low-temperature thermoplastic plate orthoses in reducing spasticity and swelling, and in improving motor function and passive range of wrist extension in stroke patients. Additionally, Lee et al. (2019) designed and manufactured a patient-specific assistive device using 3D printing techniques, optimized for the functional needs of a patient with brain injury, after assessing the patient's disability status. The subsequent step involves transferring the

acquired data to CAD software for mesh adjustment and measurement processing. Various reverse engineering software like Rhinoceros, Rapidform, Geomagic, and LeiosMesh are used, although this stage is time-consuming and demands high expertise from the user. The challenge lies not only in the orthotist-prosthetist proficiency with 3D Scanners but also in the user-friendliness of these software systems, which are not yet optimally aligned for direct orthosis construction (Baronio et al., 2016; Liu et al., 2019).

Future Research

Despite the importance of the outcomes provided by most studies on the use of 3D scanners, a notable gap is observed in the detailed description of methodologies, limiting the potential for replication and comparison by other researchers. Many studies lack comprehensive details about scanner characteristics and the types of software used, particularly for orthosis construction. Additionally, one study even fails to identify the scanner or its technology. Moreover, the involvement of actual patients in these studies is limited, with much of the research conducted on healthy individuals. Considering the anticipated future reliance on these 3D technologies, it becomes imperative to conduct more research within clinical settings.

Conclusion

Currently, it is possible to capture the human anatomy using 3D scanners. However, reducing the digitization time remains a crucial challenge to prevent any minimal movement from the patient. While the results are promising, they also highlight the challenges associated with integrating new technologies into clinical practice. Considerations such as the initial costs of equipment, training requirements, and the need to adapt clinical workflows are significant. Generally, the studies analysed suggest that photogrammetry and structured light are the most suitable 3D scanning technologies for acquiring human body data for custom orthotics. There is also a growing belief in the field that scientists will increasingly develop 360º 3D scanners capable of capturing the human limb's anatomy in a single shot. The traditional method of building custom-made orthoses with plaster casts has remained largely unchanged despite the introduction of new technologies aiding post-processing. With today's advancements, there is an opportunity to transition from the traditional method to one that better meets the needs of patients and professionals. As 3D scanners become more

affordable, their integration into clinics becomes feasible, allowing for the proper training of health professionals. However, there is a need to develop specific software to streamline the ortho-sis building process, making it both easier and faster.

Acknowledgements

The authors would like to acknowledge the support of the Fundação para a Ciência e a Tecnologia FCT/MCTES (PIDDAC) and Centro2020 through the following Projects: UIDB/04044/2020; UIDP/04044/2020; SFRH/BD/145292/2019; Associate Laboratory ARISE LA/P/0112/2020; PAMI—ROTEIRO/0328/2013 (Nº 022158) and ReinventO (POCI-01-0247-FEDER-040021).

Conflicts of Interest

The authors declare that they have no conflict of interest.

References

Agudelo-Ardila, C. P., Prada-Botía, G. C., & Rodrigues G, P. H. (2019). Orthotic prototype for upper limb printed in 3D: A efficient solution. *Journal of Physics: Conference Series*, *1388*(1), 012016. https://doi.org/10.1088/1742-6596/1388/1/012016

Ambu, R., Oliveri, S. M., & Calì, M. (2023). Neck orthosis design for 3D printing with user enhanced comfort features. *International Journal on Interactive Design and Manufacturing*. https://doi.org/10.1007/s12008-023-01507-1

Baronio, G., Harran, S., & Signoroni, A. (2016). A Critical Analysis of a Hand Orthosis Reverse Engineering and 3D Printing Process. *Applied Bionics and Biomechanics*, *2016*. https://doi.org/10.1155/2016/8347478

Belokar, R. M., Banga, H. K., & Kumar, R. (2017). A Novel Approach for Ankle Foot Orthosis Developed by Three Dimensional Technologies. *IOP Conference Series: Materials Science and Engineering*, *280*(1), 2–7. https://doi.org/10.1088/1757-899X/280/1/012030

Brognara, L., Fantini, M., Morellato, K., Graziani, G., Baldini, N., & Cauli, O. (2022). Foot Orthosis and Sensorized House Slipper by 3D Printing. *Materials*. https://doi.org/10.3390/ma15124064

Buonamici, F., Carfagni, M., Puggelli, L., Servi, M., & Volpe, Y. (2021). A Fast and Reliable Optical 3D Scanning System for Human Arm. In L. Roucoules, M. Paredes, B. Eynard, P. Morer Camo, & C. Rizzi (Eds.), *Advances on Mechanics, Design Engineering and Manufacturing III* (pp. 268–273). Springer International Publishing.

Cabrera, I. A., Zhou, Y., Ngo, E., Rao, R. R., & Lin, A. Y. (2022). *Image Segmentation Using Transfer Learning With DeepLabv3 to Facilitate Photogrammetric Limb Scanning*. https://doi.org/10.36227/techrxiv.19742488

Cha, Y. H., Lee, K. H., Ryu, H. J., Joo, I. W., Seo, A., Kim, D. H., & Kim, S. J. (2017a). Ankle-foot orthosis made by 3D printing technique and automated design software. *Applied Bionics and Biomechanics*, *2017*. https://doi.org/10.1155/2017/9610468

Cha, Y. H., Lee, K. H., Ryu, H. J., Joo, I. W., Seo, A., Kim, D. H., & Kim, S. J. (2017b). Ankle-foot orthosis made by 3D printing technique and automated design software. *Applied Bionics and Biomechanics*, *2017*. https://doi.org/10.1155/2017/9610468

Chu, C. H., Wang, I. J., Sun, J. R., & Liu, C. H. (2022). Customized designs of short thumb orthoses using 3D hand parametric models. *Assistive Technology*, *34*(1), 104–111. https://doi.org/10.1080/10400435.2019.1709917

Chudnofsky, C. R., Byers, S. R., Roberts, J. R., Hedges, J. R., & Chanmugam, A. S. (2004). *AS: Clinical Procedures in Emergency Medicine*. Philadelphia.

Ciobanu, O., Ciobanu, G., & Rotariu, M. (2013). Photogrammetric Scanning Technique and Rapid Prototyping Used for Prostheses and Ortheses Fabrication. *Applied Mechanics and Materials*, *371*, 230–234. https://doi.org/10.4028/www.scientific.net/AMM.371.230

Cullen, S., Mackay, R., Mohagheghi, A. A., & Du, X. (2021). The Use of Smartphone Photogrammetry to Digitise Transtibial Sockets: Optimisation of Method and Quantitative Evaluation of Suitability. *Sensors*. https://doi.org/10.3390/s21248405

Dal Maso, A., & Cosmi, F. (2019). 3D-printed ankle-foot orthosis: A design method. *Materials Today: Proceedings*, *12*, 252–261. https://doi.org/10.1016/j.matpr.2019.03.122

Del Corso, M., Abà, G., Vazquez, L., Dargaud, J., & Ehrenfest, D. M. D. (2009). Optical Three-Dimensional Scanning Acquisition of the Position of Osseointegrated Implants: An in vitro Study to Determine Method Accuracy and Operational Feasibility. *Clinical Implant Dentistry and Related Research*, *11*(3), 214–221. https://doi.org/10.1111/j.1708-8208.2008.00106.x

Dessery, Y., & Pallari, J. (2018). Measurements agreement between low-cost and high-level handheld 3D scanners to scan the knee for designing a 3D printed knee brace. *PLoS ONE*, *13*(1). https://doi.org/10.1371/journal.pone.0190585

Dias Hensen, J. C., Foggiatto, J. A., Ulbricht, L., & Wan Stadnik, A. M. (2018). Additive Manufacturing of Customized Lower Limb Orthoses – A Review. *International Journal for Innovation Education and Research*. https://doi.org/10.31686/ijier.vol6.iss10.1175

Dombroski, C. E., Balsdon, M. E. R., & Froats, A. (2014a). The use of a low cost 3D scanning and printing tool in the manufacture of custom-made foot orthoses: A preliminary study. *BMC Research Notes*, *7*(1), 2–5. https://doi.org/10.1186/1756-0500-7-443

Dombroski, C. E., Balsdon, M. E. R., & Froats, A. (2014b). The use of a low cost 3D scanning and printing tool in the manufacture of custom-made foot orthoses: A preliminary study. *BMC Research Notes*, *7*(1). https://doi.org/10.1186/1756-0500-7-443

Eder, M., Brockmann, G., Zimmermann, A., Papadopoulos, M. A., Schwenzer-Zimmerer, K., Zeilhofer, H. F., Sader, R., Papadopulos, N. A., & Kovacs, L. (2013). Evaluation of precision and accuracy assessment of different 3-D surface imaging systems for biomedical purposes. *Journal of Digital Imaging*, *26*(2), 163–172.

Fu, J. C. M., Chen, Y. J., Li, C. F., Hsiao, Y. H., & Chen, C. H. (2022). The effect of three dimensional printing hinged ankle foot orthosis for equinovarus control in stroke patients. *Clinical Biomechanics*, *94*. https://doi.org/10.1016/j.clinbiomech.2022.105622

Geoffroy, M., Gardan, J., Goodnough, J., & Mattie, J. (2018). Cranial Remodeling Orthosis for Infantile Plagiocephaly Created Through a 3D Scan, Topological Optimization, and 3D Printing Process. *Journal of Prosthetics and Orthotics*, *30*(4), 1. https://doi.org/10.1097/JPO.0000000000000190

Glock, F., Vogel, M., Naumann, S., Kuehnapfel, A., Scholz, M., Hiemisch, A., Kirsten, T., Rieger, K., Koerner, A., Loeffler, M., & Kiess, W. (2017). Validity and intraobserver reliability of three-dimensional scanning compared with conventional anthropometry for children and adolescents from a population-based cohort study. *Pediatric Research*, *81*(5), 736–744. https://doi.org/10.1038/pr.2016.274

Górski, F., Wichniarek, R., Kuczko, W., Żukowska, M., Lulkiewicz, M., & Zawadzki, P. (2020). Experimental Studies on 3D Printing of Automatically Designed Customized Wrist-Hand Orthoses. *Materials*. https://doi.org/10.3390/ma13184091

Grazioso, S., Selvaggio, M., & Di Gironimo, G. (2018). Design and development of a novel body scanning system for healthcare applications. *International Journal on Interactive Design and Manufacturing*, *12*(2), 611–620. https://doi.org/10.1007/s12008-017-0425-9

Ho, M., Van Nguyen, J. M., Talbot, K., Heales, L., Kean, C. O., Kong, P. W., & Stanton, R. (2021). Immediate Comfort Perception of 3d-Printed Foot Orthoses in Individuals With Unilateral Heel Pain. *Prosthetics and Orthotics International*. https://doi.org/10.1097/pxr.0000000000000068

Ismail, R., Taqriban, R. B., Ariyanto, M., Atmaja, A. T., Sugiyanto, Caesarendra, W., Glowacz, A., Irfan, M., & Głowacz, W. (2020). Affordable and Faster Transradial Prosthetic Socket Production Using Photogrammetry and 3D Printing. *Electronics*. https://doi.org/10.3390/electronics9091456

Kim, S. J., Kim, S. J., Cha, Y. H., Lee, K. H., & Kwon, J. Y. (2018). Effect of personalized wrist orthosis for wrist pain with three-dimensional scanning and printing technique: A preliminary, randomized, controlled, open-label study. *Prosthetics and Orthotics International*, *42*(6), 636–643. https://doi.org/10.1177/0309364618785725

Krajňáková, V., Rajťúková, V., Hudák, R., & Živčák, J. (2020). APPLICATION OF THE ARTEC EVA SCANNER FOR ORTHOTICS IN PRACTICE. *Lékař a Technika - Clinician and Technology*, *49*(3), 92–96. https://doi.org/10.14311/CTJ.2019.3.04

Kuo, Y. R., Fang, J. J., Wu, C. T., Lin, R. M., Su, P. F., & Lin, C. L. (2019). Analysis of a customized cervical collar to improve neck posture during smartphone usage: a comparative study in healthy subjects. *European Spine Journal*, *28*(8), 1793–1803. https://doi.org/10.1007/s00586-019-06022-0

Lee, K. H., Kim, D. K., Cha, Y. H., Kwon, J. Y., Kim, D. H., & Kim, S. J. (2019). Personalized assistive device manufactured by 3D modelling and printing techniques. *Disability and Rehabilitation: Assistive Technology*, *14*(5), 526–531. https://doi.org/10.1080/17483107.2018.1494217

Lee, S. Y., Majid, Z., & Setan, H. (2013). 3D data acquisition for indoor assets using terrestrial laser scanning. *ISPRS Annals of Photogrammetry, Remote Sensing and Spatial Information Sciences. II-2 W*, *1*, 221–226.

Liu, Z., Zhang, P., Yan, M., Xie, Y., & Huang, G. (2019). Additive manufacturing of specific ankle-foot orthoses for persons after stroke: A preliminary study based on gait analysis data. *Mathematical Biosciences and Engineering*, *16*(6), 8134–8143. https://doi.org/10.3934/mbe.2019410

Mavroidis, C., Ranky, R. G., Sivak, M. L., Patritti, B. L., DiPisa, J., Caddle, A., Gilhooly, K., Govoni, L., Sivak, S., Lancia, M., Drillio, R., & Bonato, P. (2011). Patient specific ankle-foot orthoses using rapid prototyping. *Journal of NeuroEngineering and Rehabilitation*, *8*(1), 1–11. https://doi.org/10.1186/1743-0003-8-1

Mo, S., Leung, S. H. S., Chan, Z. Y. S., Sze, L. K. Y., Mok, K. M., Yung, P. S. H., Ferber, R., & Cheung, R. T. H. (2019). The biomechanical difference between running with traditional and 3D printed orthoses. *Journal of Sports Sciences*, *37*(19), 2191–2197. https://doi.org/10.1080/02640414.2019.1626069

Munhoz, R., Moraes, C. A. da C., Tanaka, H., & Kunkel, M. E. (2016). A digital approach for design and fabrication by rapid prototyping of orthosis for developmental dysplasia of the hip. *Revista Brasileira de Engenharia Biomedica*, *32*(1), 63–73. https://doi.org/10.1590/2446-4740.00316

Murzac, R., Doicin, C. V., & Ulmeanu, M. E. (2021). Data Acquisition and Generative Design for a Smart Spinal Orthosis. *Macromolecular Symposia*, *396*(1). https://doi.org/10.1002/masy.202000297

Nam, H.-S., Seo, C. H., Joo, S. Y., 김동현, & Park, D.-S. (2018). The Application of Three-Dimensional Printed Finger Splints for Post Hand Burn Patients: A Case Series Investigation. *Annals of Rehabilitation Medicine*. https://doi.org/10.5535/arm.2018.42.4.634

Neri, P., Paoli, A., Aruanno, B., Barone, S., Tamburrino, F., & Razionale, A. V. (2023). 3D Scanning of Upper Limb Anatomy by a Depth-Camera-Based System. *International Journal on Interactive Design and Manufacturing (Ijidem)*. https://doi.org/10.1007/s12008-023-01248-1

Oud, T., Tuijtelaars, J., Bogaards, H., Nollet, F., & Brehm, M.-A. (2023). Preliminary Effectiveness of 3d-Printed Orthoses in Chronic Hand Conditions: Study Protocol for a Non-Randomised Interventional Feasibility Study. *BMJ Open*. https://doi.org/10.1136/bmjopen-2022-069424

Page, M. J., & Moher, D. (2017). Evaluations of the uptake and impact of the Preferred Reporting Items for Systematic reviews and Meta-Analyses (PRISMA) Statement and extensions: a scoping review. *Systematic Reviews*, *6*(1), 1–14.

Parry, E. J., Best, J. M., & Banks, C. E. (2020). Three-dimensional (3D) scanning and additive manufacturing (AM) allows the fabrication of customised crutch grips. *Materials Today Communications*, *25*(April), 101225. https://doi.org/10.1016/j.mtcomm.2020.101225

Powers, O. A., Palmer, J. R., & Wilken, J. M. (2022). Reliability and validity of 3D limb scanning for ankle-foot orthosis fitting. *Prosthetics and Orthotics International*, *46*(1), 84–90. https://doi.org/10.1097/PXR.0000000000000066

Pribanić, T., Petković, T., Đonlić, M., & Hrgetić, V. (2019). On Fabrication of a Shoe Insole: 3D Scanning Using a Smartphone. In *IFMBE Proceedings* (Vol. 64, pp. 111–116). https://doi.org/10.1007/978-981-10-4505-9_18

Ranaldo, D., Zonta, F., Florian, S., & Lazzaro, J. (2023). A facile, semi-automatic protocol for the design and production of 3D printed, anatomical customized orthopedic casts for forearm fractures. *Journal of Clinical Orthopaedics and Trauma*, *42*. https://doi.org/10.1016/j.jcot.2023.102206

Roberts, A., Wales, J., Smith, H., Sampson, C. J., Jones, P., & James, M. (2016). A randomised controlled trial of laser scanning and casting for the construction of ankle–foot orthoses. *Prosthetics and Orthotics International*, *40*(2), 253–261.

Rogati, G., Leardini, A., Ortolani, M., & Caravaggi, P. (2019). Validation of a novel Kinect-based device for 3D scanning of the foot plantar surface in weight-bearing. *Journal of Foot and Ankle Research*, *12*(1), 1–8. https://doi.org/10.1186/s13047-019-0357-7

Sabyrov, N., Sotsial, Z., Abilgaziyev, A., Adair, D., & Ali, H. (2021). Design of a flexible neck orthosis on Fused Deposition Modeling printer for rehabilitation on regular usage. *Procedia Computer Science*, *196*, 226–234. https://doi.org/10.1016/j.procs.2021.12.009

Salvi, J., Fernandez, S., Pribanic, T., & Llado, X. (2010). A state of the art in structured light patterns for surface profilometry. *Pattern Recognition*, *43*(8), 2666–2680. https://doi.org/10.1016/j.patcog.2010.03.004

Sansoni, G., Trebeschi, M., & Docchio, F. (2009). State-of-the-art and applications of 3D imaging sensors in industry, cultural heritage, medicine, and criminal investigation. *Sensors*, *9*(1), 568–601.

Servi, M., Volpe, Y., Uccheddu, F., Furferi, R., Governi, L., & Lazzeri, S. (2018). A Preliminary Usability Assessment of a 3D Printable Orthosis Design System. *International Conference on Human-Computer Interaction*, 273–280.

Shamata, A., & Thompson, T. (2018). Using Structured Light Three-Dimensional Surface Scanning on Living Individuals: Key Considerations and Best Practice for Forensic Medicine. *Journal of Forensic and Legal Medicine*. https://doi.org/10.1016/j.jflm.2018.02.017

Struck, R., Cordoni, S., Aliotta, S., Pérez-Pachón, L., & Gröning, F. (2019). *Application of Photogrammetry in Biomedical Science*. https://doi.org/10.1007/978-3-030-06070-1_10

Telfer, S., Abbott, M., Steultjens, M. P. M., & Woodburn, J. (2013). Dose-response effects of customised foot orthoses on lower limb kinematics and kinetics in pronated foot type. *Journal of Biomechanics*, *46*(9), 1489–1495. https://doi.org/10.1016/j.jbiomech.2013.03.036

Telfer, S., Abbott, M., Steultjens, M., Rafferty, D., & Woodburn, J. (2013). Dose-response effects of customised foot orthoses on lower limb muscle activity and plantar pressures in pronated foot type. *Gait and Posture*, *38*(3), 443–449. https://doi.org/10.1016/j.gaitpost.2013.01.012

Volonghi, P., Baronio, G., & Signoroni, A. (2018). 3D scanning and geometry processing techniques for customised hand orthotics: an experimental assessment. *Virtual and Physical Prototyping*, *13*(2), 105–116. https://doi.org/10.1080/17452759.2018.1426328

Weigert, M. C., Poier, P. H., Rosenmann, G. C., Foggiatto, J. A., Volpato, N., & Okimoto, M. L. L. R. (2016). Indirect 3D scanning of the foot plant - Comparison between a medium and low-cost tools. *Advances in Transdisciplinary Engineering*, *4*, 614–621. https://doi.org/10.3233/978-1-61499-703-0-614

Wells, J. C. K. (2019). Three-dimensional optical scanning for clinical body shape assessment comes of age. *The American Journal of Clinical Nutrition*, *110*(6), 1272–1274. https://doi.org/10.1093/ajcn/nqz258

Westoby, M., Brasington, J., Glasser, N. F., Hambrey, M. J., & Reynolds, J. M. (2012). 'Structure-From-Motion' Photogrammetry: A Low-Cost, Effective Tool for Geoscience Applications. *Geomorphology*. https://doi.org/10.1016/j.geomorph.2012.08.021

Zhang, Y., & Yilmaz, A. (2016). Structured Light Based 3d Scanning for Specular Surface by the Combination of Gray Code and Phase Shifting. *The International Archives of the Photogrammetry Remote Sensing and Spatial Information Sciences*. https://doi.org/10.5194/isprs-archives-xli-b3-137-2016

Zheng, Y., Liu, G., Yu, L., Wang, Y., Fang, Y., Shen, Y., Huang, X., Qiao, L., Yang, J., Zhang, Y., & Hua, Z. (2020). Effects of a 3D-printed orthosis compared to a low-temperature thermoplastic plate orthosis on wrist flexor spasticity in chronic hemiparetic stroke patients: a randomized controlled trial. *Clinical Rehabilitation*, *34*(2), 194–204. https://doi.org/10.1177/0269215519885174

Study 2

A Review of Additive Manufacturing Studies for Producing Customized Ankle-Foot Orthoses

Authors: **Rui Silva**, António Veloso, Nuno Alves, Cristiana Fernandes and Pedro Morouço

Abstract

Ankle-foot orthoses (AFO) are prescribed to improve the patient's quality of life. Supporting weak muscles or restraining spastic muscles leads to smoother and more stable locomotion. Commonly, AFO are made using thermoplastic vacuum forming, which requires a long time for production and limited design options. Additive manufacturing (AM) can solve this problem leading to a faster and cheaper solution. This review aimed to investigate what is the state-of-art using AM for AFO. Evaluating the used manufacturing processes, customization steps, mechanical properties, and biomechanical features in humans would provide significant insights for further research. The database searches combined AM and AFO with no year or publication type restrictions. Studies must have examined outcomes on human participants with the orthoses built by AM. Other types of orthotic devices or different manufacturing techniques were excluded. Nineteen studies met the inclusion criteria. As stated by having all studies conducted in the last nine years, this is a very recent domain. Different AM processes have been used, with the majority relying on Fused Deposition Modeling. Overall, the manuscripts' quality is deficient, which is critical to promoting further studies with higher samples. Except for one paper, AM-printed AFO was comparable or superior to the thermoplastic vacuum forming AFO in mechanical tests, kinematics, kinetics, and participant feedback.

Keywords: lower extremity; rehabilitation; walking; customization; patient-specific

Introduction

Walking is one of the most critical events in daily living, and difficulty in walking is a substantial barrier for both adults and children (Inman et al., 1981). Accordingly, ankle-foot orthoses (AFO) are prescribed to improve the patient's quality of life for several walking difficulties. It is well documented that this device may help in lower limb impairments such as stride length (Hayek et al., 2007); gait speed and walking confidence (Abd El-Kafy, 2014; Bennett et al., 2012; Brehm et al., 2008; Ginosian et al., 2013; Wren et al., 2015); equinus ankle correction (Hayek et al., 2007; Skaaret et al., 2019); energy expenditure index (Brehm et al., 2008); hip extension, dorsiflexion in the swing phase and knee extension (Hayek et al., 2007; Wren et al., 2015); correction of knee hyperextension (Kobayashi et al., 2015); correction of the foot drop (Machat et al., 2011); correction of the crouch gait (Skaaret et al., 2019); increased solear muscle activity (Gronely et al., 2010); and increased resistive moment in plantar flexion (Kobayashi et al., 2015). An AFO can support weak muscles or restrain spastic muscles, leading to smoother and more stable locomotion.

Today patients can choose between standard off-the-shelf AFO and custom-made AFO. The former is cheaper but might offer less comfort to a patient than a custom-made AFO. On the other hand, custom-made AFO may increase that comfort and be adequate, but the manufacturing process is far from optimal. The most common procedure to fabricate this type of AFO is mold. However, it takes a long time to make the mold and get the final product, which may take from 2 days to several weeks depending on the post-processing needed. Also, the technician needs to spend most of that time working on the orthosis, taking the time away from the work with patients and other aspects of their work (Totah et al., 2017). Additionally, it is not adaptable to morphologic modifications (e.g., rapid body changes during children's growth), requiring highly skilled personnel (Chen et al., 2016). These inconvenient features illustrate how much research is necessary on this topic. For instance, if society can conceive a faster and cheaper method, it may be easier to change AFO along with the children's growth. Nowadays, there is no doubt that the massive customization of products and services is a regular trend over massive production, aiming for custom mass production (Morouço, 2018). With additive manufacturing (AM) being a little-explored domain, this technology allows customizing a product since it is manufactured layer-by-layer, thus allowing com-plex architectures and formats (Morouço, 2018). These architectures are previously modeled in a

virtual environment with computer-aided design (CAD) software, which differs from traditional production processes based on removing material or the deposition of materials in molds. Customization is essential for specific biomedical applications, such as orthopedics or orthotics, in which the efficiency of treatment is strongly connected with each patient's anatomical geometry (Cha et al., 2017; Olsson et al., 2017).

To the best of our knowledge, using AM for AFO production is a recent field of research. Thus, examining the available studies, their advantages, and drawbacks may pro-vide significant further investigation insights. This review aimed to investigate the use of AM for AFO, exploring the manufacturing and customization processes and evaluating their mechanical and biomechanical properties.

Materials and Methods

Database searches were performed between October 2021 and January 2022 in Web of Science, SCOPUS, PubMed (including MEDLINE), and Scielo. Terms related to additive manufacturing (3d print, additive manufacturing, selective laser sintering, fused deposition, rapid prototyping) combined with terms to AFO (ankle-foot, orthoses, orthosis) were used, without restrictions.

Original papers were written in English with ankle-foot orthoses developed by additive manufacturing, and human participants were included. Any sample size was eligible, and there were no restrictions on the type of participants (sex, age, culture, ethnicity, healthy, non-healthy). We have included additive manufacturing types (e.g., fused deposition modeling, selective laser sintering or melting, stereolithography, digital light processing). The articles must have any outcomes by tests performed on human participants with the orthoses built by AM.

All narrative or systematic reviews were excluded, although the reference list was examined for additional references. Any full article not written in English or unpublished data were excluded. Any article with other types of orthotic devices (e.g., Foot orthosis (F.O.), knee-ankle foot orthosis (KAFO, splint), or different manufacturing techniques (e.g., mold filling) were excluded.

Data extraction was standardized after removing the excluded articles and deleting duplicates. Titles and abstracts from the search results were screened using the eligibility criteria and reviewed by two authors (R.S. and P.M.) for inclusion. We have assessed the

overall quality of evidence using the Grading of Recommendations Assessment, Development and Evaluation (GRADE) process (GRADEpro GDT) (Balshem et al., 2011).

Results

Figure III.2 illustrates the steps to identify relevant articles for the review based on PRISMA guidelines (Moher et al., 2009). The initial database search identified 1466 articles, and after duplicate removal, 540 were considered potentially related and were screened for relevant content. No additional articles were identified following a hand search of reference lists. After reading the title and abstract of the 540 articles, 63 were selected for possible inclusion in this review, and full-text articles were retrieved. 19 of the 63 articles were included in this review in the last phase because they met the inclusion criteria. The 19 studies included outcomes such as mechanical tests (Belokar et al., 2017; Cha et al., 2017; Chen et al., 2014; Dal Maso & Cosmi, 2019; Liu et al., 2019), Finite element method (FEM) simulations (Dal Maso & Cosmi, 2019; Chen et al., 2014); Sarma et al., 2019), participant feedbacks (healthy participants) (Mavroidis et al., 2011; Patar et al., 2012; Schrank & Stanhope, 2011) patient feedbacks (non-healthy participants) (Dal Maso & Cosmi, 2019; Liu et al., 2019); Wierzbicka et al., 2017), QUEST (Cha et al., 2017; Chae et al., 2020), kinematics (Cha et al., 2017; Chae et al., 2020; Choi et al., 2017; Creylman et al., 2013; Harper et al., 2014; Lin et al., 2017; Liu et al., 2019; Mavroidis et al., 2011; Ranz et al., 2016; Sarma et al., 2019; Telfer et al., 2012; Vasiliauskaite et al., 2019), kinetics (Harper et al., 2014; Mavroidis et al., 2011; Ranz et al., 2016; Sarma et al., 2019; Telfer et al., 2012; Vasiliauskaite et al., 2019), observation after trial (Deckers et al., 2018; Wierzbicka et al., 2017), dimensional accuracy (Schrank & Stanhope, 2011) and EMG (Choi et al., 2017; Harper et al., 2014; Ranz et al.,2016).

A description of the AM AFO details can be found in Table III.2. We have used the GRADE process to analyze the quality of the included studies (Table III.3). The outcomes included were: (1) walking ability through biomechanical tests (kinematics, kinetics, EMG); (2) durability through mechanical test; (3) durability through observation after trial; (4) patient satisfaction assessed with the Quebec User Evaluation of Satisfaction with assistive technology (QUEST); (5) comfort through participant/patient feedback; (6) dimensional accuracy and material strength and AFO behavior simulation assessed by FEM analysis. All the outcomes obtained overall very-low quality evidence.

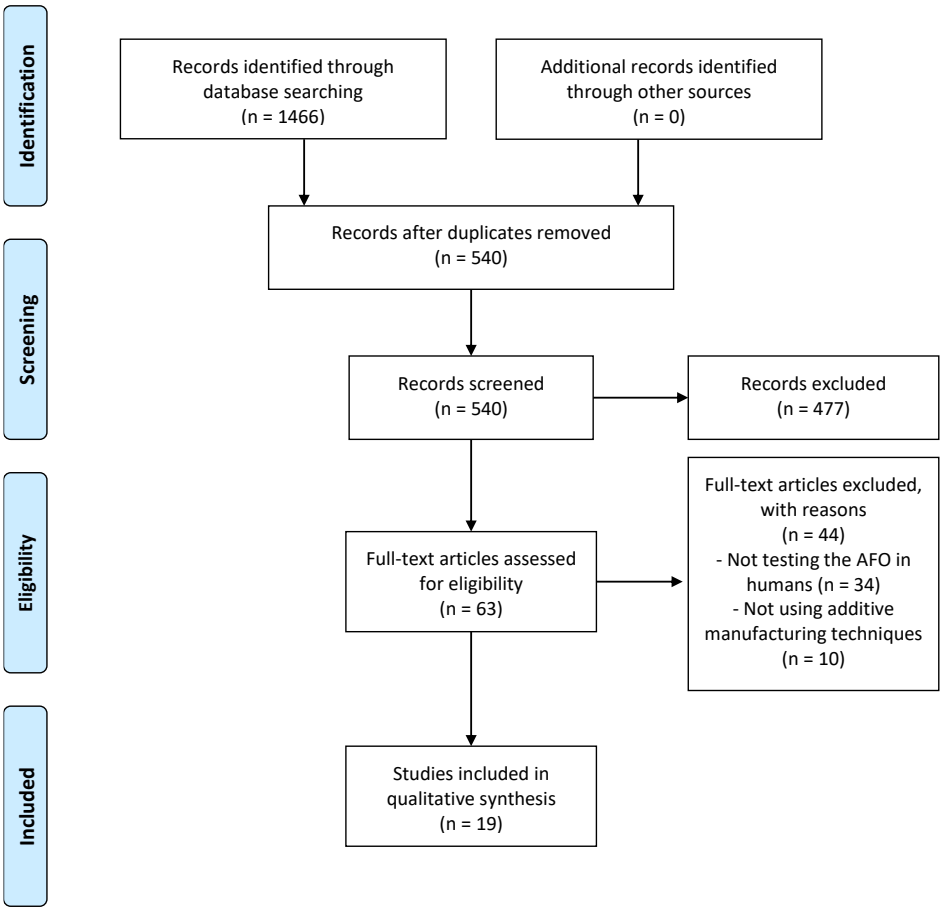

FIGURE III.2 - Flow diagram of the search history and selection process

TABLE III.2 - Included studies with AFO details, participant/patient characteristics, intervention and control conditions, outcomes, and main results

Reference	AFO Details		Participant/Patient Characteristics		Intervention vs Control Condition	Outcomes	Main Results and Conclusions
	AM Printing Method	Material	N	Condition			
Belokar et al. (2017)	FDM	ABS	1 (M; 65 kg)	Healthy	Customized ABS AFO	Mechanical test	Maximum 6.8% strain with 38.4 MPa tensile strength exerted on the AFO. Rupture of the AFO at 14.96 kJ/m^2 impact. No deformation in the inner surface with load up to 15 kN. No deformation of the AFO in hydraulic press test with 10 tons load.
Cha et al. (2017)	FDM	TPU	1 (F; 68 yrs)	Foot drop on the right side after an embolectomy	Customized TPU AFO vs TTPP AFO vs Shod Only	Mechanical test; QUEST; kinematics	No structural change, crack or damage after 300k repetitions in the durability test. Both AFO increased gait speed and stride length. Step width decreased with the FDM AFO. Higher bilateral symmetry with FDM AFO induced more stability. Better satisfaction on the FDM AFO after using both AFO for 2 months.
Chae et al. (2020)	FDM	TPU	1 (F; 72 yrs)	Foot drop on the right side after posterior lumbar interbody fusion and abscess	Customized TPU AFO vs Without AFO	Kinematics; QUEST	Using the AFO, cardiorespiratory fitness and functionality increased. Stability score with eyes open and closed improved. In QUEST items, the device and service subscore had a perfect score (5 points) showing the patient's satisfaction with the AFO.
Chen et al. (2014)	FDM	ABS; ULTEM (Polyetherimide)	1 (M; 29 yrs; 68 kg)	Healthy	Customized ABS AFOs vs TTPP AFO	Mechanical test; FEM simulations	The highest strains were found at about 50% of the gait cycle for PP (-15.3×10^{-4}), ABS (-6.4×10^{-4}), and ULTEM (-10.3×10^{-4}). The FEM estimated rotational stiffness (N.m/deg) for PP (39.1), ABS (67.7) and ULTEM (89.0). Using calculated loading conditions and FEM can help design AFO to match the patient's need and achieve desired biomechanical functions.
Choi et al. (2017)	FDM	PLA	8 (4F; 4M; 25 ± 5 yrs; 1.7 ± 0.1 m; 67 ± 9 Kg)	Healthy	Customized PLA AFO with elastic polymer bands	Kinematics, ultrasound; EMG; musculoskeletal simulation	Use of elastic polymer bands to control the stiffness of the orthosis. More stiffness led to a decrease of peak in knee extension and ankle dorsiflexion angles and maximum length of gastrocnemius and Achilles tendon. Due to medial gastrocnemius operating length

							and velocity changes, slower walking speeds may not receive the expected energy savings.
Creylman et al. (2013)	SLS	Nylon 12 (PA2201)	8 (M; 47 ± 13 yrs; 1.97 ± 0.1m; 85.30 ± 14.20 Kg)	Unilateral Foot Drop due to dorsiflexor weakness	Customized Nylon 12 AFO vs TTPP AFO vs Bare Foot	Kinematics	Similar stride duration for all interventions. Significant differences in both AFO vs barefoot for stride length of the affected (1377 vs. 1370 vs. 1213 mm) and unaffected (1373 vs. 1365 vs. 1223 mm) limb and stance phase duration of the affected limb (62.1 vs. 62.1 vs. 60.6%) for barefoot, AM AFO and TTPP. Range of Motion different between AFO due to Nylon 12 stiffer than PP.
Deckers et al. (2018)	SLS	PA12	7 (4 Adults; 3 Children)	Trauma, Neuro-muscular disorder and cerebral palsy	Customized PA12 AFO with carbon fiber strut vs TTPP AFO	Observation trial after	TTPP AFO (n = 7) survived the 6 weeks of clinical trial. For AM AFO (n = 7), 3 broke when doing sport, 1 broke while the patient walked upstairs, 1 broke due to manufacturing defect, 1 became dirty. A cracking began at the metatarsal phalangeal joint and 1 survived with no problems.
Harper et al. (2014)	SLS	Nylon 11 (PA D80—S.T.)	13 (M; 29 ± 6 yrs; 1.8 ± 0.1 m; 88 ± 11 Kg)	Unilateral lower extremity injuries	Customized Nylon 11 PD-AFO Strut (nominal vs 20% stiffer vs more compliant)	Kinematics; kinetics; EMG	Minimal effect in kinetics, kinematics and EMG gait cycle with different strut stiffness. Propulsive and medial GRF impulses were only influenced by AFO stiffness with the medial GRF impulse significantly increased in the stiff condition. Orthotists may not need to control the stiffness level precisely and may instead prescribe the AFO stiffness based on other factors.
Lin et al. (2017)	FDM	No Data	1	Healthy	Customized AFO vs TTPP AFO	Kinematics	The walking speed (367 vs. 389 mm/s), stride length (583 vs. 598 mm), cadence (76 vs. 78 steps/min) and range of motion of knee joint in flexion were similar in both AFO. TTPP AFO obtained more extended range of motion due to different footplate.
Liu et al. (2019)	MJF	PA12	12 (4F; 8M; 56 ± 9 yrs; 1.7 ± 0.1 m; 69 ± 10 Kg)	Stroke patients (6 Ischemic, 6 Hemorrhage).	Customized PA12 AFO vs Without AFO	Mechanical kinematics; patient feedback test;	Using AM AFO increased velocity (0.17 ± 0.06 vs. 0.20 ± 0.07 m/s), stride length (0.43 ± 0.10 vs. 0.48 ± 0.11 m) and cadence (47.0 ± 14.4 vs. 53.8 ± 15.5 times/min). Double limb support phase (36.3 ± 5.6 vs. 33.6 ± 5.2 %) and the step length difference decreased (0.16 ± 0.12

							vs. 0.10 ± 0.09 m). AM AFO obtained adequate dimensional accuracy, toughness, high strength, lightweight and comfort. No breakage occurred within 3 months.
Dal Maso & Cosmi (2019)	FDM	PLA	1 (F; 21 yrs)	Post-traumatic rehabilitation	Customized PLA AFO	Mechanical Test; FEM simulations; patient feedback	Great geometrical correspondence and comfort between the foot and the AM AFO. Cheap production method compared with AFO produced with other technologies. PLA material was considered excellent for manufacturing the AFO but is not the most mechanically resistant.
Mavroidis et al. (2011)	SLA	Accura 40 Resin; DSM Somos 9120 Epoxy Photopolymer	1	Healthy	Customized Accura 40 Resin AFO vs Customized DSM Somos 9120 Epoxy Photopolymer vs TTPP AFO vs Shod only	Kinematics; kinetics; participant feedback	AM AFO obtained optimal fit and great comfort. Kinetics and Kinematics gait cycle revealed that the AM AFO performed similarly to the TTPP AFO.
Patar et al. (2012)	FDM	ABS	1	Healthy	Customized ABS/PP DAFO (Dynamic Ankle-Foot Orthosis) vs No control	Participant feedback	The price reduction in producing AM DAFO was reduced 100-fold compared to the products that existed in the market. The patient considered the performance was good.
Ranz et al. (2016)	SLS	Nylon 11 (PA D80—S.T.)	13 (29.50 ± 6.28 yrs; 1.79 ± 0.09m; 87.92 ± 9.70Kg)	Lower extremity trauma resulting in unilateral ankle muscle weakness	Customized Nylon 11 PD-AFO (low vs middle vs high bending axis)	Kinematics; Kinetics; EMG	Most of the patients (7) preferred the middle bending axis. After EMG test, PD-AFO altered medial gastrocnemius activity in late single-leg support. Low bending axis resulted in the greatest medial gastrocnemius activity. Different bending axis locations had few effects on ankle and knee peak joint kinematics and kinetics.
Sarma et al. (2019)	No data	13% Kevlar Fiber reinforced ultra-high molecular weight polyethylene (UHMWPE)	>1	No data	Customized Kevlar Fiber Reinforced UHMWPE AFO	Kinematics; kinetics; FEM simulations	Based on FEM simulations Kevlar Fiber Reinforced UHMWPE-based composite material was selected as best material for fabrication of AFO compared with ABS, PLA, Nylon 6/6 and PP. The maximum ankle angle during dorsiflexion was 12° and maximum angle during plantar flexion was 23°.

Schrank & Stanhope (2011)	SLS	Nylon 11 (DuraForm EX Natural Plastic)	2 (1 M; 1 F; 34.50 ± 19.09 yrs; 1.71 ± 8.49 m ; 65.85 ± 8.41 Kg)	Healthy	Customized Nylon 11 PD-AFO	Dimensional accuracy; clinical observation; participant feedback	The dimensional accuracy of the fabricated PD-AFOs was 0.5mm. The participants demonstrated a fully accommodated, smooth, and rhythmic gait pattern following gait test and reported no discomfort. No signs of uneven pressure distribution, redness, or abrasions.
Telfer et al. (2012)	SLS	Nylon 12 (PA2200)	1 (M, 29 yrs; 1.85 m; 78.00Kg)	Healthy	Customized Nylon 12 AFO with gas spring vs Shod only	Kinematics; kinetics	Use of a gas spring to control the stiffness of the AFO. AM AFO led to a lower peak plantarflexion angle at the start stance and higher at the toe-off vs shod only. Peak ankle internal plantarflexion moment was significantly reduced in both AFO conditions compared to shod. Both AFO conditions also increased peak knee internal flexion moment during the first half of stance. AM AFO clinical performance and biomechanical changes equivalent to TTPP AFO with the advantage of the design freedom provided by AM.
Vasiliauskaite et al. (2019b)	SLS	PA12	6 (3M (1 adult, 2 children); 3F (1 adult, 2 children); 23 ± 20 yrs; 1.5 ± 0.2 m; 52 ± 33 Kg)	1 poly-trauma; 1 Charcot-Marie Tooth; 3 cerebral palsy; 1 bilateral clubfoot	Customized PA12 AFO with carbon strut vs TTPP AFO vs Shod Only	Kinematics; kinetics	AM AFO step length significantly increased vs TTPP AFO due to better energy storage properties. Push-off phase characteristics and joint work in stance became more atypical using AFO and no significant improvements in speed were observed.
Wierzbicka et al. (2017)	FDM	ABS	1 (F; 22 yrs)	Chronic ankle joint instability	Customized ABS AFO vs No control	Observation after trial; patient feedback	The AFO was comfortable and fully stabilizing the ankle joint. After gait cycle the test ended with success without no bruises or irritations on patient's skin. Limitations were found in climbing stairs, riding a bike, and driving a car.

FDM, Fused Deposition Modeling; SLS, Selective Laser Sintering; MJF, Multi-Jet Fusion; SLA, Stereolithography; ABS, Acrylonitrile Butadiene Styrene; TPU, Thermoplastic Polyurethane; PLA, Poly-Lactic Acid; PA12, Polyamide 12; PP, polypropylene; M, Male; F, Female; TTPP, Traditional thermoformed polypropylene; DAFO, Dynamic ankle-foot orthosis; PD-AFO, Passive dynamic ankle-foot orthosis; QUEST, Quebec user evaluation of satisfaction with assistive technology; FEM, finite element model; EMG, electromyography; GRF, Ground reaction force; AM, Additive manufacturing

TABLE III.3 - GRADE evidence profile

Certainty assessment							Nº of patients/participants		Effect		Certainty	Importance
Nº of studies	Study design	Risk of bias	Inconsistency	Indirectness	Imprecision	Other considerations	Customized AM AFO	Traditional Thermoformed Polypropylene AFO	Relative (95% CI)	Absolute (95% CI)		
Walking ability through biomechanical tests (kinematics, kinetics, EMG)												
12	Observational studies [1]	serious [a,b]	not serious	Serious [a]	not serious	none	66 [g]	9	--	--	⊕◯◯◯ VERY LOW	Important
Durability through a mechanical test												
5	Observational studies [2]	not serious	not serious	serious [a,c]	serious [d]	none	16	2	--	--	⊕◯◯◯ VERY LOW	Important
Durability through observation after trial												
2	Observational studies [3]	very serious [e]	not serious	not serious	serious [d]	none	8	7	--	--	⊕◯◯◯ VERY LOW	Important
Patient satisfaction assessed with the QUEST												
2	Observational studies [4]	serious [f]	not serious	not serious	serious [a,d]	none	2	1	--	--	⊕◯◯◯ VERY LOW	Important
Comfort through participant/patient feedback												
6	Observational studies [5]	very serious [b,e]	not serious	serious [a]	serious [d]	none	17	1	--	--	⊕◯◯◯ VERY LOW	Important
Dimensional accuracy through FaroArm (fit with a 3 mm spherical tip)												
1	Observational studies [6]	not serious	not serious	serious [a]	serious [d]	none	1	0	--	--	⊕◯◯◯ VERY LOW	Important
Material strength and AFO behavior simulation assessed by FEM analysis												
3	Observational studies [7]	serious [d]	not serious	serious [a]	serious [d]	none	3	1	--	--	⊕◯◯◯ VERY LOW	Important

CI Confidence Interval

[1] (Cha et al., 2017; Liu et al., 2019; Sarma et al., 2019; Mavroidis et al., 2011; Chae et al., 2020; Creylman et al., 2013; Harper et al., 2014; Vasiliauskaite et al., 2019; Telfer et al., 2012; Lin et al., 2017; Choi et al., 2017; Rans et al., 2016)
[2] (Cha et al., 2017; Dal Maso & Cosmi, 2019; Belokar et al., 2017; Chen et al., 2014; Liu et al., 2019)
[3] (Wierzbicka et al., 2017; Deckers et al., 2018)
[4] (Cha et al., 2017; Chae et al., 2020)
[5] (Dal Maso & Cosmi, 2019; Liu et al., 2019; Patar et al., 2012; Schrank et al., 2011; Mavroidis et al., 2011; Wierzbicka et al., 2017)
[6] (Schrank et al., 2011)
[7] (Dal Maso & Cosmi, 2019; Chen et al., 2014; Sarma et al., 2019)

[a] Not all studies compared to traditionally thermoformed polypropylene AFOs; [b] Differences in type of Participants / Patients conditions; [c] Differences in type of AM / Traditional AFO assessed; [d] Participants / Patients number assessed low; [e] No quantitative assessment; [f] No blinding of AFOs; [g] Sarma et al. (2019) does not reference the exact number of participants, so the value of 1 element was considered

We have compared the studies that used kinematics as an outcome with the data on the leg's ankle and knee angles with the AM AFO in the stance phase (Table III.4). The maximum angle for ankle dorsiflexion and knee flexion was 22° and 20°, respectively.

TABLE III.4 - Comparison between the different maximum angles obtained by the ankle and knee of the leg with the AFO at the stance phase

Reference	N	Healthy / Unhealthy	Ankle dorsiflexion (°)	Ankle plantarflexion (°)	Knee Flexion (°)	Knee Extension (°)
Cha et al. (2017)	1	Unhealthy	22	−8	NA	NA
Liu et al. (2019)	12	Unhealthy	0	−2	13	5
Sarma et al. (2019)	>1	No Data	10	1	NA	NA
Mavroidis et al. (2011)	1	Healthy	15	−8	NA	NA
Chae et al. (2020)	1	Unhealthy	NA	NA	NA	NA
Vasiliauskaite et al. (2019)	6	Unhealthy	13	0.2	12.8	−2
Telfer et al. (2012)	1	Healthy	18 [1]; 16 [2]	0 [1]; −3 [2]	19 [1]; 15 [2]	10 [1]; 8 [2]
Lin et al. (2017)	1	Healthy	NA	NA	20	−1
Choi et al. (2017)	8	Healthy	10	−5	17	5
Harper et al. (2014)	13	Unhealthy	6.55 [3]; 5.86 [4]; 5.68 [5]	−6.59 [3]; −6.03 [4]; −5.96 [5]	13.38 [3]; 15.71 [4]; 17.17 [5]	NA
Creylman et al. (2013)	8	Unhealthy	NA	-3	19	NA
Ranz et al. (2016)	13	Unhealthy	5.83 [6]; 5.19 [7]; 4.87 [8]	−0.68 [6]; −0.61 [7]; −0.65 [8]	17.34 [6]; 17.46 [7]; 17.85 [8]	5.21 [6]; 4.69 [7]; 4.91 [8]

NA Not Applicable

[1] AFO with high stiffness; [2] AFO with lowered stiffness; [3] AFO stifeness compliant; [4] AFO stifeness nominal; [5] AFO stifeness stiff; [6] AFO with low bending axis; [7] AFO with middle bending axis; [8] AFO with high bending axis

Discussion

Additive manufacturing methods to build ankle-foot orthoses are still in a very embryonic state, as shown by the papers' publication date. All articles reported in this review have been carried out in the past nine years, and exponential growth is expected in the next decade with the evolution of additive manufacturing printers and the type of materials used. From the nineteen studies retrieved, just seven compared the customized AM AFO with the traditional thermoformed polypropylene AFO. Similar results in biomechanical tests and comfort were observed. Accordingly, the adoption of AM may lead to faster and cheaper processes having at least the same outcomes.

Researchers have been using different types of AM printing and materials. The majority of the papers used fused deposition modeling (FDM) (Belokar et al., 2017; Cha et al., 2017; Chae et al., 2020; Chen et al., 2014; Choi et al., 2017; Dal Maso & Cosmi, 2019; Lin et al., 2017; Patar et al., 2012; Wierzbicka et al., 2017) and selective laser sintering (SLS) (Creylman et al., 2013;

Deckers et al., 2018; Harper et al., 2014; Ranz et al., 2016; Schrank & Stanhope, 2011; Telfer et al., 2012; Vasiliauskaite et al., 2019). Multi-jet fusion (MJF) (Liu et al., 2019) and stereolithography (SLA) (Mavroidis et al., 2011) were also used, and one manuscript did not describe the printing method (Sarma et al., 2019). The AM printing method will bring pros and cons to the orthoses manufacture and quality. The FDM process's main advantages are that no chemical post-processing is required. No resins are necessary to cure; less expensive machines and materials lead to a more cost-effective process. Nevertheless, the resolution on the z-axis is lower than in other additive manufacturing processes (Melchels et al., 2010), and interlayer distortion was the leading cause of mechanical weakness (Melchels et al., 2010). Four of the eight studies that used FDM did some mechanical tests using acrylonitrile butadiene styrene (ABS), polylactic acid (PLA), and thermoplastic polyurethane (TPU) materials. Belokar et al. (2017) showed that an ABS AFO could support 10 tons load, and the customized TPU AFO of Cha et al. (2017) survived 300000 repetitions in a durability test and two months of use by a foot drop 67 years old patient. Although the customized PLA AFO of Dal Maso & Cosmi (2019) was considered excellent for manufacture, it was not the most mechanically resistant.

Seven studies used the SLS printing process. Five studies used this process to build a complete AFO made of Nylon 11 (Schrank & Stanhope, 2011) and Polyamide (Nylon) 12 (PA12) (Creylman et al., 2013; Vasiliauskaite et al., 2019; Telfer et al., 2012; Deckers et al., 2018). Two studies used SLS to manufacture a strut to change the stiffness of a pre-built carbon AFO made by the traditional method. SLS is a process in which a powder is sintered or fused by applying a carbon dioxide laser beam. The chamber is heated to almost the melting point of the material. The laser fuses the powder at a specific location for each layer specified by the design (Wong & Hernandez, 2012). This technology's main advantages are the wide range of materials used; however, in these studies, they just used Polyamide (Nylon) 12 and Nylon 11, which show almost the same mechanical properties as the injected parts (Tang et al., 2011). The disadvantages are that the accuracy is limited by the size of particles of the material (Wong & Hernandez, 2012), slow process, high costs, and high porosity when the powder is fused with a binder (Ngo et al., 2018). Although seven studies manufactured SLS AFO, no mechanical tests were made, and just one (Deckers et al., 2018) did an observation in children and adults with mixed results. Five did not survive the six-week trial of the seven built SLS AFO (calf and foot connected by two carbon fiber rods to change the stiffness). Three broke when

doing sports (hiking, running, soccer), one broke while the patient walked upstairs, and one broke due to a manufacturing defect. Two survived the six weeks; nevertheless, one be-came dirty, and a cracking began at the metatarsal phalangeal joint. Telfer et al. (2012) attached off-the-shelf gas springs with AM printed components (shank, strut, slider, and foot), allowing the user to change the stiffness of the AFO that, could improve the ankle biomechanics helping day-to-day tasks reducing pain and fatigue. The results suggest that these devices may show equivalence in clinical performance compared with traditional AFOs however, their mechanical performance is far from ideal. Yet, no comparison was made using unhealthy participants or traditional AFOs.

Two studies used different printing techniques (SLA and MJF). SLA is one of the earliest additive manufacturing methods, which was developed in 1986 and uses a liquid-based process that consists of the curing or solidification of a photosensitive polymer when a ultraviolet (UV) laser contacts the resin (Wong & Hernandez, 2012). SLA prints high-quality parts at a fine resolution as low as 10 µm. However, it is relatively slow and expensive, the range of printing materials is minimal, is sensitive to long exposure to UV light and the printed parts are affected by moisture, heat, and chemicals. (Ngo et al., 2018; Wong & Hernandez, 2012). Mavroidis et al. (2011) used the SLA process with Acura 40 Resin and DSM Somos 9120 Epoxy Photopolymer. No mechanical test was done. They achieved an optimal fit of the AM AFO geometry to the participant's anatomy, and excellent comfort, and the AM AFO performed similarly to the traditional AFO. MJF combine SLS and binder jetting technologies. Compared to other AM methods, MJF has the lowest cost of 3D printed parts, quick printing, and no need for support; yet, it is limited to just two types of material, and the machines are large and expensive (Ngo et al., 2018; Wong & Hernandez, 2012). For instance, a single unit of material for MJF may be up to 4 times less expensive than for FDM. Liu et al. (2019) used the MJF process with Polyamide 12 material in stroke patients. The mechanical tests of the AFO showed toughness and high strength. They achieved a lightweight and comfortable AFO for the patient; however, further large-scale stroke samples and a long-term follow-up would be warranted to prove that MJF with PA12 could be a future solution to manufacturing custom AFO. Although different studies had utterly different methodologies and samples, the ABS and MJF AFOs obtained better durability results than the AFOs manufactured by SLS.

A GRADE evidence profile was created to assess the different outcomes in the included studies. The results analyzed had severe problems, mainly because most of them did not

compare the created AM AFO with a traditional polypropylene AFO. Moreover, the number of participants/patients assessed was low. The outcomes from the included studies were very heterogeneous. Although some studies (n = 12) had kinematics in their results, they commonly used only the ankle (n = 10) and knee (n = 8) degrees. The lack of other critical kinematic variables in most of the studies (e.g., cadence, angular velocity, hip angle, gait speed, step length, stride length, duration of stance/swing), combined with the heterogeneity in the methodology, type of patients (the kind of disease, gender, and age) and different AM AFO makes it challenging to have a reliable quantitative comparison. In the future, it is believed that because it is an area with massive potential for expansion, studies will begin to have a greater homogeneity in their methodologies.

AFO users have different ages, anatomy, gender, and lifestyle and can be found at various stages of the disease or disability. Stroke (Gök et al., 2003; Kesikburun et al., 2017), multiple sclerosis (van der Linden et al., 2018), cerebral palsy (Wren et al., 2015; Prosser et al., 2012; Ries et al., 2015), foot drop (Hayek et al., 2007; Skaaret et al., 2019; Carolus et al., 2019), Charcot-Marie tooth (Zuccarino et al., 2020), neck or spinal cord injury (Arazpour et al., 2013), sciatica (Prosser et al., 2012), muscular dystrophy (Townsend et al., 2015), or peroneal nerve injury (Carolus et al., 2019) are the most common diseases that need an AFO to improve kinematics and kinetics of the patients. Among the AFO functionality, the patient's comfort, pain, and disability reduction should be an essential factor to consider. In general, the reviewed papers present several flaws in their methodology. Of the studies, just six gave patient feedback for comfort and fit, and only two collected a QUEST. One study (Belokar et al., 2017) presented interesting mechanical test results; however, no results were shown regarding the durability of the AFO after being applied to an end-user. Almost 50% of the studies presented in this review used healthy participants. While it is the easiest solution to test durability, comfort, uneven pressure distribution, redness, abrasions, or geometry to the participant anatomy, measuring its impact on groups with dis-eases is critical. Currently, the time from the prescription to the design of traditional polypropylene AFO can take several weeks, making them often unusable due to the constant changes in anatomy, particularly in children. Custom AM AFOs could have an essential role in solving the manufacturing time (less than 1 day), as shown by the two studies using children as participants (Cha et al., 2017; Deckers et al., 2018). Together with the manufacturing time, the capacity to create complex structures could be the solution to change the aesthetics of the traditional AFOs, since part

of the patients who need AFO (mainly females and children) do not use them because of the appearance and finish of the orthosis (Holtkamp et al., 2015).

Looking at all the studies, further studies to build and test AM AFOs should include many more children and unhealthy participants. Furthermore, the studies should consist of all these steps: (1) a 3D Scan of the patient's lower leg or plaster caster model; (2) CAD Modeling of the AFO for the patient condition; (3) FEM simulations to tune and predict the properties of the AFO; (4) AM printing of the AFO with the selected material; (5) Mechanical tests of the AFO; (6) Biomechanical tests, durability, and satisfaction of the patient using the AFO.

The adoption of AM techniques for custom AFO may allow topological optimization, 4D manufacturing (manufacturing with smart materials), incorporation of multi-material leading to reduced weight and thickness, increased breathability, controlled flexibility, better fit, enhanced aesthetics, and the potential to eliminate several steps of production compared with traditional methods of AFO manufacture leading to a less cost and better AFO (Chen et al., 2016; Mueller, 2012). Furthermore, novel patient-specific AM AFO can substantially affect patient satisfaction, adherence to AFO usage, and overall health-related outcomes (Holtkamp et al., 2015).

Conclusion

Nowadays, it is possible to manufacture a custom orthosis using AM. Nevertheless, it is far from becoming the ideal solution for clinical practice. The studies have shown that AM custom-made orthoses are comparable to the Traditional AFO regarding kinematics, kinetics, and mechanics. In some cases, the AM custom-made orthoses performed better in comfort, performance, and optimal fit. However, the lack of more participants in studies with some diseases, the lack of more mechanical tests (e.g., durability and stiffness), no feedback from the participants, and more pediatric populations' tests bring the additive manufactured orthoses far from being used by the masses.

Acknowledgments

The authors would like to acknowledge the support of the Fundação para a Ciência e a Tecnologia FCT/MCTES (PIDDAC) and Centro2020 through the following Projects: UIDB/04044/2020; UIDP/04044/2020; SFRH/BD/145292/2019; Associate Laboratory ARISE

LA/P/0112/2020; PAMI—ROTEIRO/0328/2013 (Nº 022158) and ReinventO (POCI-01-0247-FEDER-040021).

Conflicts of Interest

The authors declare that they have no conflict of interest.

References

Abd El-Kafy, E. M. (2014). The clinical impact of orthotic correction of lower limb rotational deformities in children with cerebral palsy: A randomized controlled trial. Clinical Rehabilitation, 28(10), 1004–1014. https://doi.org/10.1177/0269215514533710

Arazpour, M., Tajik, H. R., Aminian, G., Bani, M. A., Ghomshe, F. T., & Hutchins, S. W. (2013). Comparison of the effects of solid versus hinged ankle foot orthoses on select temporal gait parameters in patients with incomplete spinal cord injury during treadmill walking. Prosthetics and Orthotics International, 37(1), 70–75.

Balshem, H., Helfand, M., Schünemann, H. J., Oxman, A. D., Kunz, R., Brozek, J., Vist, G. E., Falck-Ytter, Y., Meerpohl, J., & Norris, S. (2011). GRADE guidelines: 3. Rating the quality of evidence. Journal of Clinical Epidemiology, 64(4), 401–406.

Belokar, R. M., Banga, H. K., & Kumar, R. (2017). A Novel Approach For Ankle Foot Orthosis Developed By Three Dimensional Technologies. IOP Conference Series: Materials Science and Engineering, 280, 12030. https://doi.org/10.1088/1757-899x/280/1/012030

Bennett, B. C., Russell, S. D., & Abel, M. F. (2012). The effects of ankle foot orthoses on energy recovery and work during gait in children with cerebral palsy. Clinical Biomechanics, 27(3), 287–291. https://doi.org/10.1016/j.clinbiomech.2011.09.005

Brehm, M. A., Harlaar, J., & Schwartz, M. (2008). Effect of ankle-foot orthoses on walking efficiency and gait in children with cerebral palsy. Journal of Rehabilitation Medicine, 40(7), 529–534. https://doi.org/10.2340/16501977-0209

Carolus, A. E., Becker, M., Cuny, J., Smektala, R., Schmieder, K., & Brenke, C. (2019). The interdisciplinary management of foot drop. Deutsches Ärzteblatt International, 116(20), 347.

Cha, Y. H., Lee, K. H., Ryu, H. J., Joo, I. W., Seo, A., Kim, D. H., & Kim, S. J. (2017). Ankle-foot orthosis made by 3D printing technique and automated design software. Applied Bionics and Biomechanics, 2017. https://doi.org/10.1155/2017/9610468

Chae, D.-S., Kim, D.-H., Kang, K.-Y., Kim, D.-Y., Park, S.-W., Park, S.-J., & Kim, J.-H. (2020). The functional effect of 3D-printing individualized orthosis for patients with peripheral nerve injuries: Three case reports. Medicine, 99(16), e19791.

Chen, R. K., Chen, L., Tai, B. L., Wang, Y., Shih, A. J., & Wensman, J. (2014). Additive manufacturing of personalized ankle-foot orthosis. Transactions of the North American Manufacturing Research Institution of SME, 42(January), 381–389.

Chen, R. K., Jin, Y.-A., Wensman, J., & Shih, A. (2016). Additive manufacturing of custom orthoses and prostheses—A review. Additive Manufacturing, 12, 77–89. https://doi.org/10.1016/j.addma.2016.04.002

Choi, H., Peters, K. M., MacConnell, M. B., Ly, K. K., Eckert, E. S., & Steele, K. M. (2017). Impact of ankle foot orthosis stiffness on Achilles tendon and gastrocnemius function during

unimpaired gait. Journal of Biomechanics, 64, 145–152. https://doi.org/10.1016/j.jbiomech.2017.09.015

Creylman, V., Muraru, L., Pallari, J., Vertommen, H., & Peeraer, L. (2013). Gait assessment during the initial fitting of customized selective laser sintering ankle foot orthoses in subjects with drop foot. Prosthetics and Orthotics International, 37(2), 132–138. https://doi.org/10.1177/0309364612451269

Dal Maso, A., & Cosmi, F. (2019). 3D-printed ankle-foot orthosis: A design method. Materials Today: Proceedings, 12, 252–261. https://doi.org/10.1016/j.matpr.2019.03.122

Deckers, J. P., Vermandel, M., Geldhof, J., Vasiliauskaite, E., Forward, M., & Plasschaert, F. (2018). Development and clinical evaluation of laser-sintered ankle foot orthoses. Plastics, Rubber and Composites, 47(1), 42–46. https://doi.org/10.1080/14658011.2017.1413760

Ginosian, J., Kluding, P. M., McBride, K., Feld, J., Wu, S. S., O'Dell, M. W., & Dunning, K. (2013). Foot Drop Stimulation Versus Ankle Foot Orthosis After Stroke. Stroke, 44(6), 1660–1669. https://doi.org/10.1161/strokeaha.111.000334

Gök, H., Küçükdeveci, A., Altinkaynak, H., Yavuzer, G., & Ergin, S. (2003). Effects of ankle-foot orthoses on hemiparetic gait. Clinical Rehabilitation, 17(2), 137–139. https://doi.org/10.1191/0269215503cr605oa

Gronely, J. K., Weiss, W., Newsam, C. J., Mulroy, S. J., & Eberly, V. J. (2010). Effect of AFO Design on Walking after Stroke: Impact of Ankle Plantar Flexion Contracture. Prosthetics and Orthotics International, 34(3), 277–292. https://doi.org/10.3109/03093646.2010.501512

Harper, N. G., Esposito, E. R., Wilken, J. M., & Neptune, R. R. (2014). The influence of ankle-foot orthosis stiffness on walking performance in individuals with lower-limb impairments. Clinical Biomechanics, 29(8), 877–884. https://doi.org/10.1016/j.clinbiomech.2014.07.005

Hayek, S., Hemo, Y., Chamis, S., Bat, R., Segev, E., Wientroub, S., & Yzhar, Z. (2007). The effect of community-prescribed ankle-foot orthoses on gait parameters in children with spastic cerebral palsy. Journal of Children's Orthopaedics, 1(6), 325–332. https://doi.org/10.1007/s11832-007-0055-z

Holtkamp, F. C., Wouters, E. J. M., Van Hoof, J., van Zaalen, Y., & Verkerk, M. J. (2015). Use of and satisfaction with ankle foot orthoses. Clinical Research on Foot & Ankle.

Inman, V. T., Ralston, H. J., & Todd, F. (1981). Human walking. Williams & Wilkins.

Kesikburun, S., Yavuz, F., Güzelküçük, Ü., Yaşar, E., & Balaban, B. (2017). Effect of ankle foot orthosis on gait parameters and functional ambulation in patients with stroke. Turkiye Fiziksel Tip ve Rehabilitasyon Dergisi, 63(2), 143–148. https://doi.org/10.5606/tftrd.2017.129

Kobayashi, T., Singer, M. L., Orendurff, M. S., Gao, F., Daly, W. K., & Foreman, K. B. (2015). The effect of changing plantarflexion resistive moment of an articulated ankle-foot orthosis on ankle and knee joint angles and moments while walking in patients post stroke. Clinical Biomechanics, 30(8), 775–780. https://doi.org/10.1016/j.clinbiomech.2015.06.014

Lin, Y.-C., Lin, K.-W., & Chen, C.-S. (2017). Evaluation of the walking performance between 3D-printed and traditional fabricated ankle-foot orthoses— A prospective study. Gait & Posture, 57, 366–367. https://doi.org/10.1016/j.gaitpost.2017.06.471

Liu, Z., Zhang, P., Yan, M., Xie, Y., & Huang, G. (2019). Additive manufacturing of specific ankle-foot orthoses for persons after stroke: A preliminary study based on gait analysis data.

Mathematical Biosciences and Engineering, 16(6), 8134–8143. https://doi.org/10.3934/mbe.2019410

Machat, H., Mazaux, J. M., de Sèze, M.-P., Rousseaux, M., Daviet, J.-C., Bonhomme, C., & Burguete, E. (2011). Effect of early compensation of distal motor deficiency by the Chignon ankle-foot orthosis on gait in hemiplegic patients: a randomized pilot study. Clinical Rehabilitation, 25(11), 989–998. https://doi.org/10.1177/0269215511410730

Mavroidis, C., Ranky, R. G., Sivak, M. L., Patritti, B. L., DiPisa, J., Caddle, A., Gilhooly, K., Govoni, L., Sivak, S., Lancia, M., Drillio, R., & Bonato, P. (2011). Patient specific ankle-foot orthoses using rapid prototyping. Journal of NeuroEngineering and Rehabilitation, 8(1), 1–11. https://doi.org/10.1186/1743-0003-8-1

Melchels, F. P. W., Feijen, J., & Grijpma, D. W. (2010). A review on stereolithography and its applications in biomedical engineering. Biomaterials, 31(24), 6121–6130.

Moher, D., Liberati, A., Tetzlaff, J., & Altman, D. G. (2009). Preferred Reporting Items for Systematic Reviews and Meta-Analyses: The PRISMA Statement. PLoS Medicine, 89(9), e1000097. https://doi.org/10.1371/journal.pmed.1000097

Morouço, P. (2018). The Usefulness of Direct Digital Manufacturing for Biomedical Applications. Green Chemistry Series, 55, 478–487.

Mueller, B. (2012). Additive manufacturing technologies–Rapid prototyping to direct digital manufacturing. Assembly Automation.

Ngo, T. D., Kashani, A., Imbalzano, G., Nguyen, K. T. Q., & Hui, D. (2018). Additive manufacturing (3D printing): A review of materials, methods, applications and challenges. Composites Part B: Engineering, 143, 172–196.

Olsson, A., Hellsing, M. S., & Rennie, A. R. (2017). New possibilities using additive manufacturing with materials that are difficult to process and with complex structures. Physica Scripta, 92(5), 53002.

Patar, A., Jamlus, N., Makhtar, K., Mahmud, J., & Komeda, T. (2012). Development of dynamic ankle foot orthosis for therapeutic application. Procedia Engineering, 41(Iris), 1432–1440. https://doi.org/10.1016/j.proeng.2012.07.332

Prosser, L. A., Curatalo, L. A., Alter, K. E., & Damiano, D. L. (2012). Acceptability and potential effectiveness of a foot drop stimulator in children and adolescents with cerebral palsy. Developmental Medicine & Child Neurology, 54(11), 1044–1049.

Ranz, E. C., Russell Esposito, E., Wilken, J. M., & Neptune, R. R. (2016). The influence of passive-dynamic ankle-foot orthosis bending axis location on gait performance in individuals with lower-limb impairments. 37, 13–21. https://doi.org/10.1016/j.clinbiomech.2016.05.001

Sarma, T., Pandey, D., Sahai, N., & Tewari, R. P. (2019). Material selection and development of ankle foot orthotic device. Materials Today: Proceedings, 18, 2509–2514. https://doi.org/10.1016/j.matpr.2019.07.107

Schrank, E. S., & Stanhope, S. J. (2011). Dimensional accuracy of ankle-foot orthoses constructed by rapid customization and manufacturing framework. Journal of Rehabilitation Research and Development, 48(1), 31–42. https://doi.org/10.1682/JRRD.2009.12.0195

Skaaret, I., Steen, H., Terjesen, T., & Holm, I. (2019). Impact of ankle-foot orthoses on gait 1 year after lower limb surgery in children with bilateral cerebral palsy. Prosthetics and Orthotics International, 43(1), 12–20. https://doi.org/10.1177/0309364618791615

Tang, H.-H., Chiu, M.-L., & Yen, H.-C. (2011). Slurry-based selective laser sintering of polymer-coated ceramic powders to fabricate high strength alumina parts. Journal of the European Ceramic Society, 31(8), 1383–1388.

Telfer, S., Pallari, J., Munguia, J., Dalgarno, K., McGeough, M., & Woodburn, J. (2012). Embracing additive manufacture: Implications for foot and ankle orthosis design. BMC Musculoskeletal Disorders, 13(May). https://doi.org/10.1186/1471-2474-13-84

Totah, D., Kovalenko, I., Saez, M., & Barton, K. (2017). Manufacturing Choices for Ankle-Foot Orthoses: A Multi-objective Optimization. Procedia CIRP, 65, 145–150. https://doi.org/10.1016/j.procir.2017.04.014

Townsend, E. L., Tamhane, H., & Gross, K. D. (2015). Effects of AFO Use on Walking in Boys With Duchenne Muscular Dystrophy: A Pilot StudyA Pilot Study. Pediatric Physical Therapy, 27(1), 24–29.

van der Linden, M. L., Andreopoulou, G., Scopes, J., Hooper, J. E., & Mercer, T. H. (2018). Ankle kinematics and temporal gait characteristics over the duration of a 6-minute walk test in people with multiple sclerosis who experience foot Drop. Rehabilitation Research and Practice, 2018.

Vasiliauskaite, E., Ielapi, A., De Beule, M., Van Paepegem, W., Deckers, J. P., Vermandel, M., Forward, M., & Plasschaert, F. (2019). A study on the efficacy of AFO stiffness prescriptions. Disability and Rehabilitation: Assistive Technology, 0(0), 1–13. https://doi.org/10.1080/17483107.2019.1629114

Wierzbicka, N., Górski, F., Wichniarek, R., & Kuczko, W. (2017). Prototyping of Individual Ankle Orthosis Using Additive Manufacturing Technologies. Advances in Science and Technology Research Journal, 11(3), 283–288. https://doi.org/10.12913/22998624/76070

Wong, K. V, & Hernandez, A. (2012). A review of additive manufacturing. International Scholarly Research Notices, 2012.

Wren, T. A. L., Dryden, J. W., Mueske, N. M., Dennis, S. W., Healy, B. S., & Rethlefsen, S. A. (2015). Comparison of 2 Orthotic Approaches in Children With Cerebral Palsy. Pediatric Physical Therapy, 27(3), 218–226. https://doi.org/10.1097/pep.0000000000000153

Zuccarino, R., Anderson, K. M., Shy, M. E., & Wilken, J. M. (2020). Satisfaction with Ankle Foot Orthoses in Individuals with Charcot-Marie-Tooth. Muscle & Nerve.

Study 3

Innovative Design and Development of Personalized Ankle-Foot Orthoses for Stroke Survivors with Equinovarus Foot: A Feasibility and Comparative Trial Protocol

Authors: **Rui Silva**, Pedro Morouço, Jorge Lains, Paula Amorim, Nuno Alves and António Veloso

Abstract

Background: Ankle-Foot Orthoses (AFOs) are vital in gait rehabilitation for stroke patients. However, many conventional AFO designs may not offer the required precision for optimized patient outcomes. With the advent of 3D scanning and printing technology, there exists potential for more individualized AFO solutions, aiming to enhance the rehabilitative process. Objective: This non-randomized trial seeks to introduce and validate a novel system for AFO design tailored to stroke patients. By leveraging the capabilities of 3D scanning and bespoke software solutions, the aim is to produce orthoses that might surpass conventional designs in terms of biomechanical effectiveness and patient satisfaction.

Methods: A distinctive 3D scanner, complemented by specialized software, will be developed to accurately capture the biomechanical data of leg movements during gait in stroke patients. The acquired data will subsequently guide the creation of patient specific AFO designs. These personalized orthoses will be provided to participants, and their efficacy will be compared with traditional AFO models. The qualitative dimensions of this experience will be evaluated using the QUEST assessment tool. Feedback from healthcare professionals and the participants will be considered throughout the trial to ensure a rounded understanding of the system's implications.

Results: Spatial-temporal parameters will be statistically compared using paired t-tests to determine significant differences between walking with the personalized orthosis, the existing orthosis, and barefoot conditions. Significant differences will be identified based on p-values, with $p < 0.05$ indicating statistical significance. The Statistical Parametric Mapping (SPM) method will be applied to graphically compare kinematic and kinetic data across the entire gait cycle. QUEST responses will undergo statistical analysis to evaluate patient satisfaction, with scores ranging from 1 (not satisfied) to 5 (very satisfied). Satisfaction scores will be presented as mean values ± standard deviations. Significant variations in satisfaction levels between the personalized and existing orthosis will be assessed using a Wilcoxon signed-rank test. The anticipation is that the AFOs crafted through this innovative system will either match or outperform existing orthoses in use, with higher patient satisfaction rates.

Conclusions: Embracing the synergy of technology and biomechanics may hold the key to revolutionizing orthotic design, with the potential to set new standards in patient-centered orthotic solutions. However, as with all innovations, a balanced approach, considering both

the technological possibilities and individual patient needs, will be paramount to achieve optimal outcomes.

Keywords: 3D Scanner; 3D Printing; Ankle Foot Orthosis; Equinovarus foot; Biomechanical Analysis

Introduction

Stroke, often termed as a cerebrovascular accident, poses a monumental global health issue and stands as the second leading cause of mortality worldwide (Vos et al., 2016). In addition to the grave concern of mortality, survivors of stroke frequently grapple with substantial morbidity, most notably neurological impairments that substantially hamper their quality of life. Among these impairments, a prevalent issue is equinovarus foot a symptom characterized by the foot being plantarflexed (downward) and inverted (turned inward), often resulting from muscle imbalances or neurological impairments (Fietzek et al., 2014; Ward, 2014)

In the management and rehabilitation of equinovarus foot, Ankle-Foot Orthoses (AFOs) serve as a foundational element, supporting and aligning the ankle and foot, suppressing spastic and overpowering muscles, and assisting weak or paralyzed muscles (Cakar et al., 2010). While these devices are indispensable in aiding patients in regaining some semblance of normal gait, they come with their own sets of limitations. Broadly speaking, AFOs are categorized into two primary types: traditional off-the-shelf models and custom-crafted versions. Traditional AFOs, designed for a broad patient demographic, offer widespread accessibility but often miss the mark in addressing the unique biomechanical needs of each patient. This one-size-fits-all approach has drawn criticism for its rigidity and lack of individual customization (Zhang et al., 2013). Conversely, custom-made AFOs are meticulously tailored to fit a specific patient's anatomical structure. While they provide a more individualized fit, the process of creating these orthoses is time-consuming and very laborious. In addition, the process is also wasteful of materials, as the plaster molds and other excess fabrication materials are discarded during the fabrication process (Liu et al., 2019). This gap between age-old craftsmanship and cutting-edge precision sets the stage for technological intervention, aiming to meld the advantages of both approaches.

The concept of reverse engineering in orthotics involves capturing a patient's limb anatomy in detail, translating this information into a digital model, and then crafting an orthotic device to perfectly align with the individual's biomechanical demands (Lunsford et al., 2016; Silva et al., 2022). Utilizing 3D scanning techniques allows for a highly accurate representation of human anatomy. This digital replica serves as a blueprint upon which orthotic devices can be meticulously designed, thereby ensuring that the device is tailored to an individual's unique biomechanical requirements. Nevertheless, the integration of 3D scanning technology into

the orthotic field is fraught with challenges. Capturing a comprehensive scan, particularly of the plantar region of the foot, proves to be problematic. The quality of the scan is often compromised due to patient movements, exacerbated by the extended duration needed for the scanning process (Gefen, 2003). This prolonged duration can be uncomfortable for the patient, thereby leading to unintended movements and consequential errors in the scan data. Moreover, there are ongoing debates over the computational workload and adaptability of the resulting digital models. Such pitfalls, whether arising from anatomical complexities, patient movements, or technological limitations, could culminate in an improperly fitting orthotic device.

The science of photogrammetry, which involves making measurements based on photographs, offers a potential solution. Initially used for mapping and topographical studies (Magnani et al., 2020) its application in the medical realm, particularly in orthotics and prosthetics, has only recently been explored. The capacity to transform photographs into intricate 3D models offers quicker scan times and could minimize errors induced by patient movements (Grazioso et al., 2019). However, the full-scale integration of this promising technology into the orthopedic field is still in its infancy (Ciobanu et al., 2013; Dal Maso & Cosmi, 2019; Grazioso et al., 2018; Munhoz et al., 2016; Weigert et al., 2016). Ensuring that the resulting 3D models are an accurate reflection of patient anatomy and that the resultant devices are both functional and comfortable remains a challenge. Furthermore, orthopedics is a multi-disciplinary field that includes physicians, physical therapists, and engineers. Consequently, any new technological adoption must be orchestrated carefully to ensure effective utility across all these professions (Dickinson et al., 2019). Armed with these technological advancements, the field of orthotics is poised for a transformative evolution—a shift toward a more patient-centric and technologically-integrated paradigm. This fusion of traditional orthotic craftsmanship with cutting-edge computational tools heralds a new era in patient care, targeting both precision and broad accessibility.

Goal of this study

This research protocol delineates our approach to develop a next-generation AFO system tailored to meet the specific needs of stroke survivors. The primary objective is to harness advanced scanning tools and bespoke software for a holistic orthotic solution. By innovatively integrating technology and medical expertise, we envision a transformation in the rehabilitation journey, creating a more refined and effective recovery pathway for individuals

with post-stroke motor challenges. Our methodological framework will guide us from the initial stages of scanner and software development to a culminating phase of validation, where the proposed orthotic devices will undergo rigorous patient trials. Through this initiative, we aim to chart a progressive path in the realm of post-stroke orthotic care.

Methods

Study Design

This non-randomized feasibility study aims to harness advanced scanning technologies and innovative software for the design and refinement of orthotics tailored specifically to the unique anatomical and biomechanical needs of stroke survivors presenting with equinovarus deformity. Following a non-inferiority trial design for biomechanical outcomes and a superiority trial design for qualitative outcomes, our methodology focuses on the development of a novel AFO system. The goal is to ensure its biomechanical performance is at least as effective as off-the-shelf AFOs, while also enhancing patient satisfaction. Feedback from patients and clinical observations will serve as the primary indicators of success.

Ethics Approval

The approval for the protocol of this study was granted by the Health Ethics Committee of Centro de Medicina de Reabilitação da Região Centro – Rovisco Pais (Tocha, Portugal) in August 2022.

Consent to Participate and Consent for Publication

A document was developed at the request of the Health Ethics Committee for informed, clear, and voluntary consent for participation in research studies. The document outlines the research study's objective and assures that there will be no detriment to treatments and clinical follow-up should the patient choose to withdraw. It also guarantees the anonymity and confidentiality of all collected data, including photographs, results from the Quebec User Evaluation of Satisfaction with Assistive Technology (QUEST) (Demers et al., 1996) and biomechanical analysis data. The consent form must be signed by both the attending physician and the patient.

This protocol was prepared according to the SPIRIT (Standard Protocol Items: Recommendations for Interventional Trials) 2013 checklist for reporting a protocol study (Chan et al., 2013)

Eligibility Criteria and Recruitment Procedures

The inclusion criteria for this study have been defined with precision to select the most suitable candidates in alignment with the study objectives. We are targeting stroke survivors, both male and female, aged between 18 to 75 years, who exhibit equinovarus foot secondary to hemiparesia, affecting either the left or right side. A prerequisite for potential participants is their current utilization of AFOs. Furthermore, the concurrent use of any assistive technologies such as tripods, crutches, or canes is deemed acceptable. Essential criteria include the capacity to provide informed consent and the ability to ambulate, either independently or with the support of aforementioned devices. Conversely, candidates with concomitant neurological or orthopedic conditions that might confound the study outcomes, those with active dermatological conditions, or and severe communication impairments potentially hindering consistent participation will be excluded.

The recruitment process will be at the Centro de Medicina de Reabilitação da Região Centro. Attending physicians will review patient profiles to identify individuals meeting the stipulated criteria. Those aligning with our research parameters will be briefed on the study's aims and subsequently provided with the detailed consent document. Upon granting written consent, these individuals will be enlisted as participants, ensuring a systematic and ethically rigorous approach to data acquisition and feedback.

Clinical Outcomes

In the pursuit of developing an optimized orthotic design system, an array of clinical metrics is implemented to gauge its efficiency, efficacy, and the comfort it bestows on both patients and healthcare professionals. Ensuring a comfortable experience for the patient during the photography process is paramount, given its pivotal role in the orthotic design. This precision not only benefits the patient but also ensures that the system healthcare professionals navigate is intuitive.

Biomechanical assessments employ the Qualisys Miqus M3 system, paired with Bertec force platforms. Patients will wear the CAST lower body marker set, which consists of 36 reflective

markers, as prescribed by Cappozzo (Cappozzo et al., 1995). Observations cover three walking conditions for each participant: unaided (where possible), with the current orthosis, and with the newly designed orthosis. This methodology provides an in-depth understanding of the orthosis's efficacy, drawing from ten walking cycles for each leg, analyzing both kinematics and kinetics.

The biomechanical data under scrutiny spans temporal-Spatial parameters, which capture walking speed, gait cycle duration, step length, step time, time in stance, and time in swing. Kinematic parameters delve into pelvic movements such as anterior tilt, up obliquity, and internal rotation. Hip parameters include flexion, adduction, and internal rotation, while knee parameters assess flexion, varus, and internal rotation. Ankle and foot evaluations note dorsiflexion, inversion, pitch, and internal progression. Kinetic parameters are marked by the internal moments at the hip (extensor and valgus), knee (extensor and valgus), and ankle (plantarflexor and extensor), accompanied by the Vertical Ground Reaction Force.

The qualitative patient analysis will also incorporate the QUEST assessment. QUEST focuses on understanding the user's satisfaction with assistive technology. It evaluates a range of aspects, from device functionality to user confidence. This offers insights into patients' perceptions and benefits derived from the new orthosis in comparison to conventional models. Incorporating QUEST ensures the orthosis not only meets clinical requirements but also aligns with patient preferences and comfort levels.

Through these comprehensive evaluations, the study aims to offer an enriched perspective on the potential and effectiveness of the innovative orthotic system.

Data Analysis

The forthcoming data analysis is designed to provide an in-depth understanding of the impact of personalized orthoses on gait parameters in relation to both the pre-existing orthosis and barefoot walking. The sample size was estimated for a prespecified power of 90%, while the α value was set at $<.05$. The primary outcomes will be represented through spatial-temporal data tables and normalized gait graphs, spanning from 0 to 100% of the gait cycle for the left and right legs.

Spatial-temporal parameters will undergo statistical comparisons utilizing paired t-tests. This will discern any significant differences between walking with the personalized orthosis, the

pre-existing orthosis, and walking barefoot. Significant distinctions will be recognized based on p-values, with a threshold set at 95% indicating statistical significance.

Graphical comparisons of kinematic and kinetic data will employ the Statistical Parametric Mapping (SPM) method. SPM is tailored for the analysis of one-dimensional biomechanical data series, such as kinematic curves, yielding a nuanced understanding of differences across the entire gait cycle, rather than mere isolated time points. The analysis will leverage the SPM1D script. By employing SPM1D, it becomes feasible to pinpoint regions in the gait cycle where palpable differences between conditions (existing orthosis, personalized orthosis, and barefoot) arise. This rigorous method offers a continuous evaluation over the entire time or space continuum, safeguarding against missing subtle yet clinically pivotal variations.

Simultaneously, the QUEST responses will be statistically analyzed to evaluate patient satisfaction. Scores from the QUEST, which range from 1 (not satisfied) to 5 (very satisfied), will be presented as mean values ± standard deviations for each question. A one-sample t-test will be employed to determine if the mean satisfaction scores significantly differ from a neutral value. Additionally, a Wilcoxon signed-rank test may be used to determine differences in satisfaction levels between using the personalized orthosis and the pre-existing orthosis. Any statistically significant variations in user satisfaction between the two orthoses will provide insight into the preferential utility and comfort of the personalized design.

In essence, this multifaceted statistical approach aims to quantify not only the possible biomechanical advantages of personalized orthoses over standard ones but also the subjective satisfaction of users, ensuring a holistic assessment of the new system's efficacy.

Results

The methodology and approach of this research harbor specific expectations concerning its outcomes. We will use the Qualisys Track Manager (QTM) from Qualisys® to capture biomechanical data with unparalleled accuracy. Once gathered, the data will be processed and analyzed rigorously. With the integration of the PAF framework from Qualisys® and Visual 3D from C-Motion®, the raw biomechanical data will be transformed into actionable insights that promise to inform and refine orthotic design.

One of the primary quantitative expectations is that the orthosis developed through the new system will either match or surpass the performance of the patient's current orthosis. This benchmark stems from the belief that the integration of state-of-the-art technology and

personalized biomechanical data can achieve superior orthotic design. On the qualitative front, using QUEST assessment, the expectation leans towards higher satisfaction rates with the new orthosis. Since the orthosis is tailored specifically to the patient's leg, it is anticipated that its unique design will resonate more with patients, ensuring better fit, comfort, and overall user experience. To ensure comprehensive results, feedback from healthcare professionals and participants will be actively sought throughout the trial phases. This blend of qualitative and quantitative data aims to present a holistic perspective on the impact of the new orthotic design, setting the stage for potential breakthroughs in patient-centered orthotic solutions. In summary, while this research protocol lays out the groundwork and anticipated outcomes, the subsequent study will seek to not just present numbers but to demonstrate the tangible and intangible benefits of a personalized orthotic approach.

Discussion

Over the years, the field of gait rehabilitation has witnessed significant advancements, with orthoses taking center stage in many innovative solutions. As such, they have played a pivotal role in enhancing gait and laying the foundation for more customized interventions (Hurwitz et al., 2002; Menz et al., 2005) In the chronicle of medical interventions, the present times showcase a blend of time-tested traditional methods coexisting with avant-garde technologies. It's within this dynamic backdrop that the new system emerges, positioning itself as a game changer in the realm of orthoses. With a design methodology that captures the transformative essence of technology, this system aims to usher in a new epoch where AFOs are no longer generic but are sculpted based on the detailed biomechanical nuances of individual patients (Oosterwaal et al., 2011)

A key component of this innovation lies in the use of 3D scanning and 3D printing techniques. Particularly, AFOs crafted through such state-of-the-art processes have been thrust under the academic microscope. In recent years, various studies have examined multiple outcomes with the use of these technologies for the fabrication of AFOs. Belokar et al and Cha et al (Belokar et al., 2017; Cha et al., 2017) conducted numerous mechanical tests to understand the strength and deformation of the AFO, while other studies focused on gait analysis (Chae et al., 2020; Choi et al., 2017; Lin et al., 2017) while others on a qualitative analysis of patient comfort (Dal Maso & Cosmi, 2019; Mavroidis et al., 2011). The allure of these techniques is evident, offering unparalleled precision coupled with the prospects of personalization. However, as with all innovations, there exists a spectrum of opinions. While numerous

research endeavors highlight the undeniable advantages of 3D methodologies, others have voiced concerns — touching upon biomechanical compatibility, the robustness of materials used, and the overall comfort on prolonged usage studies (Silva et al., 2022)

While contrasting the biomechanics of barefoot walking with orthotic-assisted gait yields valuable insights, our central focus is on the differences between traditionally designed orthoses and those created using the novel system. Contemporary research reinforces the merits of tailored medical interventions, suggesting that custom orthoses can lead to enhanced foot function, pain relief, and overall improved mobility (Jin et al., 2015; Shih et al., 2017) For patients, the benefits of this approach are substantial. Custom-made orthoses, derived from comprehensive biomechanical analyses, not only promise greater comfort but also accelerate gait rehabilitation and minimize complications arising from poorly fitted orthoses (Cha et al., 2017; Liu et al., 2019; Lunsford et al., 2016). Such initiatives are in tune with the broader shift in healthcare towards patient-centered treatments, ensuring holistic and efficacious therapeutic outcomes (Epstein & Street, 2011).

Nonetheless, potential limitations exist. While the novel system promises tailored orthoses, individual patient responses, adaptation periods, and unique rehabilitation timelines could present challenges. The variability in individual reactions to orthoses, both in terms of comfort and therapeutic outcomes, remains a critical factor to consider.

This proposed research protocol marks a pivotal juncture between technology and biomechanics in the healthcare landscape. It signals a shift in orthotic design, embracing recent advancements and a nuanced understanding of biomechanics. The endeavors are not merely about gait rehabilitation recovery but also about setting a new benchmark for precision and efficacy in patient care.

Acknowledgements

The authors would like to acknowledge the support of the Portuguese Foundation for Science and Technology (FCT) through the following projects: SFRH/BD/145292/2019, UIDB/04044/2020, UIDP/04044/2020, PAMI ROTEIRO /0328/2013 (CENTRO2020: N 22158), and the support of the National Innovation Agency (ANI) through the project ReinventO (POCI-01-0247-FEDER-040021).

Conflicts of Interest

The authors declare that they have no conflict of interest.

References

Belokar, R. M., Banga, H. K., & Kumar, R. (2017). A Novel Approach for Ankle Foot Orthosis Developed by Three Dimensional Technologies. IOP Conference Series: Materials Science and Engineering, 280(1), 2–7. https://doi.org/10.1088/1757-899X/280/1/012030

Cakar, E., Durmus, O., Tekin, L., Dincer, U., & Kiralp, M. Z. (2010). The ankle-foot orthosis improves balance and reduces fall risk of chronic spastic hemiparetic patients (Vol. 46).

Cappozzo, A., Catani, F., Della Croce, U., & Leardini, A. (1995). Position and orientation in space of bones during movement: anatomical frame definition and determination. Clinical Biomechanics, 10(4), 171–178.

Cha, Y. H., Lee, K. H., Ryu, H. J., Joo, I. W., Seo, A., Kim, D. H., & Kim, S. J. (2017). Ankle-foot orthosis made by 3D printing technique and automated design software. Applied Bionics and Biomechanics, 2017. https://doi.org/10.1155/2017/9610468

Chae, D.-S., Kim, D.-H., Kang, K.-Y., Kim, D.-Y., Park, S.-W., Park, S.-J., & Kim, J.-H. (2020). The functional effect of 3D-printing individualized orthosis for patients with peripheral nerve injuries: Three case reports. Medicine, 99(16), e19791.

Chan, A.-W., Tetzlaff, J. M., Altman, D. G., Laupacis, A., Gøtzsche, P. C., Krleža-Jeric, K., Hró bjartsson, A., Mann, H., Dickersin, K., Berlin, J. A., Doré, C. J., Parulekar, W. R., Summerskill, W. S., Groves, T., Schulz, K. F., Sox, H. C., Rockhold, F. W., Rennie, D., & Moher, D. (2013). SPIRIT 2013 Statement: Defining Standard Protocol Items for Clinical Trials DEVELOPMENT OF THE SPIRIT 2013 STATEMENT. In Ann Intern Med (Vol. 158). www.annals.org

Choi, H., Peters, K. M., MacConnell, M. B., Ly, K. K., Eckert, E. S., & Steele, K. M. (2017). Impact of ankle foot orthosis stiffness on Achilles tendon and gastrocnemius function during unimpaired gait. Journal of Biomechanics, 64, 145–152. https://doi.org/10.1016/j.jbiomech.2017.09.015

Ciobanu, O., Ciobanu, G., & Rotariu, M. (2013). Photogrammetric Scanning Technique and Rapid Prototyping Used for Prostheses and Ortheses Fabrication. Applied Mechanics and Materials, 371, 230–234. https://doi.org/10.4028/www.scientific.net/AMM.371.230

Dal Maso, A., & Cosmi, F. (2019). 3D-printed ankle-foot orthosis: A design method. Materials Today: Proceedings, 12, 252–261. https://doi.org/10.1016/j.matpr.2019.03.122

Demers, L., Weiss-Lambrou, R., Demers, L., & Ska, B. (1996). Development of the Quebec User Evaluation of Satisfaction with assistive Technology (QUEST). Assistive Technology, 8(1), 3–13. https://doi.org/10.1080/10400435.1996.10132268

Dickinson, A., Donovan-Hall, M., Kheng, S., Wiegand, S., Wills, G., Ostler, C., Srors, S., Tech, A., Granat, M., Kenney, L., Pathak, P., Harte, C., Worsley, P., & Metcalf, C. (2019). Technologies to Enhance Quality and Access to Prosthetics & Orthotics: the importance of a multidisciplinary, user-centred approach. Global Report on Assistive Technology (GReAT) Consultation, 22–23. https://doi.org/10.5258/SOTON/P0014

Epstein, R. M., & Street, R. L. (2011). The values and value of patient-centered care. In Annals of Family Medicine (Vol. 9, Issue 2, pp. 100–103). Annals of Family Medicine, Inc. https://doi.org/10.1370/afm.1239

Fietzek, U. M., Kossmehl, P., Schelosky, L., Ebersbach, G., & Wissel, J. (2014). Early botulinum toxin treatment for spastic pes equinovarus - a randomized double-blind placebo-

controlled study. European Journal of Neurology, 21(8), 1089–1095. https://doi.org/10.1111/ene.12381

Gefen, A. (2003). Plantar soft tissue loading under the medial metatarsals in the standing diabetic foot. Medical Engineering and Physics, 25(6), 491–499. https://doi.org/10.1016/S1350-4533(03)00029-8

Grazioso, S., Selvaggio, M., Caporaso, T., & Di Gironimo, G. (2019). A Digital Photogrammetric Method to Enhance the Fabrication of Custom-Made Spinal Orthoses. Journal of Prosthetics and Orthotics, 31(2), 140–144. https://doi.org/10.1097/JPO.0000000000000244

Grazioso, S., Selvaggio, M., & Di Gironimo, G. (2018). Design and development of a novel body scanning system for healthcare applications. International Journal on Interactive Design and Manufacturing, 12(2), 611–620. https://doi.org/10.1007/s12008-017-0425-9

Hurwitz, D. E., Ryals, A. B., Case, J. P., Block, J. A., & Andriacchi, T. P. (2002). The knee adduction moment during gait in subjects with knee osteoarthritis is more closely correlated with static alignment than radiographic disease severity, toe out angle and pain. Journal of Orthopaedic Research, 20(1), 101–107. https://doi.org/10.1016/S0736-0266(01)00081-X

Jin, Y. A., Plott, J., Chen, R., Wensman, J., & Shih, A. (2015). Additive manufacturing of custom orthoses and prostheses - A review. Procedia CIRP, 36, 199–204. https://doi.org/10.1016/j.procir.2015.02.125

Lin, Y.-C., Lin, K.-W., & Chen, C.-S. (2017). Evaluation of the walking performance between 3D-printed and traditional fabricated ankle-foot orthoses— A prospective study. Gait & Posture, 57, 366–367. https://doi.org/10.1016/j.gaitpost.2017.06.471

Liu, Z., Zhang, P., Yan, M., Xie, Y., & Huang, G. (2019). Additive manufacturing of specific ankle-foot orthoses for persons after stroke: A preliminary study based on gait analysis data. Mathematical Biosciences and Engineering, 16(6), 8134–8143. https://doi.org/10.3934/mbe.2019410

Lunsford, C., Grindle, G., Salatin, B., & Dicianno, B. E. (2016). Innovations With 3-Dimensional Printing in Physical Medicine and Rehabilitation: A Review of the Literature. In PM and R (Vol. 8, Issue 12, pp. 1201–1212). Elsevier Inc. https://doi.org/10.1016/j.pmrj.2016.07.003

Magnani, M., Douglass, M., Schroder, W., Reeves, J., & Braun, D. R. (2020). The Digital Revolution to Come: Photogrammetry in Archaeological Practice. American Antiquity, 85(4), 737–760. https://doi.org/10.1017/aaq.2020.59

Mavroidis, C., Ranky, R. G., Sivak, M. L., Patritti, B. L., DiPisa, J., Caddle, A., Gilhooly, K., Govoni, L., Sivak, S., Lancia, M., Drillio, R., & Bonato, P. (2011). Patient specific ankle-foot orthoses using rapid prototyping. Journal of NeuroEngineering and Rehabilitation, 8(1), 1–11. https://doi.org/10.1186/1743-0003-8-1

Menz, H. B., Morris, M. E., & Lord, S. R. (2005). Foot and Ankle Characteristics Associated With Impaired Balance and Functional Ability in Older People. https://academic.oup.com/biomedgerontology/article/60/12/1546/558012

Munhoz, R., Moraes, C. A. da C., Tanaka, H., & Kunkel, M. E. (2016). A digital approach for design and fabrication by rapid prototyping of orthosis for developmental dysplasia of the hip. Revista Brasileira de Engenharia Biomedica, 32(1), 63–73. https://doi.org/10.1590/2446-4740.00316

Oosterwaal, M., Telfer, S., Tørholm, S., Carbes, S., Van Rhijn, L. W., MacDuff, R., Meijer, K., & Woodburn, J. (2011). Generation of subject-specific, dynamic, multisegment ankle and

foot models to improve orthotic design: A feasibility study. BMC Musculoskeletal Disorders, 12. https://doi.org/10.1186/1471-2474-12-256

Shih, A., Park, D. W., Yang, Y. Y., Chisena, R., & Wu, D. (2017). Cloud-based Design and Additive Manufacturing of Custom Orthoses. Procedia CIRP, 63, 156–160. https://doi.org/10.1016/j.procir.2017.03.355

Silva, R., Veloso, A., Alves, N., Fernandes, C., & Morouço, P. (2022). A Review of Additive Manufacturing Studies for Producing Customized Ankle-Foot Orthoses. In Bioengineering (Vol. 9, Issue 6). MDPI. https://doi.org/10.3390/bioengineering9060249

Vos, T., Allen, C., Arora, M., Barber, R. M., Brown, A., Carter, A., Casey, D. C., Charlson, F. J., Chen, A. Z., Coggeshall, M., Cornaby, L., Dandona, L., Dicker, D. J., Dilegge, T., Erskine, H. E., Ferrari, A. J., Fitzmaurice, C., Fleming, T., Forouzanfar, M. H., … Zuhlke, L. J. (2016). Global, regional, and national incidence, prevalence, and years lived with disability for 310 diseases and injuries, 1990–2015: a systematic analysis for the Global Burden of Disease Study 2015. The Lancet, 388(10053), 1545–1602. https://doi.org/10.1016/S0140-6736(16)31678-6

Ward, A. B. (2014). Managing spastic foot drop after stroke. In European Journal of Neurology (Vol. 21, Issue 8, pp. 1053–1054). Blackwell Publishing Ltd. https://doi.org/10.1111/ene.12404

Weigert, M. C., Poier, P. H., Rosenmann, G. C., Foggiatto, J. A., Volpato, N., & Okimoto, M. L. L. R. (2016). Indirect 3D scanning of the foot plant - Comparison between a medium and low-cost tools. Advances in Transdisciplinary Engineering, 4, 614–621. https://doi.org/10.3233/978-1-61499-703-0-614

Zhang, M., Davies, C., & Xie, S. (2013). Effectiveness of robot-assisted therapy on ankle rehabilitation-a systematic review. Journal of Neuroengineering and Rehabilitation, 10(1), 1–16. http://www.jneuroengrehab.com/content/10/1/30

Study 4

Photogrammetry in Ankle Foot Orthoses: A Revolutionary System for Rapid 3D Scanning and Modelling

Authors: **Rui Silva**, Pedro Morouço, Diogo Ricardo, Inês Campos, Nuno Alves, Filipe Perdigoto, Moisés Domingues and António Veloso

Abstract

As the technological landscape for orthotics evolves, there's an increasing emphasis on precision tools that capture the intricacies of foot anatomy, including the often overlooked sole. This research introduces a novel 3D photogrammetric scanner tailored for this task and assesses its integration with a tailored orthotic design process. The system integrates the 3D scanner with a custom-developed web-based interface, linking it to established design platforms for which specific scripts were crafted to aid orthosis construction. The adaptability and user-friendliness of the system in a clinical setting were assessed, and a comparative case study was conducted to evaluate a patient's traditional prefabricated AFO against a new 3D printed version produced using the system. The clinical application showcased a minimal learning curve, while the case study provided insights into the nuances between the traditional and 3D printed AFOs. The rapid 3D photogrammetric scanner, capturing detailed foot anatomy in under 2 seconds, coupled with its integrated software framework, provides a novel approach in orthotic design, hinting at the potentialities of 3D printed orthoses. This study serves as a foundational step for future research focused on optimized and efficient orthotic designs.

Keywords: 3D Scanner, Orthoses, Photogrammetry System

Introduction

Orthotic devices stand as pillars in today's healthcare landscape, addressing diverse physiological disorders and physical impairments. Spanning from spinal supports to limb orthoses, these tools have brought relief to conditions such as muscular dystrophy, cerebral palsy, and post-stroke rehabilitation (Ricardo et al., 2021). Among these biomechanical devices, Ankle Foot Orthosis (AFO) have carved a distinctive niche. Primarily crafted from durable plastics, AFOs offer essential support to the foot and ankle, focusing on motion regulation, deformity correction, and counteracting muscular weaknesses (Lintanf et al., 2018). Despite the innovations in AFO design, off-the-shelf orthoses—readily available and non-customized—continue to find a market. Often chosen for immediate accessibility and affordability, these generic devices might not deliver the same level of comfort and specificity as their tailored counterparts. However, they offer a viable option for many. Conversely, customized AFOs traditionally relied on labor-intensive methods. A common approach was manually casting the patient's limb in plaster. While this technique was effective, it often led to extended production times, inconsistent outcomes, and occasional discomfort during the casting process (Silva et al., 2022; Totah et al., 2017)

But technological advancements have ushered in a new chapter for AFO production. A growing recognition highlights the advantages of patient-specific orthoses over their standard commercial counterparts (Telfer et al., 2012). Tailored for individual needs, these AFOs pledge improved comfort and superior functionality. Enhanced by modern technologies, the journey from design to production has seen significant time reductions (R. K. Chen et al., 2014; Morouço, 2018) Central to this shift is photogrammetry, which merges photography with precise measurements. In orthotics, it's the conduit converting two-dimensional images into tangible three-dimensional limb models. This shift, while intricate, offers perks like cost efficiency, precision, and quicker production cycles (Ciobanu et al., 2013; Dal Maso & Cosmi, 2019; Grazioso et al., 2019) Concurrently, the advancements in 3D scanning technologies have allowed for capturing the human form in its intricate detail. Modern 3D scanners deliver high-resolution outputs, offering increased precision in AFO designs and fabrications (Baronio et al., 2016; Krajňáková et al., 2020; Rogati et al., 2019). Yet, weaving photogrammetry and 3D scanning into the fabric of orthotics is not challenge-free. The upfront costs of cutting-edge equipment and software, coupled with the need for specialized training, often pose barriers (R. K. Chen et al., 2016) These technologies, though demanding significant initial

investments, vindicate their worth in the long run with consistent and high-quality outputs (Silva et al., 2022). However, as the winds of healthcare veer towards a more digital and remote direction, accelerated by global events like the pandemic, these technological tools emerge as frontrunners in shaping the orthotics landscape. Their potential shines particularly in realms like remote patient care and telemedicine, showcasing a promising future (Bitar & Alismail, 2021)

Methods

The most pertinent factors for the conception of the entire system were: (i) cost and (ii) patient comfort. To achieve this objective, preliminary tests were conducted using 16 synchronized Raspberry Pi units with 16 Raspberry Pi Camera Module V2 8MP (Silva et al., 2019). By this approach, it was feasible to gauge the effectiveness of capturing the patient's lower limb surface using the photogrammetry technique and understand the potential of this technology in swiftly acquiring the intended surface.

Designing a New Printed Circuit Board

After conducting preliminary tests, the potential of photogrammetry in achieving the proposed objective became evident. However, the extensive wiring required for power and data transmission posed a challenge. To address this, a new Printed Circuit Board (PCB) was designed using Altium Designer software (Altium Limited®, Australia). The industrial version of Raspberry Pi, the Compute Module 3+, was selected for integration. This new design allowed the inclusion of both an input and output connectors, to share the 24V DC power between boards, the incorporation of an internal switch to support two Ethernet LAN ports, and the addition of two MIPI camera interfaces to connect the Raspberry Pi Camera Module. With this configuration, all PCBs can be connected in series, and each PCB can support two cameras (Fig.III.3).

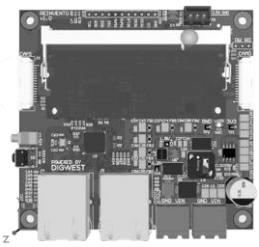

FIGURE III.3 - Design of the printed circuit board. The upper rectangular area is where the Raspberry Pi Compute Module 3+ is integrated. The lower area is where the network and power cables are connected.

Designing a New Application Programming Interface and User Interface

Microsoft's Visual Studio 2022 and Visual Studio Code were utilized for the comprehensive development of the API and the Web-based User Interface (UI). The API facilitates all communication, handling request-response interactions between the user and the scanner. The Web UI provides users (e.g., physicians, orthotists) with the capability to control the scanner and navigate the entire workflow, from capturing data to orthosis fabrication. An SQL database was also established to store essential patient details and to document the orthosis construction process.

Designing a Tool for Orthotics Design and Leg Postural Correction

The Rhinoceros® software from Robert McNeel & Associates was employed, in conjunction with the Grasshopper® plugin, to develop algorithms for parametric orthotics design. The "HumanUI" plugin for Grasshopper® was utilized to craft the graphical user interface, enhancing user interaction. To facilitate leg postural correction, a dedicated plugin was created in Blender. This leg postural correction plugin empowers users to adjust angles in both the frontal and sagittal planes.

Designing a Tool for Orthotics Design and Leg Postural Correction

The Rhinoceros® software from Robert McNeel & Associates was employed, in conjunction with the Grasshopper® plugin, to develop algorithms for parametric orthotics design. The "HumanUI" plugin for Grasshopper® was utilized to craft the V2 8MP.

Designing the 3D Photogrammetry Scanner for Lower Limbs

Solidworks (Dassault Systèmes®, France) software was utilized to draft the prototype, incorporating the new PCBs. The primary aim of this prototype was to comprehensively capture the surface of the patient's leg and foot. For a holistic scan that ensures the optimal crafting of a customized orthosis, it was essential to include the capture of the patient's foot sole. The prototype was conceptualized, placing particular emphasis on cost-effectiveness, patient comfort, and optimal leg capture. This design employed 30 PCBs connected to 60 cameras for an enhanced scanning precision (Fig.III.4). Various tests were conducted to evaluate the scanner. The temporal acquisition test for images was conducted using commands embedded in the Application Programming Interface (API) developed. The time

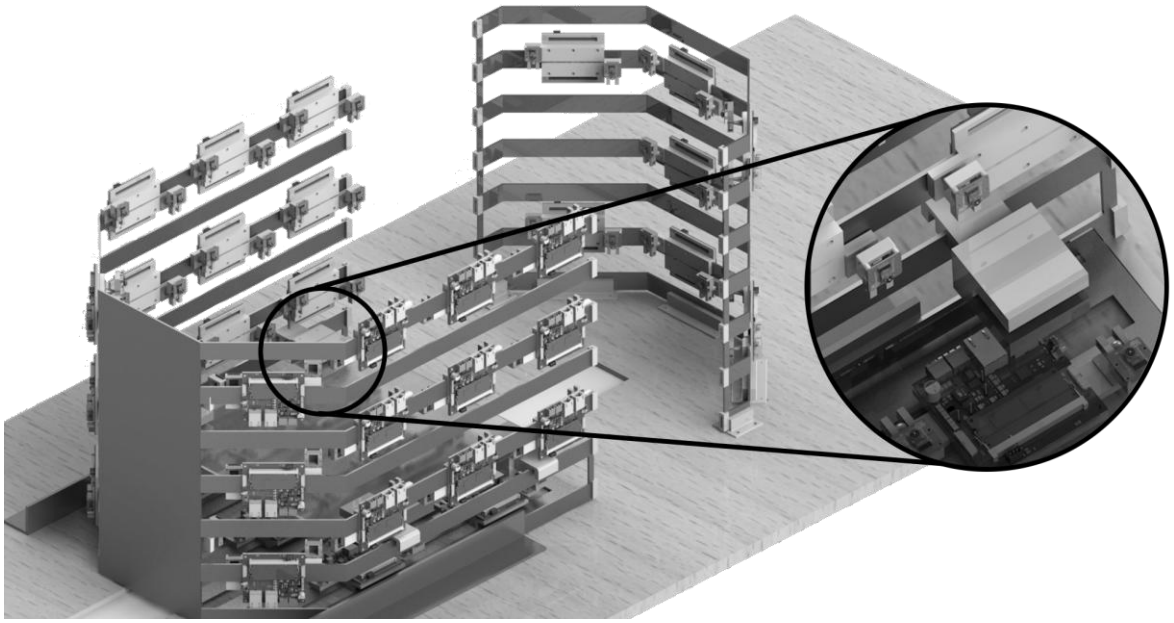

FIGURE III.4 - Design of the new scanner created to capture the surface of the patient's leg and foot using photogrammetry technology. It is possible to see in detail the connection between the acrylic and the scanner's structure, with the capability to adjust its position horizontally and vertically for an optimal fit to the patient's leg.

from the HTTP GET request for capturing the photographs to receiving the confirmation that all photos were taken was measured using the Postman® software from Postman, Inc. The scanner's precision test was carried out using CloudCompare. The mesh and deviation of an object plaster cast model of a foot) were analyzed by comparing scans from the custom-built scanner and the Steinbichler Comet 5 1.4M scanner (Zeiss Group, Oberkochen, Germany) through overlay.

Case Study of a Stroke Patient

To validate the entire system, a case study was undertaken with a male patient suffering from left-sided hemiplegia due to a stroke that occurred 1.5 years earlier. The study was conducted over two days: the left leg was scanned on the first day, and a biomechanical (kinematic) gait assessment was performed on the second day. Table III.5 shows the subject's clinical characteristics. Ethical clearance for the study was obtained from the Ethical Committee of Centro de Medicina de Reabilitação da Região Centro-Rovisco Pais and the subject signed an informed consent form. During the work process, all methods were performed in accordance with the relevant guidelines and regulations. A clinical staff consisting of physiatrists and a certified prosthetist and orthotist, were responsible for monitoring the clinical status of the patient during the trials and for the fitting of the AFO. Prior to data collection, an informed consent was acquired from the patient.

TABLE III.5 - Clinical characteristics of the subject

Parameters	Value
Age (years)	67
Height (cm)	169
Weight (Kg)	69
Diagnosis	Cerebral hemorrhage
Paretic Side	Left Side
Fugl-Meyer Scale (lower extremity) [17]	78
Tinetti POMA	24 (with AFO)
Modified ash worth scale of ankle joint muscles	1

Day One

The surface of the left lower limb was captured. This capture was achieved using the new 3D photogrammetry scanner detailed in this study. The patient was requested to wear loose-fitting track pants to allow easy access to the affected leg. To ensure a cleaner scan and reduce surface noise (like leg hair) on the mesh, the patient donned a stocking to achieve a more consistent model. The time required to position the patient within the scanner was 5 minutes, while the actual capture time was just 2 seconds. In the patient's absence, the physiatrist then utilized the workflow and software outlined in this study. Always using the web interface, they generated the 3D model from the photos taken with the scanner. This step was executed using the Reality Capture® software by Capturing Reality. In practice, the user never interacts directly with the software due to the presence of a command-line script that automates the entire

process. Subsequently, the physician performed the foot-leg postural correction using the Blender script and then designed the orthosis on the 3D leg model using the tool developed in Rhinoceros + Grasshopper. The total time required for these tasks was approximately 35 minutes (10 minutes for 3D model creation, 5 minutes for postural correction, and 20 minutes for orthosis design and STL format export). The orthosis model was then printed using the Fused Deposition Modeling process with Nylon 12 material employing a Stratasys Fortus 450 printer by Stratasys®. The decision to use Nylon 12 material for the AFOs was based on extensive mechanical testing of various materials, including Acrylonitrile Styrene Acrylate (ASA), Polycarbonate-Acrylonitrile Butadiene Styrene (PC-ABS), Polyethylene Terephthalate Glycol (PETG), Thermoplastic Polyurethane (TPU), Polylactic Acid (PLA), Polycarbonate (PC), ULTEM 1010, and ULTEM 9085. The printing process took approximately 10 hours.

Day Two

The gait dynamics were captured using a Qualisys® motion analysis system, equipped with 12 high-speed Miqus M3 cameras (Frequency: 120-Hz). The locations of markers were recorded with the Qualisys Track Manager® software. The patient's lower limbs were digitally reconstructed in a 3D environment using the Visual 3D™ software developed by C-motion Inc, leveraging the Project Automation Framework from Qualisys®. For accurate data acquisition, thirty-six markers, each 10 mm in diameter, were affixed according to the CAST lower body marker protocol (Capozzo et al., 1995).

The subject was instructed to walk on a flat surface to gather data. The acquired data were processed using a Butterworth low-pass filter with a cutoff frequency of 10 Hz and segmented into phases of the gait cycle based on heel strike events. Tests were repeated to obtain 6 successful trials for both the orthoses, i.e., the developed AFO using this system (Custom Orthosis - CO) and the AFO the patient uses in his daily life (Pre-existing Orthosis - PO). The spatiotemporal gait parameters from both limbs evaluated in this study included speed, step length, step time, stance time, swing time, cycle time, steps/minute and strides/minute, as well as the kinematics of the hips, knees, and ankles. For the statistical analysis of the spatiotemporal parameters, GraphPad Prism version 9 (GraphPad Software, San Diego, CA, USA) was utilized. Initially, a test for the normality of data distribution was conducted. Due to the non-normal distribution of the data, the non-parametric Wilcoxon test was employed to

compare values between PO left vs. CO left and PO right vs. CO right. A significance level of $p<0.05$ was used for all statistical tests, corresponding to a confidence level of 95%.

Results

3D Photogrammetry Scanner

The prototype (Fig.III.5) utilized materials such as: wood (scanner base), stainless steel (scanner base structure), 3D printed PLA parts (camera and customized PCB supports), and

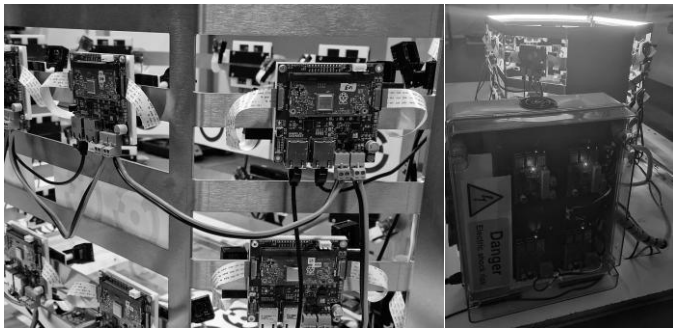

FIGURE III.5 - View of the rear of the scanner with all modules connected in series for data transmission and power supply.

acrylic (patient's foot support). The 60 cameras were strategically positioned around the scanner, all focused on a central point within the scanner. Each camera is equipped with a Sony IMX219 sensor, boasting a resolution of 3280 × 2464 pixels, a Horizontal Field of View (FoV) of 62.2 degrees, and a Vertical FoV of 48.8 degrees. Given the cameras' diverse placements around the scanner, including some at its base to capture the sole of the foot, a high degree of image overlap is achieved—optimal for effective photogrammetry. Integrated into the scanner are circular markers (dual ring, 12-bit) placed on the acrylic base and distributed throughout the scanner. These markers streamline the photogrammetry process and facilitate the precise alignment of various photos. Additionally, an LED strip with a color rendering index of over 85% was installed around the scanner. This arrangement effectively eliminates potential shadows, reflexes, and dark spots during the leg surface capture. A box was also constructed to house the electrical setup and the network hub.

The capture time over the 30 tests conducted was 1.76 ± 0.11 s. For the scanner precision test (Fig.III.6), the mean deviation spectrum of the object between the scanners ranged from 0.001516m on the positive side to -0.002506m on the negative side, with most of the deviation centered around 0.00008m.

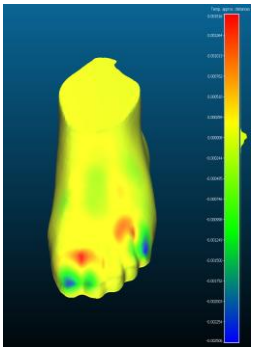

FIGURE III.6 - Accuracy test comparing the new scanner with the Steinbichler Comet 5 scanner. The yellow areas represent identical zones, the red areas indicate positive deviations, and the blue areas indicate negative deviations.

Web-based User Interface

The API underwent rigorous testing to eliminate all potential bugs. Over time, 20 distinct versions were developed, each with specific fixes and enhancements to ensure comprehensive control of the scanner. For a more streamlined and user-friendly experience, a "Dashboard" interface was created. This dashboard allows users to navigate between the 'Scanner' page and the 'Patient Management' page (Fig.III.7).

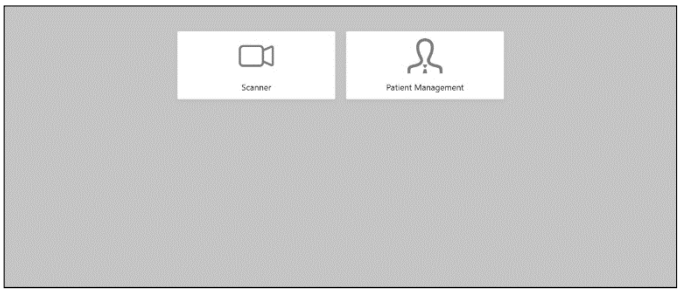

FIGURE III.7 - Main page of the web module with options to select either the scanner page or the patient management page.

The scanner page offers various requests based on the desired tests or configurations by the technician. It provides options to adjust all capture settings and monitor every component of the scanner. Features include the ability to modify camera capture settings, adjust LED intensity, stream live camera feeds, and initiate captures (Fig. III.8).

FIGURE III.8 - Main scanner page, where it is possible to view or change the associated settings. A live preview from all 60 cameras can also be accessed.

For patient management, users can either create a new patient profile or edit an existing one. Subsequently, there is a workflow in place to guide the technician through a straightforward and intuitive process for orthosis creation. This workflow encompasses patient leg scanning, photogrammetry, preliminary alignment, orthosis design, and finally, orthosis printing (Fig.III.9).

FIGURE III.9 - Workflow from the scanner to the orthotic printout. The user can view all the steps that have been completed or are yet to be done. It's possible to preview the 3D model of the leg or the orthosis.

The script created for Blender provides tools for technicians to adjust specific attributes of the leg model mesh. Upon importing the model (which is automated when using the web interface), the foot's sole must be aligned with the ground by selecting three reference points. For mesh manipulation, five leg points must be selected: Head of the 2nd Metatarsal, Lateral and Medial Malleolus Center, and Lateral and Medial Epicondyle Center (Fig. III.10). If the Epicondyles are not present in the model, the closest approximate point should be chosen. Subsequently, several tools are available for use. The user can align the leg relative to the foot using angle units (considering inversion/eversion and dorsiflexion/plantar flexion), create inflate or deflate points on the mesh which might be crucial for subsequent AFO fabrication

to alleviate potential pressure points, smooth out the mesh, and perform linear and angular measurements on the leg model.

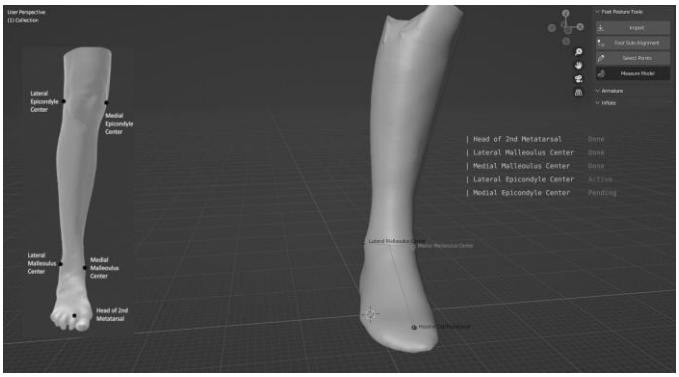

FIGURE III.10 - Blender module for leg alignment, mesh modifications, or leg measurement. In this 3D model, the patient was wearing a stocking for smoother surface rendering, avoiding defects from veins or leg hair.

To enable users to interact with Rhino3D easily and without requiring advanced CAD knowledge, a user-friendly interface was developed using the HumanUI plugin. This interface dynamically updates its content based on the user's current step in the orthosis design process (Fig. III.11).

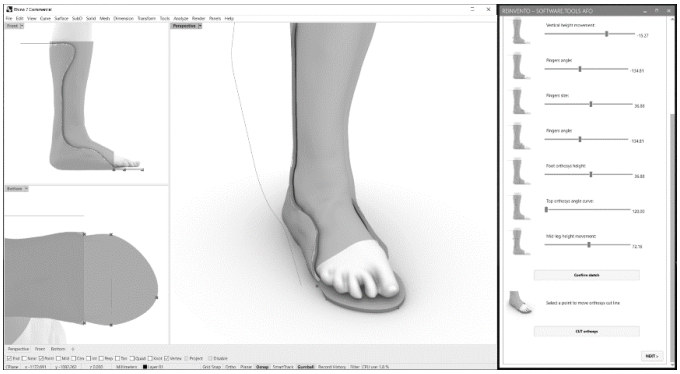

FIGURE III.11 - Module for constructing the AFO in Rhinoceros. All features of the orthosis can be adjusted using sliders located on the right.

Upon importing the limb data, the user proceeds with the lower limb alignment process, starting by marking three points on the sole of the foot. They then follow steps to define the orthosis thickness, its offset, design the main structure, and potentially add straps (Fig. III.12). Any modifications made in the HumanUI prompt an automatic update of the orthosis design, allowing users to see real-time changes on the patient's leg model. It is feasible to construct an AFO with or without metatarsal support.

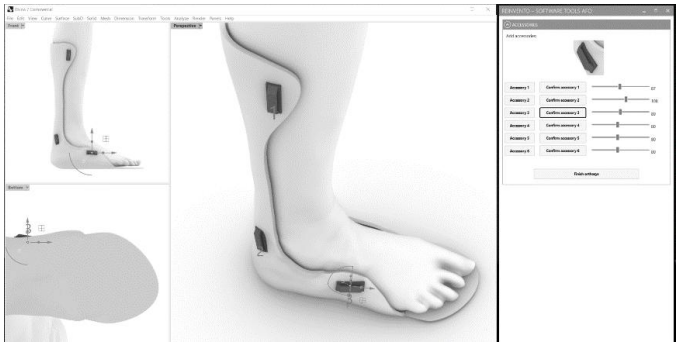

FIGURE III.12 - Design of the final orthosis overlaid on the patient's leg model, with incorporation of eyelets for future placement of velcro straps.

Case Study of a Stroke Patient

On day one of testing, the patient arrived at Rehabilitation Center for the scanning of the affected limb (Fig.III.13).

After acquiring the surface scan of the patient's leg, the steps for photogrammetric reconstruction, orthosis design, and printing were undertaken (Fig.III.14). The decision was made to fabricate the orthosis without the insole extension for metatarsal support to ensure it was identical to the AFO the patient was already using. On day two, a kinematic biomechanical assessment was conducted on the patient.

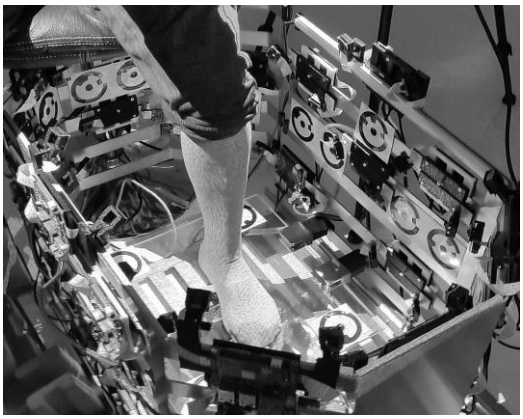

FIGURE III.14 - Patient with the left lower limb in the scanner to capture the 3D model of the leg and foot surface (including the sole).

FIGURE III.13 - 3D printed AFO in Nylon 12 material.

Spatiotemporal parameters

Table III.6 shows the spatiotemporal parameters for both conditions, Pre-existing Orthosis - PO and Custom Orthosis – CO for both limbs.

TABLE III.6 - Spatiotemporal parameters for both conditions

Parameters	PO Left (Mean±SD)	CO Left (Mean±SD)	PO Right (Mean±SD)	CO Right (Mean±SD)
Step Length (m)	0.23±0.01	0.25±0.01	0.12±0.01	0.14±0.01
Step Time (s)	0.78±0.03	0.79±0.03	0.59±0.02[1]	0.63±0.04
Stance Time (s)	0.93±0.05	0.96±0.04	1.05±0.06	1.13±0.05
Swing Time (s)	0.45±0.06	0.45±0.03	0.30±0.04	0.29±0.02
Cycle Time (s)	1.37±0.04	1.41±0.06	1.36±0.07	1.42±0.05
Steps / Minute	80.24±6.59	75.27±3.25	102.69±3.97[2]	95.49±5.23
Strides / Minute	43.86±0.88	42.57±1.86	44.38±2.39	42.40±1.51

Abbreviations: m - meters. s - seconds.
All values where statistically significant differences were found with a confidence level above 95% are represented with superscript numbers.
[1]p<0.001 for the step time between PO right and CO right
[2]p<0.001 for the steps/minute between PO right and CO right

Gait analysis revealed an average walking speed of 0.26 m/s with the PO and 0.28 m/s with the CO. Notable differences between the orthoses were found in step time and steps/minute for the unaffected right leg. The step time for PO right was 0.59±0.02s, compared to 0.63±0.04s for CO right. Similarly, steps/minute was 102.69±3.97 for PO right and 95.49±5.23 for CO right. These parameters showed the only statistically significant differences between the orthoses.

Kinematic Parameters

The graphs display the mean of normalized gait cycles from 0 to 100% (Fig. III.15) between the Heel Strike events for left side (dot line) and right side (solid line).

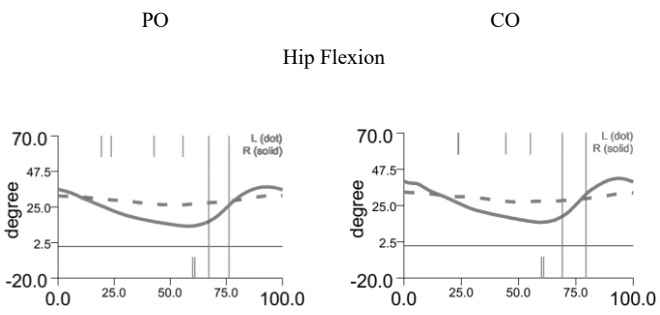

Hip Adduction

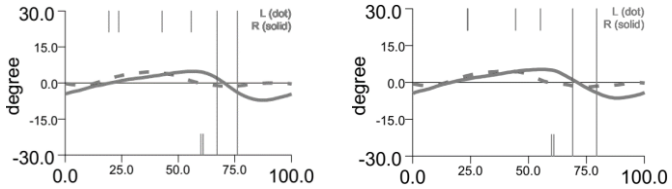

Hip Internal Rotation

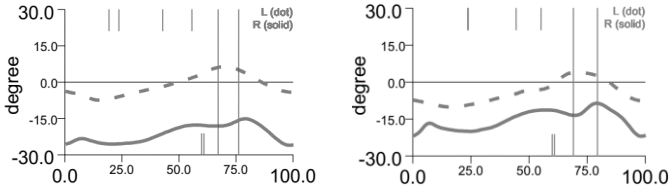

Knee Flexion

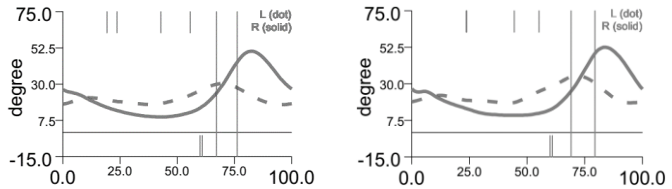

Knee Varus

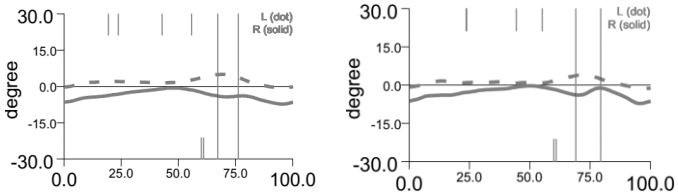

Knee Internal Rotation

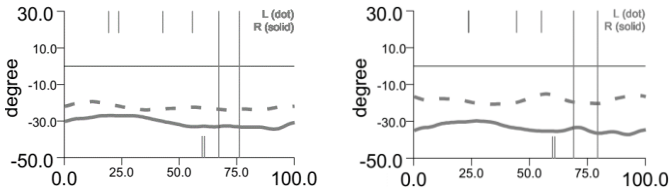

Ankle Dorsiflexion

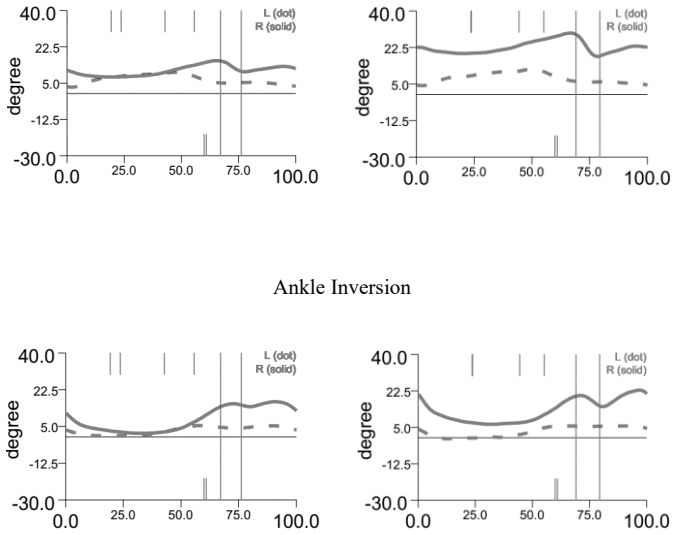

FIGURE III.15 - Representation of the angles from the average of the 6 gait cycles for the left foot and right foot.

Visually, there are no significant differences in the kinematic graph curves when comparing PO and CO. The most notable differences lie in the internal rotation of the thigh in PO for the right leg, which demonstrates a more negative internal rotation. There is also a discernibly higher angle in dorsiflexion and inversion of the ankle during the CO moment for the right leg. For all variables analyzed in the leg with the AFO, no differences were observed between the patient wearing the pre-existing orthosis and the new customized orthosis constructed through 3D printing using this new system.

Discussion

Photogrammetry, historically used in cartography and geology to map topographies from photographic images, has its origins in the pre-digital age (Ackermann, 1999) This technique creates three-dimensional models from two-dimensional photos. Due to the rise of technology and increased availability of high-resolution imaging equipment, its application has expanded into various domains including archaeology, architecture, and medicine (El-Hakim et al., 2004). More recently, the integration of photogrammetry with modern techniques like 3D printing has opened novel avenues, especially in the healthcare sector. In the realm of orthotics, the fusion of these technologies promises to redefine the creation and delivery of orthopedic devices by allowing clinicians to capture intricate anatomical details and subsequently craft personalized orthotic solutions (Silva et al., 2022; Wojciechowski et al., 2019)

Amidst this technological evolution, a variety of different scanners have been developed, each with its own strengths and limitations. However, a common oversight in many of these devices is the inability to capture the entire foot anatomy, notably the sole – a critical component for comprehensive orthotic design (Telfer & Woodburn, 2010)

Advancements in technology have led to various scanning methodologies, each presents unique challenges. Popular scanning technologies such as Magnetic Resonance Imaging (MRI), CT scans, laser triangulation, and structured light scanning offer different benefits. However, they often come with their own sets of challenges (Fantini et al., 2017; Mercuri et al., 2005).

Laser triangulation provides high-resolution images, but the scanning process can be prolonged, especially for larger anatomical regions. Also, the reflective properties of the skin can sometimes interfere with the accuracy of laser scanners (Grazioso et al., 2018). On the other hand, structured light scanning, while being rapid and non-invasive, requires optimal lighting conditions and patient immobilization to ensure model accuracy (Baronio et al., 2016; Geoffroy et al., 2018). From a patient's perspective, staying still during prolonged scanning can be challenging, especially for those with mobility issues or pain-related conditions. Even slight, involuntary movements during scanning can introduce discrepancies, affecting the quality of the final model (Grazioso et al., 2019) Thus, in the face of these challenges the design of our 3D scanner emerges as a calculated response to longstanding challenges. The diverse combination of materials, encompassing wood, stainless steel, 3D printed PLA, and acrylic, not only underscores the system's resilience but also hints at its modularity. However, not all was straightforward during development. While the inclusion of acrylic optimized patient support, it occasionally proved intrusive for imaging. Yet, this very challenge underscored the critical nature of the scanner's camera placement. With 60 cameras, especially those at the base, capturing the elusive sole became feasible. Overcoming the interference from the acrylic, a seemingly simple material, underscores the intricate ballet that is photogrammetry.

The use of LED strips, characterized by their high color rendering index, effectively addressed the issue of shadows, a limitation often seen in traditional scanners according to (Nam & Kim, 2014). The notion of integrating projectors, emitting patterns to enhance depth perception, hints at the continuous evolution and potential augmentation of this system.

Patient comfort was paramount. Their seated position not only provided stability but ensured minimal movement, further enhanced by this scanner's rapid image-capturing capability, a swift two seconds. This rapidity not only augments comfort but ensures a crisp, movement-free image. PLA's incorporation, chosen for 3D printed components, stands out as a boon for swift and economical part replacement, echoing its reputation for adaptability. The flexibility with camera positioning adds another layer of adaptability, suggesting that this scanner is not static but ever evolving.

During the orthotic software development phase, a combination of Rhinoceros® and Grasshopper®, integrated with HumanUI, was employed due to their recognized precision, versatility, and adaptability in the design and engineering landscape. Such tools offer the advantage of precision modeling and crafting intuitive user interfaces, critical for tailoring orthotic designs (Barrios-Muriel et al., 2020). The challenge of harmoniously aligning the foot model with the leg necessitated the use of a platform adept at intricate three-dimensional manipulation. Proper orientation of these models is paramount for the creation of a functional and patient-specific orthosis. Blender, with its advanced 3D modeling and object manipulation capabilities, was deemed most suitable for this alignment phase (Morinaga et al., 2019). The integration of Blender into the process not only facilitated the alignment but also offered extended features. Its architecture made it possible to integrate additional tools, such as a measurement ruler, enabling users to take precise measurements across any section of the anatomical leg model. Moreover, the inflate and deflate functionalities were incorporated, granting users an intuitive mechanism to adjust the mesh structure seamlessly. These features are paramount, allowing orthotic specialists to refine the design to ensure the optimal fit and functionality in the final orthotic device. Moving forward, one of our primary objectives is to centralize the process further, aiming for a more unified solution. The ambition is to integrate all functionalities into either Blender or Rhinoceros®/Grasshopper®, streamlining the user experience and the orthotic development process even more.

In the clinical setting where the scanner and software were tested, the user - a physiatrist - reported a notably effortless experience across multiple stages of the process. From positioning the patient for the scan to the software utilization, spanning the creation of a patient's clinical record, conducting the leg scan, performing the vital pre-alignment, and finally drafting the orthotic design, the system demonstrated seamless operability. Notably,

the physiatrist required only a brief introduction to the system's workings, underpinned by a singular demonstration. Yet, post this brief orientation, the physician managed to navigate and operate the entire process independently. Beyond the immediacy of its operation, the software offers a strategic advantage in data management. It is capable of securely storing patient data, facilitating global accessibility. Such a feature ensures that a patient's orthotic design and medical records can be accessed and replicated with precision from any corner of the world, fostering a continuity of care that's paramount in modern medicine (Roberts et al., 2017). Moreover, the ability to reproduce the AFOs with exactitude promises consistent patient outcomes, eliminating variables that might arise from manual or disparate design processes (Silva et al., 2022).

The case study highlighted similarities in the results of various AFOs. Similar findings were reported by (Chen et al., 2010; Lewallen et al., 2010), where they found no significant differences in the spatiotemporal gait variables among stroke patients wearing different types of AFOs. However, this case study presents some unique results. The gait speed was identical with the PO (0.26m/s) compared to the CO (0.28m/s), but the cadence was higher in the PO (102.69 steps/min) than in the CO (95.49 steps/min). This difference can be attributed to an improvement in the step length of the unaffected leg, a result of enhanced ankle stability (Bouchalová et al., 2016), provided by the CO orthosis. Such results suggest that this approach could be beneficial in the prescription process for individuals suffering from foot drop or ankle instability that compromises their gait function (Daryabor et al., 2018). The design of the AFO developed through this novel method (i.e., CO) maintained a consistent joint restriction in the range of dorsiflexion. As such, the median dorsiflexion during stance was 8.4° and during the swing was 5.2°, suggesting that the support provided under the forefoot effectively neutralized any plantarflexion during these gait phases (Gasq et al., 2023).

Conclusion

The transition of photogrammetry from its foundational role in mapping to its contemporary applications in orthotic solutions illustrates the adaptability of such technology. This new 3D scanner, tailored for the precise scanning of lower limbs and foot sole, showcases ongoing advancements in this domain. Capable of capturing 60 images in less than two seconds, this scanner represents a significant stride in orthotic technology. Integrating established software

tools with a custom-developed web interface has resulted in a more unified and easy-to-use system. While promising results have been observed clinically, the path of refinement and enhancement remains ongoing. The fundamental aim is to optimize the confluence of technology and orthotic care, ensuring both accuracy and wide-reaching accessibility.

Acknowledgements
The authors would like to acknowledge the support of the Portuguese Foundation for Science and Technology (FCT) through the following projects: SFRH/BD/145292/2019, UIDB/04044/2020, UIDP/04044/2020, PAMI ROTEIRO /0328/2013 (CENTRO2020: N 22158), and the support of the National Innovation Agency (ANI) through the project ReinventO (POCI-01-0247-FEDER-040021).

Conflicts of Interest
The authors declare that they have no conflict of interest.

References
Ackermann, F. (1999). Airborne laser scanning-present status and future expectations. In ISPRS Journal of Photogrammetry & Remote Sensing (Vol. 54).

Baronio, G., Harran, S., & Signoroni, A. (2016). A Critical Analysis of a Hand Orthosis Reverse Engineering and 3D Printing Process. Applied Bionics and Biomechanics, 2016. https://doi.org/10.1155/2016/8347478

Barrios-Muriel, J., Romero-Sánchez, F., Alonso-Sánchez, F. J., & Salgado, D. R. (2020). Advances in orthotic and prosthetic manufacturing: A technology review. Materials, 13(2). https://doi.org/10.3390/ma13020295

Bitar, H., & Alismail, S. (2021). The role of eHealth, telehealth, and telemedicine for chronic disease patients during COVID-19 pandemic: A rapid systematic review. In Digital Health (Vol. 7). SAGE Publications Inc. https://doi.org/10.1177/20552076211009396

Bouchalová, V., Houben, E., Tancsik, D., Schaekers, L., Meuws, leni, & Feys, P. (2016). The influence of an ankle-foot orthosis on the spatiotemporal gait parameters and functional balance in chronic stroke patients. The Journal of Physical Therapy Science, 28, 1621–1628.

Cappozzo, A., Catani, F., Della Croce, U., & Leardini, A. (1995). Position and orientation in space of bones during movement: anatomical frame definition and determination. Clinical Biomechanics, 10(4), 171–178.

Chen, C. C., Hong, W. H., Wang, C. M., Chen, C. K., Wu, K. P. H., Kang, C. F., & Tang, S. F. (2010). Kinematic features of rear-foot motion using anterior and posterior ankle-foot orthoses in stroke patients with hemiplegic gait. Archives of Physical Medicine and Rehabilitation, 91(12), 1862–1868. https://doi.org/10.1016/j.apmr.2010.09.013

Chen, R. K., Chen, L., Tai, B. L., Wang, Y., Shih, A. J., & Wensman, J. (2014). Additive manufacturing of personalized ankle-foot orthosis. Transactions of the North American Manufacturing Research Institution of SME, 42(January), 381–389.

Chen, R. K., Jin, Y. an, Wensman, J., & Shih, A. (2016). Additive manufacturing of custom orthoses and prostheses-A review. Additive Manufacturing, 12, 77–89. https://doi.org/10.1016/j.addma.2016.04.002

Ciobanu, O., Ciobanu, G., & Rotariu, M. (2013). Photogrammetric Scanning Technique and Rapid Prototyping Used for Prostheses and Ortheses Fabrication. Applied Mechanics and Materials, 371, 230–234. https://doi.org/10.4028/www.scientific.net/AMM.371.230

Dal Maso, A., & Cosmi, F. (2019). 3D-printed ankle-foot orthosis: A design method. Materials Today: Proceedings, 12, 252–261. https://doi.org/10.1016/j.matpr.2019.03.122

Daryabor, A., Arazpour, M., & Aminian, G. (2018). Effect of different designs of ankle-foot orthoses on gait in patients with stroke: A systematic review. In Gait and Posture (Vol. 62, pp. 268–279). Elsevier B.V. https://doi.org/10.1016/j.gaitpost.2018.03.026

El-Hakim, S., Beraldin, J. A., Picard, M., & Godin, G. (2004). Detailed 3D Reconstruction of Large-Scale Heritage Sites with Integrated Techniques. IEEE Computer Graphics and Applications, 24(3), 21–29.

Fantini, M., De Crescenzio, F., Brognara, L., & Baldini, N. (2017). Design and rapid manufacturing of a customized foot orthosis: A first methodological study. Lecture Notes in Mechanical Engineering, 0, 457–467. https://doi.org/10.1007/978-3-319-45781-9_46

Fugl-Meyer, A. R., Jääskö, L., & Norlin, V. (1975). The post-stroke hemiplegic patient. II. Incidence, mortality, and vocational return in Göteborg, Sweden with a review of the literature. Scandinavian Journal of Rehabilitation Medicine, 7(2), 73–83.

Gasq, D., Dumas, R., Caussé, B., Scandella, M., Cintas, P., Acket, B., & Arné-Bes, M. C. (2023). Comparison between a novel helical and a posterior ankle–foot orthosis on gait in people with unilateral foot drop: a randomised crossover trial. Journal of NeuroEngineering and Rehabilitation, 20(1). https://doi.org/10.1186/s12984-023-01184-x

Geoffroy, M., Gardan, J., Goodnough, J., & Mattie, J. (2018). Cranial Remodeling Orthosis for Infantile Plagiocephaly Created Through a 3D Scan, Topological Optimization, and 3D Printing Process. Journal of Prosthetics and Orthotics, 30(4), 1. https://doi.org/10.1097/JPO.0000000000000190

Grazioso, S., Selvaggio, M., Caporaso, T., & Di Gironimo, G. (2019). A Digital Photogrammetric Method to Enhance the Fabrication of Custom-Made Spinal Orthoses. Journal of Prosthetics and Orthotics, 31(2), 140–144. https://doi.org/10.1097/JPO.0000000000000244

Grazioso, S., Selvaggio, M., & Di Gironimo, G. (2018). Design and development of a novel body scanning system for healthcare applications. International Journal on Interactive Design and Manufacturing, 12(2), 611–620. https://doi.org/10.1007/s12008-017-0425-9

Habiba, R., Amaro, A., Moura, C., Silva, R., Trindade, D., Antão, A., Martins, R., Malça, C., & Branco, R. (2023). splnproc1703_v4. Proceedings of the 10th Congress of the Portuguese Society of Biomechanics: CNB 2023.

Krajňáková, V., Rajťúková, V., Hudák, R., & Živčák, J. (2020). APPLICATION OF THE ARTEC EVA SCANNER FOR ORTHOTICS IN PRACTICE. Lékař a Technika - Clinician and Technology, 49(3), 92–96. https://doi.org/10.14311/CTJ.2019.3.04

Lewallen, J., Miedaner, J., Amyx, S., & Sherman, J. (2010). Effect of Three Styles of Custom Ankle Foot Orthoses on the Gait of Stroke Patients While Walking on Level and Inclined Surfaces.

Lintanf, M., Bourseul, J. S., Houx, L., Lempereur, M., Brochard, S., & Pons, C. (2018). Effect of ankle-foot orthoses on gait, balance and gross motor function in children with cerebral palsy: a systematic review and meta-analysis. In Clinical Rehabilitation (Vol. 32, Issue 9, pp. 1175–1188). SAGE Publications Ltd. https://doi.org/10.1177/0269215518771824

Mercuri, E., Jungbluth, H., & Muntoni, F. (2005). Muscle imaging in clinical practice: diagnostic value of muscle magnetic resonance imaging in inherited neuromuscular disorders. In Current Opinion in Neurology (Vol. 18). Lippincott Williams & Wilkins.

Morinaga, K., Takeue, K., Ishihara, T., Ishihara, S., Hirano, M., Arizono, H., Tsuji, T., Francis, A., & Anderson, S. (2019). Kansei Based Evaluation of 3D CG Material Surface in Children's Lower Leg Orthotics.

Morouço, P. (2018). The Usefulness of Direct Digital Manufacturing for Biomedical Applications. Green Chemistry Series, 55, 478–487.

Nam, G., & Kim, M. H. (2014). The Next Big Thing Multispectral Photometric Stereo for Acquiring High-Fidelity Surface Normals.

Ricardo, D., Raposo, M. R., Cruz, E. B., Oliveira, R., Carnide, F., Veloso, A. P., & João, F. (2021). Effects of ankle foot orthoses on the gait patterns in children with spastic bilateral cerebral palsy: A scoping review. In Children (Vol. 8, Issue 10). MDPI. https://doi.org/10.3390/children8100903

Roberts, K., Boland, M. R., Pruinelli, L., Dcruz, J., Berry, A., Georgsson, M., Hazen, R., Sarmiento, R. F., Backonja, U., Yu, K. H., Jiang, Y., & Brennan, P. F. (2017). Biomedical informatics advancing the national health agenda: The AMIA 2015 year-in-review in clinical and consumer informatics. Journal of the American Medical Informatics Association, 24(e1), e185–e190. https://doi.org/10.1093/jamia/ocw103

Rogati, G., Leardini, A., Ortolani, M., & Caravaggi, P. (2019). Validation of a novel Kinect-based device for 3D scanning of the foot plantar surface in weight-bearing. Journal of Foot and Ankle Research, 12(1), 1–8. https://doi.org/10.1186/s13047-019-0357-7

Silva, R., Morouço, P., & Veloso, A. (2019). Desenvolvimento de um sistema one-shot de baixo custo para aquisição de modelos 3D. Proceedings Do 8o Congresso Nacional de Biomecânica, 239–240.

Silva, R., Veloso, A., Alves, N., Fernandes, C., & Morouço, P. (2022). A Review of Additive Manufacturing Studies for Producing Customized Ankle-Foot Orthoses. In Bioengineering (Vol. 9, Issue 6). MDPI. https://doi.org/10.3390/bioengineering9060249

Telfer, S., Pallari, J., Munguia, J., Dalgarno, K., McGeough, M., & Woodburn, J. (2012). Embracing additive manufacture: Implications for foot and ankle orthosis design. BMC Musculoskeletal Disorders, 13(May). https://doi.org/10.1186/1471-2474-13-84

Telfer, S., & Woodburn, J. (2010). The use of 3D surface scanning for the measurement and assessment of the human foot. http://www.jfootankleres.com/content/3/1/19

Totah, D., Kovalenko, I., Saez, M., & Barton, K. (2017). Manufacturing Choices for Ankle-Foot Orthoses: A Multi-objective Optimization. Procedia CIRP, 65, 145–150. https://doi.org/10.1016/j.procir.2017.04.014

Wojciechowski, E., Chang, A. Y., Balassone, D., Ford, J., Cheng, T. L., Little, D., Menezes, M. P., Hogan, S., & Burns, J. (2019). Feasibility of designing, manufacturing and delivering 3D printed ankle-foot orthoses: A systematic review. Journal of Foot and Ankle Research, 12(1), 1–12. https://doi.org/10.1186/s13047-019-0321-6

Study 5

From Scans to Steps: Elevating Stroke Rehabilitation with 3D-Printed Ankle-Foot Orthoses

Authors: **Rui Silva**, Pedro Morouço, Diogo Ricardo, Inês Campos, Nuno Alves and António Veloso

Abstract

Background: The integration of advanced 3D scanning and additive manufacturing technologies in stroke rehabilitation offers promising advancements in the design and production of ankle-foot orthoses. These technological innovations are progressively recognized for their potential to provide more precise and customized orthotic solutions for individuals with stroke-related impairments.

Objectives: The primary aim of this study was to biomechanically test and validate the effectiveness of custom ankle foot orthoses produced through additive manufacturing technology using data captured by a novel photogrammetric scanning system. The customized orthosis was compared with a standard prefabricated orthosis to assess their relative effectiveness in improving gait dynamics and patient satisfaction in stroke rehabilitation.

Methods: Participants with equinovarus deformity, a common consequence of stroke, were fitted with custom ankle foot orthosis, alongside conventional prefabricated orthosis. The study utilized the Qualisys® motion analysis system for a comprehensive biomechanical gait analysis, and the QUEST questionnaire was employed to capture participant feedback on both types of orthoses. Detailed comparisons of gait dynamics were conducted using Statistical Parametric Mapping under each orthosis.

Results: The study revealed notable kinematic and kinetic differences between the custom and prefabricated orthoses. The custom orthosis, demonstrated superior performance in enhancing gait efficiency, symmetry, and safety. Patient feedback favoured the customized orthosis over the prefabricated variant, with higher scores in comfort, fit, and overall effectiveness.

Conclusions: This research underscores the effectiveness of custom orthoses produced through additive manufacturing technology for stroke rehabilitation. By offering a comprehensive evaluation of orthotic interventions and establishing a comparative framework, the study serves as a reference point for future research, advocating for a more personalized and evidence-based approach in orthotic design for improving the quality of life of stroke survivors.

Keywords: Kinematics, Kinetics, Gait Profile Score, Spatiotemporal, Stroke, 3D Scanner, Additive Manufacturing, QUEST, Ankle Foot, Orthosis

Introduction

Rehabilitation plays a crucial role in helping individuals regain mobility and enhance their quality of life after debilitating health events, particularly in the context of stroke patients with significant motor impairments (S. Tyson & Kent, 2013). It has been demonstrated that the use of ankle-foot orthoses (AFOs) can profoundly improve walking patterns, offering stability, and preventing equinovarus foot in stroke survivors (S. Tyson & Kent, 2013; Wada et al., 2021). Studies have evaluated the effects of AFOs on balance, walking, energy expenditure, and gait performance in stroke patients, demonstrating their potential therapeutic effect in the recovery phase (Daryabor et al., 2022; Daryabor, Yamamoto, et al., 2020; Doğan et al., 2011; Kobayashi et al., 2017; S.-H. Lee et al., 2018; Maeda et al., 2009; Zarezadeh et al., 2022). Additionally, different AFO designs have been compared, highlighting their clinical efficacy in subjects with foot drop after stroke (Mohanty et al., 2020). Case reports and feasibility studies have also explored novel AFO designs and their impact on gait changes in hemiplegic patients (Daryabor, Arazpour, et al., 2020; Yamamoto, 2014). However, it is essential to consider the long-term usage and patient-specific customization of AFOs to ensure their acceptability and effectiveness in stroke rehabilitation (S. Tyson & Kent, 2013; Wada et al., 2021).

Over time, the realm of rehabilitation has witnessed an evolution in the techniques and applications associated with AFOs. Traditionally, these orthoses were crafted through methods that relied extensively on the skills and expertise of orthotists-prosthetists. While these methods were functional, they sometimes fell short in terms of customization due to the limitations inherent in these processes. These traditional methods were time-consuming and occasionally resulted in discomfort for the patients (Silva et al., 2022), still, this handmade AFOs also had its advantages. One of the primary benefits are the in-depth understanding it provided of each patient's specific requirements, ensuring a highly personalized and tailored approach to treatment. Furthermore, the materials used in crafting these orthoses are selected based on years of experience and consideration, ensuring that the final products are not only functional but also long-lasting (Wojciechowski et al., 2019).

With technological advancements, the potential for achieving higher levels of precision and customization in AFO production has become increasingly higher. The manufacturing of AFOs has undergone significant transformations, particularly with the integration of additive manufacturing (AM) and cutting-edge 3D scanning technologies. Innovative techniques like

Fused Deposition Modelling (FDM), Selective Laser Sintering (SLS), and Stereolithography (SLA) have marked a new era in orthotics production (Choi et al., 2017; Creylman et al., 2013; Mavroidis et al., 2011). Each of these AM techniques brings its unique strengths, enabling diverse designs, versatile material options, and accelerated production cycles. Both SLA and SLS offer capabilities specifically tailored to meet the intricate demands of orthotic production (Mavroidis et al., 2011; Telfer et al., 2012; Vasiliauskaite et al., 2019). For instance, the adaptability and cost-effectiveness of FDM have made it a preferred choice for various applications (Boparai et al., 2016). In addition to these technological advancements, the popularity of prefabricated orthoses has also increased significantly, as they offer a cost-effective and readily available solution (Böhm & Dussa, 2021; Wojciechowski et al., 2019). These off-the-shelf options often result in cost savings; conversely, their design approach might not always provide the perfect fit for every individual, which can sometimes compromise both the comfort and overall effectiveness of the device (Morrissey et al., 2020). To address the need for customization in orthotics, 3D scanning technologies have emerged as revolutionary tools in the field. These technologies, adept at capturing the complex anatomical details necessary for creating personalized orthotics, have significantly altered the landscape of orthotic design and fabrication (Barrios-Muriel et al., 2020). The spectrum of available 3D scanning techniques has broadened, encompassing not only laser scanners (Parry et al., 2020; Roberts et al., 2016) but also structured light scanners (Ambu et al., 2023; Cha et al., 2017), photogrammetry (Dal Maso & Cosmi, 2019; Sabyrov et al., 2021), and handheld optical scanners (Ciobanu et al., 2013; Roucoules et al., 2021). Each of these technologies offers unique advantages and contributes to an unprecedented level of accuracy in data capture. For instance, laser scanners provide high precision and are excellent for capturing complex geometries, making them ideal for detailed orthotic design. Structured light scanners, on the other hand, offer a balance between speed and accuracy, useful for quickly capturing the shape and size of a limb. Photogrammetry, utilizing photographic images from different angles, is beneficial for its versatility and ease of use, especially in remote or resource-limited settings. Handheld scanners add the convenience of portability and flexibility, enabling clinicians to perform scans in various clinical environments. This wide array of scanning options has made personalized orthotics more accessible and feasible for a diverse range of individuals (Eder et al., 2013; Rogati et al., 2019). These scanners have been instrumental in creating tailored orthoses that meet patient-specific needs, as evidenced in

various case studies (Baronio et al., 2016; Krajňáková et al., 2020; Ranaldo et al., 2023). Their ability to accurately capture the unique contours of an individual's anatomy ensures that the resulting orthoses are not just functionally superior but also comfortable, thereby enhancing patient compliance and therapeutic outcomes (R. K. Chen et al., 2016). Nevertheless, it is important to recognize that while this method offers precision and customization, challenges remain in integrating this technology into existing clinical workflows and providing adequate training for medical professionals.

The potential of combining AM with 3D scanning for orthotic fabrication is incredibly exciting. The literature presents a range of perspectives on this integration; some studies enthusiastically highlight the benefits and practical applications of this synergy (Belokar et al., 2017; Grazioso et al., 2018; Parry et al., 2020), while other research studies point to challenges, gaps, and inconsistencies in this field (Baronio et al., 2016; Liu et al., 2019). What becomes increasingly clear is the need for comprehensive evaluations and assessments. Unfortunately, a sizeable portion of existing research lacks these assessments, sometimes leading to gaps in understanding any potential obstacles in real-world implementation. A closer look at the studies provides insights into how these technologies have real-world implications. Several studies have tested their AFOs only on healthy individuals (Belokar et al., 2017; R. K. Chen et al., 2014; Lin et al., 2017), or used moulds for digitization, bypassing direct scanning of the patient's limb (Pérez Pico et al., 2023). Others have limitations, such as lacking biomechanical analyses or qualitative assessments (R. K. Chen et al., 2014; Deckers et al., 2018). Despite these methodological variations and limitations, each study holds its merit and contributes valuable insights to the field of personalized orthoses using AM. These investigations, whether focusing on the intricacies of manufacturing techniques, the precision of 3D scanning methods, or exploring the capabilities of these technologies in real-world clinical settings, have laid a crucial foundation for future research endeavours. The dynamic nature of this field is further highlighted by the diverse approaches in different studies. While some researchers prioritize exploring the capabilities of manufacturing techniques and 3D scanners, others concentrate on evaluating their applications in clinical scenarios (Ciobanu et al., 2013). Within the realm of manufacturing, ongoing discussions and research are centered around finding the most suitable materials for orthotic fabrication, balancing durability, flexibility, patient comfort, and cost-effectiveness. This challenge has led to various research projects searching for the best materials based on specific clinical requirements (Dal Maso &

Cosmi, 2019; Liu et al., 2019). Despite their flaws, these studies pave the way for new discoveries and advancements, significantly contributing to a field that has the potential to aid millions worldwide with more effective and personalized orthotic solutions.

In contrast, when it comes to 3D scanning, a unique set of challenges and complexities arise. While the potential for accuracy is high, implementing these technologies in real-world scenarios can sometimes bring unexpected obstacles. Factors such as movement during scanning procedures (Grazioso et al., 2018), scanner resolution quality (Baronio et al., 2016), and the software algorithms (Cha et al., 2017) used for data processing can significantly impact the quality of the orthotic products. Another crucial aspect to consider in this discussion is the perspectives and feedback from patients, who are the end-users of these orthotic devices. The comfort, experiences, and adherence to treatment plans of patients are crucial in determining the success of any intervention. Several studies (Silva et al., 2022; Wojciechowski et al., 2019) have focused on this aspect by comparing feedback on traditional orthoses versus those produced using AM techniques. While most of the feedback has been positive, these studies also point out potential areas for improvement, particularly concerning the weight and aesthetic design of these devices (Cha et al., 2017; Chae et al., 2020).

Moreover, it is important to consider the implications associated with integrating 3D scanning and AM into orthotic fabrication processes. The initial investments in equipment, training, and infrastructure changes may be substantial. However, the potential long-term benefits, such as reduced production times, minimized material waste, and increased customization options, present a promising outlook for return on investment (Silva et al., 2022). While it becomes clear that the field of rehabilitation is on the verge of a meaningful change, it comes with its share of challenges. Like any transition, incorporating AM and 3D scanning technologies into the orthotics field requires a comprehensive approach. This approach should cover aspects such as understanding capabilities, aligning with clinical needs, gathering patient feedback, considering economic implications, and ensuring long-term sustainability.

This study aimed to biomechanically test and validate the effectiveness of custom ankle-foot orthoses produced through additive manufacturing technology, using data captured by a novel photogrammetric scanning system. It sought to bridge the gap between traditional craftsmanship and modern technology, leveraging the precision of 3D scanning and the versatility of AM. In doing so, the study addressed the challenges of integrating these

technologies into clinical practice, from ensuring high-quality scanning to a perfect fit AFO. While the primary focus was on biomechanical outcomes and patient feedback, a brief overview of the scanning system was also provided to contextualize the customization process. Ultimately, this research aimed to contribute to the transformative change in the field of rehabilitation, promising more effective, personalized orthotic solutions for millions worldwide.

Materials and Methods

This research expands on the development of a scanner and software system used to create 3D printed AFOs for stroke survivors experiencing equinovarus deformity, as detailed in an upcoming paper by R. S., P. M., D. R., I. C., N. A., Filipe Perdigoto, Moisés Domingues, and A. V. To validate the entire system was necessary to ensure its biomechanical performance was at least as effective as standard AFOs, while also enhancing patient satisfaction. Feedback from patients and clinical observations served as the primary indicators of success.

Participant Recruitment and Ethical Considerations

The approval for the protocol of this study was granted by the Health Ethics Committee of Centro de Medicina de Reabilitação da Região Centro – Rovisco Pais (Tocha, Portugal) in August 2022. All experiments and procedures were performed in accordance with the relevant guidelines and regulations. Additionally, all aspects of the research involving human participants were performed in accordance with the Declaration of Helsinki. In line with a request from the Health Ethics Committee a specific document was created. The purpose of this document was to ensure that the participants gave their consent freely with understanding. This document detailed the objectives of the research study and provided assurances that there would be no negative impact on the patient's treatment and clinical follow-up should they choose to withdraw from the study. It also guaranteed the anonymity and confidentiality of all collected data, including photographs, results from the Quebec User Evaluation of Satisfaction with Assistive Technology (QUEST) (Demers et al., 1996), and biomechanical analysis data. Both the physician and the patient signed the consent form, validating their participation in the study. The research protocol was crafted in accordance with the SPIRIT (Standard Protocol Items: Recommendations for Interventional Trials) 2013 checklist, a recognized standard for reporting protocol studies (Chan et al., 2013). Also, a research protocol was created for this study (Silva, 2023).

The participant selection criteria for this study were meticulously defined to ensure the inclusion of individuals whose profiles were optimally aligned with the objectives of the research. The study targeted a cohort of stroke survivors, both genders, within an age range of 18 to 75 years. The subjects in the study were required to exhibit signs of equinovarus foot caused by a stroke, impacting either the left or right lower extremity. A critical criterion for inclusion was the daily use of the subjects with off-the-shelf AFOs as a component of their rehabilitation regimen. The concurrent use of auxiliary assistive devices such as tripods, crutches, or canes was not a disqualifying factor. Foremost, among the inclusion criteria were the ability of participants to provide informed consent and demonstrate ambulatory capabilities, either independently or with the aid of the assistive devices. Exclusion criteria encompassed individuals presenting with coexisting neurological or orthopaedic conditions and impairing gait that could potentially obfuscate the study's results. Additionally, candidates exhibiting active dermatological conditions in distal lower limbs or severe communicative limitations that could impede consistent and effective participation were deemed ineligible. The recruitment phase was conducted at the Centro de Medicina de Reabilitação da Região Centro. Physicians undertook a rigorous examination of patient profiles to ascertain congruence with the predefined selection criteria. A total of ten eligible candidates (Table III.7) were comprehensively briefed about the study's objectives and methodology, followed by the dissemination of a detailed informed consent document. Ensuring adherence to ethical standards and the integrity of the data collection process, the enrolment of these participants proceeded after their provision of written informed consent.

TABLE III.7 - Demographic and Clinical Profile of Stroke Patients: A Detailed Overview of Gender, Age, Physical Characteristics, Stroke Type, Affected Side, and Orthotic Preferences

Patient	Gender	Age (years)	Height (cm)	Weight (Kg)	Diagnosis	Time since Stroke (months)	Paretic Side	Fugl-Meyer Scale (lower extremity)	Tinetti POMA	Current AFO Type
1	F	48	168	68.0	Ischemic Stroke	3	Left	69	17	PLS
2	M	67	169	69.3	Ischemic Stroke	5	Left	78	24	PLS
3	M	26	175	75.1	Hemorrhagic Stroke	5	Left	74	21	PLS
4	M	65	163	69.1	Ischemic Stroke	8	Right	53	13	Leaf Spring
5	F	54	166	77.3	Hemorrhagic Stroke	140	Right	65	18	PLS
6	F	56	147	78.0	Hemorrhagic Stroke	13	Left	67	18	Leaf Spring
7	F	36	165	63.7	Ischemic Stroke	5	Right	58	24	PLS
8	M	70	185	77.8	Hemorrhagic Stroke	5	Left	73	20	PLS
9	M	64	167	70.1	Hemorrhagic Stroke	5	Right	71	20	PLS
10	M	54	168	73.5	Ischemic Stroke	5	Right	75	21	PLS

AFO Fabrication Process

The novel photogrammetric 3D scanner(Silva et al., 2019) as employed for the precise capture of the surface topology of the hemiparetic lower limb. The patients were requested to wear loose-fitting track pants to allow easy access to the affected leg. To ensure a cleaner scan and reduce surface noise, like leg hair on the mesh, the patients used a stocking to achieve a more consistent model. The preparatory phase for positioning each patient within the scanning apparatus required approximately five minutes, with the actual data capture process concluding in less than two seconds (Fig. III.16).

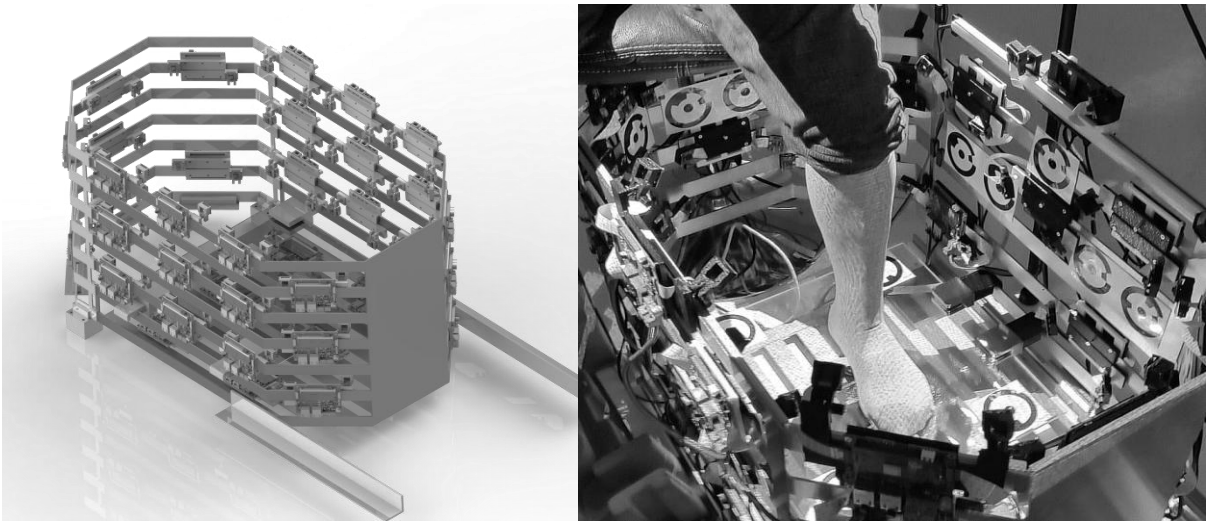

FIGURE III.16 – On the left side – Virtual image of the novel photogrammetric 3D Scanner. On the right side – Left hemiparetic lower limb of the patient on the scanner

In the patient's absence, the physiatrist utilized a newly developed software to construct the custom AFO on the virtual leg of the subject. The decision to use Nylon 12 material for the AFOs was based on extensive mechanical testing of various materials (Habiba et al., 2023), including Acrylonitrile Styrene Acrylate (ASA), Polycarbonate-Acrylonitrile Butadiene Styrene (PC-ABS), Polyethylene Terephthalate Glycol (PETG), Thermoplastic Polyurethane (TPU), Polylactic Acid (PLA), Polycarbonate (PC), ULTEM 1010, and ULTEM 9085. The models for the AFOs were then printed using the FDM process, ensuring a uniform thickness of 3mm across all printed orthoses (Fig.2). This thickness was selected based on the mechanical tests conducted with various thicknesses, as well as the typical thicknesses found in off-the-shelf AFOs. The design of these AM custom AFOs was influenced by the Posterior Leaf Spring (PLS)

model, tailored to the gait requirements post-stroke, with the objective of mitigating excessive equinus or foot drop during the swing phase and augmenting push-off during stance (Ounpuu et al., 1996). The upper proximal portion was delimited to 5cm below the fibular head and surrounding the posterior portion of the leg to form the upper band of the AFO where a velcro strap was fixed later. From this point downwards the width of the posterior trim lines was narrowed onto the ankle without covering the medial and lateral malleoli. A medial arch was included in the orthosis to enhance the medial plane control of the foot and ankle. These supports were also used to place velcro straps at the ankle when needed. The trim lines for the foot plate were just behind the metatarsal heads. The AFOs were initially fitted to each subject, with fine tuning performed as necessary. This fine tuning included the use of a very fine sandpaper to smooth any sharp edges or vertices that could potentially cause discomfort or injure the patient. A period was given for AFO acclimatization. To avoid bias, standardized sport shoes in different sizes were available during the testing for each subject (Fig. III.17).

Figure III.17 - 3D printed AFO in Nylon 12 material

Biomechanical Assessment and Data Collection

Following the acclimatization period with the customized AFO (CO), subjects were instructed to walk along a 10-meter corridor, completing a total of 10 repetitions. This process was conducted with both their regularly used standard AFO (off-the-shelf) (PO) and the new CO AFO. To ensure the accuracy and consistency of the biomechanical data, the six most representative gait cycles from each set of AFOs were selected for detailed analysis. This selection criterion was applied to mitigate variability and focus on the highest quality data sets.

The gait dynamics were captured using a Qualisys® motion analysis system (Qualisys AB, Gothenburg, Sweden), equipped with 12 high-speed Miqus M3 cameras (Frequency: 120-Hz) and 2 Bertec force

platforms (FP4060-07, FP4060-10, Bertec, Columbus, OH, USA) was utilized to capture precise movement data (Fig. 3). Subjects were fitted with the CAST lower body marker set, which includes 36 reflective markers (10mm diameter) following the protocol prescribed by Cappozzo et al. (Cappozzo et al., 1995). It is important to note that all markers were placed directly on the skin of the patients to accurately capture their movements, with the exception of the foot markers. For the feet, markers were placed on standardized sports shoes provided to the patients. These shoes, consistent in design but varying in size to fit each patient, were used to minimize variability in data collection related to different footwear. The patient's lower limbs were digitally reconstructed in a 3D environment using the Visual 3D™ software developed (C-Motion, Inc., Rockville, MD, USA), using the Project Automation Framework (PAF) from Qualisys®. The acquired data were processed using a Butterworth low-pass filter with a cutoff frequency of 10 Hz and segmented into phases of the gait cycle based on heel strike events.

For the kinematic data analysis, several parameters were extracted for future analysis, including Pelvic Anterior Tilt, Pelvic Up Obliquity, Pelvic Internal Rotation, Hip Flexion, Hip Adduction, Hip Internal Rotation, Knee Flexion, Knee Varus, Knee Internal Rotation, Ankle Dorsiflexion, Ankle Inversion, Foot Pitch, and Foot Internal Progression. Regarding the kinetic data, parameters such as Internal Hip Extensor Moment, Internal Hip Valgus Moment, Internal Knee Extensor Moment, Internal Knee Valgus Moment, Internal Ankle Plantarflexor Moment, and Internal Ankle Extensor Moment were selected. For spatiotemporal data, values including Speed, Stride Width, Stride Length, Cycle Time, Step Length, Step Time, Stance Time, Swing Time, Steps per Minute, Strides per Minute, and Double Limb Support were extracted. Additionally, Gait Profile Score (GPS) (R. J. Baker et al., 2018) values were also retrieved. These data were collected for both the affected and unaffected limbs, using both AFOs (PO vs CO).

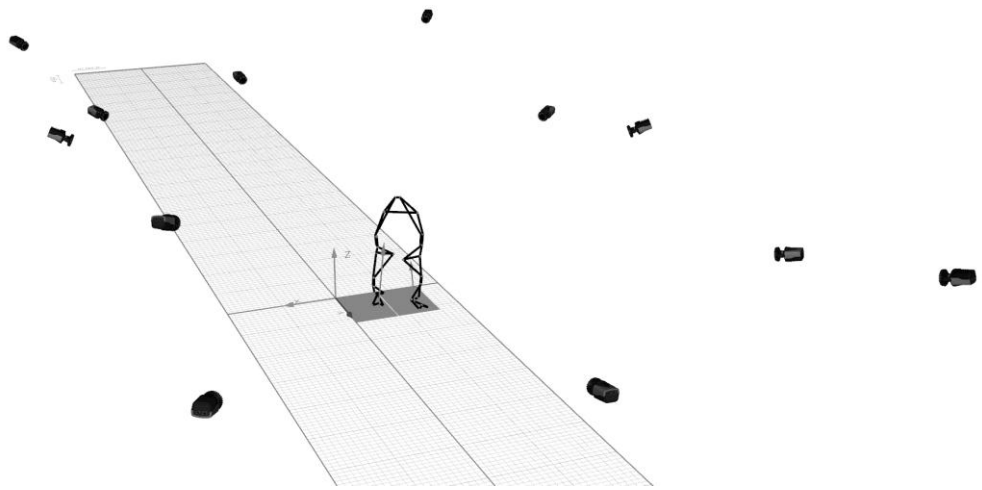

FIGURE III.18 - Testing environment. Representation of test environment with twelve infrared highspeed cameras and two force platforms during the gait cycle of the patient in the Qualisys Track Manager software

Quality assessment from Subjects

In this study, significant emphasis was placed on the subjective feedback from the subjects, in addition to the analysis of biomechanical data. A structured questionnaire, based on the QUEST, was utilized to rate various parameters of both AFOs. Subjects rated Dimensions, Weight, Fit, Safety, Usability, Comfort, and Effectiveness on a scale from 1 to 5, where 1 represented 'Not Satisfied at All' and 5 signified 'Very Satisfied'.

Statistical Analysis

The statistical analysis of the data was conducted both individually for each subject and globally for all patients of the normalized gait cycle (heel strike to heel strike).

For kinematic and kinetic data, graphical comparisons were made using the Statistical Parametric Mapping (SPM) method. The analysis utilized the SPM1D script and MatLab v2023b (MathWorks, Natick, MA, USA). SPM1D v0.4 allows for identifying specific regions in the gait cycle where noticeable differences between conditions (PO and CO) occur, offering continuous evaluation over the entire cycle and highlighting subtle yet clinically important variations. Individual comparisons were made using paired t-tests for each subject's legs (left leg PO vs. left leg CO and right leg PO vs. right leg CO). The global analysis involved two-sample t-tests for comparing the affected limb with the unaffected limb. All GPS data were collected and analyzed to observe mean differences between each set.

A symmetry test and an intra-subject symmetry index were conducted to compare the left and right legs using Microsoft Excel (Microsoft Corporation, Redmond, WA, USA) to detect deviations on 50%. Intra-subject leg comparison tests in both PO and CO conditions involved normality tests followed by Wilcoxon tests for all variables, using GraphPad Prism 10.0.2 software (GraphPad Software, San Diego, CA, USA). For the global analysis, Mann-Whitney tests were performed.

For the analysis of the quality assessment from subjects all mean values were analyzed both individually and globally, incorporating all findings from the QUEST questionnaire.

Significant differences were recognized based on p-values, with a threshold set at 95% indicating statistical significance.

Results

The Results section herein provides a comprehensive analysis of the gathered data, encompassing kinematic and kinetic parameters, spatiotemporal metrics, and patient satisfaction levels as measured by the QUEST. The global outcomes derived from these data sets are synthesized and presented in the main body of this paper. To facilitate a thorough understanding and transparency, the individual results for each patient have been detailed in the Supplementary Material.

Kinematics

The graphs on the top display the means of normalized gait cycles, ranging from 0 to 100%, for all patients' kinematics (Fig. III.19), comparing Heel Strike events between AFO CO (black line) and AFO PO (red line). The lightly shaded grey area provided by PAF software represents the normative data standard deviation for a healthy adult demographic. The graphs on the bottom show the SPM comparison between both means.

Affected Limb		
X	**Y**	**Z**
Pelvic Anterior Tilt	Pelvic Up Obliquity	Pelvic Int. Rotation
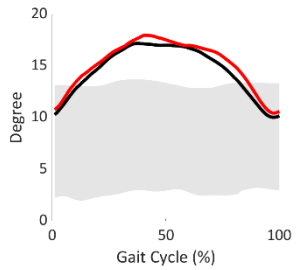	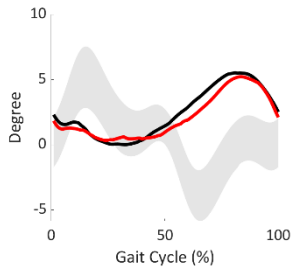	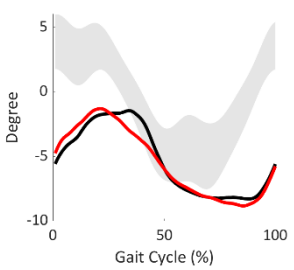
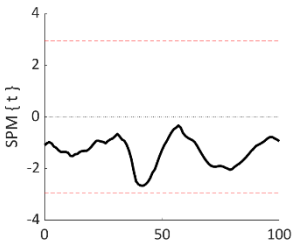	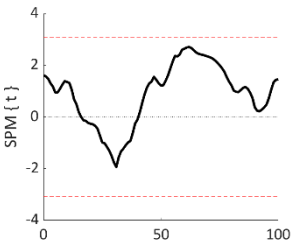	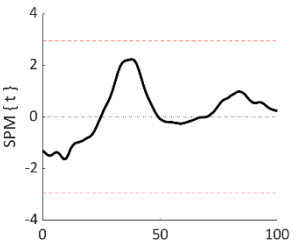
Hip Flexion	Hip Adduction	Hip Int. Rotation

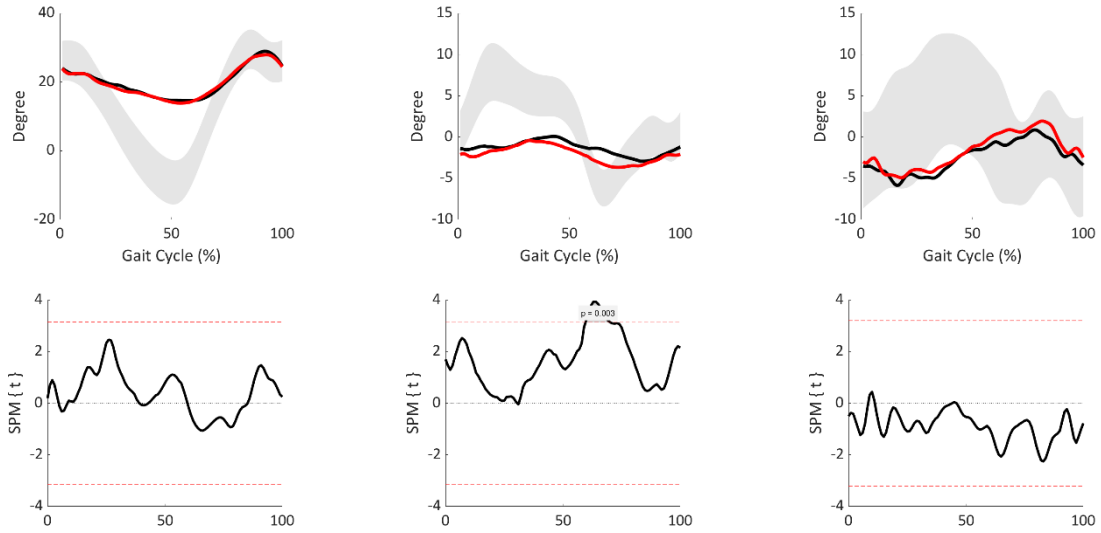

Knee Flexion | Knee Varus | Knee Int. Rotation

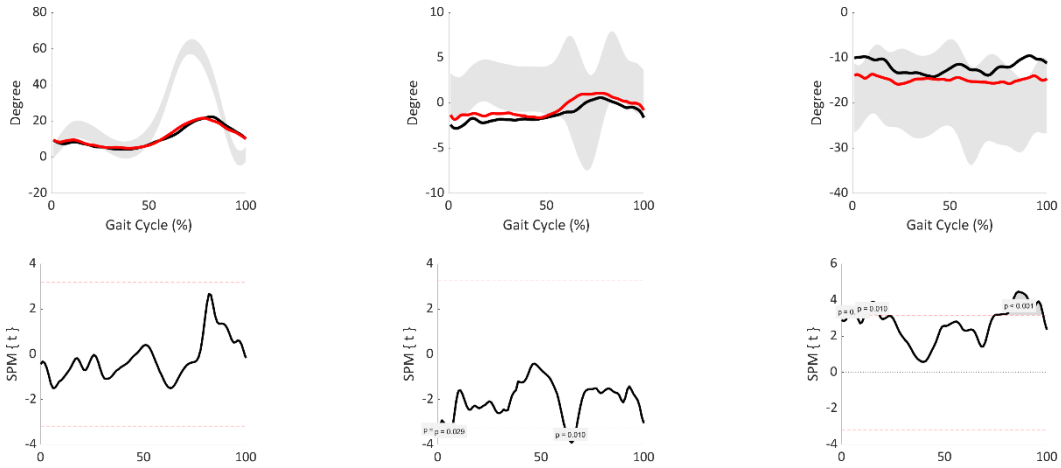

Ankle Dorsiflexion | Ankle Inversion

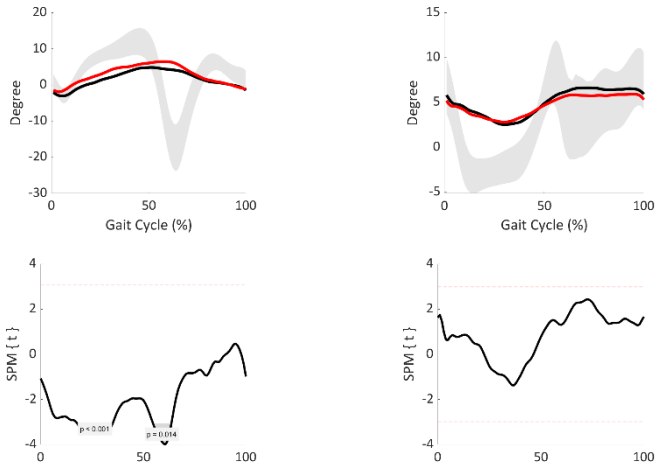

Foot Pitch | Foot Int. Progression

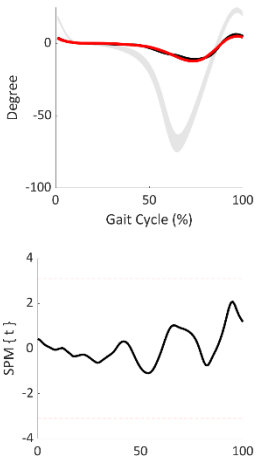

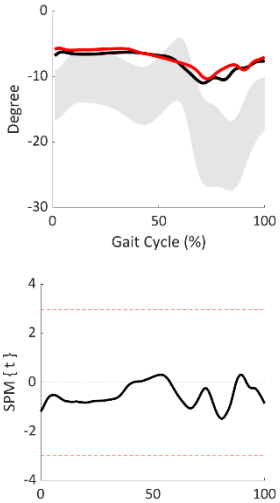

Unaffected Limb

Pelvic Anterior Tilt

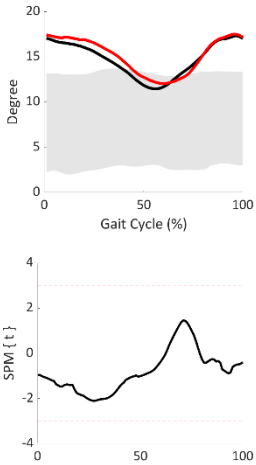

Pelvic Up Obliquity

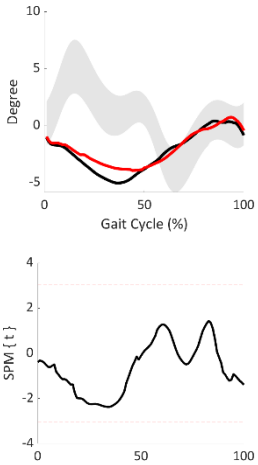

Pelvic Int. Rotation

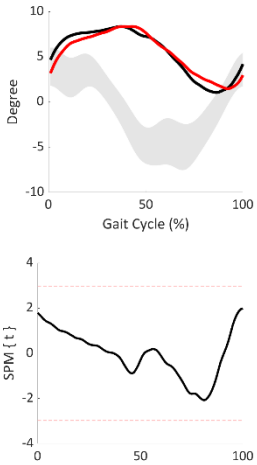

Hip Flexion

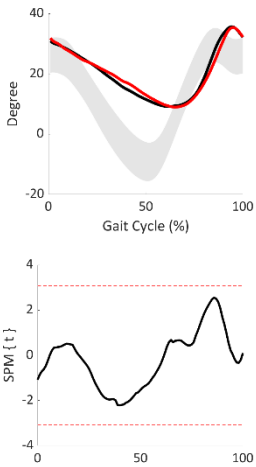

Hip Adduction

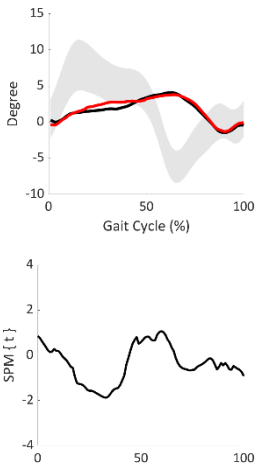

Hip Int. Rotation

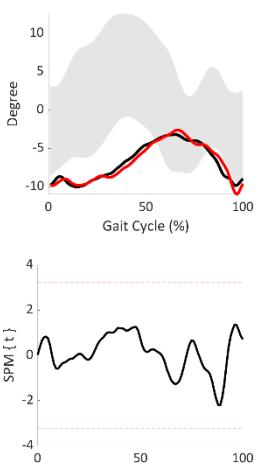

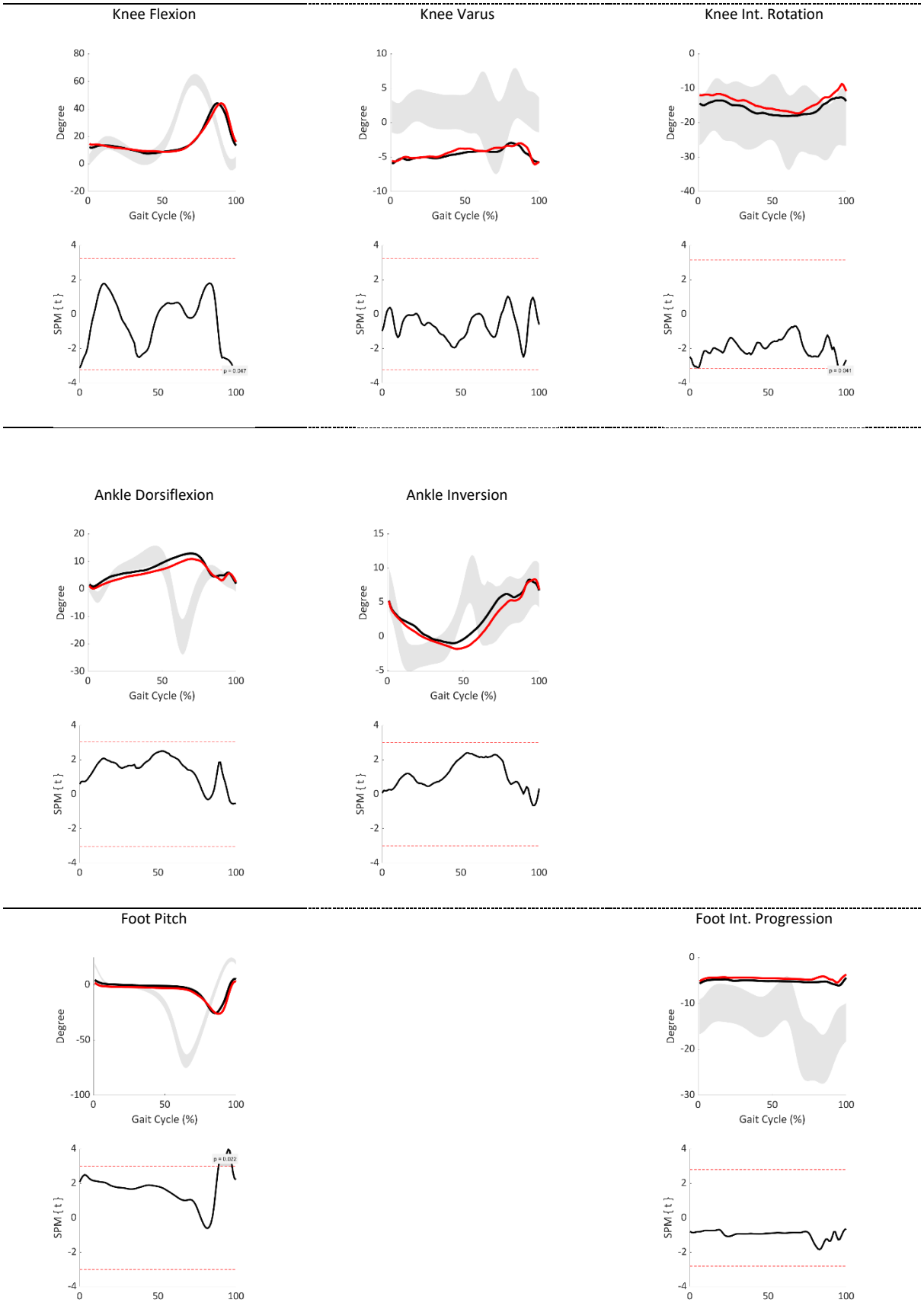

FIGURE III.19 – Mean Joint angles of all patients (top) and the respective 1D-SPM analysis (bottom) during the gait cycle, for the PO AFO (red line) and the CO AFO (black line). Grey shaded regions on the top side shows the normative data for the gait cycle of healthy patients and grey shaded regions on the bottom side indicate where differences were statistically significant

Kinetics

On the top, the graphics display the average kinetic profiles of normalized gait cycles from heel strike to heel strike (Fig. III.20), contrasting the kinetics of AFO PO (red line) with AFO CO (black line). The shaded grey region provided by PAF software delineates the standard deviation of normative kinetic data for a healthy adult demographic. On the bottom, the graphics present the results of the Statistical Parametric Mapping (SPM) analysis comparing the two kinetic curves.

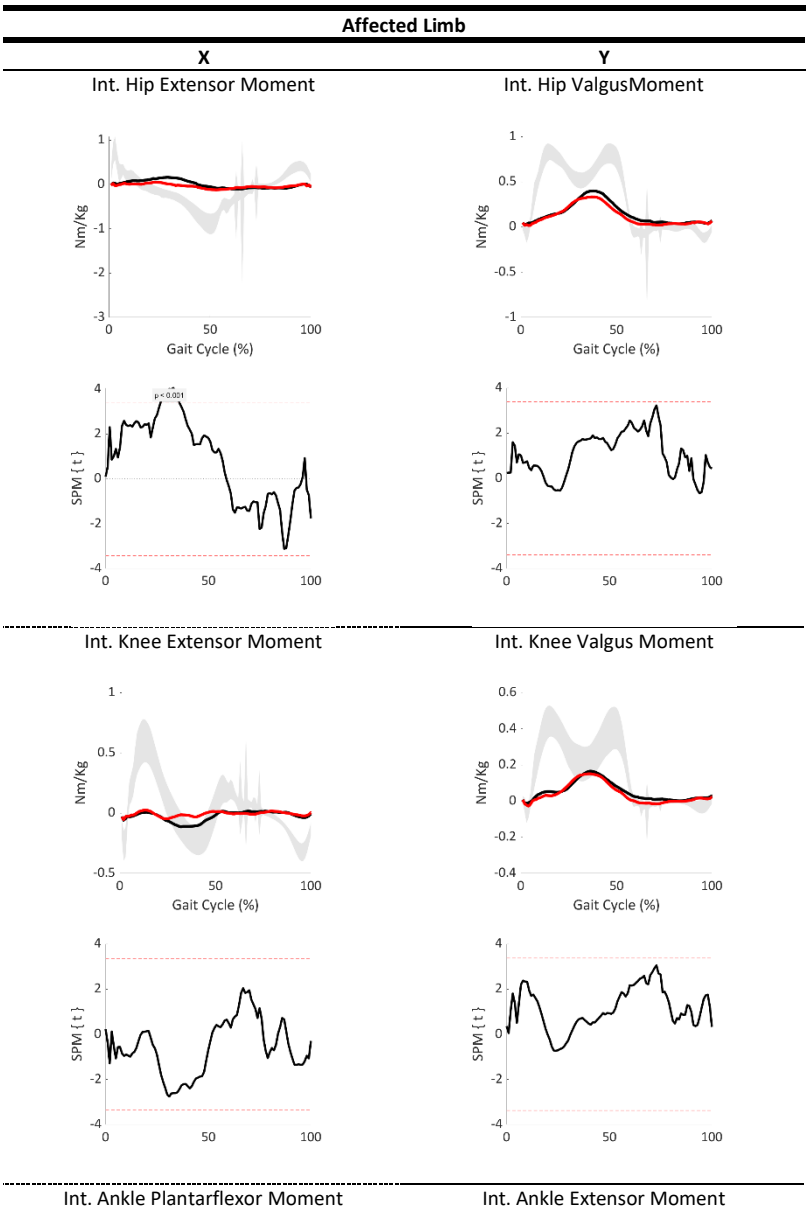

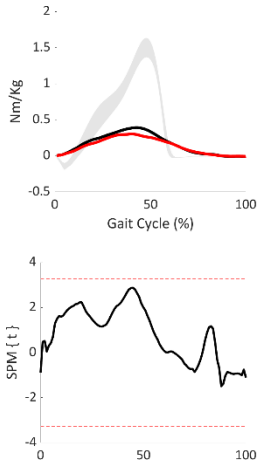

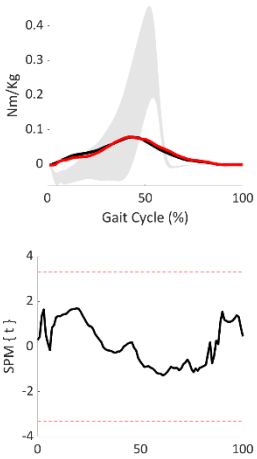

Unaffected Limb

Int. Hip Extensor Moment

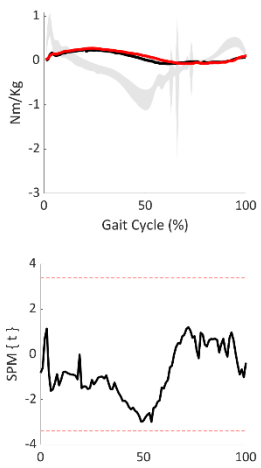

Int. Hip Valgus Moment

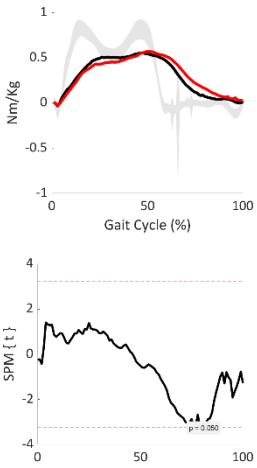

Int. Knee Extensor Moment

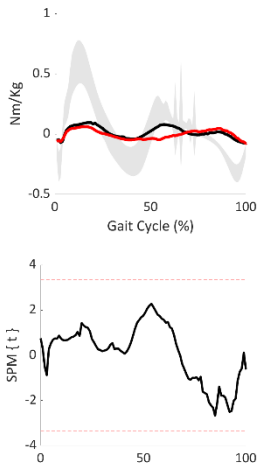

Int. Knee Valgus Moment

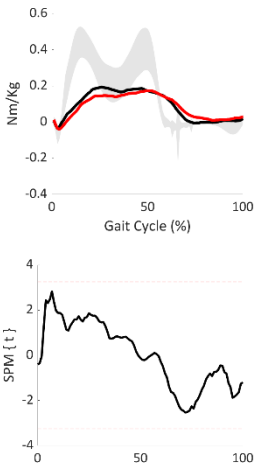

Int. Ankle Plantarflexor Moment

Int. Ankle Extensor Moment

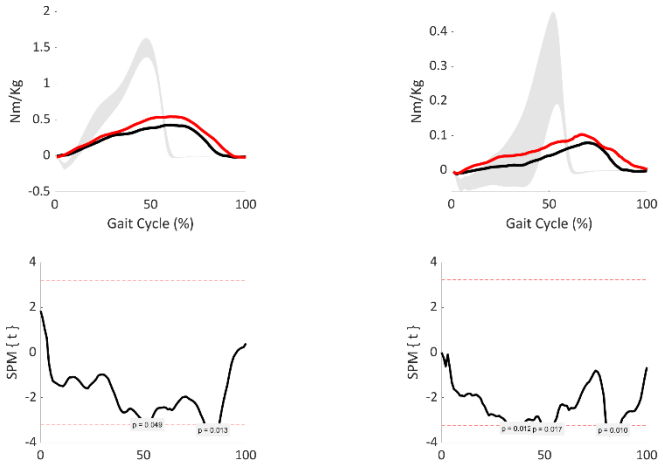

FIGURE III.20 - Mean Moments of all patients (top) and the respective 1D-SPM analysis (bottom) during the gait cycle, for the PO AFO (red line) and the CO AFO (black line). Grey shaded regions on the top side shows the normative data for the gait cycle of healthy patients and grey shaded regions on the bottom side indicate where differences were statistically significant

Spatiotemporal

The forthcoming analysis presents a detailed examination of spatiotemporal gait parameters, which are integral to understanding locomotive efficiency and symmetry in human movement. Initially, the symmetry between affected and unaffected limbs is assessed (Figure III.20), revealing compensatory strategies that may emerge due to gait alterations. Subsequently, Gait Symmetry Indices are analyzed (Table III.8), providing a quantitative measure of bilateral coordination, and identifying potential asymmetries. The breakdown of gait cycles further elucidates the timing and consistency of walking patterns, essential for recognizing deviations from typical gait (Table III.9). Also, a comparative analysis between the affected and unaffected limbs for PO and CO (Table III.10), delineating the influence of orthotic intervention on gait mechanics. These comparisons are pivotal for assessing the orthosis' role in gait modification and its relevance to rehabilitative strategies.

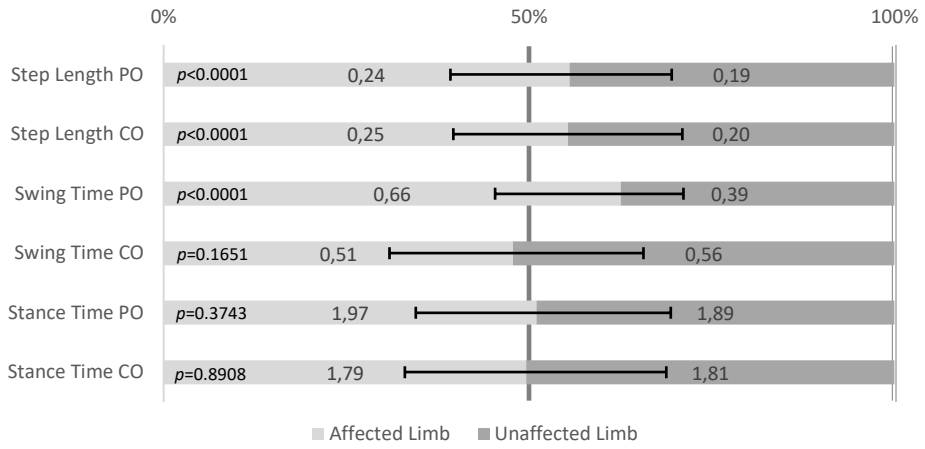

FIGURE III.21 – Mean and standard deviation of Symmetry vs Asymmetry of all patients for Step Length, Swing Time and Stance Time lor affected limb (light grey) and unaffected limb (dark grey). *P value* indicates if differences were statistically significant

TABLE III.8 - Comparative Analysis of Gait Symmetry Indices: Assessing Step Length, Swing Time, and Stance Time for PO and CO in Stroke Patients

Parameters	PO (mean±SD)	CO (mean±SD)	*p value*
Symmetric Index Step Length (%)	54.61 ± 13.55	55.16 ± 12.07	0.7359
Symmetric Index Swing Time (%)	62.11 ± 5.80	48.09 ± 12.36	<0.0001*
Symmetric Index Stance Time (%)	51.24 ± 5.15	50.00 ± 4.97	0.2188

TABLE III.9 - Comparative Analysis of Gait Parameters: PO and CO in Stroke Patients

Parameters	PO (mean±SD)	CO (mean±SD)	*p value*
Speed (m/s)	0.18±0.06	0.21±0.07	0.0485*
Stride Width (m)	0.20±0.04	0.20±0.04	0.8681
Stride Length (m)	0.44±0.09	0.45±0.10	0.6824
Double Limb Support (s)	1.40±0.64	1.32±0.63	0.5174
Cycle Time (s)	2.46±0.72	2.43±0.78	0.7586

TABLE III.10 - Detailed Gait Analysis Comparing Affected and Unaffected Limbs for PO and CO Use in Stroke Patients: Step Length, Time, Stride, Stance, Swing, Cycle Time, and Frequency

Parameters	Affected Limb PO (mean±SD)	Affected Limb CO (mean±SD)	*p value*	Unaffected Limb PO (mean±SD)	Unaffected Limb CO (mean±SD)	*p value*
Step Length (m)	0.24±0.07	0.25±0.07	0.5379	0.19±0.06	0.20±0.07	0.9677
Step Time (s)	1.51±0.63	1.42±0.62	0.3347	0.96±0.23	0.97±0.24	0.9677
Stride Length (m)	0.43±0.09	0.45±0.11	0.3501	0.43±0.09	0.44±0.10	0.7998
Stance Time (s)	1.79±0.67	1.78±0.71	0.9718	2.08±0.67	1.99±0.68	0.2801
Swing Time (s)	0.66±0.18	0.66±0.17	0.7487	0.39±0.09	0.40±0.09	0.5998
Cycle Time (s)	2.46±0.75	2.42±0.78	0.5927	2.45±0.70	2.38±0.78	0.4342
Steps / Minute	47.53±18.94	49.73±18.04	0.3426	67.46±17.06	65.30±17.14	0.5413
Strides / Minute	26.80±9.03	27.42±8.36	0.5207	26.72±8.62	27.83±9.26	0.4576

Gait Profile Score

Table III.11 presents the Gait Profile Score (GPS) results for all patients. The GPS is a recognized measure for assessing gait abnormalities and offers valuable insights into the effectiveness of various orthotic interventions. This table focuses on comparing the affected and unaffected limbs of patients by evaluating the median values of overall GPS scores. Additionally, it details individual values for each of the nine variables that constitute the GPS, for both affected and unaffected limbs under PO and CO conditions. This data provides a comprehensive understanding of the impact of each AFO type on specific gait aspects in both limb types. Furthermore, the table highlights the median differences between the AFO conditions, providing an analytical perspective on their comparative effectiveness.

GPS

TABLE III.11 - Comprehensive Gait Profile Score (GPS). Analysis for Stroke Patients: Comparing Affected and Unaffected Limbs for PO and CO with Median and Interquartile range with median differences

PO

Subject	Global (median)			Affected Limb (median)									Unaffected Limb (median)								
	GPS Affected Limb	GPS Unaffected Limb	GPS Overall	Pelvis Tilt	Hip Flexion	Knee Flexion	Ankle Dorsiflexion	Pelvis Obliquity	Hip Abduction	Pelvis Rotation	Hip Rotation	Foot Progression	Pelvis Tilt	Hip Flexion	Knee Flexion	Ankle Dorsiflexion	Pelvis Obliquity	Hip Abduction	Pelvis Rotation	Hip Rotation	Foot Progression
1	12.4	13	15.5	6.1	11.9	19.2	9.2	3.4	6	11.7	7.1	19.7	6.2	16.8	23.9	12.7	3.9	8.8	13.1	8.6	9
2	10.1	13.8	12.9	8	18.1	16.6	8.4	2.7	3.4	8.4	8.3	3	5.3	10.3	17.9	15.4	3.2	5.6	8.8	26	9.4
3	11.3	9.6	11.3	1.7	10.6	19.4	9.9	4.5	13.1	9	10.5	12.4	1.8	7.9	21	11.8	3.6	4.4	7.8	5.9	7.1
4	9.4	11.6	11	9.7	12.1	16.3	10.3	4	3	7.9	5.8	7.1	9.4	12.6	23.3	12.4	4.2	4.8	8.6	7.9	8.8
5	14.3	14.8	14.9	17.5	13.6	29.8	11.8	7.8	6.2	7.4	9.7	7.1	17.3	26.7	20.8	11.1	7.1	5.5	10.7	6.7	12.1
6	15.7	16.2	16.7	14.9	20.4	21	8.5	5	12.7	10.5	6.2	26.7	15.2	23.7	18.9	11.2	4.4	9.5	11.9	8.4	27.7
7	13.4	11	13.3	4.4	10.9	31.4	12	5.3	5.7	5.7	8.4	13.3	4.7	10.3	24.6	11.3	6.2	5	6.8	9.2	5.7
8	14.9	12.6	14.5	14.5	17.8	23.8	8.4	6.1	6.4	5.1	23.2	12.8	14.5	22.1	17.3	11.7	6.6	5.4	6.4	9	8.5
9	11	14.7	14.1	1.5	13.7	21.9	9.7	3	6.1	7.1	7.9	12.7	1.5	12.1	29.8	6.4	2.9	4.8	8.6	18.7	20.2
10	9.4	12.1	11.6	4.9	8.7	20.3	6.7	6.3	3.7	3.7	11.7	5.5	5.5	9.7	28.6	9.5	6.4	6.5	6.2	6.7	10.2
Median	**11.9**	**12.8**	**13.7**	**7.1**	**12.9**	**20.7**	**9.5**	**4.8**	**6.1**	**7.7**	**8.4**	**12.6**	**5.9**	**12.4**	**22.2**	**11.5**	**4.3**	**5.5**	**8.6**	**8.5**	**9.2**
IQR	**10.3 – 14.1**	**11.7 – 14.5**	**11.9 – 14.8**	**4.5 – 13.3**	**11.2 – 16.8**	**19.3 – 23.3**	**8.4 – 10.2**	**3.6 – 5.9**	**4.2 – 6.4**	**6.1 – 8.9**	**7.3 – 10.3**	**7.1 – 13.2**	**4.9 – 13.2**	**10.3 – 20.8**	**19.4 – 24.4**	**11.1 – 12.3**	**3.7 – 6.4**	**4.9 – 6.3**	**7.1 – 10.2**	**7.0 – 9.2**	**8.6 – 11.6**

CO

Subject	Global (median)			Affected Limb (median)									Unaffected Limb (median)								
	GPS Affected Limb	GPS Unaffected Limb	GPS Overall	Pelvis Tilt	Hip Flexion	Knee Flexion	Ankle Dorsiflexion	Pelvis Obliquity	Hip Abduction	Pelvis Rotation	Hip Rotation	Foot Progression	Pelvis Tilt	Hip Flexion	Knee Flexion	Ankle Dorsiflexion	Pelvis Obliquity	Hip Abduction	Pelvis Rotation	Hip Rotation	Foot Progression
1	11.2	10.4	11.7	4.1	10.3	22.7	9	3.8	4.6	7.7	6.2	15.1	3.4	11.9	17.9	14.3	3.9	7.6	7.4	7.7	6.6
2	9.8	13.6	12.6	8.6	18.9	14.5	8.3	3	3.7	5.3	8.2	3	8.7	15.7	17.9	15.3	3.5	6	6.9	17.9	4.2
3	11.8	9.3	11.4	4.9	9.4	21.4	10.5	4.8	13	8.5	13.9	10.1	3.8	9.1	18.6	13.4	5	4	9.1	3.2	5.4
4	9.1	11.2	10.8	9.1	12.5	16.5	9.8	4.6	2.9	6.9	6.4	3.5	9.5	13.2	22.1	11.2	4.4	4.3	7.3	7	9.5
5	13.4	13	13.6	11.7	12.6	27.3	15.1	10.1	8.1	10.3	5.8	5	11.7	18.8	17.2	15.8	10.8	8.5	13	6	8.5
6	15.4	14.9	16.1	11.4	17.1	22.8	8.6	4	8.6	7.8	5.7	30.3	11.6	20	19.3	11.2	3.9	8.6	10	8.9	25.6
7	12.7	11.2	12.9	4	9.9	29.9	11.6	5.1	5.5	5.7	5.7	13.1	4.1	11.1	24.4	11.2	5.7	5	7.1	10.4	5.8
8	13.6	13	13.8	14.8	22.1	20.7	8.6	6.1	6.9	6.5	13.2	10.4	14.9	22.2	17.8	11.8	6.6	5.9	7.6	9.2	9.8
9	10.9	14.6	14	1.4	13.4	21	10.5	3.1	6.4	6.8	9.5	11.6	1.4	11.6	27.4	7	2.8	4.9	8	22.7	18.9
10	9.7	11.9	11.6	5.2	10	19	12.8	5.7	4.3	4	10	4.3	5.3	8.7	28	9.5	5.9	6	6.4	8.6	9.3
Median	**11.5**	**12.5**	**12.8**	**6.9**	**12.6**	**21.2**	**10.2**	**4.7**	**6.0**	**6.9**	**7.3**	**10.3**	**7.0**	**12.6**	**19.0**	**11.5**	**4.7**	**6.0**	**7.5**	**8.8**	**8.9**
IQR	**10.1 – 13.2**	**11.2 – 13.5**	**11.6 – 13.8**	**4.3 – 10.8**	**10.1 – 16.2**	**19.4 – 22.8**	**8.7 – 11.3**	**3.9 – 5.6**	**4.4 – 7.8**	**5.9 – 7.8**	**5.9 – 9.9**	**4.5 – 12.7**	**3.9 – 11.1**	**11.2 – 18.0**	**17.9 – 23.8**	**11.2 – 14.1**	**3.9 – 5.9**	**4.9 – 7.2**	**7.2 – 8.8**	**7.2 – 10.1**	**6.0 – 9.7**

MEDIAN DIFFERENCE PO vs CO

	0.4	**0.3**	**0.9**	**0.2**	**0.3**	**-0.5**	**-0.7**	**0.1**	**0.1**	**0.8**	**1.1**	**2.3**	**-1.1**	**-0.2**	**3.2**	**0**	**-0.4**	**-0.5**	**1.1**	**-0.3**	**0.3**

QUEST

Table III.12 displays the QUEST results for all patients. QUEST is an established tool for evaluating user satisfaction with assistive technologies, covering essential aspects such as Dimension, Weight, Adjustment, Safety, Usage, Comfort, and Effectiveness. The table compares individual patient responses across all these variables. Additionally, the table provides average scores and standard deviations for each variable under PO and CO conditions.

TABLE III.12 - Assessment of AFO Satisfaction: Comparison of User Experience with QUEST

Subject	Dimensions		Weight		Adjustment		Safety		Usage		Comfort		Effectiveness	
	PO	**CO**	**PO**	**CO**	**PO**	**CO**	**PO**	**CO**	**PO**	**CO**	**PO**	**CO**	**PO**	**CO**
1	3	5	3	5	4	5	4	5	3	5	2	5	4	5
2	3	3	3	3	3	3	3	3	3	3	3	4	3	3
3	3	5	4	5	4	3	5	5	4	5	4	5	5	5
4	4	5	4	4	4	4	5	5	4	4	4	4	4	4
5	4	4	4	4	4	3	4	4	4	3	4	3	3	3
6	4	5	5	5	5	5	5	5	5	5	4	4	3	3
7	Unable to perform QUEST due to Aphasia													
8	2	4	2	4	3	4	3	4	3	4	2	4	2	5
9	5	5	5	5	4	5	5	3	4	5	4	5	4	3
10	5	5	5	5	5	5	5	5	5	5	5	5	5	5
Mean	3.67	4.56	3.89	4.44	4.00	4.11	4.33	4.33	3.89	4.33	3.56	4.33	3.67	4.00
SD	0.89	0.65	0.94	0.65	0.63	0.83	0.77	0.77	0.70	0.77	0.91	0.63	0.89	0.89

Discussion

This study represents a significant step forward for neurorehabilitation, particularly in the development and application of AFOs for stroke survivors. This study, integrating a 3D scanning and AM technologies, aimed to bridge the gap between traditional orthotic craftsmanship and prefabricated orthosis with modern precision-driven fabrication methods. This integration not only promised a higher level of customization but also sought to enhance the functional effectiveness of AFOs. The implementation of a novel photogrammetric 3D scanner for capturing the intricate details of the hemiparetic lower limb was instrumental in achieving a high degree of precision in orthosis design. This precision was critical in addressing the unique anatomical and biomechanical needs of each participant, as reflected in their feedback and the biomechanical data collected. The customization process was further augmented by employing FDM with Nylon 12 material, ensuring uniformity and durability in the final AFO product. According to our previous review (Silva et al., 2022) and Wojciechowski et al. (2019), several studies have built their orthoses using Nylon 12 (Creylman et al., 2013; Deckers et al., 2018; Faustini et al., 2008; Liu et al., 2019; Telfer et al., 2012). However, this study marks the first instance of employing Nylon 12 in conjunction with FDM technology, setting it apart from previous research. For instance, Liu et al. (2019) utilized MJF technology, while other studies

predominantly employed Selective SLS. This distinction is crucial, as the manufacturing process can significantly influence the material properties of the final product. While it is feasible to draw parallels with studies that used the same material, the divergent fabrication techniques employed - FDM in this case versus MJF and SLS in others - can lead to variances in the mechanical and structural characteristics of the Nylon 12. These variations can affect everything from the AFOs flexibility and durability to its comfort and fit. Therefore, while the use of Nylon 12 as a material remains a common thread, the application of different manufacturing technologies introduces a layer of complexity in direct comparisons. This emphasizes the importance of considering both material and fabrication method in assessing the efficacy and functionality of AFOs in clinical settings.

Kinematics Data Analysis

The SPM1D method, a Python/MATLAB package, has been developed for introducing SPM to biomechanics for the analysis of time-varying human movement, particularly in gait analysis (Alhossary et al., 2021). This method is particularly useful in gait analysis as it allows for the detailed examination of entire gait cycles, providing a comprehensive view of kinematic and kinetic patterns.

This study contributes significantly to the field of gait analysis in stroke rehabilitation by focusing on the kinematic differences using SPM. Notably, to date, only two other studies have employed SPM in the analysis of gait in stroke patients. Wang et al. (2022) study aimed to validate a new three-dimensional gait analysis system, concentrating on the ankle, knee, and hip joints in stroke patients but solely in barefoot conditions. Cicarello et al. (2023), meanwhile, was focused on analysing vertical and mediolateral centre of mass displacement in barefoot stroke patients. Both these studies provided valuable insights but did not explore the effects of AFOs on gait dynamics. In contrast, the present study specifically examines the kinematic impacts of PO and CO in stroke patients. The SPM analysis conducted, a pioneering approach in this context, revealed some deviations in parts of the gait cycle when comparing PO and CO. These deviations were observed in areas such as the affected limb hip adduction, unaffected limb knee internal rotation, affected limb knee varus, affected limb knee internal rotation, affected limb ankle dorsiflexion, and unaffected limb foot pitch. These deviations offer new insights into how different AFOs can influence gait kinematics in stroke patients. For instance, variations in hip adduction and knee varus on the affected side may indicate how each AFO type affects lateral stability and limb alignment, which are crucial for effective and safe walking. Additionally, most studies have established that the use of AFOs typically results in an increase in dorsiflexion during the initial stages of the stance phase in stroke patients (Kim & Won, 2019; Mulroy et al., 2010). The findings of this study support these observations, showing improvements in ankle motion from initial contact to the three rockers of the foot, both with PO and CO. Notably, subject 5, who is detailed in the

supplementary material, demonstrated a significant statistical difference between the two types of AFOs on the affected side ($p<0.001$), emphasizing the importance of AFO design and material in influencing gait. What makes the results for patient 5 even more intriguing is that being the patient with the longest time since stroke and having always used the PO orthosis, it is possible that they had developed specific gait mechanisms. Interestingly, upon using the CO orthosis for the first time, significant and promising results were immediately observed. This suggests that switching to the CO orthosis helped to counteract some of the less optimal gait patterns that had developed over time with the consistent use of the PO orthosis. Supporting this, Kobayashi et al. (2018) indicated that different AFO resistances at the ankle joints are particularly notable in the early stance phase. These findings suggest that differences in AFO design and material, which lead to variations in stiffness applied, can restrict the subject's ankle motion in stance, impacting overall gait mechanics. Alterations in these areas can significantly impact the balance and overall gait mechanics, particularly in stroke patients where muscle control and coordination are often compromised. Similarly, differences in ankle dorsiflexion and foot pitch provide a window into how these orthoses modify foot-ground interactions.

It is commonly observed that stroke patients exhibit a peak extension at initial contact and during the loading response, leading to increased gait difficulty due to the interruption of fluidity between sub-phases of gait. Yet, studies including Kobayashi et al. (2018) indicate that AFOs can enhance either the initial or terminal stance phase. Notably, patient 8 (data on supplementary material) showed an improved sagittal knee pattern with the CO AFO, as the joint range of motion remained within the flexion spectrum, effectively eliminating certain extension peaks observed with the PO AFO. This was particularly significant (p=0.016) in the stance phase but was evident throughout the entire gait cycle. Such improvement in knee angle at heel strike and facilitation of limb clearance during the swing phase are crucial for gait fluidity (Esquenazi et al., 2009). Previous studies have suggested that greater plantar flexion resistance can induce increased knee flexion in the early stance phase of gait (Yamamoto et al., 2018), implying that the PO AFO may offer more flexibility than the CO AFO.

While only a few studies have directly investigated the impact of AFOs on hip kinematics, reviews of existing research, such as the one conducted by Tyson et al. (2013), report no significant differences, especially in initial contact and peak hip extension during the stance phase. In contrast, this study observed improvements across all three hip planes on both the affected and unaffected sides in most subjects when using both types of AFOs. Remarkably, subject 5's hip sagittal parameters (data on supplementary material) during the stance phase exhibited statistically significant changes, not only on the affected side but predominantly on the unaffected side with the CO AFO. It is conceivable that the enhancement in knee flexion at clearance facilitated by the CO AFO allowed for a decrease in hip abduction and ultimately reduced the hip flexion normally required to successfully swing between

steps. These observations further demonstrate the intricate interplay between lower limb joint kinematics in stroke patients and the influence of AFO design. The kinematic changes observed with different AFO types highlight the need for personalized orthotic solutions in stroke rehabilitation to address individual biomechanical deviations and enhance overall gait quality.

Kinetics Data Analysis

In addition to the kinematic analysis, this study also delved into the kinetic aspects of gait in stroke patients using PO and CO. Notably, the use of Statistical SPM for kinetic data analysis is a pioneering approach in this area, as to date, no studies have employed SPM for kinetic gait analysis in stroke patients. One significant deviation was observed in the affected limb internal hip extensor moment between 27 and 36% of the gait cycle. This deviation suggests a variation in the hip's capacity to generate or control force during the mid-stance phase of walking. In stroke patients, the hip moment plays a critical role in maintaining balance and stability (Kobayashi et al., 2018). Therefore, the observed variation indicates that the type of AFO, can substantially influence the hip's biomechanical function, affecting the patient's stability and propulsion during the gait cycle. Further analysis revealed deviations in the unaffected limb internal ankle plantarflexor moment between 80 and 87% of the gait cycle. The variance in ankle moment on the unaffected side could be indicative of how each AFO type influences these compensatory strategies, impacting the overall balance and load distribution during walking. Additionally, a deviation was noted in the unaffected limb internal ankle extensor moment during the toe-off phase, between 80 and 87% of the gait cycle. A potential explanation for this difference lies in the normalization of gait with the use of CO AFO in the affected limb. The more normalized gait pattern with CO AFO leads to an earlier toe-off, around 75% of the gait cycle, compared to the toe-off occurring around 85% with PO. This suggests that CO AFO may contribute to a more efficient and natural gait pattern in the affected limb, which in turn influences the kinetic behaviour of the unaffected limb during the toe-off phase.

Interestingly, only four studies have conducted kinetic analyses using AM-produced AFOs, none of which involved stroke patients (Harper et al., 2014; Ranz et al., 2016; Telfer et al., 2012; Vasiliauskaite et al., 2019). Vasiliauskaite et al. (2019) study, which explored the efficacy of AFO stiffness prescriptions in various patients, compared Nylon 12 AFOs produced via SLS with conventional polypropylene AFOs. They found Peak AFO plantarflexion moments of 0.497 (0.171) and 0.587 (0.281) N.m/Kg for conventional polypropylene and SLS AFOs, respectively, higher than those observed in this study for PO AFO-0.303 (0.215) and CO AFO-0.392 (0.189). While Vasiliauskaite's study reported an 18% increase in moment between the two AFO types, this study observed a 29% increase. This difference may be attributed to the unique biomechanical and anatomical characteristics of stroke patients. Stroke-

induced muscular and neural impairments can profoundly influence how the body interacts with orthotic devices, potentially leading to more significant changes in kinetic parameters when different AFO types are used. Harper et al. (2014) study involved thirteen active military personnel with unilateral lower extremity injuries, comparing various SLS-produced AFOs with Nylon 11 and different strut stiffnesses. Though a direct comparison is challenging due to different patient demographics and AFO materials, understanding how AFO stiffness influences joint moments in the hip, knee, and ankle, as investigated by Telfer et al. (2012), is valuable. These studies observed that variations in AFO stiffness can significantly impact the ankle's range of motion and the body's support mechanics, highlighting the complex interplay between AFO design and gait biomechanics. Furthermore, Ranz et al. (2016) delved into the influence of passive-dynamic ankle-foot orthosis bending axis location on gait performance in individuals with lower-limb impairments. Similar to Harper et al. (2014) and Telfer et al. (2012), the values found in Ranz's study were higher than those in this research. Although a direct comparison is not feasible, the insights provided by Ranz study are crucial. They observed that the bending axis condition influenced various aspects of gait in the first half of the stance, with participant preferences for bending axis conditions correlating strongly with peak joint moments and kinematics. This diversity in preferences, influenced by individual aetiologies, underscores the need for personalized AFO prescriptions, a principle that is also central to this study.

Spatiotemporal Data Analysis

Gait parameters such as walking speed, stride width, stride length, cycle time, step length, and double limb support offer a quantitative measure of gait efficiency and fluidity. This study utilized these parameters to compare the effectiveness of custom and off-the-shelf AFOs in enhancing gait dynamics. Reductions in gait speed are a prevalent characteristic among stroke survivors experiencing hemiparesis. According to Verma et al. (2012), average gait speeds in this population may vary from a slow 0.23 m/s to a relatively faster 0.73 m/s, reflecting a wide range of mobility impairments. Furthermore, Perry et al. (1995) have demonstrated that gait speed is a critical marker in differentiating stroke patients based on the severity of their comorbid conditions. Specifically, those experiencing greater ambulatory challenges exhibited gait velocities between a markedly reduced 0.1 m/s and 0.23 m/s. This aligns with the findings of the current study, which focused on a sample primarily comprising hospital inpatients, none of whom could ambulate without the assistance of a walking aid or an AFO. Consequently, the observed gait speeds in these patients were generally lower compared to those reported in other studies (Abe et al., 2009; R.-Y. Wang et al., 2005). In the present research, a statistically significant difference ($p=0.0485$) was observed in gait speeds between different types of AFOs, with an average speed of 0.18 m/s recorded for patients using PO AFOs and 0.21 m/s for those using CO AFOs. This finding is particularly noteworthy in the context of existing literature, which offers

mixed results. For instance, Chen et al. (2010) did not report significant differences in gait speeds when comparing similar types of AFOs, while Gök et al. (2003) observed a notable variation, with plastic AFOs yielding a gait speed of 0.37 m/s ($p<0.05$) and metal AFOs resulting in a speed of 0.41 m/s ($p<0.05$). It is evident that the design elements of AFOs, such as material composition, shaft construction, movement restriction at the ankle, and footplate length, can profoundly influence gait biomechanics (S. Tyson & Kent, 2013). In this study, the primary design and material of the PO AFOs differed significantly from the CO AFOs used. Although patients were accustomed to using their personal AFOs (PO) in daily activities, it is plausible that the mechanical properties of the CO AFO may have provided enhanced stability during the gait cycle, thereby contributing to the observed improvement in the walking speed. While other spatiotemporal parameters such as stride length and double limb support time also showed trends towards improvement with the AM custom AFOs, these changes did not reach statistical significance in this study as observed in other studies (Creylman et al., 2013; Daryabor, Arazpour, et al., 2020; Mavroidis et al., 2011; Momosaki et al., 2015; Telfer et al., 2012; S. Tyson & Kent, 2013).

The assessment of symmetry and asymmetry in gait is crucial for understanding the effectiveness of orthotic interventions in stroke rehabilitation. In this study, symmetry tests, along with intra- and inter-subject symmetry indices, provided valuable insights into the bilateral balance achieved by patients. The analysis revealed notable improvements in symmetry when participants used the CO AFO. A more individualized analysis of each patient (detailed in the supplementary material) reveals nuanced trends in response to the use of CO AFOs. In this individualized analysis, a trend towards increased walking speed was observed in 5 out of 10 patients when using the CO AFO, with only 2 experiencing a reduction. Regarding Stride Width, there was a tendency for a reduction in 5 of the 10 patients, with only 2 showing an increase. For Stride Length, an increase in step size was found in 5 patients, while a decrease was observed in 3 patients. Double Limb Support times showed mixed results, with an increase and decrease in 3 patients each, and no change in 4 patients. Cycle Time increased in 5 patients and decreased in 2 patients. These varied responses underscore the heterogeneity inherent in stroke patients (Alexander et al., 2009). The variability in gait adaptations among individuals can be attributed to several factors, including the extent and location of the brain injury, the duration since stroke onset, pre-existing motor skills, the severity of motor impairments and the degree of access to rehabilitation treatments (Alexander et al., 2009; Cruz et al., 2009). Stroke impacts motor control and gait in diverse ways, leading to a wide range of compensatory mechanisms and recovery trajectories (D. G. Lee & Lee, 2022; Nam et al., 2022). This heterogeneity highlights the complexity of stroke rehabilitation and the need for personalized treatment plans.

Concerning step length symmetry mean of all patients, both PO and CO AFOs demonstrated similar patterns with an increased step length for the affected limb. A significant improvement was observed in the swing time symmetry when patients used the CO AFO, making the swing phase much more symmetrical, with negligible statistical differences between the affected and unaffected limbs ($p=0.1651$). This indicates that the use of CO AFO may contribute to a more balanced and coordinated gait, reducing the discrepancies in limb movement timing often seen in stroke patients. In terms of stance time symmetry, no significant differences were found between the PO and CO AFOs. Yet, with the CO AFO, the stance time achieved perfect symmetry, with a mean value of 50.00 ± 4.97. In contrast, Cha et al.(Cha et al., 2017) conducted tests on stance time symmetry and found differences between 3D Printed AFO vs Conventional AFO, with favourable results for the 3D AFO, but they did not present the symmetry values between AFOs. Creylman et al. (2013), found identical values for polypropylene AFO and SLS-AFO yet, there is an associated asymmetry for both of 62.1%. Normally, stroke patients tend to spend more time in contact with the ground with the unaffected limb indicating extended weight transfer to the unaffected side to compensate for the weakness of the affected side (Creylman et al., 2013). Nevertheless, in this study, the use of both PO AFO and CO AFO demonstrated very good symmetry values, contributing significantly to a more physiological gait pattern in this group of patients.

Gait Profile Score Analysis

The GPS offers a comprehensive assessment of gait quality, encapsulating various aspects of movement into a single measure. In mathematical terms, the GPS represents the root mean square difference between the individual joint's curve and the mean curve calculated for a reference population of unaffected individuals (Bigoni et al., 2021). Originally developed to assess the gait of children with cerebral palsy (R. Baker et al., 2009, 2012; Beynon et al., 2010; Ricardo et al., 2022), its application has significantly broadened in recent years. Contemporary studies have extended the use of GPS to evaluate populations with diverse conditions, notably including those with lower limb amputations (Kark et al., 2012), Parkinson's disease (Speciali et al., 2014), and multiple sclerosis (Pau et al., 2014). This expansion reflects the GPS's versatility and adaptability in various clinical scenarios. Moreover, some investigations have employed the GPS to assess mixed samples, encompassing adults with a range of orthopaedic and neurological disorders (Schweizer et al., 2014) and children diagnosed with multiple clinical conditions (McMulkin & MacWilliams, 2015). This approach highlights the tool's capability to provide valuable insights across a spectrum of gait abnormalities. Despite its expanding application, the use of GPS in assessing patients with stroke remains relatively unexplored. To date, and to the best of our knowledge, only four studies have focused on the application of GPS in stroke patients (Bigoni et al., 2021; Devetak et al., 2016; Fukuchi & Duarte, 2019; Jarvis et al., 2022). These

studies represent a crucial step in understanding the gait characteristics and alterations in this patient population. However, all these four studies have evaluated this metric with the stroke patient walking in barefoot. Given the critical role that AFOs play in supporting gait rehabilitation in stroke patients, this lack of research represents a notable oversight. This study addresses this gap by being the first to conduct a comprehensive GPS analysis of stroke patients using AFOs. We extend the scope of existing research by not only analysing the gait of stroke patients with the aid of AFOs but also by comparing the GPS outcomes when using a prefabricated AFO versus a custom-made AFO fabricated through AM. By comparing the GPS values for both the affected and unaffected limbs in participants wearing the PO and CO, it's possible to discern the specific impact of the personalized design on gait normalization. These results indicated an improvement in the gait quality (GPS Overall: PO-13.7 vs CO-12.8) when patients used the CO AFOs compared to the PO AFO models. This was particularly evident in the reduced deviation from the normative gait patterns, as the GPS values approached those of healthy adult gait standards. Such improvements are indicative of a more balanced and physiologically accurate walking pattern, which is crucial for reducing the risk of falls and enhancing mobility in stroke survivors. The closer alignment of GPS values with normative data in the CO condition highlights the effectiveness of the personalized design in addressing gait abnormalities associated with post-stroke hemiparesis. When comparing the PO and CO results, both AFOs obtained lower values for affected limb than Devetak et al. (2016) (13.9) but higher than Fukuchi & Duarte (2019) (8.0), Bigoni et al. (2021) (10.07) and Jarvis et al. (2022) (9.4). This could be explained by the temporal differences between the date of analysis and date of stroke and level of neurological impairments only defined by CT scan or MRI (Jarvis et al., 2022). In the reviewed studies, all except Devetak et al. (2016) research exhibit differences exceeding one year in terms of time since stroke. As time progresses, patients tend to stabilize their gait through rehabilitation, often resulting in a more homogeneous and normalized walking pattern. The same (Devetak et al., 2016) study, with a time difference of 6.0 months, aligns more closely with the patient demographics of this study. Consequently, it can be inferred that the use of AFOs generally contributes to the improvement of the patient's gait. This is particularly evident with AFOs fabricated using AM, which appear to offer enhanced benefits in gait rehabilitation.

QUEST Analysis

In this study, the QUEST effectively delineated patient satisfaction regarding the custom and standard AFOs, particularly emphasizing comfort, fit, and efficacy. Notably, the weight of the orthoses emerged as the second-highest rated aspect in our study, surpassed only by dimensions. This significant score in the weight category is largely attributable to the strategic selection of Nylon 12 as the material for 3D printing, which, with its mere 3mm thickness, contributed substantially to the orthoses' lightweight attribute while maintaining essential durability. Moreover, the high scores in dimensions and comfort

can be directly linked to the bespoke nature of the custom orthoses. The utilization of advanced 3D scanning technology ensured an impeccable contouring to the patients' limbs and foot sole, thereby eliminating unnecessary pressure points and achieving optimal fit. This precision in customization not only elevates user comfort but also enhances the functional efficacy of the orthoses in facilitating mobility and ensuring gait stability. Comparative studies, such as those by Cha et al. (2017) and Chae et al. (2020), have similarly reported a preference for 3D-printed AFOs in terms of comfort and fit. Conversely, the study by Fu et al. (2022), comparing standard hinged AFOs with those produced via AM, underscores the necessity for improvements in certain areas, particularly the orthoses' weight. The lower score observed for weight in Fu et al. (2022) study highlights the ongoing imperative to refine material selection and design in the AM of AFOs. Collectively, these findings underscore the critical role of patient-centred design in orthotic development, where customization and material choice are key to improving user experience. The integration of tools like the QUEST into clinical practice offers invaluable insights for healthcare professionals, allowing for a deeper understanding of patient needs and preferences. This understanding is crucial in guiding the selection and design of more effective and comfortable orthotic solutions in rehabilitation contexts.

Cost of Fabrication

While the results are promising, they also underscore the challenges associated with integrating new technologies into clinical practice. The initial costs of equipment and training, along with the need to adapt clinical workflows to accommodate these technologies, are significant considerations. However, the long-term benefits – improved patient outcomes, reduced material waste, and faster production times – suggest a favourable return on investment. In the context of AFOs, the financial implications are particularly noteworthy. Traditional custom AFOs, tailored to each patient's specific needs through a manual process, are notably expensive (Silva et al., 2022). These custom devices, designed for a precise fit and maximum efficacy, reflect the extensive assessment, moulding, and adjustments performed by prosthetic-orthotic professionals. On the other hand, prefabricated AFOs present a more economical option (Choo & Lee, 2021). These mass-produced units, available in standard sizes, are significantly more affordable than custom AFOs, catering to less complex conditions or serving as temporary solutions. Nevertheless, they offer less customization. For instance, in creating CO AFO using with Nylon 12, the average material cost was determined to be 2.87 euros. This value, however, does not account for other expenses such as the cost of the printer, design software, operator training, and time. Despite these additional costs, the use of AM in AFO production has the potential to drastically reduce material waste and expedite the manufacturing process (Kumar & Banwait, 2020), thereby offering a more sustainable and efficient approach in the long run.

Adopting these new technologies in clinical settings, therefore, represents a balance between initial investment and long-term gains. While the upfront costs for equipment and training are significant, the advantages – particularly in terms of personalized patient care and resource efficiency – indicate a promising future for AM in orthopaedic applications. As the technology matures and becomes more integrated into clinical practice, it is expected that the costs will become more manageable, further enhancing its viability as a tool for orthotic fabrication.

Conclusion

This research marks a transformative stride in the field of stroke rehabilitation, showcasing the extraordinary potential of integrating advanced 3D scanning and additive manufacturing technologies in the creation of Ankle-Foot Orthoses. The application of a novel photogrammetric 3D scanner in the fabrication of custom orthoses with AM not only embodies the cutting edge of technological advancement but also represents a significant leap in personalized patient care. By meticulously comparing these AM custom orthoses with standard prefabricated orthoses, this study offers an unparalleled insight into the biomechanical and qualitative differences, illuminating the profound impact of tailored orthotic solutions on stroke survivors' gait dynamics and overall quality of life. We acknowledge that while the insights derived from this study are meaningful, they are drawn from a relatively small sample size. A larger cohort would undoubtedly enhance the robustness of the findings and their applicability to a broader stroke survivor population. Furthermore, it is important to clarify that the absence of a functional evaluation with patients walking barefoot was not an oversight but a necessary adaptation to the inherent limitations faced by this study population. Stroke patients often cannot walk without the support of an AFO, making such assessments unfeasible.

Despite these limitations, this study provides a pivotal foundation for future research, encouraging further exploration into the benefits of custom AFOs fabricated using cutting-edge technologies.

Acknowledgements

The authors would like to acknowledge the support of the Portuguese Foundation for Science and Technology (FCT) through the following projects: SFRH/BD/145292/2019, UIDB/04044/2020, UIDP/04044/2020, PAMI ROTEIRO /0328/2013 (CENTRO2020: N 22158), and the support of the National Innovation Agency (ANI) through the project ReinventO (POCI-01-0247-FEDER-040021) and Project: INOV.AM—Innovation in Additive Manufacturing (02-C05-i01.01-2022.PC644865234-00000004), funded by European Union—Next Generation EU, PRR—Plano de Recuperação e Resiliência.

Conflicts of Interest

The authors declare that they have no conflict of interest.

References

Abe, H., Michimata, A., Sugawara, K., Sugaya, N., & Izumi, S.-I. (2009). Improving gait stability in stroke hemiplegic patients with a plastic ankle-foot orthosis. *The Tohoku Journal of Experimental Medicine*, *218*(3), 193–199.

Alexander, L. D., Black, S. E., Patterson, K. K., Gao, F., Danells, C., & McIlroy, W. E. (2009). Association Between Gait Asymmetry and Brain Lesion Location in Stroke Patients. *Stroke*. https://doi.org/10.1161/strokeaha.108.527374

Alhossary, A. A., Pataky, T., ANG, W. T., CHUA, K. S. G., & Donnelly, C. J. (2021). *MovementRx: Versatile clinical movement analysis using Statistical Parametric Mapping*.

Ambu, R., Oliveri, S. M., & Calì, M. (2023). Neck orthosis design for 3D printing with user enhanced comfort features. *International Journal on Interactive Design and Manufacturing*. https://doi.org/10.1007/s12008-023-01507-1

Baker, R. J., Leboeuf, F. Y., Reay, J., & Sangeux, M. (2018). *The conventional gait model-success and limitations*. Springer.

Baker, R., McGinley, J. L., Schwartz, M. H., Beynon, S., Rozumalski, A., Graham, H. K., & Tirosh, O. (2009). The gait profile score and movement analysis profile. *Gait & Posture*, *30*(3), 265–269.

Baker, R., McGinley, J. L., Schwartz, M., Thomason, P., Rodda, J., & Graham, H. K. (2012). The minimal clinically important difference for the Gait Profile Score. *Gait & Posture*, *35*(4), 612–615.

Baronio, G., Harran, S., & Signoroni, A. (2016). A Critical Analysis of a Hand Orthosis Reverse Engineering and 3D Printing Process. *Applied Bionics and Biomechanics*, *2016*. https://doi.org/10.1155/2016/8347478

Barrios-Muriel, J., Romero-Sánchez, F., Alonso-Sánchez, F. J., & Salgado, D. R. (2020). Advances in orthotic and prosthetic manufacturing: A technology review. *Materials*, *13*(2). https://doi.org/10.3390/ma13020295

Belokar, R. M., Banga, H. K., & Kumar, R. (2017). A Novel Approach for Ankle Foot Orthosis Developed by Three Dimensional Technologies. *IOP Conference Series: Materials Science and Engineering*, *280*(1), 2–7. https://doi.org/10.1088/1757-899X/280/1/012030

Beynon, S., McGinley, J. L., Dobson, F., & Baker, R. (2010). Correlations of the gait profile score and the movement analysis profile relative to clinical judgments. *Gait & Posture*, *32*(1), 129–132.

Bigoni, M., Cimolin, V., Vismara, L., Tarantino, A. G., Clerici, D., Baudo, S., Galli, M., & Mauro, A. (2021). Relationship between gait profile score and clinical assessments of gait in post-stroke patients. *Journal of Rehabilitation Medicine*, *53*(5). https://doi.org/10.2340/16501977-2809

Böhm, H., & Dussa, C. U. (2021). Prefabricated ankle-foot orthoses for children with cerebral palsy to overcome spastic drop-foot: does orthotic ankle stiffness matter? *Prosthetics and Orthotics International*, *45*(6), 491–499.

Boparai, K. S., Singh, R., & Singh, H. (2016). Development of Rapid Tooling Using Fused Deposition Modeling: A Review. *Rapid Prototyping Journal*. https://doi.org/10.1108/rpj-04-2014-0048

Cappozzo, A., Catani, F., Della Croce, U., & Leardini, A. (1995). Position and orientation in space of bones during movement: anatomical frame definition and determination. *Clinical Biomechanics*, *10*(4), 171–178.

Cha, Y. H., Lee, K. H., Ryu, H. J., Joo, I. W., Seo, A., Kim, D. H., & Kim, S. J. (2017). Ankle-foot orthosis made by 3D printing technique and automated design software. *Applied Bionics and Biomechanics*, *2017*. https://doi.org/10.1155/2017/9610468

Chae, D.-S., Kim, D.-H., Kang, K.-Y., Kim, D.-Y., Park, S.-W., Park, S.-J., & Kim, J.-H. (2020). The functional effect of 3D-printing individualized orthosis for patients with peripheral nerve injuries: Three case reports. *Medicine*, *99*(16), e19791.

Chan, A.-W., Tetzlaff, J. M., Altman, D. G., Laupacis, A., Gøtzsche, P. C., Krleža-Jeric, K., Hró bjartsson, A., Mann, H., Dickersin, K., Berlin, J. A., Doré, C. J., Parulekar, W. R., Summerskill, W. S., Groves, T., Schulz, K. F., Sox, H. C., Rockhold, F. W., Rennie, D., & Moher, D. (2013). SPIRIT 2013 Statement: Defining Standard Protocol Items for Clinical Trials DEVELOPMENT OF THE SPIRIT 2013 STATEMENT. In *Ann Intern Med* (Vol. 158). www.annals.org

Chen, C.-C., Hong, W.-H., Wang, C.-M., Chen, C.-K., Wu, K. P.-H., Kang, C.-F., & Tang, S. F. (2010). Kinematic features of rear-foot motion using anterior and posterior ankle-foot orthoses in stroke patients with hemiplegic gait. *Archives of Physical Medicine and Rehabilitation*, *91*(12), 1862–1868.

Chen, R. K., Chen, L., Tai, B. L., Wang, Y., Shih, A. J., & Wensman, J. (2014). Additive manufacturing of personalized ankle-foot orthosis. *Transactions of the North American Manufacturing Research Institution of SME*, *42*(January), 381–389.

Chen, R. K., Jin, Y. an, Wensman, J., & Shih, A. (2016). Additive manufacturing of custom orthoses and prostheses-A review. *Additive Manufacturing*, *12*, 77–89. https://doi.org/10.1016/j.addma.2016.04.002

Choi, H., Peters, K. M., MacConnell, M. B., Ly, K. K., Eckert, E. S., & Steele, K. M. (2017). Impact of ankle foot orthosis stiffness on Achilles tendon and gastrocnemius function during unimpaired gait. *Journal of Biomechanics*, *64*, 145–152. https://doi.org/10.1016/j.jbiomech.2017.09.015

Choo, Y. J., & Lee, H. J. (2021). Commonly Used Types and Recent Development of Ankle-Foot Orthosis: A Narrative Review. *Healthcare*. https://doi.org/10.3390/healthcare9081046

Cicarello, N. D. S., Bohrer, R. C. D., Devetak, G. F., Rodacki, A. L. F., Loureiro, A. P. C., & Manffra, E. F. (2023). Control of center of mass during gait of stroke patients: Statistical parametric mapping analysis. *Clinical Biomechanics*, *107*. https://doi.org/10.1016/j.clinbiomech.2023.106005

Ciobanu, O., Ciobanu, G., & Rotariu, M. (2013). Photogrammetric Scanning Technique and Rapid Prototyping Used for Prostheses and Ortheses Fabrication. *Applied Mechanics and Materials*, *371*, 230–234. https://doi.org/10.4028/www.scientific.net/AMM.371.230

Creylman, V., Muraru, L., Pallari, J., Vertommen, H., & Peeraer, L. (2013). Gait assessment during the initial fitting of customized selective laser sintering ankle foot orthoses in subjects with drop foot. *Prosthetics and Orthotics International*, *37*(2), 132–138. https://doi.org/10.1177/0309364612451269

Cruz, T. H., Lewek, M. D., & Dhaher, Y. Y. (2009). Biomechanical Impairments and Gait Adaptations Post-Stroke: Multi-Factorial Associations. *Journal of Biomechanics*. https://doi.org/10.1016/j.jbiomech.2009.04.015

Dal Maso, A., & Cosmi, F. (2019). 3D-printed ankle-foot orthosis: A design method. *Materials Today: Proceedings*, *12*, 252–261. https://doi.org/10.1016/j.matpr.2019.03.122

Daryabor, A., Arazpour, M., Aminian, G., Baniasad, M., & Yamamoto, S. (2020). Design and Evaluation of an Articulated Ankle Foot Orthosis With Plantarflexion Resistance on the Gait: A Case Series of 2 Patients With Hemiplegia. *Journal of Biomedical Physics and Engineering*. https://doi.org/10.31661/jbpe.v0i0.1159

Daryabor, A., Yamamoto, S., Motojima, N., & Tanaka, S. (2022). Therapeutic Effect of Gait Training With Two Types of Ankle-Foot Orthoses on the Gait of the Stroke Patients in the Recovery Phase. *Turkish Journal of Physical Medicine and Rehabilitation*. https://doi.org/10.5606/tftrd.2022.7866

Daryabor, A., Yamamoto, S., Orendurff, M. S., & Kobayashi, T. (2020). Effect of Types of Ankle-Foot Orthoses on Energy Expenditure Metrics During Walking in Individuals With Stroke: A Systematic Review. *Disability and Rehabilitation*. https://doi.org/10.1080/09638288.2020.1762767

Deckers, J. P., Vermandel, M., Geldhof, J., Vasiliauskaite, E., Forward, M., & Plasschaert, F. (2018). Development and clinical evaluation of laser-sintered ankle foot orthoses. *Plastics, Rubber and Composites*, *47*(1), 42–46. https://doi.org/10.1080/14658011.2017.1413760

Demers, L., Weiss-Lambrou, R., Demers, L., & Ska, B. (1996). Development of the Quebec User Evaluation of Satisfaction with assistive Technology (QUEST). *Assistive Technology*, *8*(1), 3–13. https://doi.org/10.1080/10400435.1996.10132268

Devetak, G. F., Martello, S. K., de Almeida, J. C., Correa, K. P., Iucksch, D. D., & Manffra, E. F. (2016). Reliability and minimum detectable change of the gait profile score for post-stroke patients. *Gait and Posture*, *49*, 382–387. https://doi.org/10.1016/j.gaitpost.2016.07.149

Doğan, A., Mengüllüoğlu, M., & Özgirgin, N. (2011). Evaluation of the Effect of Ankle-Foot Orthosis Use on Balance and Mobility in Hemiparetic Stroke Patients. *Disability and Rehabilitation*. https://doi.org/10.3109/09638288.2010.533243

Eder, M., Brockmann, G., Zimmermann, A., Papadopoulos, M. A., Schwenzer-Zimmerer, K., Zeilhofer, H. F., Sader, R., Papadopulos, N. A., & Kovacs, L. (2013). Evaluation of precision and accuracy assessment of different 3-D surface imaging systems for biomedical purposes. *Journal of Digital Imaging*, *26*(2), 163–172.

Esquenazi, A., Ofluoglu, D., Hirai, B., & Kim, S. (2009). The effect of an ankle-foot orthosis on temporal spatial parameters and asymmetry of gait in hemiparetic patients. *PM&R*, *1*(11), 1014–1018.

Faustini, M. C., Neptune, R. R., Crawford, R. H., & Stanhope, S. J. (2008). Manufacture of passive dynamic ankle-foot orthoses using selective laser sintering. *IEEE Transactions on Biomedical Engineering*, *55*(2), 784–790. https://doi.org/10.1109/TBME.2007.912638

Fu, J. C. M., Chen, Y. J., Li, C. F., Hsiao, Y. H., & Chen, C. H. (2022). The effect of three dimensional printing hinged ankle foot orthosis for equinovarus control in stroke patients. *Clinical Biomechanics*, *94*. https://doi.org/10.1016/j.clinbiomech.2022.105622

Fukuchi, C. A., & Duarte, M. (2019). Gait Profile Score in able-bodied and post-stroke individuals adjusted for the effect of gait speed. *Gait and Posture*, *69*, 40–45. https://doi.org/10.1016/j.gaitpost.2019.01.018

Gök, H., Küçükdeveci, A., Altinkaynak, H., Yavuzer, G., & Ergin, S. (2003). Effects of ankle-foot orthoses on hemiparetic gait. *Clinical Rehabilitation*, *17*(2), 137–139.

Grazioso, S., Selvaggio, M., & Di Gironimo, G. (2018). Design and development of a novel body scanning system for healthcare applications. *International Journal on Interactive Design and Manufacturing*, *12*(2), 611–620. https://doi.org/10.1007/s12008-017-0425-9

Habiba, R., Amaro, A., Moura, C., Silva, R., Trindade, D., Antão, A., Martins, R., Malça, C., & Branco, R. (2023). Impact Resistance of Additively Manufactured Polymeric Materials for Biomedical Applications. In A. Martins Amaro, L. Roseiro, A. L. Messias, B. Gomes, H. Almeida, M. António Castro, M. A. Neto, M. de Fátima Paulino, & V. Maranha (Eds.), *Proceedings of the 10th Congress of the Portuguese Society of Biomechanics* (pp. 333–341). Springer Nature Switzerland.

Harper, N. G., Esposito, E. R., Wilken, J. M., & Neptune, R. R. (2014). The influence of ankle-foot orthosis stiffness on walking performance in individuals with lower-limb impairments. *Clinical Biomechanics*, *29*(8), 877–884. https://doi.org/10.1016/j.clinbiomech.2014.07.005

Jarvis, H. L., Brown, S. J., Butterworth, C., Jackson, K., Clayton, A., Walker, L., Rees, N., Price, M., Groenevelt, R., & Reeves, N. D. (2022). The gait profile score characterises walking performance impairments in young stroke survivors. *Gait and Posture*, *91*, 229–234. https://doi.org/10.1016/j.gaitpost.2021.10.037

Kark, L., Vickers, D., McIntosh, A., & Simmons, A. (2012). Use of gait summary measures with lower limb amputees. *Gait & Posture*, *35*(2), 238–243.

Kim, J. H., & Won, B. H. (2019). Kinematic on Ankle and Knee Joint of Post-Stroke Elderly Patients by Wearing Newly Elastic Band-Type Ankle–Foot Orthosis in Gait. *Clinical Interventions in Aging*, 2097–2104.

Kobayashi, T., Orendurff, M. S., Hunt, G., Gao, F., LeCursi, N., Lincoln, L. S., & Foreman, K. B. (2018). The effects of an articulated ankle-foot orthosis with resistance-adjustable joints on lower limb joint kinematics and kinetics during gait in individuals post-stroke. *Clinical Biomechanics*, *59*, 47–55.

Kobayashi, T., Orendurff, M. S., Hunt, G., Lincoln, L., Gao, F., LeCursi, N., & Foreman, K. B. (2017). An Articulated Ankle–foot Orthosis With Adjustable Plantarflexion Resistance, Dorsiflexion Resistance and Alignment: A Pilot Study on Mechanical Properties and Effects on Stroke Hemiparetic Gait. *Medical Engineering & Physics*. https://doi.org/10.1016/j.medengphy.2017.02.012

Krajňáková, V., Rajťúková, V., Hudák, R., & Živčák, J. (2020). APPLICATION OF THE ARTEC EVA SCANNER FOR ORTHOTICS IN PRACTICE. *Lékař a Technika - Clinician and Technology*, *49*(3), 92–96. https://doi.org/10.14311/CTJ.2019.3.04

Kumar, M. S. K., & Banwait, S. S. (2020). Reducing Cost of Walking W Ith Fused Deposition Modelling Rendering Point Cloud Data. *International Journal of Innovative Technology and Exploring Engineering*. https://doi.org/10.35940/ijitee.e2739.039520

Lee, D. G., & Lee, G. (2022). Correlation Among Motor Function and Gait Velocity, and Explanatory Variable of Gait Velocity in Chronic Stroke Survivors. *Physical Therapy Rehabilitation Science*. https://doi.org/10.14474/ptrs.2022.11.2.181

Lee, S.-H., Choi, C.-M., Lee, D., Lee, S.-H., Song, S., Pyo, S., Hong, S., & Lee, G. (2018). A Novel Hinged Ankle Foot Orthosis for Gait Performance in Chronic Hemiplegic Stroke Survivors: A Feasibility Study. *Biomedical Engineering Letters*. https://doi.org/10.1007/s13534-018-0074-3

Lin, Y.-C., Lin, K.-W., & Chen, C.-S. (2017). Evaluation of the walking performance between 3D-printed and traditional fabricated ankle-foot orthoses— A prospective study. *Gait & Posture*, *57*, 366–367. https://doi.org/10.1016/j.gaitpost.2017.06.471

Liu, Z., Zhang, P., Yan, M., Xie, Y., & Huang, G. (2019). Additive manufacturing of specific ankle-foot orthoses for persons after stroke: A preliminary study based on gait analysis data. *Mathematical Biosciences and Engineering*, *16*(6), 8134–8143. https://doi.org/10.3934/mbe.2019410

Maeda, N., Kato, J., Azuma, Y., Okuyama, S., Yonei, S., Murakami, M., & Shimada, T. (2009). Energy Expenditure and Walking Ability in Stroke Patients: Their Improvement by Ankle-Foot Orthoses. *Isokinetics and Exercise Science*. https://doi.org/10.3233/ies-2009-0333

Mavroidis, C., Ranky, R. G., Sivak, M. L., Patritti, B. L., DiPisa, J., Caddle, A., Gilhooly, K., Govoni, L., Sivak, S., Lancia, M., Drillio, R., & Bonato, P. (2011). Patient specific ankle-foot orthoses using rapid prototyping. *Journal of NeuroEngineering and Rehabilitation*, *8*(1), 1–11. https://doi.org/10.1186/1743-0003-8-1

McMulkin, M. L., & MacWilliams, B. A. (2015). Application of the gillette gait index, gait deviation index and gait profile score to multiple clinical pediatric populations. *Gait & Posture*, *41*(2), 608–612.

Mohanty, R. K., Behera, P., Sahoo, P. K., & Das, S. (2020). Clinical Efficacy of Different Ankle Foot Orthosis Design in Subjects With Foot Drop After Stroke: A Review and Comparison. *Engineering and Scientific International Journal*. https://doi.org/10.30726/esij/v7.i3.2020.73012

Momosaki, R., Abo, M., Watanabe, S., Kakuda, W., Yamada, N., & Kinoshita, S. (2015). Effects of Ankle–Foot Orthoses on Functional Recovery After Stroke: A Propensity Score Analysis Based on Japan Rehabilitation Database. *Plos One*. https://doi.org/10.1371/journal.pone.0122688

Morrissey, D., Cotchett, M., J'Bari, A. S., Prior, T. D., Vicenzino, B., Griffiths, I. B., Rathleff, M. S., Gülle, H., & Barton, C. J. (2020). *Management of Plantar Heel Pain: A Best Practice Guide Synthesising Systematic Review With Expert Clinical Reasoning and Patient Values*. https://doi.org/10.21203/rs.3.rs-36329/v1

Mulroy, S. J., Eberly, V. J., Gronely, J. K., Weiss, W., & Newsam, C. J. (2010). Effect of AFO design on walking after stroke: impact of ankle plantar flexion contracture. *Prosthetics and Orthotics International*, *34*(3), 277–292.

Nam, Y. G., Ko, M. J., Bok, S.-K., Paik, N.-J., Lim, C.-Y., Lee, J., & Kwon, B. S. (2022). Efficacy of Electromechanical-Assisted Gait Training on Clinical Walking Function and Gait Symmetry After Brain Injury of Stroke: A Randomized Controlled Trial. *Scientific Reports*. https://doi.org/10.1038/s41598-022-10889-3

Ounpuu, S., Bell, K. J., Davis III, R. B., & DeLuca, P. A. (1996). An evaluation of the posterior leaf spring orthosis using joint kinematics and kinetics. *Journal of Pediatric Orthopaedics*, *16*(3), 378–384.

Parry, E. J., Best, J. M., & Banks, C. E. (2020). Three-dimensional (3D) scanning and additive manufacturing (AM) allows the fabrication of customised crutch grips. *Materials Today Communications*, *25*(April), 101225. https://doi.org/10.1016/j.mtcomm.2020.101225

Pau, M., Coghe, G., Atzeni, C., Corona, F., Pilloni, G., Marrosu, M. G., Cocco, E., & Galli, M. (2014). Novel characterization of gait impairments in people with multiple sclerosis by means of the gait profile score. *Journal of the Neurological Sciences*, *345*(1–2), 159–163.

Pérez Pico, A. M., Marcos Tejedor, F., de Cáceres Orellana, L. C., de Cáceres Orellana, P., & Mayordomo, R. (2023). Using Photogrammetry to Obtain 3D-Printed Positive Foot Casts Suitable for Fitting Thermoconformed Plantar Orthoses. *Processes*, *11*(1). https://doi.org/10.3390/pr11010024

Perry, J., Garrett, M., Gronley, J. K., & Mulroy, S. J. (1995). Classification of walking handicap in the stroke population. *Stroke*, *26*(6), 982–989.

Ranaldo, D., Zonta, F., Florian, S., & Lazzaro, J. (2023). A facile, semi-automatic protocol for the design and production of 3D printed, anatomical customized orthopedic casts for forearm fractures. *Journal of Clinical Orthopaedics and Trauma*, *42*. https://doi.org/10.1016/j.jcot.2023.102206

Ranz, E. C., Russell Esposito, E., Wilken, J. M., & Neptune, R. R. (2016). The influence of passive-dynamic ankle-foot orthosis bending axis location on gait performance in individuals with lower-limb impairments. *Clinical Biomechanics*, *37*, 13–21. https://doi.org/10.1016/j.clinbiomech.2016.05.001

Ricardo, D., Raposo, M. R., Veloso, A., & João, F. (2022). The gait profile score to assess the effects of ankle-foot orthoses in the gait of children with cerebral palsy. *Gait & Posture*, *97*, S204–S205.

Roberts, A., Wales, J., Smith, H., Sampson, C. J., Jones, P., & James, M. (2016). A randomised controlled trial of laser scanning and casting for the construction of ankle–foot orthoses. *Prosthetics and Orthotics International*, *40*(2), 253–261.

Rogati, G., Leardini, A., Ortolani, M., & Caravaggi, P. (2019). Validation of a novel Kinect-based device for 3D scanning of the foot plantar surface in weight-bearing. *Journal of Foot and Ankle Research*, *12*(1), 1–8. https://doi.org/10.1186/s13047-019-0357-7

Roucoules, L., Paredes, M., Eynard, B., Camo, P. M., & Rizzi, C. (2021). *Advances on Mechanics, Design Engineering and Manufacturing III: Proceedings of the International Joint Conference on Mechanics, Design Engineering & Advanced Manufacturing, JCM 2020, June 2-4, 2020*. Springer Nature.

Sabyrov, N., Sotsial, Z., Abilgaziyev, A., Adair, D., & Ali, H. (2021). Design of a flexible neck orthosis on Fused Deposition Modeling printer for rehabilitation on regular usage. *Procedia Computer Science*, *196*, 226–234. https://doi.org/10.1016/j.procs.2021.12.009

Schweizer, K., Romkes, J., Coslovsky, M., & Brunner, R. (2014). The influence of muscle strength on the gait profile score (GPS) across different patients. *Gait & Posture*, *39*(1), 80–85.

Silva, R. (2023). *Innovative Design and Development of Personalized Ankle-Foot Orthoses for Stroke Survivors With Equinovarus Foot: A Feasibility and Comparative Trial Protocol (Preprint)*. https://doi.org/10.2196/preprints.52365

Silva, R., Morouço, P., & Veloso, A. (2019). Desenvolvimento de um sistema one-shot de baixo custo para aquisição de modelos 3D. *Proceedings Do 8º Congresso Nacional de Biomecânica*, 239–240.

Silva, R., Veloso, A., Alves, N., Fernandes, C., & Morouço, P. (2022). A Review of Additive Manufacturing Studies for Producing Customized Ankle-Foot Orthoses. In *Bioengineering* (Vol. 9, Issue 6). MDPI. https://doi.org/10.3390/bioengineering9060249

Speciali, D. S., Oliveira, E. M., Cardoso, J. R., Correa, J. C. F., Baker, R., & Lucareli, P. R. G. (2014). Gait profile score and movement analysis profile in patients with Parkinson's disease during concurrent cognitive load. *Brazilian Journal of Physical Therapy*, *18*, 315–322.

Telfer, S., Pallari, J., Munguia, J., Dalgarno, K., McGeough, M., & Woodburn, J. (2012). Embracing additive manufacture: Implications for foot and ankle orthosis design. *BMC Musculoskeletal Disorders*, *13*(May). https://doi.org/10.1186/1471-2474-13-84

Tyson, S. F., Sadeghi-Demneh, E., & Nester, C. J. (2013). A systematic review and meta-analysis of the effect of an ankle-foot orthosis on gait biomechanics after stroke. *Clinical Rehabilitation*, *27*(10), 879–891.

Tyson, S., & Kent, R. (2013). Effects of an Ankle-Foot Orthosis on Balance and Walking After Stroke: A Systematic Review and Pooled Meta-Analysis. *Archives of Physical Medicine and Rehabilitation*. https://doi.org/10.1016/j.apmr.2012.12.025

Vasiliauskaite, E., Ielapi, A., De Beule, M., Van Paepegem, W., Deckers, J. P., Vermandel, M., Forward, M., & Plasschaert, F. (2019). A study on the efficacy of AFO stiffness prescriptions. *Disability and Rehabilitation: Assistive Technology*, *0*(0), 1–13. https://doi.org/10.1080/17483107.2019.1629114

Verma, R., Arya, K. N., Sharma, P., & Garg, R. K. (2012). Understanding gait control in post-stroke: implications for management. *Journal of Bodywork and Movement Therapies*, *16*(1), 14–21.

Wada, Y., Otaka, Y., Mukaino, M., Tsujimoto, Y., Shiroshita, A., Kawate, N., & Taito, S. (2021). The Effect of Ankle-foot Orthosis on Ankle Kinematics in Individuals After Stroke: A Systematic Review and Meta-analysis. *Pm&r*. https://doi.org/10.1002/pmrj.12687

Wang, R.-Y., Yen, L.-L., Lee, C.-C., Lin, P.-Y., Wang, M.-F., & Yang, Y.-R. (2005). Effects of an ankle-foot orthosis on balance performance in patients with hemiparesis of different durations. *Clinical Rehabilitation*, *19*(1), 37–44.

Wang, Y., Tang, R., Wang, H., Yu, X., Li, Y., Wang, C., Wang, L., & Qie, S. (2022). The Validity and Reliability of a New Intelligent Three-Dimensional Gait Analysis System in Healthy Subjects and Patients with Post-Stroke. *Sensors*, *22*(23). https://doi.org/10.3390/s22239425

Wojciechowski, E., Chang, A. Y., Balassone, D., Ford, J., Cheng, T. L., Little, D., Menezes, M. P., Hogan, S., & Burns, J. (2019). Feasibility of designing, manufacturing and delivering 3D printed ankle-foot orthoses: A systematic review. In *Journal of Foot and Ankle Research* (Vol. 12, Issue 1). BioMed Central Ltd. https://doi.org/10.1186/s13047-019-0321-6

Yamamoto, S. (2014). Gait Changes in a Hemiplegic Patient Using an Ankle-Foot Orthosis With an Oil Damper: A Case Report. *Clinical Research on Foot & Ankle*. https://doi.org/10.4172/2329-910x.1000136

Yamamoto, S., Tanaka, S., & Motojima, N. (2018). Comparison of ankle–foot orthoses with plantar flexion stop and plantar flexion resistance in the gait of stroke patients: A randomized controlled trial. *Prosthetics and Orthotics International*, *42*(5), 544–553.

Zarezadeh, R., Arazpour, M., & Aminian, G. (2022). The Effect of Anterior Ankle-Foot Orthosis and Posterior Ankle-Foot Orthosis on Functional Ambulation in Stroke Patients. *Journal of Rehabilitation and Assistive Technologies Engineering*. https://doi.org/10.1177/20556683221082451

IV. General Discussion

Stroke is a major public health issue, often leading to significant long-term motor impairments among survivors. One common consequence of stroke is hemiparesis, which disrupts normal gait and necessitates assistive devices such as AFOs to improve walking ability. Traditional AFO fabrication methods—typically involving plaster casting and manual crafting—have served patients for decades, but they come with limitations in precision, comfort, and efficiency. Considering these challenges, the present work introduced and evaluated a novel system that combines photogrammetry-based 3D scanning with AM to produce custom AFOs. The development of a photogrammetry-based 3D scanning system integrated with AM represents a paradigm shift in orthotic fabrication for stroke rehabilitation. The use of additive manufacturing enables the precise tailoring of orthoses to each patient's unique anatomical and biomechanical profile, a critical improvement over the constraints of traditional AFO manufacturing methods. In the conventional process, creating a custom AFO can be labour-intensive and dependent on the skill of the orthotist, often resulting in variations in fit and function. By contrast, AM provides a digital, precision-driven workflow: once a patient's limb geometry is captured in detail, an AFO can be computationally designed to mirror that anatomy and then 3D-printed with minimal loss of fidelity. Central to this innovation is the incorporation of a novel photogrammetry-based 3D scanning technique. Photogrammetry uses a series of photographs from multiple angles to reconstruct a highly accurate 3D model of the limb. This method is non-invasive and rapid, offering a comfortable experience for patients compared to plaster casting or even some structured-light scanning methods. A complete digital scan can be obtained within minutes, eliminating the need for patients to endure long periods of immobilization or contact with casting materials. The resulting digital model captures fine anatomical details, ensuring that the fabricated orthosis will conform closely to the patient's morphology. This high level of accuracy enhances the interface between the AFO and the limb, thereby improving both the functional efficacy of the device and the comfort for the wearer. The combination of precise 3D scanning and AM allows for a degree of customization and design complexity that is difficult to achieve with traditional techniques. For example, the thickness, rigidity, and contour of different sections of the AFO can be algorithmically optimized to provide support where needed while reducing bulk elsewhere. The adaptability of the digital design process means that orthoses can be iteratively refined: clinicians can adjust the AFO model based on patient feedback or gait

analysis results, and an updated version can be rapidly prototyped without starting from scratch. This iterative capability is particularly valuable in stroke rehabilitation, where patients often undergo changes in muscle tone and gait pattern over time—custom devices can be adjusted to their evolving needs with relative ease. In implementing this system, the present research also explored materials and manufacturing techniques that balance performance with practicality. Notably, the custom AFOs in this work were produced using FDM 3D printer with Nylon-12 thermoplastic filament. Previous studies on 3D-printed AFOs have predominantly employed SLS and various polymer powders. The choice of Nylon-12 FDM in this thesis is significant: it demonstrates that a more accessible and potentially cost-effective desktop printing technology can be leveraged to fabricate robust orthotic devices. This choice of fabrication method influences the final material properties of the AFO (such as strength, flexibility, and weight) as well as the economic cost and speed of production. The success of Nylon-12 FDM in producing functional AFOs highlights the importance of evaluating different AM technologies and materials for medical use. It suggests that with careful material selection and printer calibration, lower-cost AM systems could meet clinical requirements, which is crucial for the broader feasibility of adopting this technology in healthcare settings. Overall, the technological innovation presented—combining high-resolution photogrammetry and versatile AM—lays the groundwork for revolutionizing AFO fabrication by making it more precise, patient-specific, and adaptable than ever before.

Clinical and Biomechanical Outcomes of the Custom 3D-Printed AFOs

A central question in adopting any new orthotic fabrication method is whether the resulting devices measurably improve patient outcomes. This research addressed that question through comprehensive gait analysis, comparing the performance of custom-made, 3D-printed AFOs against standard prefabricated AFOs in stroke survivors. The results provide strong evidence of the clinical and biomechanical benefits of the new system. Using motion analysis techniques, including SPM1D for continuous data, the gait kinematics of stroke patients were examined across the full gait cycle under different orthotic conditions. The analysis revealed that walking with the custom AM-fabricated AFO led to significant differences in joint kinematics when compared to walking with a conventional off-the-shelf AFO. In particular, deviations in ankle and knee motion patterns were observed, indicating that the custom AFO altered gait dynamics in ways that are conducive to a more stable and

physiological walking pattern. For example, improvements in lateral stability and limb alignment were noted. These kinematic changes are important because stroke survivors often exhibit gait asymmetries and instability (such as excessive mediolateral sway or knee hyperextension) that can increase their risk of falls. The customized AFOs, being tailored to the individual's deformities and weaknesses, appear to provide targeted support that helps correct or compensate for these abnormal movements, contributing to safer and more effective ambulation. In addition to kinematics, this research was among the first to investigate gait kinetics (forces and moments) in stroke patients using 3D-printed AFOs. The kinetic analysis unveiled noteworthy variations in joint moments at the hip and ankle between the prefabricated and custom AFO conditions. For instance, patients wearing the custom AFO exhibited different ankle moment profiles during stance, suggesting a more controlled ankle behaviour and improved push-off compared to when they wore a generic device. At the hip, changes in moment patterns implied better support and balance. These findings suggest that the type and design of AFO can modulate the distribution of forces and the propulsion mechanics during gait. A custom AFO that closely fits the patient’s anatomy may provide more effective leverage and support at critical phases of gait (such as toe-off and mid-stance), thereby reducing compensatory movements and allowing a more normal momentum transfer through the limbs. The ability to influence gait kinetics is clinically relevant: it provides insight into how custom orthoses might reduce the effort of walking or the strain on certain joints, potentially decreasing fatigue and improving endurance for stroke survivors. Spatiotemporal gait parameters further quantified the functional advantages of the custom-fabricated AFOs. Patients using the custom devices demonstrated faster comfortable walking speeds, longer stride lengths, and more symmetric step times in comparison to the prefabricated AFO condition. An increase in walking speed is a key indicator of enhanced gait efficiency and confidence. Even modest improvements in gait speed can translate to significantly better mobility in daily life, enabling patients to walk farther and participate more fully in activities. The observation of improved spatiotemporal metrics with the custom AFOs indicates that these devices not only alter the mechanics of gait but also confer a tangible performance benefit that could enhance a patient’s independence and safety. Gait became generally more fluid and closer to a normal walking pattern, reflecting the effective support and facilitation provided by an orthosis designed specifically for the user’s impairments. To synthesize the overall impact on gait quality, GPS analysis was employed. The GPS is a

composite measure that captures the deviation of a patient's gait from normative (able-bodied) gait patterns across multiple dimensions. In this study, the GPS revealed that stroke patients walking with a custom 3D-printed AFO had gait patterns that were more closely aligned with those of healthy individuals than when the same patients used a standard prefabricated AFO. This is a notable outcome: post-stroke hemiparetic gait is typically characterized by a combination of temporal asymmetry, altered joint motions, and compensatory strategies, and achieving even partial normalization is challenging. The custom AFOs, by virtue of their tailored support (for example, correcting foot drop and stabilizing the ankle in the frontal plane for each specific patient), seem to address multiple aspects of the pathological gait. The improved GPS suggests that these orthoses can mitigate common post-stroke gait abnormalities such as drop foot, knee instability, or hip hiking, thereby contributing to a gait pattern that is closer to the natural, pre-stroke condition. In summary, the biomechanical evaluation provides compelling evidence that photogrammetry-designed, AM-produced AFOs offer superior gait outcomes for stroke survivors when compared to generic devices. The kinematic improvements (better joint alignment and stability), kinetic adjustments (favorable redistribution of forces), and spatiotemporal gains (speed and symmetry increases) all converge on the conclusion that a personalized AFO can more effectively support the complex needs of gait rehabilitation. These objective improvements are crucial from a clinical perspective: safer and more efficient gait reduces the risk of secondary complications (like falls or joint degeneration) and can accelerate the rehabilitation process by enabling patients to practice a more correct walking pattern during therapy sessions.

Patient-Centred Outcomes: Comfort, Usability, and Satisfaction

While quantitative gait measures are essential for demonstrating biomechanical efficacy, the ultimate success of an orthotic intervention also hinges on patient acceptance and comfort. Stroke survivors will only wear and benefit from AFOs if the devices are tolerable and meet their daily needs. In this context, the present research placed strong emphasis on patient-centred outcomes, gathering user feedback to evaluate comfort, usability, and overall satisfaction with the custom 3D-printed AFOs relative to traditional ones. Using the QUEST questionnaire and other qualitative feedback methods, the study assessed key aspects of the user experience. The findings consistently favoured the custom-fabricated AFOs in terms of

user satisfaction. Patients reported higher levels of comfort with the 3D-printed orthoses, which can be attributed to the improved fit and anatomical conformity. Unlike off-the-shelf AFOs that often have generic shapes and may require padding or manual adjustments to accommodate individual limb variations, the custom devices were designed from the start to mirror each patient's leg and foot contours. This precise fit likely led to fewer pressure points, better weight distribution, and a more natural feel when walking or standing. As a result, patients experienced less discomfort over prolonged use, which is crucial for an orthosis that might be worn for many hours each day. Another important dimension of satisfaction was the perceived usability and convenience of the AFOs. Participants noted that the custom AFOs were generally easier to don and doff, and they interfaced better with footwear. The design could be optimized to individual needs—for example, adjusting the stiffness or including relief areas for bony prominences—enhancing the usability in everyday activities. The research also highlighted the significance of device weight and aesthetics (dimensions) in user satisfaction. Many stroke patients are older adults who may have limited strength; a lighter AFO reduces the energy required for leg swing during gait and places less strain on the limb. The use of Nylon-12 and the ability to incorporate cut-outs or thinner sections in the 3D-printed design might have contributed to a lighter device without sacrificing strength. Indeed, participants identified weight as a significant factor: a bulky or heavy orthosis can feel encumbering, whereas a lightweight one is more easily accepted as part of the body during movement. The relatively compact dimensions of the custom AFO (achieved by avoiding unnecessary material and tailoring the shape) also meant it fit more comfortably inside shoes and under clothing, which is important for discretion and practicality. Patient confidence and psychological acceptance were additional, less tangible benefits observed with the custom AFOs. Knowing that the device was custom-made for them, patients often expressed greater trust in its effectiveness and a willingness to wear it regularly. This psychological comfort is an important outcome: if patients believe in and prefer their assistive device, they are more likely to use it consistently, which in turn reinforces the positive effects on mobility. Some individuals reported feeling more stable and secure while wearing the custom AFO, reflecting both the physical support provided and the subjective reassurance that the device was optimized for their condition. In summary, the patient-centred assessments demonstrated that the advantages of the new AFO system extend beyond objective gait improvements—they also create a more comfortable and acceptable user experience. Comfort, ease of use, and

personal preference are all pivotal for long-term adherence to orthotic use. The high satisfaction scores for the custom 3D-printed AFOs underscore a critical point: rehabilitation technologies must ultimately align with patient needs and lifestyles. An intervention that is biomechanically effective but uncomfortable will likely fail in practice. The present work shows that through careful design and customization, it is possible to achieve both biomechanical efficacy and user satisfaction, thereby maximizing the real-world impact of the orthotic device on stroke rehabilitation.

Practical Advantages Over Traditional Methods

Adopting this photogrammetry-AM workflow for AFO production also offers several practical advantages and demonstrates feasibility when compared to traditional orthotic fabrication. One of the most immediate benefits is the streamlined production process. Traditional custom AFO fabrication typically requires taking a plaster cast of the patient's limb (or using foam impressions), waiting for the cast to harden, creating a positive model, and then moulding or laminating materials over the model. This multi-step process is time-consuming and labour-intensive. In contrast, the digital workflow developed in this thesis dramatically reduces manual labour: after a quick scanning session, the design and fabrication steps are largely automated. The orthotist can use CAD software to finalize the AFO design, and the 3D printer fabricates the device, potentially within the same day. This could shorten the turnaround time from measurement to delivery, meaning patients receive their orthoses faster. For stroke patients, who typically begin gait rehabilitation soon after the acute phase, minimizing delays in obtaining a properly fitted AFO can be crucial for early mobilization. Another significant practical advantage lies in the reproducibility and consistency of the digital process. Human techniques like plaster casting are subject to variability (different technicians might produce slightly different results, and the casts can deform). In contrast, a digital scan is highly repeatable, and the design file for an AFO can be saved and re-used or modified precisely. If a patient needs a replacement AFO months later (due to wear or changes in condition), the same digital model can be reprinted, or quickly adjusted if, for example, minor swelling or atrophy has occurred. This ability to efficiently create consistent duplicates or updated versions of an orthosis is an important practical benefit, improving the continuity of care. Resource efficiency is another key consideration. While there is an initial cost in acquiring a high-quality camera or scanner and a 3D printer, these tools can produce many

devices once in place. Over the long term, the cost per device may decrease, especially when factoring in the reduction of manual labour and the potential for less wasted material (AM can be more material-efficient, adding material only where needed). The use of FDM with Nylon-12, as demonstrated, is relatively cost-effective because filament materials are less expensive than specialized polymers for SLS, and FDM printers are widely available at moderate cost. This approach could make custom AFO production more economically feasible for smaller clinics or resource-limited settings, which often cannot invest in expensive moulding equipment or industrial 3D printers. Furthermore, as AM technology continues to mature, it is expected that printers will become faster and more affordable, and materials will diversify, further tipping the cost-benefit balance in favour of digital fabrication. From a practical workflow perspective, integrating photogrammetry and AM can also enhance multidisciplinary collaboration. The digital nature of the process means that data (the 3D limb models and orthosis designs) can be easily shared among clinicians, orthotists, and engineers. For instance, a rehabilitation team can review a digital model to discuss pressure points or support areas, and adjustments can be made virtually before printing. This collaborative tuning of the device is harder to achieve once a traditional AFO is fabricated, because changes would require physically modifying or remaking the device. Thus, the new system supports a more iterative and collaborative approach to orthosis design, potentially leading to better outcomes. It is also worth noting that the patient experience during the fabrication process is improved. Photogrammetric scanning is relatively comfortable – patients can sit or stand briefly while photos are taken, without the need to coat the limb in plaster or endure awkward casting postures for extended periods. This reduces discomfort and anxiety, making the process more patient-friendly. Such improvements in the clinical procedure can increase patient willingness to be fitted for orthoses and return for follow-up fittings if needed. In summary, the transition to a photogrammetry and AM-based fabrication method provides tangible practical benefits: quicker production times, consistent quality, ease of reproduction, cost-effectiveness in the long run, and a more patient-friendly experience. These factors all contribute to the feasibility of implementing this new system in real clinical settings. While the initial setup requires investment in technology and training, the day-to-day workflow can become more efficient and adaptable than the traditional paradigm. This positions the innovative approach not just as a theoretical improvement, but as a realistic advancement that can be adopted in modern orthotic clinics.

Implications for Rehabilitation and Clinical Implementation

The successful development and testing of the custom photogrammetry-AM AFO system carry important implications for stroke rehabilitation and highlight potential pathways for implementing this technology in clinical practice. Fundamentally, this work demonstrates that embracing modern engineering solutions in rehabilitation can lead to measurable improvements in patient outcomes. For stroke survivors, even incremental enhancements in gait stability, speed, or endurance can have a profound impact on their rehabilitation trajectory and quality of life. By delivering a more effective orthotic device, this approach can facilitate more intensive and effective rehabilitation. Patients walking with a well-fitted custom AFO can practice gait with proper form, which reinforces correct movement patterns in therapy sessions. Over time, this could translate to greater improvements in walking independence and a reduction in secondary musculoskeletal issues, thereby accelerating functional recovery. Clinically, the introduction of a digital fabrication workflow implies some changes in practice that are important to consider. Orthotists and clinicians will need to be trained in using 3D scanning equipment and software for modelling orthoses. This is a shift from hands-on fabrication skills to more computer-aided design and engineering skills. However, once trained, practitioners might find that the ability to visualize and adjust a patient's orthosis in a digital environment opens new possibilities for creative and precise interventions. For example, clinicians could simulate how slight changes in AFO angle or stiffness might affect gait or easily customize cut-outs to relieve pressure on an area of concern, before ever printing the device. The collaborative planning of AFOs could become a standard part of multidisciplinary rehabilitation team meetings. The integration into clinical workflow would also necessitate logistical planning. In a busy rehabilitation hospital or clinic, scheduling a scanning session and then scheduling a fitting session once the AFO is printed would need to be as streamlined as current casting and fitting appointments. Encouragingly, the speed of scanning and automated fabrication can make this feasible. In fact, if the process is well-organized, it may reduce the number of visits: patients might be scanned and then return a few days later to receive the finished AFO, whereas traditional methods might require intermediate steps (cast removal, test fitting of a plastic mould, etc.). The new system could thus fit within standard rehabilitation timelines or even shorten them, ensuring that patients are not kept waiting for assistive devices during critical periods of recovery. From a

broader healthcare perspective, the findings of improved gait and patient satisfaction with custom AM AFOs provide evidence-based support for adopting such technology. Clinicians and decision-makers are more likely to embrace a new system if it demonstrably enhances patient outcomes. The positive results can be used to justify investments in 3D printing infrastructure and training, framing them as investments in quality of care and long-term cost savings (through reduced device remake rates, fewer complications, and better rehab results). There is also an implication for personalized medicine in rehabilitation: this work aligns with the growing trend of tailoring interventions to individual patient profiles. As healthcare moves towards personalization, having in-house capabilities to produce custom devices quickly can become a competitive advantage for clinics and a hallmark of advanced patient care. In terms of policy and guidelines, widespread implementation of photogrammetry and AM for AFO production may require updating clinical practice guidelines and regulatory frameworks. Rehabilitation professionals will need clear protocols for how and when to use these technologies. The current research serves as a pioneering example that others can build upon, helping to establish best practices—such as optimal scanning procedures, design principles for printed AFOs, and recommended outcome evaluation metrics. Importantly, the success of this system suggests potential applicability beyond just stroke-related AFOs. The framework of digitally scanning a body part and printing a custom orthosis could be extended to other types of orthotic and prosthetic devices in rehabilitation medicine (such as wrist splints, knee braces, or even prosthetic sockets). Thus, the implications of this research resonate with a broader innovation wave in rehabilitative care: it exemplifies how engineering advancements can be translated into clinical solutions that are more effective and patient friendly. By thoroughly researching and documenting the process and outcomes, this thesis contributes to building the trust and knowledge base necessary for clinicians to adopt these new tools. In the long run, the integration of such technologies is expected to raise the standard of rehabilitative care, making personalized assistive devices more accessible and commonplace, much to the benefit of patients who rely on them for regaining independence.

V. General Conclusion

This thesis marks a notable advancement in orthotic care for stroke survivors. It focuses on the role of additive manufacturing in improving the design and production of AFOs. The introduction of a new 3D scanning system, based on photogrammetry, enhances accuracy in orthotic fabrication. This method is not just a technical improvement; it also makes the orthoses more comfortable for patients and speeds up their production.

Following this technological improvement, the research explores the effectiveness of AFOs produced using AM. The results show increased patient satisfaction, a critical factor as the healthcare industry seeks to improve stroke rehabilitation methods. These findings provide a strong foundation for future developments in orthotic technology, potentially leading to better patient care and more innovative practices.

Also, the advancements presented in this thesis are expected to influence clinical practices, enhance patient outcomes, and a new wave of innovation in rehabilitative care. By combining thorough research with practical application, this work contributes significantly to the collective effort to improve mobility and quality of life for stroke survivors. It exemplifies the successful combination of clinical expertise, engineering innovation, and a focus on patient-centred rehabilitation. It’s clear that the impact of this research could extend beyond academic circles, influencing real-world clinical practices and guiding the future direction of orthotic care.

VI. Methodological Considerations

Despite the detailed exposition of materials and methods in chapter III, additional methodological aspects warrant a more comprehensive elucidation in the subsequent paragraphs.

Motion Capture

An optoelectronic system with 12 cameras Qualisys Micus M3 (Qualisys AB, Gothenburg, Sweden) with with 2 Bertec Force Plates (Models: 4060-07 and 4060-10) (Bertec, Columbus, OH, USA) was employed to capture kinematic and kinetic data, a prevalent choice for recording human motion. This system encompasses a network of cameras synchronized with the force plates that define the measurement volume. The cameras accurately locate point markers, either emitting or reflecting light, placed on the skin. These markers' locations, in Cartesian coordinates relative to a global system, are deduced through mathematical transformations of the 2-D coordinates captured by at least two cameras at each instant (Baker et al., 2018).

The frame rate selected for capturing motion should be adequately high to accurately document both maximal and minimal displacements of joints and limbs. This is particularly vital for analyzing critical events in gait cycles. While higher frame rates are beneficial for enhancing data precision and accuracy in motion capture, the specific requirements vary depending on the activity being studied. Given the nature of the gait movements in stroke patients, a lower frame rate was deemed sufficient. Therefore, a 120Hz capture rate was employed. This rate was found to be adequate for capturing the nuances of both clinical and pathological gait cycles in stroke patients, who typically exhibit slower and more varied movement patterns. This frequency provides a balanced approach, ensuring the capture of detailed gait dynamics without unnecessary data complexity. This methodological decision is supported by the literature, where similar frame rates have been effectively utilized in the kinematic study of gait in stroke patients, thereby validating the approach in this context.

Marker Set

The marker configuration adhered to the Calibrated Anatomical System Protocol (CAST) (Cappozzo et al., 1995; Kaufman et al., 2016) and the CODA pelvis model (Cappozzo et al., 1995), as depicted in Fig. VIII.21. This setup facilitated the reconstruction of the pelvis and both lower limbs (Monaghan et al., 2007). The system comprised 20 individual markers and four clusters, each containing four embedded markers. This arrangement enabled the detailed reconstruction of seven distinct body segments: feet, shanks, thighs, and pelvis. It was considered each segment independently with six degrees of freedom, as per biomechanical standards (Bell et al., 1990).

Palpation was the primary method for identifying subcutaneous anatomical landmarks on the patients (Chiari et al., 2005), which then guided the precise placement of the marker set. The markers used were 10 mm spherical reflective markers, each affixed to a base. Four marker clusters were strategically attached to the lateral aspects of the thigh and shank. This configuration was crucial for independently tracking the anatomical landmarks of each segment, thus allowing for both rotational and translational movements at the joints (Collins et al., 2009).

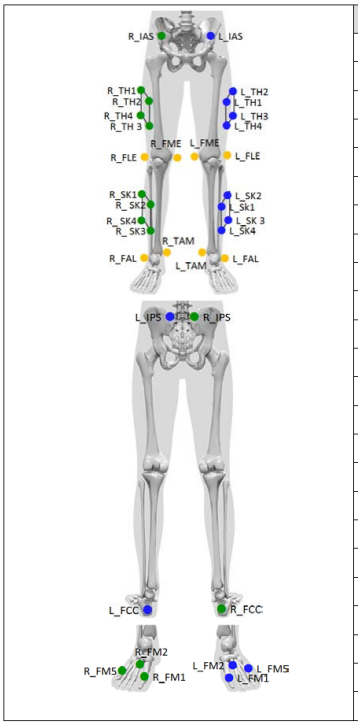

Name	Ref. [2]	Location	Static (36)	Dyn. (28)
L_IAS	IAS	Anterior superior iliac spine	X	X
L_IPS	IPS	Posterior superior iliac spine	X	X
R_IPS	IPS	Posterior superior iliac spine	X	X
R_IAS	IAS	Right anterior superior iliac spine	X	X
L_TH1-4		Cluster	X	X
L_FLE	FLE	Lateral epicondyle	X	
L_FME	FME	Medial epicondyle	X	
L_SK1-4		Cluster	X	X
L_FAL	FAL	Lateral prominence of the lateral malleolus	X	
L_TAM	TAM	Medial prominence of the medial malleolus	X	
L_FCC	FCC	Aspect of the Achilles tendon insertion on the calcaneus	X	X
L_FM1	FM1	Dorsal margin of the first metatarsal head	X	X
L_FM2	FM2	Dorsal aspect of the second metatarsal head	X	X
L_FM5	FM5	Dorsal margin of the fifth metatarsal head	X	X
R_TH1-4		Cluster	X	X
R_FLE	FLE	Lateral epicondyle	X	
R_FME	FME	Medial epicondyle	X	
R_SK1-4		Cluster	X	X
R_FAL	FAL	Lateral prominence of the lateral malleolus	X	
R_TAM	TAM	Medial prominence of the medial malleolus	X	
R_FCC	FCC	Aspect of the Achilles tendon insertion on the calcaneus	X	X
R_FM1	FM1	Dorsal margin of the first metatarsal head	X	X
R_FM2	FM2	Dorsal aspect of the second metatarsal head	X	X
R_FM5	FM5	Dorsal margin of the fifth metatarsal head	X	X

FIGURE VII.22 – Model and location of the retroreflective markers

Filter Cut-off Frequency

In biomechanical recordings, signal and noise often overlap within the frequency domain, necessitating the selection of an appropriate cut-off frequency to filter out noise while preserving as much signal as possible. Kinematic data generally possess higher error margins due to skin movement artifacts and marker vibration, in contrast to the more stable force platform measures. Consequently, researchers typically employ a lower cut-off frequency (e.g., 10-20Hz) for kinematic data, whereas force platform data are presented either raw or with a higher cut-off frequency (50-100Hz) (Baker et al., 2018). For this study kinematic signals were filtered at 10 Hz, and kinetic data were presented in raw, following previous literature and research focusing on different pathologic gait.

VII. Recommendations for Future Research

Despite the promising outcomes, it is important to acknowledge the limitations of this research and the areas that warrant further investigation. First, the sample size of patients in the evaluation was relatively modest. While the observed improvements in gait and satisfaction are encouraging, a larger cohort would strengthen the generalizability of the conclusions. Future studies should include a more diverse and extensive population of stroke survivors, encompassing different ages, degrees of impairment, and time since stroke. Such studies would not only verify the consistency of the benefits seen with custom 3D-printed AFOs but also help identify any subgroup-specific effects—perhaps certain categories of patients (e.g., those with very severe gait deficits) benefit the most, while others see more moderate gains. Larger trials could also facilitate statistically robust comparisons and subgroup analyses, thereby providing more nuanced guidance for clinicians about who is likely to benefit most from this technology. Another limitation pertains to the long-term durability and performance of the 3D-printed AFOs. The current evaluation focused on relatively short-term use and immediate effects. However, orthoses are typically worn for many hours a day over months or years. The durability of devices produced by FDM with Nylon-12 (or any AM process) under continuous stress, exposure to sweat, varying temperatures, and general wear-and-tear remains an open question. Traditional polypropylene AFOs are known for their toughness and longevity; it must be demonstrated that printed AFOs can match or exceed this durability for routine clinical use. Future research should include longitudinal studies where patients use the custom AFOs for extended periods, with regular follow-ups to inspect the devices for signs of material degradation (such as cracks, loss of rigidity, or wear in straps and joints) and to ensure that the initial patient benefits are maintained over time. Additionally, mechanical testing of the printed AFOs (e.g., fatigue testing, load failure testing) would provide valuable data on how these devices hold up under forces similar to those experienced during gait. If any weaknesses are found, they could guide design optimizations or material enhancements (for instance, reinforcing high-stress areas or exploring alternative filaments/composites for greater strength). The design of the AFOs themselves offers many avenues for future improvement. Although the custom devices produced were effective, design optimization can continue to refine their performance and user experience. One direction is to further reduce the weight and profile of the AFO without compromising

support, using generative design algorithms or lattice structures made possible by AM. Another direction is to tailor the mechanical properties of the orthosis, such as tuning the flexibility at the ankle or the stiffness along the foot plate, to better mimic natural limb function or to provide dynamic assistance at certain gait phases. Advances in multi-material 3D printing might even allow sections of the AFO to have varying hardness or elasticity, providing rigidity where stability is needed and flexibility where movement should be allowed. Future prototypes could incorporate ventilation channels for breathability or interchangeable components to accommodate changes in swelling. Patient feedback should continue to inform design tweaks, ensuring that each iteration of the device addresses any shortcomings noted in real-world use (for example, if some patients still experience minor discomfort at a particular spot, the design could be altered locally to relieve pressure there). When considering implementation on a larger scale, regulatory and safety considerations become significant. Custom 3D-printed orthoses for medical use likely fall under medical device regulations, which means they must meet certain safety, efficacy, and quality control standards before being routinely provided to patients. Regulators will be interested in issues such as the consistency of production (does each printed device reliably match the design without defects?), the biocompatibility of the materials (to ensure no adverse skin reactions or toxicity), and the risk management of the digital process (for example, ensuring that the software used to create the orthosis does not introduce errors, and that patient data is handled securely). Future work should engage with these regulatory frameworks, perhaps by developing standardized protocols for validation of each custom device (e.g., a quick stress test or fit verification before dispensing to the patient). Additionally, there may be a need for creating guidelines or best practices at the industry or national level, to help clinics safely adopt 3D printing for orthoses. This could involve training certification for practitioners, maintenance protocols for the equipment, and traceability of the digital models and printed products. Addressing these regulatory and quality assurance aspects will be crucial for transitioning from research prototypes to approved medical products that can be covered by health insurance and prescribed widely. Finally, another future direction is to explore the broader impact on rehabilitation outcomes beyond gait metrics. It would be valuable to investigate whether the use of a superior custom AFO translates into improvements in patients' overall rehabilitation progress and daily function. For instance, do patients with custom AFOs show better balance confidence, fewer falls, or greater participation in

community activities over time compared to those with standard AFOs? Long-term follow-up studies and perhaps randomized controlled trials could examine outcomes such as fall rates, functional independence scores, and health-related quality of life measures. These data would help solidify the argument that investing in personalized, digitally fabricated orthoses yields tangible benefits in patients' lives and justifies any additional upfront costs. In conclusion, the introduction of photogrammetry-based 3D scanning combined with additive manufacturing has been shown to markedly improve the customization and effectiveness of ankle-foot orthoses for stroke patients. The research presented in this thesis demonstrates enhancements in gait function and patient satisfaction while also highlighting practical feasibility. By addressing the remaining challenges—expanding sample sizes, validating long-term durability, optimizing designs, and navigating regulatory pathways—this innovative approach is poised to transition from a cutting-edge concept into a standard of care. The implications of this work suggest a positive shift in stroke rehabilitation practice: one that embraces technological innovation to deliver individualized therapy solutions, ultimately aiming to improve mobility and quality of life for stroke survivors on a broad scale.

VIII. General References

All References are in Alphabetical Order

- Abd El-Kafy, E.M. The clinical impact of orthotic correction of lower limb rotational deformities in children with cerebral palsy: A randomized controlled trial. Clin. Rehabil. 2014, 28, 1004–1014, doi:10.1177/0269215514533710.
- Abe, H., Michimata, A., Sugawara, K., Sugaya, N., & Izumi, S.-I. (2009). Improving gait stability in stroke hemiplegic patients with a plastic ankle-foot orthosis. The Tohoku Journal of Experimental Medicine, 218(3), 193–199.
- Adamczyk, M., Liberadzki, P., & Sitnik, R. (2020). . Temperature compensation method for mechanical base of 3d-structured light scanners. Sensors, 20(2). , 362. https://doi.org/10.3390/s20020362
- Adiputra, D., Nazmi, N., Bahiuddin, I., Ubaidillah, U., Imaduddin, F., Rahman, M., … & Zamzuri, H. (2019). . A review on the control of the mechanical properties of ankle foot orthosis for gait assistance. Actuators, 8(1). , 10. https://doi.org/10.3390/act8010010
- Agudelo-Ardila, C.P.; Prada-Botía, G.C.; Rodrigues G, P.H. Orthotic Prototype for Upper Limb Printed in 3. D: A Efficient Solution. J Phys Conf Ser 2019, 1388, 012016, doi:10.1088/1742-6596/1388/1/012016.
- Alam, M., Choudhury, I., Mamat, A., & Hussain, S. (2015). . Computer aided design and fabrication of a custom articulated ankle foot orthosis. Journal of Mechanics in Medicine and Biology, 15(04). , 1550058. https://doi.org/10.1142/s021951941550058x
- Alexander, L. D., Black, S. E., Patterson, K. K., Gao, F., Danells, C., & McIlroy, W. E. (2009). Association Between Gait Asymmetry and Brain Lesion Location in Stroke Patients. Stroke. https://doi.org/10.1161/strokeaha.108.527374
- Alhossary, A. A., Pataky, T., Ang, W. T., Chua, K. S. G., & Donnelly, C. J. (2021). MovementRx: Versatile clinical movement analysis using Statistical Parametric Mapping.
- Ambu, R.; Oliveri, S.M.; Calì, M. Neck Orthosis Design for 3. D Printing with User Enhanced Comfort Features. International Journal on Interactive Design and Manufacturing 2023, doi:10.1007/s12008-023-01507-1.
- Anderson, S., Barnett, C., & Rusaw, D. (2021). . Exploring the perspectives of prosthetic and orthotic users: past and present experiences and insights for the future. Disability and Rehabilitation, 44(18). , 5284-5290. https://doi.org/10.1080/09638288.2021.1928777
- Arazpour, M.; Tajik, H.R.; Aminian, G.; Bani, M.A.; Ghomshe, F.T.; Hutchins, S.W. Comparison of the effects of solid versus hinged ankle foot orthoses on select temporal gait parameters in patients with incomplete spinal cord injury during treadmill walking. Prosthet. Orthot. Int. 2013, 37, 70–75.
- Baghbanbashi, A., Farahmand, B., Azadinia, F., & Jalali, M. (2022). . Evaluation of user's satisfaction with orthotic and prosthetic devices and services in orthotics and prosthetics center of iran university of medical sciences. Canadian Prosthetics & Orthotics Journal, 5(1). . https://doi.org/10.33137/cpoj.v5i1.37981

- Baker, R. J., Leboeuf, F. Y., Reay, J., & Sangeux, M. (2018). The conventional gait model-success and limitations. Springer.
- Baker, R., McGinley, J. L., Schwartz, M. H., Beynon, S., Rozumalski, A., Graham, H. K., & Tirosh, O. (2009). The gait profile score and movement analysis profile. Gait & Posture, 30(3), 265–269.
- Baker, R., McGinley, J. L., Schwartz, M., Thomason, P., Rodda, J., & Graham, H. K. (2012). The minimal clinically important difference for the Gait Profile Score. Gait & Posture, 35(4), 612–615.
- Bakhsh, H., Franchignoni, F., Bravini, E., Ferriero, G., Giordano, A., & Foti, C. (2014). . Validation of the arabic version of the client satisfaction with device module of the "orthotics and prosthetics users" survey. Annals of Saudi Medicine, 34(4). , 320-327. https://doi.org/10.5144/0256-4947.2014.320
- Balshem, H.; Helfand, M.; Schünemann, H.J.; Oxman, A.D.; Kunz, R.; Brozek, J.; Vist, G.E.; Falck-Ytter, Y.; Meerpohl, J.; Norris, S. G. RADE guidelines: 3. Rating the quality of evidence. J. Clin. Epidemiol. 2011, 64, 401–406.
- Banga, H., Belokar, R., Kalra, P., & Kumar, R. (2018). . Fabrication and stress analysis of ankle foot orthosis with additive manufacturing. Rapid Prototyping Journal, 24(2). , 301-312. https://doi.org/10.1108/rpj-08-2016-0125
- Baker, R. J., Leboeuf, F. Y., Reay, J., & Sangeux, M. (2018). The conventional gait model-success and limitations. Springer.
- Barnett, J. (2018). . Integrating technological advances into clinical training and practice: the future is now!. Clinical Psychology Science and Practice, 25(2). . https://doi.org/10.1111/cpsp.12233
- Baronio, G.; Harran, S.; Signoroni, A. A Critical Analysis of a Hand Orthosis Reverse Engineering and 3. D Printing Process. Appl Bionics Biomech 2016, 2016, doi:10.1155/2016/8347478.
- Barrios-Muriel, J., Romero-Sánchez, F., Alonso-Sánchez, F. J., & Salgado, D. R. (2020). Advances in orthotic and prosthetic manufacturing: A technology review. Materials, 13(2). https://doi.org/10.3390/ma13020295
- Bell, A. L., Pedersen, D. R., & Brand, R. A. (1990). A comparison of the accuracy of several hip center location prediction methods. Journal of Biomechanics, 23(6), 617–621.
- Belokar R. M, Banga H. K, Kumar R. A Novel Approach for Ankle Foot Orthosis Developed by Three Dimensional Technologies. I. OP Conf Ser Mater Sci Eng. 2017;280(1). :2-7. doi:10.1088/1757-899X/280/1/012030
- Bennett, B.C.; Russell, S.D.; Abel, M.F. The effects of ankle foot orthoses on energy recovery and work during gait in children with cerebral palsy. Clin. Biomech. 2012, 27, 287–291, doi:10.1016/j.clinbiomech.2011.09.005.
- Beynon, S., McGinley, J. L., Dobson, F., & Baker, R. (2010). Correlations of the gait profile score and the movement analysis profile relative to clinical judgments. Gait & Posture, 32(1), 129–132.
- Bigoni, M., Cimolin, V., Vismara, L., Tarantino, A. G., Clerici, D., Baudo, S., Galli, M., & Mauro, A. (2021). Relationship between gait profile score and clinical assessments of gait in post-

stroke patients. Journal of Rehabilitation Medicine, 53(5). https://doi.org/10.2340/16501977-2809

- Böhm, H., & Dussa, C. U. (2021). Prefabricated ankle-foot orthoses for children with cerebral palsy to overcome spastic drop-foot: does orthotic ankle stiffness matter? Prosthetics and Orthotics International, 45(6), 491–499.
- Boparai, K. S., Singh, R., & Singh, H. (2016). Development of Rapid Tooling Using Fused Deposition Modeling: A Review. Rapid Prototyping Journal. https://doi.org/10.1108/rpj-04-2014-0048
- Brehm, M.A.; Harlaar, J.; Schwartz, M. Effect of ankle-foot orthoses on walking efficiency and gait in children with cerebral palsy. J. Rehabil. Med. 2008, 40, 529–534, doi:10.2340/16501977-0209.
- Briko, A., Kapravchuk, V., Kobelev, A., Hammoud, A., Leonhardt, S., Ngo, C., … & Shchukin, S. (2021). . A way of bionic control based on ei, emg, and fmg signals. Sensors, 22(1). , 152. https://doi.org/10.3390/s22010152
- Brognara, L.; Fantini, M.; Morellato, K.; Graziani, G.; Baldini, N.; Cauli, O. Foot Orthosis and Sensorized House Slipper by 3. D Printing. Materials 2022, doi:10.3390/ma15124064.
- Cakar E, Durmus O, Tekin L, Dincer U, Kiralp M. Z. The Ankle-Foot Orthosis Improves Balance and Reduces Fall Risk of Chronic Spastic Hemiparetic Patients. Vol 46.; 2010.
- Cappozzo A, Catani F, Della Croce U, Leardini A. Position and orientation in space of bones during movement: anatomical frame definition and determination. Clinical biomechanics. 1995;10(4). :171-178.
- Carolus, A.E.; Becker, M.; Cuny, J.; Smektala, R.; Schmieder, K.; Brenke, C. The interdisciplinary management of foot drop. Dtsch. Arztebl. Int. 2019, 116, 347.
- Cha Y. H, Lee K. H, Ryu H. J, et al. Ankle-foot orthosis made by 3. D printing technique and automated design software. Appl Bionics Biomech. 2017;2017. doi:10.1155/2017/9610468
- Chae D. S, Kim D. H, Kang K. Y, et al. The functional effect of 3. D-printing individualized orthosis for patients with peripheral nerve injuries: Three case reports. Medicine. 2020;99(16). :e19791.
- Chan A. W, Tetzlaff J. M, Altman D. G, et al. S. PIRIT 2013 Statement: Defining Standard Protocol Items for Clinical Trials D. EVELOPMENT O. F T. HE S. PIRIT 2013 S. TATEMENT. Vol 158.; 2013. www.annals.org
- Chen, C.-C., Hong, W.-H., Wang, C.-M., Chen, C.-K., Wu, K. P.-H., Kang, C.-F., & Tang, S. F. (2010). Kinematic features of rear-foot motion using anterior and posterior ankle-foot orthoses in stroke patients with hemiplegic gait. Archives of Physical Medicine and Rehabilitation, 91(12), 1862–1868
- Chen, R.K.; Chen, L.; Tai, B.L.; Wang, Y.; Shih, A.J.; Wensman, J. Additive manufacturing of personalized ankle-foot orthosis. Trans. North Am. Manuf. Res. Inst. S. ME 2014, 42, 381–389.
- Chen, R. K., Jin, Y. an, Wensman, J., & Shih, A. (2016). Additive manufacturing of custom orthoses and prostheses-A review. Additive Manufacturing, 12, 77–89. https://doi.org/10.1016/j.addma.2016.04.002

- Chiari, L., Della Croce, U., Leardini, A., & Cappozzo, A. (2005). Human movement analysis using stereophotogrammetry: Part 2: Instrumental errors. Gait & Posture, 21(2), 197–211.
- Chimento, J., Highsmith, M., & Crane, N. (2011). . 3d printed tooling for thermoforming of medical devices. Rapid Prototyping Journal, 17(5). , 387-392. https://doi.org/10.1108/13552541111156513
- Choi H, Peters K. M, MacConnell M. B, Ly K. K, Eckert E. S, Steele K. M. Impact of ankle foot orthosis stiffness on Achilles tendon and gastrocnemius function during unimpaired gait. J Biomech. 2017;64:145-152. doi:10.1016/j.jbiomech.2017.09.015
- Choo, Y. J., & Lee, H. J. (2021). Commonly Used Types and Recent Development of Ankle-Foot Orthosis: A Narrative Review. Healthcare. https://doi.org/10.3390/healthcare9081046
- Chu, C. H., Wang, I. J., Sun, J. R., & Liu, C. H. (2022). Customized designs of short thumb orthoses using 3D hand parametric models. Assistive Technology, 34(1), 104–111. https://doi.org/10.1080/10400435.2019.1709917
- Chudnofsky, C.R.; Byers, S.R.; Roberts, J.R.; Hedges, J.R.; Chanmugam, A.S. A. S: Clinical Procedures in Emergency Medicine 2004.
- Cicarello, N. D. S., Bohrer, R. C. D., Devetak, G. F., Rodacki, A. L. F., Loureiro, A. P. C., & Manffra, E. F. (2023). Control of center of mass during gait of stroke patients: Statistical parametric mapping analysis. Clinical Biomechanics, 107. https://doi.org/10.1016/j.clinbiomech.2023.106005
- Ciobanu O, Ciobanu G, Rotariu M. Photogrammetric Scanning Technique and Rapid Prototyping Used for Prostheses and Ortheses Fabrication. Applied Mechanics and Materials. 2013;371:230-234. doi:10.4028/www.scientific.net/A. MM.371.230
- Collins, T. D., Ghoussayni, S. N., Ewins, D. J., & Kent, J. A. (2009). A six degrees-of-freedom marker set for gait analysis: repeatability and comparison with a modified Helen Hayes set. Gait & Posture, 30(2), 173–180.
- Creylman, V., Muraru, L., Pallari, J., Vertommen, H., & Peeraer, L. (2013). . Gait assessment during the initial fitting of customized selective laser sintering ankle foot orthoses in subjects with drop foot. Prosthetics and Orthotics International, 37(2). , 132-138. https://doi.org/10.1177/0309364612451269
- Cruz, T. H., Lewek, M. D., & Dhaher, Y. Y. (2009). Biomechanical Impairments and Gait Adaptations Post-Stroke: Multi-Factorial Associations. Journal of Biomechanics. https://doi.org/10.1016/j.jbiomech.2009.04.015
- Cui, Y., Cheng, S., Chen, X., Xu, G., Ma, N., Li, H., … & Li, Z. (2023). . Advances in the clinical application of orthotic devices for stroke and spinal cord injury since 2013. Frontiers in Neurology, 14. https://doi.org/10.3389/fneur.2023.1108320
- Dal Maso A, Cosmi F. 3. D-printed ankle-foot orthosis: A design method. Mater Today Proc. 2019;12:252-261. doi:10.1016/j.matpr.2019.03.122
- Daryabor, A., Arazpour, M., Aminian, G., Baniasad, M., & Yamamoto, S. (2020). Design and Evaluation of an Articulated Ankle Foot Orthosis With Plantarflexion Resistance on the Gait: A Case Series of 2 Patients With Hemiplegia. Journal of Biomedical Physics and Engineering. https://doi.org/10.31661/jbpe.v0i0.1159

- Daryabor, A., Yamamoto, S., Motojima, N., & Tanaka, S. (2022). Therapeutic Effect of Gait Training With Two Types of Ankle-Foot Orthoses on the Gait of the Stroke Patients in the Recovery Phase. Turkish Journal of Physical Medicine and Rehabilitation. https://doi.org/10.5606/tftrd.2022.7866
- Daryabor, A., Yamamoto, S., Orendurff, M. S., & Kobayashi, T. (2020). Effect of Types of Ankle-Foot Orthoses on Energy Expenditure Metrics During Walking in Individuals With Stroke: A Systematic Review. Disability and Rehabilitation. https://doi.org/10.1080/09638288.2020.1762767
- Deckers, J.P.; Vermandel, M.; Geldhof, J.; Vasiliauskaite, E.; Forward, M.; Plasschaert, F. Development and clinical evaluation of laser-sintered ankle foot orthoses. Plast. Rubber Compos. 2018, 47, 42–46, doi:10.1080/14658011.2017.1413760.
- Del Corso, M.; Abà, G.; Vazquez, L.; Dargaud, J.; Ehrenfest, D.M.D. Optical Three-Dimensional Scanning Acquisition of the Position of Osseointegrated Implants: An in Vitro Study to Determine Method Accuracy and Operational Feasibility. Clin Implant Dent Relat Res 2009, 11, 214–221, doi:10.1111/j.1708-8208.2008.00106.x.
- Demers L, Weiss-Lambrou R, Demers L, Ska B. Development of the Quebec User Evaluation of Satisfaction with assistive Technology (Q. UEST). . Assistive Technology. 1996;8(1). :3-13. doi:10.1080/10400435.1996.10132268
- Dessery, Y.; Pallari, J. Measurements Agreement between Low-Cost and High-Level Handheld 3. D Scanners to Scan the Knee for Designing a 3. D Printed Knee Brace. P. LoS One 2018, 13, doi:10.1371/journal.pone.0190585.
- Deverka, P., Doksum, T., & Carlson, R. (2007). . Integrating molecular medicine into the us health-care system: opportunities, barriers, and policy challenges. Clinical Pharmacology & Therapeutics, 82(4). , 427-434. https://doi.org/10.1038/sj.clpt.6100319
- Devetak, G. F., Martello, S. K., de Almeida, J. C., Correa, K. P., Iucksch, D. D., & Manffra, E. F. (2016). Reliability and minimum detectable change of the gait profile score for post-stroke patients. Gait and Posture, 49, 382–387. https://doi.org/10.1016/j.gaitpost.2016.07.149
- Dias Hensen, J.C.; Foggiatto, J.A.; Ulbricht, L.; Wan Stadnik, A.M. Additive Manufacturing of Customized Lower Limb Orthoses – A Review. Int J Innov Educ Res 2018, doi:10.31686/ijier.vol6.iss10.1175.
- Dickinson A, Donovan-Hall M, Kheng S, et al. Technologies to Enhance Quality and Access to Prosthetics & Orthotics: the importance of a multidisciplinary, user-centred approach. Global Report on Assistive Technology (G. ReAT). Consultation. Published online 2019:22-23. doi:10.5258/S. OTON/P0014
- Doern, C. (2013). . Integration of technology into clinical practice. Clinics in Laboratory Medicine, 33(3). , 705-729. https://doi.org/10.1016/j.cll.2013.03.004
- Dombroski, C.E.; Balsdon, M.E.R.; Froats, A. The Use of a Low Cost 3. D Scanning and Printing Tool in the Manufacture of Custom-Made Foot Orthoses: A Preliminary Study. B. MC Res Notes 2014, 7, 2–5, doi:10.1186/1756-0500-7-443.

- Doğan, A., Mengüllüoğlu, M., & Özgirgin, N. (2011). Evaluation of the Effect of Ankle-Foot Orthosis Use on Balance and Mobility in Hemiparetic Stroke Patients. Disability and Rehabilitation. https://doi.org/10.3109/09638288.2010.533243
- Dutta, R., Kumar, N., & Bora, D. (2017). . Development of algorithm for different programmable modes for a prototype of orthotic ambulatory device for gait rehabilitation. International Journal of System Control and Information Processing, 2(1). , 51. https://doi.org/10.1504/ijscip.2017.084261
- Eder, M.; Brockmann, G.; Zimmermann, A.; Papadopoulos, M.A.; Schwenzer-Zimmerer, K.; Zeilhofer, H.F.; Sader, R.; Papadopulos, N.A.; Kovacs, L. Evaluation of Precision and Accuracy Assessment of Different 3-D Surface Imaging Systems for Biomedical Purposes. J Digit Imaging 2013, 26, 163–172.
- El-Hakim, S.; Beraldin, J.A.; Picard, M.; Godin, G. Detailed 3. D Reconstruction of Large-Scale Heritage Sites with Integrated. I. EEE Comput Graph Appl 2004, 24, 21–29.
- Epstein R. M, Street R. L. The values and value of patient-centered care. Ann Fam Med. 2011;9(2). :100-103. doi:10.1370/afm.1239
- Esquenazi, A., Ofluoglu, D., Hirai, B., & Kim, S. (2009). The effect of an ankle-foot orthosis on temporal spatial parameters and asymmetry of gait in hemiparetic patients. PM&R, 1(11), 1014–1018.
- Faustini, M. C., Neptune, R. R., Crawford, R. H., & Stanhope, S. J. (2008). Manufacture of passive dynamic ankle-foot orthoses using selective laser sintering. IEEE Transactions on Biomedical Engineering, 55(2), 784–790. https://doi.org/10.1109/TBME.2007.912638
- Feigin, V., Krishnamurthi, R., Parmar, P., Norrving, B., Mensah, G., Bennett, D., … & Roth, G. (2015). . Update on the global burden of ischemic and hemorrhagic stroke in 1990-2013: the gbd 2013 study. Neuroepidemiology, 45(3). , 161-176. https://doi.org/10.1159/000441085
- Feigin, V., Nguyen, G., Cercy, K., Johnson, C., Alam, T., Parmar, P., … & Roth, G. (2018). . Global, regional, and country-specific lifetime risks of stroke, 1990 and 2016. New England Journal of Medicine, 379(25). , 2429-2437. https://doi.org/10.1056/nejmoa1804492
- Fietzek U. M, Kossmehl P, Schelosky L, Ebersbach G, Wissel J. Early botulinum toxin treatment for spastic pes equinovarus - a randomized double-blind placebo-controlled study. Eur J Neurol. 2014;21(8). :1089-1095. doi:10.1111/ene.12381
- Filho, I., Medola, F., Sandnes, F., & Paschoarelli, L. (2019). . Manufacturing technology in rehabilitation practice: implications for its implementation in assistive technology production., 328-336. https://doi.org/10.1007/978-3-030-20216-3_31
- Fu, J. C. M., Chen, Y. J., Li, C. F., Hsiao, Y. H., & Chen, C. H. (2022). The effect of three dimensional printing hinged ankle foot orthosis for equinovarus control in stroke patients. Clinical Biomechanics, 94. https://doi.org/10.1016/j.clinbiomech.2022.105622
- Fukuchi, C. A., & Duarte, M. (2019). Gait Profile Score in able-bodied and post-stroke individuals adjusted for the effect of gait speed. Gait and Posture, 69, 40–45. https://doi.org/10.1016/j.gaitpost.2019.01.018
- Funes-Lora, M., Posh, R., Wensman, J., & Shih, A. (2021). . Design of a segmented custom ankle foot orthosis with custom-made metal strut and 3d-printed footplate and calf shell.

Prosthetics and Orthotics International, 46(1). , 37-41. https://doi.org/10.1097/pxr.0000000000000071

- Garvey, C. and Hanlon, R. (2002). . Computed tomography in clinical practice. B. MJ, 324(7345). , 1077-1080. https://doi.org/10.1136/bmj.324.7345.1077
- Gefen A. Plantar soft tissue loading under the medial metatarsals in the standing diabetic foot. Med Eng Phys. 2003;25(6). :491-499. doi:10.1016/S1350-4533(03). 00029-8
- Geoffroy, M.; Gardan, J.; Goodnough, J.; Mattie, J. Cranial Remodeling Orthosis for Infantile Plagiocephaly Created Through a 3. D Scan, Topological Optimization, and 3. D Printing Process. Journal of Prosthetics and Orthotics 2018, 30, 1, doi:10.1097/J. PO.0000000000000190.
- Ginosian, J.; Kluding, P.M.; McBride, K.; Feld, J.; Wu, S.S.; O'Dell, M.W.; Dunning, K. Foot Drop Stimulation Versus Ankle Foot Orthosis After Stroke. Stroke 2013, 44, 1660–1669, doi:10.1161/strokeaha.111.000334.
- Glock, F.; Vogel, M.; Naumann, S.; Kuehnapfel, A.; Scholz, M.; Hiemisch, A.; Kirsten, T.; Rieger, K.; Koerner, A.; Loeffler, M.; et al. Validity and Intraobserver Reliability of Three-Dimensional Scanning Compared with Conventional Anthropometry for Children and Adolescents from a Population-Based Cohort Study. Pediatr Res 2017, 81, 736–744, doi:10.1038/pr.2016.274.
- Goda, K., Mahjoubfar, A., Wang, C., Fard, A., Adam, J., Gossett, D., … & Jalali, B. (2012). . Hybrid dispersion laser scanner. Scientific Reports, 2(1). . https://doi.org/10.1038/srep00445
- Grazioso S, Selvaggio M, Caporaso T, Di Gironimo G. A Digital Photogrammetric Method to Enhance the Fabrication of Custom-Made Spinal Orthoses. Journal of Prosthetics and Orthotics. 2019;31(2). :140-144. doi:10.1097/J. PO.0000000000000244
- Grazioso S, Selvaggio M, Di Gironimo G. Design and development of a novel body scanning system for healthcare applications. International Journal on Interactive Design and Manufacturing. 2018;12(2). :611-620. doi:10.1007/s12008-017-0425-9
- Grazioso, S.; Selvaggio, M.; Di Gironimo, G. Design and Development of a Novel Body Scanning System for Healthcare Applications. International Journal on Interactive Design and Manufacturing 2018, 12, 611–620, doi:10.1007/s12008-017-0425-9.
- Gronely, J.K.; Weiss, W.; Newsam, C.J.; Mulroy, S.J.; Eberly, V.J. Effect of A. FO Design on Walking after Stroke: Impact of Ankle Plantar Flexion Contracture. Prosthet. Orthot. Int. 2010, 34, 277–292, doi:10.3109/03093646.2010.501512.
- Górski, F.; Wichniarek, R.; Kuczko, W.; Żukowska, M.; Lulkiewicz, M.; Zawadzki, P. Experimental Studies on 3. D Printing of Automatically Designed Customized Wrist-Hand Orthoses. Materials 2020, doi:10.3390/ma13184091.
- Gök, H.; Küçükdeveci, A.; Altinkaynak, H.; Yavuzer, G.; Ergin, S. Effects of ankle-foot orthoses on hemiparetic gait. Clin. Rehabil. 2003, 17, 137–139, doi:10.1191/0269215503cr605oa.
- Harper, N.G.; Esposito, E.R.; Wilken, J.M.; Neptune, R.R. The influence of ankle-foot orthosis stiffness on walking performance in individuals with lower-limb impairments. Clin. Biomech. 2014, 29, 877–884, doi:10.1016/j.clinbiomech.2014.07.005.
- Hartley, R.; Zisserman, A. Multiple View Geometry in Computer Vision; Cambridge university press, 2003; I. SBN 0521540518.

- Hayek, S.; Hemo, Y.; Chamis, S.; Bat, R.; Segev, E.; Wientroub, S.; Yzhar, Z. The effect of community-prescribed ankle-foot orthoses on gait parameters in children with spastic cerebral palsy. J. Child. Orthop. 2007, 1, 325–332, doi:10.1007/s11832-007-0055-z.
- Ho, M.; Van Nguyen, J.M.; Talbot, K.; Heales, L.; Kean, C.O.; Kong, P.W.; Stanton, R. Immediate Comfort Perception of 3d-Printed Foot Orthoses in Individuals With Unilateral Heel Pain. Prosthet Orthot Int 2021, doi:10.1097/pxr.0000000000000068.
- Holtkamp, F.C.; Wouters, E.J.M.; Van Hoof, J.; van Zaalen, Y.; Verkerk, M.J. Use of and satisfaction with ankle foot orthoses. Clin. Res. Foot Ankle 2015.
- Hurwitz D. E, Ryals A. B, Case J. P, Block J. A, Andriacchi T. P. The knee adduction moment during gait in subjects with knee osteoarthritis is more closely correlated with static alignment than radiographic disease severity, toe out angle and pain. Journal of Orthopaedic Research. 2002;20(1). :101-107. doi:10.1016/S0736-0266(01). 00081-X
- Hwang, Y. (2020). . Effects of an elastic afo on the walking patterns of foot-drop patients with stroke. Journal of the Korean Society of Physical Medicine, 15(1). , 1-9. https://doi.org/10.13066/kspm.2020.15.1.1
- Inman, V.T.; Ralston, H.J.; Todd, F. Human walking; Williams & Wilkins, 1981; I. SBN 068304348X.
- Ivarsson, B., Wiinberg, S., & Svensson, M. (2016). . Information and/or medical technology staff experience with regulations for medical information systems and medical devices. Health Policy and Technology, 5(4). , 383-388. https://doi.org/10.1016/j.hlpt.2016.07.008
- Jarvis, H. L., Brown, S. J., Butterworth, C., Jackson, K., Clayton, A., Walker, L., Rees, N., Price, M., Groenevelt, R., & Reeves, N. D. (2022). The gait profile score characterises walking performance impairments in young stroke survivors. Gait and Posture, 91, 229–234. https://doi.org/10.1016/j.gaitpost.2021.10.037
- Jin Y. A, Plott J, Chen R, Wensman J, Shih A. Additive manufacturing of custom orthoses and prostheses - A review. In: Procedia C. IRP. Vol 36. Elsevier B.V.; 2015:199-204. doi:10.1016/j.procir.2015.02.125
- Johnson, A., Palit, S., Terry, E., Thompson, O., Powell-Roach, K., Dyal, B., … & Booker, S. (2021). . Managing osteoarthritis pain with smart technology: a narrative review. Rheumatology Advances in Practice, 5(1). . https://doi.org/10.1093/rap/rkab021
- Kafle, A., Luis, E., Silwal, R., Pan, H., Shrestha, P., & Bastola, A. (2021). . 3d/4d printing of polymers: fused deposition modelling (fdm). , selective laser sintering (sls). , and stereolithography (sla). . Polymers, 13(18). , 3101.
- Kark, L., Vickers, D., McIntosh, A., & Simmons, A. (2012). Use of gait summary measures with lower limb amputees. Gait & Posture, 35(2), 238–243.
- Karunakaran, K., Pilkar, R., Ehrenberg, N., Bentley, K., Cheng, J., & Nolan, K. (2019). . Kinematic and functional gait changes after the utilization of a foot drop stimulator in pediatrics. Frontiers in Neuroscience, 13. https://doi.org/10.3389/fnins.2019.00732
- Kaufman, K., Miller, E., Kingsbury, T., Esposito, E. R., Wolf, E., Wilken, J., & Wyatt, M. (2016). Reliability of 3D gait data across multiple laboratories. Gait & Posture, 49, 375–381.

- Kesikburun, S.; Yavuz, F.; Güzelküçük, Ü.; Yaşar, E.; Balaban, B. Effect of ankle foot orthosis on gait parameters and functional ambulation in patients with stroke. Turkiye Fiz. Tip ve Rehabil. Derg. 2017, 63, 143–148, doi:10.5606/tftrd.2017.129.
- Kilmartin, T. and Wallace, W. (1994). . The scientific basis for the use of biomechanical foot orthoses in the treatment of lower limb sports injuries--a review of the literature.. British Journal of Sports Medicine, 28(3). , 180-184. https://doi.org/10.1136/bjsm.28.3.180
- Kim, J. H., & Won, B. H. (2019). Kinematic on Ankle and Knee Joint of Post-Stroke Elderly Patients by Wearing Newly Elastic Band-Type Ankle–Foot Orthosis in Gait. Clinical Interventions in Aging, 2097–2104.
- Kim, S. J., Kim, S. J., Cha, Y. H., Lee, K. H., & Kwon, J. Y. (2018). Effect of personalized wrist orthosis for wrist pain with three-dimensional scanning and printing technique: A preliminary, randomized, controlled, open-label study. Prosthetics and Orthotics International, 42(6), 636–643. https://doi.org/10.1177/0309364618785725
- Kobayashi, T., Orendurff, M. S., Hunt, G., Gao, F., LeCursi, N., Lincoln, L. S., & Foreman, K. B. (2018). The effects of an articulated ankle-foot orthosis with resistance-adjustable joints on lower limb joint kinematics and kinetics during gait in individuals post-stroke. Clinical Biomechanics, 59, 47–55.
- Kobayashi, T., Orendurff, M. S., Hunt, G., Lincoln, L., Gao, F., LeCursi, N., & Foreman, K. B. (2017). An Articulated Ankle–foot Orthosis With Adjustable Plantarflexion Resistance, Dorsiflexion Resistance and Alignment: A Pilot Study on Mechanical Properties and Effects on Stroke Hemiparetic Gait. Medical Engineering & Physics. https://doi.org/10.1016/j.medengphy.2017.02.012
- Kobayashi, T.; Singer, M.L.; Orendurff, M.S.; Gao, F.; Daly, W.K.; Foreman, K.B. The effect of changing plantarflexion resistive moment of an articulated ankle-foot orthosis on ankle and knee joint angles and moments while walking in patients post stroke. Clin. Biomech. 2015, 30, 775–780, doi:10.1016/j.clinbiomech.2015.06.014.
- Konttila, J., Siira, H., Kyngäs, H., Lahtinen, M., Elo, S., Kääriäinen, M., … & Mikkonen, K. (2018). . Healthcare professionals' competence in digitalisation: a systematic review. Journal of Clinical Nursing, 28(5-6). , 745-761. https://doi.org/10.1111/jocn.14710
- Krajňáková, V.; Rajťúková, V.; Hudák, R.; Živčák, J. A. PPLICATION O. F T. HE A. RTEC E. VA S. CANNER F. OR O. RTHOTICS I. N P. RACTICE. Lékař a technika - Clinician and Technology 2020, 49, 92–96, doi:10.14311/C. TJ.2019.3.04.
- Krishnamurthi, R., Feigin, V., Forouzanfar, M., Mensah, G., Connor, M., Bennett, D., … & Murray, C. (2013). . Global and regional burden of first-ever ischaemic and haemorrhagic stroke during 1990–2010: findings from the global burden of disease study 2010. The Lancet Global Health, 1(5). , e259-e281. https://doi.org/10.1016/s2214-109x(13). 70089-5
- Kumar, M. S. K., & Banwait, S. S. (2020). Reducing Cost of Walking W Ith Fused Deposition Modelling Rendering Point Cloud Data. International Journal of Innovative Technology and Exploring Engineering. https://doi.org/10.35940/ijitee.e2739.039520

- Kumar, A. (2021). . Current status of prosthetic and orthotic rehabilitation services in india: its issues and challenges. Frontiers in Health Informatics, 10(1). , 55. https://doi.org/10.30699/fhi.v10i1.258
- Kuo, Y. R., Fang, J. J., Wu, C. T., Lin, R. M., Su, P. F., & Lin, C. L. (2019). Analysis of a customized cervical collar to improve neck posture during smartphone usage: a comparative study in healthy subjects. European Spine Journal, 28(8), 1793–1803. https://doi.org/10.1007/s00586-019-06022-0
- Lazaridis, K., McAllister, T., Babovic-Vuksanovic, D., Beck, S., Borad, M., Bryce, A., … & Farrugia, G. (2014). . Implementing individualized medicine into the medical practice. American Journal of Medical Genetics Part C Seminars in Medical Genetics, 166(1). , 15-23. https://doi.org/10.1002/ajmg.c.31387
- Lee, H., Nam, Y., & Lee, K. (2015). . Development-assistance strategies for stroke in low- and middle-income countries. Journal of Korean Medical Science, 30(Suppl 2). , S139. https://doi.org/10.3346/jkms.2015.30.s2.s139
- Lee, S.Y.; Majid, Z.; Setan, H. 3. D Data Acquisition for Indoor Assets Using Terrestrial Laser Scanning. I. SPRS Annals of Photogrammetry, Remote Sensing and Spatial Information Sciences. I. I-2 W 2013, 1, 221–226.
- Lee, D. G., & Lee, G. (2022). Correlation Among Motor Function and Gait Velocity, and Explanatory Variable of Gait Velocity in Chronic Stroke Survivors. Physical Therapy Rehabilitation Science. https://doi.org/10.14474/ptrs.2022.11.2.181
- Lee, S.-H., Choi, C.-M., Lee, D., Lee, S.-H., Song, S., Pyo, S., Hong, S., & Lee, G. (2018). A Novel Hinged Ankle Foot Orthosis for Gait Performance in Chronic Hemiplegic Stroke Survivors: A Feasibility Study. Biomedical Engineering Letters. https://doi.org/10.1007/s13534-018-0074-3
- Lee, K. H., Kim, D. K., Cha, Y. H., Kwon, J. Y., Kim, D. H., & Kim, S. J. (2019). Personalized assistive device manufactured by 3D modelling and printing techniques. Disability and Rehabilitation: Assistive Technology, 14(5), 526–531. https://doi.org/10.1080/17483107.2018.1494217
- Liao, C., Zuo, Y., Xu, S., Law, R., & Zhang, M. (2023). . Dimensions of the health benefits of wellness tourism: a review. Frontiers in Psychology, 13. https://doi.org/10.3389/fpsyg.2022.1071578
- Lin Y. C, Lin K. W, Chen C. S. Evaluation of the walking performance between 3. D-printed and traditional fabricated ankle-foot orthoses— A prospective study. Gait Posture. 2017;57:366-367. doi:10.1016/j.gaitpost.2017.06.471
- Liu Z, Zhang P, Yan M, Xie Y, Huang G. Additive manufacturing of specific ankle-foot orthoses for persons after stroke: A preliminary study based on gait analysis data. Mathematical Biosciences and Engineering. 2019;16(6). :8134-8143. doi:10.3934/mbe.2019410
- Lowry, C. and Jin, A. (2020). . Improving the social relevance of experimental stroke models: social isolation, social defeat stress and stroke outcome in animals and humans. Frontiers in Neurology, 11. https://doi.org/10.3389/fneur.2020.00427

- Lu, M. and Zhan, X. (2018). . The crucial role of multiomic approach in cancer research and clinically relevant outcomes. The Epma Journal, 9(1). , 77-102. https://doi.org/10.1007/s13167-018-0128-8
- Lunsford C, Grindle G, Salatin B, Dicianno B. E. Innovations With 3-Dimensional Printing in Physical Medicine and Rehabilitation: A Review of the Literature. P. M and R. 2016;8(12). :1201-1212. doi:10.1016/j.pmrj.2016.07.003
- Machat, H.; Mazaux, J.M.; de Sèze, M.-P.; Rousseaux, M.; Daviet, J.-C.; Bonhomme, C.; Burguete, E. Effect of early compensation of distal motor deficiency by the Chignon ankle-foot orthosis on gait in hemiplegic patients: a randomized pilot study. Clin. Rehabil. 2011, 25, 989–998, doi:10.1177/0269215511410730.
- Maeda, N., Kato, J., Azuma, Y., Okuyama, S., Yonei, S., Murakami, M., & Shimada, T. (2009). Energy Expenditure and Walking Ability in Stroke Patients: Their Improvement by Ankle-Foot Orthoses. Isokinetics and Exercise Science. https://doi.org/10.3233/ies-2009-0333
- Magnani M, Douglass M, Schroder W, Reeves J, Braun D. R. The Digital Revolution to Come: Photogrammetry in Archaeological Practice. Am Antiq. 2020;85(4). :737-760. doi:10.1017/aaq.2020.59
- Magnusson, L., Shangali, H., & Ahlström, G. (2016). . Graduates' perceptions of prosthetic and orthotic education and clinical practice in tanzania and malawi. African Journal of Disability, 5(1). . https://doi.org/10.4102/ajod.v5i1.142
- Martín-Montal, J., Pernas-Sánchez, J., & Varas, D. (2021). . Experimental characterization framework for sla additive manufacturing materials. Polymers, 13(7). , 1147. https://doi.org/10.3390/polym13071147
- Mavroidis, C.; Ranky, R.G.; Sivak, M.L.; Patritti, B.L.; DiPisa, J.; Caddle, A.; Gilhooly, K.; Govoni, L.; Sivak, S.; Lancia, M.; et al. Patient specific ankle-foot orthoses using rapid prototyping. J. Neuroeng. Rehabil. 2011, 8, 1–11, doi:10.1186/1743-0003-8-1.
- McDonald, C., Larbi, H., McCoy, S., & Kartin, D. (2020). . Information access and sharing among prosthetics and orthotics faculty in ghana and the united states. Prosthetics and Orthotics International, 45(2). , 123-130. https://doi.org/10.1177/0309364620958828
- McMulkin, M. L., & MacWilliams, B. A. (2015). Application of the gillette gait index, gait deviation index and gait profile score to multiple clinical pediatric populations. Gait & Posture, 41(2), 608–612.
- Meadmore, K., Hallewell, E., Freeman, C., & Hughes, A. (2018). . Factors affecting rehabilitation and use of upper limb after stroke: views from healthcare professionals and stroke survivors. Topics in Stroke Rehabilitation, 26(2). , 94-100. https://doi.org/10.1080/10749357.2018.1544845
- Medeiros, E., Doraiswamy, H., Berger, M., & Silva, C. (2014). . Using physically based rendering to benchmark structured light scanners. Computer Graphics Forum, 33(7). , 71-80. https://doi.org/10.1111/cgf.12475
- Melchels, F.P.W.; Feijen, J.; Grijpma, D.W. A review on stereolithography and its applications in biomedical engineering. Biomaterials 2010, 31, 6121–6130.

- Menz H. B, Morris M. E, Lord S. R. Foot and Ankle Characteristics Associated With Impaired Balance and Functional Ability in Older People.; 2005. https://academic.oup.com/biomedgerontology/article/60/12/1546/558012
- Mo, S., Leung, S. H. S., Chan, Z. Y. S., Sze, L. K. Y., Mok, K. M., Yung, P. S. H., Ferber, R., & Cheung, R. T. H. (2019). The biomechanical difference between running with traditional and 3D printed orthoses. Journal of Sports Sciences, 37(19), 2191–2197. https://doi.org/10.1080/02640414.2019.1626069
- Moher, D.; Liberati, A.; Tetzlaff, J.; Altman, D.G. Preferred Reporting Items for Systematic Reviews and Meta-Analyses: The P. RISMA Statement. P. LoS Med. 2009, 89, e1000097, doi:10.1371/journal.pmed.1000097.
- Mohanty, R. K., Behera, P., Sahoo, P. K., & Das, S. (2020). Clinical Efficacy of Different Ankle Foot Orthosis Design in Subjects With Foot Drop After Stroke: A Review and Comparison. Engineering and Scientific International Journal. https://doi.org/10.30726/esij/v7.i3.2020.73012
- Momosaki, R., Abo, M., Watanabe, S., Kakuda, W., Yamada, N., & Kinoshita, S. (2015). . Effects of ankle–foot orthoses on functional recovery after stroke: a propensity score analysis based on japan rehabilitation database. Plos One, 10(4). , e0122688. https://doi.org/10.1371/journal.pone.0122688
- Monaghan, K., Delahunt, E., & Caulfield, B. (2007). Increasing the number of gait trial recordings maximises intra-rater reliability of the CODA motion analysis system. Gait & Posture, 25(2), 303–315.
- Morouço, P. The Usefulness of Direct Digital Manufacturing for Biomedical Applications. Green Chem. Ser. 2018, 478–487.
- Morrissey, D., Cotchett, M., J'Bari, A. S., Prior, T. D., Vicenzino, B., Griffiths, I. B., Rathleff, M. S., Gülle, H., & Barton, C. J. (2020). Management of Plantar Heel Pain: A Best Practice Guide Synthesising Systematic Review With Expert Clinical Reasoning and Patient Values. https://doi.org/10.21203/rs.3.rs-36329/v1
- Mueller, B. Additive manufacturing technologies–Rapid prototyping to direct digital manufacturing. Assem. Autom. 2012.
- Mulroy, S. J., Eberly, V. J., Gronely, J. K., Weiss, W., & Newsam, C. J. (2010). Effect of AFO design on walking after stroke: impact of ankle plantar flexion contracture. Prosthetics and Orthotics International, 34(3), 277–292.
- Munhoz R, Moraes C. A da C, Tanaka H, Kunkel M. E. A digital approach for design and fabrication by rapid prototyping of orthosis for developmental dysplasia of the hip. Revista Brasileira de Engenharia Biomedica. 2016;32(1). :63-73. doi:10.1590/2446-4740.00316
- Murzac, R.; Doicin, C.V.; Ulmeanu, M.E. Data Acquisition and Generative Design for a Smart Spinal Orthosis. Macromol Symp 2021, 396, doi:10.1002/masy.202000297.
- Nam, H.-S.; Seo, C.H.; Joo, S.Y.; 김동현; Park, D.-S. The Application of Three-Dimensional Printed Finger Splints for Post Hand Burn Patients: A Case Series Investigation. Ann Rehabil Med 2018, doi:10.5535/arm.2018.42.4.634.

- Nam, Y. G., Ko, M. J., Bok, S.-K., Paik, N.-J., Lim, C.-Y., Lee, J., & Kwon, B. S. (2022). Efficacy of Electromechanical-Assisted Gait Training on Clinical Walking Function and Gait Symmetry After Brain Injury of Stroke: A Randomized Controlled Trial. Scientific Reports. https://doi.org/10.1038/s41598-022-10889-3
- Navarro-Martínez, O., Igual-García, J., & Traver-Salcedo, V. (2023). . Bridging the educational gap in terms of digital competences between healthcare institutions' demands and professionals' needs. B. MC Nursing, 22(1). . https://doi.org/10.1186/s12912-023-01284-y
- Netten, J., Jarl, G., Postema, K., & Williams, A. (2020). . A toolkit for prosthetists and orthotists to facilitate progress in professional communication over the next 50 years. Prosthetics and Orthotics International, 44(6). , 408-415. https://doi.org/10.1177/0309364620962325
- Ngo, T.D.; Kashani, A.; Imbalzano, G.; Nguyen, K.T.Q.; Hui, D. Additive manufacturing (3. D printing). : A review of materials, methods, applications and challenges. Compos. Part B Eng. 2018, 143, 172–196.
- Nishimwe, A., Mbarushimana, V., Ngenzi, J., & Nyssen, M. (2016). . Assessment of health informatics competencies in undergraduate training of healthcare professionals in rwanda. Rwanda Journal, 3(1). , 36. https://doi.org/10.4314/rj.v3i1.6f
- Okçu, M., Tuncay, F., Koçak, F., D. OĞRU, Y., GÜNGÖR, Z., & K. AYA, S. (2022). . Factors affecting compliance with lower and upper extremity orthoses in patients with disability due to neurological diseases. Fiziksel Tıp Ve Rehabilitasyon Bilimleri Dergisi, 25(2). , 240-247. https://doi.org/10.31609/jpmrs.2021-86851
- Olsson, A.; Hellsing, M.S.; Rennie, A.R. New possibilities using additive manufacturing with materials that are difficult to process and with complex structures. Phys. Scr. 2017, 92, 53002.
- Oosterwaal M, Telfer S, Tørholm S, et al. Generation of subject-specific, dynamic, multisegment ankle and foot models to improve orthotic design: A feasibility study. B. MC Musculoskelet Disord. 2011;12. doi:10.1186/1471-2474-12-256
- Ormond, K. and Cho, M. (2014). . Translating personalized medicine using new genetic technologies in clinical practice: the ethical issues. Personalized Medicine, 11(2). , 211-222. https://doi.org/10.2217/pme.13.104
- Oud, T.; Tuijtelaars, J.; Bogaards, H.; Nollet, F.; Brehm, M.-A. Preliminary Effectiveness of 3d-Printed Orthoses in Chronic Hand Conditions: Study Protocol for a Non-Randomised Interventional Feasibility Study. B. MJ Open 2023, doi:10.1136/bmjopen-2022-069424.
- Ounpuu, S., Bell, K. J., Davis III, R. B., & DeLuca, P. A. (1996). An evaluation of the posterior leaf spring orthosis using joint kinematics and kinetics. Journal of Pediatric Orthopaedics, 16(3), 378–384.
- Page, M.J.; Moher, D. Evaluations of the Uptake and Impact of the Preferred Reporting Items for Systematic Reviews and Meta-Analyses (P. RISMA). Statement and Extensions: A Scoping Review. Systematic reviews 2017, 6, 1–14.
- Parry, E.J.; Best, J.M.; Banks, C.E. Three-Dimensional (3. D). Scanning and Additive Manufacturing (A. M). Allows the Fabrication of Customised Crutch Grips. Mater Today Commun 2020, 25, 101225, doi:10.1016/j.mtcomm.2020.101225.

- Patar, A.; Jamlus, N.; Makhtar, K.; Mahmud, J.; Komeda, T. Development of dynamic ankle foot orthosis for therapeutic application. Procedia Eng. 2012, 41, 1432–1440, doi:10.1016/j.proeng.2012.07.332.
- Pau, M., Coghe, G., Atzeni, C., Corona, F., Pilloni, G., Marrosu, M. G., Cocco, E., & Galli, M. (2014). Novel characterization of gait impairments in people with multiple sclerosis by means of the gait profile score. Journal of the Neurological Sciences, 345(1–2), 159–163.
- Pérez Pico, A. M., Marcos Tejedor, F., de Cáceres Orellana, L. C., de Cáceres Orellana, P., & Mayordomo, R. (2023). Using Photogrammetry to Obtain 3D-Printed Positive Foot Casts Suitable for Fitting Thermoconformed Plantar Orthoses. Processes, 11(1). https://doi.org/10.3390/pr11010024
- Perry, J., Garrett, M., Gronley, J. K., & Mulroy, S. J. (1995). Classification of walking handicap in the stroke population. Stroke, 26(6), 982–989.
- Pons, C., Brochard, S., Gallien, P., Nicolas, B., Duruflé, A., Roquet, M., … & Garlantézec, R. (2016). . Medication, rehabilitation and health care consumption in adults with cerebral palsy: a population based study. Clinical Rehabilitation, 31(7). , 957-965. https://doi.org/10.1177/0269215516663286
- Powers, O., Palmer, J., & Wilken, J. (2021). . Reliability and validity of 3d limb scanning for ankle-foot orthosis fitting. Prosthetics and Orthotics International, 46(1). , 84-90. https://doi.org/10.1097/pxr.0000000000000066
- Pribanić, T.; Petković, T.; Đonlić, M.; Hrgetić, V. On Fabrication of a Shoe Insole: 3. D Scanning Using a Smartphone. In I. FMBE Proceedings; 2019; Vol. 64, pp. 111–116 I. SBN 9789811045042.
- Prosser, L.A.; Curatalo, L.A.; Alter, K.E.; Damiano, D.L. Acceptability and potential effectiveness of a foot drop stimulator in children and adolescents with cerebral palsy. Dev. Med. Child Neurol. 2012, 54, 1044–1049.
- Ranaldo, D.; Zonta, F.; Florian, S.; Lazzaro, J. A Facile, Semi-Automatic Protocol for the Design and Production of 3. D Printed, Anatomical Customized Orthopedic Casts for Forearm Fractures. J Clin Orthop Trauma 2023, 42, doi:10.1016/j.jcot.2023.102206.
- Ranz, E.C.; Russell Esposito, E.; Wilken, J.M.; Neptune, R.R. The influence of passive-dynamic ankle-foot orthosis bending axis location on gait performance in individuals with lower-limb impairments. 2016, 37, 13–21, doi:10.1016/j.clinbiomech.2016.05.001.
- Rao, N., Wening, J., Hasso, D., Gnanapragasam, G., Perera, P., Srigiriraju, P., … & Aruin, A. (2014). . The effects of two different ankle-foot orthoses on gait of patients with acute hemiparetic cerebrovascular accident. Rehabilitation Research and Practice, 2014, 1-7. https://doi.org/10.1155/2014/301469
- Rasenberg, N., Riel, H., Rathleff, M., Bierma-Zeinstra, S., & Middelkoop, M. (2018). . Efficacy of foot orthoses for the treatment of plantar heel pain: a systematic review and meta-analysis. British Journal of Sports Medicine, 52(16). , 1040-1046. https://doi.org/10.1136/bjsports-2017-097892

- Ricardo, D., Raposo, M. R., Veloso, A., & João, F. (2022). The gait profile score to assess the effects of ankle-foot orthoses in the gait of children with cerebral palsy. Gait & Posture, 97, S204–S205.
- Ries, A.J.; Novacheck, T.F.; Schwartz, M.H. The Efficacy of Ankle-Foot Orthoses on Improving the Gait of Children With Diplegic Cerebral Palsy: A Multiple Outcome Analysis. P. M R 2015, 7, 922–929, doi:10.1016/j.pmrj.2015.03.005.
- Roberts, A.; Wales, J.; Smith, H.; Sampson, C.J.; Jones, P.; James, M. A Randomised Controlled Trial of Laser Scanning and Casting for the Construction of Ankle–Foot Orthoses. Prosthet Orthot Int 2016, 40, 253–261.
- Roberts, M., Mensah, G., & Khoury, M. (2019). . Leveraging implementation science to address health disparities in genomic medicine: examples from the field. Ethnicity & Disease, 29(Suppl 1). , 187-192. https://doi.org/10.18865/ed.29.s1.187
- Rogati, G.; Leardini, A.; Ortolani, M.; Caravaggi, P. Validation of a Novel Kinect-Based Device for 3. D Scanning of the Foot Plantar Surface in Weight-Bearing. J Foot Ankle Res 2019, 12, 1–8, doi:10.1186/s13047-019-0357-7.
- Roucoules, L.; Paredes, M.; Eynard, B.; Camo, P.M.; Rizzi, C. Advances on Mechanics, Design Engineering and Manufacturing I. II: Proceedings of the International Joint Conference on Mechanics, Design Engineering & Advanced Manufacturing, J. CM 2020, June 2-4, 2020; Springer Nature, 2021; I. SBN 3030705668.
- Sabyrov, N.; Sotsial, Z.; Abilgaziyev, A.; Adair, D.; Ali, H. Design of a Flexible Neck Orthosis on Fused Deposition Modeling Printer for Rehabilitation on Regular Usage. In Proceedings of the Procedia Computer Science; Elsevier B.V., 2021; Vol. 196, pp. 226–234.
- Saenger, A. and Christenson, R. (2010). . Stroke biomarkers: progress and challenges for diagnosis, prognosis, differentiation, and treatment. Clinical Chemistry, 56(1). , 21-33. https://doi.org/10.1373/clinchem.2009.133801
- Salvi, J.; Fernandez, S.; Pribanic, T.; Llado, X. A State of the Art in Structured Light Patterns for Surface Profilometry. Pattern Recognit 2010, 43, 2666–2680, doi:10.1016/j.patcog.2010.03.004.
- Sansoni, G.; Trebeschi, M.; Docchio, F. State-of-the-Art and Applications of 3. D Imaging Sensors in Industry, Cultural Heritage, Medicine, and Criminal Investigation. Sensors 2009, 9, 568–601.
- Sarma, T.; Pandey, D.; Sahai, N.; Tewari, R.P. Material selection and development of ankle foot orthotic device. Mater. Today Proc. 2019, 18, 2509–2514, doi:10.1016/j.matpr.2019.07.107.
- Schrank, E.S.; Stanhope, S.J. Dimensional accuracy of ankle-foot orthoses constructed by rapid customization and manufacturing framework. J. Rehabil. Res. Dev. 2011, 48, 31–42, doi:10.1682/J. RRD.2009.12.0195.
- Schweizer, K., Romkes, J., Coslovsky, M., & Brunner, R. (2014). The influence of muscle strength on the gait profile score (GPS) across different patients. Gait & Posture, 39(1), 80–85.
- Servi, M.; Volpe, Y.; Uccheddu, F.; Furferi, R.; Governi, L.; Lazzeri, S. A Preliminary Usability Assessment of a 3. D Printable Orthosis Design System. In Proceedings of the International Conference on Human-Computer Interaction; Springer, 2018; pp. 273–280.

- Shih A, Park D. W, Yang Y. Y, Chisena R, Wu D. Cloud-based Design and Additive Manufacturing of Custom Orthoses. In: Procedia C. IRP. Vol 63. Elsevier B.V.; 2017:156-160. doi:10.1016/j.procir.2017.03.355
- Silva, R. (2023). Innovative Design and Development of Personalized Ankle-Foot Orthoses for Stroke Survivors With Equinovarus Foot: A Feasibility and Comparative Trial Protocol (Preprint). https://doi.org/10.2196/preprints.52365
- Silva, R., Morouço, P., & Veloso, A. (2019). Desenvolvimento de um sistema one-shot de baixo custo para aquisição de modelos 3D. Proceedings Do 8o Congresso Nacional de Biomecânica, 239–240.
- Silva R, Veloso A, Alves N, Fernandes C, Morouço P. A Review of Additive Manufacturing Studies for Producing Customized Ankle-Foot Orthoses. Bioengineering. 2022;9(6). . doi:10.3390/bioengineering9060249
- Simpkins, A., Janowski, M., Oz, H., Roberts, J., Bix, G., Doré, S., … & Stowe, A. (2019). . Biomarker application for precision medicine in stroke. Translational Stroke Research, 11(4). , 615-627. https://doi.org/10.1007/s12975-019-00762-3
- Skaaret, I.; Steen, H.; Terjesen, T.; Holm, I. Impact of ankle-foot orthoses on gait 1 year after lower limb surgery in children with bilateral cerebral palsy. Prosthet. Orthot. Int. 2019, 43, 12–20, doi:10.1177/0309364618791615.
- Spaulding, S., Yamane, A., McDonald, C., & Spaulding, S. (2019). . A conceptual framework for orthotic and prosthetic education. Prosthetics and Orthotics International, 43(4). , 369-381. https://doi.org/10.1177/0309364619852455
- Speciali, D. S., Oliveira, E. M., Cardoso, J. R., Correa, J. C. F., Baker, R., & Lucareli, P. R. G. (2014). Gait profile score and movement analysis profile in patients with Parkinson's disease during concurrent cognitive load. Brazilian Journal of Physical Therapy, 18, 315–322.
- Struck, R., Cordoni, S., Aliotta, S., Pérez-Pachón, L., & Gröning, F. (2019). . Application of photogrammetry in biomedical science., 121-130. https://doi.org/10.1007/978-3-030-06070-1_10
- Swinnen, E., Lafosse, C., Nieuwenhoven, J., Ilsbroukx, S., Beckwée, D., & Kerckhofs, E. (2017). . Neurological patients and their lower limb orthotics. Prosthetics and Orthotics International, 41(1). , 41-50. https://doi.org/10.1177/0309364615592696
- Tang, H.-H.; Chiu, M.-L.; Yen, H.-C. Slurry-based selective laser sintering of polymer-coated ceramic powders to fabricate high strength alumina parts. J. Eur. Ceram. Soc. 2011, 31, 1383–1388.
- Telfer, S., Abbott, M., Steultjens, M. P. M., & Woodburn, J. (2013a). Dose-response effects of customised foot orthoses on lower limb kinematics and kinetics in pronated foot type. Journal of Biomechanics, 46(9), 1489–1495. https://doi.org/10.1016/j.jbiomech.2013.03.036
- Telfer, S., Abbott, M., Steultjens, M., Rafferty, D., & Woodburn, J. (2013b). Dose-response effects of customised foot orthoses on lower limb muscle activity and plantar pressures in pronated foot type. Gait and Posture, 38(3), 443–449. https://doi.org/10.1016/j.gaitpost.2013.01.012

- Telfer, S.; Pallari, J.; Munguia, J.; Dalgarno, K.; McGeough, M.; Woodburn, J. Embracing additive manufacture: Implications for foot and ankle orthosis design. B. MC Musculoskelet. Disord. 2012, 13, doi:10.1186/1471-2474-13-84.
- Teng, Y., Lou, S., Lin, C., Chen, F., & Yeung, K. (2014). . User satisfaction with orthotic devices and service in taiwan. Plos One, 9(10). , e110661. https://doi.org/10.1371/journal.pone.0110661
- Totah, D.; Kovalenko, I.; Saez, M.; Barton, K. Manufacturing Choices for Ankle-Foot Orthoses: A Multi-objective Optimization. Procedia C. IRP 2017, 65, 145–150, doi:10.1016/j.procir.2017.04.014.
- Townsend, E.L.; Tamhane, H.; Gross, K.D. Effects of A. FO Use on Walking in Boys With Duchenne Muscular Dystrophy: A Pilot StudyA Pilot Study. Pediatr. Phys. Ther. 2015, 27, 24–29.
- Tyson, S. F., Sadeghi-Demneh, E., & Nester, C. J. (2013). A systematic review and meta-analysis of the effect of an ankle-foot orthosis on gait biomechanics after stroke. Clinical Rehabilitation, 27(10), 879–891.
- Tyson, S. and Kent, R. (2013). . Effects of an ankle-foot orthosis on balance and walking after stroke: a systematic review and pooled meta-analysis. Archives of Physical Medicine and Rehabilitation, 94(7). , 1377-1385. https://doi.org/10.1016/j.apmr.2012.12.025
- Vasiliauskaite, E.; Ielapi, A.; De Beule, M.; Van Paepegem, W.; Deckers, J.P.; Vermandel, M.; Forward, M.; Plasschaert, F. A study on the efficacy of A. FO stiffness prescriptions. Disabil. Rehabil. Assist. Technol. 2019, 0, 1–13, doi:10.1080/17483107.2019.1629114.
- Verma, R., Arya, K. N., Sharma, P., & Garg, R. K. (2012). Understanding gait control in post-stroke: implications for management. Journal of Bodywork and Movement Therapies, 16(1), 14–21.
- Voisin, S., Foufou, S., Truchetet, F., Page, D., & Abidi, M. (2007). . Study of ambient light influence for three-dimensional scanners based on structured light. Optical Engineering, 46(3). , 030502.
- Volonghi, P.; Baronio, G.; Signoroni, A. 3. D Scanning and Geometry Processing Techniques for Customised Hand Orthotics: An Experimental Assessment. Virtual Phys Prototyp 2018, 13, 105–116, doi:10.1080/17452759.2018.1426328.
- Vos T, Allen C, Arora M, et al. Global, regional, and national incidence, prevalence, and years lived with disability for 310 diseases and injuries, 1990–2015: a systematic analysis for the Global Burden of Disease Study 2015. The Lancet. 2016;388(10053). :1545-1602. doi:10.1016/S0140-6736(16). 31678-6
- Wada, Y., Otaka, Y., Mukaino, M., Tsujimoto, Y., Shiroshita, A., Kawate, N., … & Taito, S. (2021). . The effect of ankle-foot orthosis on ankle kinematics in individuals after stroke: a systematic review and meta-analysis. Pm&r, 14(7). , 828-836. https://doi.org/10.1002/pmrj.12687
- Wang, K., Shi, Y., He, W., Yuan, J., Li, Y., Pan, X., & Zhao, C. (2018). The research on 3D printing fingerboard and the initial application on cerebral stroke patient's hand spasm. BioMedical Engineering Online, 17(1). https://doi.org/10.1186/s12938-018-0522-4

- Wang, R.-Y., Yen, L.-L., Lee, C.-C., Lin, P.-Y., Wang, M.-F., & Yang, Y.-R. (2005). Effects of an ankle-foot orthosis on balance performance in patients with hemiparesis of different durations. Clinical Rehabilitation, 19(1), 37–44.
- Wang, Y., Tang, R., Wang, H., Yu, X., Li, Y., Wang, C., Wang, L., & Qie, S. (2022). The Validity and Reliability of a New Intelligent Three-Dimensional Gait Analysis System in Healthy Subjects and Patients with Post-Stroke. Sensors, 22(23). https://doi.org/10.3390/s22239425
- Ward A. B. Managing spastic foot drop after stroke. Eur J Neurol. 2014;21(8). :1053-1054. doi:10.1111/ene.12404
- Weigert, M.C.; Poier, P.H.; Rosenmann, G.C.; Foggiatto, J.A.; Volpato, N.; Okimoto, M.L.L.R. Indirect 3. D Scanning of the Foot Plant - Comparison between a Medium and Low-Cost Tools. Advances in Transdisciplinary Engineering 2016, 4, 614–621, doi:10.3233/978-1-61499-703-0-614.
- Wells, J.C.K. Three-Dimensional Optical Scanning for Clinical Body Shape Assessment Comes of Age. Am J Clin Nutr 2019, 110, 1272–1274, doi:10.1093/ajcn/nqz258.
- Wierzbicka, N.; Górski, F.; Wichniarek, R.; Kuczko, W. Prototyping of Individual Ankle Orthosis Using Additive Manufacturing Technologies. Adv. Sci. Technol. Res. J. 2017, 11, 283–288, doi:10.12913/22998624/76070.
- Wilkins, R., Chapman, L., Emmel, J., Flannery, T., Chapman, G., Walwyn, R., … & Siddle, H. (2022). . A systematic review and narrative synthesis of footwear and orthotic devices used in the management of ankle haemarthrosis and haemarthropathy in haemophilia. Haemophilia, 28(3). , 422-436. https://doi.org/10.1111/hae.14521
- Williams, J. and Butters, J. (1991). . A population-based planning approach to professional dental education. Journal of Continuing Education in the Health Professions, 11(1). , 29-41. https://doi.org/10.1002/chp.4750110105
- Wong, K. V; Hernandez, A. A review of additive manufacturing. Int. Sch. Res. Not. 2012, 2012.
- Woodcock, J. (2007). . Molecular medicine: how, what, and when?. Clinical Pharmacology & Therapeutics, 82(4). , 376-378. https://doi.org/10.1038/sj.clpt.6100349
- Wojciechowski, E., Chang, A. Y., Balassone, D., Ford, J., Cheng, T. L., Little, D., Menezes, M. P., Hogan, S., & Burns, J. (2019). Feasibility of designing, manufacturing and delivering 3D printed ankle-foot orthoses: A systematic review. In Journal of Foot and Ankle Research (Vol. 12, Issue 1). BioMed Central Ltd. https://doi.org/10.1186/s13047-019-0321-6
- Wren, T.A.L.; Dryden, J.W.; Mueske, N.M.; Dennis, S.W.; Healy, B.S.; Rethlefsen, S.A. Comparison of 2 Orthotic Approaches in Children With Cerebral Palsy. Pediatr. Phys. Ther. 2015, 27, 218–226, doi:10.1097/pep.0000000000000153.
- Yamamoto, S. (2014). Gait Changes in a Hemiplegic Patient Using an Ankle-Foot Orthosis With an Oil Damper: A Case Report. Clinical Research on Foot & Ankle. https://doi.org/10.4172/2329-910x.1000136
- Yamamoto, S., Tanaka, S., & Motojima, N. (2018). Comparison of ankle–foot orthoses with plantar flexion stop and plantar flexion resistance in the gait of stroke patients: A randomized controlled trial. Prosthetics and Orthotics International, 42(5), 544–553.

- Yan, T., Chopp, M., & Chen, J. (2015). . Experimental animal models and inflammatory cellular changes in cerebral ischemic and hemorrhagic stroke. Neuroscience Bulletin, 31(6). , 717-734. https://doi.org/10.1007/s12264-015-1567-z
- Yeung, S. (2013). . Do orthotics work as an injury prevention strategy for the military? a systematic review. Physical Therapy Reviews, 18(1). , 49-50. https://doi.org/10.1179/1743288x12y.0000000037
- Zarezadeh, R., Arazpour, M., & Aminian, G. (2022). . The effect of anterior ankle-foot orthosis and posterior ankle-foot orthosis on functional ambulation in stroke patients. Journal of Rehabilitation and Assistive Technologies Engineering, 9, 205566832210824. https://doi.org/10.1177/20556683221082451
- Zhang M, Davies C, Xie S. Effectiveness of robot-assisted therapy on ankle rehabilitation-a systematic review. J Neuroeng Rehabil. 2013;10(1). :1-16. http://www.jneuroengrehab.com/content/10/1/30
- Zhang, Q., Liao, Y., Liu, Z., Dai, Y., Li, Y., & Tang, Y. (2020). . Interleukin-17 and ischaemic stroke. Immunology, 162(2). , 179-193.
- Zheng, Y., Liu, G., Yu, L., Wang, Y., Fang, Y., Shen, Y., Huang, X., Qiao, L., Yang, J., Zhang, Y., & Hua, Z. (2020). Effects of a 3D-printed orthosis compared to a low-temperature thermoplastic plate orthosis on wrist flexor spasticity in chronic hemiparetic stroke patients: a randomized controlled trial. Clinical Rehabilitation, 34(2), 194–204. https://doi.org/10.1177/0269215519885174
- Zuccarino, R.; Anderson, K.M.; Shy, M.E.; Wilken, J.M. Satisfaction with Ankle Foot Orthoses in Individuals with Charcot-Marie-Tooth. Muscle Nerve 2020.
- van der Linden, M.L.; Andreopoulou, G.; Scopes, J.; Hooper, J.E.; Mercer, T.H. Ankle kinematics and temporal gait characteristics over the duration of a 6-minute walk test in people with multiple sclerosis who experience foot Drop. Rehabil. Res. Pract. 2018, 2018.

IX. Other Publications (Conference Papers and Secondary Publications)

Conference Paper 1

Development of a low-cost one-shot system for acquiring 3D models

Authors: **Rui Silva,** Pedro Morouço, Nuno Alves and António Veloso

Abstract
The objective of this study was to compare two 3D scanner systems. A box with predefined measurements was used as the study object, and the Sense 3D system and a system developed by the authors, consisting of 16 RaspBerry Pi Module V2 cameras for obtaining the 3D virtual object, were employed. Five variables were selected for this pilot study: virtual length, virtual width, mesh, object texture, and average deviation between models through overlay. Differences were found when comparing the two systems for mesh, object texture, and average deviation through overlay. Further studies are needed, including comparisons with other 3D scanner systems, to better understand the advantages of using a one-shot photogrammetry system for obtaining 3D models.

Keywords: Orthoses, 3D scanner, meshes, 3D models

Introduction
Orthoses are medical devices used to enhance performance in individuals with difficulties and/or disabilities [1]. Widely prescribed to address various pathologies, custom orthoses are widely recognized for their medical functionality and the comfort they provide, allowing patients to use them continuously during the recommended treatment period. The adaptation of the geometric shape to the patient allows for greater efficiency in immobilization or restriction of movement. To obtain the patient's geometric shape, increasingly different methods of obtaining three-dimensional contactless information are used, which can be simplified into triangulation and photometry.

Among triangulation-based techniques are photogrammetry, structured light projection, and laser line scanning. Projection techniques (structured light or laser scanning) enable the determination of depth (distance relative to the image formation plane) from a single image. The knowledge of the spatial position of the laser beam or a lighting pattern, along with image formation parameters, resolves the ambiguity present in the two-dimensional image. Photogrammetry uses the correspondence between points in different views of the same scene to infer the position of that point in space, thus always requiring two or more views [2].

The study's objective is to compare an existing market system that uses structured light technology with a low-cost one-shot system developed by the authors, utilizing photogrammetry techniques.

Materials and Methods

A study was conducted using a box measuring 120mm x 75mm, measured with a Neiko 01407A digital caliper (Neiko Tools USA, La Porte, Indiana, USA). For result comparison, two types of 3D image capture scanners with different capture methods were used. The Sense 3D Scanner system (3D Systems, South Carolina, USA), which utilizes structured light, and a photogrammetry system with 16 Raspberry Pi Module V2 8MP cameras (Raspberry Pi Foundation, Cambridge, United Kingdom). Each camera was connected to a Single Board Computer (SBC) Raspberry Pi 3 Model B+ 1Gb (Raspberry Pi Foundation, Cambridge, United Kingdom), synchronized and networked.

For capturing the 3D model of the box using the Sense 3D, proprietary Sense software from 3D Systems was employed. For the Raspberry Pi system, 16 photos were taken in a single shot, and the 3D model was created using RealityCapture software (CapturingReality, Bratislava, Slovakia). Both 3D models in .obj format were then analyzed using 3D Builder software (Microsoft, Washington, USA) for comparison of length, width, and textures, and Geomagic Studio 12 software (3D Systems, South Carolina, USA) for mesh analysis and the deviation between models through overlay.

Results and Discussion

Using the 3D Builder software, tests were conducted to obtain the difference in virtual sizes for comparison with the real sizes. The 3D model extracted from the Sense 3D yielded a box length of 120.94 mm and a width of 75.10 mm, while the model from the Raspberry Pi system resulted in a length of 120.13 mm and a width of 74.97 mm, being closer in terms of both length and width to the actual box measurement. For the texture test, as indicated in Figure 1, visible differences are observed in both color and resolution. In the Raspberry Pi test, a texture with a color closer to the real value of the box was obtained, allowing for the legibility of all text on the surface.

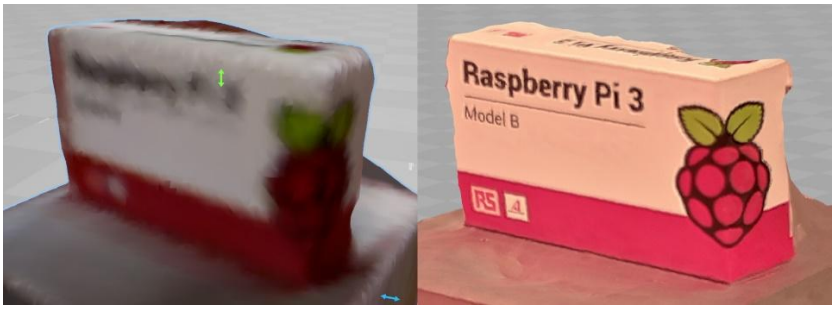

FIGURE 1 - Comparison of textures between the Sense 3D system (left) and Raspberry Pi (right).

For the mesh study, the triangle count on the front face for the Raspberry Pi system was 545% higher than that found in the Sense 3D system (28318 triangles vs. 5196 triangles). No filters, cleaning, or mesh repair were applied to either model, and these values were directly extracted from the initially created file. The higher number of triangles indicates greater image resolution, translating to more surface information. The deviation test between models through model overlay, as indicated in Figure 2, shows an average deviation between models of 1mm, reaching a maximum of 3mm in the lower area of the surface. The deviation in the lower area is explained by being the region where the object intersects with the supporting surface. The Sense 3D system does not recognize the surface change, merging them and creating a rounded surface between them, leading to the disappearance of the contact edge.

In addition to being able to capture a complete 3D model with a single shot in less than 1 second, the mesh and texture quality are much superior in the Raspberry Pi system compared to the Sense 3D system. Further studies are necessary, involving different variables, objects, and various systems to better understand the advantages of this system for future Full Body 3D scans of the human body.

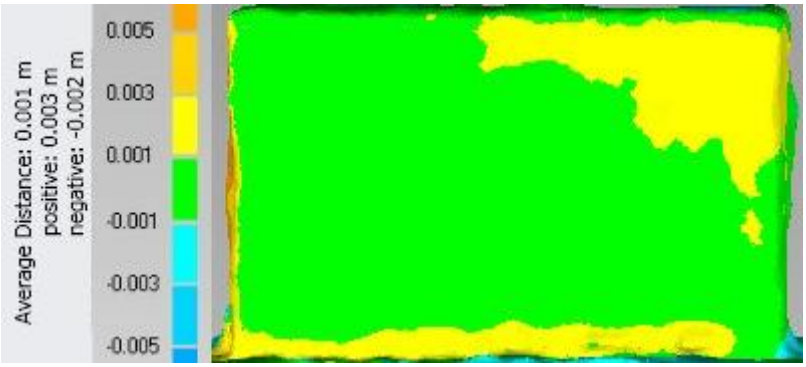

FIGURE 2 - Spectrum of the average deviation of the object between the Sense 3D system and Raspberry Pi.

References

[1] Faustini, M. C., Neptune, R. R., Crawford, R. H., & Stanhope, S. J. (2008). Manufacture of passive dynamic ankle–foot orthoses using selective laser sintering. IEEE transactions on biomedical engineering, 55(2), 784-790.

[2] Langguth, F., Sunkavalli, K., Hadap, S., & Goesele, M. (2016, October). Shading-aware multi-view stereo. In European Conference on Computer Vision (pp. 469-485). Springer, Cham.

Conference Paper 2

Photogrammetric Scanner for Lower Limbs

Authors: **Rui Silva,** Pedro Morouço, Nuno Alves, Artur Mateus and António Veloso

Abstract
Foot-Ankle Orthoses (AFOs) can be prescribed to improve a patient's quality of life. Nowadays, AFOs are constructed using molds with thermoplastic materials, leading to long waiting times and limited design options. Reverse engineering, particularly the use of 3D scanners, has the potential to address this issue, resulting in a faster and more economical construction solution. This study aims to construct a 3D scanner capable of employing photogrammetry techniques to capture the surface of a patient's leg and foot.

Keywords: Foot-Ankle Orthoses / Scanner / Photogrammetry

Introduction
The challenges in mobility present a significant barrier for both adults and children, where an Ankle-Foot Orthosis (AFO) may be prescribed to enhance the patient's quality of life. It is well-documented that this medical device can assist in various lower limb (LL) impairments. Currently, patients have the option to choose between standard AFOs and custom AFOs. The former is more cost-effective but may provide less comfort to the patient. On the other hand, custom AFOs can enhance comfort and be more suitable, but the manufacturing process is far from ideal.

Custom AFOs are typically handmade from a plaster cast of the patient's lower limb [1]. This negative impression is removed and filled with liquid plaster to form a positive model, which is manually modified by adding or removing plaster. Subsequently, thermoformed plastic is vacuum formed over the positive model using polypropylene. This traditional approach is labor-intensive, offers limited design options, is expensive, and is often associated with long waiting times, prompting the search for non-invasive alternatives for acquiring the patient's anatomical shape.

Reverse engineering is a method that can be explored, generally consisting of three steps: (1) scanning anatomical parts; (2) processing the acquired geometry; (3) manufacturing the device using additive manufacturing technologies. With the available 3D data acquisition technologies, optical scanning has proven to be the most suitable for manual data acquisition in terms of accuracy, resolution, patient safety, cost, speed, and efficiency [2]. The most relevant scanner requirements for orthoses include scanning time, as well as practicality and

versatility. In particular, as the target is a living being, the scan must be safe, fast, and comfortable, even at the expense of a (relatively and acceptable) loss of precision.

The different types of 3D scanners available are divided into photogrammetry, structured light, time of flight, and laser triangulation. Photogrammetry uses multiple 2D images taken from different positions of the object and triangulates different pixels in the images to discover their location in a three-dimensional space. This study aimed to develop a photogrammetric 3D scanner for the lower limbs of a human being.

Description

SolidWorks software (Dassault Systèmes®) was used for modeling and simulating the structure (Figure 1). The scanner was designed to achieve a surface scan of the patient's lower limb using photogrammetry techniques. In a previous study [3], employing 16 synchronized RaspBerry Pi units with 16 RaspBerry Pi Module V2 8MP cameras demonstrated the potential of this technology in quickly obtaining the surface to be used. The scanner will have 60 cameras positioned to capture a 360º model of the leg and foot in a single shot (including the sole).

Due to the limited mobility of many patients requiring AFOs, a robotic arm with 2 rotational degrees of freedom will be connected to an ergonomic chair for patient reception and positioning during the lower limb scan. The camera support structure will include a linear guide to position the cameras accurately, and for foot support, there will be a glass-built structure to minimize interference between the cameras and the limb being scanned. This structure will be removable and adjustable in height for correct patient positioning, allowing its use for both adults and children.

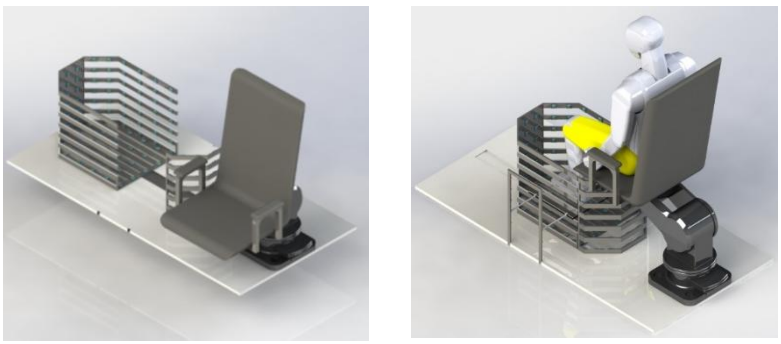

FIGURE 1 - 3D Scanner in the initial position (left) and final position for limb scanning (right).

Conclusions

Based on the conducted simulations, it was concluded that this design is functional and comfortable for the patient. It will be possible, through a single shot (<1s), to capture the necessary photographs for obtaining the complete 3D model for orthosis construction. The significant advantage of the speed in image acquisition will eliminate the issue present in other 3D scanner technologies, which require the patient to remain still for several minutes.

References

[1] A. Orthosis, "Manufacturing Guidelines for Ankle-Foot Orthosis," 2006, [Online]. Available: https://www.icrc.org/eng/assets/files/other/eng-afo-2010.pdf.

[2] A. M. J. Paterson, R. J. Bibb, and R. I. Campbell, "A review of existing anatomical data capture methods to support the mass customisation of wrist splints," Virtual Phys. Prototyp., vol. 5, no. 4, pp. 201–207, 2010.

[3] R. Silva, P. Morouço, and A. Veloso, "Desenvolvimento de um sistema one-shot de baixo custo para aquisição de modelos 3D," in Proceedings do 8o Congresso Nacional de Biomecânica, 2019, pp. 239–240.

Conference Paper 3

Flexible 3D Scanning Apparatus for Anatomic Applications: Concept and Preliminary Results

Authors: **Rui Silva,** António Veloso, Pedro Morouço and Nuno Alves

Abstract
Ankle-foot orthoses are prescribed to improve the Patient's quality of life. Supporting weak muscles or restraining spastic muscles, they lead to smoother and more stable locomotion. Commonly, these devices are handmade using thermoplastic vacuum forming, which becomes time-consuming and error prone. From another point-of-view, it is possible to use image-based techniques (e.g. computed tomography; magnetic resonance) to scan the human body, which help orthoses manufacturing, however, they are time-consuming and computed tomography induces radiation to the patient. To overcome these disadvantages, two novel photogrammetric 3D scanner was specifically designed to obtain anatomic surfaces of a patient´s body. Preliminary results of the full body scanner validate the concept that can lead to a faster and economic solution. Moreover, the concept of the second scanner to acquire the Ankle-foot anatomical shape is also presented.

Introduction
Walking is one of the most critical events in daily-living, and difficulty in walking is a significant barrier for both adults and children [1]. An Ankle-foot orthoses (AFO) can be prescribed to improve the patient's quality of life. It is well documented that this medical device can help with different impairments of the lower limbs (LL) [2–5]. Currently, patients can choose between standard AFO and custom AFO. The former are cheaper but may offer less patient comfort. On the other hand, custom AFO may increase this comfort and be more suitable, but the manufacturing process is far from ideal. Custom AFOs are usually handcrafted from a plaster cast of the patient's LL [6]. The negative print is removed and filled with liquid plaster to form a positive model, which is modified by manual addition or removal of plaster, followed by thermoplastic vacuum formation over the positive model with polypropylene. This traditional approach is labor-intensive, expensive, often associated with long waiting times and offers limited design options, which motivates the search for non-invasive alternatives for acquiring the patient's anatomical shape. To overcome these limitations, reverse engineering can be used following three steps: (1) digitization of anatomical parts; (2) processing of acquired geometry; (3) device fabrication using additive manufacturing technologies. With the available three-dimensional (3D) data acquisition technologies, the optical scanner has proven to be the most suitable for manual data acquisition in terms of accuracy, resolution, patient safety, cost, speed and efficiency [7]. The most relevant scanner requirements for

orthotics include scanning time as well as practicality and versatility. In particular, as the target is a living being, scanning must be safe, fast and comfortable, even at the expense of a (relative and acceptable) loss of accuracy. The different types of 3D scanners available are divided into photogrammetry, structured light, time of flight and triangulation laser. Photogrammetry uses several 2D images, taken at different positions of the object, and triangulates different pixels in the images to find their location in a 3D space. This study aimed to develop two photogrammetric 3D scanners to obtain anatomic surfaces of a patient´s body.

Development of Photogrammetric 3D Scanners

Solidworks (Dassault Systèmes®, France) software was used to model the prototype structures. Two prototypes were created. The first one, a full body scanner, was created to test the reliability and accuracy of using photogrammetry on a human body. This scanner (Figure 1) with an oval shape, was built using wood in the base, aluminum in the vertical bars and several 3D printed parts (also designed in Solidworks) to fix the custom printed circuit boards (PCB) and cameras (RaspBerry Pi Camera Module V2). The second scanner, a lower limb scanner, was created to specifically capture the leg, and foot (include sole) surface. This prototype was built using wood in the base, stainless steel in the core frame and several 3D printed parts to fix the PCB and cameras (Figure 2). To create the custom PCB, Altium Designer (Altium Limited®, Australia) software was used.

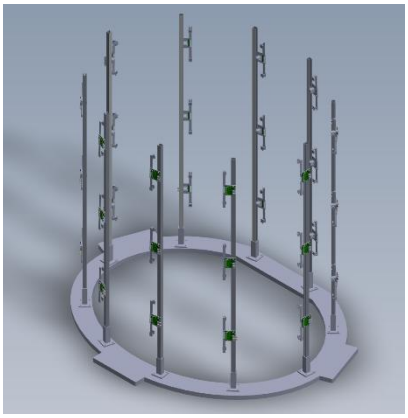

FIGURE 1 - Full body scanner prototype

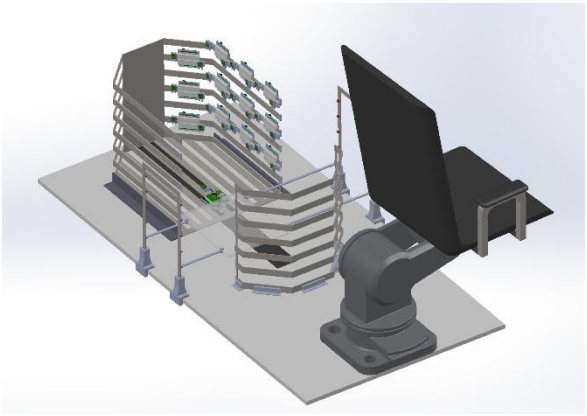

FIGURE 2 - Lower Limb scanner prototype

The scanners were designed to obtain a scan of the patient's body surface using the photogrammetry technique. In a previous study [8] using 16 RaspBerry Pi synchronized with 16 RaspBerry Pi Module V2 8MP cameras, which allowed us to understand the potential of this technology in quickly obtaining the surface to be used. The biggest problem found in that previous study was the quantity and organization of cables for power supply and data transmission from the RaspBerry Pi to the computer. So, a custom PCB with a RaspBerry Pi Zero processor core was designed and built (Figure 3) that allowed not only to connect 2 cameras to only 1 device, but also to connect all the PCB in parallel, solving the problem with the cables.

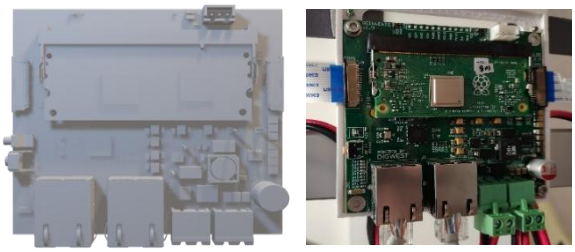

FIGURE 3 - Custom PCB with RaspBerry Pi Zero processor core with 2 cameras connectors (in), 2 RJ45 connectors (in and out) and 2 power connectors (in and out)

The full body scanner (Figure 4) has 60 cameras positioned in order to obtain the 360º model of the whole body, in a single shot. The first tests were already conducted with promising results (Figure 5).

FIGURE 4 - Full Body Scanner structure with 60 cameras

FIGURE 5 - 3D model without texture (left) and with texture (right)

To acquire the 3D model of the leg and foot (to create the AFO), with a Full Body scanner would be impossible to scan the structure of the sole of the foot. Furthermore, due to the mobility limitation of patients, the need to stand still while acquiring the shot was not practical. So, for the LL scanner, a robotic arm with 2 rotational degrees of freedom will be connected to an ergonomic chair for receiving and positioning the patient for LL scanning. This scanner (Figure 6) will have 60 cameras positioned in order to obtain the 360º model of the leg and foot (including the sole), in a single shot. The structure that supports the cameras will have a linear guide that will place the cameras in position and to support the foot there will be a structure built in glass for minimal noise between the cameras and the member to be scanned. This structure will be removable and adjustable in height for the correct positioning of the patient, being possible its use in adults and children.

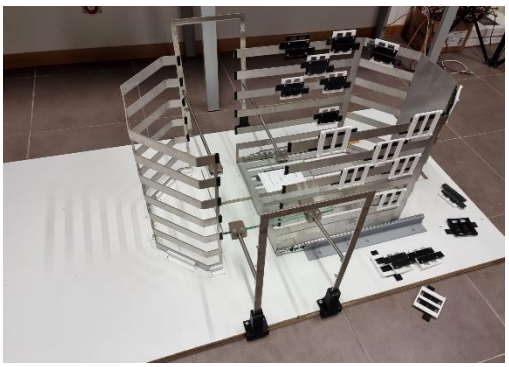

FIGURE 6 - Prototype of Lower limb Scanner

Conclusion

Through the simulations carried out, it was concluded that this design is functional and comfortable for the patient. It will be possible, through a single shot (<1s), take the required photographs to obtain the complete 3D model for the construction of an orthosis. The great advantage of fast body's surface acquisition will solve the problem existing in other 3D scanner technologies in which the patient is required to be immobile for several minutes.

References

[1] Inman VT, Ralston HJ, Todd F. Human walking. Williams & Wilkins; 1981.

[2] Wren TAL, Dryden JW, Mueske NM, Dennis SW, Healy BS, Rethlefsen SA. Comparison of 2 Orthotic Approaches in Children With Cerebral Palsy. Pediatric Physical Therapy 2015;27:218–26. https://doi.org/10.1097/pep.0000000000000153.

[3] Abd El-Kafy EM. The clinical impact of orthotic correction of lower limb rotational deformities in children with cerebral palsy: A randomized controlled trial. Clinical Rehabilitation 2014;28:1004–14. https://doi.org/10.1177/0269215514533710.
[4] Bennett BC, Russell SD, Abel MF. The effects of ankle foot orthoses on energy recovery and work during gait in children with cerebral palsy. Clinical Biomechanics 2012;27:287–91. https://doi.org/10.1016/j.clinbiomech.2011.09.005.
[5] Skaaret I, Steen H, Terjesen T, Holm I. Impact of ankle-foot orthoses on gait 1 year after lower limb surgery in children with bilateral cerebral palsy. Prosthetics and Orthotics International 2019;43:12–20. https://doi.org/10.1177/0309364618791615.
[6] Baronio G. A critical analysis of a hand orthosis reverse engineering and 3d printing process. Appl. Bion. Biomech. 2016, 8347478 (2016) n.d.
[7] Paterson AMJ, Bibb RJ, Campbell RI. A review of existing anatomical data capture methods to support the mass customisation of wrist splints. Virtual and Physical Prototyping 2010;5:201–7.
[8] Silva R, Morouço P, Veloso A. Desenvolvimento de um sistema one-shot de baixo custo para aquisição de modelos 3D. Proceedings do 8º Congresso Nacional de Biomecânica, 2019, p. 239–40.

Conference Paper 4

Impact Resistance of Additively Manufactured Polymeric Materials for Biomedical Applications

Authors: Rachel Habiba, Ana Amaro, Carla Moura, **Rui Silva**, Daniela Trindade, André Antão, Rui Martins, Cândida Malça and Ricardo Branco

Abstract

This paper studies the impact resistance of nine polymeric materials to be used in orthosis manufacturing. The study aims to understand the behavior of these materials under different conditions to improve their performance and durability. The materials were additive manufactured in both vertical and horizontal directions, and their impact properties were evaluated through Charpy pendulum impact tests.

The tests were conducted in air and wet environment to simulate native conditions, dry, and sweat, respectively. Results show that the impact resistance of the materials is influenced by material type, printing direction, and environmental conditions. Nylon 12 demonstrates superior impact resistance. ULTEM™ 9085 exhibited a clear anisotropic behavior with significantly different absorbed energy between the vertically and horizontally printed samples. The immersion in artificial sweat (wet environment) reduced the absorbed energy, which was more pronounced for longer immersion times. The fracture surface analysis revealed different failure mechanisms for the different materials ranging from ductile to brittle failure.

Introduction

Orthoses are medical devices designed to prevent, support, align, and improve the function of the human body [1]. Customization is key in orthosis manufacturing, as it allows for the adaptation of these devices to accommodate specific anatomical variations and activity levels [3]. Furthermore, orthoses must prioritize comfort, high quality, and durability to ensure optimal performance and patient satisfaction [3].

With the advance of additive manufacturing (AM) and the use of polymeric materials, orthosis production has undergone a significant transformation. AM techniques enable the creation of patient-adapted orthoses, customized to meet the unique needs of everyone [2, 3]. This approach also facilitates the integration of innovative materials and streamlines the fabrication of complex shapes, optimizing the design and manufacturing process. Polymeric materials show characteristics that make them particularly suitable for orthosis applications. Their flexibility allows for the creation of orthoses that conform to the body's contours, providing a comfortable and supportive fit [3]. Additionally, these materials are biocompatible, minimizing the risk of adverse reactions. The lightweight nature of polymeric

materials further enhances patient comfort and mobility, while their cost-effectiveness contributes to the accessibility and affordability of orthosis devices. The impact resistance of polymeric materials is a key point in biomedical applications, including orthoses. Understanding how these materials withstand sudden shocks or forces is vital to ensure the durability and performance of orthoses. Factors such as humidity, sweat, and environmental conditions may influence the materials behavior and affect their overall mechanical performance and durability. Through comprehensive testing and analysis, valuable insights can be gained to prevent and mitigate potential damages in the future. Nevertheless, there is little research in the literature regarding this topic.

This paper aims to investigate the impact resistance of nine polymeric materials produced by AM. The samples were printed in two directions, vertical and horizontal, and were evaluated in air and in wet environments. By studying the mechanical behavior and failure mechanisms of these materials, it will be possible to better understand their performance, durability, and suitability for orthosis applications. The findings of this research will contribute to the development of more effective and reliable orthoses, improving patient outcomes and quality of life. The paper is organized as follows. Section 2 presents the methodology employed to evaluate the impact resistance of polymeric materials. Section 3 presents and discusses the experimental results. The paper ends with some concluding remarks.

Materials and Methods

This investigation studies the impact resistance of nine polymer materials that were 3D printed in both vertical (V) and horizontal (H) directions. The materials studied were: Acrylonitrile Butadiene Styrene (ABS); NYLON 12; Polycarbonate (PC); PC ABS, Polyethylene Terephthalate Glycol (PETG); Polylactic Acid (PLA); Thermo-plastic Polyurethane (TPU); ULTEM™ 1010; and ULTEM™ 9085. Rectangular cross-section specimens (90 × 10 × 4 mm3) were used. Impact tests were performed in a Charpy pendulum impact testing machine, model Instron CEAST 9050, equipped with a 5 J hammer. Two environmental conditions were evaluated: (i) air; and (ii) immersion in artificial sweat (phosphate buffered saline with pH 6.3) for 30 days [4, 5]. Three specimens were tested for each condition, and the average absorbed energy was calculated. The samples immersed in artificial sweat were regularly monitored to evaluate mass changes which provided insights into the potential absorption of the solution

by the polymer materials. After the impact tests, the fracture surfaces of the different specimens were examined using optical microscopy. This evaluation aimed to identify the main failure mechanisms and understand how the different environmental conditions affected the mechanical behavior of the polymeric materials.

Results and Discussion

This section is organized into two subsections. Firstly, the impact tests are addressed. Then, it is analyzed the failure mechanisms found in fracture surfaces.

Impact Tests

The results of the impact tests for the different materials are shown in Table 1. These values correspond to the average absorbed energy resulting from at least three valid tests performed for each tested condition. Upon careful examination of the Table 1, it becomes evident that the impact resistance is significantly influenced not only by the material type, but also by the printing direction. A comparison between NYLON 12 (H) and TPU (H) tested in air reveals a significant variation in impact resistance. The former exhibited the highest value while the latter exhibited the lowest values observed in the experiments for the vertical direction.

Furthermore, an analysis of both the horizontally and the vertically printed specimens of ULTEM™ 9085 shows a remarkable difference regarding the absorbed energy. The ULTEM™ 9085 (V) absorbed 40.9% more energy than the horizontal one. However, the greatest difference between the vertical and the horizontal directions is observed for the PETG, where the vertical sample has an absorbed energy value 68.3% higher than the horizontal one. This clearly shows the high level of anisotropy presented in these polymeric materials.

The tests conducted in wet environments with the samples immersed in artificial sweat for 30 days led to similar conclusions. Nevertheless, it was observed that the absorbed energy was lower when compared to the tests without immersion for most materials. However, for the PLA cases, an increase of 78.3 and 72.7% in the absorbed energy was observed for the immersed samples. The same trend was detected for the PETG with an increase of 81.9% and 32.3% relative to the non-immersed ones, for H and V, respectively. The reason behind this phenomenon was attributed to the varying hydrophilic and hydrophobic properties of the AM polymeric materials used in this study.

Table 1 - Average absorbed energy in air (left side) and wet environments (right side).

Material	Absorbed energy in air (J)	Absorbed energy in sweat (J)
ABS (H)	1.201 ± 0.110	0.825 ± 0.050
ABS (V)	1.336 ± 0.084	1.268 ± 0.166
NYLON 12 (H)	3.402 ± 0.153	3.011 ± 0.068
NYLON 12 (V)	3.233 ± 0.007	3.220 ± 0.062
PC ABS (H)	2.095 ± 0.727	2.416 ± 0.179
PC ABS (V)	1.923 ± 0.080	2.581 ± 0.158
PETG (H)	0.656 ± 0.314	3.587 ± 0.474
PETG (V)	2.070 ± 0.179	3.056 ± 0.106
PLA (H)	0.557 ± 0.014	2.556 ± 0.201
PLA (V)	0.668 ± 0.109	2.445 ± 0.178
PC (H)	3.230 ± 0.099	3.512 ± 0.179
PC (V)	2.947 ± 0.217	1.514 ± 0.158
TPU (H)	0.244 ± 0.009	0.212 ± 0.013
TPU (V)	0.320 ± 0.018	0.260 ± 0.006
ULTEM™ 1010 (H)	1.078 ± 0.103	1.491 ± 0.233
ULTEM™ 1010 (V)	1.677 ± 0.496	2.483 ± 0.163
ULTEM™ 9085 (H)	1.760 ± 0.173	1.852 ± 0.171
ULTEM™ 9085 (V)	2.979 ± 0.822	3.584 ± 0.090

The hydrophilic property refers to the affinity to absorb or attract water, while the hydrophobic property refers to the resistance to water absorption. In the case of the tested AM polymers, they exhibited different levels of hydrophilicity and hydrophobicity. TPU showed a hydrophobic property while the others were hydrophilic. The hydrophobic behaviour can be associated with a higher ability to repel liquids to a greater extent, while the hydrophilic response is characterised by a greater tendency to absorb liquids. Therefore, the differences in the hydrophilic and hydrophobic characteristics of the tested AM polymers led to variations in their response to immersion in artificial sweat. The material states with a more hydrophilic response exhibited a greater reduction in absorbed energy. Thus, thesweat absorptionaffectedthemechanical properties and reduced their capacity to absorb energy. Figure 1 shows the mass changes over time for four selected materials: ABS (Fig. 1a); Nylon 12 (Fig. 1b); PETG (Fig. 1c); and PC ABS (Fig. 1d).

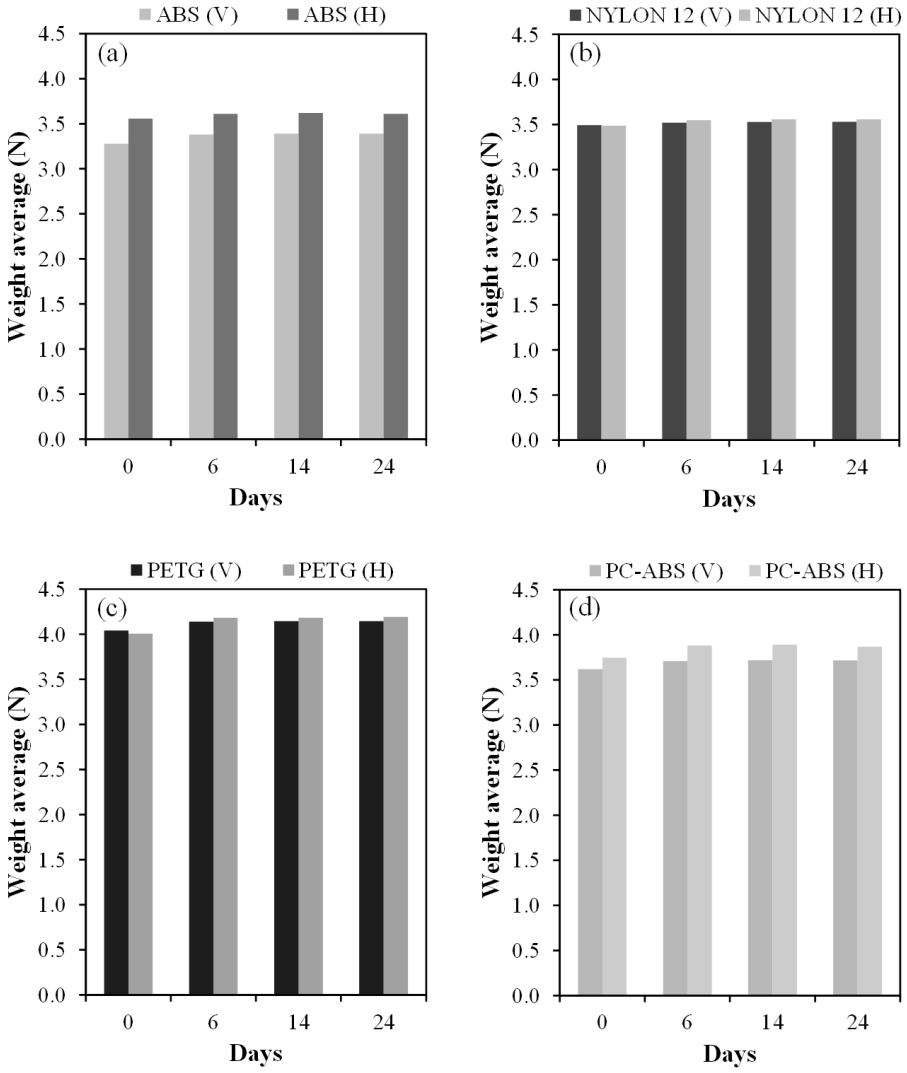

FIGURE 1 - Weight measurement for: (a) ABS; (b) Nylon 12; (c) PETG; and (d) PC ABS

Based on these results, it is suggested that when the material is printed in a vertical direction, it generally shows better results in terms of high absorption rates than the horizontally printed version. Nevertheless, it should be noted that there16 were some materials that showed good energy absorption even when printed in the horizontal direction. Table 2 summarizes which materials have the best energy absorption according to their printing direction (the green color represents the best impact performance).

Table 2 - Best impact performance (marked in green) in air and wet environments.

Material	In air		In sweat	
	Vertical	Horizontal	Vertical	Horizontal
ABS				
NYLON 12				
PC ABS				
PETG				
PLA				
PC				
TPU				
ULTEM 1010				
ULTEM 9085				

Despite the energy absorbed is quite different, based on the experimental findings, both Nylon 12 and TPU materials showed resistance to failure. Nylon 12 demonstrated a tendency to bend rather than fail under the applied testing conditions. This suggests that Nylon 12 possesses excellent flexibility, allowing it to withstand high deformation without fracturing or breaking. On the other hand, TPU was observed to be excessively flexible, indicating a high degree of elasticity and a low degree of energy absorption. While this flexibility can be advantageous in certain applications requiring materials with stretchability and resilience, it may also suggest limitations in terms of rigidity and structural integrity.

Before immersion, Nylon 12 (H), PC ABS (H), and PC (H) showed the best energy absorption. After immersion, PC (H), PETG (H), and PLA (H) demonstrated the best energy absorption. On average, vertically printed materials displayed superior energy2 absorption. By analyzing the results before and after immersion for the same material, PC (H) consistently showed the best absorption rate in both cases (see Table 2). Nylon 12 (H) and PC ABS (H) showed greater liquid absorption (see Fig. 1b, d). After immersion, PETG (H) and PLA (H) had greater energy absorption compared to the vertical condition (see Table 2). The reason why PETG (H) outperformed PETG (V) can be attributed to the presence of more molten areas noticed on the fracture surface (see Fig. 2).

In general, greater damage is associated with higher values of absorbed energy. However, in the case of materials for use in medical devices, it is often not important that all the energy is elastic (less energy absorbed), since in this case it is the organism that absorbs the energy that

is not absorbed by the material. There must be a trade-off between the values of absorbed energy and elastic energy [13].

Fractography of Selected Materials

The analysis of fracture surfaces of tested materials revealed different failure mechanisms. As exhibited brittle fracture, due to the presence of pores or spaces between layers, along with surface cracks(see Fig. 2a). Thefracture surfaces of PC ABS exhibited voids, resulting in both ductile and brittle fracture behaviour.

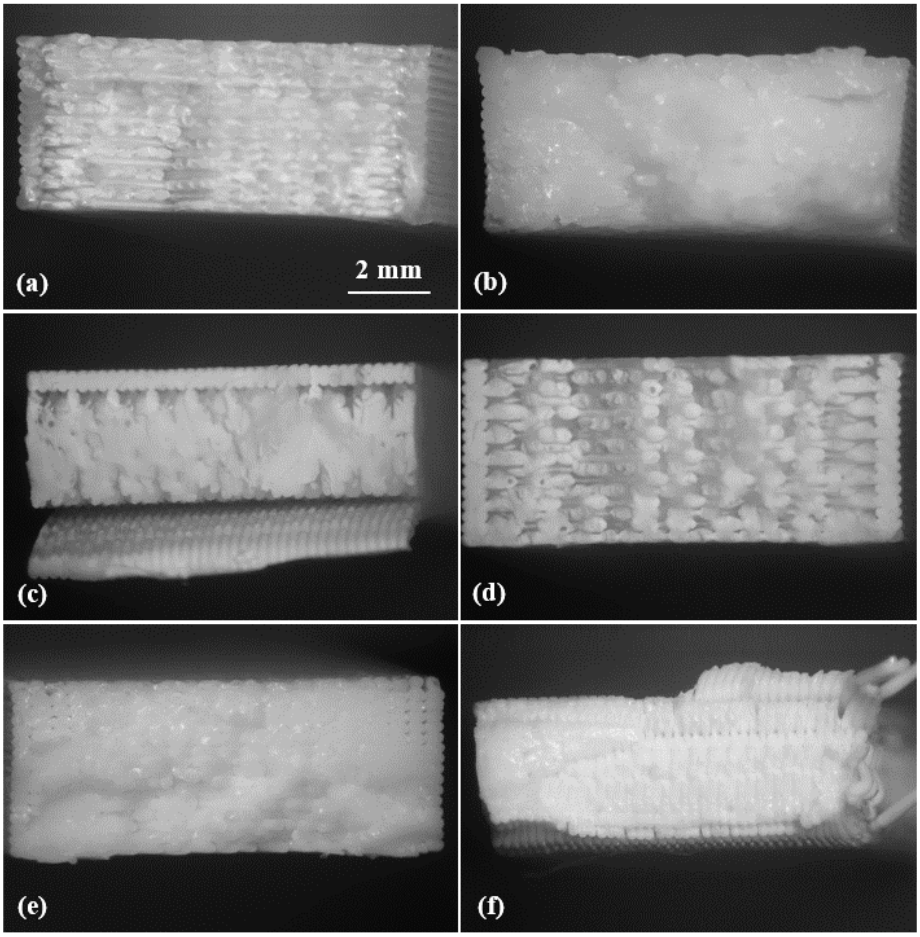

FIGURE 2 - Fracture surfaces: (a) ULTEM™ 9085 (H); (b) PC (H); (c) ABS (V); (d) ABS (H); (e) PETG (H); and (f) PETG (V).

PETG experienced brittle fracture primarily caused by crack propagation, accompanied by visible voids on the fractured surface. PLA (H) and PLA (V) failures were attributed to crack propagation with initial crack formations and filament fusion on the fractured surfaces facilitating brittle fracture. PC (H) and PC (V) failures resulted from cracks with brittle fractures

facilitated by filament fusion during the printing process which led to the formation of pores. The fracture surface of ULTEM™ 1010 (V) and ULTEM™ 1010 (H) showed crack formations, increased crack propagation, and pores caused by lack of fusion between dropped adjacent rasterizations. ULTEM™ 9085 (V) and ULTEM™ 9085 (H) showed crack propagation resulting in brittle fractures, and the presence of pores between the upper and interior layers (see Fig. 2). Materials like NYLON 12 and TPU did not fail during the impact tests. Thus, there is no fractography for these materials because they were prone to bend and did not exhibit total failure.

Conclusions

Impact resistance of nine polymeric materials printed by AM on both vertical and horizontal conditions was tested. Two environments were studied: in air and wet conditions (artificial sweat for 30 days). After the tests, fracture surfaces were assessed by optical microscopy. In summary, the tested polymeric materials exhibited an anisotropic behavior and susceptibility to impact and wet environments. This study revealed that materials with higher weight gain tend to absorb reduced energy. Additionally, results indicated that vertically printed materials displayed the best performance regarding energy absorption. Moreover, when considering the effects of immersion, Nylon 12 (V) emerged as the most suitable material, exhibiting superior energy absorption properties. These findings provide valuable insights for material selection and design, emphasizing the importance of considering and adequate printing orientation and post-immersion behavior to optimize energy absorption in polymeric materials produced by AM.

References

1. A. Kumar & D. Chhabra, “Adopting additive manufacturing as a cleaner fabrication framework for topologically optimized orthotic devices: Implications over sustainable rehabilitation”, Cleaner Engineering and Technology, Volume 10, 100559, 2022.
2. M. Boolos, S. Corbin, A. Herrmann & B. Regez, “3D printed orthotic leg brace with movement assist”, Annals of 3D Printed Medicine, Volume 7, 100062, 2022.
3. Paterson, A M, R J Bibb, and R I Campbell. 2012. “Evaluation of a Digitised Splinting Ap-proach with Multiple-Material Functionality Using Additive Manufacturing Technologies.” In Thirteenth Conference on Rapid Design, Prototyping and Manufacturing, 17.
4. Jadoon, S., Karim, S., Akram, M. R., Kalsoom Khan, A., Zia, M. A., Siddiqi, A. R., & Murtaza, G. (2015). Recent developments in sweat analysis and its applications. International Journal of analytical chemistry, 2015.

5. Russell, E., Koren, G., Rieder, M., & Van Uum, S. H. M. (2013). The Detection of Cortisol in Human Sweat. Therapeutic Drug Monitoring, 1. doi: 10.1097/ftd.0b013e31829daa0a
6. Carla M. Ferreira, Carlos M.S.V., Manuel S., Marco L., Luis R., ‘‘Characterization of 3D printed ABS specimens under static and cyclic torsional loadings’’, ScienceDirect, Structural Integrity 34 (2021)205–210.
7. C. W. Ziemiana, D.E. Cipolettia, S. N. Ziemianb, M. N. Okwarac, K. V. Haile, ‘‘Monotonic and Cyclic Tensile Properties of ABS Components Fabricated by Additive Manufacturing’’, review version, pp. 1-17
8. Janusz K., Ireneusz S., J. Torzewskia, L. Sniézeka, K. Grzelaka, G. Budzikb, Ł. Przeszłowskib, M. Małekc, Jakub Ł., ‘‘Fatigue and fracture of additively manufactured polyethylene terephthalate glycol and acrylonitrile butadiene styrene polymers’’, International Journal of Fatigue 165 (2022) 107212.
9. LNCS Homepage, https://doi.org/10.1007/s11665-021-06032-4, 19 July 2021.
10. M. R. Ayatollahia, A. Nabavi-Kivia, B. Bahramia, M. Yazid Y., M. Reza K., ‘‘The influence of in-plane raster angle on tensile and fracture strengths of 3D-printed PLA specimens’’, Engineering Fracture Mechanics, Volume 237, 107225, 1 October 2020.
11. Umesh Kizhakkinana, David W. Rosena, N. Raghavan, ‘‘Experimental investigation of frac-ture toughness of fused deposition modeling 3D-printed PLA parts’, Materials Today: Proceedings, Volume 70, Pages 631-637, 2022.
12. Soran Hassanifard, Seyed M. Hashemi, ‘‘On the strain-life fatigue parameters of additive manufactured plastic materials through fused filament fabrication process’’, Additive Manufacturing, Volume 32, 100973, March 2020.
13. Maria Moreira, João Carlos Ramos, Ana Messias, Maria Augusta Neto, Ana Amaro, Paulo Reis, “Impact response of different materials for sports mouthguards” Frattura ed Integrità Strutturale, Volume 57, Pages 63-69, 2021.

Secondary Publication

Material Performance Evaluation for Customized Orthoses: Compression, Flexural, and Tensile Tests combined with Finite Element Analysis

Authors: Daniela Trindade, Rachel Habiba, Cristiana Fernandes, André Antão, **Rui Silva**, Nuno Alves, Rui Martins, Rui Martins, Cândida Malça, Ricardo Branco and Carla Moura

Abstract
Orthoses are commonly used for treating injuries to improve the quality of life of patients, with customized orthoses offering significant benefits. Additive manufacturing, especially Fused Deposition Modelling, enhances these benefits by providing faster, more precise, and more comfortable orthoses. The present study evaluates nine polymeric materials printed in horizontal and vertical directions, by assessing their performance through compressive, flexural, and tensile tests. Among all materials, polycarbonate, polylactic acid, and ULTEMTM 1010 showed the most promising results, not only because they had the highest mechanical values, but also due to their minimal or no difference in performance between printing directions, making them advantageous in orthoses fabrication. Based on this, a finite element model of an Ankle-Foot orthosis was developed to simulate the deformation, strain, and stress fields under static conditions. The findings aim to optimize material selection for orthotic fabrication, where ULTEMTM 1010 is presented as the material with improved performance and durability.

Keywords: Customized Orthoses; Additive Manufacturing; Polymeric Materials; Ankle-Foot Orthosis; Mechanical Properties; Static Conditions

Introduction
Orthopaedic devices are commonly used for treating injuries that can be caused by falls, age-related illnesses, or accidents. Orthoses are a type of assistive device, that can be used in patients with physical impairments. The main function of these devices is to provide support and correct a certain segment of the body, confine joint movement, and minimize the risk of malformations by distributing the loading forces [1,2]. They can be categorized depending on (I) the body portion: upper limb, spinal, and lower limb, or (ii) the joint involved: wrist-hand, lumbar, and ankle-foot [3].

Customized orthoses present good outcomes in patients, such as comfort and pain reduction [4], but as they are handmade, their quality highly depends on the competence and expertise of the specialist [5]. Additive manufacturing (AM) presents several advantages to the time-consuming and laborious conventional fabrication of custom orthoses, such as plaster casting [3,6]. The production of the orthoses is faster; the patient's experience is more comfortable since scanners can be used to aid in obtaining the desired geometry; the number of technicians and the manual work is reduced; the model of the orthoses can be archived and

reproduced when necessary; and there is less need for production equipment, therefore less storage space [7].

Fused deposition modeling (FDM) is an AM technology that allows the production of three-dimensional objects through the extrusion of a material layer by layer. This technique allows for high precision in creating complex geometries that are challenging to achieve with traditional methods. Consequently, it can enhance orthoses' performance, durability, and modern aesthetics [8–10]. Furthermore, FDM offers greater accuracy, ease of use, and cost-effectiveness compared to other AM strategies, such as selective laser sintering [11]. Despite these advantages, the benefits of FDM technology are still underexplored [3]. One major challenge is selecting the right material for orthoses, which must meet various mechanical and physical properties [5,12,13]. No single material can meet all adequate criteria, but the final product should be lightweight, user-friendly, cost-effective, durable, body-compatible, and suitable for its intended use (e.g., rehabilitation or support). Using a hard material or an improper design can result in an uncomfortable or biomechanically incorrect orthosis [1,5,13–15].

The primary objective of this study is to evaluate nine polymeric materials printed in two printing directions (horizontal and vertical relative to the base plate) by analysing their compressive, flexural, and tensile properties. The second objective is the development of a three-dimensional finite element model of a real Ankle-Foot orthosis for simulating its deformation, stress, and strain fields under static loading conditions considering daily usage.

Materials and Methods

Materials Production

The study evaluated nine polymeric materials: acrylonitrile butadiene styrene (ABS), Nylon 12, polycarbonate (PC), polycarbonate/acrylonitrile butadiene styrene (PC-ABS), polyethylene terephthalate glycol (PETG), polylactic acid (PLA), thermoplastic polyurethane (TPU), and high-performance polytherimide (PEI) thermoplastics ULTEM™ 1010, and ULTEM™ 9085. Materials were provided by Stratasys and the specimens were manufactured using a 3D printer by FDM (Stratasys F170 printer, Stratasys, Eden Prairie, MN, USA) with an infill density of 100%, infill

angle of 45°, and a slice height of 254 µm. Each material was printed in two directions: horizontal (H) and vertical (V) relative to the base plate, as shown in Figure 1.

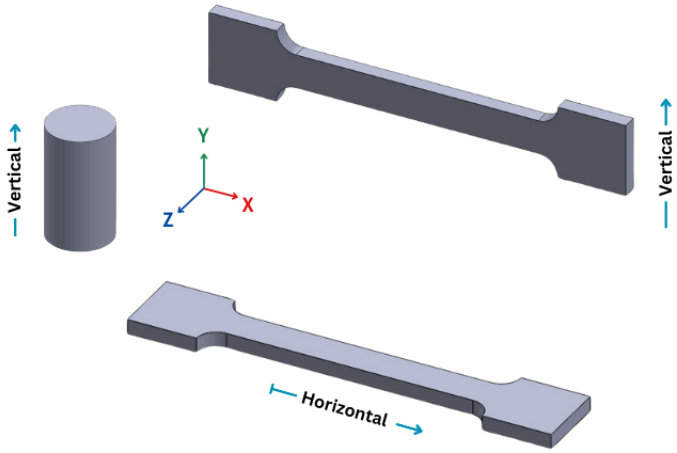

Figure 1. Horizontal (H) and vertical (V) printing directions of the tested specimens.

Tensile Testing

Tensile tests were conducted following ASTM D638-14 standards [16]. The tested specimens were printed in both H and V orientations. The tests were performed using a universal testing machine (Instron Model 5544, Norwood, MA, USA) equipped with a 100 kN load cell. The test speed was set to 5 mm/min.

Flexural Testing

Flexural tests were conducted using the same universal testing machine, but with a speed test of 2 mm/min according to ISO 178 standard [17]. The specimens used for this test were the same as those used in the tensile test since their specifications correspond to those used for this standard.

Compression Testing

Compression tests were performed according to ASTM D695-23 standards [18]. The cylindrical specimens tested were printed in the V direction. Testing was conducted using the same universal testing machine, with a speed test of 1 mm/min.

Data analysis of the mechanical assays

Tests were conducted at room temperature and for each test type and material, five specimens were tested to ensure statistical reliability. The tensile/flexural/compressive strength, Young's modulus, and strain at break were recorded for each specimen, where the results were averaged, and standard deviations were calculated. The influence of printing direction on flexural and tensile properties was evaluated on GraphPad Prism 9 software with multiple unpaired t-test. All tests were calculated with a confidence interval of 95%, where statistically significant differences are represented by * $p<0.05$, ** $p<0.01$ and *** $p<0.001$. Correlations for the mechanical assays were also calculated with Pearson correlation test on GraphPad using the same software and confidence interval above-mentioned.

Static Structural Test

The static structural analysis of the ankle-foot orthosis was performed for the PC, PLA, and ULTEM™ 1010 due to their minimal or low differences in printing direction mechanical results. In this analysis, it was simulated a real ankle-foot orthosis. The three-dimensional model was created using SolidWorks 2023, a software from Dassault Systèmes Corporation (Waltham, MA, USA). The model was imported as a Parasolid file (.x_t) into Ansys Workbench 19.2 software (Canonsburg, PA, USA) which provides a common platform integrating various Ansys applications for multi-physics simulations and design optimization. The finite element mesh contained 23440 nodes and 11758 elements, the element size was set at 5 mm and the mesh type is tetrahedral. The physical model and the corresponding assembled meshed can be seen in Figure 2, where different perspective views of the ankle-foot orthosis are shown. The Ankle-Foot orthosis was designed with an increase in the length of the lever arm and the calf surface area to assure comfort and efficiency [19].

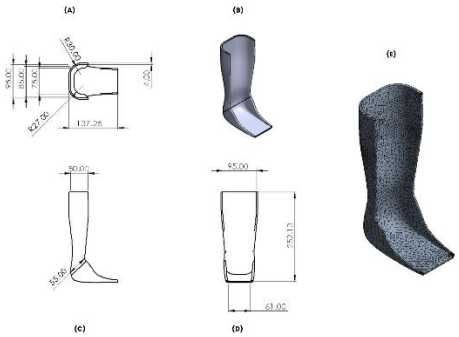

Figure 2. Ankle-Foot Orthosis Design model: Up view (A), 3D projection view (B), Front view (C), Right view (D), and Mesh model (E).

The simulation of the real-life effects can be seen in Figure 3: the area where the foot will be placed was assigned a ground-to-part relation with a fixed joint (in blue); to simulate the contact and force that the body may apply on the Ankle-Foot orthosis in real life when subjected to static conditions, a force of 490.03N was used with force vector components (-3,5,490) N in X, Y, and Z directions. The force was applied to the entire model as shown in Figure 3. The applied force is according to Marques et al [19] and Ali et al [20] investigations describing the full contact moment in the gait cycle when the sole fully touches the ground.

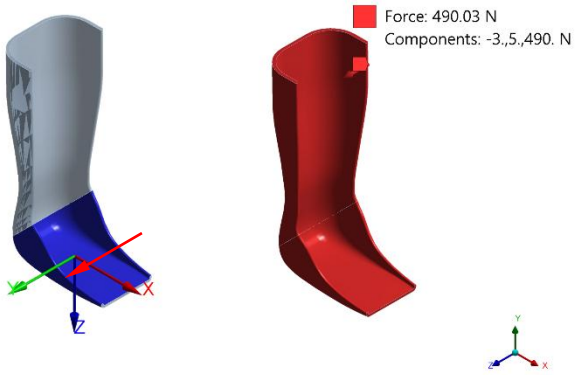

Figure 3. Fixed joint ground to part in blue and applied force in red.

The finite element model was assumed to be linear-elastic, homogeneous, and isotropic. The information about the isotropic elasticity, yield, and ultimate strength of the tested materials according to the material's supplier (Stratasys, Eden Prairie, MN, USA) is shown in Table 1.

Table 1. Material data.

Material	Young's modulus (MPa)	Poisson's Ratio	Tensile Yield Strength (MPa)	Tensile Ultimate Strength (MPa)
PC	2250	0.39	57.9	57.3
PLA	3039	0.39	45.0	48.0
ULTEM™ 1010	2770	0.36	64.0	81.0

A static structural analysis was performed to obtain results relative to the total deformation, equivalent elastic strain, equivalent von Mises stress, and factor of safety defined based on

maximum equivalent stress theory and tensile yield. The structural analyses were carried out for the three materials used in the numerical simulations.

Results

Tensile Tests

The tensile properties of the nine polymeric materials, printed in both H and V directions were evaluated. The three parameters analysed were tensile strength (Figure 4-A), tensile Young's modulus (Figure 4-B), and strain at break (Figure 4-C). For tensile strength in the H direction, ULTEMTM 1010 gave the highest value of 69.99 ± 1.23 MPa, and TPU was the lowest with a value of 3.97 ± 0.03 MPa. For the V direction, ULTEM™ 8095 gave the highest value with 73.17 ± 0.33 MPa and TPU led to the lowest with a value of 4.36 ± 0.03 MPa. Statistically significant differences were found for most of the materials when comparing the printing directions, such as ABS, PC-ABS, PETG, Nylon12, TPU, and ULTEM™ 9085, where the V direction was the one with the highest values.

For tensile Young's modulus, TPU was the material with the lowest value for both directions, with a modulus of 20.04 ± 0.93 MPa and 24.18 ± 0.54 MPa for the H and V directions, respectively. The highest values were found in PLA, with a tensile Young´s modulus of 2451.36 ± 81.12 MPa and 2245.74 ± 114.80 MPa, for the H and V direction, respectively. Statistically significant differences were found between directions for the same materials as for tensile strength, where the V direction was the one with the highest values, except for PLA where the H direction gave rise to a higher modulus.

Finally, for strain at break, TPU was the only material that did not lead to a break fracture. PLA was the material with the lower extension with a value of 4.07 ± 0.17 % and 4.48 ± 0.31 % for the H and V direction, respectively. For the higher values, in the H direction, ABS presented an extension of 11.41 ± 0.60 %, and in the V direction, Nylon presented an extension of 21.89 ± 5.46 %. Comparing printing directions, all materials led to statistically significant differences, except PC-ABS and PETG. For ABS, PLA, Nylon, and ULTEM™ 9085, the V direction led to higher values, whereas for PC and ULTEM™ 1010, the maximum values were found in the H direction.

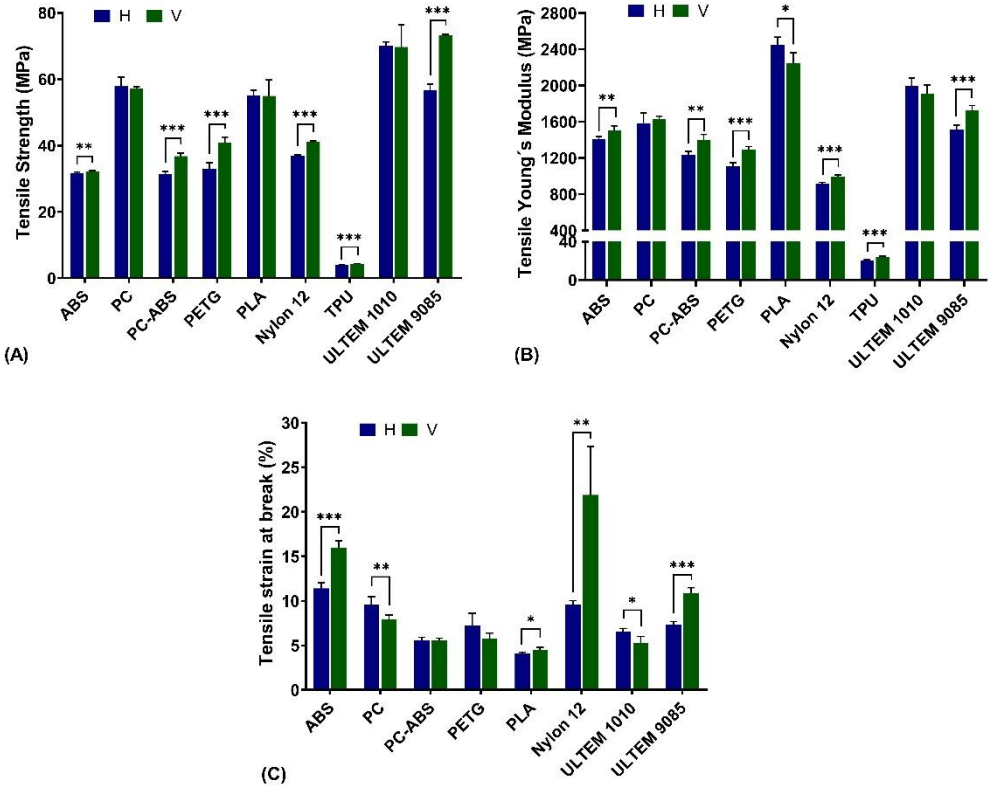

Figure 4. Tensile Strength (A), Young´s modulus (B), and strain at break (C) for all materials in both printing directions: horizontal (H) and vertical (V). Statistical analysis was conducted with multiple unpaired t-test and differences are represented by * $p<0.05$, ** $p<0.01$, and *** $p<0.001$.

Flexural Tests

Similar to tensile testing, the flexural strength (Figure 5-A), flexural Young's modulus (Figure 5-B), and flexural strain at break (Figure 5-C) were evaluated for the nine tested materials in both H and V printing directions. It should be noted that in this research it was not possible to evaluate the TPU in our equipment due to its high flexibility, which led to some instability issues resulting in very unreliable graphs.

For the flexural strength in the H direction, the highest value was attributed to ULTEM™ 1010 with a strength of 114 ± 3.27 MPa, and the lowest value to PETG with a value of 55.56 ± 2.26 MPa. In the V direction, ULTEM™ 9085 led to the highest value of 115 ± 1.44 MPa, and ABS exhibited the lowest value with 59.18 ± 0.92 MPa. Focusing on printing direction, statistically significant differences were found for the PC-ABS, PETG, ULTEM™ 1010, and ULTEM™ 9085, where the V direction gave origin to higher values.

For flexural Young's modulus, in both printing directions, PLA gave the highest values, whereas Nylon gave the lowest values: PLA-H was 1181.00 ± 39.36 MPa, PLA-V was 1236.32 ± 127.28 MPa, Nylon-H was 3313.68 ± 142.03 MPa and Nylon-V was 3343.27 ± 219.58 MPa. Between directions, the statistically significant differences were similar to flexural strength, where PC-ABS, PETG, ULTEM™ 1010, and ULTEM™ 9085 gave rise to higher values in the V direction.

Strain at break was lower for PLA, in both printing directions, with values of 4.86 ± 0.33 % for the H direction, and 5.89 ± 0.26 % for the V direction. Nylon led to an extension of 14.93 ± 0.36 %, being the material with the higher value in the H direction, whereas the in the V direction was ULTEM™ 9085 with a value of 15.98 ± 1.77 %. Once again, TPU also did not lead to a fracture. Between printing directions, statistically significant differences were found for ABS, PLA, ULTEM™ 1010and ULTEM™ 9085, where the V direction was the one with the higher values.

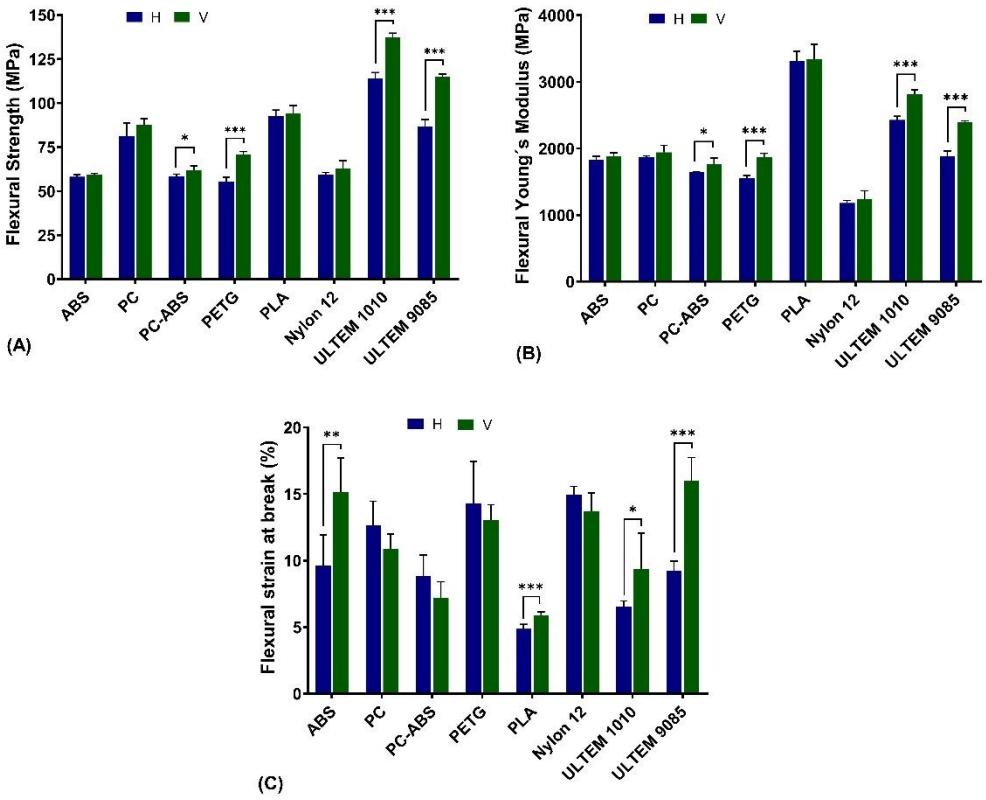

Figure 5. Flexural Strength (A), Young´s modulus (B), and strain at break (C) for all materials in both printing directions: horizontal (H) and vertical (V). Statistical analysis was conducted with multiple unpaired t-test and differences are represented by * $p<0.05$, ** $p<0.01$, and *** $p<0.001$.

Compressive Tests

Compression properties were only evaluated in the V direction. The values of compressive strength, compressive Young's modulus, and compressive strain at break obtained in the tests are displayed in Figure 6-A, Figure 6-B, and Figure 6-C, respectively.

As far as the compression strength is concerned, the material that led to higher values was PETG with 680.7 ± 155.1 MPa and the lower was TPU with 16.9 ± 1.1 MPa. For compression Young´s modulus, PLA had the higher values with 2264.0 ± 34.0 MPa, and PETG exhibited the lower value with 1008.8 ± 38.3 MPa. For compressive strain at break, the material that had a higher strain value was PETG with 85.1 ± 1.3%, while ULTEM™ led to the lower compressive strain at break with 63.2 ± 0.7MPa.

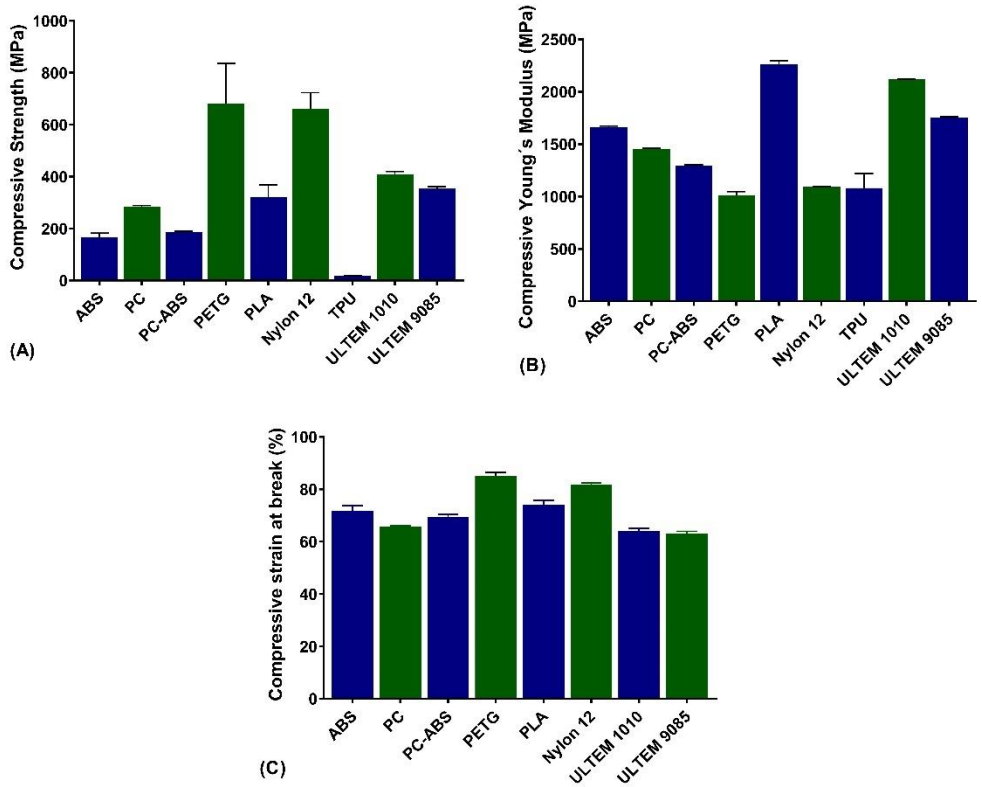

Figure 6. Compression Strength (A), Young´s modulus (B), and strain at break (C) for all materials.

Correlation Assays

Analysing the correlation studies for the tensile tests, see Figure 7-Ai, Aii, it is possible to conclude that the strain at break is not associated with the tensile strength for both printing directions as the correlation coefficients are close to 0 (r=-0.2900 and r=-0.2946, for H and V

direction, respectively). On the contrary, the tensile Young´s modulus, showed a negative correlation with the tensile strain at break for both printing directions (r=-0.529 and r=-0.562 for H and V direction, respectively), meaning that when the tensile Young´s modulus increases, the strain at break decreases. This was also confirmed by the $p<0.001$ which confirmed that this negative correlation is not due to random sampling. As for tensile strength versus tensile Young´s modulus, a positive correlation was found (r=0.602, and r=0.597 for H and V direction, respectively, and $p<0.001$), meaning that when one parameter increases the other also increases.

Regarding the flexural tests, see Figure 7-Bi, Bii similar results with the tensile assays were found for the V direction. Flexural strength vs flexural strain at break presented no relationship (r=-0.123, NS), flexural Young´s modulus versus flexural strain at break presented a negative correlation (r=-0.469, $p<0.01$), and flexural strength versus flexural Young´s modulus presented a positive correlation (r=0.702, $p<0.001$). As for the H direction, interestingly, flexural strength versus flexural strain at break presented a negative correlation (r=-0.586, $p<0.001$). The remaining analyses, were similar to the V direction as flexural Young´s modulus vs flexural strain at break presented a negative correlation (r=-0.781, $p<0.001$), despite being a must stronger correlation as value as close to -1. Finally, flexural strength vs flexural Young´s modulus also presented a positive correlation (r=0.697, $p<0.001$).

For compression assays, see Figure 7-C, as similar to the other mechanical tests, compressive Young´s modulus presented a negative association with compressive strain at break (r=-0.577, $p<0.001$). The differences were found for the remaining correlations. Compressive strength versus compressive strain at break presented a positive correlation (r=0.669, $p<0.001$) and compressive strength versus compressive Young´s modulus presented a negative correlation (r=-0.435, $p<0.01$).

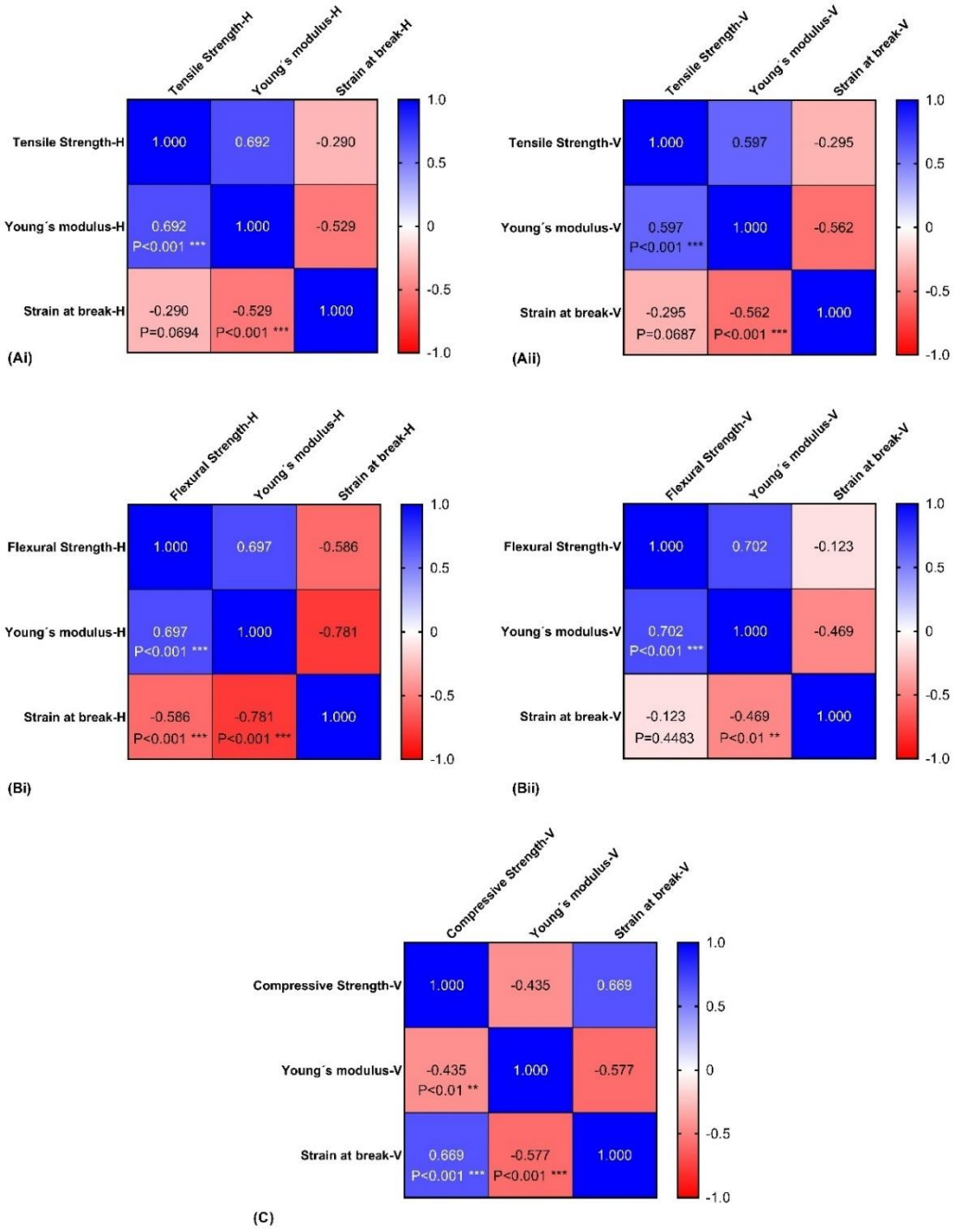

Figure 7. Correlation matrix for each mechanical assay: tensile test in the vertical (Ai) and horizontal direction (Aii), flexural test in the vertical (Bi) and horizontal direction (Bii), and compression test (C). The correlation coefficient is presented, as well as statistical differences by * p<0.05, ** p<0.01 and *** p<0.001.

Static Structural analysis

Static structural analysis was carried out for PC, PLA, and ULTEM™ 1010 due to their minimal or low differences in mechanical results between printing directions, and also because they are the materials with the highest mechanical properties of all the materials, making them

suitable for the production of orthotics. The results are represented in colour varying from blue to red, which correspond from the lower to the higher values of the plotted variable. For each material, equivalent stresses (Figure 8-A), equivalent strains (Figure 8-B), total deformation (Figure 8-C), and safety factors (Figure 8-D) are presented. Regarding stresses, for the three materials (PC, PLA, and ULTEM™ 1010), the maximum von Mises stresses are around 25 MPa and stress concentrations are more located in the area covering the ankle. The elastic strains are also more visible in that area where PC showed the highest maximum elastic strain followed by ULTEM™ 1010 and PLA. The upper area of the Ankle-Foot orthosis showed a significant deformation for the three materials with red indicating maximum total deformation. PLA showed the lowest deformation compared to ULTEM™ 1010 and PC, while PC showed the highest deformation. All three materials demonstrated a minimum safety factor greater than 1. Among them, ULTEM™ 1010 had the highest safety factor, followed by PC. PLA showed the lowest safety factor. Table 2 summarises the main results obtained in the numerical simulations for the three materials (maximum von Mises stress, maximum elastic strain, maximum total deformation, and minimum safety factor).

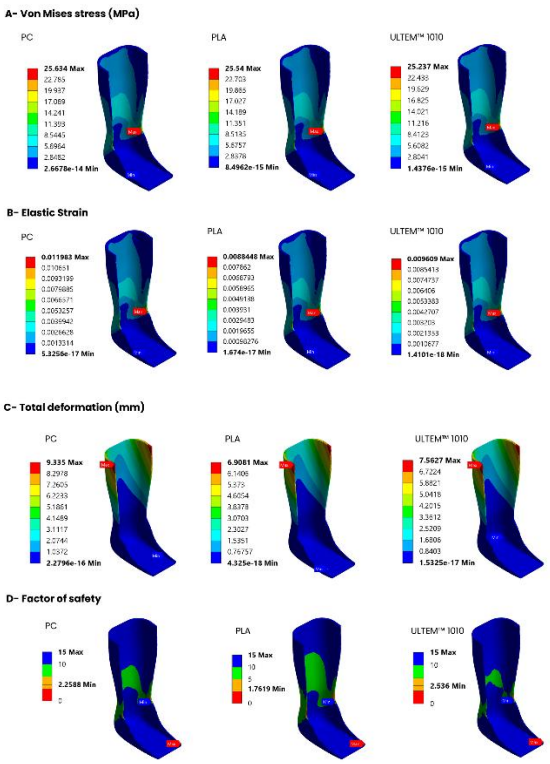

Figure 8. Static structural analysis of the Ankle-Foot ankle orthosis: (A) equivalent von Mises stress; (B) equivalent strain; (C) total deformation, and (D) safety factor for the three tested materials (PC, PLA, and ULTEM™ 1010).

Table 2. Result summary for the PC, PLA, and ULTEM™ 1010.

Material	Maximum von Mises stress (MPa)	Maximum elastic strain (mm/mm)	Maximum total deformation (mm)	Minimum safety factor
PC	25.63	11.98×10^{-03}	9.34	2.26
PLA	25.54	8.85×10^{-03}	6.91	1.76
ULTEM™ 1010	25.24	9.61×10^{-03}	7.56	2.54

Discussion

For orthotic AM production, it is essential that the chosen materials can withstand distinct mechanical stresses, including those resulting from flexural, compression, and tensile forces. These properties ensure that the orthosis will be durable and reliable for the patient while maintaining its structural integrity and functionality over time. Different authors have investigated different materials for orthotic production such as PC, PC-ABS, ULTEM, PLA, ABS, and PETG [22–29]. However, a consensus on the most suitable material is still debatable.

FDM-manufactured parts are known to be anisotropic due to the specificities inherent to this AM process, including the printing orientation [30,31]. This is why the mechanical properties of printed materials must be addressed in different orientations to achieve the desired results. Camargo et al. showed that the tensile and flexural strength of PLA-graphene material increases with the increase of the infill, while impact energy decreases. An increase in layer thickness also led to higher values in the referred mechanical properties [32]. Moreover, PLA also exhibited varying flexural strengths depending on the type of filling, such as rectangular, triangular, and honeycomb [33].

In the V direction, the layers of the printed materials are aligned parallel to the loads, while in the H direction, they are aligned perpendicularly. This characteristic resulted in better mechanical performance in the flexural tests, for all the analysed materials. For the tensile tests, the best performance was associated with the V direction, except for the PLA's Young´s modulus, and for PC and ULTEM™ 1010 strain at break, where the H direction showed higher values. Various studies have reported that printing directions affect the flexural properties of resins [34,35]. Similar findings have been reported for thermoplastics, aligning with the results found in the present study. The specimens printed parallel to the loads, presented higher flexural strength in ULTEM™ 9085 and ABS [36], and higher tensile strength in ABS [37]. The same was also observed for Nylon and ULTEM™ 9085 tensile strength, tensile Young´s

modulus, and tensile strain at break [38,39]. Curiously, ULTEM™ 1010´s tensile strength and tensile Young´s modulus presented similar results between printing directions, but tensile strain at break was also higher for the H direction [40]. Although PLA [41] and PC [42] presented higher tensile strength values for specimens printed parallel to the loads in other studies, this was not observed in the present study. This discrepancy may occur likely due to variations in printing speed and temperature, which can affect the adhesion between layers and the consistency of the filament diameter and its quality, leading to differences in mechanical performance [6,43]. The rapid cooling from the FDM process can leave behind empty spaces due to a very rapid shrinkage of the material which leads to a deficiency in the adhesion between material layers, leading to residual stresses in the material [30].

The strength-ductility of the materials produced can be more effectively analysed through correlation studies of mechanical properties [44]. It is known that Young´s modulus is defined as the ability of a material to resist deformation [45]. The ultimate strength, used in this study as tensile/flexural/compression strength, is the maximum value that an object can resist without breaking [46], and strain at break is the point the material fractures [47]. Results of correlation demonstrated that there is no association between tensile strain at break and tensile strength. This means that the material´s ability to withstand stress in both printing directions does not predict its elongation. As for tensile Young´s modulus and tensile strain at break, there is a negative correlation. This means that materials with a higher Young´s modulus (stiffer materials) are often more brittle. Tensile strength vs tensile Young´s modulus presented a positive correlation, as both are related to the material´s ability to bear loads. For flexural tests, the same conclusions can be drawn, as similar results were obtained. The only difference was found in the H direction, where a negative correlation was found between flexural strength and flexural strain at break. In this direction, not only does a stiffer disc lead to a brittle material but so does its load-bearing capacity. Lastly, the failure mechanisms of compressive loads led to differences when compared to the tensile and flexural tests: a positive correlation was found between compressive strength and compressive strain at break, meaning that the materials can withstand higher loads and also elongate more; and negative correlation between compressive strength and compressive Young´s modulus, where a material that can withstand more loads does not necessarily exhibit greater stiffness.

Regarding Ankle-Foot orthosis manufacturing, Raj et al. highlighted the advantages of using AM to produce ankle-foot orthosis compared to conventional manufacturing [48]. Overall PC, PLA, and ULTEM^{TM} 1010 demonstrated the most promising outcomes. Not only do they present a higher superior mechanical properties, but also their consistent results in the different printing directions, make them particularly advantageous for orthosis fabrication due to a higher printing flexibility. Thus, their choice for the simulations. The simulation of the Ankle-Foot orthosis designed in this study gives realistic results relative to its mechanical performance under real-world conditions while allowing for reduction of the amount of prototype iterations for validation. The results of static structural analysis give an insight into the mechanical performance of the Ankle-Foot orthoses produced using three distinct materials. The stress distribution patterns are comparable to each other allowing us to identify the concentrated high-stress regions where potential failures can occur. The maximum stresses for PC, PLA, and ULTEM™ 1010 are below their tensile yield strengths which ensures that the material behaves predictably, within its safe operating limits. PC showed the highest maximum elastic strain, which means that it is prone to deform more compared to ULTEM™ 1010 and PLA. The total deformation results show that PC is prone to significant deformation while PLA has a lower deformation, whereas ULTEM™ 1010 balances between them. Regarding the safety factor, a value lower than 1 indicates potential failure. In the three cases, the safety factor is higher than 1 which indicates that these materials are in the acceptable range. The safety factors of PC and ULTEM™ 1010 are greater than 2, indicating that the model can handle twice the force applied without failing. Based on the simulation results, it is clear that the current orthoses design will experience high stress levels in specific areas, regardless of the material used.

Conclusions

Through these tests, we can select materials that will optimize the performance of orthoses, contributing to better patient outcomes and satisfaction. The present study led to a better understanding of 9 polymeric materials under various mechanical conditions. The correlation studies emphasized the importance of considering different mechanical properties for evaluating material performance. Nylon12, PC, PLA, and ULTEM^{TM} 1010 presented the most interesting results because there are no differences in values between the print directions, making them more advantageous for orthosis printing. This led to the choice of virtual ankle-foot orthosis based on these three materials. The FEA of the Ankle-Foot orthosis gives insight

into the mechanical behavior of an ankle-foot orthosis under static conditions. This result from the static structural analysis can help in optimizing ankle-foot orthoses for better performance under real loading conditions. Based on the numerical simulations, ULTEM™ 1010 exhibited the best performance.

Author Contributions: Conceptualization: DT, CM (Carla Moura); Methodology; DT, RH, CF, AAC, RB, CM (Carla Moura); Formal analysis: DT, RH, CF, AAC; Validation: RS, NA, RM, CM (Cândida Malça), RB, CM (Carla Moura); Writing and revising of the article: DT, RH, CF, AAC, RS, NA, RM, CM (Cândida Malça), RB, CM (Carla Moura). All authors have read and agreed to the published version of the manuscript.

Funding: The authors acknowledge Fundação para a Ciência e a Tecnologia (FCT, I.P.) for its financial support through the CDRSP projects: UIDB/04044/2020, UIDP/04044/2020 and Associate Laboratory ARISE LA/P/0112/2020; and CEMMPRE projects: UIDB/00285/2020 and LA/P/0112/2020. This research was also funded through the institutional scientific employment program-contract (CEECINST/00077/2021).

References

1. Alqahtani, M.S.; Al-Tamimi, A.; Almeida, H.; Cooper, G.; Bartolo, P. A Review on the Use of Additive Manufacturing to Produce Lower Limb Orthoses. *Prog. Addit. Manuf.* 2020, *5*, 85–94, doi:10.1007/s40964-019-00104-7.

2. Hensen, J.C.D. dos S.F.; Foggiatto, J.A.; Ulbricht, L.; Stadnik, A.M.W. Additive Manufacturing of Customized Lower Limb Orthoses – A Review. *Int. J. Innov. Educ. Res.* 2018, *6*, 141–152, doi:10.31686/ijier.Vol6.Iss10.1175.

3. Wang, Y.; Tan, Q.; Pu, F.; Boone, D.; Zhang, M. A Review of the Application of Additive Manufacturing in Prosthetic and Orthotic Clinics from a Biomechanical Perspective. *Engineering* 2020, *6*, 1258–1266, doi:10.1016/j.eng.2020.07.019.

4. Aydin, L.; Kucuk, S. A Method for More Accurate FEA Results on a Medical Device Developed by 3D Technologies. *Polym. Adv. Technol.* 2018, *29*, 2281–2286, doi:10.1002/pat.4339.

5. Barrios-Muriel, J.; Romero-Sánchez, F.; Alonso-Sánchez, F.J.; Rodríguez Salgado, D. Advances in Orthotic and Prosthetic Manufacturing: A Technology Review. *Materials (Basel).* 2020, *13*, 295, doi:10.3390/ma13020295.

6. Mian, S.H.; Abouel Nasr, E.; Moiduddin, K.; Saleh, M.; Alkhalefah, H. An Insight into the Characteristics of 3D Printed Polymer Materials for Orthoses Applications: Experimental Study. *Polymers (Basel).* 2024, *16*, 403, doi:10.3390/polym16030403.

7. Pallari, J.H.P.; Dalgarno, K.W.; Munguia, J.; Muraru, L.; Peeraer, L.; Telfer, S.; Woodburn, J. Design and Additive Fabrication of Foot and Ankle-Foot Orthoses. In Proceedings of the Proceedings of the 21st Annual International Solid Freeform Fabrication Symposium–An Additive Manufacturing Conference; 2010; pp. 9–11.

8. Chhikara, K.; Singh, G.; Gupta, S.; Chanda, A. Progress of Additive Manufacturing in Fabrication of Foot Orthoses for Diabetic Patients: A Review. *Ann. 3D Print. Med.* 2022, *8*, 100085, doi:10.1016/j.stlm.2022.100085.

9. Butt, J.; Bhaskar, R.; Mohaghegh, V. Investigating the Influence of Material Extrusion Rates and Line Widths on FFF-Printed Graphene-Enhanced PLA. *J. Manuf. Mater. Process.* 2022, *6*.

10. Walbran, M.; Turner, K.; McDaid, A.J. Customized 3D Printed Ankle-Foot Orthosis with Adaptable Carbon Fibre Composite Spring Joint. *Cogent Eng.* 2016, *3*, 1227022, doi:10.1080/23311916.2016.1227022.

11. Rengier, F.; Mehndiratta, A.; von Tengg-Kobligk, H.; Zechmann, C.M.; Unterhinninghofen, R.; Kauczor, H.-U.; Giesel, F.L. 3D Printing Based on Imaging Data: Review of Medical Applications. *Int. J. Comput. Assist. Radiol. Surg.* 2010, *5*, 335–341, doi:10.1007/s11548-010-0476-x.

12. Wong, M.S.; Hassan Beygi, B.; Zheng, Y. Materials for Exoskeletal Orthotic and Prosthetic Systems. In *Encyclopedia of Biomedical Engineering*; Narayan, R., Ed.; Elsevier, 2019; pp. 352–367.

13. Sarma, T.; Pandey, D.; Sahai, N.; Tewari, R.P. Material Selection And Development Of Ankle Foot Orthotic Device. *Mater. Today Proc.* 2019, *18*, 2509–2514.

14. Shahar, F.S.; Hameed Sultan, M.T.; Lee, S.H.; Jawaid, M.; Md Shah, A.U.; Safri, S.N.A.; Sivasankaran, P.N. A Review on the Orthotics and Prosthetics and the Potential of Kenaf Composites as Alternative Materials for Ankle-Foot Orthosis. *J. Mech. Behav. Biomed. Mater.* 2019, *99*, 169–185, doi:10.1016/j.jmbbm.2019.07.020.

15. Portnova, A.A.; Mukherjee, G.; Peters, K.M.; Yamane, A.; Steele, K.M. Design of a 3D-Printed, Open-Source Wrist-Driven Orthosis for Individuals with Spinal Cord Injury. *PLoS One* 2018, *13*, e0193106, doi:10.1371/journal.pone.0193106.

16. ASTM International ASTM D638-14 - Standard Test Method for Tensile Properties of Plastics. *Am. Soc. Test. Mater.* 2022, doi:10.1520/D0638-14.

17. 178:2019, B.E.I. Plastics—Determination of Flexural Properties. *British, Eur. Int. Stand.* 2019.

18. ASTM International ASTM D695-23 - Standard Test Method for Compressive Properties of Rigid Plastics. *Am. Soc. Test. Mater.* 2023, doi:10.1520/D0695-23.

19. Ferreira, P.D.P. Development of a Two-Dimensional Biomechanical Multibody Model for the Analysis of the Human Gait with an Ankle-Foot Orthosis/Desenvolvimento de Um Modelo Biomecânico Multibody Bidimensional Para a Análise Da Marcha Humana Com Uma Ortótese Do Tornozelo, Universidade do Minho (Portugal), 2012.

20. Marques, M.A.; Mendes, E.; Ramos, N. V; Pinto, V.C.; Vaz, M.A. Finite-Element Analysis of Ankle-Foot Orthosis to Predict Fracture Conditions during Gait. *Proc. 1st ICH Gaia-Porto, Porto, Port.* 2010, *1*.

21. Ali, M.H.; Smagulov, Z.; Otepbergenov, T. Finite Element Analysis of the CFRP-Based 3D Printed Ankle-Foot Orthosis. *Procedia Comput. Sci.* 2021, *179*, 55–62, doi:10.1016/j.procs.2020.12.008.

22. Blaya, F.; Pedro, P.S.; Silva, J.L.; D'Amato, R.; Heras, E.S.; Juanes, J.A. Design of an Orthopedic Product by Using Additive Manufacturing Technology: The Arm Splint. *J. Med. Syst.* 2018, *42*, 54, doi:10.1007/s10916-018-0909-6.

23. Chen, R.K.; Chen, L.; Tai, B.L.; Wang, Y.; Shih, A.J.; Wensman, J. Additive Manufacturing of Personalized Ankle-Foot Orthosis. *Proc. NAMRI/SME* 2014, *42*.

24. Schrank, E.S.; Hitch, L.; Wallace, K.; Moore, R.; Stanhope, S.J. Assessment of a Virtual Functional Prototyping Process for the Rapid Manufacture of Passive-Dynamic Ankle-Foot Orthoses. *J. Biomech. Eng.* 2013, *135*, doi:10.1115/1.4024825.

25. Varga, P.; Lorinczy, D.; Toth, L.; Pentek, A.; Nyitrai, M.; Maroti, P. Novel PLA-CaCO 3 Composites in Additive Manufacturing of Upper Limb Casts and Orthotics—A Feasibility Study. *Mater. Res. Express* 2019, *6*, 045317, doi:10.1088/2053-1591/aafdbc.

26. Arulmozhi, R.S.; Vaidya, M.; Poojalakshmi, M.G.; Ashok Kumar, D.; Anuraag, K. 3D DESIGN AND PRINTING OF CUSTOM-FIT FINGER SPLINT. *Biomed. Eng. Appl. Basis Commun.* 2018, *30*, 1850032, doi:10.4015/S1016237218500321.

27. Łukaszewski, K.; Wichniarek, R.; Górski, F. Determination of the Elasticity Modulus of Additively Manufactured Wrist Hand Orthoses. *Materials (Basel).* 2020, *13*, 4379, doi:10.3390/ma13194379.

28. Santos, M.A.R.D.; Tokimatsu, R.C.; Treichel, T.L.E.; Prado, T.D.D.; C. D. S. Junior, A. Orthosis and Prosthesis Development for Large and Medium Animals Using Reverse Engineering and Additive Manufacturing Techniques. *Int. J. Adv. Eng. Res. Sci.* 2020, *7*, 169–177, doi:10.22161/ijaers.75.23.

29. Habiba, R.; Amaro, A.; Trindade, D.; Moura, C.; Silva, R.; Antão, A.; Martins, R.F.; Malça, C.; Branco, R. Comparative Analysis of Impact Strength among Various Polymeric Materials for Orthotic Production. *Polymers (Basel).* 2024, *16*, 1843, doi:10.3390/polym16131843.

30. Butt, J.; Oxford, P.; Sadeghi-Esfahlani, S.; Ghorabian, M.; Shirvani, H. Hybrid Manufacturing and Mechanical Characterization of Cu/PLA Composites. *Arab. J. Sci. Eng.* 2020, *45*, 9339–9356, doi:10.1007/s13369-020-04778-y.

31. Butt, J.; Bhaskar, R.; Mohaghegh, V. Non-Destructive and Destructive Testing to Analyse the Effects of Processing Parameters on the Tensile and Flexural Properties of FFF-Printed Graphene-Enhanced PLA. *J. Compos. Sci.* 2022, *6*.

32. Camargo, J.C.; Machado, Á.R.; Almeida, E.C.; Silva, E.F.M.S. Mechanical Properties of PLA-Graphene Filament for FDM 3D Printing. *Int. J. Adv. Manuf. Technol.* 2019, *103*, 2423–2443, doi:10.1007/s00170-019-03532-5.

33. Rebenaque, A.G.; González-Requena, I. STUDY OF BENDING TEST OF SPECIMENS OBTAINED THROUGH FDM PROCESSES OF ADDITIVE MANUFACTURING. *Procedia Manuf.* 2019, *41*, 859–866, doi:10.1016/j.promfg.2019.10.008.

34. Derban, P.; Negrea, R.; Rominu, M.; Marsavina, L. Influence of the Printing Angle and Load Direction on Flexure Strength in 3D Printed Materials for Provisional Dental Restorations. *Materials (Basel).* 2021, *14*, 3376, doi:10.3390/ma14123376.

35. KEßLER, A.; HICKEL, R.; ILIE, N. In Vitro Investigation of the Influence of Printing Direction on the Flexural Strength, Flexural Modulus and Fractographic Analysis of 3D-Printed Temporary Materials. *Dent. Mater. J.* 2021, *40*, 641–649, doi:10.4012/dmj.2020-147.

36. Maroti, P.; Varga, P.; Abraham, H.; Falk, G.; Zsebe, T.; Meiszterics, Z.; Mano, S.; Csernatony, Z.; Rendeki, S.; Nyitrai, M. Printing Orientation Defines Anisotropic Mechanical Properties in Additive Manufacturing of Upper Limb Prosthetics. *Mater. Res. Express* 2018, *6*, 035403, doi:10.1088/2053-1591/aaf5a9.

37. Dwiyati, S.T.; Kholil, A.; Riyadi, R.; Putra, S.E. Influence of Layer Thickness and 3D Printing Direction on Tensile Properties of ABS Material. *J. Phys. Conf. Ser.* 2019, *1402*, 066014, doi:10.1088/1742-6596/1402/6/066014.

38. Zaldivar, R.J.; Witkin, D.B.; McLouth, T.; Patel, D.N.; Schmitt, K.; Nokes, J.P. Influence of Processing and Orientation Print Effects on the Mechanical and Thermal Behavior of 3D-Printed ULTEM® 9085 Material. *Addit. Manuf.* 2017, *13*, 71–80, doi:10.1016/j.addma.2016.11.007.

39. Appalsamy, T.; Hamilton, S.L.; Kgaphola, M.J. Tensile Test Analysis of 3D Printed Specimens with Varying Print Orientation and Infill Density. *J. Compos. Sci.* 2024, *8*, 121, doi:10.3390/jcs8040121.

40. Appalsamy, T.; Hamilton, S.L.; Kgaphola, M.J. Tensile Test Analysis of 3D Printed Specimens with Varying Print Orientation and Infill Density. *J. Compos. Sci.* 2024, *8*, 121, doi:10.3390/jcs8040121.

41. Liu, H.; He, H.; Peng, X.; Huang, B.; Li, J. Three-dimensional Printing of Poly(Lactic Acid) Bio-based Composites with Sugarcane Bagasse Fiber: Effect of Printing Orientation on Tensile Performance. *Polym. Adv. Technol.* 2019, *30*, 910–922, doi:10.1002/pat.4524.

42. Akgümüş Gök, D. Determination of Optimum Printing Direction of the Polycarbonate Parts Produced by Additive Manufacturing. *Mater. Res. Express* 2024, *11*, 045302, doi:10.1088/2053-1591/ad3f79.

43. Tymrak, B.M.; Kreiger, M.; Pearce, J.M. Mechanical Properties of Components Fabricated with Open-Source 3-D Printers under Realistic Environmental Conditions. *Mater. Des.* 2014, *58*, 242–246, doi:10.1016/j.matdes.2014.02.038.

44. Xie, X.; Bennett, J.; Saha, S.; Lu, Y.; Cao, J.; Liu, W.K.; Gan, Z. Mechanistic Data-Driven Prediction of as-Built Mechanical Properties in Metal Additive Manufacturing. *npj Comput. Mater.* 2021, *7*, 86, doi:10.1038/s41524-021-00555-z.

45. Long, H.; Lin, H.; Li, S.; Bai, Y.; Qin, L.; Xiao, T.; Qin, A. Nanomechanical Properties of CH4-Containing Coal during CO2 Storage under Different Injection Pressures Based on Molecule Dynamics. *Appl. Surf. Sci.* 2022, *590*, 153126, doi:10.1016/j.apsusc.2022.153126.

46. Parsajoo, M.; Armaghani, D.J.; Mohammed, A.S.; Khari, M.; Jahandari, S. Tensile Strength Prediction of Rock Material Using Non-Destructive Tests: A Comparative Intelligent Study. *Transp. Geotech.* 2021, *31*, 100652, doi:10.1016/j.trgeo.2021.100652.

47. Subramanian, S.M. Mechanical Properties of Materials: Definition, Testing and Application. *Int. J. Mod. Stud. Mech. Eng.* 2020, *6*, 28–38, doi:10.20431/2454-9711.0602003.

48. Raj, R.; Dixit, A.R.; Łukaszewski, K.; Wichniarek, R.; Rybarczyk, J.; Kuczko, W.; Górski, F. Numerical and Experimental Mechanical Analysis of Additively Manufactured Ankle–Foot Orthoses. *Materials (Basel).* 2022, *15*, 6130, doi:10.3390/ma15176130.

X. Datasets

All kinematic, kinetic, and spatiotemporal data are presented for each of the patients, as well as the global data. Additionally, the results of the mechanical tests performed on different materials are also presented.

Patient	Affected Limb
1	Left
2	Left
3	Left
4	Right
5	Right
6	Left
7	Right
8	Left
9	Right
10	Right
GLOBAL	Left / Right

Graphics Lines:

___ - CO

___ - PO

▒▒▒ - Normative Data Healthy Adult

Statistical Analyses Performed:

Kinematics - SPM Paired (Patient); SPM Unpaired (Global)

Kinetics - SPM Paired (Patient); SPM Unpaired (Global)

Spatiotemporal - Wilcoxon Test [Paired – Non-Parametric] (Patient); Mann-Whitney Test [Unpaired-Non-Parametric] (Global)

Graphic Name	Actual Name of the Joint / Moment
Kinematics	
Pelvic Angles X	Pelvic Anterior Tilt
Pelvic Angles Y	Pelvic Up Obliquity
Pelvic Angles Z	Pelvic Int. Rotation
Hip Angles X	Hip Flexion
Hip Angles Y	Hip Adduction
Hip Angles Z	Hip Int. Rotation
Knee Angles X	Knee Flexion
Knee Angles Y	Knee Varus
Knee Angles Z	Knee Int. Rotation
Ankle Angles X	Ankle Dorsiflexion
Ankle Angles Y	Ankle Inversion
Foot Pitch Angles X	Foot Pitch
Foot Progression Z	Foot Int. Progression
Kinetics	
Hip Moment X	Int Hip Extensor Moment
Hip Moment Y	Int. Hip Valgus Moment
Knee Moment X	Int. Knee Extensor Moment
Knee Moment Y	Int. Knee Valgus Moment
Ankle Moment X	Int. Ankle Plantarflexor Moment
Ankle Moment Y	Int. Ankle Extensor Moment

Kinematics, Kinetics and Spatiotemporal

PATIENT 1

Right Pelvic Angles X

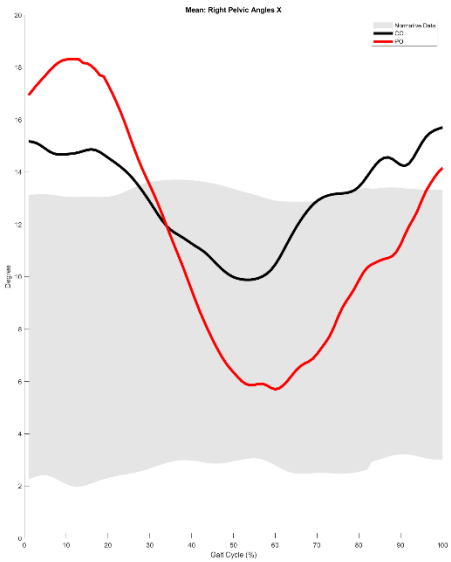

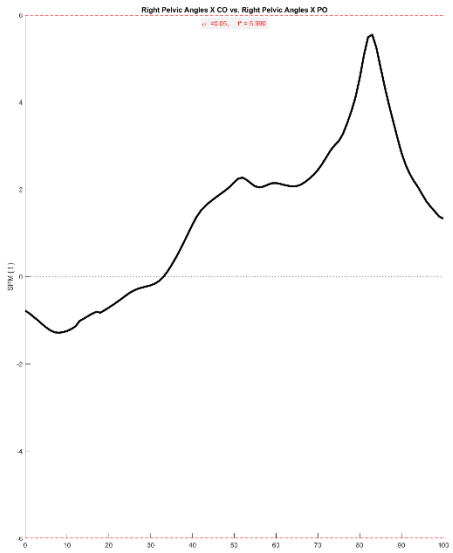

Right Pelvic Angles Y

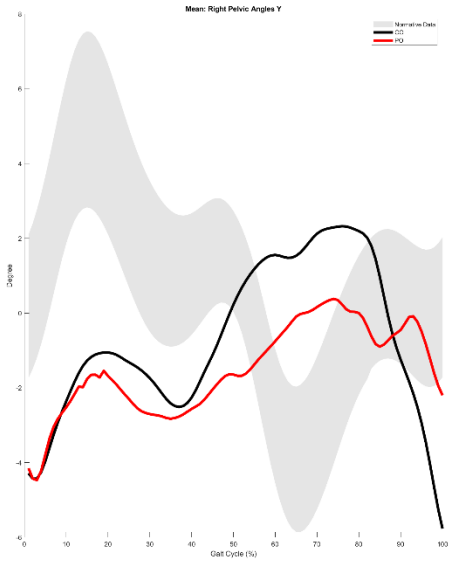

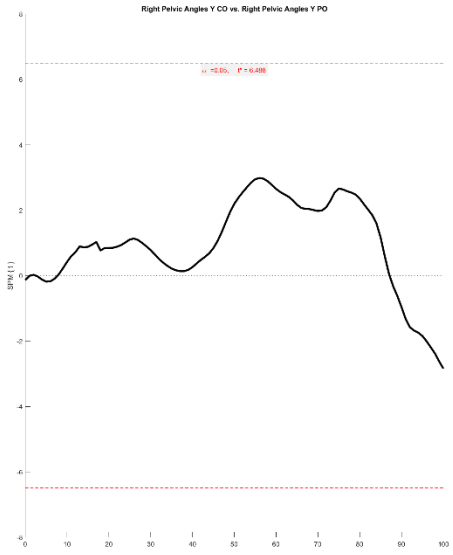

Right Pelvic Angles Z

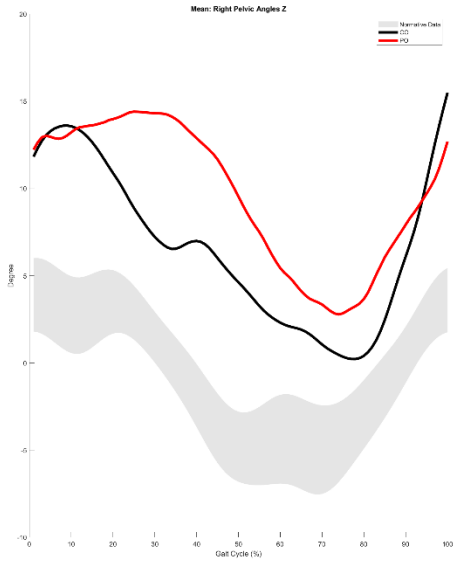

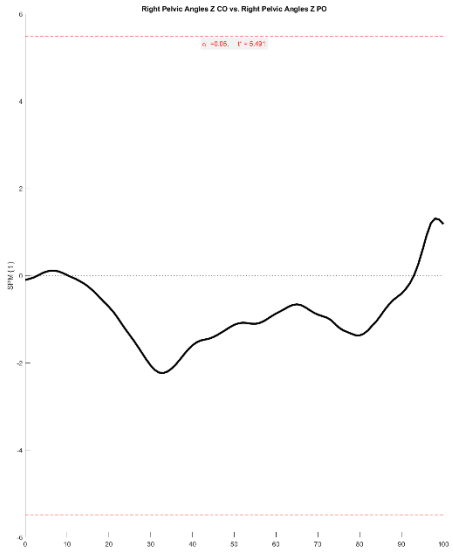

Left Pelvic Angles X

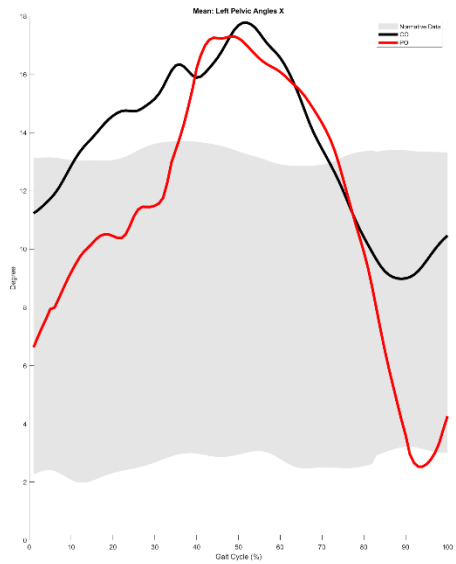

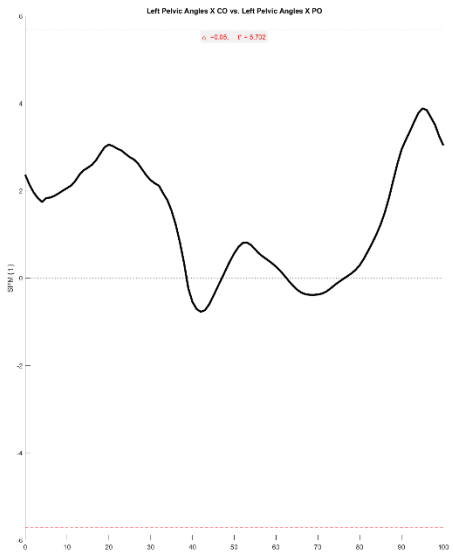

Left Pelvic Angles Y

11.8-14.6%

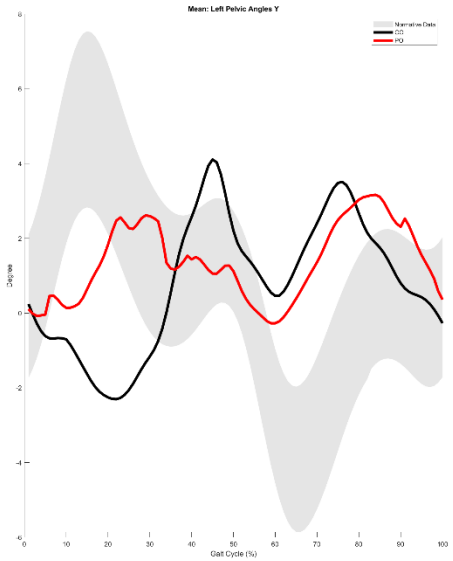

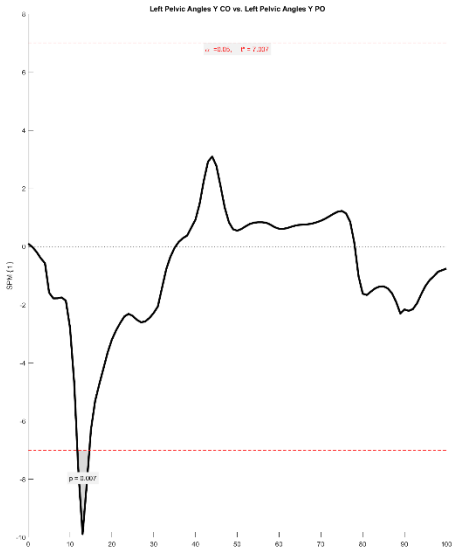

Left Pelvic Angles Z

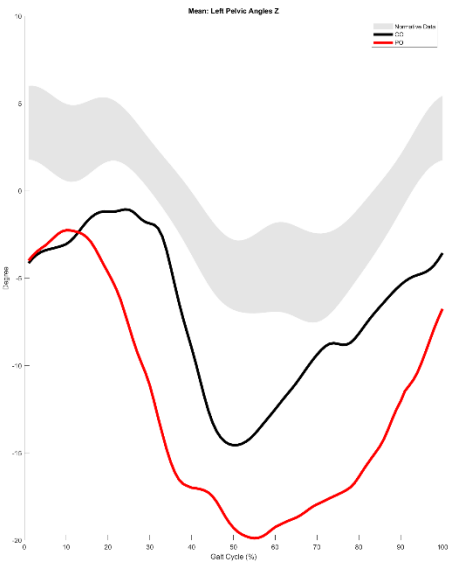

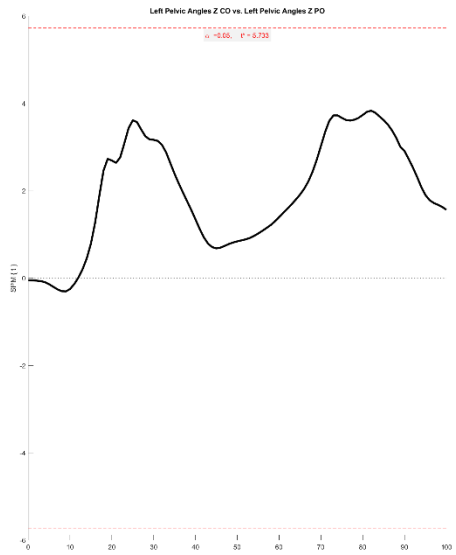

Right Hip Angles X

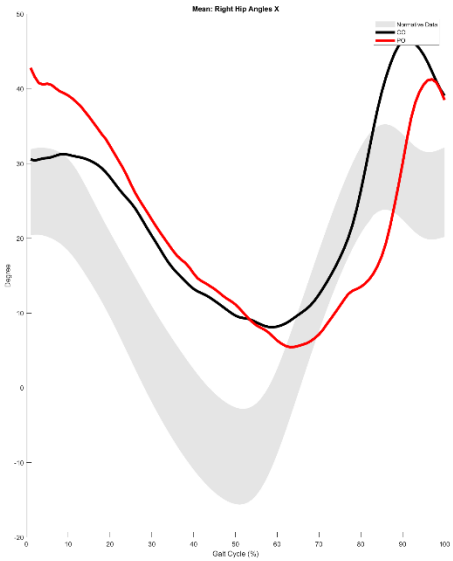

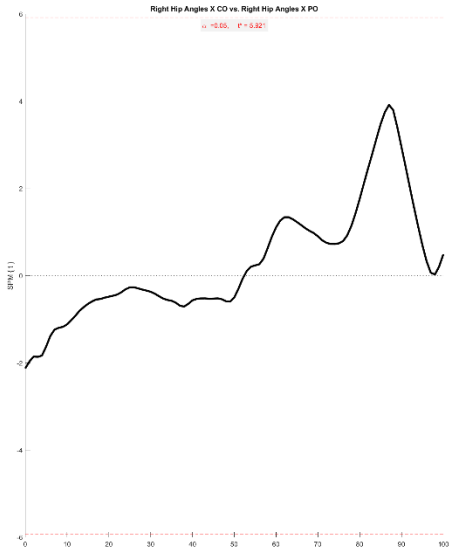

Right Hip Angles Y

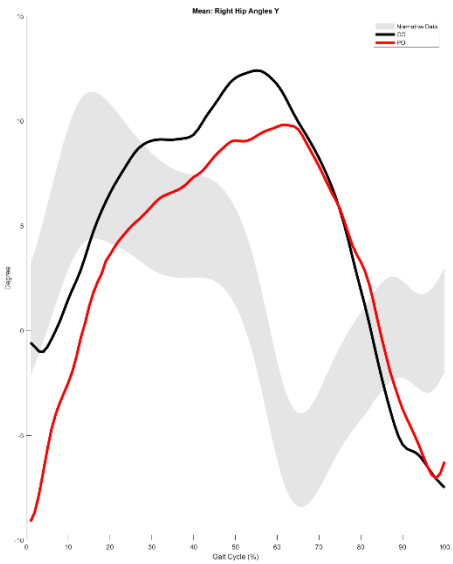

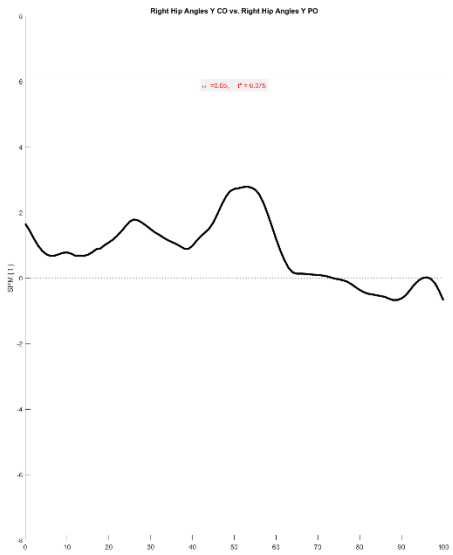

Right Hip Angles Z

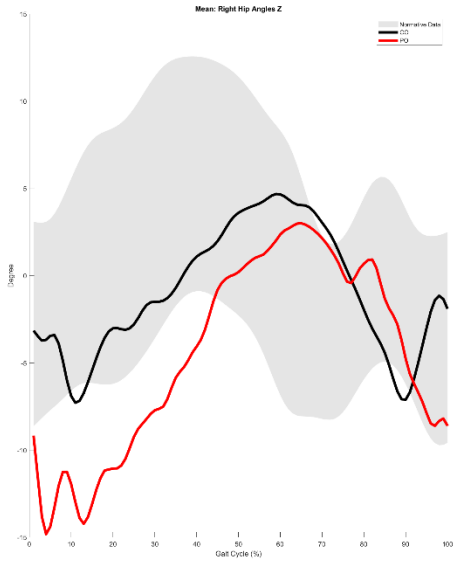

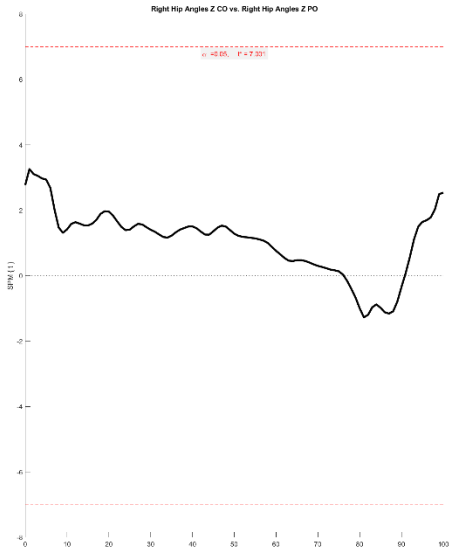

Left Hip Angles X

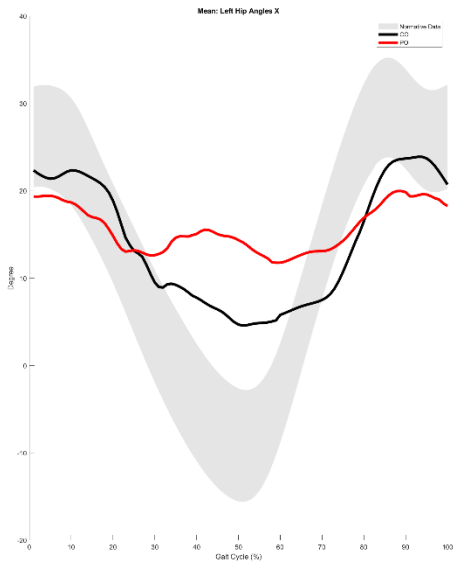

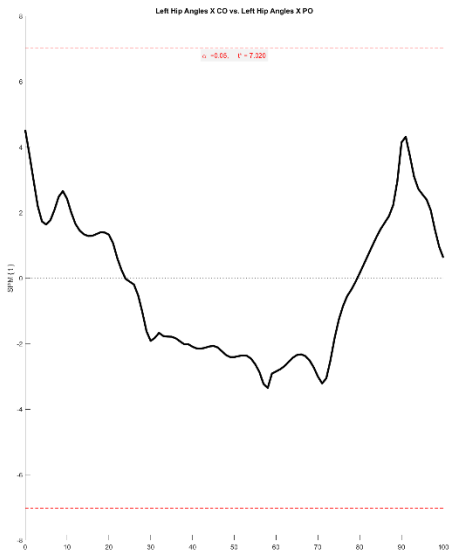

Left Hip Angles Y

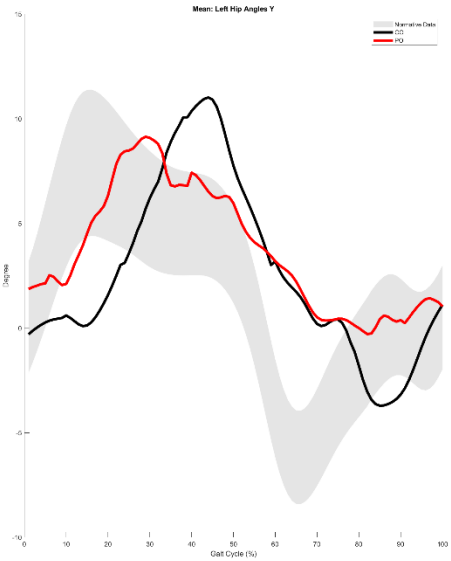

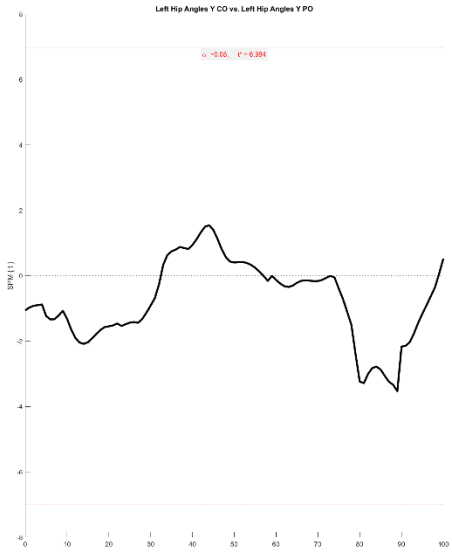

Left Hip Angles Z

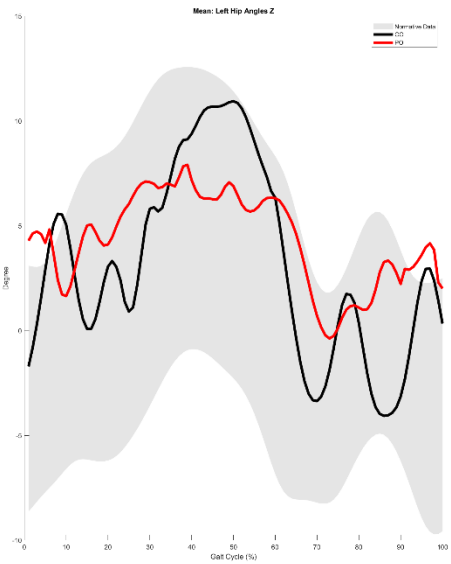

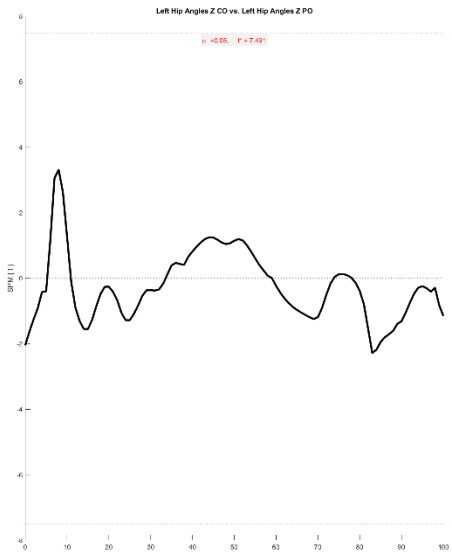

Right Knee Angles X

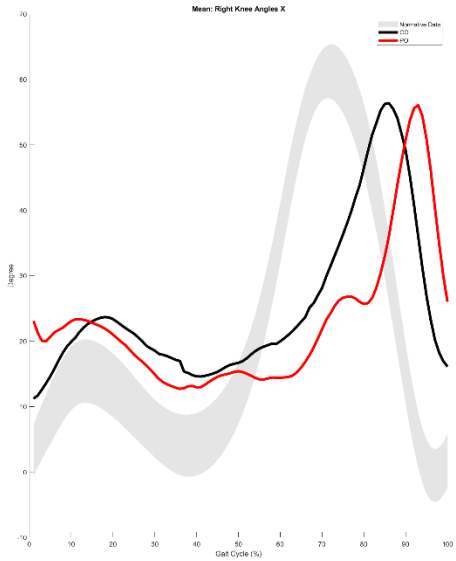

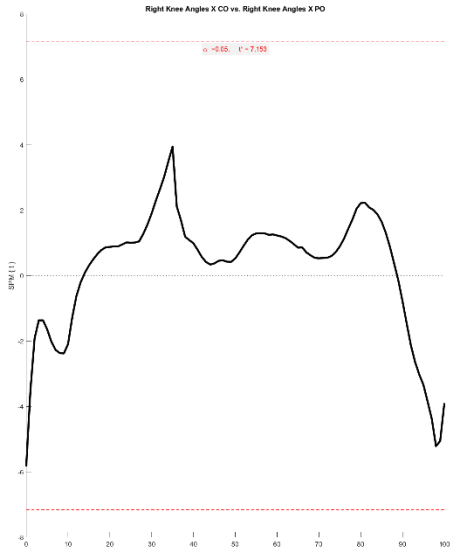

Right Knee Angles Y

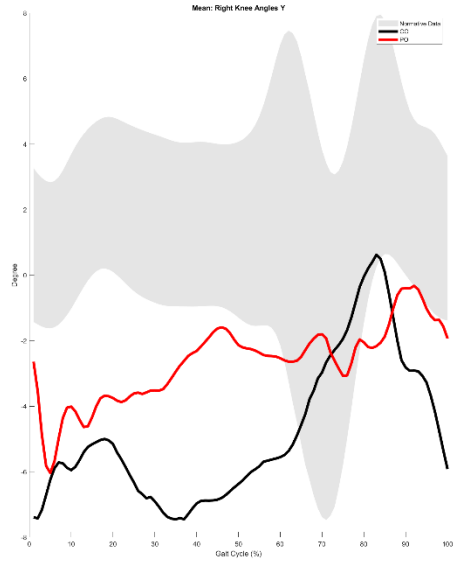

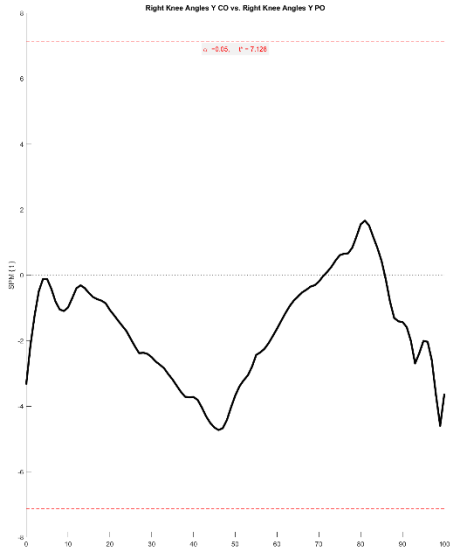

Right Knee Angles Z

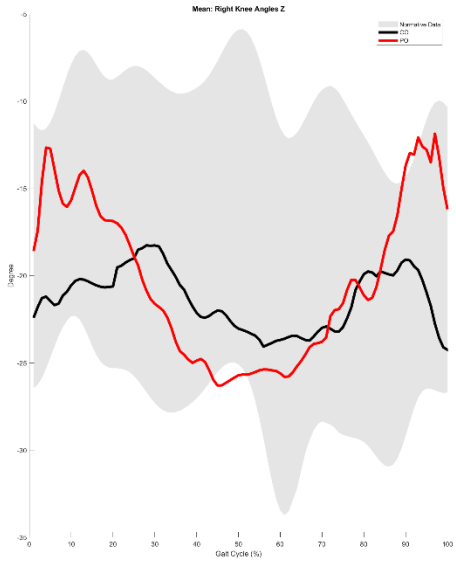

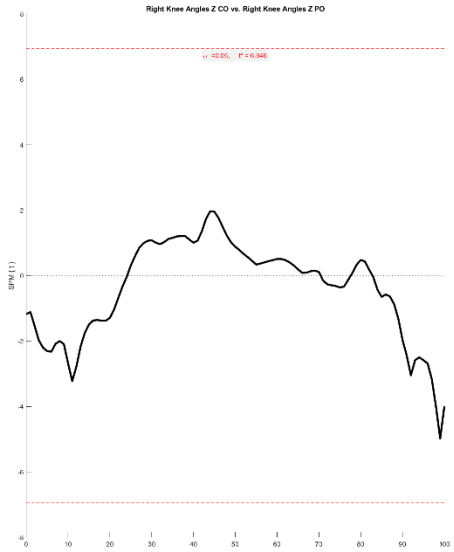

Left Knee Angles X

90.9-91.2%

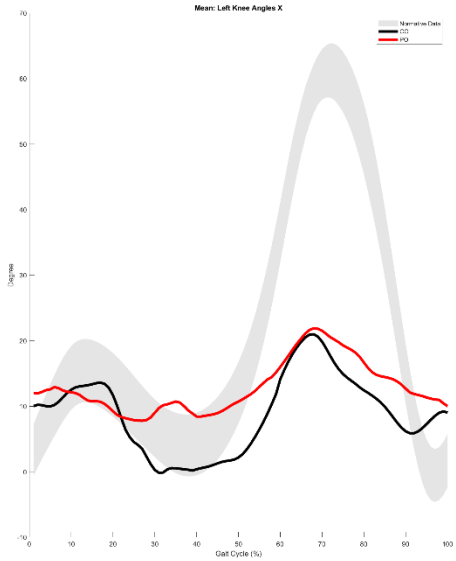

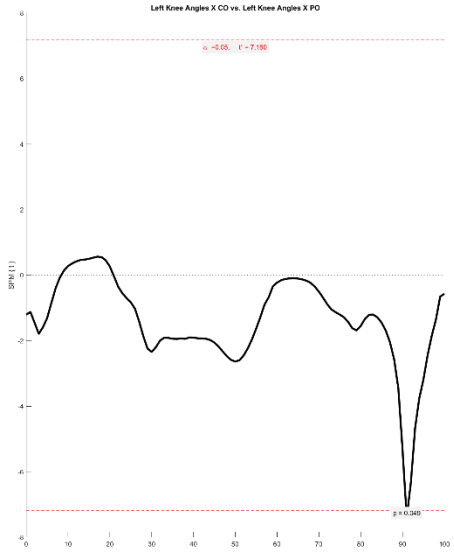

Left Knee Angles Y

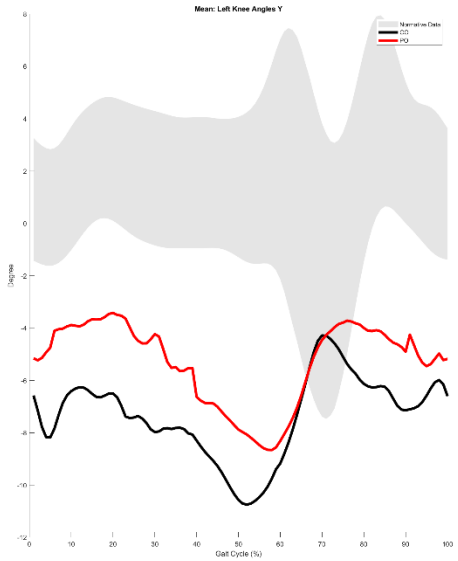

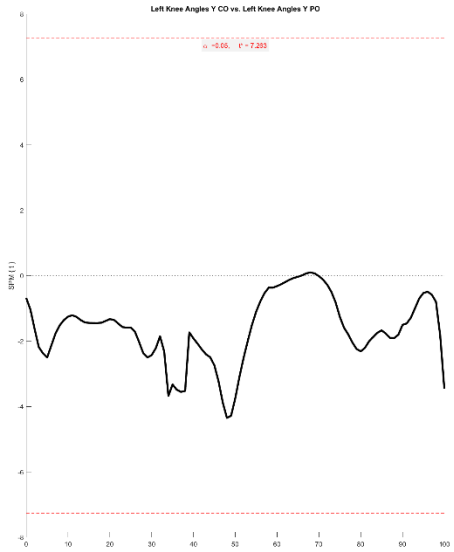

Left Knee Angles Z

84.2-92.8%

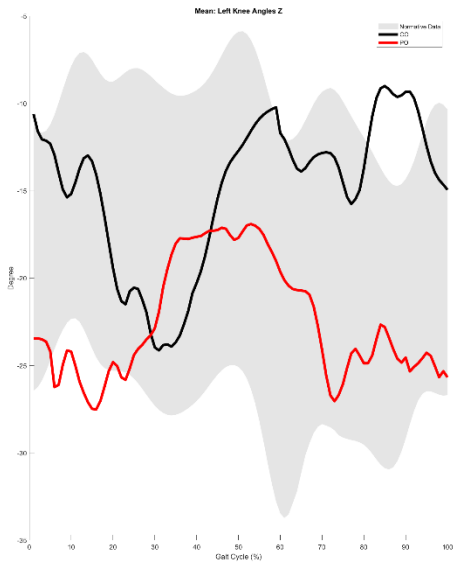

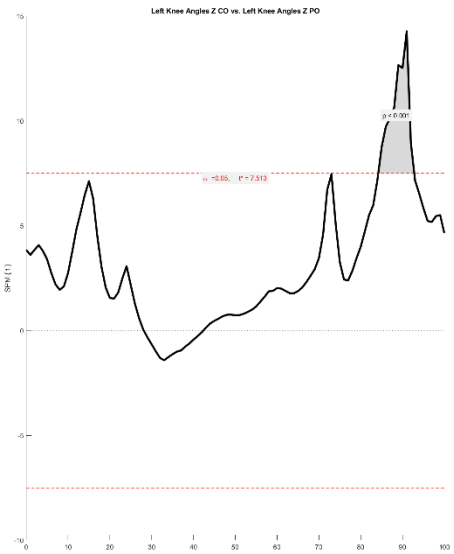

Right Ankle Angles X

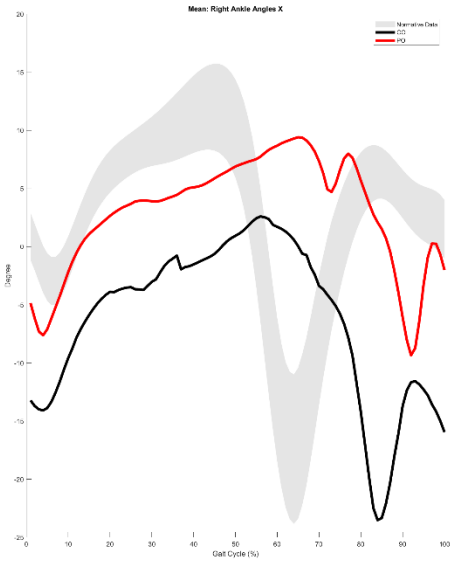

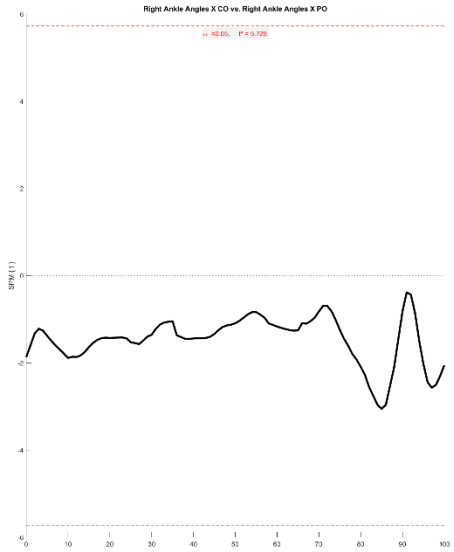

Right Ankle Angles Y

7.4-36.3%, 39.5-41.5%, 80.9-89.6%, 99.7-100.0%

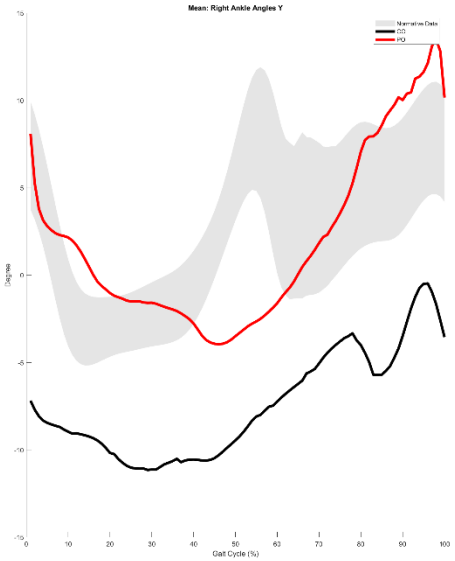

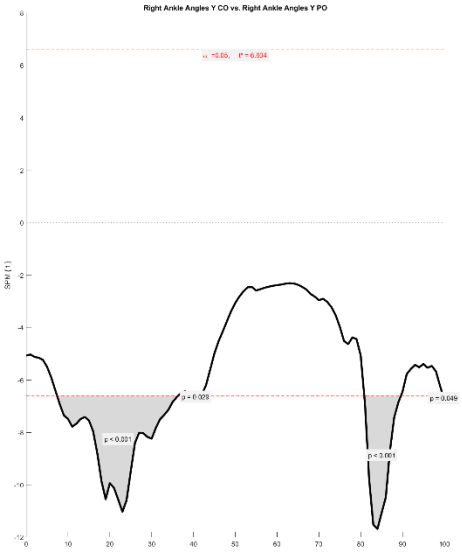

Left Ankle Angles X

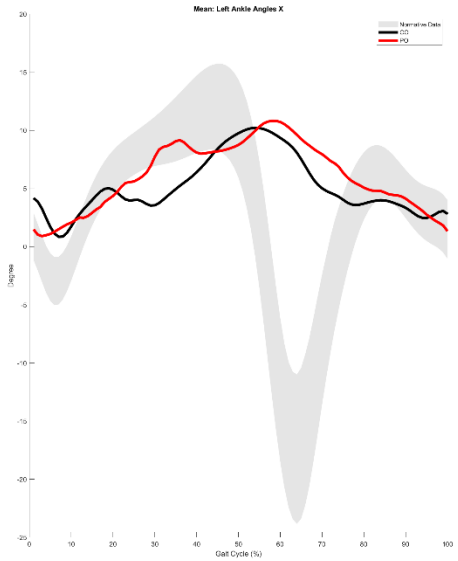

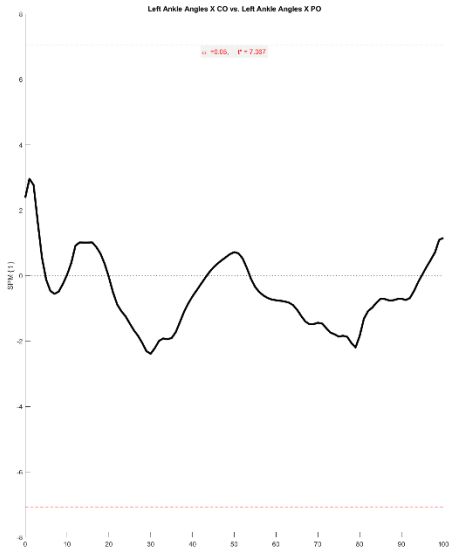

Left Ankle Angles Y

10.9-11.0%, 21.9-22.2%, 71.1-73.7%, 80.4-86.4%, 89.4-95.2%

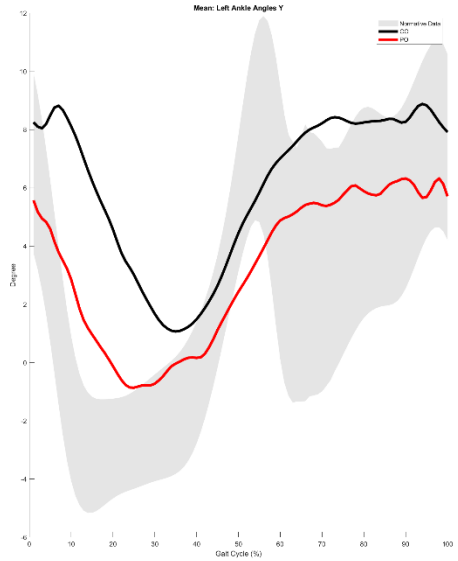

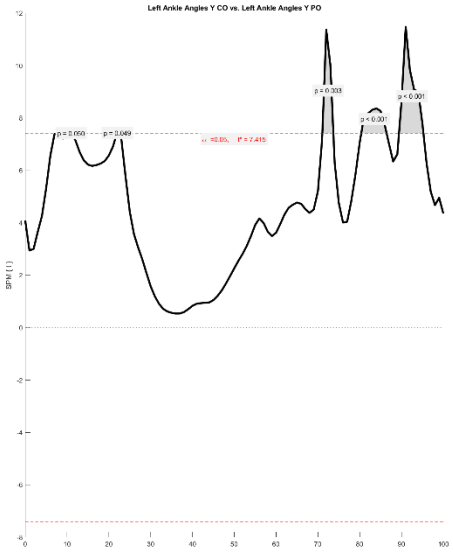

Right Foot Pitch Angles X

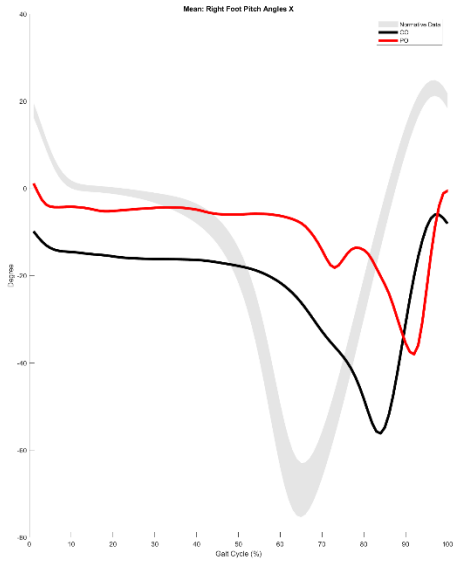

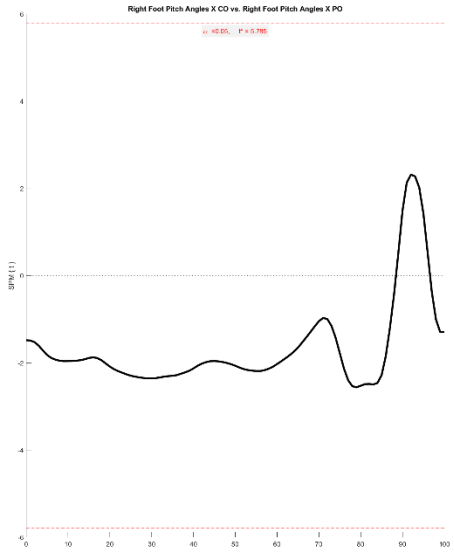

Left Foot Pitch Angles X

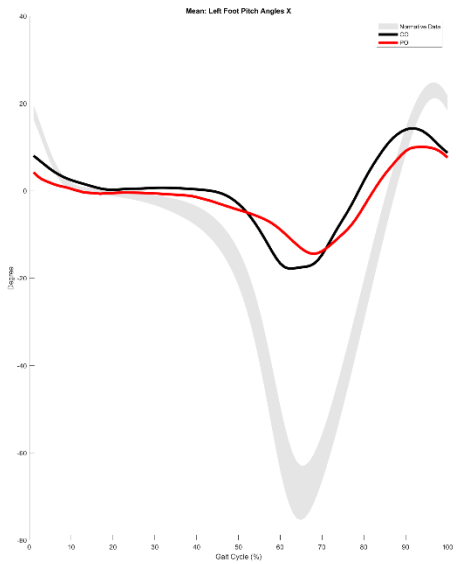

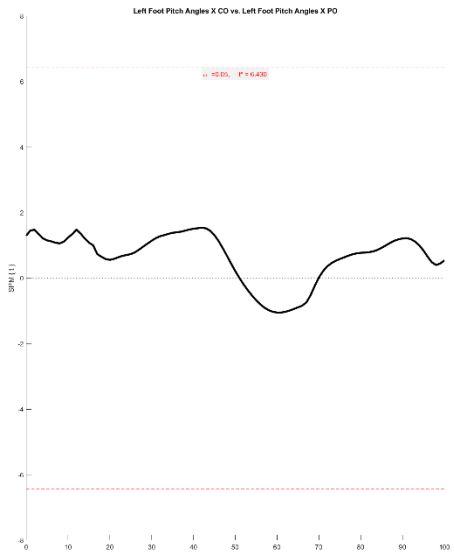

Right Foot Progression Z

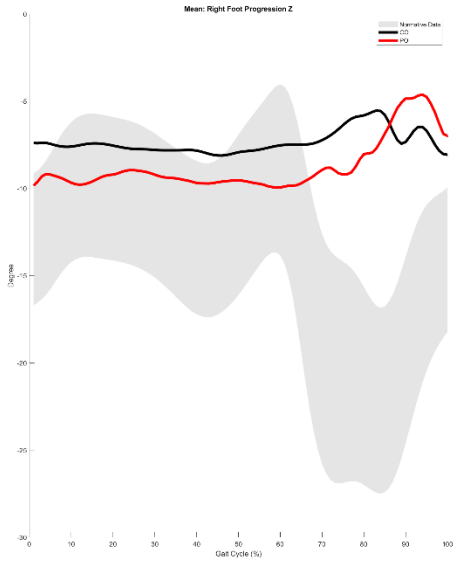

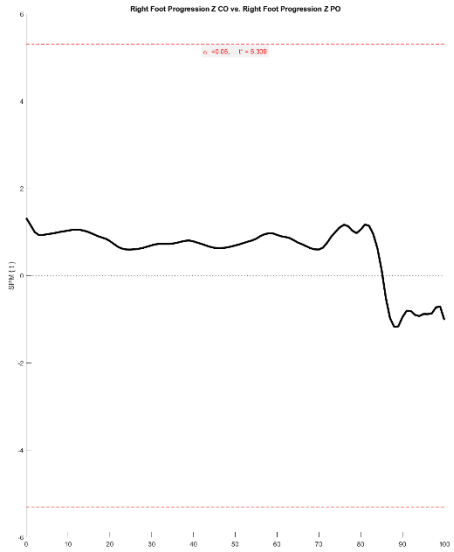

Left Foot Progression Z

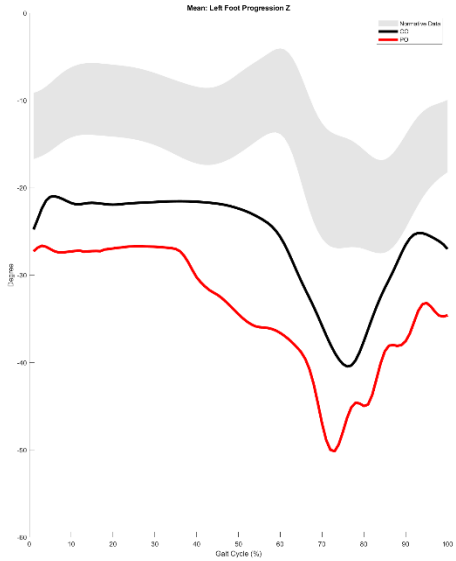

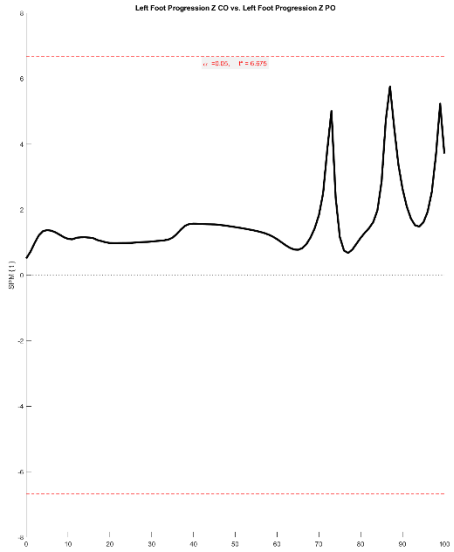

Right Hip Moment X

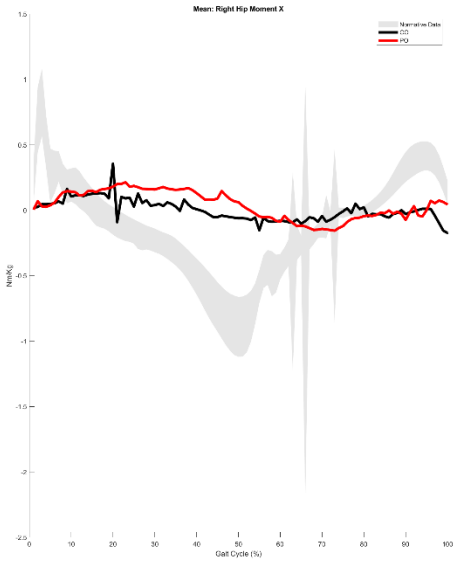

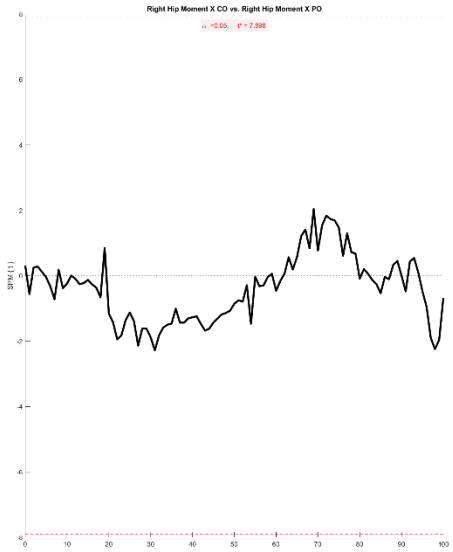

Right Hip Moment Y

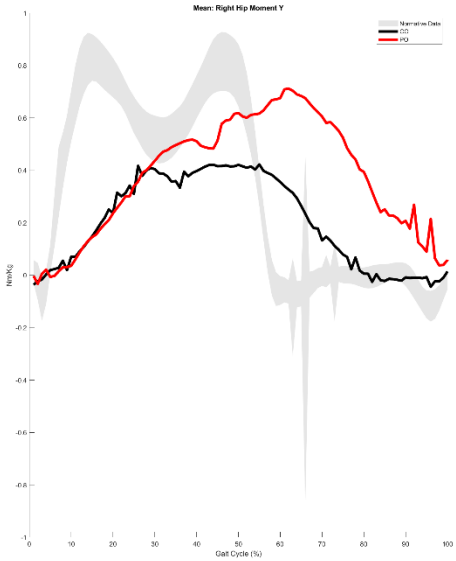

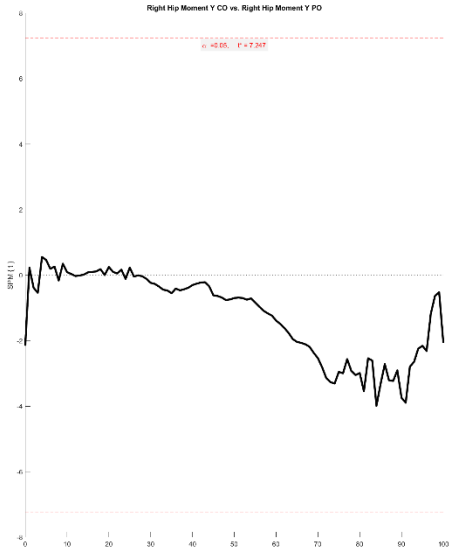

Left Hip Moment X

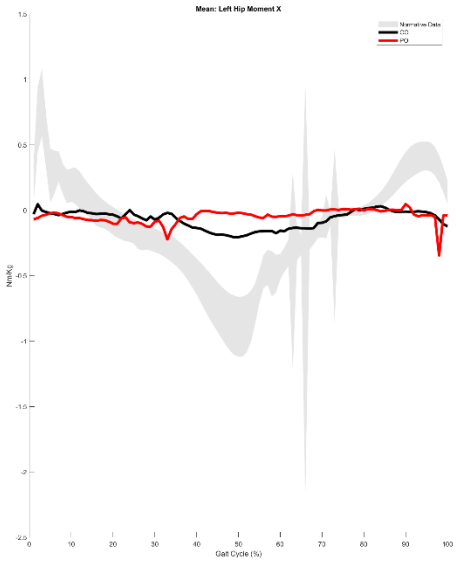

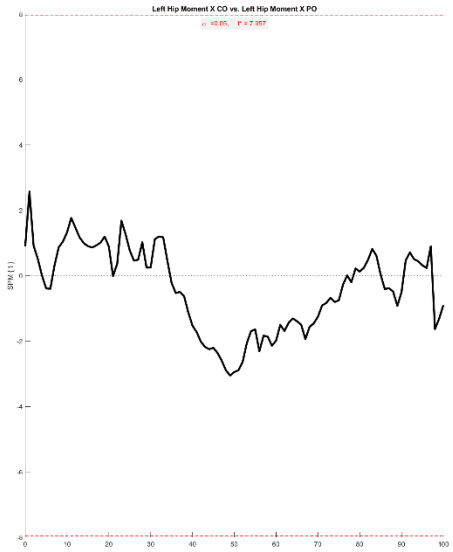

Left Hip Moment Y

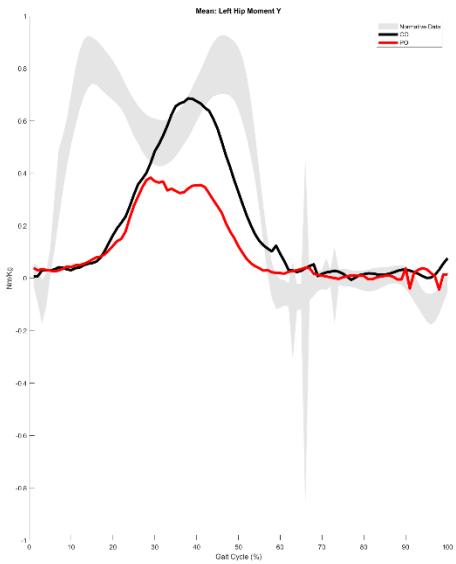

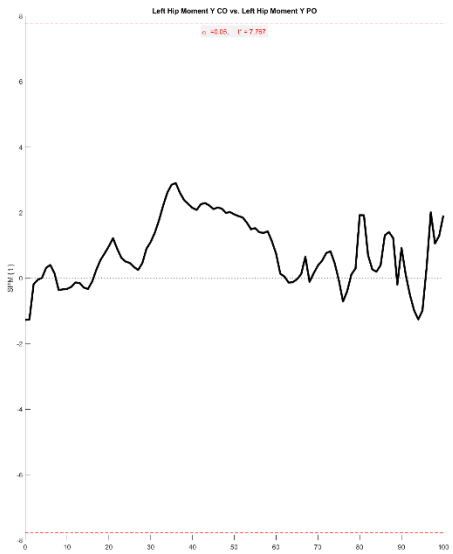

Right Knee Moment X

95.0-95.0%

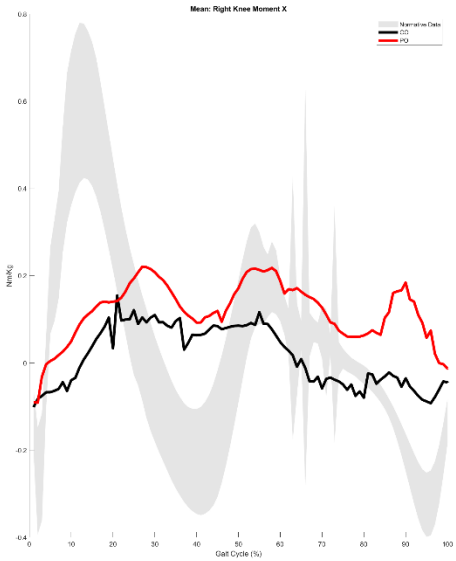

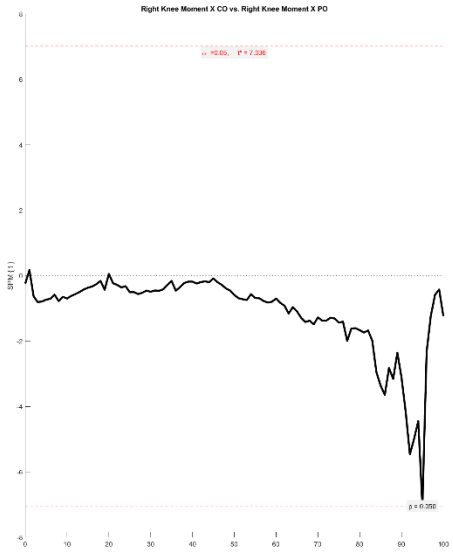

Right Knee Moment Y

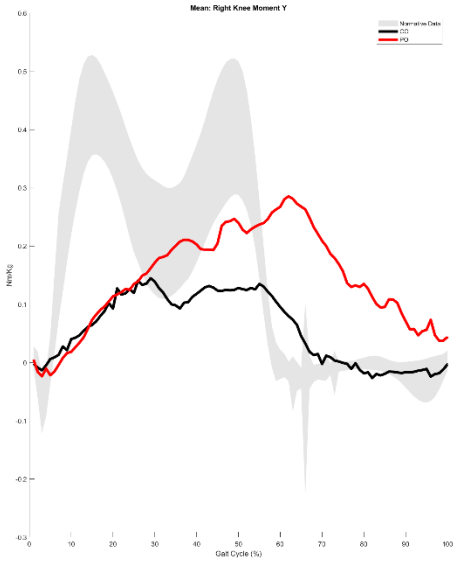

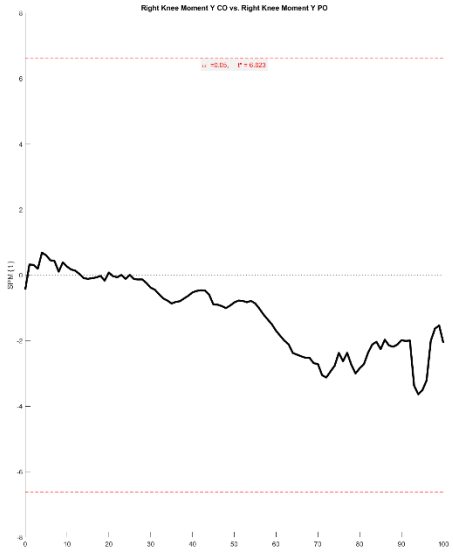

Left Knee Moment X

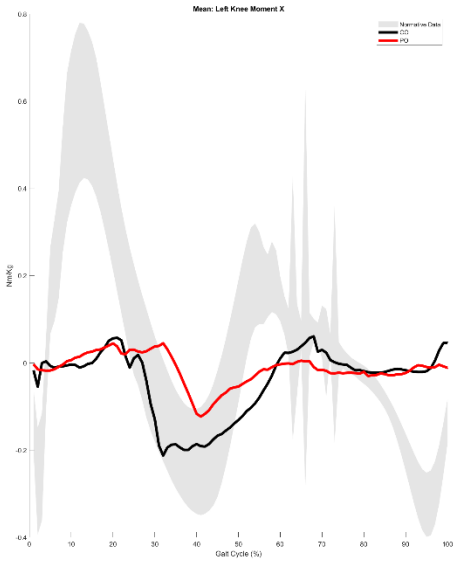

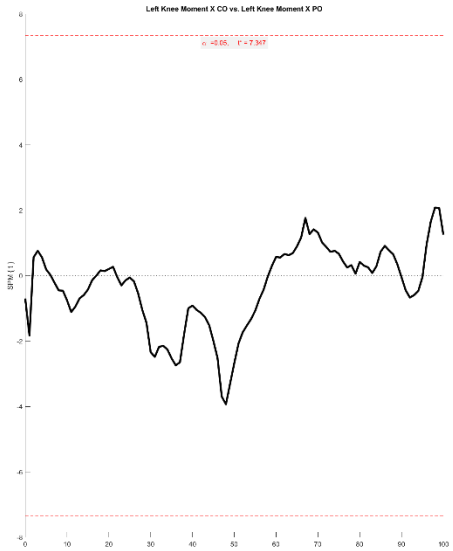

Left Knee Moment Y

21.5-22.7%

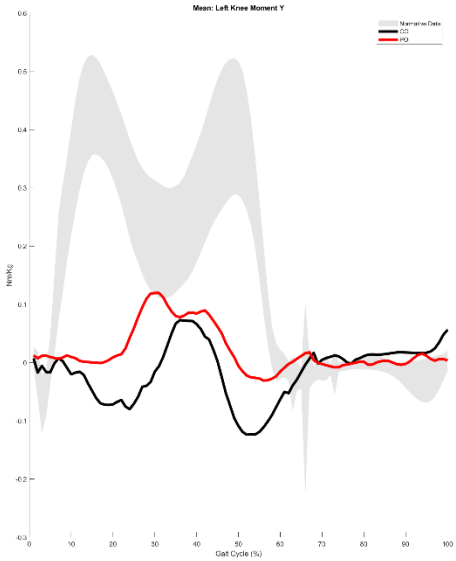

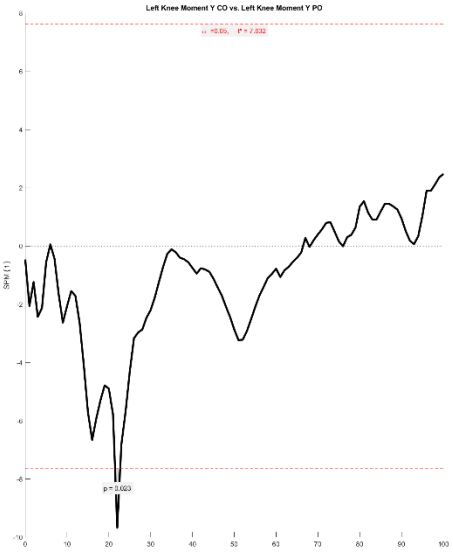

Right Ankle Moment X

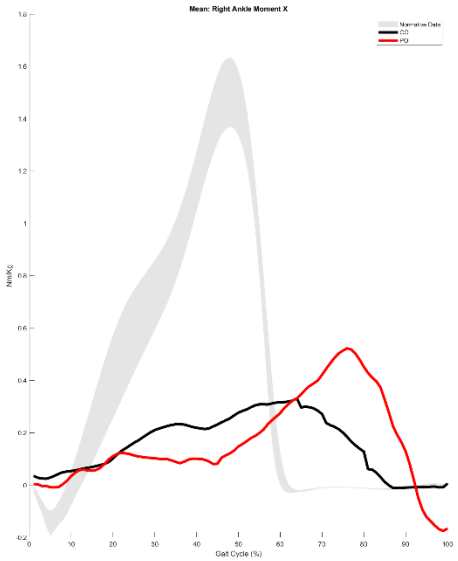

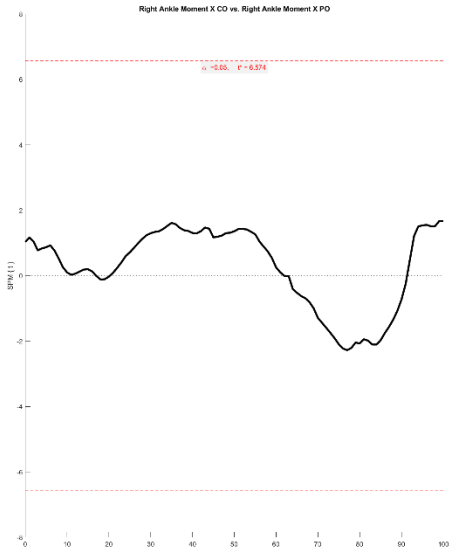

Right Ankle Moment Y

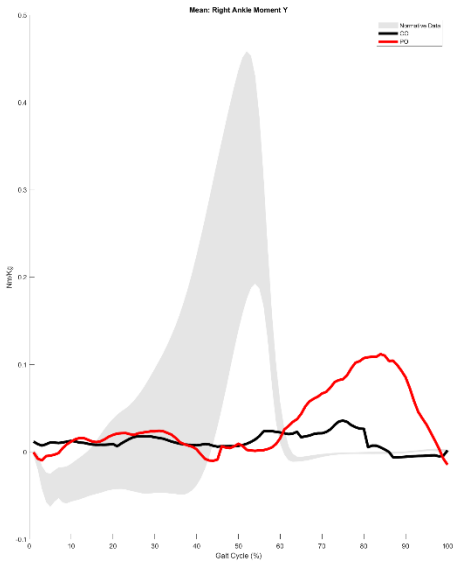

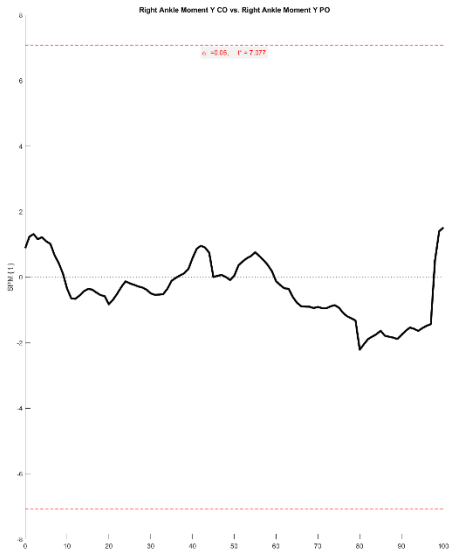

Left Ankle Moment X

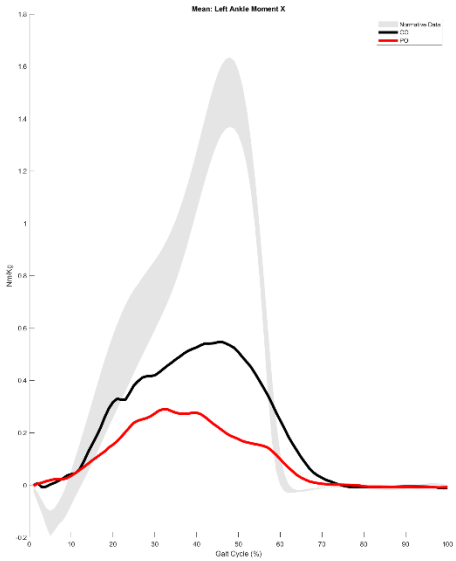

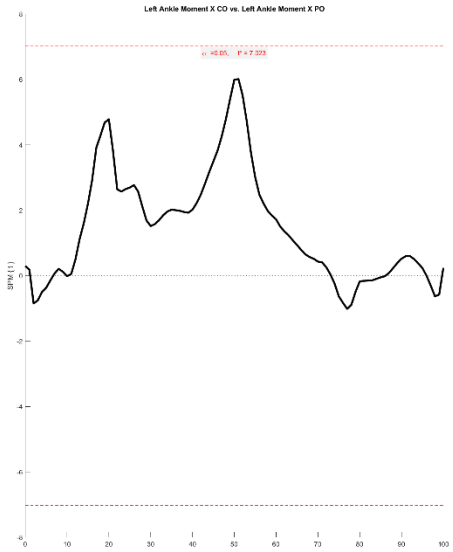

Left Ankle Moment Y

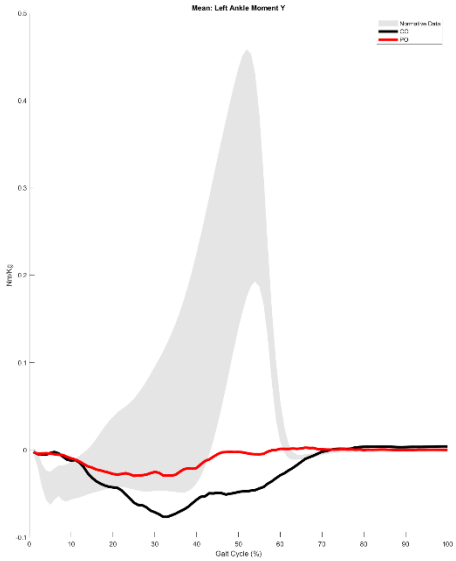

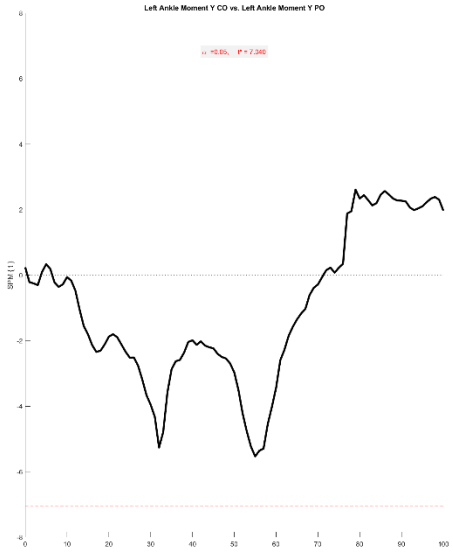

PO

Step Length

REP	Left	Right	IS (50%)	IS (0%)
1	0.21238	0.32345	39.6357	41.4572
2	0.21046	0.31968	39.6989	41.2042
3	0.19398	0.30221	39.0939	43.6244
4	0.19287	0.29782	39.3059	42.7765
5	0.189	0.29558	39.0028	43.9886
6	0.18186	0.22925	44.2363	23.0547
Mean	0.196758	0.294665	40.1623	39.3509
SD	0.011081	0.0310944	1.83979	7.35917

CO

Step Length

REP	Left	Right	IS (50%)	IS (0%)
1	0.26541	0.39947	39.9185	40.3261
2	0.26442	0.39387	59.8323	39.3292
3	0.22154	0.38621	63.5475	54.19
4	0.20939	0.38284	64.6438	58.5752
5	0.20912	0.37691	64.3158	57.2633
6	0.18943	0.34139	64.3137	57.2548
Mean	0.2265517	0.380115	59.4286	51.1564
SD	0.0287098	0.0187896	8.87619	8.12307

PO

Swing Time

REP	Left	Right	IS (50%)	IS (0%)
1	0.91	0.49	35	60
2	0.91	0.45	33.0882	67.6471
3	0.83	0.39	31.9672	72.1311
4	0.8	0.36	31.0345	75.8621
5	0.77	0.32	29.3578	82.5688
6	0.75	0.31	29.2453	83.0189
Mean	0.828333	0.3866667	31.6155	73.538
SD	0.062827	0.0654896	2.03307	8.13228

CO

Swing Time

REP	Left	Right	IS (50%)	IS (0%)
1	0.86	0.54	38.5714	45.7143
2	0.79	0.47	37.3016	50.7937
3	0.77	0.44	36.3636	54.5455
4	0.74	0.43	36.7521	52.9915
5	0.62	0.36	36.7347	53.0612
6	0.55	0.33	37.5	50
Mean	0.7216667	0.4283333	37.2039	51.1843
SD	0.1051058	0.0691416	0.71852	2.87409

PO

Stance Time

REP	Left	Right	IS (50%)	IS (0%)
1	2.38	2.85	54.4933	17.9732
2	2.01	2.47	55.1339	20.5357
3	1.86	2.37	56.0284	24.1135
4	1.84	2.36	56.1905	24.7619
5	1.77	2.09	54.1451	16.5803
6	1.74	2.09	54.5692	18.2768
Mean	1.933333	2.3716667	55.0934	20.3736
SD	0.217383	0.2573206	0.77606	3.10424

CO

Stance Time

REP	Left	Right	IS (50%)	IS (0%)
1	1.79	1.97	52.3936	9.57447
2	1.74	1.97	53.0997	12.3989
3	1.65	1.9	53.5211	14.0845
4	1.63	1.87	53.4286	13.7143
5	1.5	1.85	55.2239	20.8955
6	1.31	1.68	56.1873	24.7492
Mean	1.6033333	1.8733333	53.9757	15.9028
SD	0.1597568	0.0977525	1.30546	5.22185

	Left	Right
Step Length PO	0.20	0.29
Step Length CO	0.23	0.38
Swing Time PO	0.83	0.39
Swing Time CO	0.72	0.43
Stance Time PO	1.93	2.37
Stance Time CO	1.60	1.87

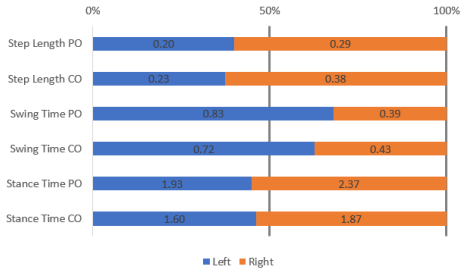

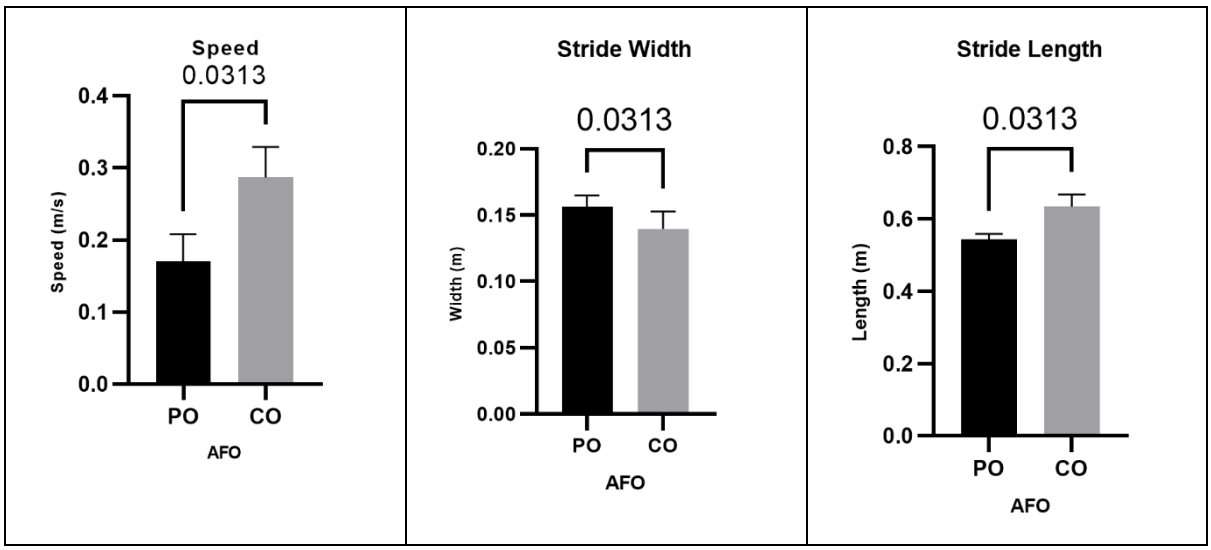

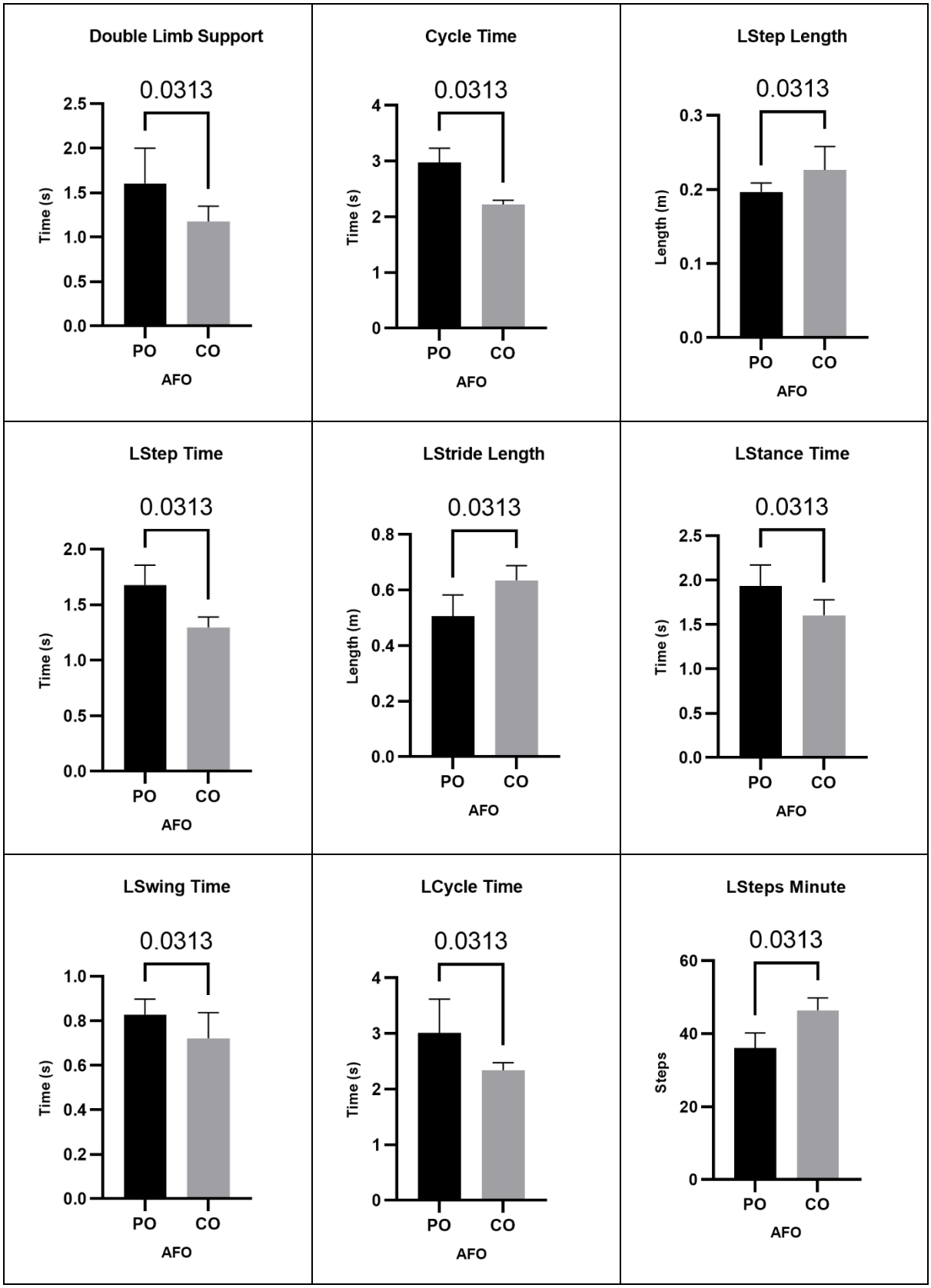
Double Limb Support
0.0313
Time (s)
2.5
2.0
1.5
1.0
0.5
0.0
PO
CO
AFO
Cycle Time
0.0313
Time (s)
4
3
2
1
0
PO
CO
AFO
LStep Length
0.0313
Length (m)
0.3
0.2
0.1
0.0
PO
CO
AFO
LStep Time
0.0313
Time (s)
2.0
1.5
1.0
0.5
0.0
PO
CO
AFO
LStride Length
0.0313
Length (m)
0.8
0.6
0.4
0.2
0.0
PO
CO
AFO
LStance Time
0.0313
Time (s)
2.5
2.0
1.5
1.0
0.5
0.0
PO
CO
AFO
LSwing Time
0.0313
Time (s)
1.0
0.8
0.6
0.4
0.2
0.0
PO
CO
AFO
LCycle Time
0.0313
Time (s)
4
3
2
1
0
PO
CO
AFO
LSteps Minute
0.0313
Steps
60
40
20
0
PO
CO
AFO

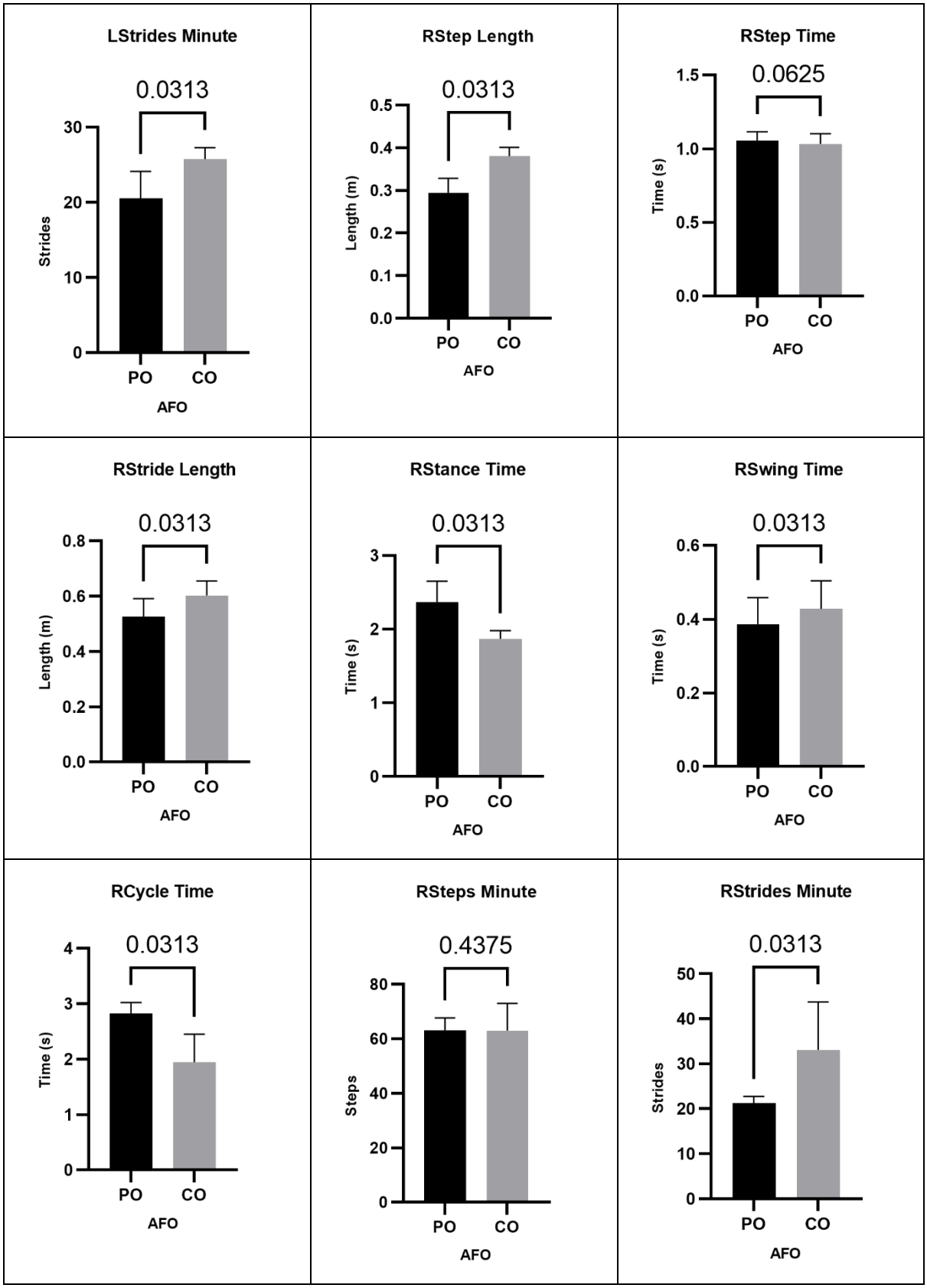
LStrides Minute
0.0313
Strides
30
20
10
0
PO
CO
AFO
RStep Length
0.0313
Length (m)
0.5
0.4
0.3
0.2
0.1
0.0
PO
CO
AFO
RStep Time
0.0625
Time (s)
1.5
1.0
0.5
0.0
PO
CO
AFO
RStride Length
0.0313
Length (m)
0.8
0.6
0.4
0.2
0.0
PO
CO
AFO
RStance Time
0.0313
Time (s)
3
2
1
0
PO
CO
AFO
RSwing Time
0.0313
Time (s)
0.6
0.4
0.2
0.0
PO
CO
AFO
RCycle Time
0.0313
Time (s)
4
3
2
1
0
PO
CO
AFO
RSteps Minute
0.4375
Steps
80
60
40
20
0
PO
CO
AFO
RStrides Minute
0.0313
Strides
50
40
30
20
10
0
PO
CO
AFO

PATIENT 2

Right Pelvic Angles X

1.2-7.5%

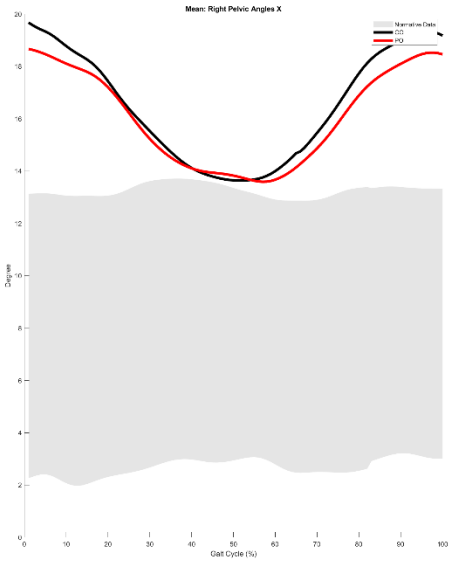

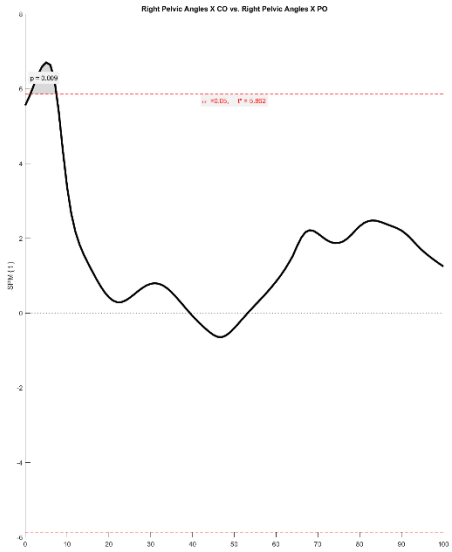

Right Pelvic Angles Y

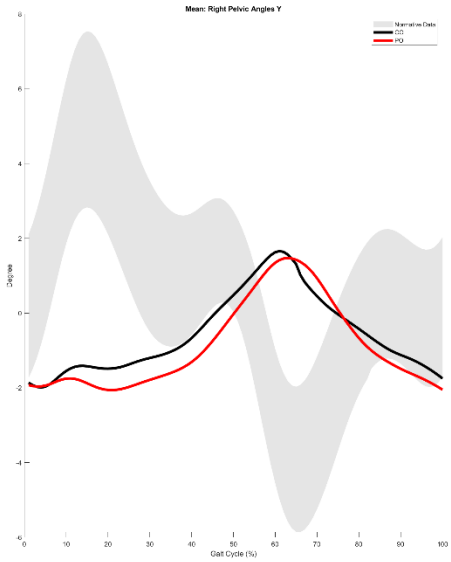

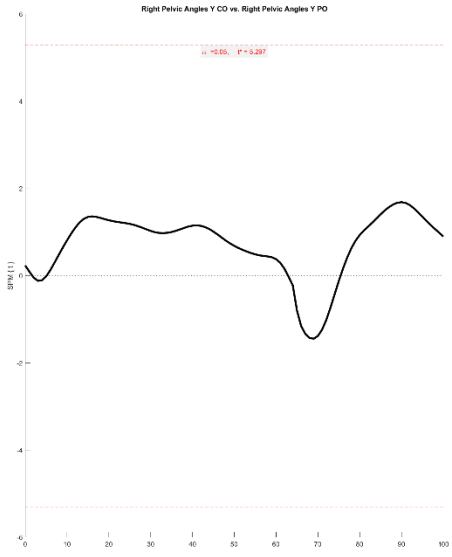

Right Pelvic Angles Z

46.2-60.4%, 67.9-75.5%

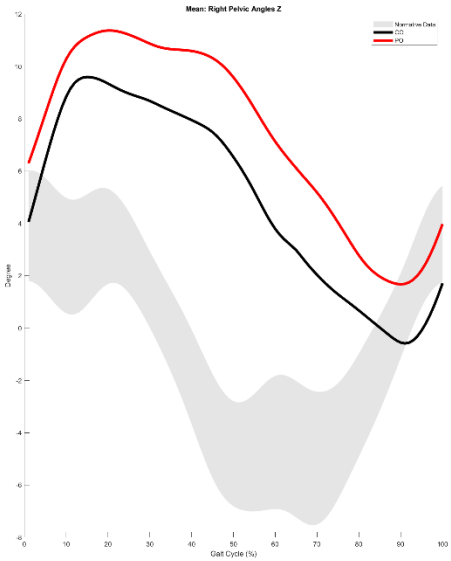

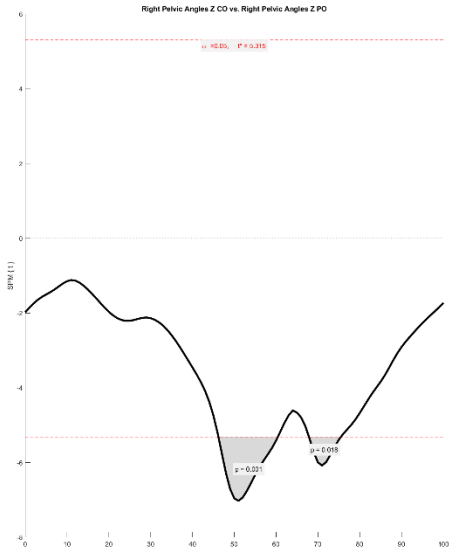

Left Pelvic Angles X

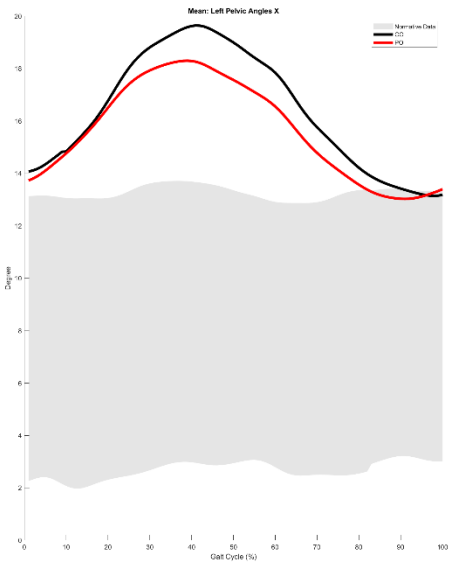

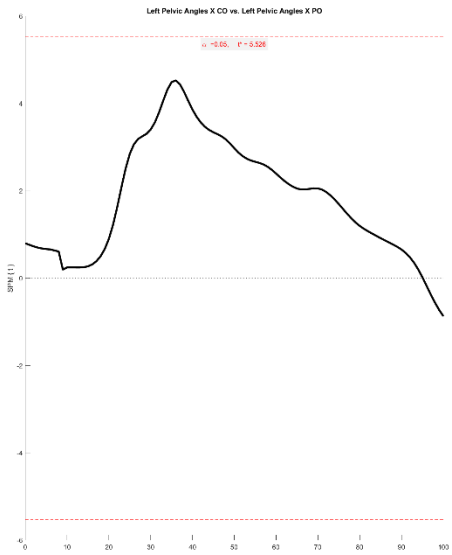

Left Pelvic Angles Y

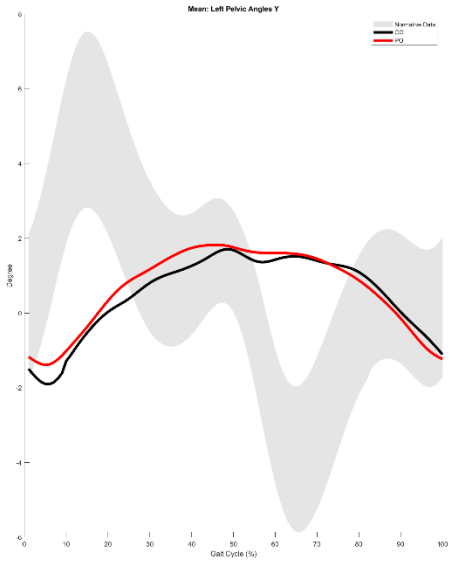

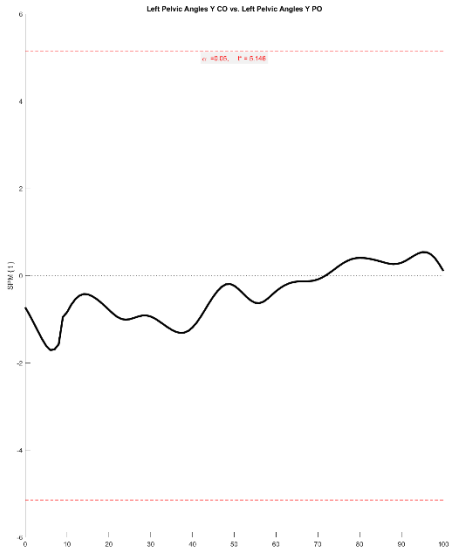

Left Pelvic Angles Z

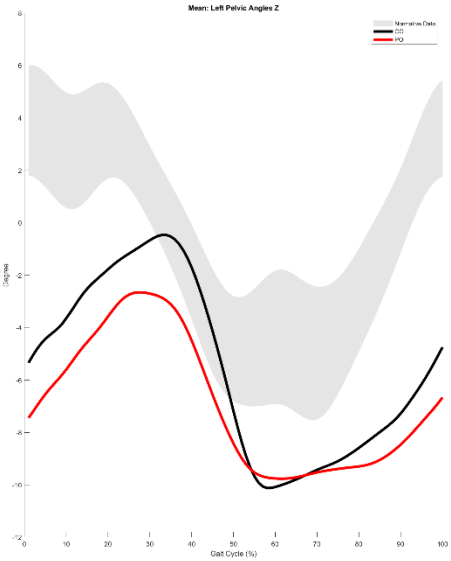

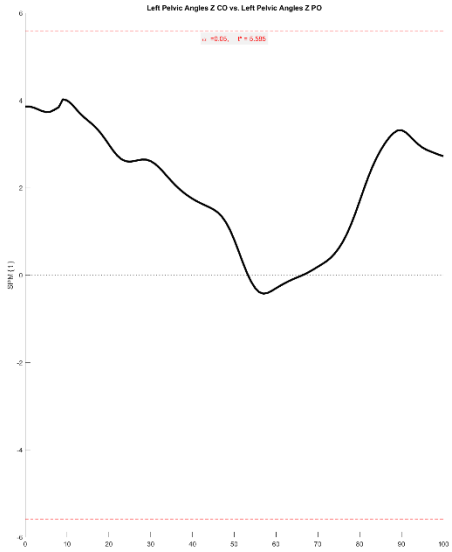

Right Hip Angles X

0.0-25.6%

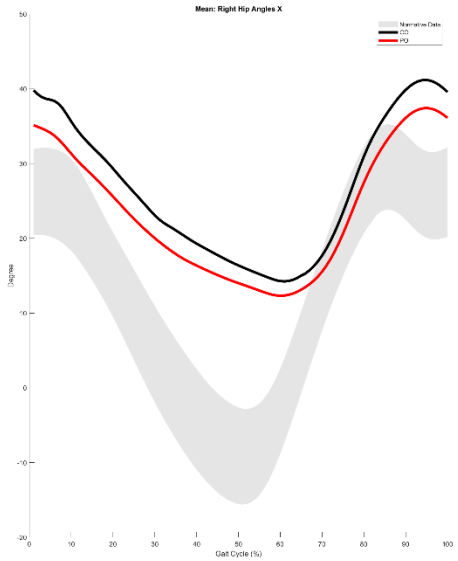

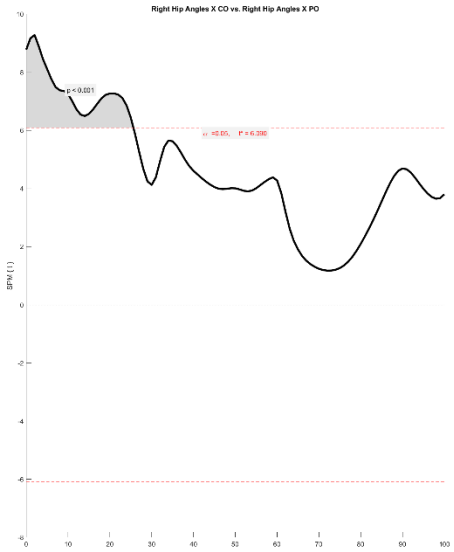

Right Hip Angles Y

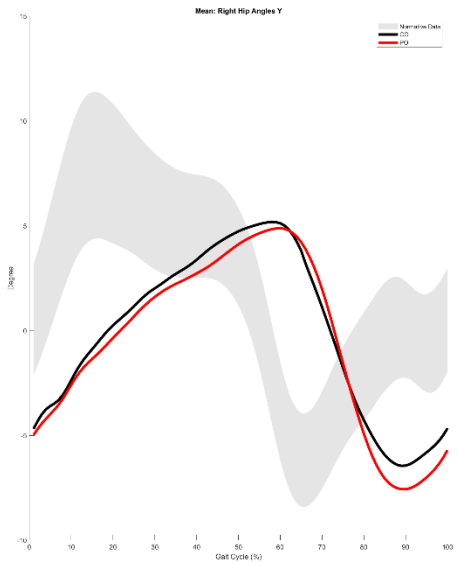

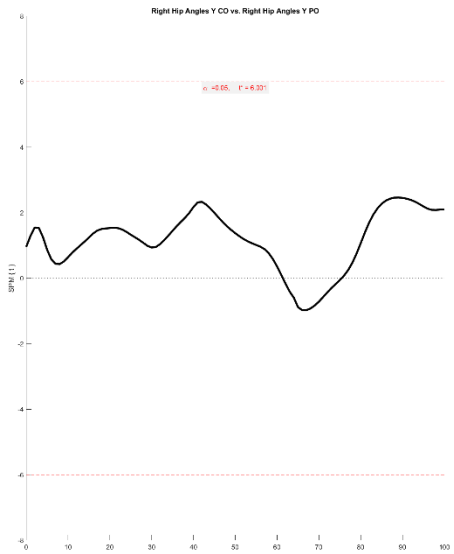

Right Hip Angles Z

6.3-12.0%, 62.0-89.3%

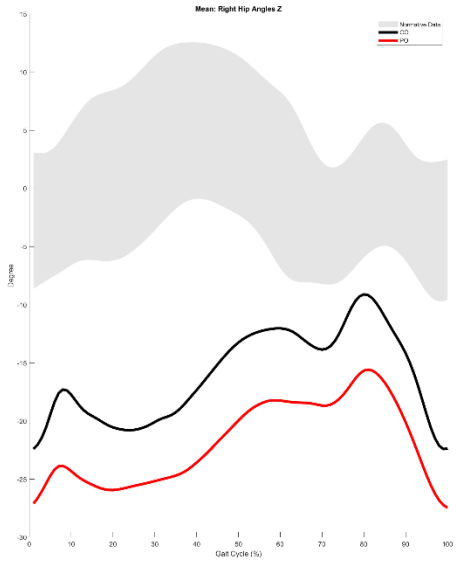

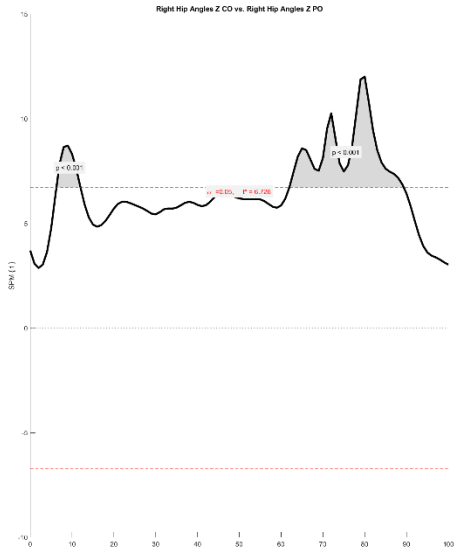

Left Hip Angles X

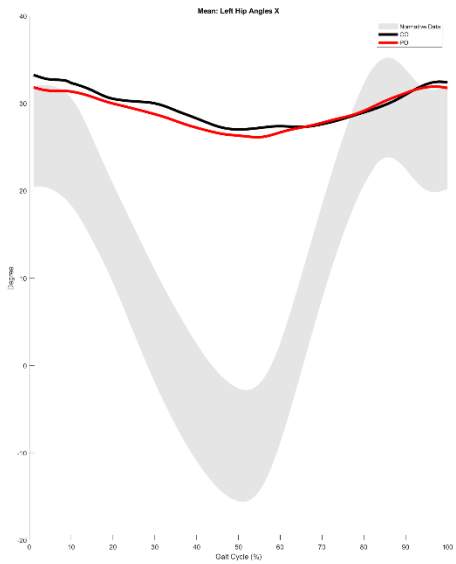

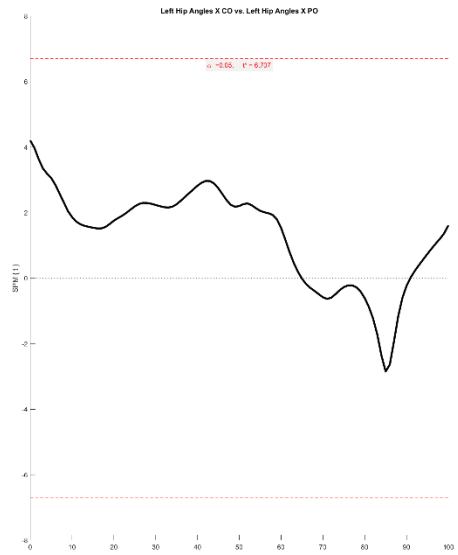

Left Hip Angles Y

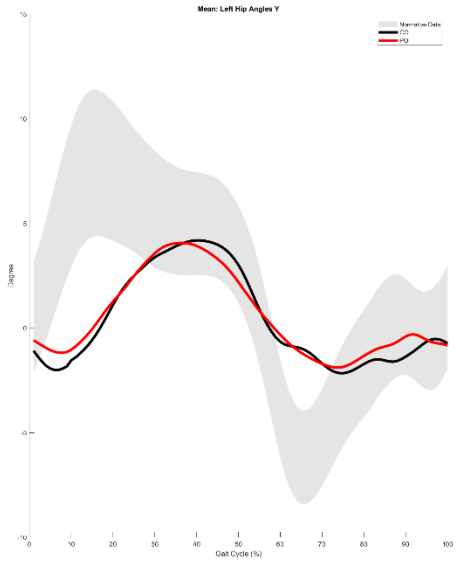

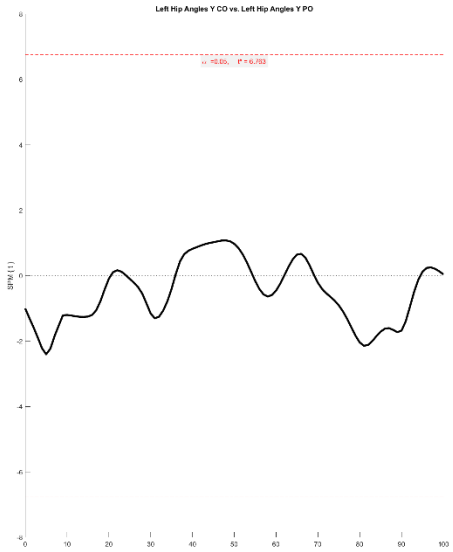

Left Hip Angles Z

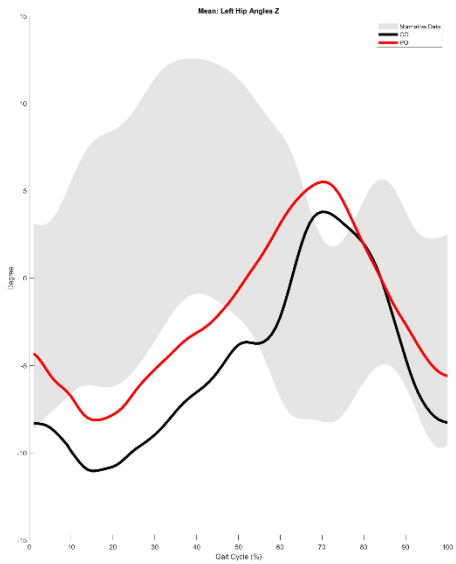

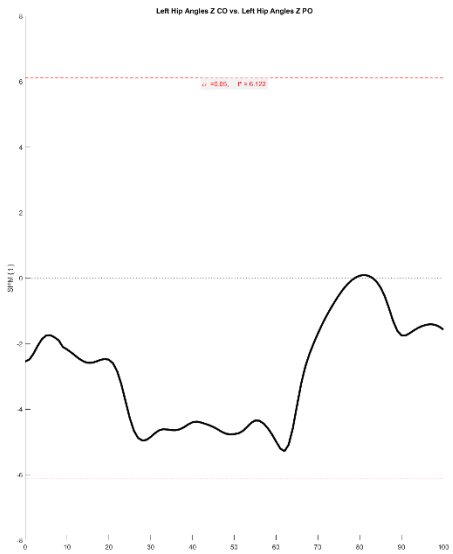

Right Knee Angles X

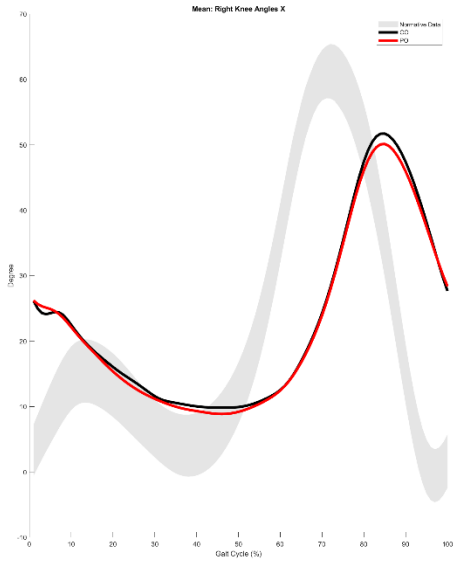

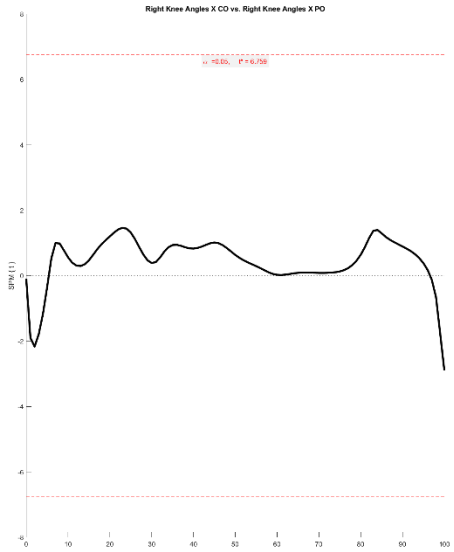

Right Knee Angles Y

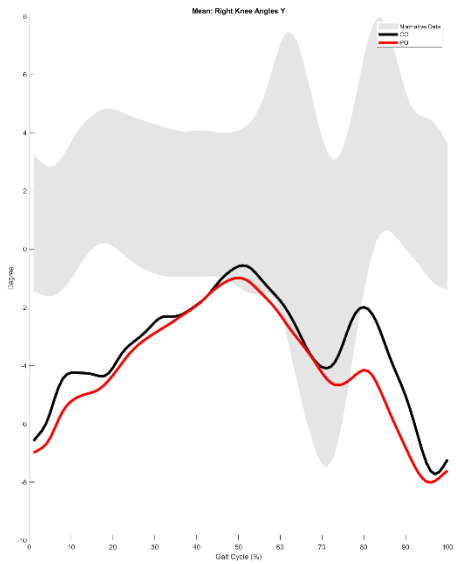

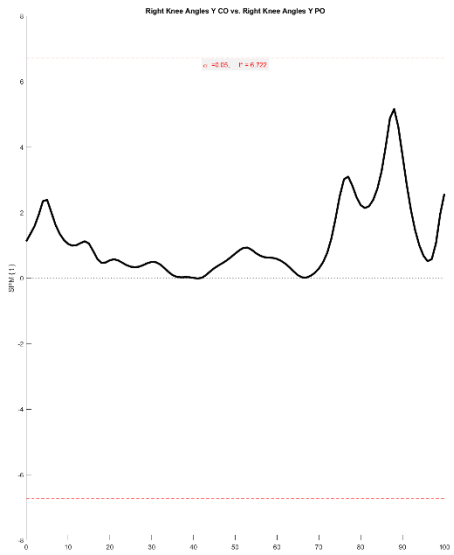

Right Knee Angles Z

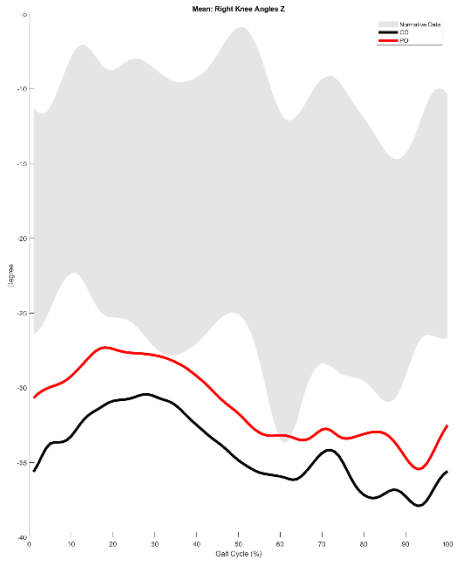

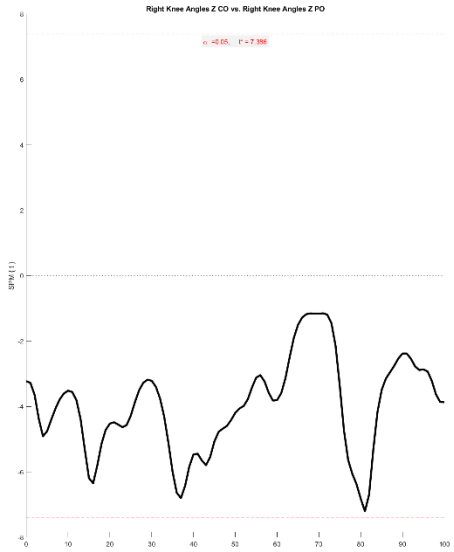

Left Knee Angles X

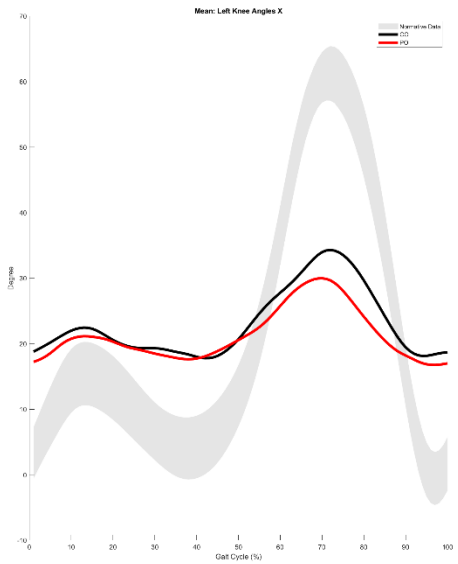

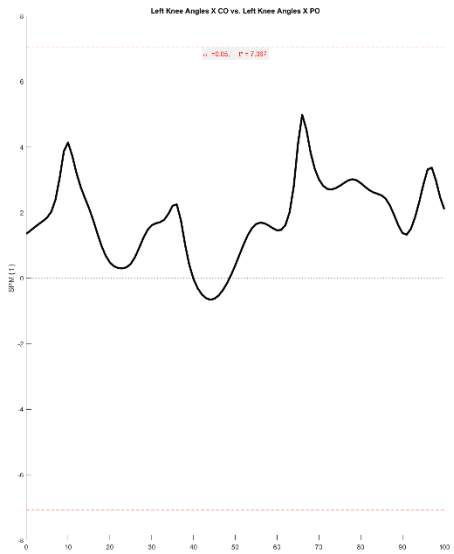

Left Knee Angles Y

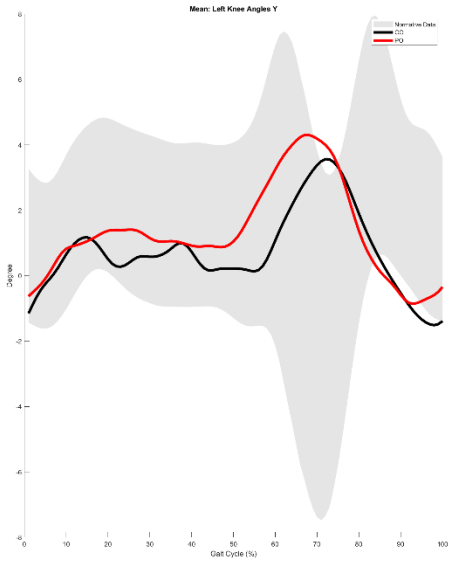

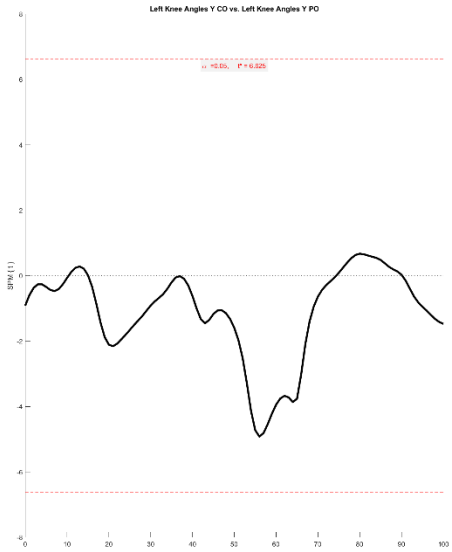

Left Knee Angles Z

9.2-11.7%, 84.9-88.2%

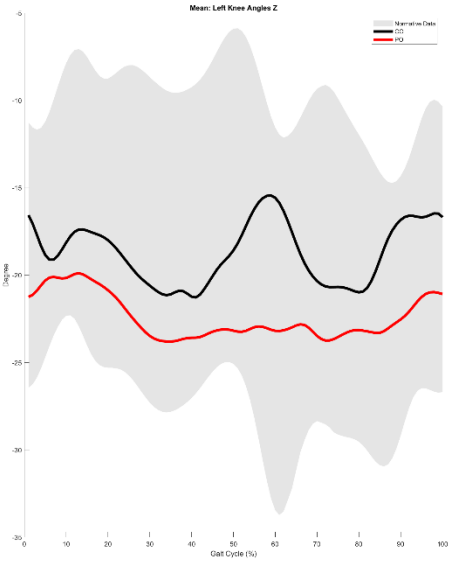

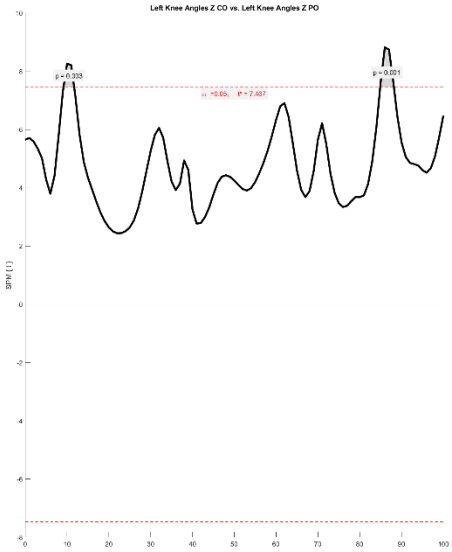

Right Ankle Angles X

0.0-70.0%, 78.6-100.0%

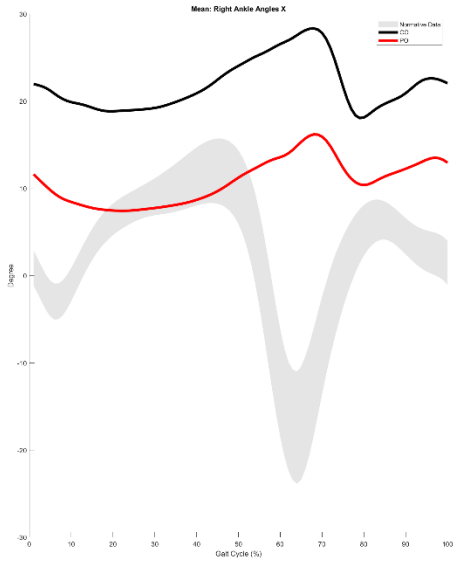

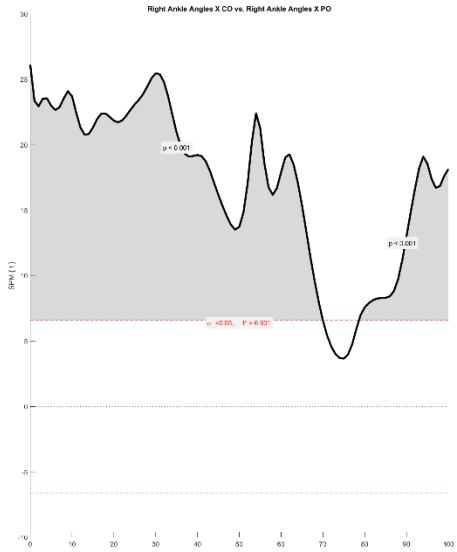

Right Ankle Angles Y

1.1-6.9%, 11.4-13.8%, 87.9-100.0%

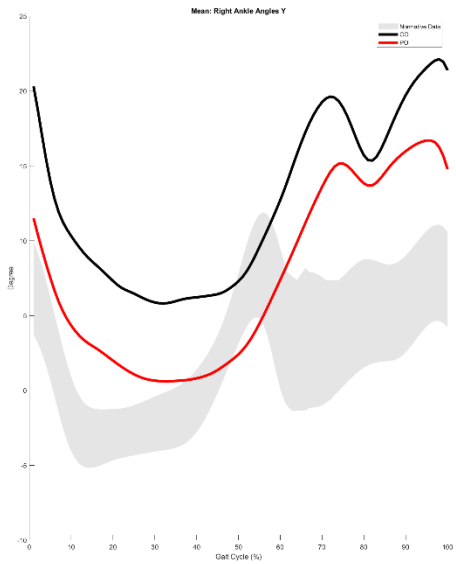

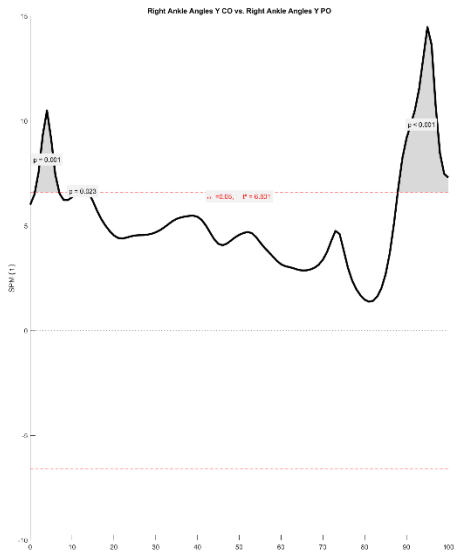

Left Ankle Angles X

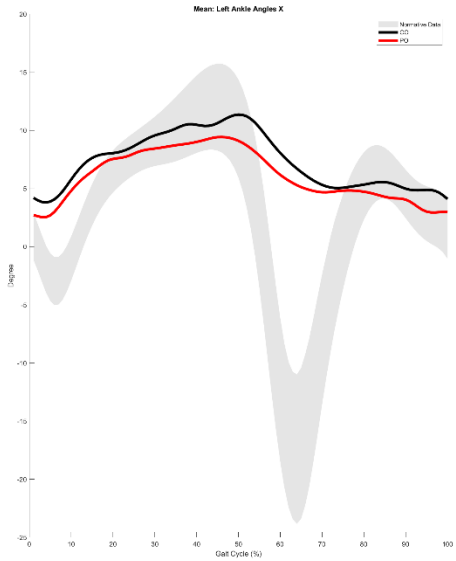

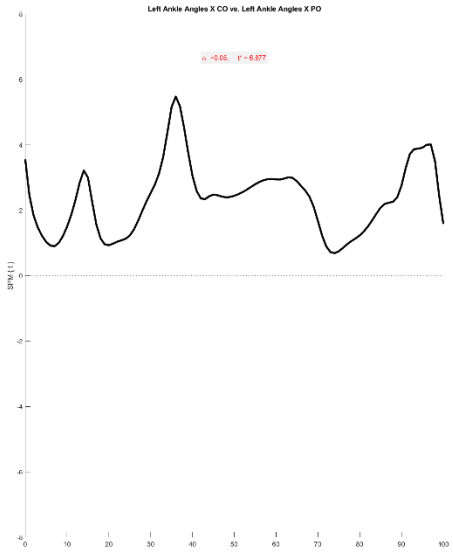

Left Ankle Angles Y

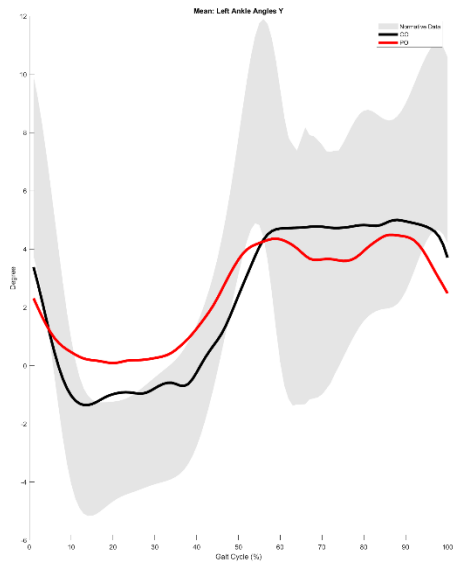

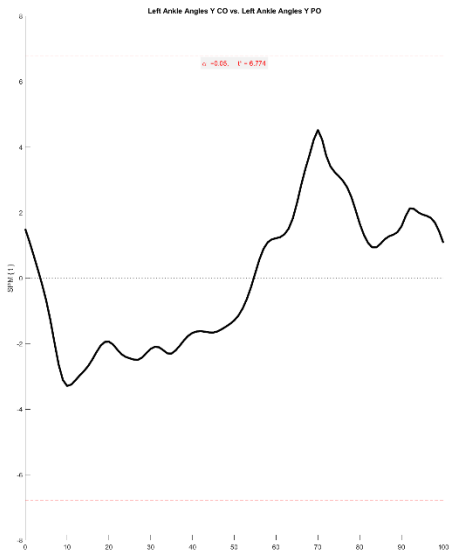

Right Foot Pitch Angles X

0.0-68.3%, 91.7-100.0%

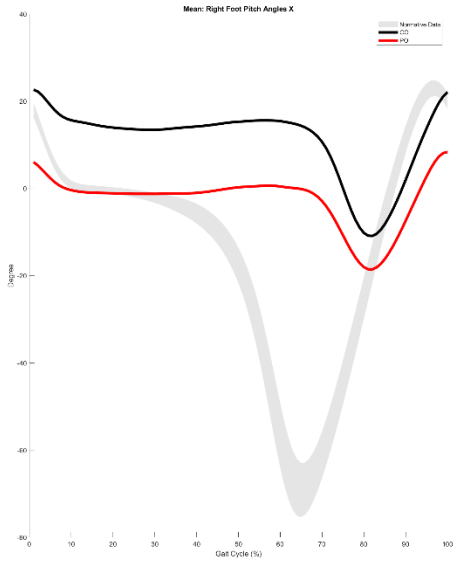

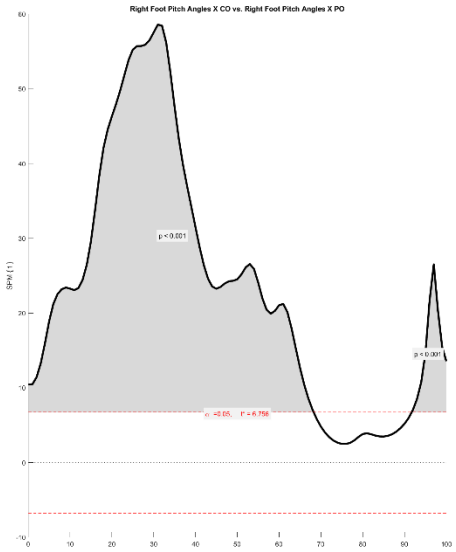

Left Foot Pitch Angles X

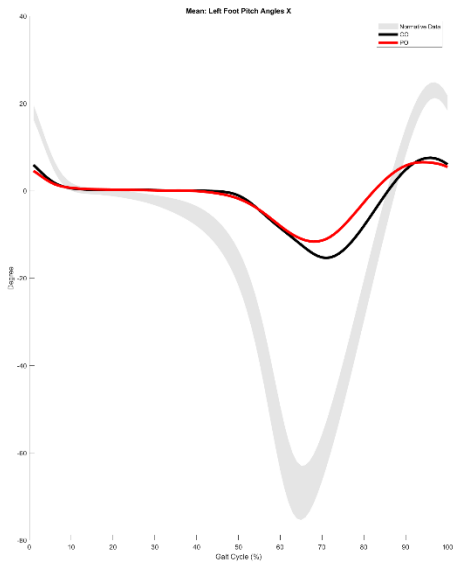

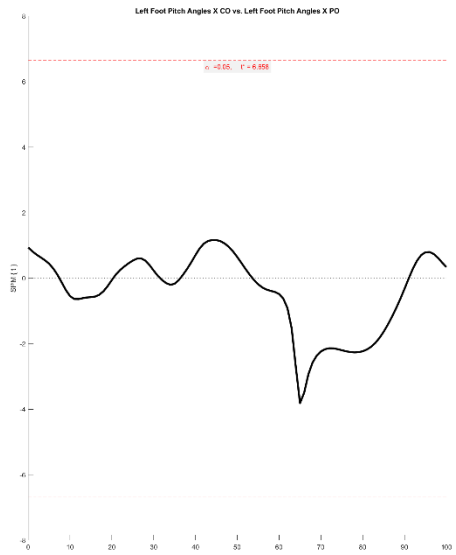

Right Foot Progression Z

1.1-70.9%, 75.0-100.0%

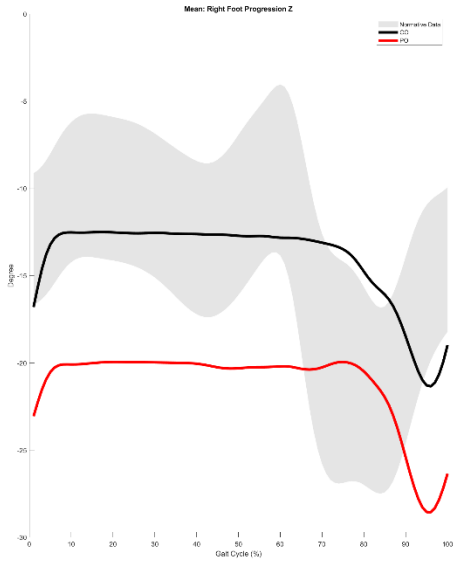

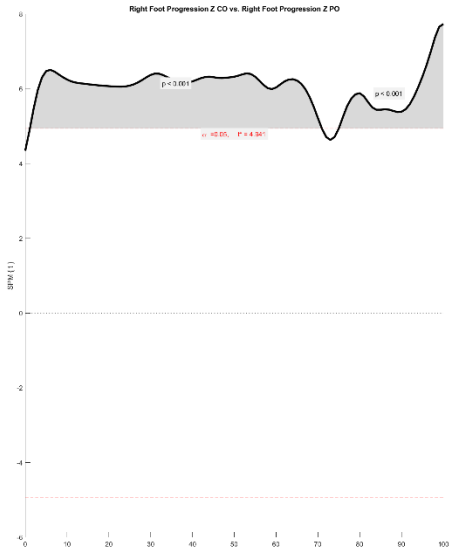

Left Foot Progression Z

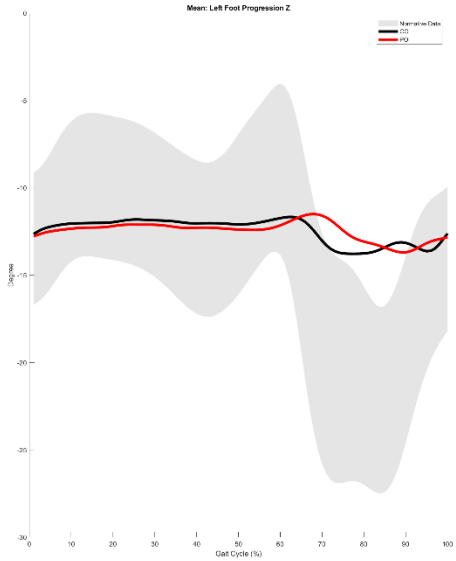

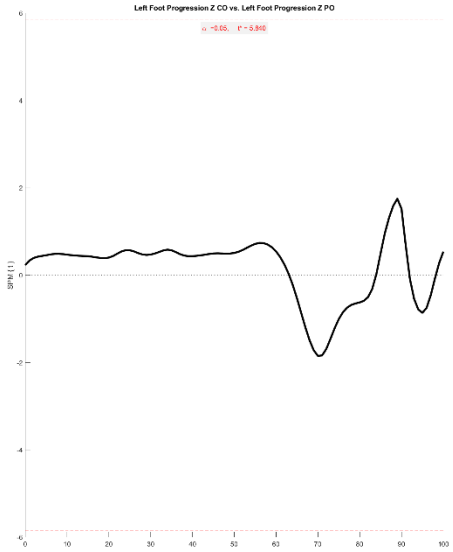

Right Hip Moment X

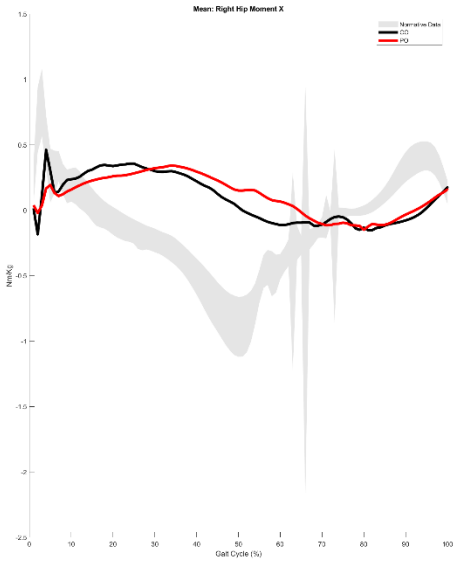

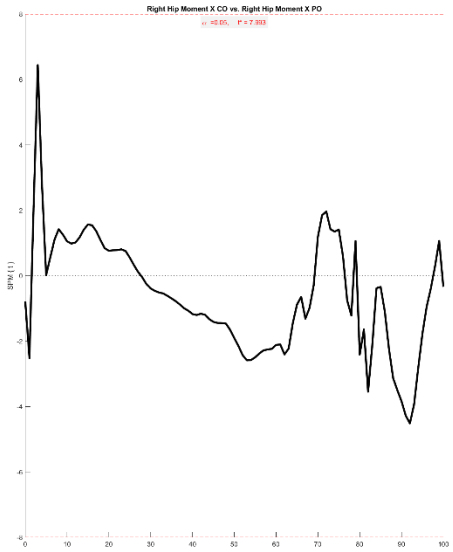

Right Hip Moment Y

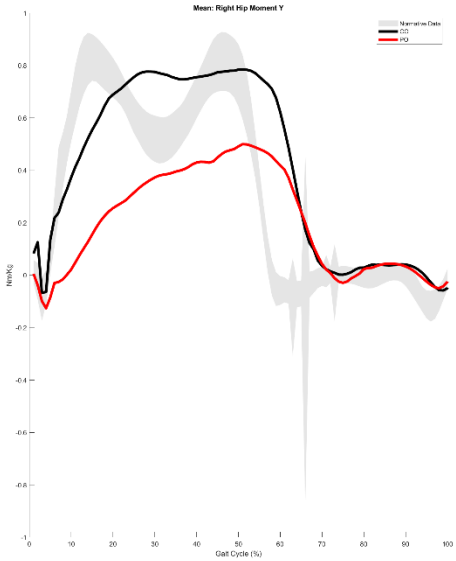

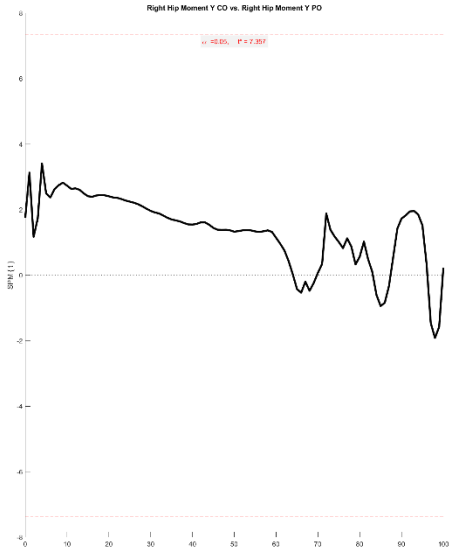

Left Hip Moment X

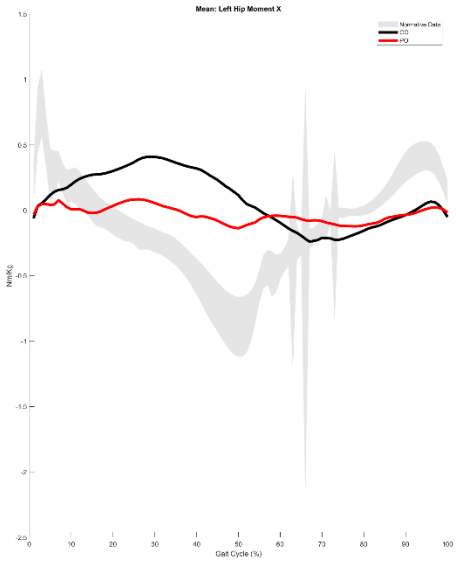

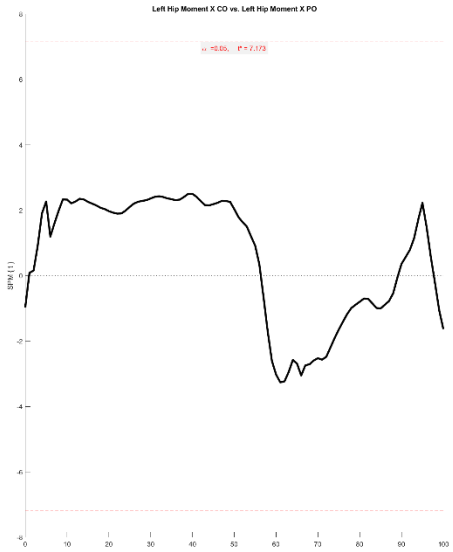

Left Hip Moment Y

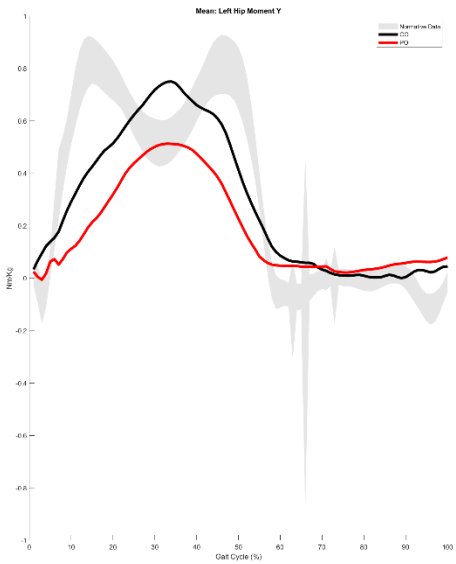

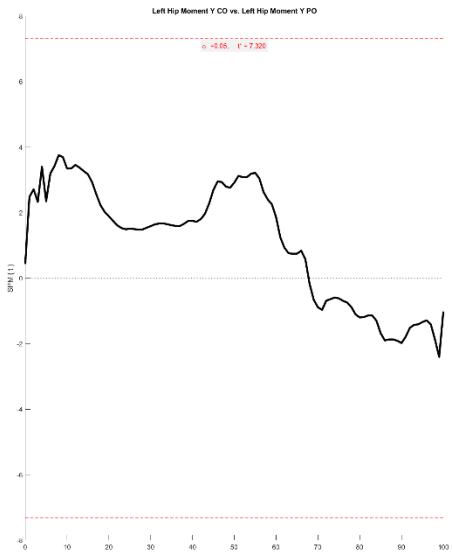

Right Knee Moment X

69.9-70.2%

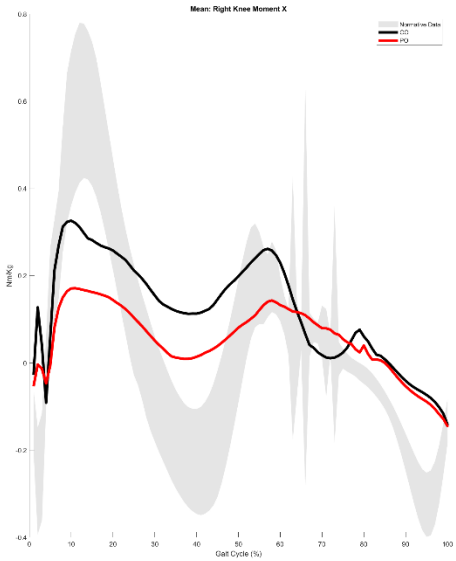

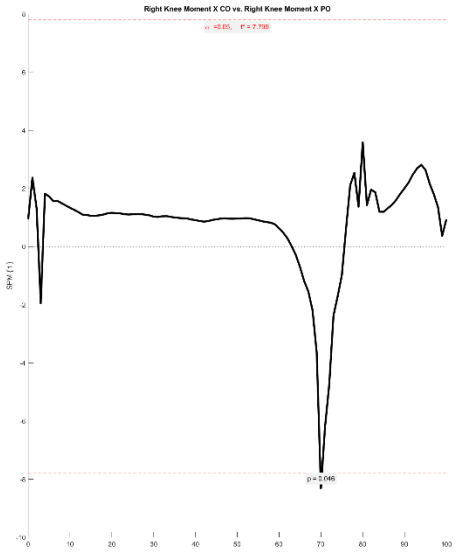

Right Knee Moment Y

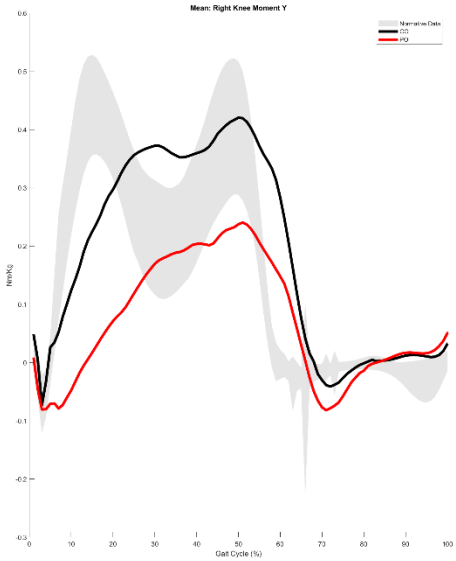

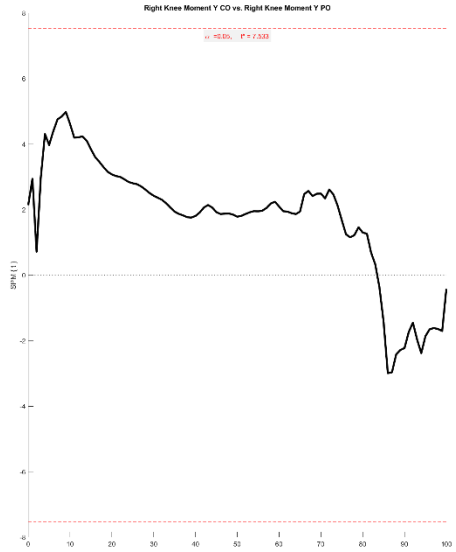

Left Knee Moment X

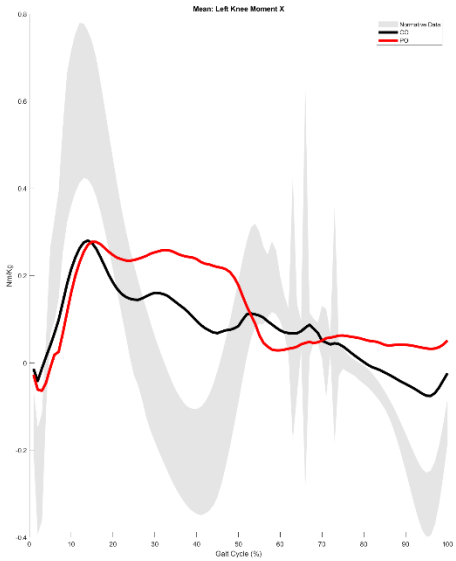

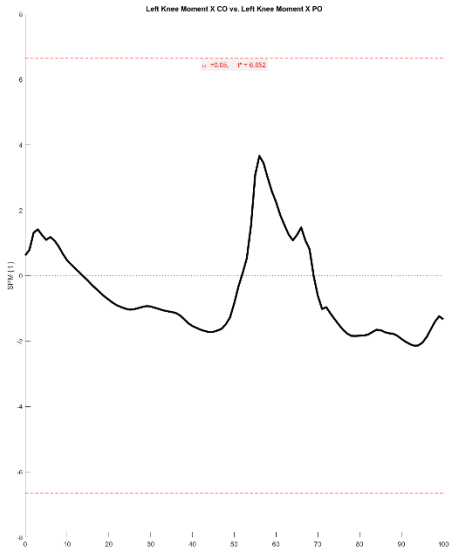

Left Knee Moment Y

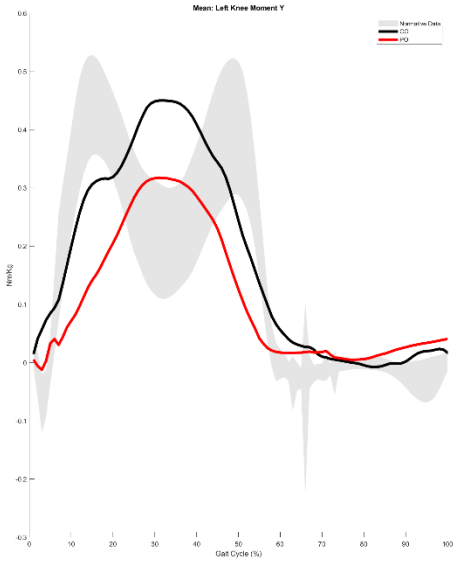

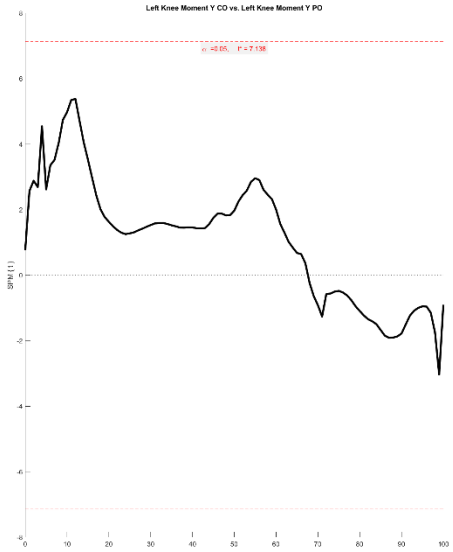

Right Ankle Moment X

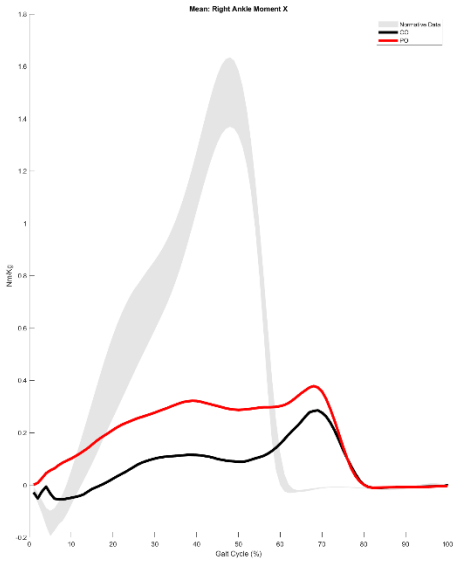

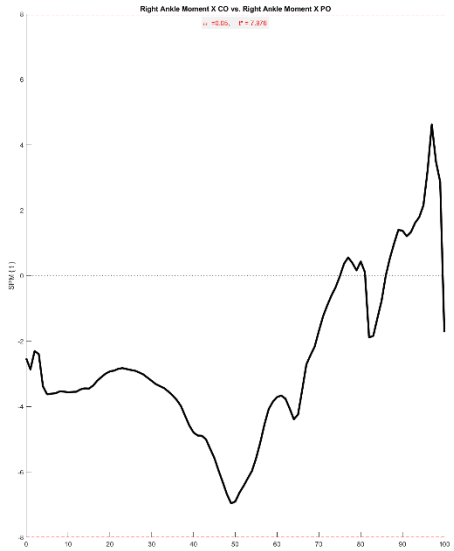

Right Ankle Moment Y

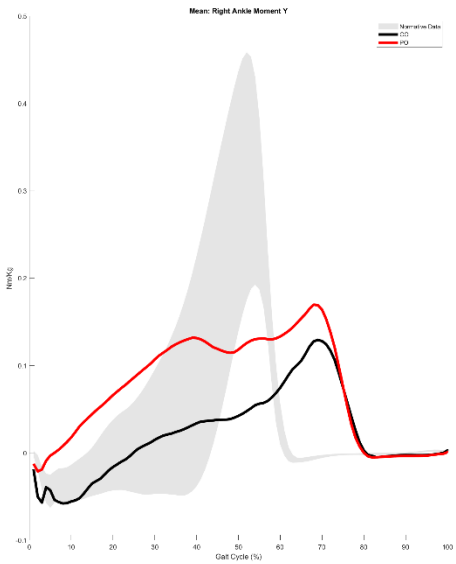

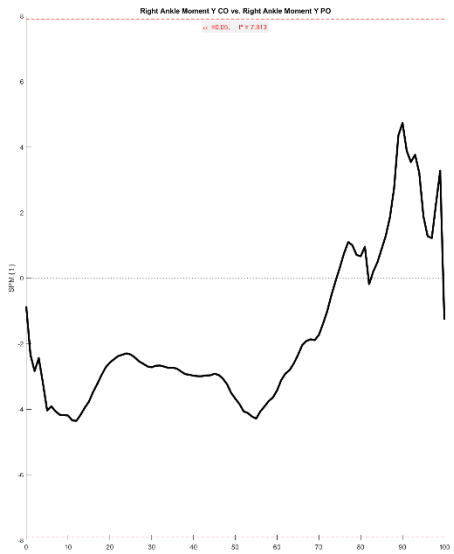

Left Ankle Moment X

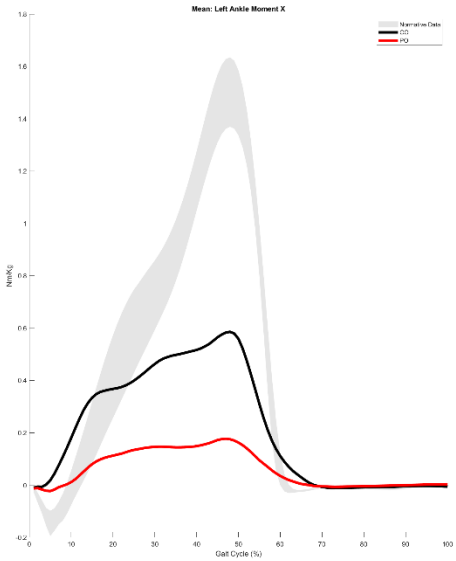

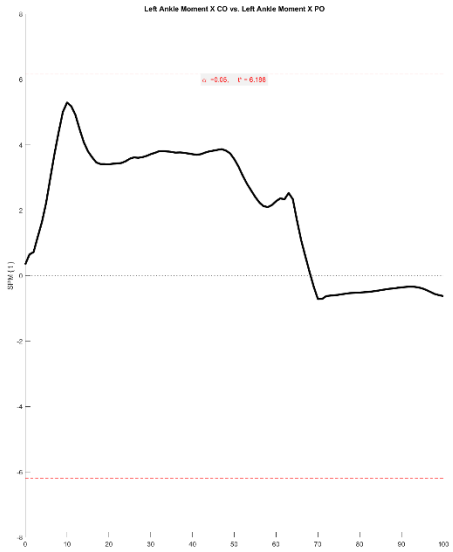

Left Ankle Moment Y

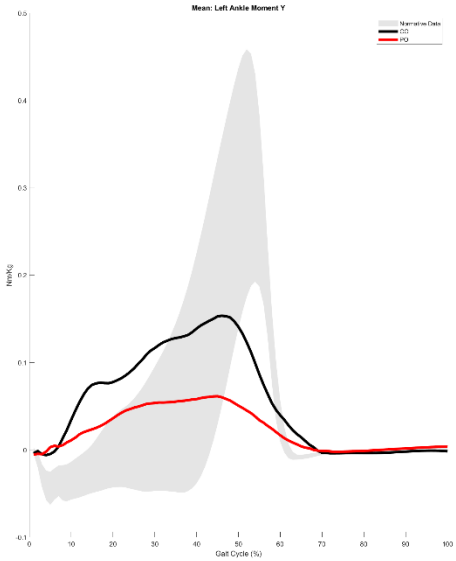

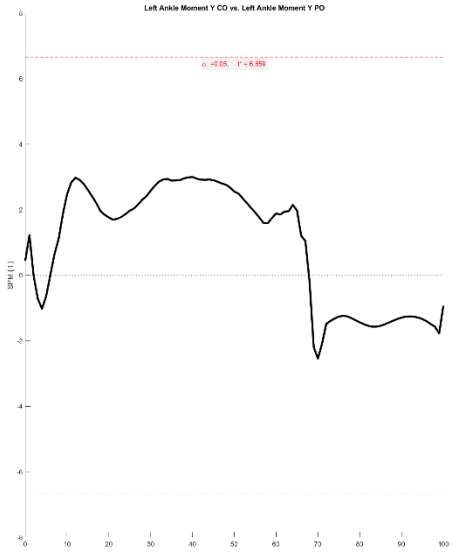

PO

Step Length

REP	Left	Right	IS (50%)	IS (0%)
1	0.24646	0.13351	35.137	59.4521
2	0.24257	0.13183	35.211	59.156
3	0.24148	0.13149	35.2548	58.9806
4	0.23987	0.11642	32.6756	69.2975
5	0.23577	0.11545	32.8711	68.5155
6	0.23556	0.11106	32.0409	71.8366
Mean	0.240285	0.1232933	33.8651	64.5397
SD	0.003822	0.0091547	1.35961	5.43844

CO

Step Length

REP	Left	Right	IS (50%)	IS (0%)
1	0.25432	0.15423	37.7506	48.9977
2	0.25105	0.15345	37.9357	48.2571
3	0.24825	0.15276	38.0938	47.6247
4	0.24802	0.14221	36.4426	54.2296
5	0.24611	0.13707	35.7717	56.9132
6	0.24355	0.13062	34.9093	60.3629
Mean	0.24855	0.1450567	36.8173	52.7309
SD	0.0034367	0.009076	1.199	4.79601

PO

Swing Time

REP	Left	Right	IS (50%)	IS (0%)
1	0.47	0.35	42.6829	29.2683
2	0.46	0.34	42.5	30
3	0.45	0.33	42.3077	30.7692
4	0.43	0.33	43.4211	26.3158
5	0.43	0.32	42.6667	29.3333
6	0.42	0.3	41.6667	33.3333
Mean	0.443333	0.3283333	42.5408	29.8367
SD	0.017951	0.0157233	0.52138	2.08551

CO

Swing Time

REP	Left	Right	IS (50%)	IS (0%)
1	0.47	0.32	40.5063	37.9747
2	0.47	0.31	39.7436	41.0256
3	0.45	0.3	40	40
4	0.45	0.28	38.3562	46.5753
5	0.42	0.28	40	40
6	0.42	0.28	40	40
Mean	0.4466667	0.295	39.7677	40.9293
SD	0.020548	0.0160728	0.67088	2.68352

PO

Stance Time

REP	Left	Right	IS (50%)	IS (0%)
1	0.96	1.07	52.7094	10.8374
2	0.94	1.06	53	12
3	0.91	1.06	53.8071	15.2284
4	0.91	1.04	53.3333	13.3333
5	0.9	1.04	53.6082	14.433
6	0.88	1.02	53.6842	14.7368
Mean	0.916667	1.0483333	53.357	13.4282
SD	0.026247	0.0167498	0.39163	1.56651

CO

Stance Time

REP	Left	Right	IS (50%)	IS (0%)
1	0.99	1.14	53.5211	14.0845
2	0.97	1.14	54.0284	16.1137
3	0.96	1.13	54.067	16.2679
4	0.96	1.13	54.067	16.2679
5	0.96	1.11	53.6232	14.4928
6	0.95	1.1	53.6585	14.6341
Mean	0.965	1.125	53.8275	15.3102
SD	0.0125831	0.015	0.23067	0.92266

	Left	Right
Step Length PO	0.24	0.12
Step Length CO	0.25	0.15
Swing Time PO	0.44	0.33
Swing Time CO	0.45	0.30
Stance Time PO	0.92	1.05
Stance Time CO	0.97	1.13

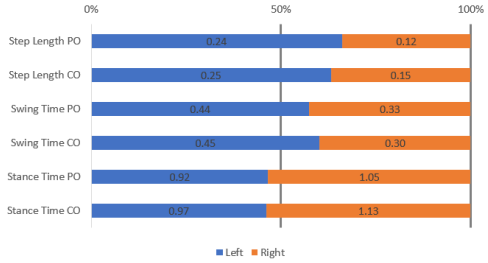

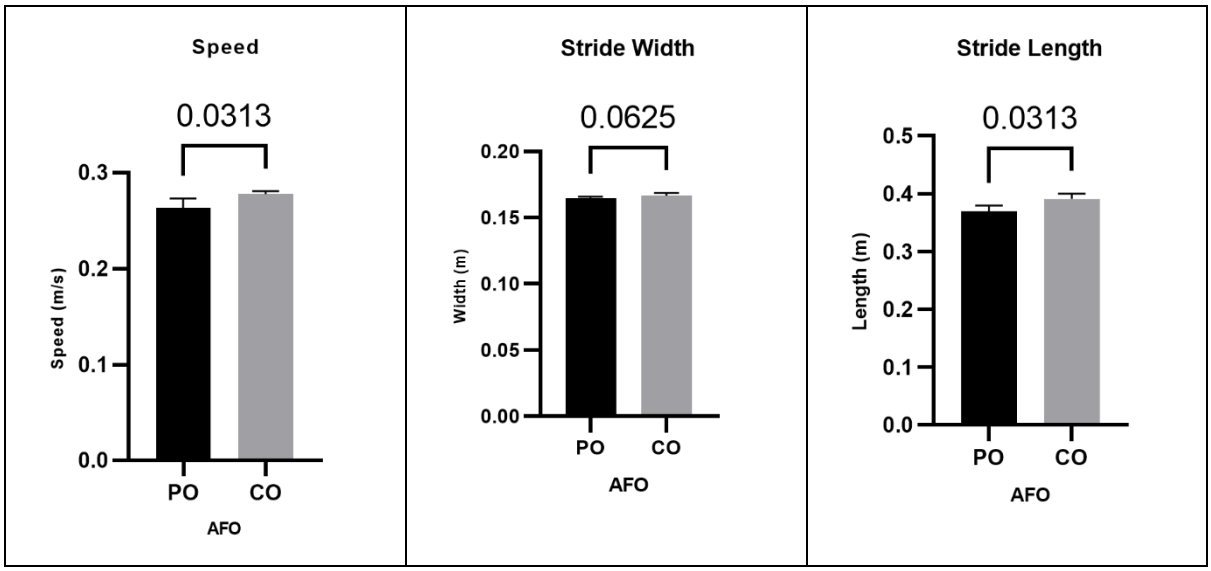

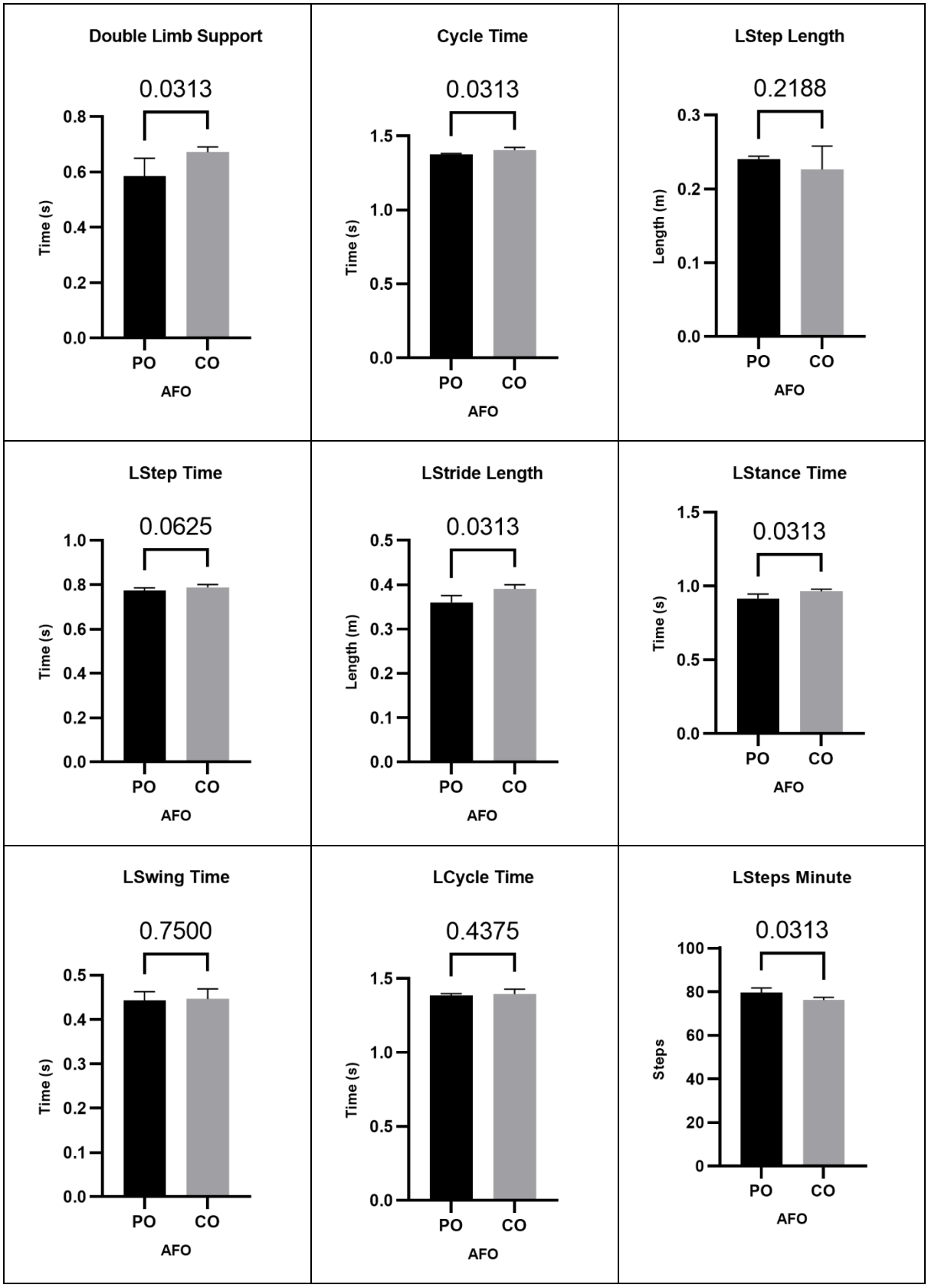
Double Limb Support
0.0313
Time (s)
0.8
0.6
0.4
0.2
0.0
PO
CO
AFO
Cycle Time
0.0313
Time (s)
1.5
1.0
0.5
0.0
PO
CO
AFO
LStep Length
0.2188
Length (m)
0.3
0.2
0.1
0.0
PO
CO
AFO
LStep Time
0.0625
Time (s)
1.0
0.8
0.6
0.4
0.2
0.0
PO
CO
AFO
LStride Length
0.0313
Length (m)
0.5
0.4
0.3
0.2
0.1
0.0
PO
CO
AFO
LStance Time
0.0313
Time (s)
1.5
1.0
0.5
0.0
PO
CO
AFO
LSwing Time
0.7500
Time (s)
0.5
0.4
0.3
0.2
0.1
0.0
PO
CO
AFO
LCycle Time
0.4375
Time (s)
1.5
1.0
0.5
0.0
PO
CO
AFO
LSteps Minute
0.0313
Steps
100
80
60
40
20
0
PO
CO
AFO

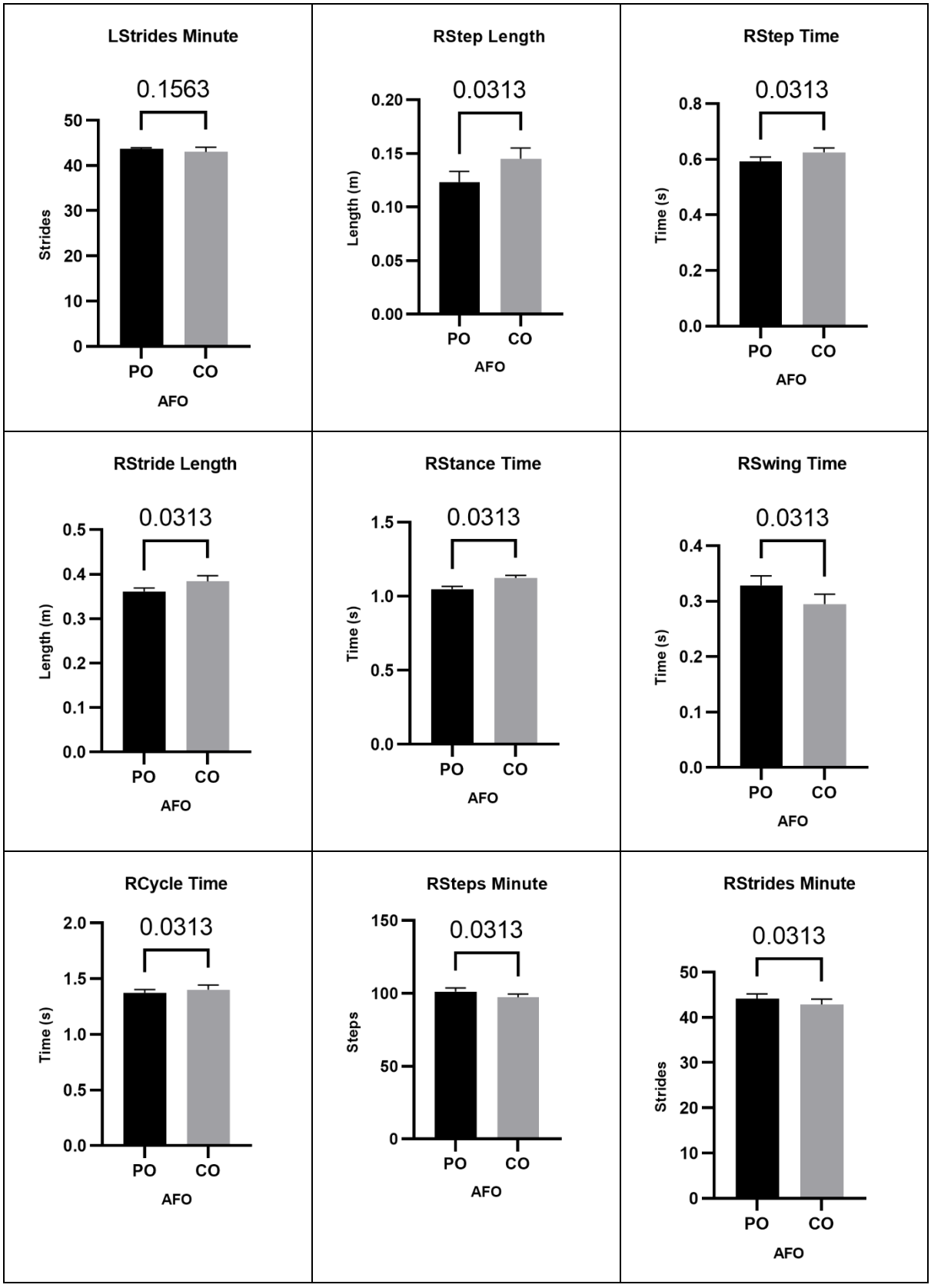
LStrides Minute
0.1563
Strides
50
40
30
20
10
0
PO
CO
AFO
RStep Length
0.0313
Length (m)
0.20
0.15
0.10
0.05
0.00
PO
CO
AFO
RStep Time
0.0313
Time (s)
0.8
0.6
0.4
0.2
0.0
PO
CO
AFO
RStride Length
0.0313
Length (m)
0.5
0.4
0.3
0.2
0.1
0.0
PO
CO
AFO
RStance Time
0.0313
Time (s)
1.5
1.0
0.5
0.0
PO
CO
AFO
RSwing Time
0.0313
Time (s)
0.4
0.3
0.2
0.1
0.0
PO
CO
AFO
RCycle Time
0.0313
Time (s)
2.0
1.5
1.0
0.5
0.0
PO
CO
AFO
RSteps Minute
0.0313
Steps
150
100
50
0
PO
CO
AFO
RStrides Minute
0.0313
Strides
50
40
30
20
10
0
PO
CO
AFO

PATIENT 3

Right Pelvic Angles X

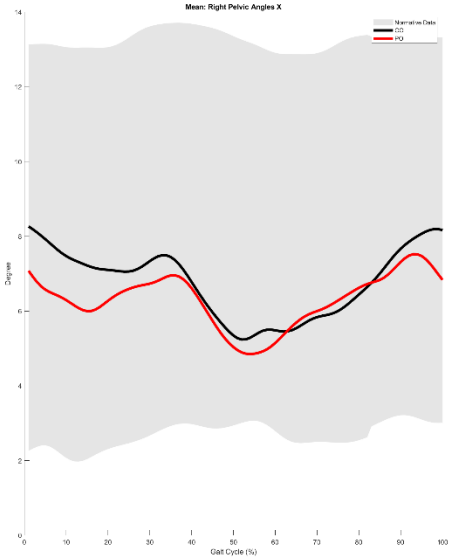

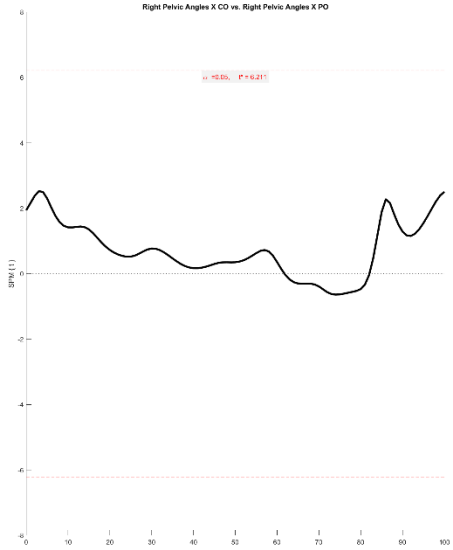

Right Pelvic Angles Y

10.2-12.5%

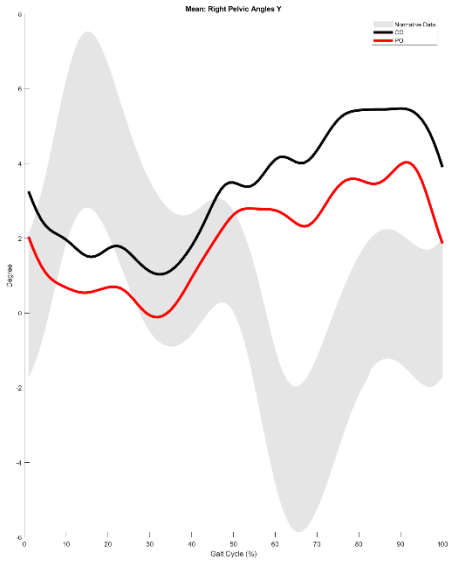

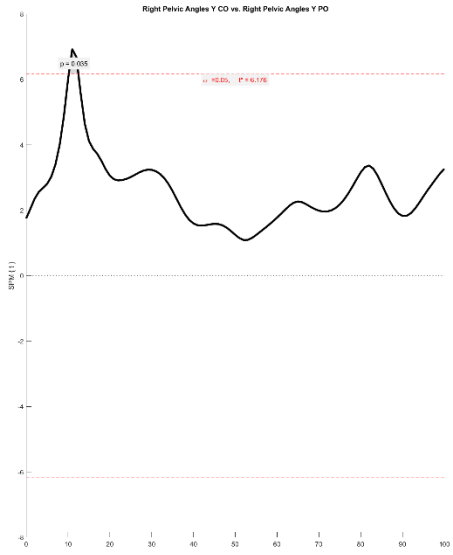

Right Pelvic Angles Z

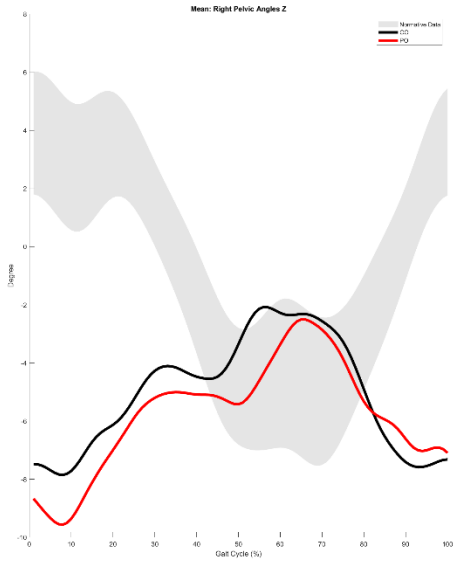

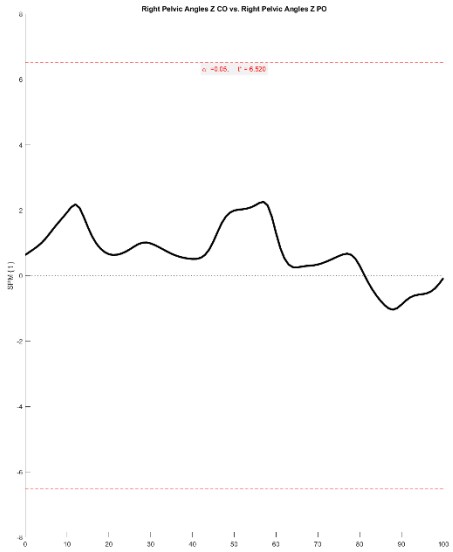

Left Pelvic Angles X

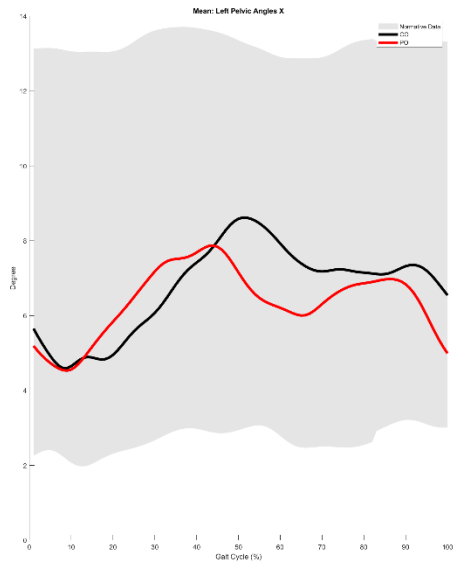

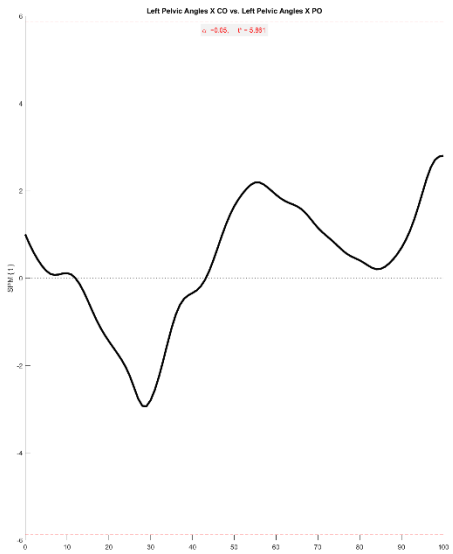

Left Pelvic Angles Y

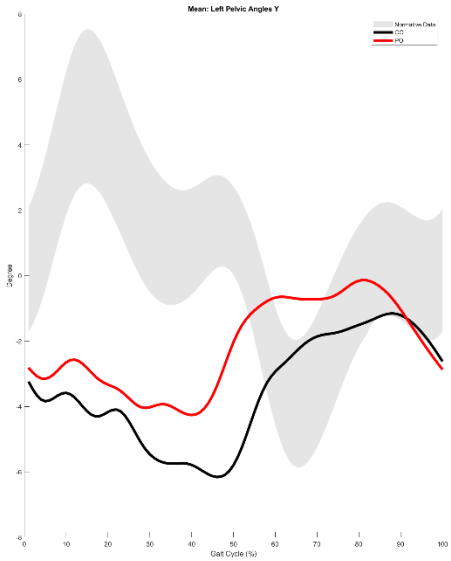

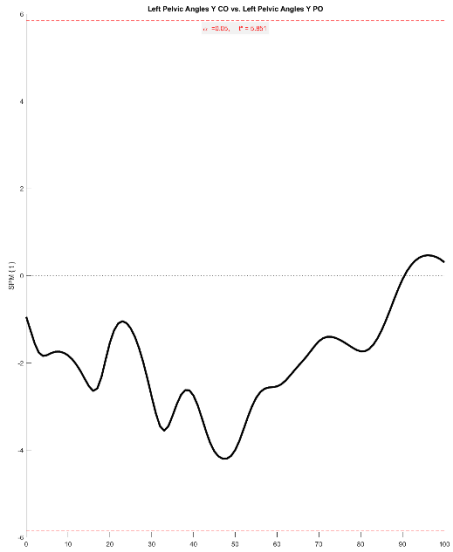

Left Pelvic Angles Z

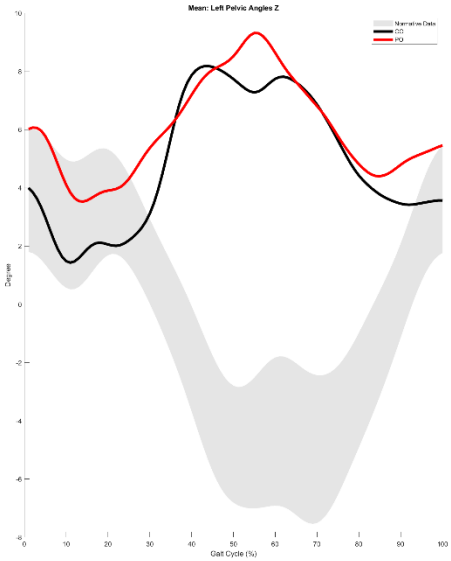

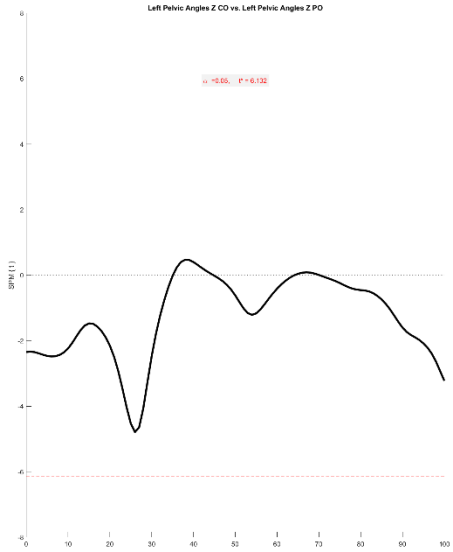

Right Hip Angles X

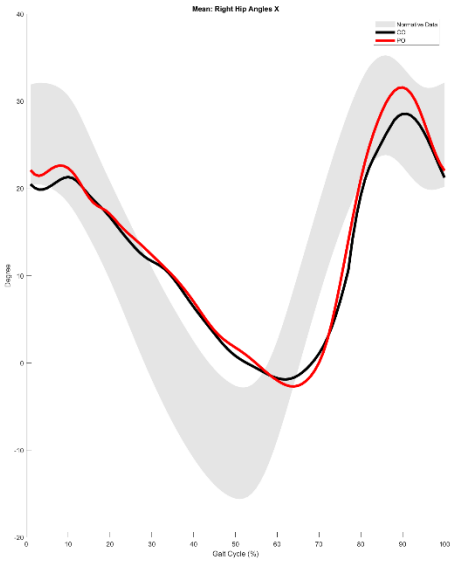

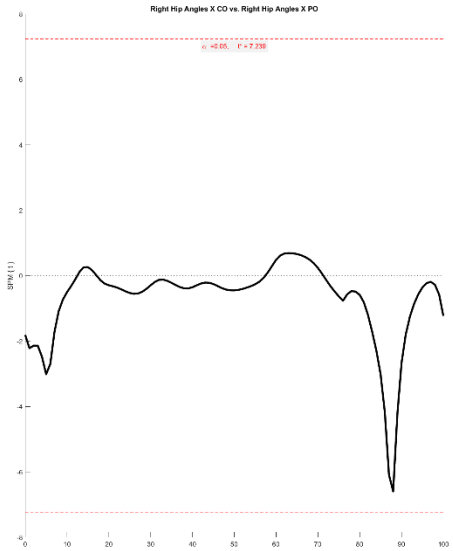

Right Hip Angles Y

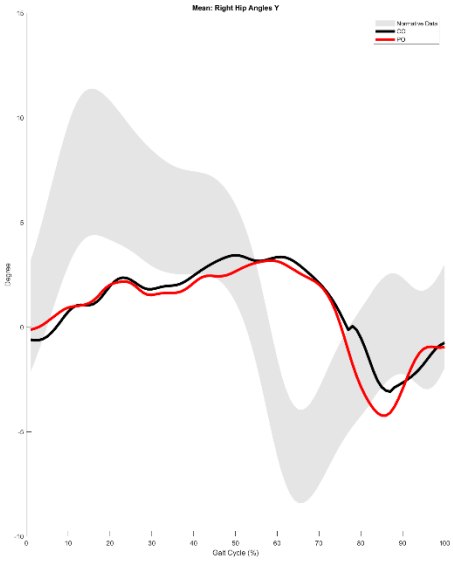

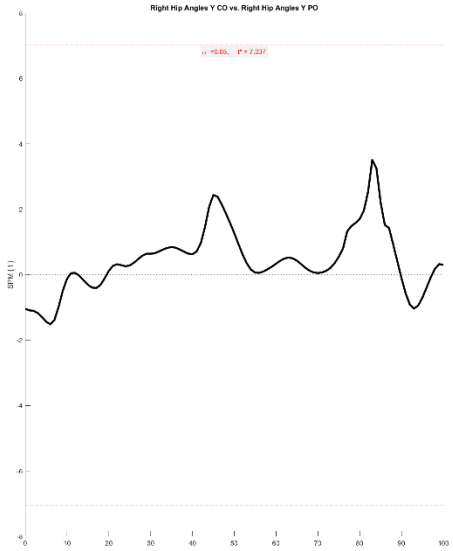

Right Hip Angles Z

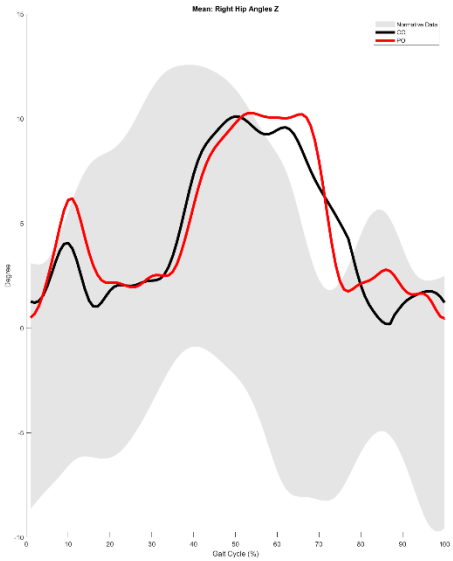

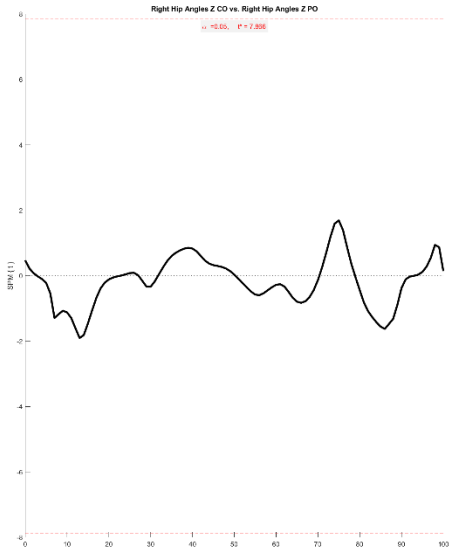

Left Hip Angles X

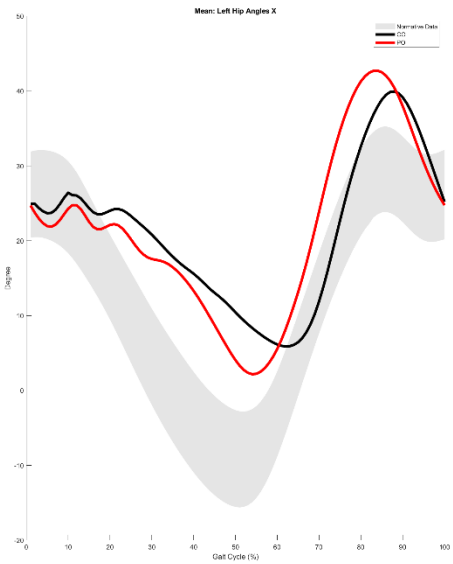

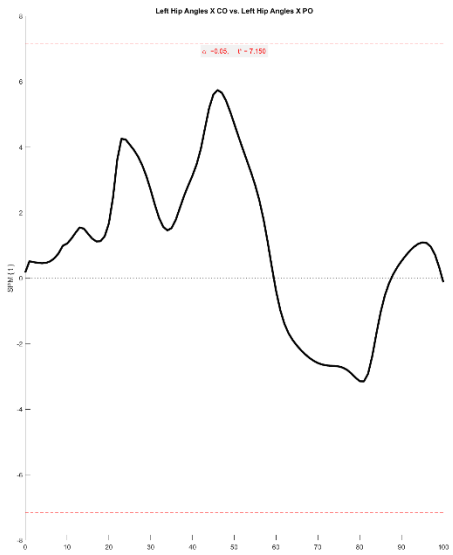

Left Hip Angles Y

3.5-7.8%

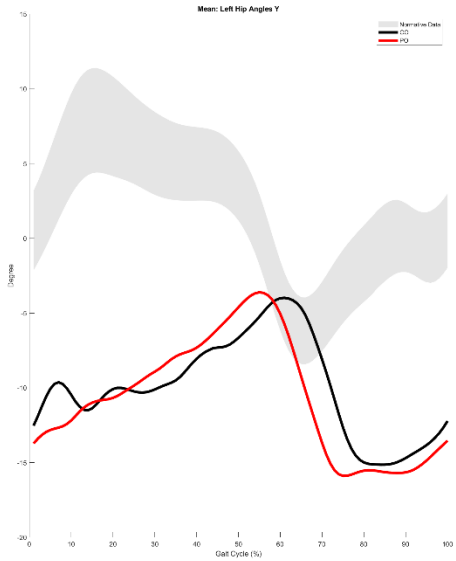

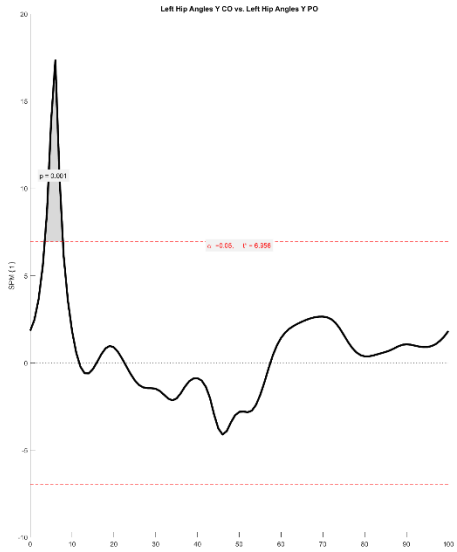

Left Hip Angles Z

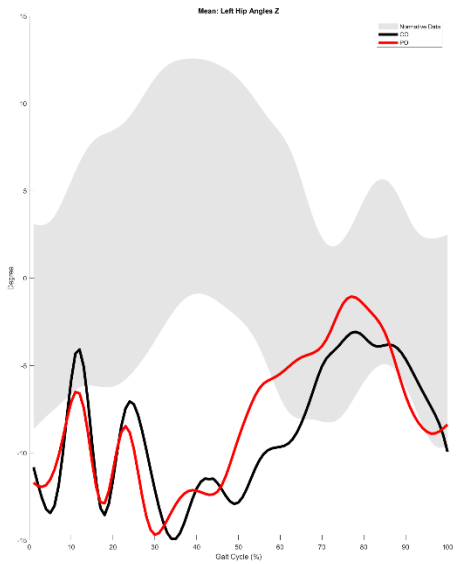

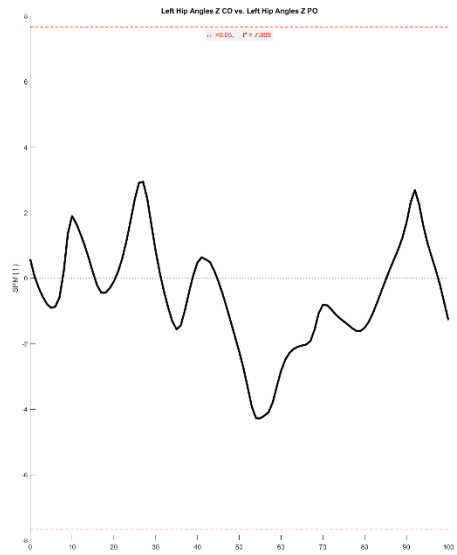

Right Knee Angles X

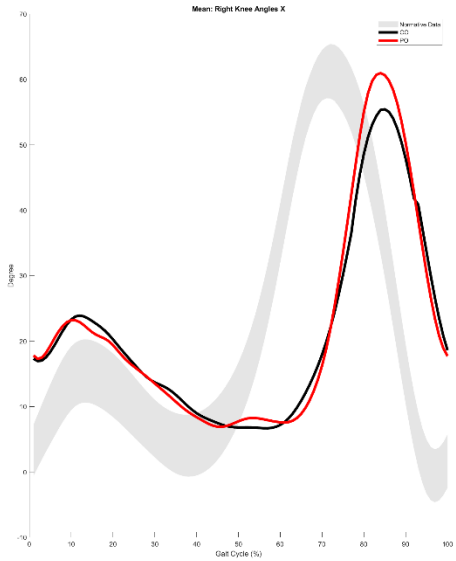

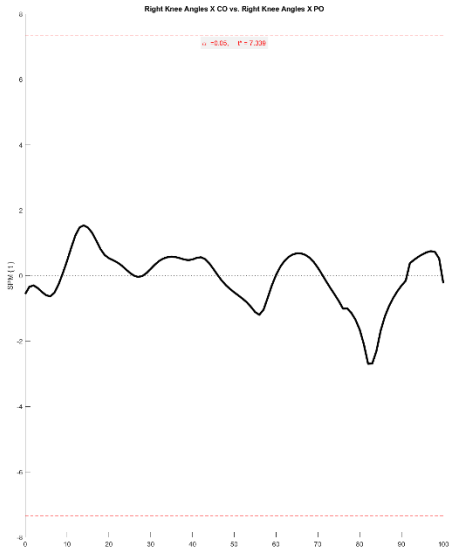

Right Knee Angles Y

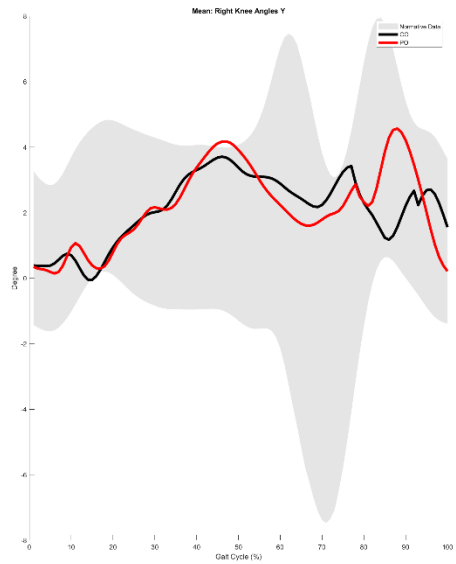

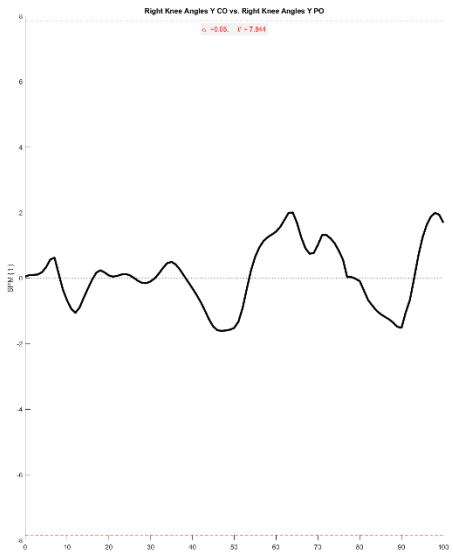

Right Knee Angles Z

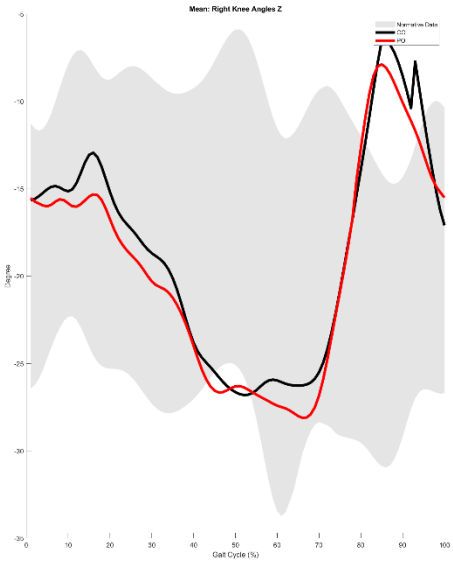

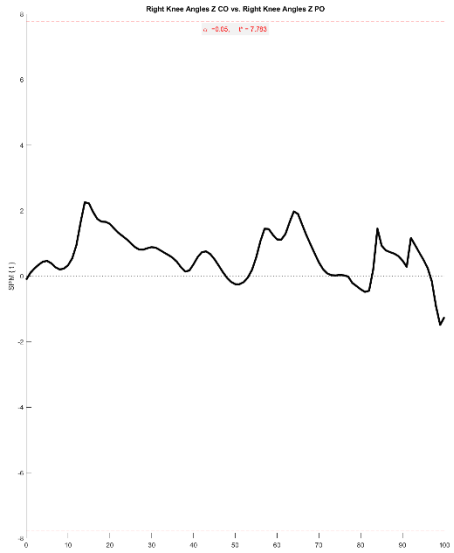

Left Knee Angles X

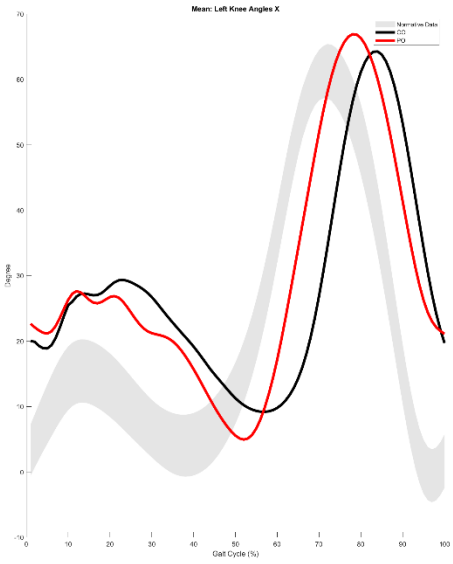

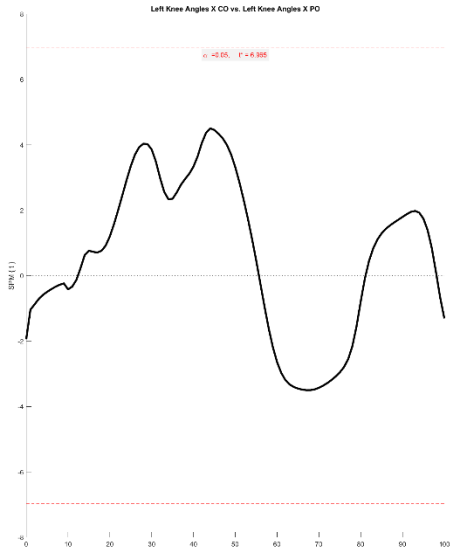

Left Knee Angles Y

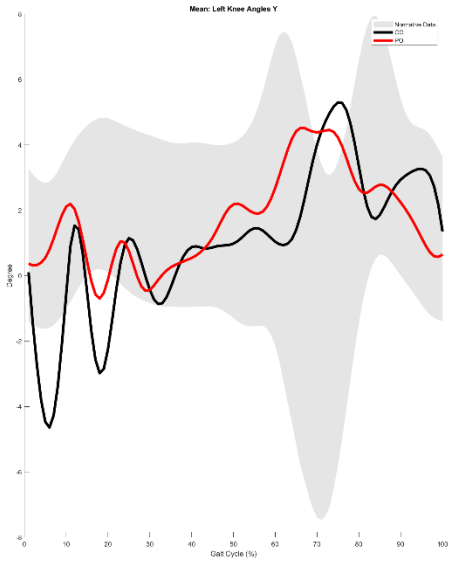

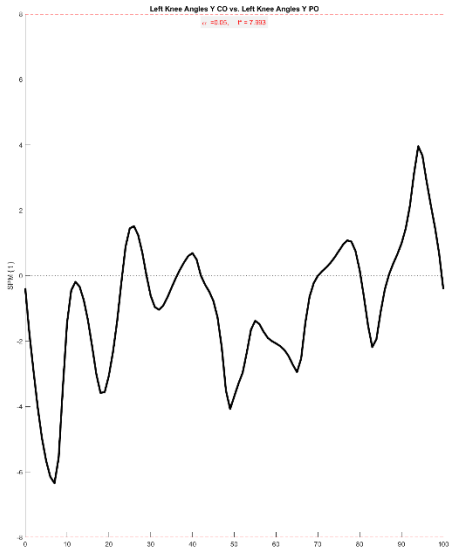

Left Knee Angles Z

7.8-8.2%

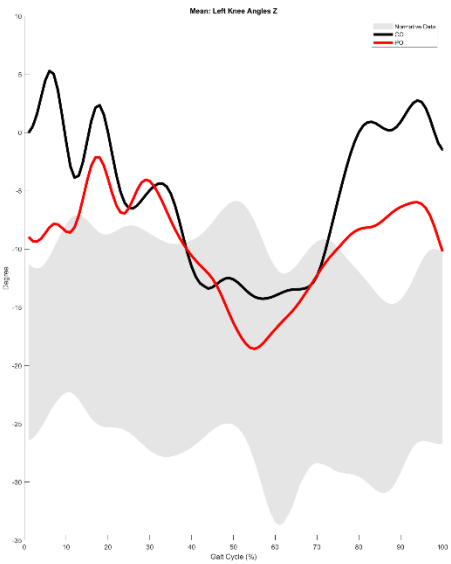

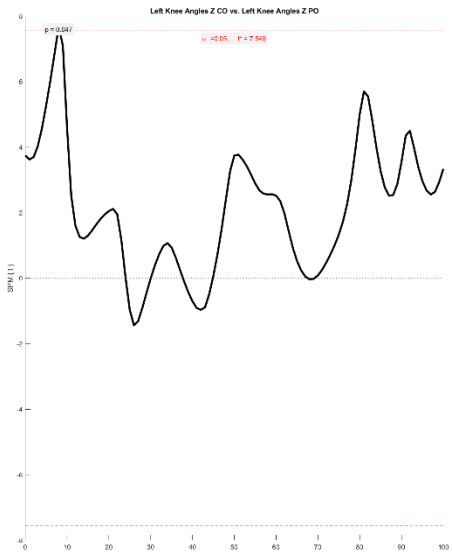

Right Ankle Angles X

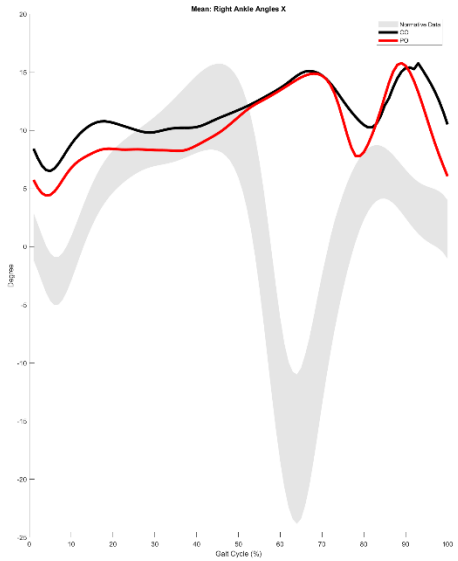

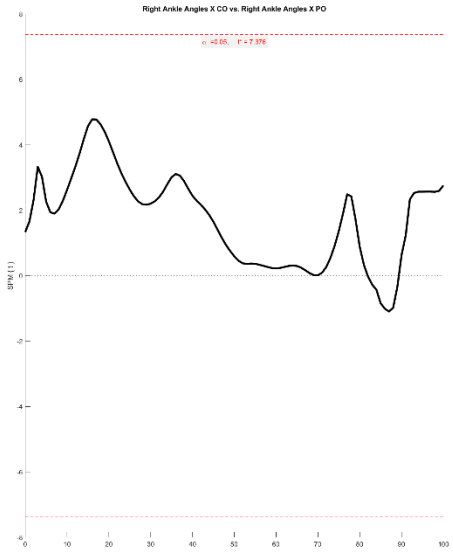

Right Ankle Angles Y

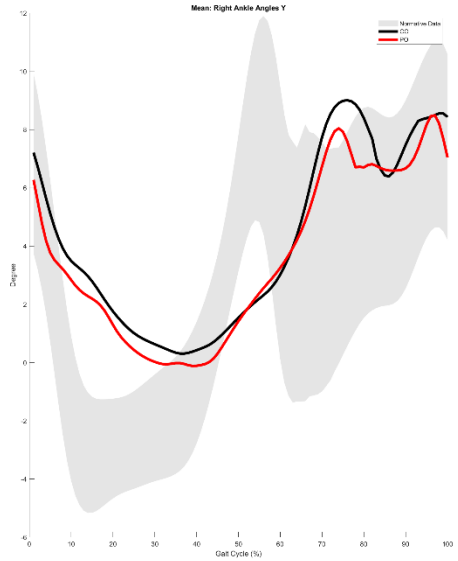

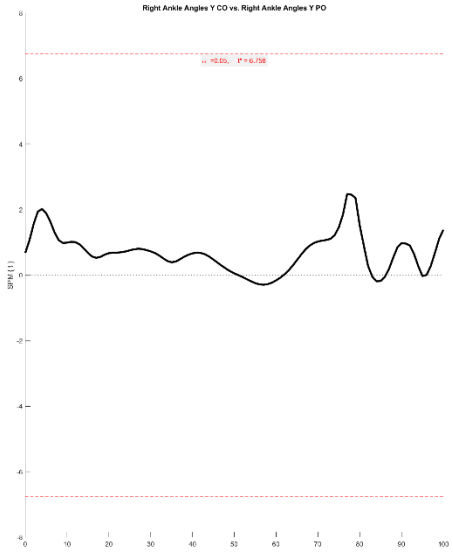

Left Ankle Angles X

80.8-100.0%

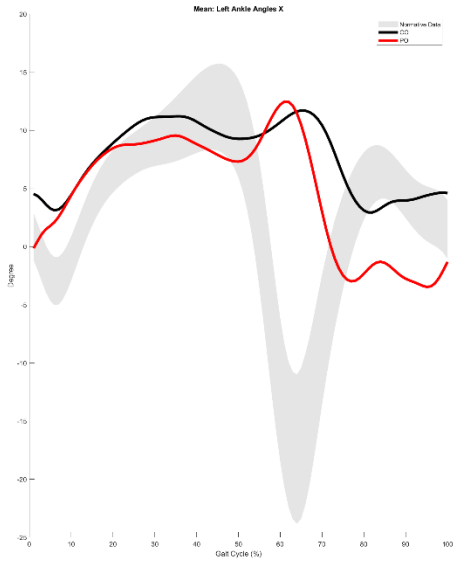

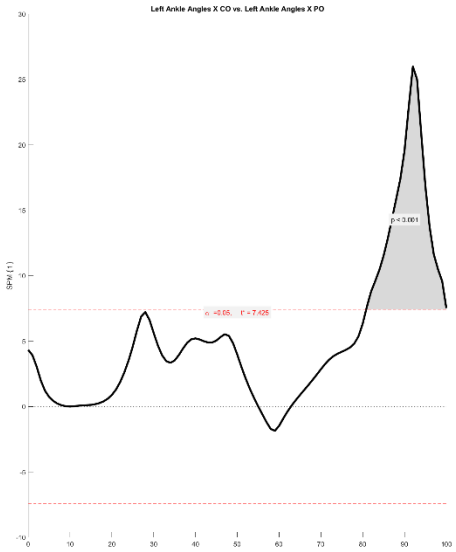

Left Ankle Angles Y

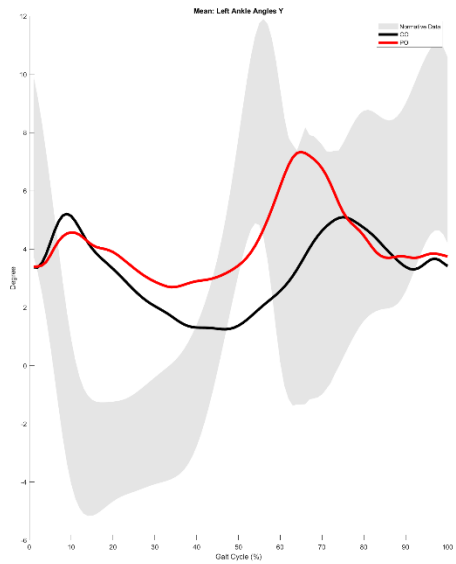

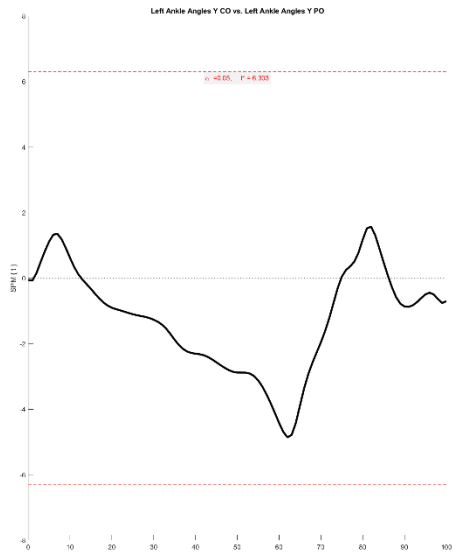

Right Foot Pitch Angles X

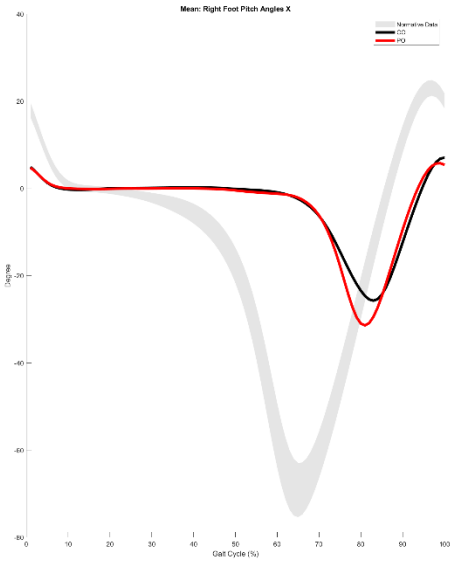

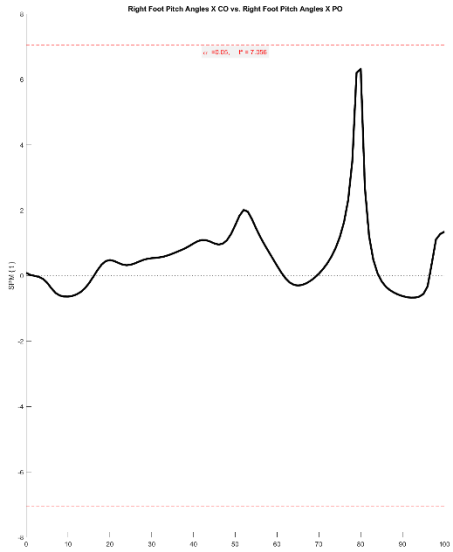

Left Foot Pitch Angles X

0.0-4.6%

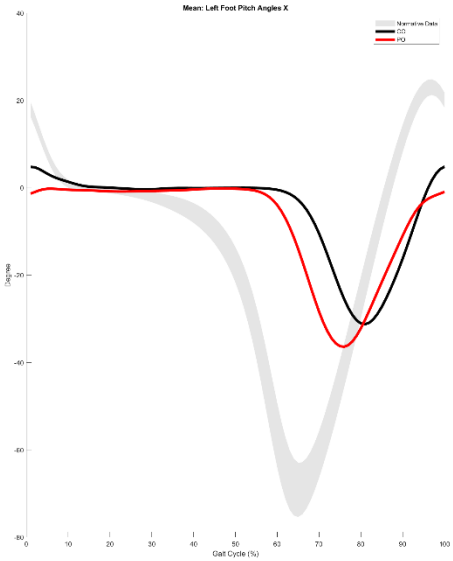

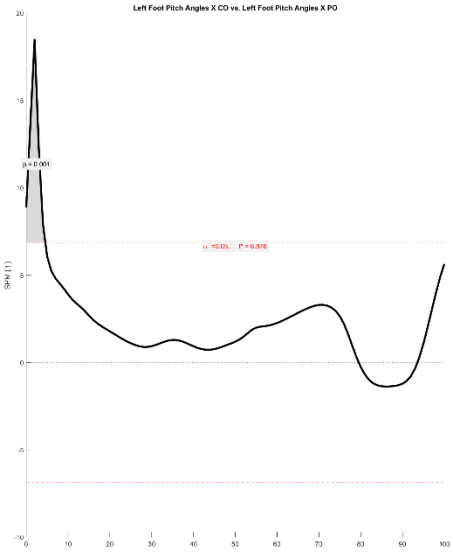

Right Foot Progression Z

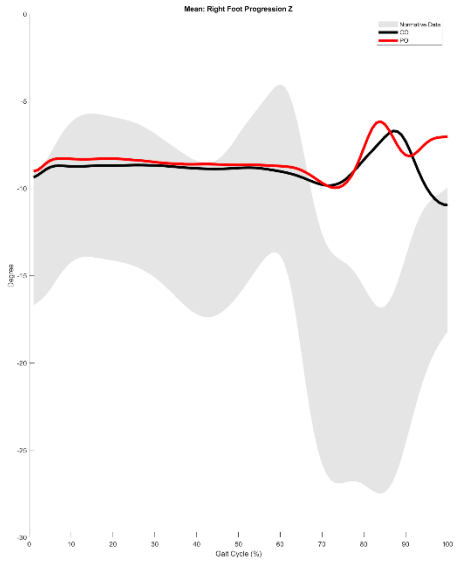

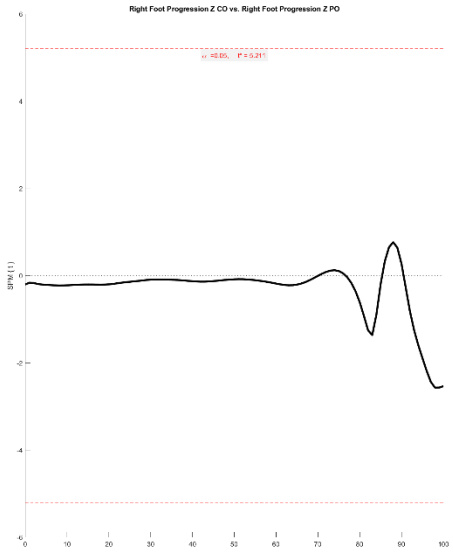

Left Foot Progression Z

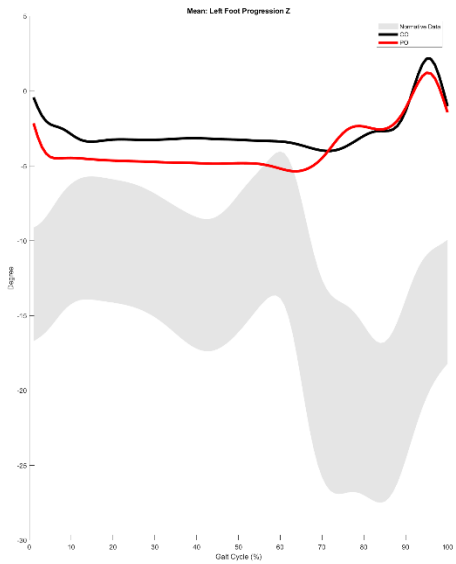

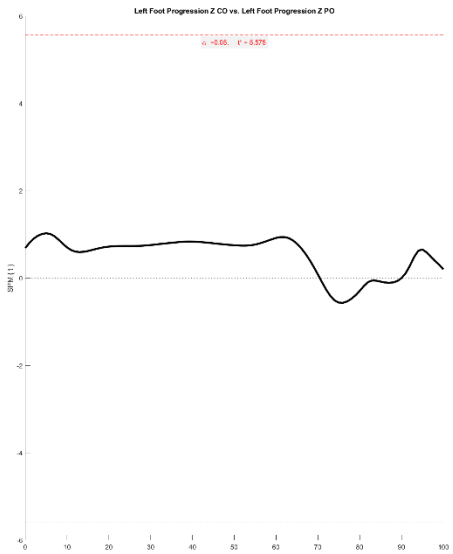

Right Hip Moment X

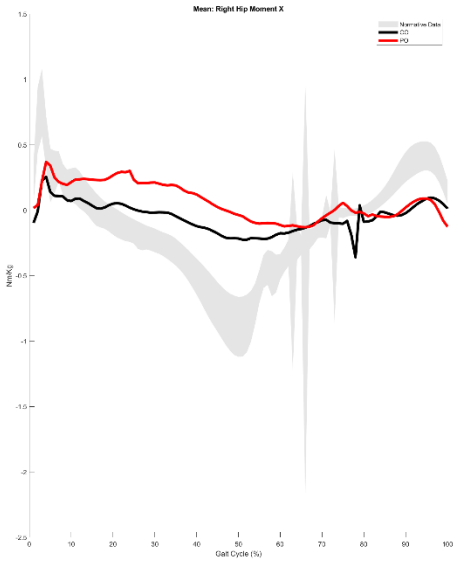

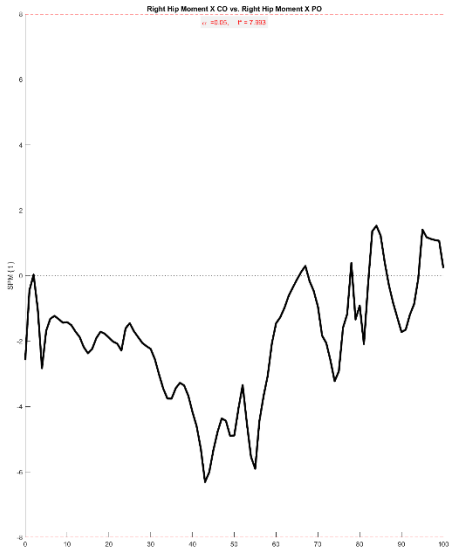

Right Hip Moment Y

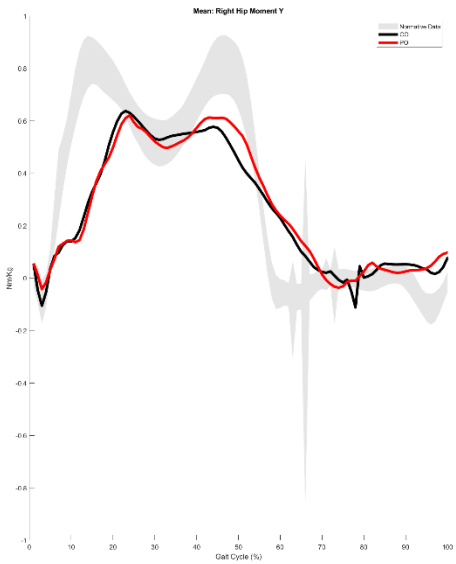

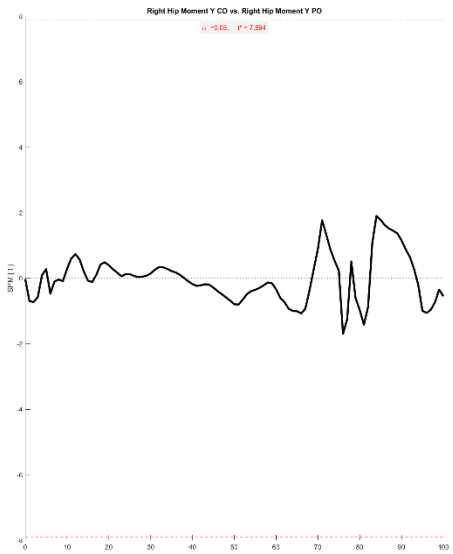

Left Hip Moment X

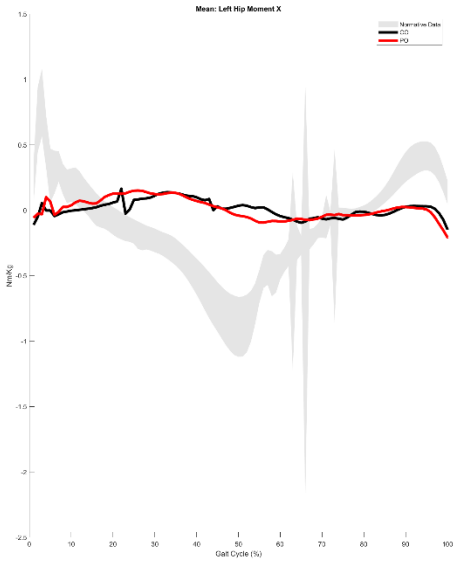

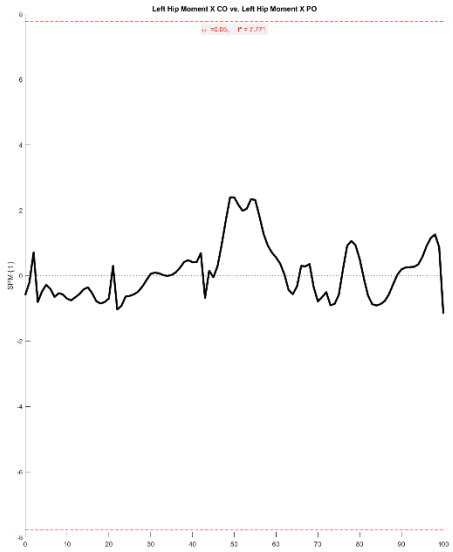

Left Hip Moment Y

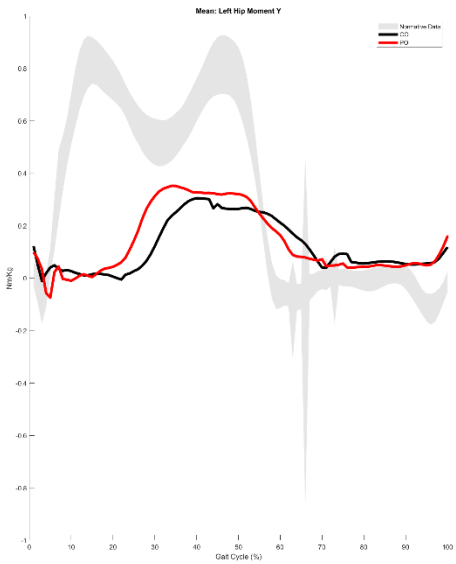

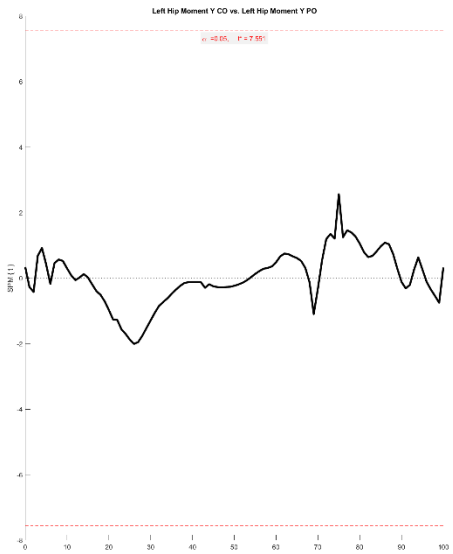

Right Knee Moment X

73.2-74.8%

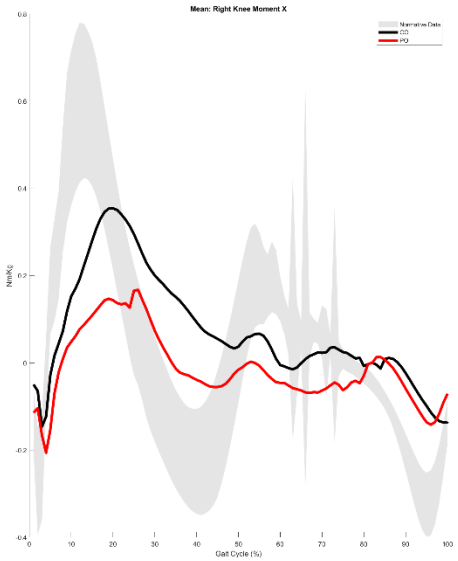

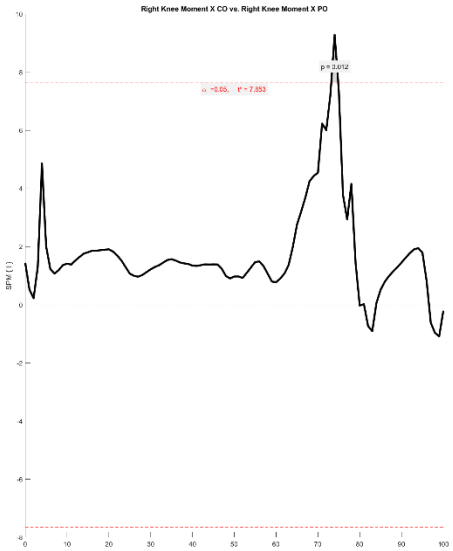

Right Knee Moment Y

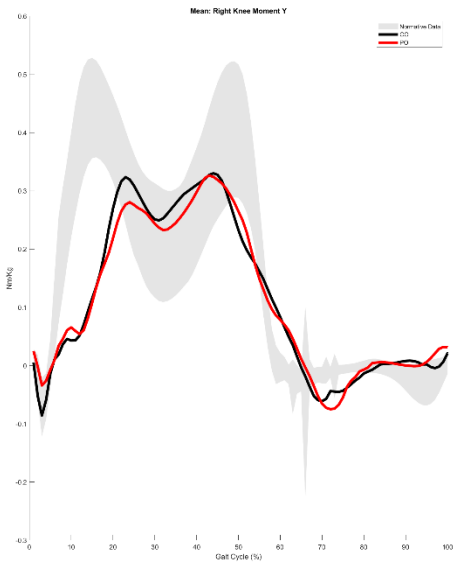

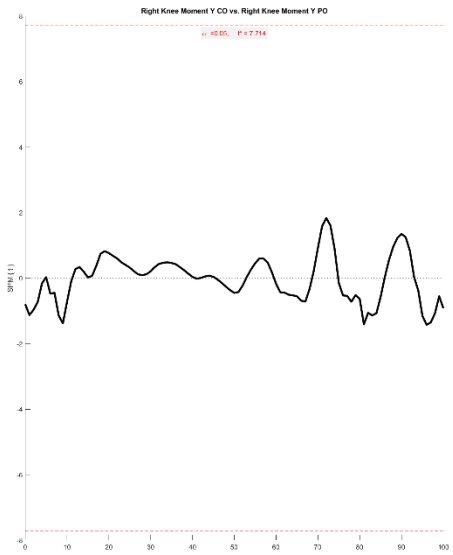

Left Knee Moment X

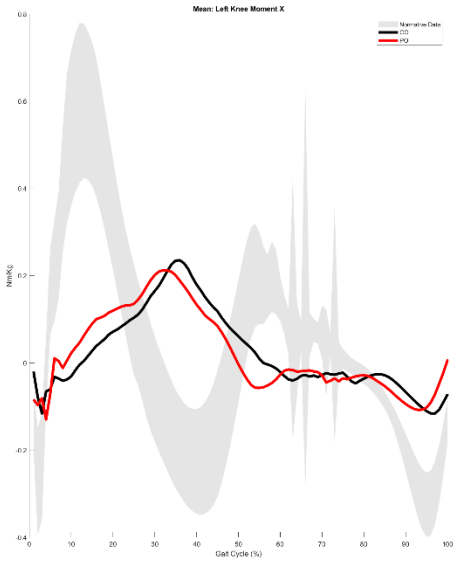

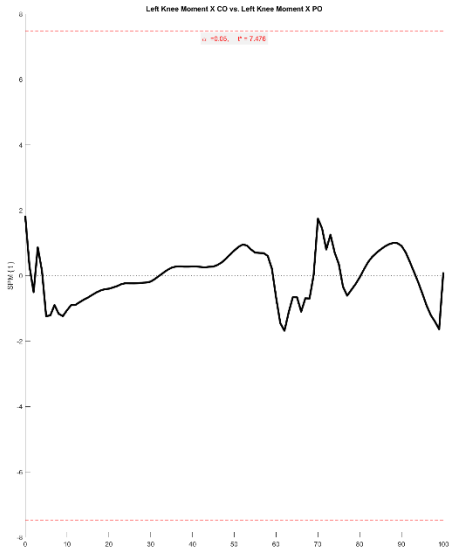

Left Knee Moment Y

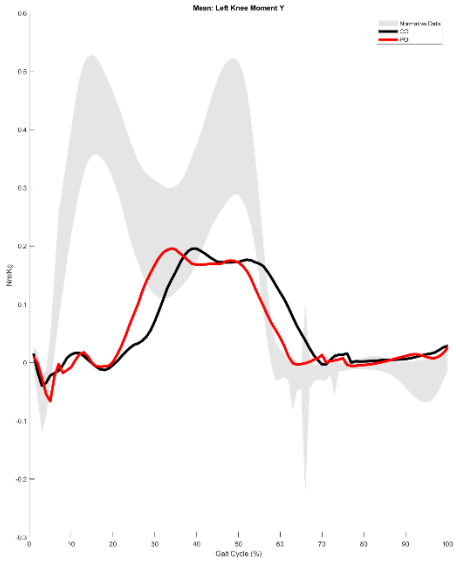

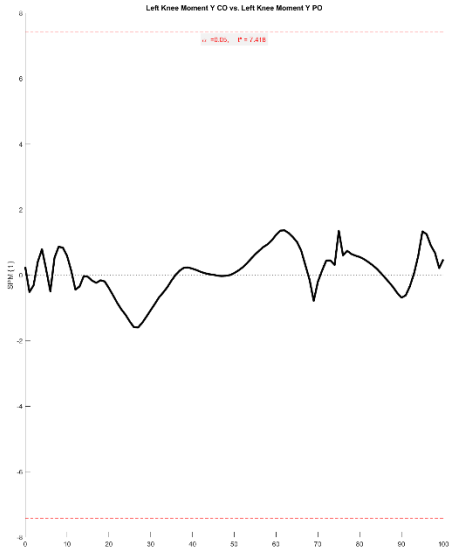

Right Ankle Moment X

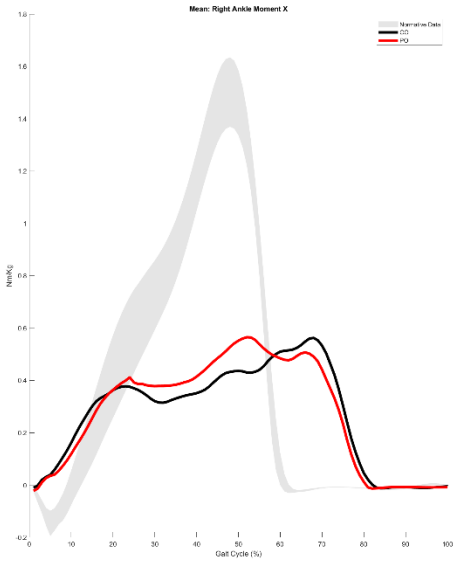

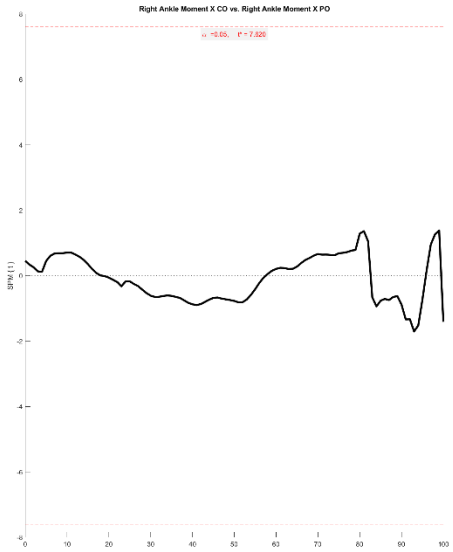

Right Ankle Moment Y

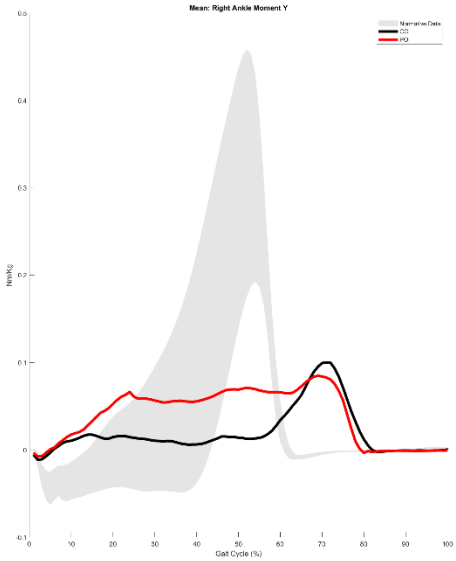

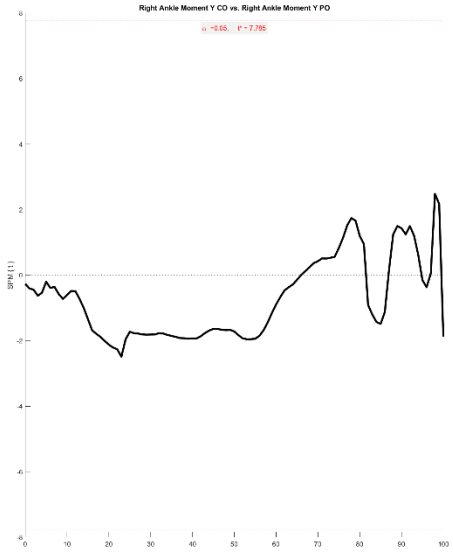

Left Ankle Moment X

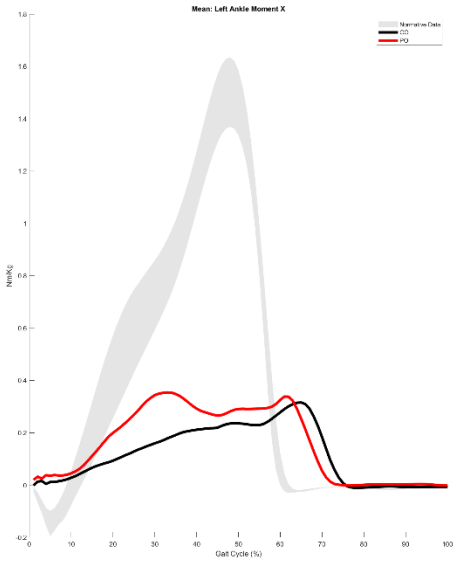

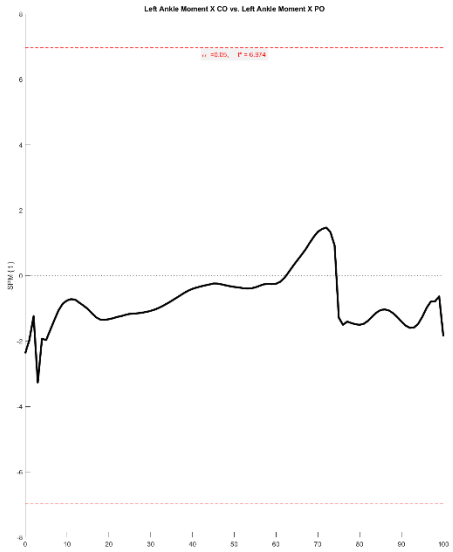

Left Ankle Moment Y

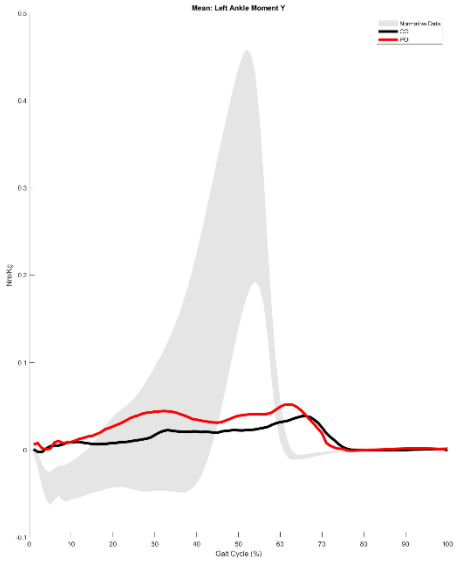

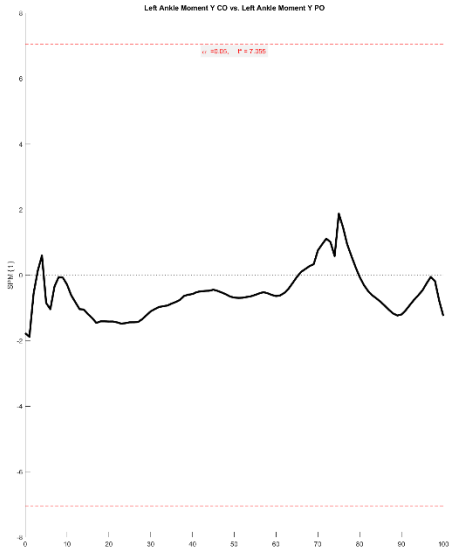

PO

Step Length

REP	Left	Right	IS (50%)	IS (0%)
1	0.28932	0.19744	40.5621	37.7517
2	0.28903	0.18466	38.9833	44.0668
3	0.27429	0.17494	38.9422	44.2312
4	0.27411	0.17328	38.7313	45.0748
5	0.26715	0.17309	39.3172	42.7312
6	0.26611	0.16854	38.776	44.8959
Mean	0.276668	0.1786583	39.2187	43.1253
SD	0.009373	0.0097032	0.62978	2.51913

CO

Step Length

REP	Left	Right	IS (50%)	IS (0%)
1	0.26634	0.16644	38.4583	46.1666
2	0.2659	0.16046	37.6349	49.4605
3	0.2654	0.15718	37.1953	51.2187
4	0.25428	0.15158	37.3479	50.6086
5	0.24922	0.14209	36.3114	54.7545
6	0.24889	0.13765	35.6108	57.5568
Mean	0.2583383	0.1525667	37.0931	51.6276
SD	0.0077455	0.0100772	0.91661	3.66644

	Left	Right
Step Length PO	0.28	0.18
Step Length CO	0.26	0.15
Swing Time PO	0.41	0.35
Swing Time CO	0.38	0.32
Stance Time PO	1.02	1.18
Stance Time CO	1.16	1.22

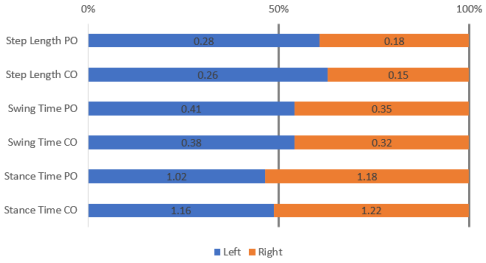

PO

Swing Time

REP	Left	Right	IS (50%)	IS (0%)
1	0.48	0.37	43.5294	25.8824
2	0.41	0.36	46.7532	12.987
3	0.41	0.36	46.7532	12.987
4	0.4	0.35	46.6667	13.3333
5	0.39	0.34	46.5753	13.6986
6	0.37	0.3	44.7761	20.8955
Mean	0.41	0.3466667	45.8423	16.6306
SD	0.034157	0.0228522	1.24918	4.99674

CO

Swing Time

REP	Left	Right	IS (50%)	IS (0%)
1	0.44	0.38	46.3415	14.6341
2	0.38	0.34	47.2222	11.1111
3	0.38	0.33	46.4789	14.0845
4	0.38	0.3	44.1176	23.5294
5	0.38	0.29	43.2836	26.8657
6	0.33	0.29	46.7742	12.9032
Mean	0.3816667	0.3216667	45.703	17.188
SD	0.0318416	0.0323608	1.46242	5.84968

PO

Stance Time

REP	Left	Right	IS (50%)	IS (0%)
1	0.8	1.22	60.396	41.5842
2	1.03	1.21	54.0179	16.0714
3	1.17	1.18	50.2128	0.85106
4	1.16	1.15	49.7835	0.8658
5	0.9	1.15	56.0976	24.3902
6	1.07	1.15	51.8018	7.20721
Mean	1.021667	1.1766667	53.7183	15.1617
SD	0.133843	0.0292499	3.69204	14.4717

CO

Stance Time

REP	Left	Right	IS (50%)	IS (0%)
1	1.35	1.25	48.0769	7.69231
2	1.21	1.24	50.6122	2.44898
3	1.18	1.23	51.0373	4.14938
4	1.15	1.23	51.6807	6.72269
5	1.05	1.19	53.125	12.5
6	1.02	1.18	53.6364	14.5455
Mean	1.16	1.22	51.3614	8.0098
SD	0.1086278	0.0258199	1.8185	4.29068

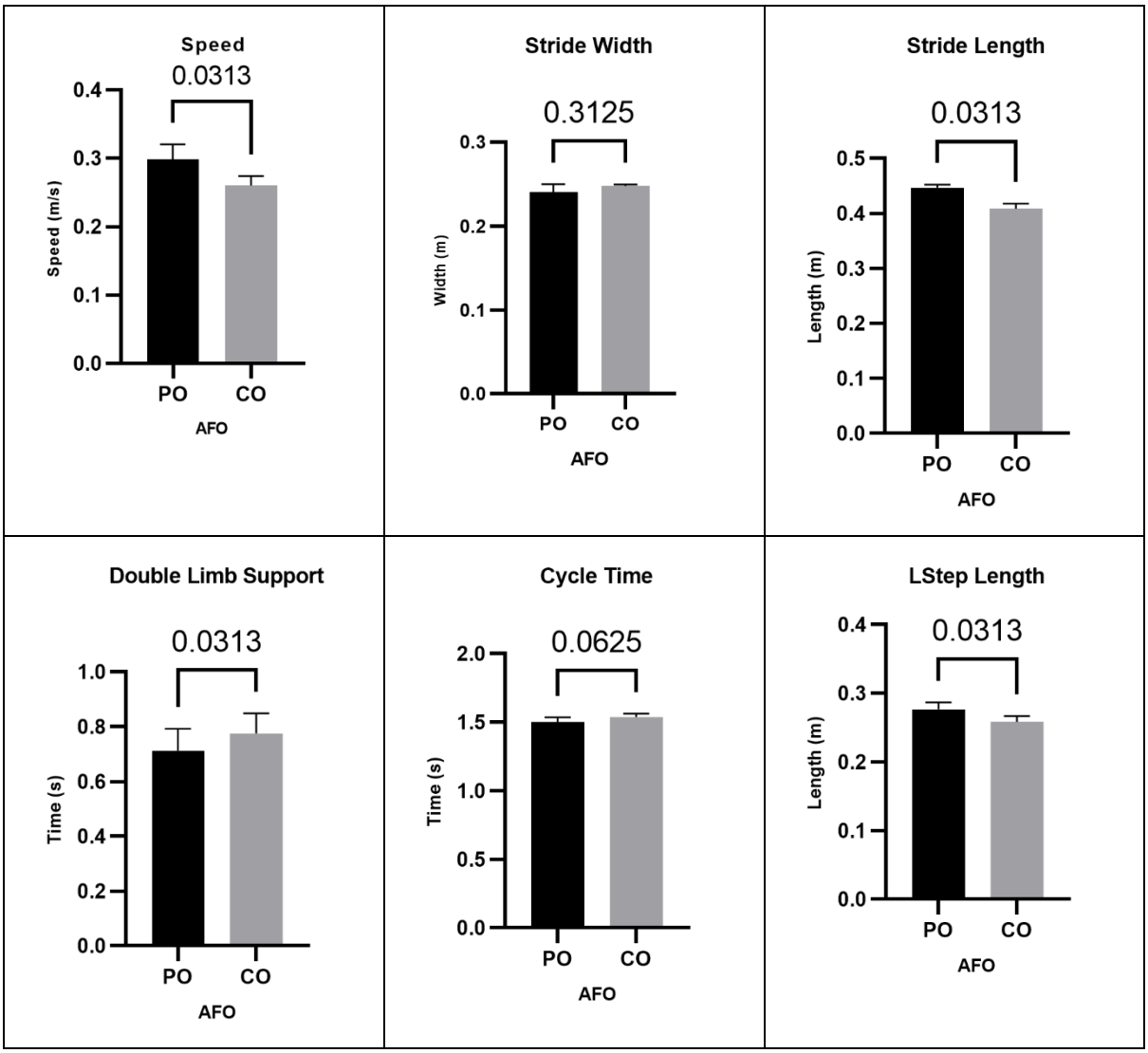

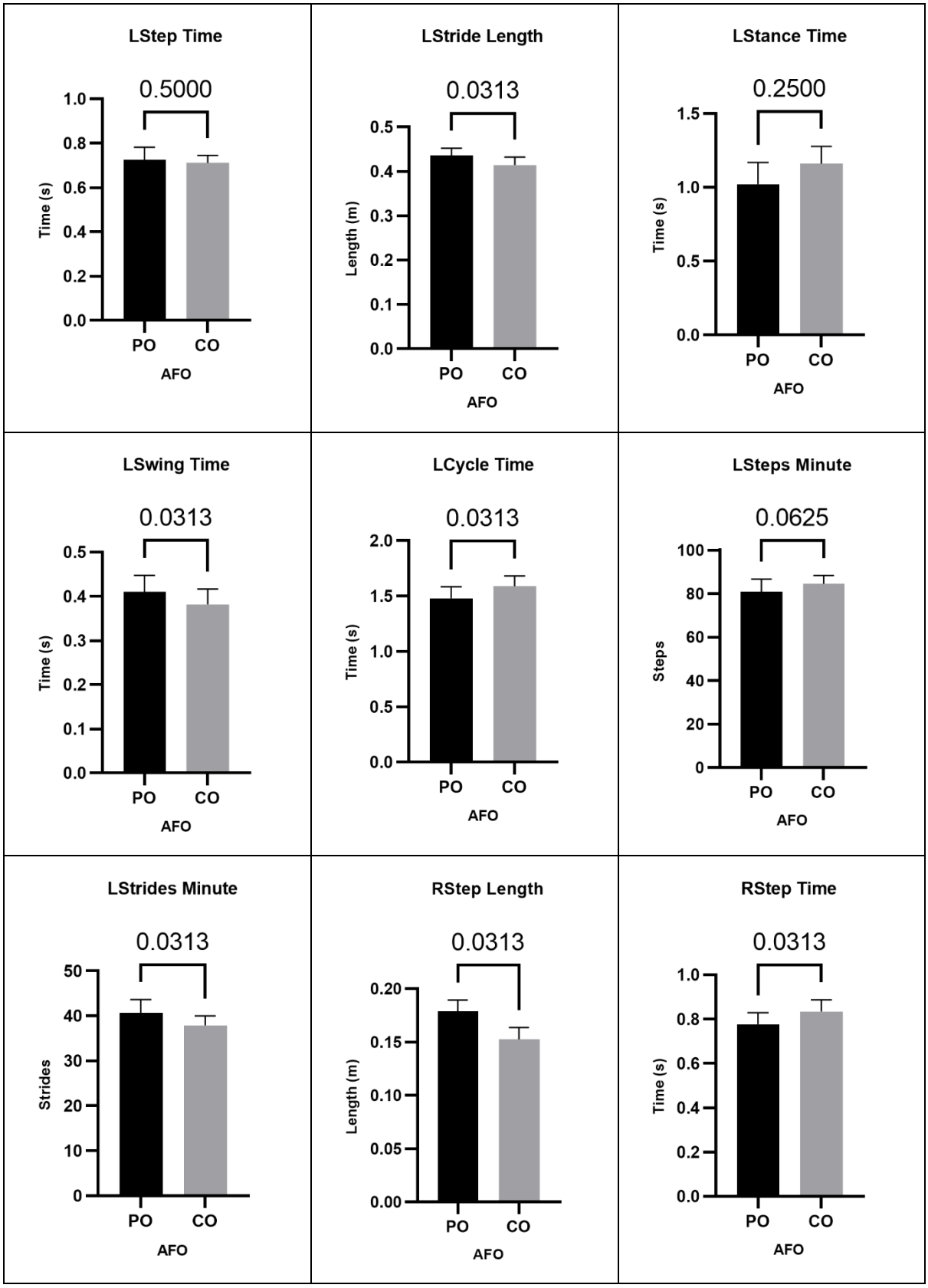
LStep Time
0.5000
Time (s)
1.0
0.8
0.6
0.4
0.2
0.0
PO
CO
AFO
LStride Length
0.0313
Length (m)
0.5
0.4
0.3
0.2
0.1
0.0
PO
CO
AFO
LStance Time
0.2500
Time (s)
1.5
1.0
0.5
0.0
PO
CO
AFO
LSwing Time
0.0313
Time (s)
0.5
0.4
0.3
0.2
0.1
0.0
PO
CO
AFO
LCycle Time
0.0313
Time (s)
2.0
1.5
1.0
0.5
0.0
PO
CO
AFO
LSteps Minute
0.0625
Steps
100
80
60
40
20
0
PO
CO
AFO
LStrides Minute
0.0313
Strides
50
40
30
20
10
0
PO
CO
AFO
RStep Length
0.0313
Length (m)
0.20
0.15
0.10
0.05
0.00
PO
CO
AFO
RStep Time
0.0313
Time (s)
1.0
0.8
0.6
0.4
0.2
0.0
PO
CO
AFO

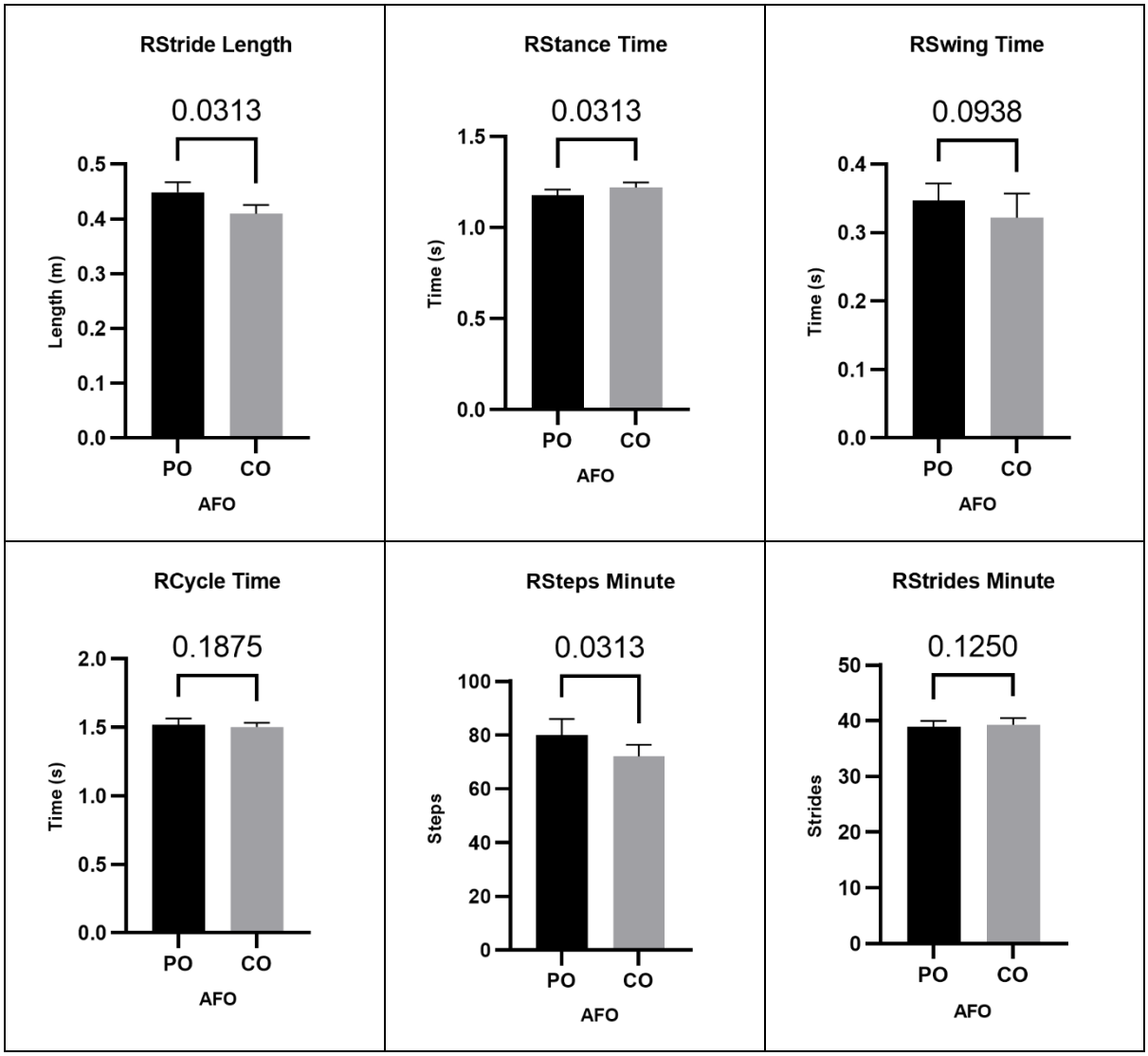
RStride Length
0.0313
Length (m)
0.5
0.4
0.3
0.2
0.1
0.0
PO
CO
AFO
RStance Time
0.0313
Time (s)
1.5
1.0
0.5
0.0
PO
CO
AFO
RSwing Time
0.0938
Time (s)
0.4
0.3
0.2
0.1
0.0
PO
CO
AFO
RCycle Time
0.1875
Time (s)
2.0
1.5
1.0
0.5
0.0
PO
CO
AFO
RSteps Minute
0.0313
Steps
100
80
60
40
20
0
PO
CO
AFO
RStrides Minute
0.1250
Strides
50
40
30
20
10
0
PO
CO
AFO

PATIENT 4

Right Pelvic Angles X

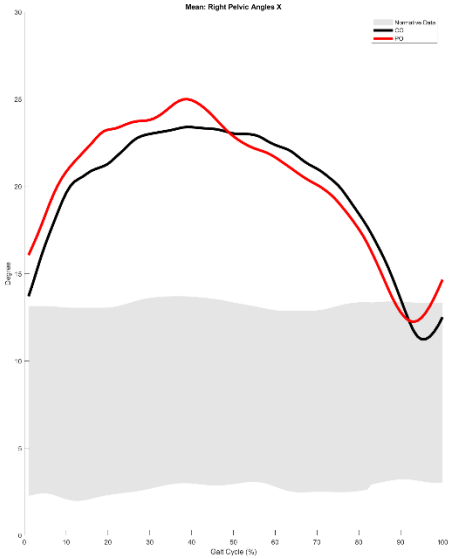

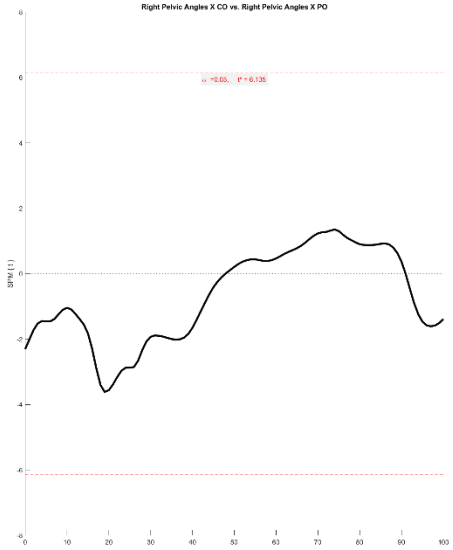

Right Pelvic Angles Y

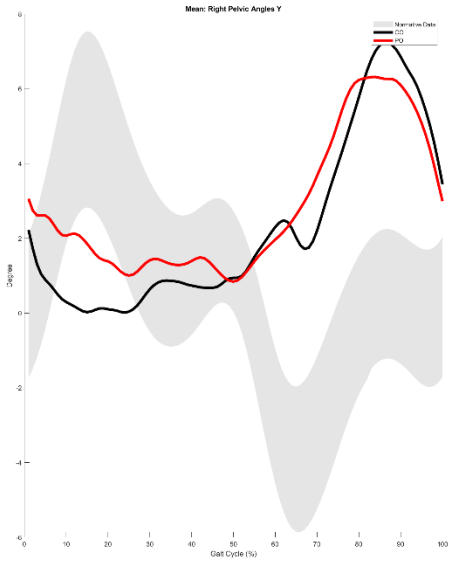

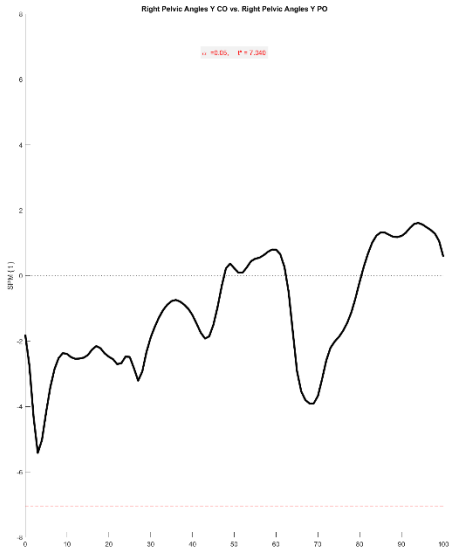

Right Pelvic Angles Z

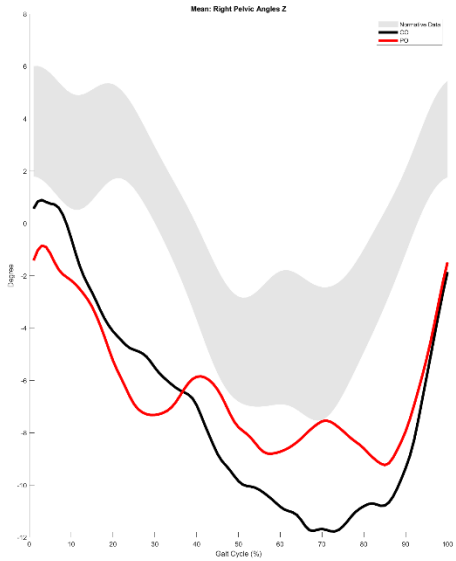

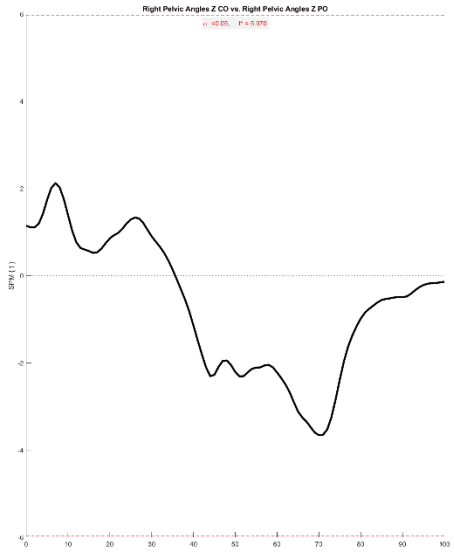

Left Pelvic Angles X

48.9-55.4%

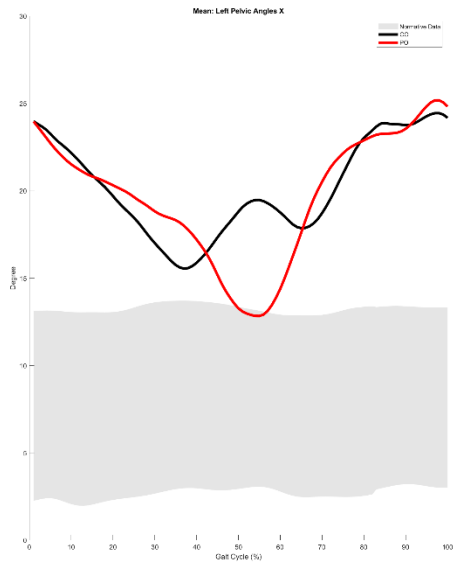

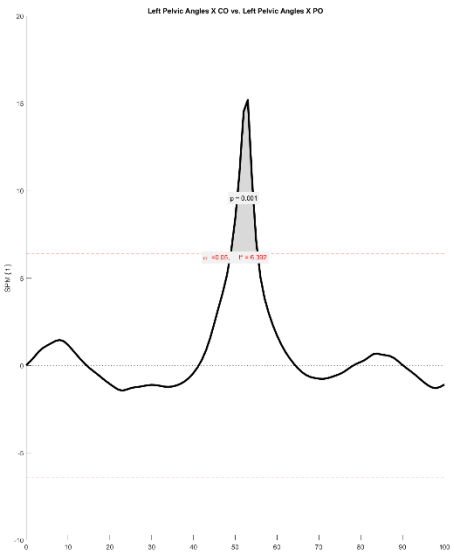

Left Pelvic Angles Y

40.1-45.0%

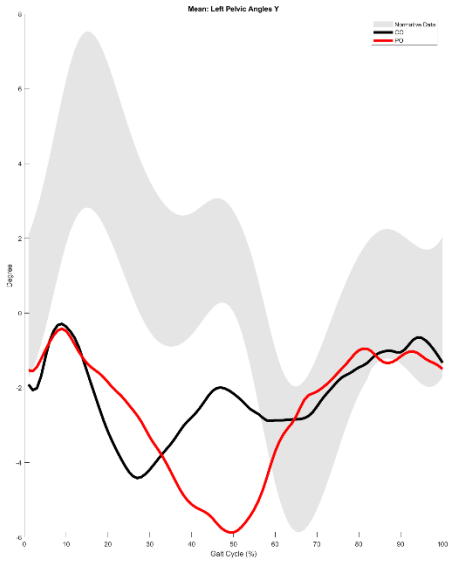

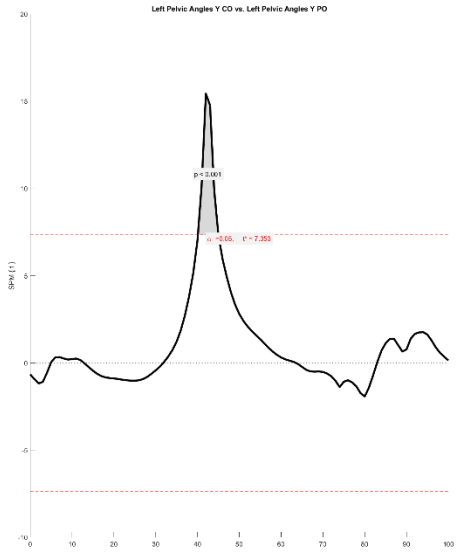

Left Pelvic Angles Z

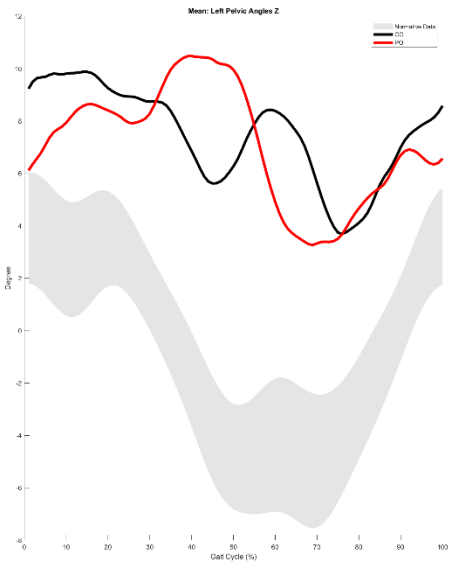

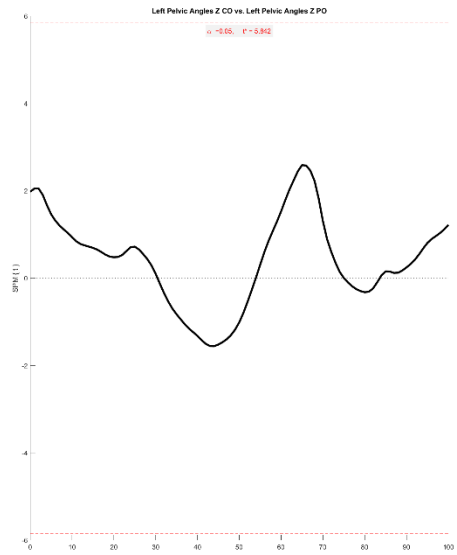

Right Hip Angles X

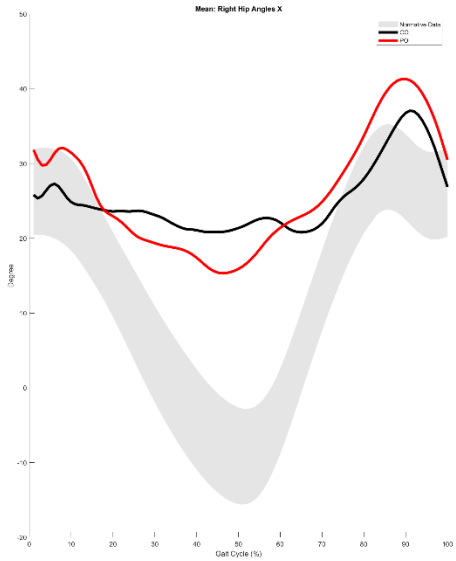

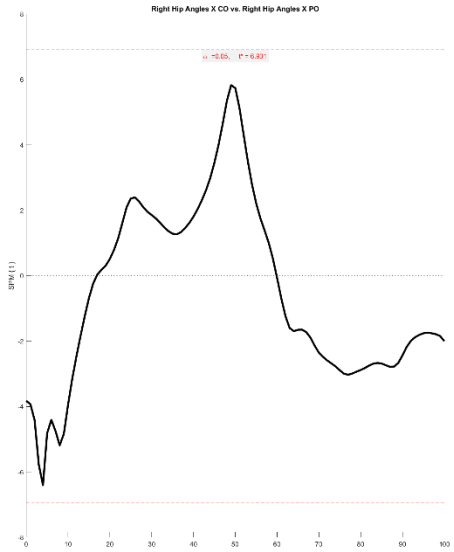

Right Hip Angles Y

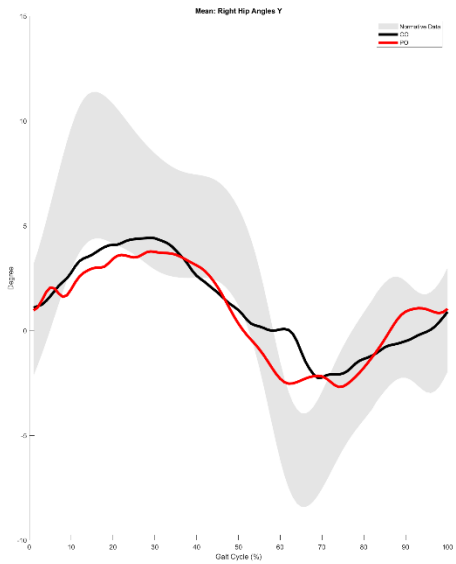

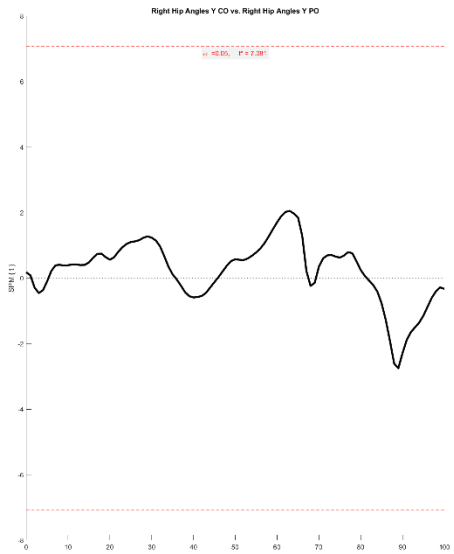

Right Hip Angles Z

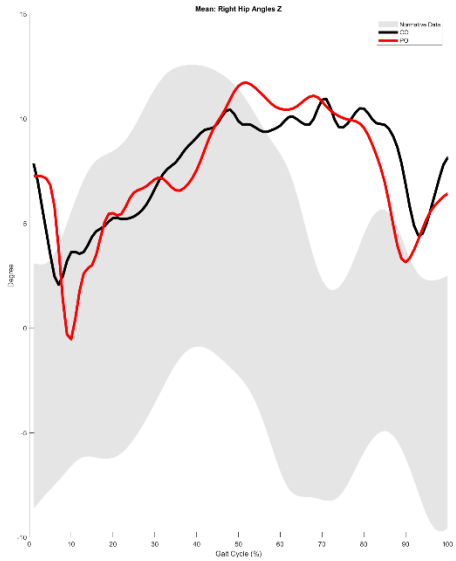

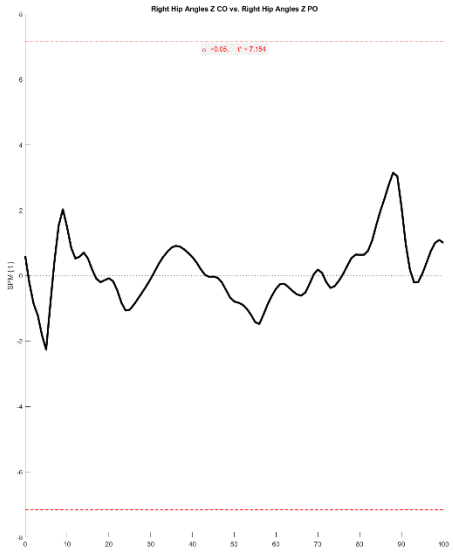

Left Hip Angles X

55.9-61.5%

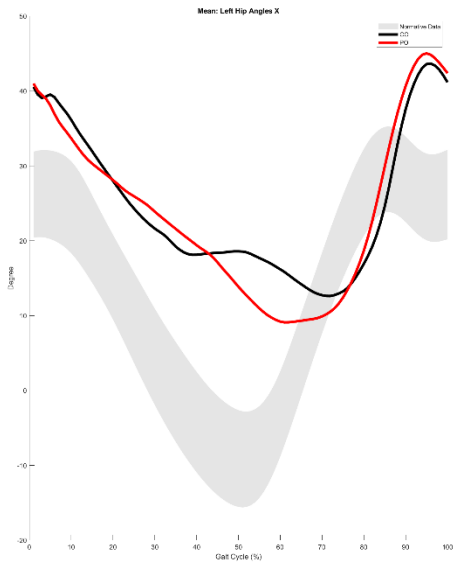

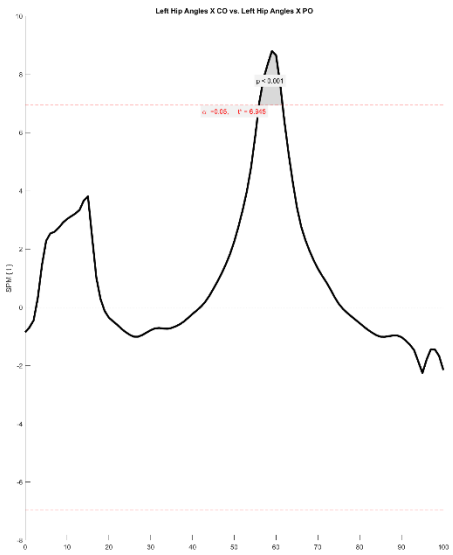

Left Hip Angles Y

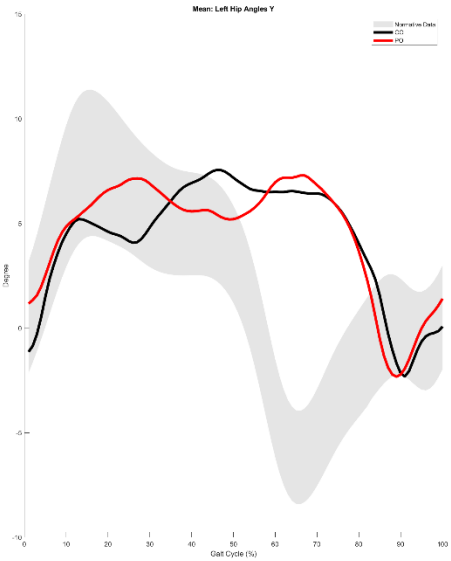

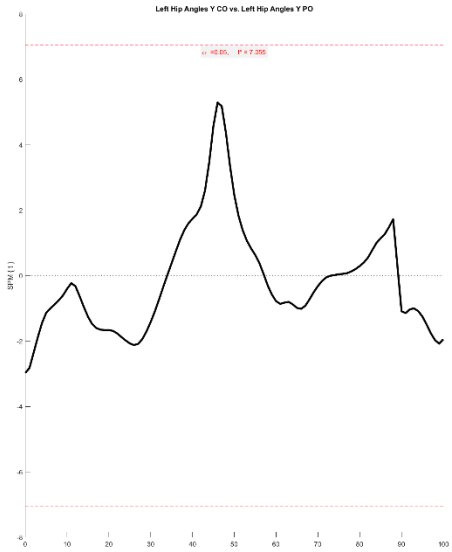

Left Hip Angles Z

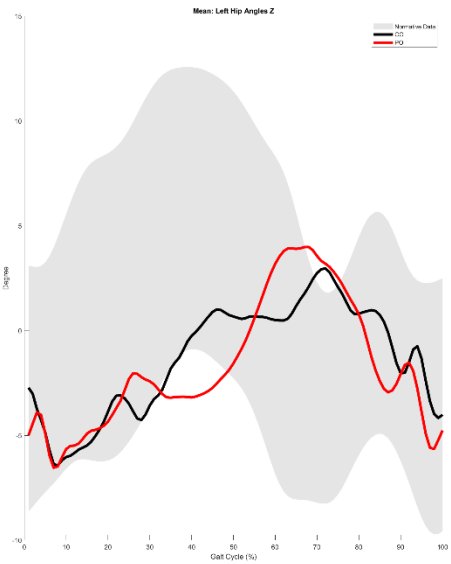

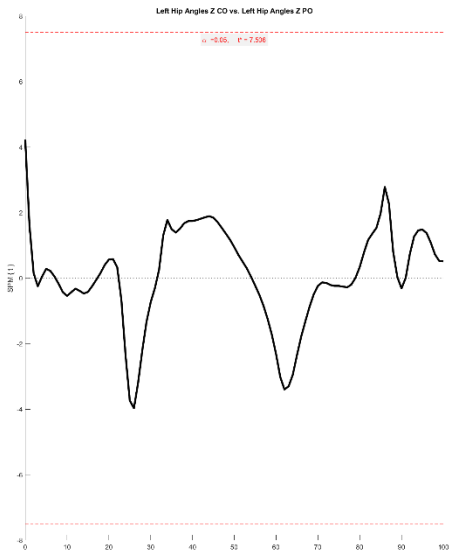

Right Knee Angles X

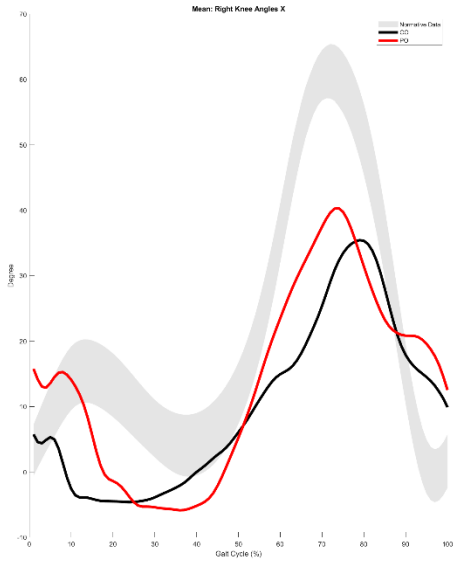

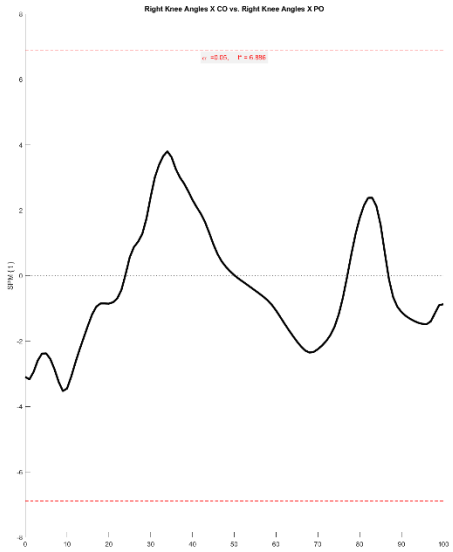

Right Knee Angles Y

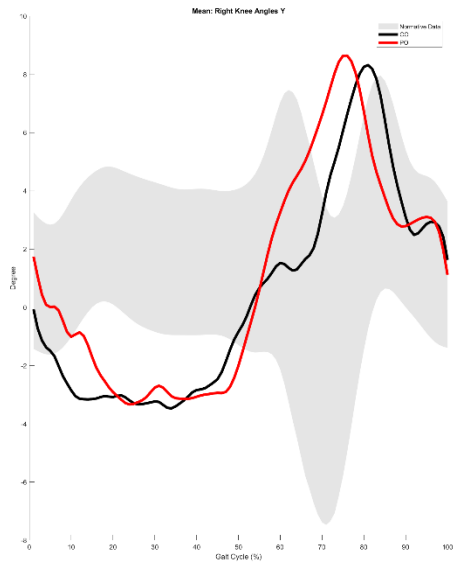

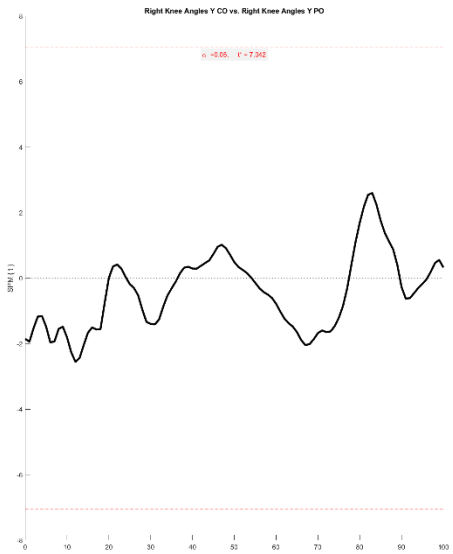

Right Knee Angles Z

0.0-1.2%, 4.8-6.6%, 7.2-10.1%, 37.4-39.1%, 45.7-49.0%, 51.1-55.6%, 56.8-58.5%, 89.4-92.1%, 94.3-100.0%

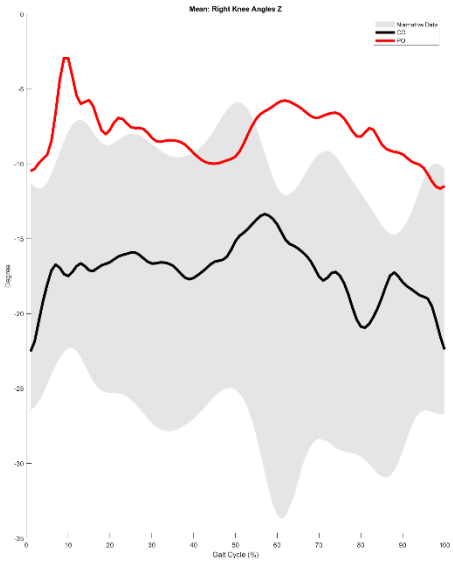

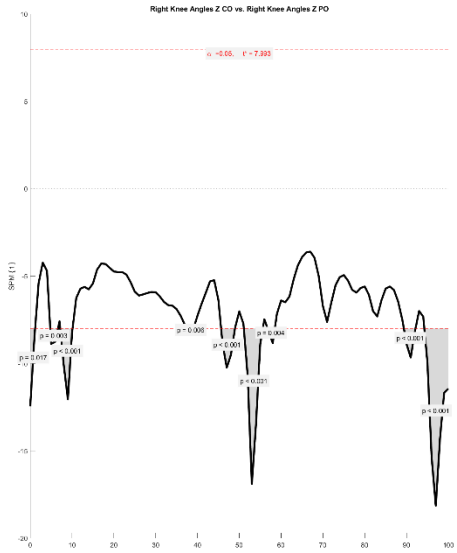

Left Knee Angles X

54.8-55.1%, 85.9-86.2%

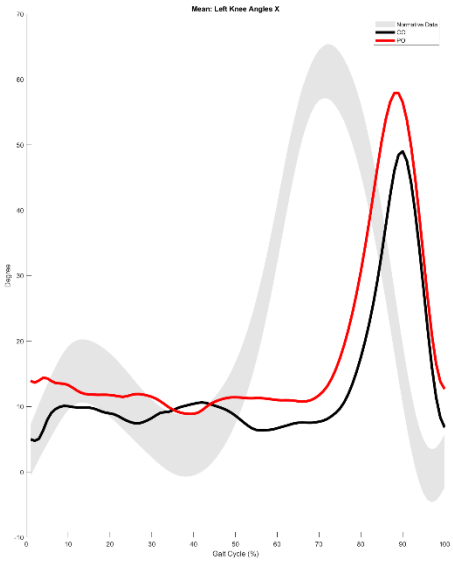

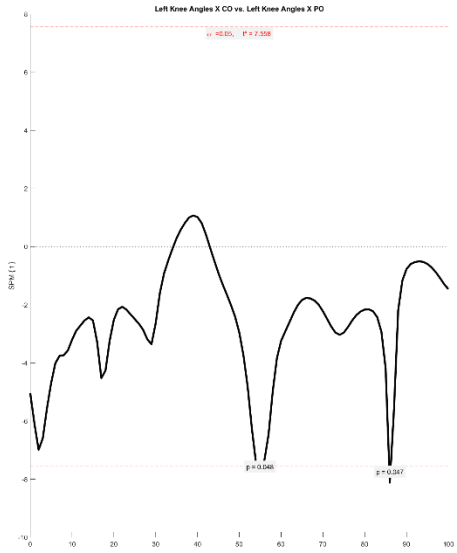

Left Knee Angles Y

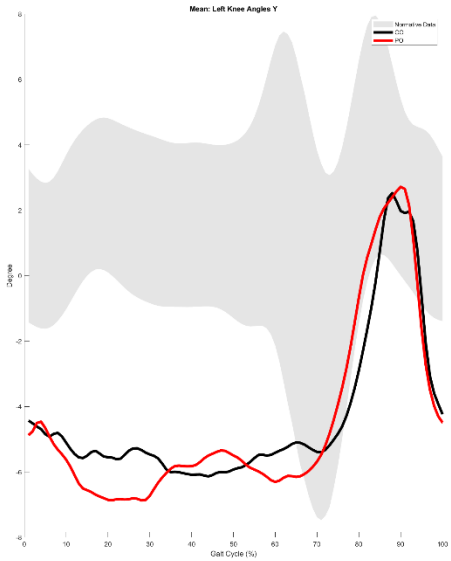

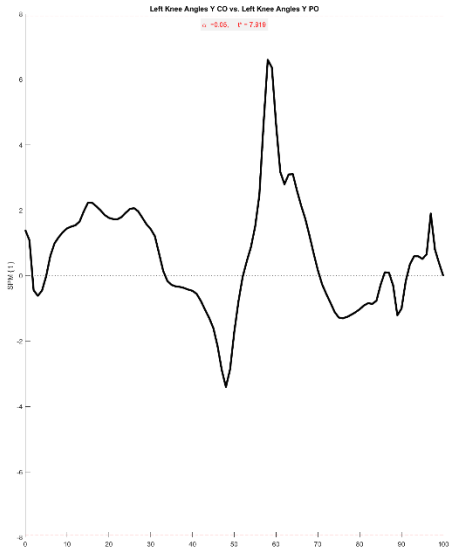

Left Knee Angles Z

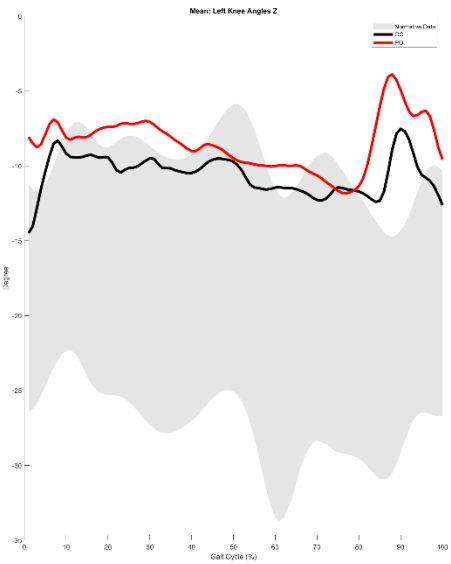

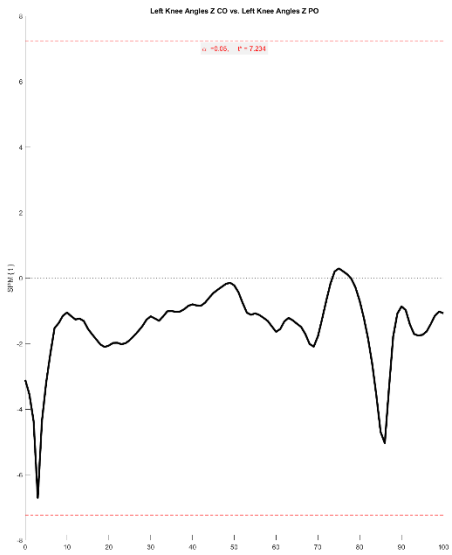

Right Ankle Angles X

21.5-24.3%, 61.8-62.2%

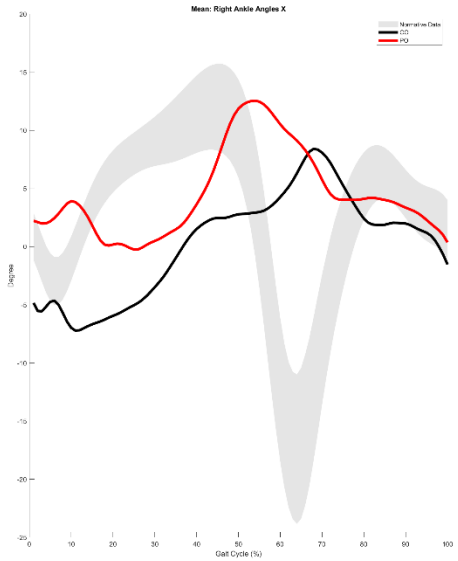

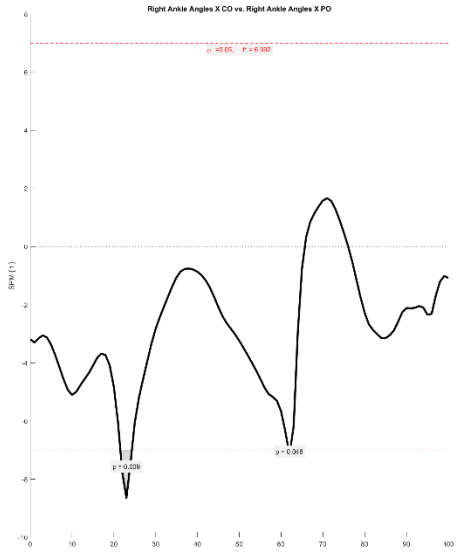

Right Ankle Angles Y

1.6-7.5%, 12.9-20.4%, 25.0-31.4%, 78.4-87.7%, 90.8-92.4%, 95.0-97.6%

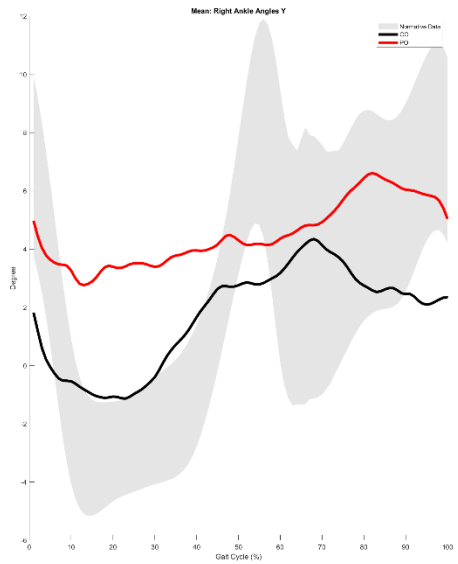

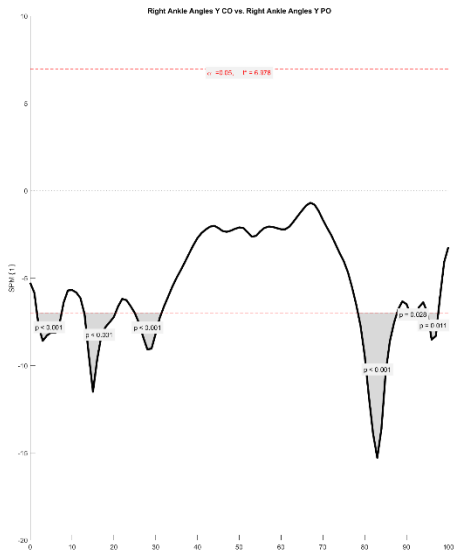

Left Ankle Angles X

0.8-6.8%, 7.1-9.2%, 57.2-63.0%

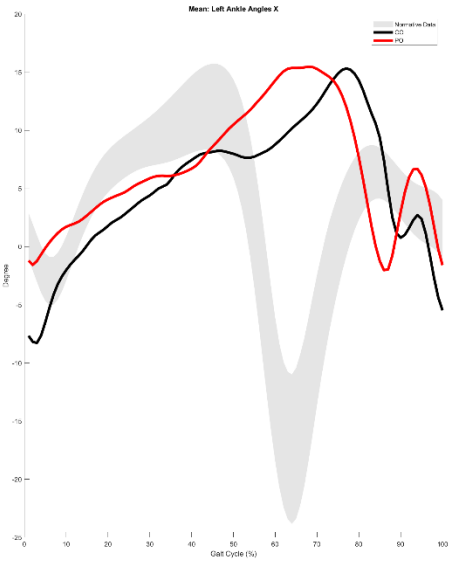

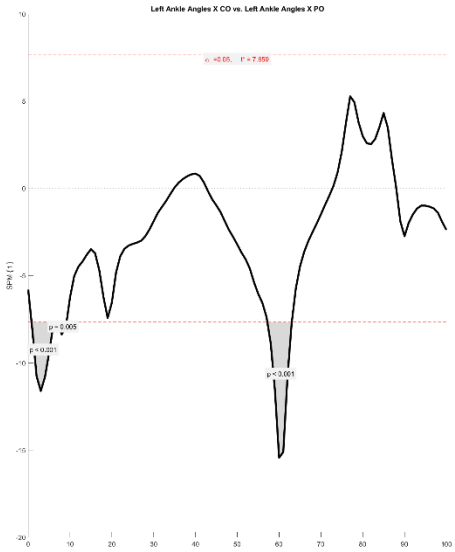

Left Ankle Angles Y

25.8-30.6%

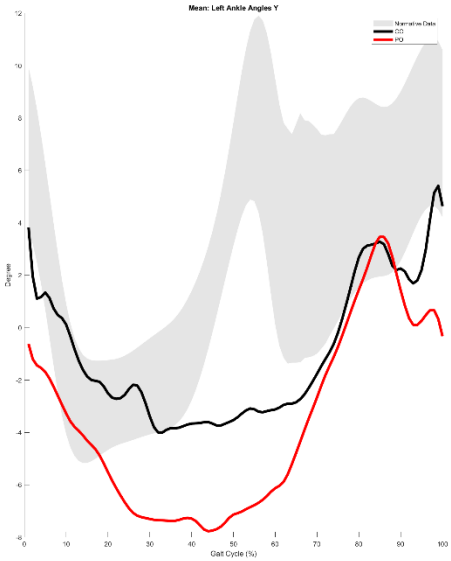

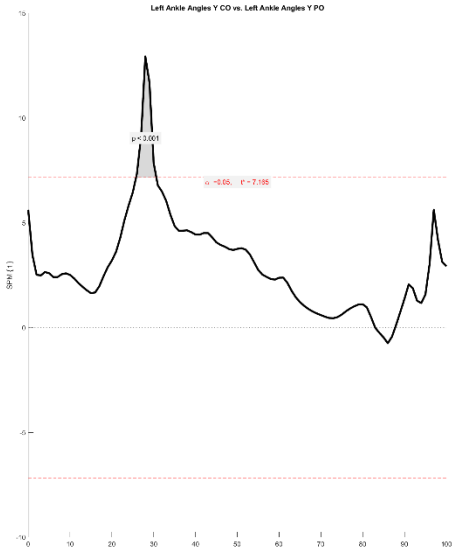

Right Foot Pitch Angles X

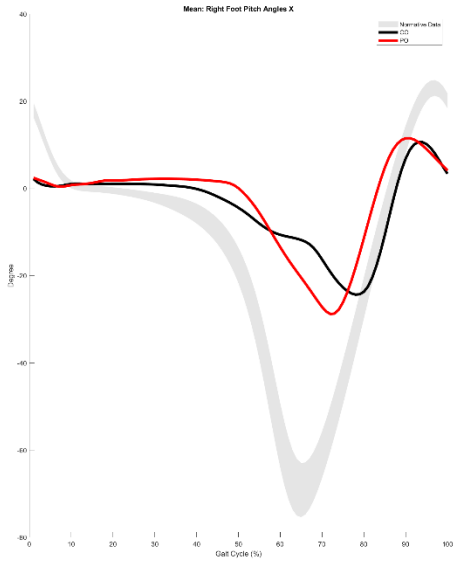

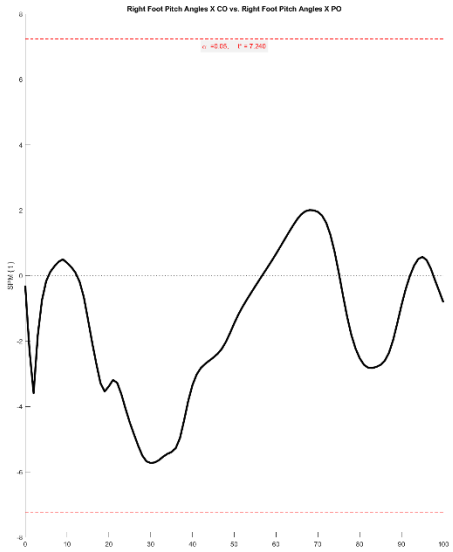

Left Foot Pitch Angles X

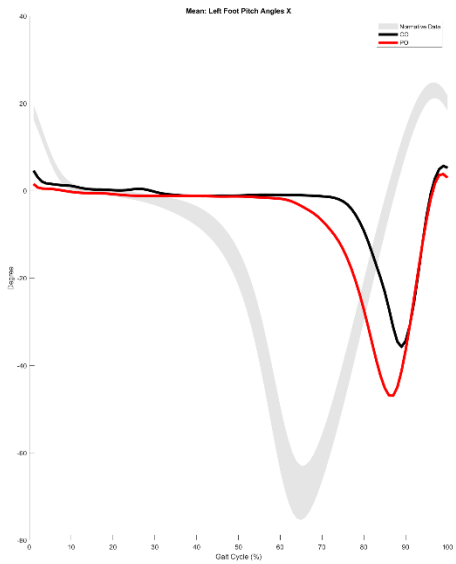

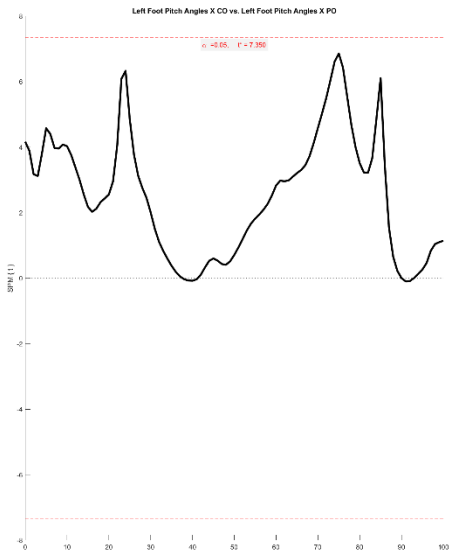

Right Foot Progression Z

7.0-17.9%, 37.8-48.8%

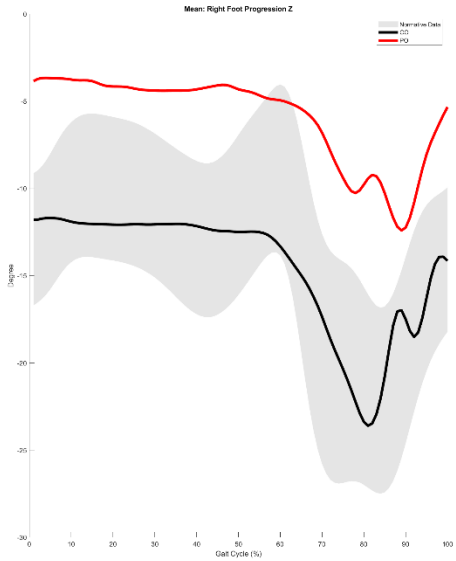

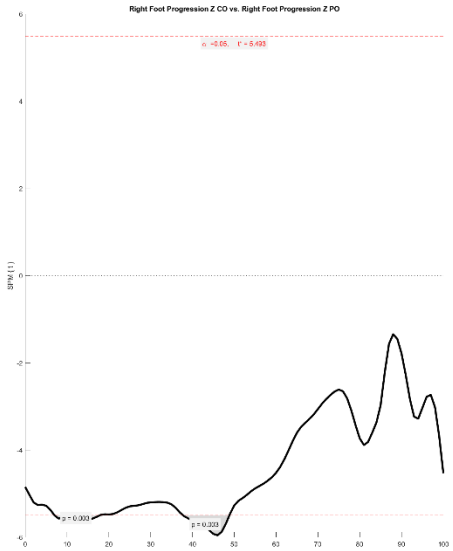

Left Foot Progression Z

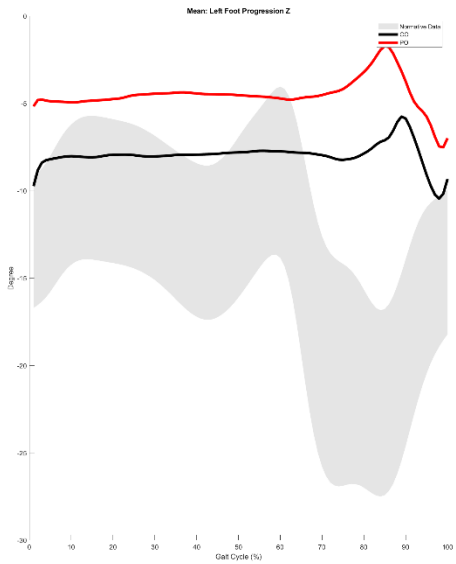

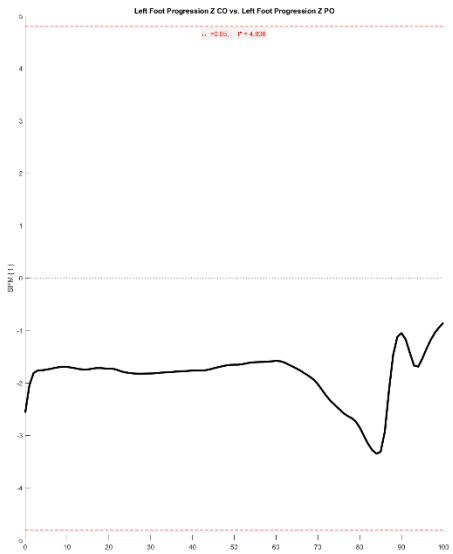

PO

Step Length

REP	Left	Right	IS (50%)	IS (0%)
1	0.23779	0.32046	57.4044	29.6176
2	0.2305	0.31248	57.5491	30.1963
3	0.223	0.30987	58.1511	32.6046
4	0.22129	0.30089	57.6219	30.4876
5	0.20541	0.29314	58.7985	35.1941
6	0.2022	0.28858	58.8003	35.2011
Mean	0.220032	0.3042367	58.0542	32.2169
SD	0.012696	0.0111232	0.57508	2.30033

CO

Step Length

REP	Left	Right	IS (50%)	IS (0%)
1	0.26941	0.34624	56.2397	24.959
2	0.23522	0.33083	58.4454	33.7815
3	0.22539	0.31671	58.4228	33.6912
4	0.19457	0.31518	61.8303	47.3212
5	0.18601	0.30185	61.8723	47.489
6	0.17858	0.27418	60.5575	42.2299
Mean	0.2148633	0.314165	59.5613	38.2453
SD	0.0317841	0.0225998	2.04351	8.17402

	Left	Right
Step Length PO	0.22	0.30
Step Length CO	0.21	0.31
Swing Time PO	0.51	0.92
Swing Time CO	0.55	0.89
Stance Time PO	2.30	1.79
Stance Time CO	1.60	2.19

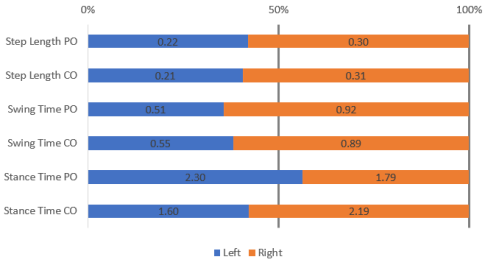

PO

Swing Time

REP	Left	Right	IS (50%)	IS (0%)
1	0.55833	0.95	62.9836	51.9343
2	0.54166	0.94167	63.4835	53.9341
3	0.525	0.93333	63.9999	55.9997
4	0.48333	0.91667	65.4764	61.9057
5	0.48333	0.90833	65.2695	61.0781
6	0.46667	0.88333	65.4319	61.7274
Mean	0.50972	0.9222217	64.4408	57.7632
SD	0.03382	0.0223965	0.99798	3.99193

CO

Swing Time

REP	Left	Right	IS (50%)	IS (0%)
1	0.61667	0.96667	61.0526	44.2103
2	0.58333	0.94167	61.7489	46.9954
3	0.54167	0.86667	61.5384	46.1536
4	0.525	0.86667	62.2755	49.1022
5	0.50834	0.85833	62.8045	51.2179
6	0.50833	0.83334	62.1121	48.4486
Mean	0.5472233	0.8888917	61.922	47.688
SD	0.0401577	0.0480323	0.55871	2.23483

PO

Stance Time

REP	Left	Right	IS (50%)	IS (0%)
1	2.43333	2.1	46.3236	14.7057
2	2.375	1.85833	43.8976	24.4096
3	2.325	1.80833	43.75	25.0002
4	2.30833	1.78333	43.5845	25.662
5	2.25	1.65	42.3077	30.7692
6	2.13334	1.51667	41.5525	33.79
Mean	2.304167	1.78611	43.5693	25.7228
SD	0.095103	0.1804476	1.49364	5.97457

CO

Stance Time

REP	Left	Right	IS (50%)	IS (0%)
1	1.79	2.475	58.0305	32.1219
2	1.74	2.4	57.971	31.8841
3	1.65	2.35	58.75	35
4	1.63	2.01667	55.3017	21.2067
5	1.5	1.96667	56.7308	26.9232
6	1.31	1.91667	59.4009	37.6035
Mean	1.6033333	2.1875017	57.6975	30.7899
SD	0.1597568	0.2256533	1.34594	5.38376

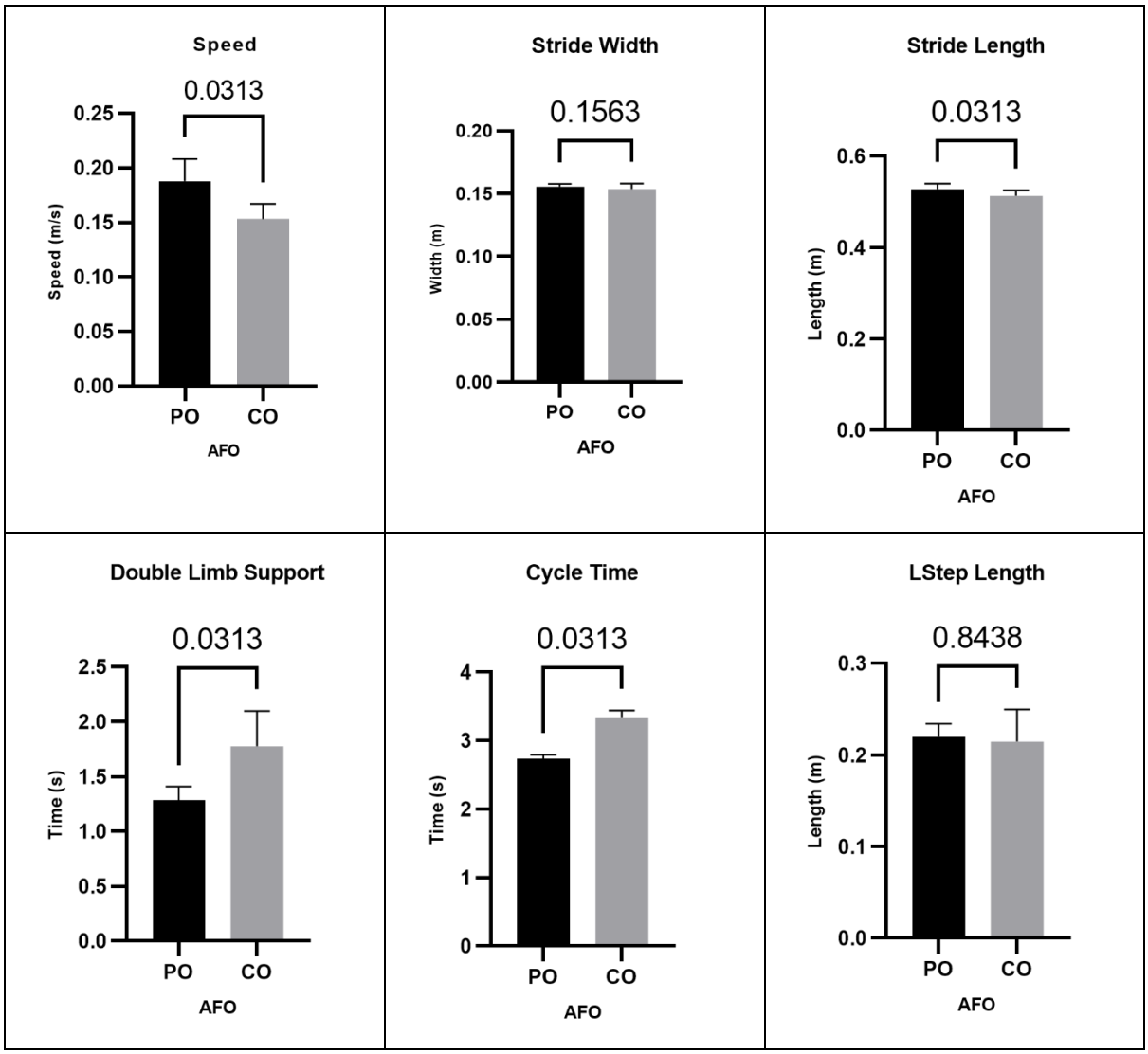

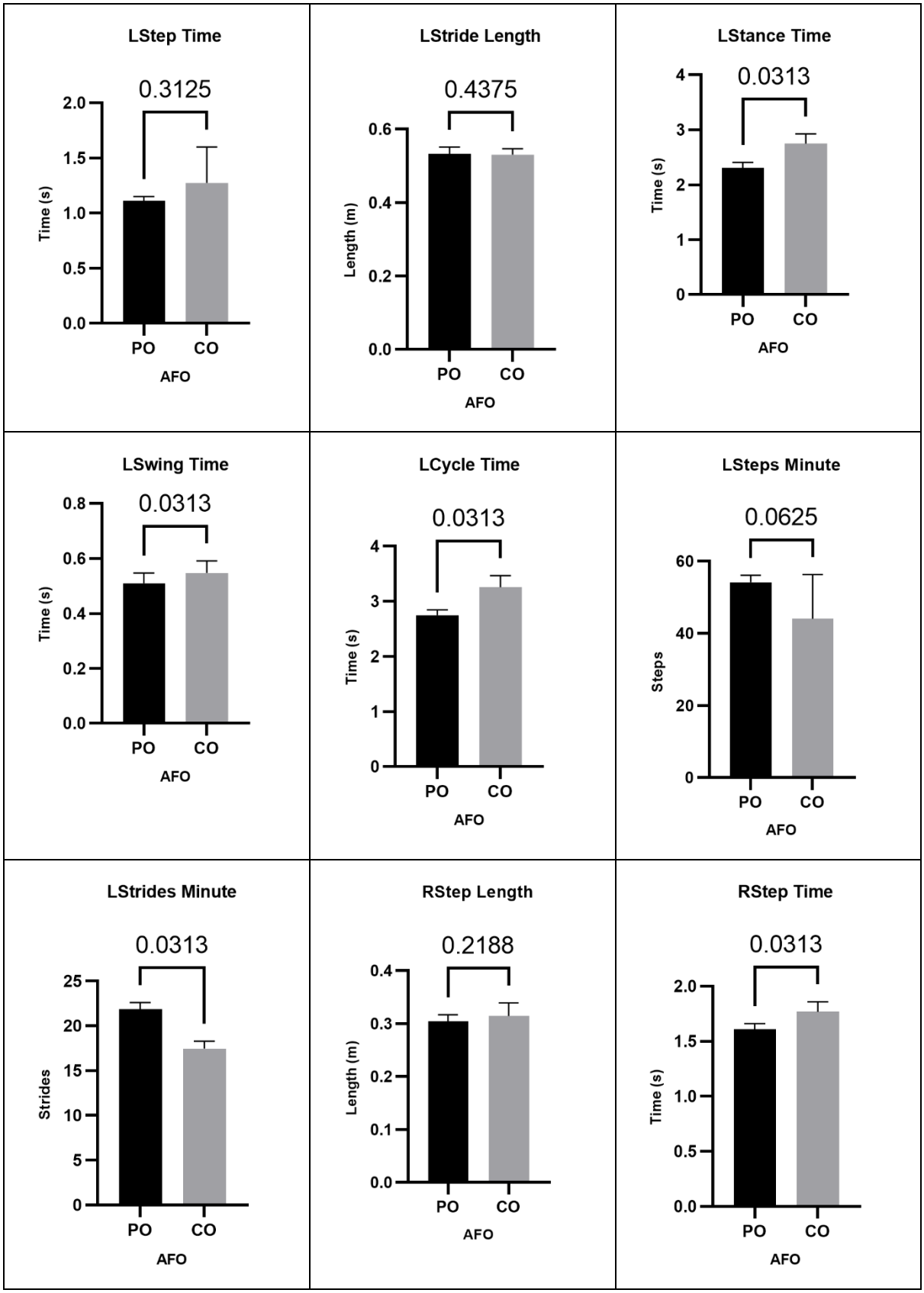
LStep Time
0.3125
Time (s)
2.0
1.5
1.0
0.5
0.0
PO
CO
AFO
LStride Length
0.4375
Length (m)
0.6
0.4
0.2
0.0
PO
CO
AFO
LStance Time
0.0313
Time (s)
4
3
2
1
0
PO
CO
AFO
LSwing Time
0.0313
Time (s)
0.8
0.6
0.4
0.2
0.0
PO
CO
AFO
LCycle Time
0.0313
Time (s)
4
3
2
1
0
PO
CO
AFO
LSteps Minute
0.0625
Steps
60
40
20
0
PO
CO
AFO
LStrides Minute
0.0313
Strides
25
20
15
10
5
0
PO
CO
AFO
RStep Length
0.2188
Length (m)
0.4
0.3
0.2
0.1
0.0
PO
CO
AFO
RStep Time
0.0313
Time (s)
2.0
1.5
1.0
0.5
0.0
PO
CO
AFO

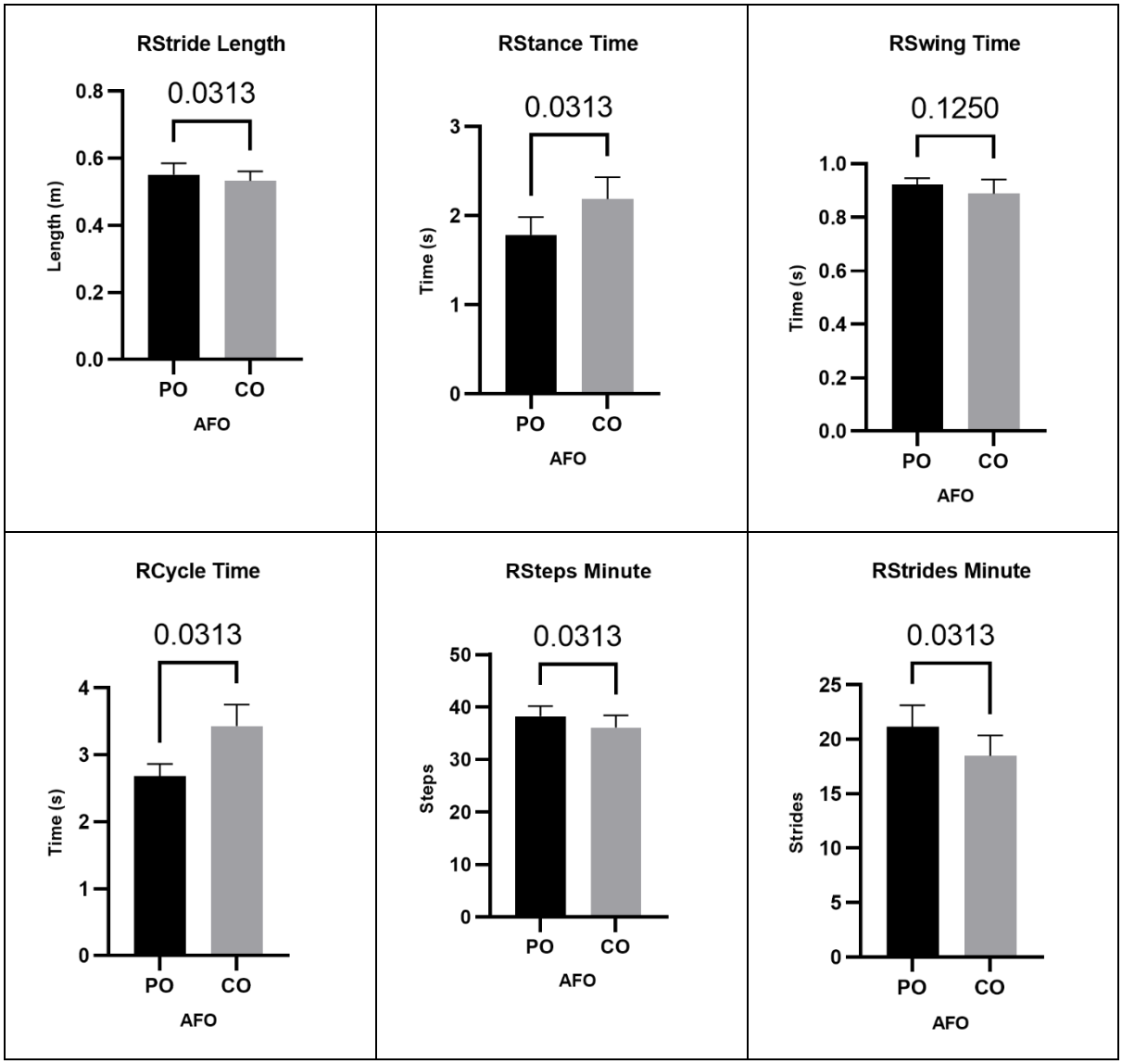
RStride Length
0.0313
Length (m)
0.0
0.2
0.4
0.6
0.8
PO
CO
AFO
RStance Time
0.0313
Time (s)
0
1
2
3
PO
CO
AFO
RSwing Time
0.1250
Time (s)
0.0
0.2
0.4
0.6
0.8
1.0
PO
CO
AFO
RCycle Time
0.0313
Time (s)
0
1
2
3
4
PO
CO
AFO
RSteps Minute
0.0313
Steps
0
10
20
30
40
50
PO
CO
AFO
RStrides Minute
0.0313
Strides
0
5
10
15
20
25
PO
CO
AFO

PATIENT 5

Right Pelvic Angles X

0.5-85.0%, 92.2-100.0%

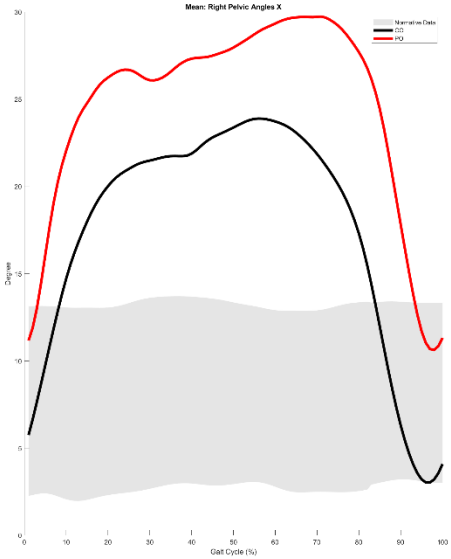

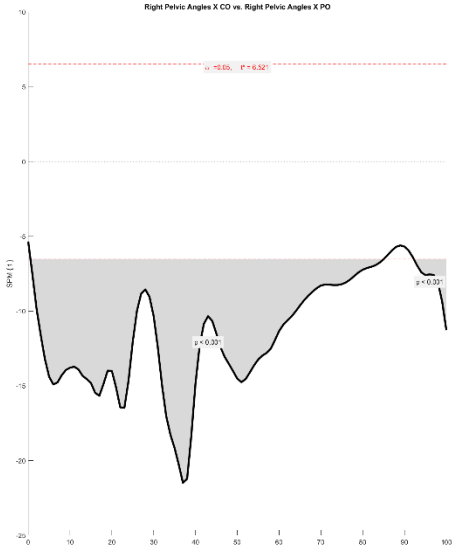

Right Pelvic Angles Y

14.6-22.6%, 58.7-71.6%

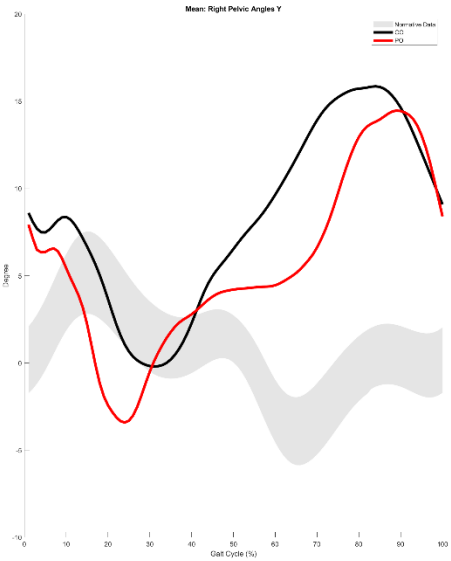

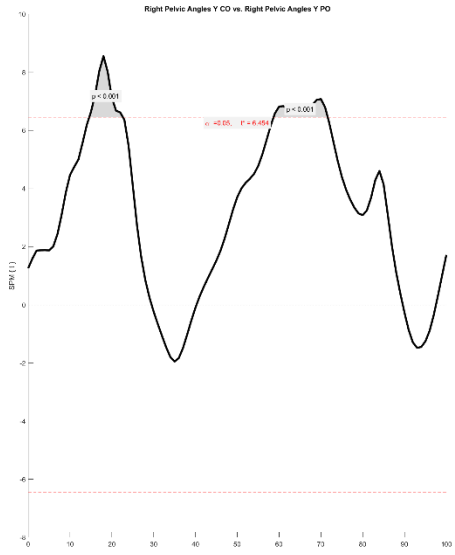

Right Pelvic Angles Z

15.5-23.1%, 49.1-89.6%, 94.6-95.8%, 99.9-100.0%

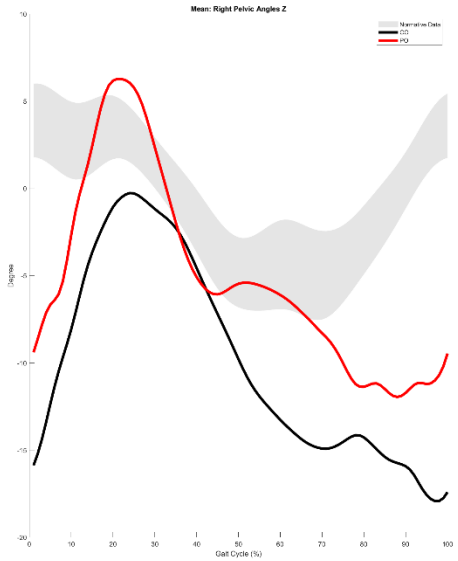

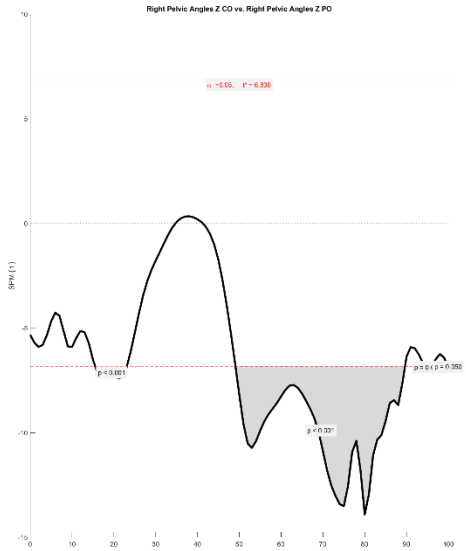

Left Pelvic Angles X

0.0-57.1%, 83.6-100.0%

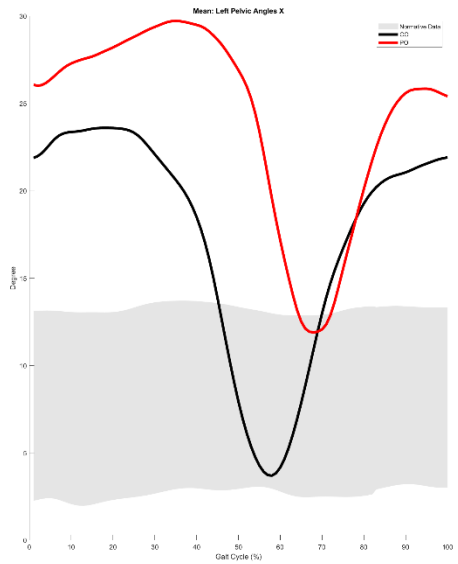

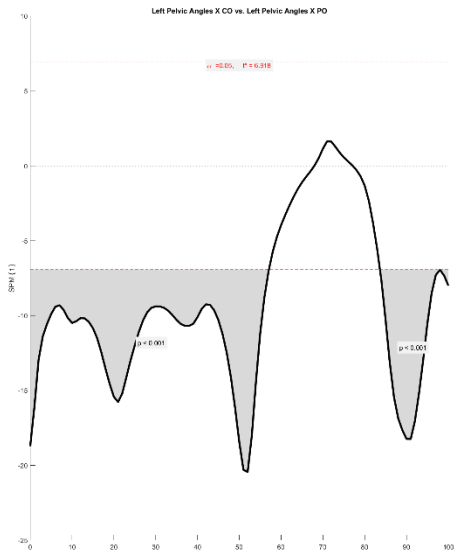

Left Pelvic Angles Y

2.1-44.1%, 61.6-64.3%

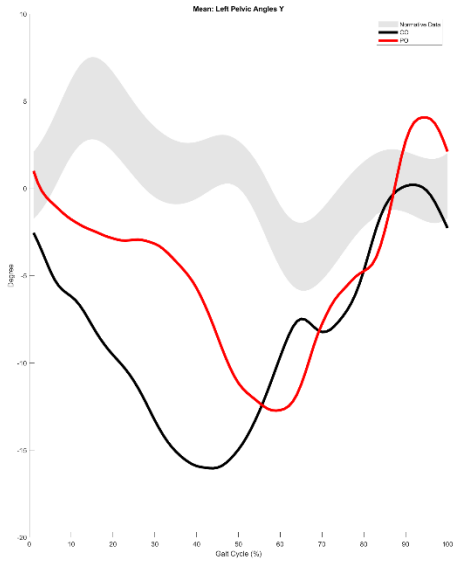

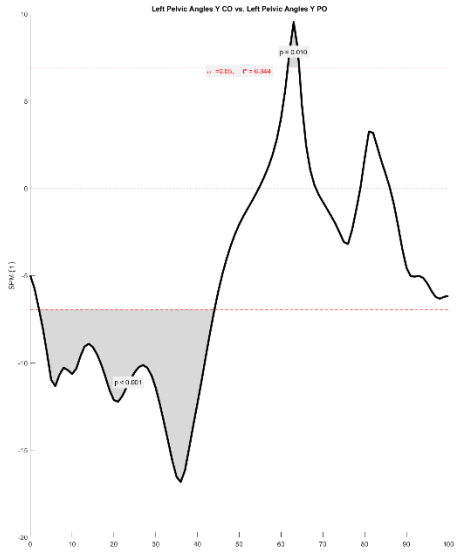

Left Pelvic Angles Z

88.8-100.0%

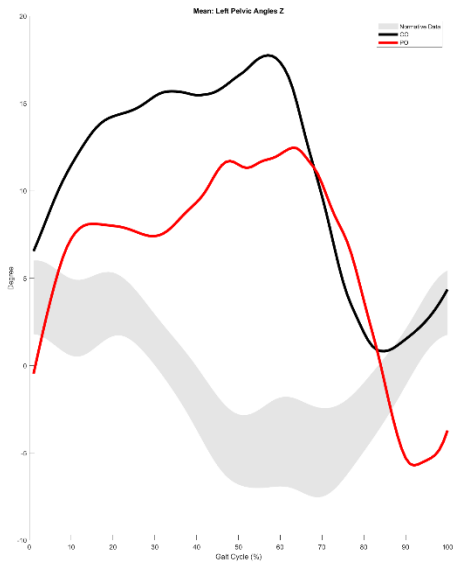

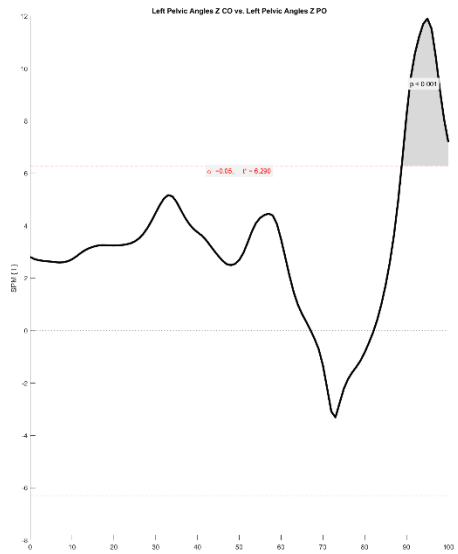

Right Hip Angles X

39.8-48.1%, 89.6-90.2%

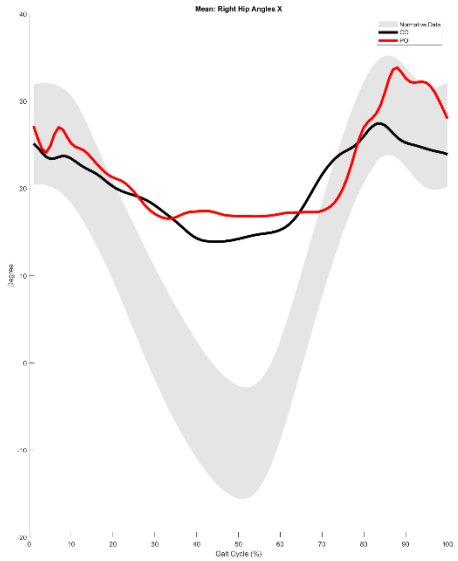

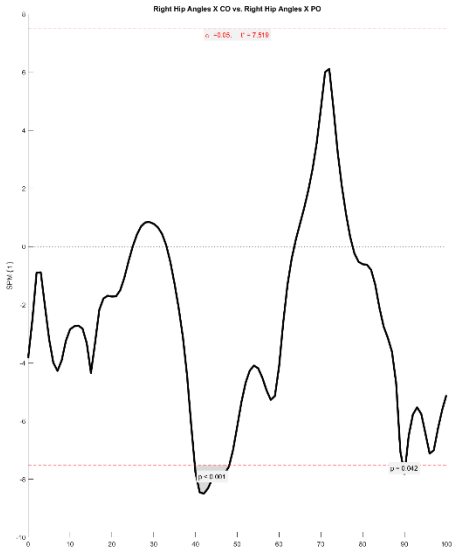

Right Hip Angles Y

18.3-24.9%, 58.1-62.2%, 67.4-72.2%, 79.8-87.7%

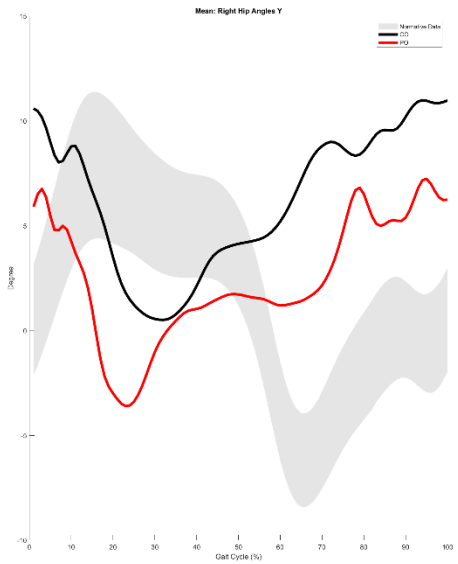

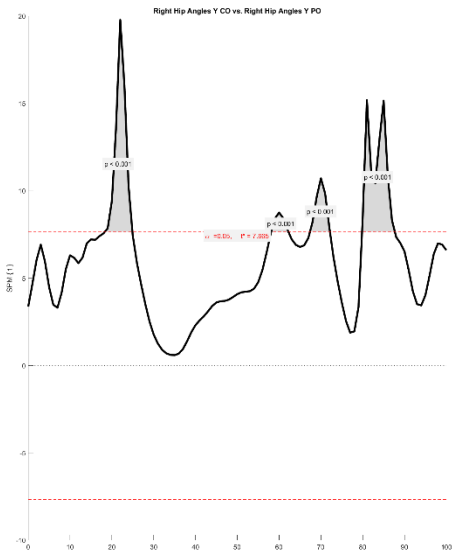

Right Hip Angles Z

0.0-8.4%, 11.5-27.2%, 29.7-89.5%, 92.2-94.7%, 95.2-100.0%

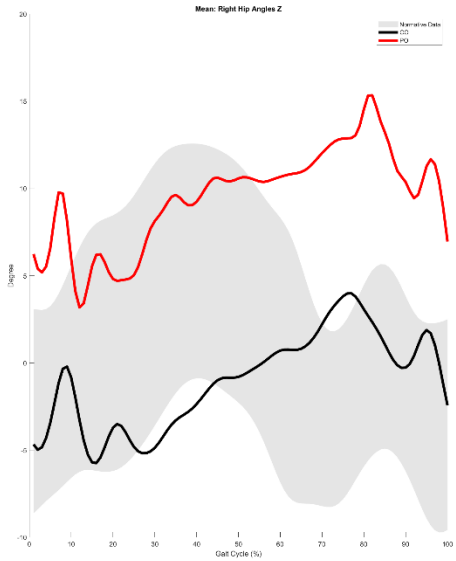

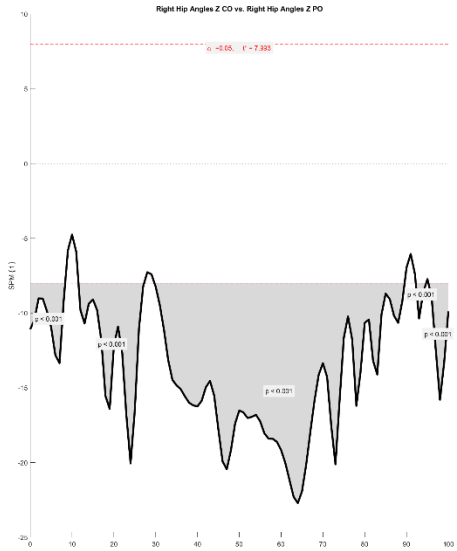

Left Hip Angles X

35.7-54.3%, 82.5-84.3%

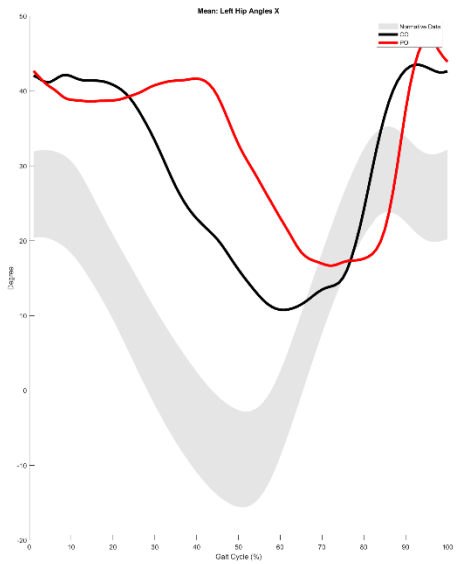

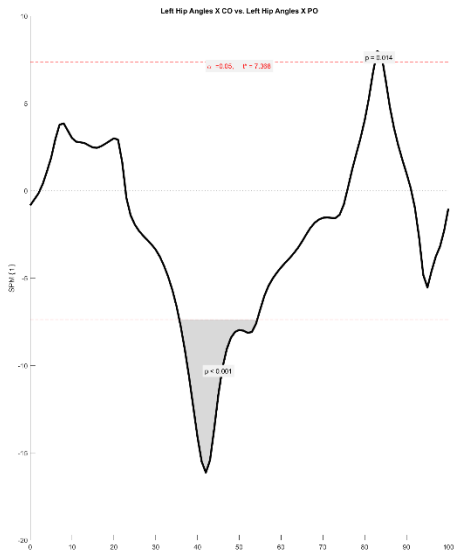

Left Hip Angles Y

29.3-38.6%, 61.3-65.2%, 92.8-96.3%

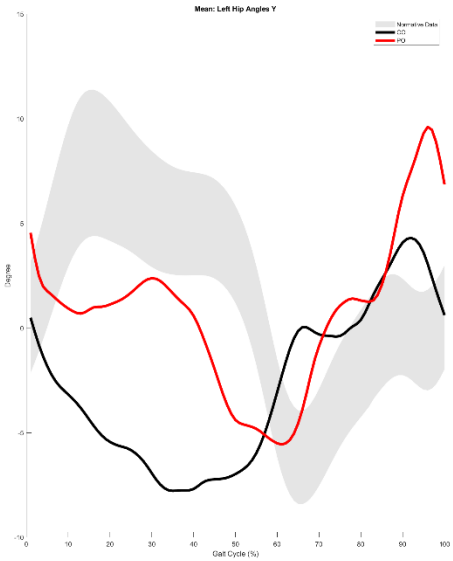

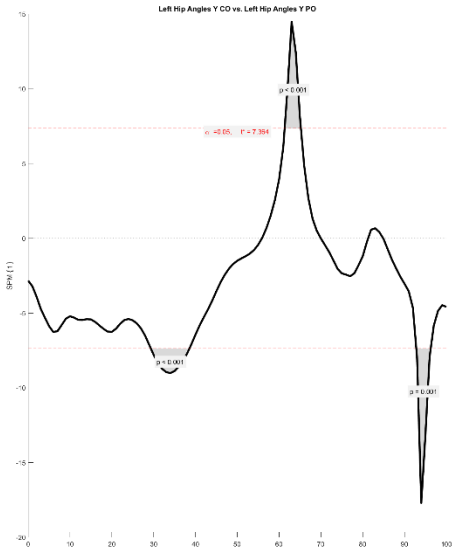

Left Hip Angles Z

36.1-40.5%, 56.4-59.3%, 63.9-65.7%, 93.7-94.5%

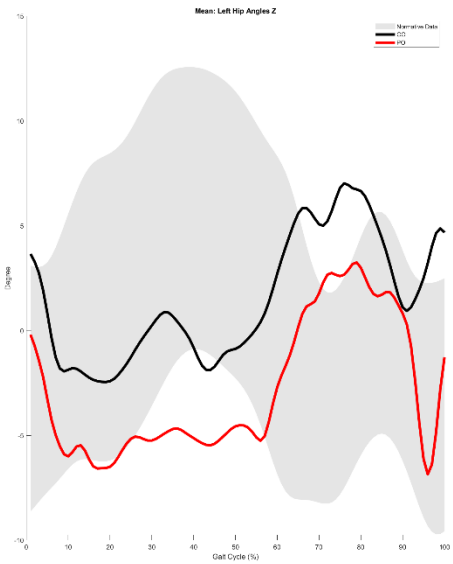

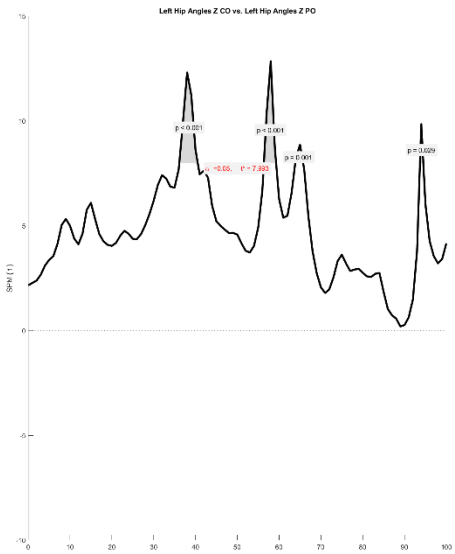

Right Knee Angles X

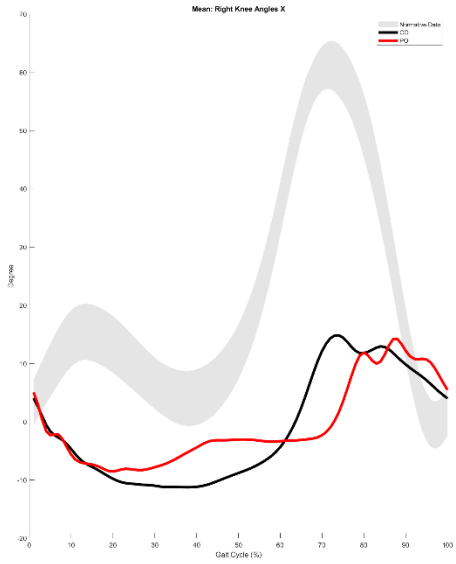

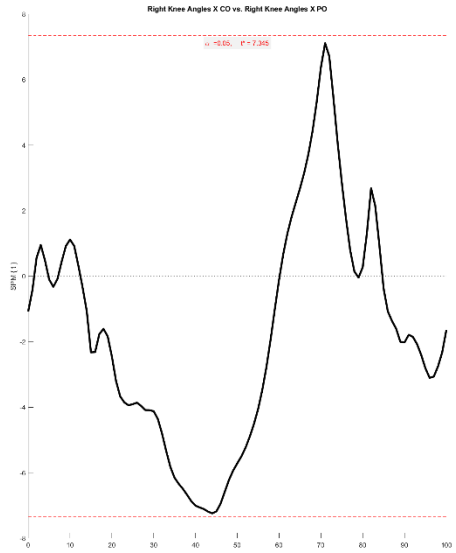

Right Knee Angles Y

68.6-74.6%, 78.1-80.8%, 81.7-94.9%, 96.7-97.3%

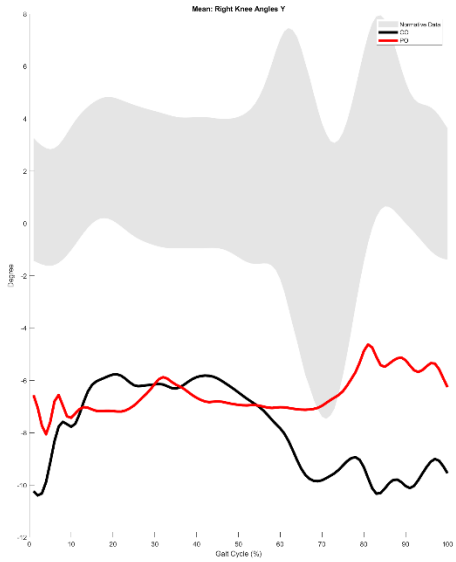

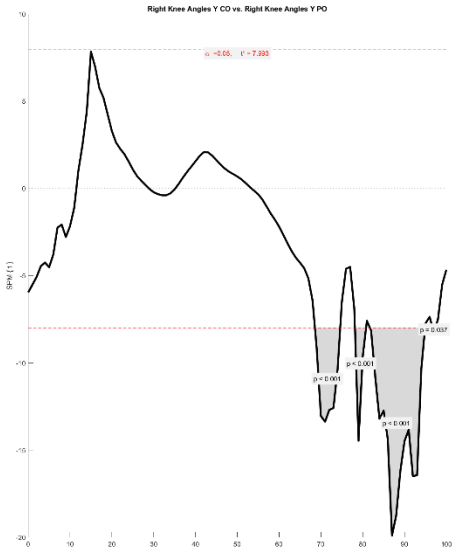

Right Knee Angles Z

0.0-6.9%, 12.9-22.6%, 24.2-34.5%, 47.5-71.8%, 75.3-86.7%, 92.3-100.0%

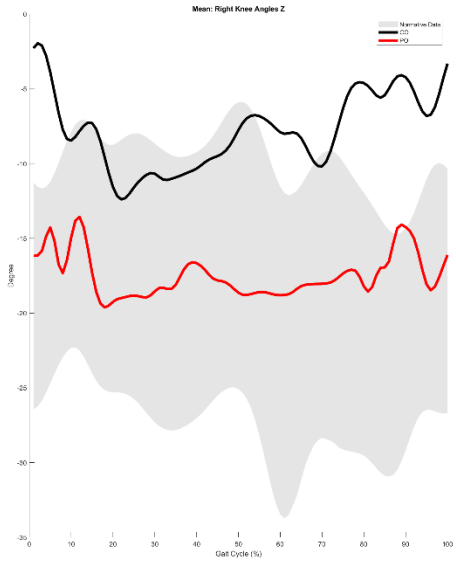

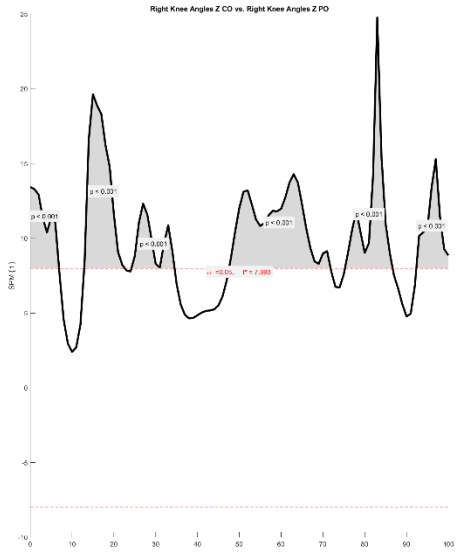

Left Knee Angles X

6.8-9.1%, 20.9-22.9%, 37.0-42.5%, 80.4-83.9%

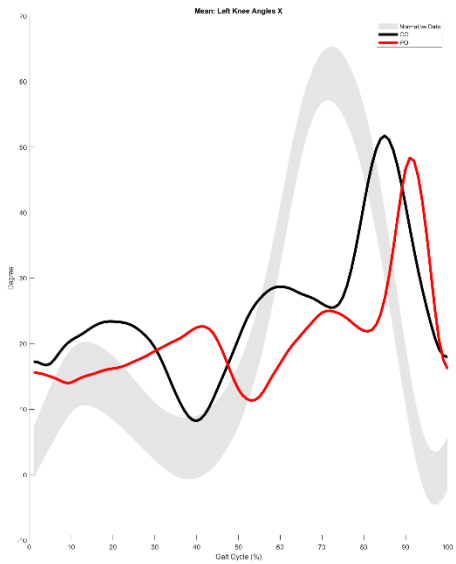

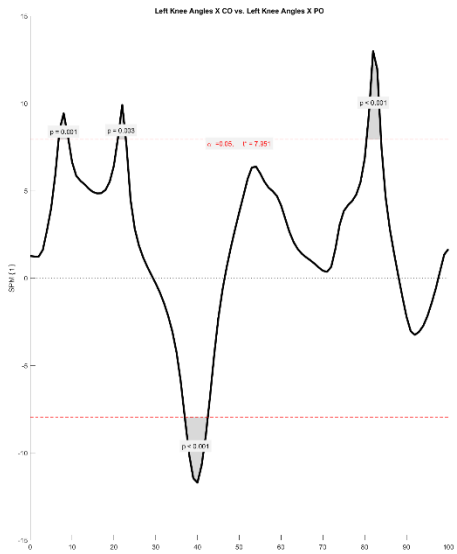

Left Knee Angles Y

19.9-20.0%, 29.0-31.5%, 52.5-61.6%, 83.9-84.1%, 93.4-95.3%

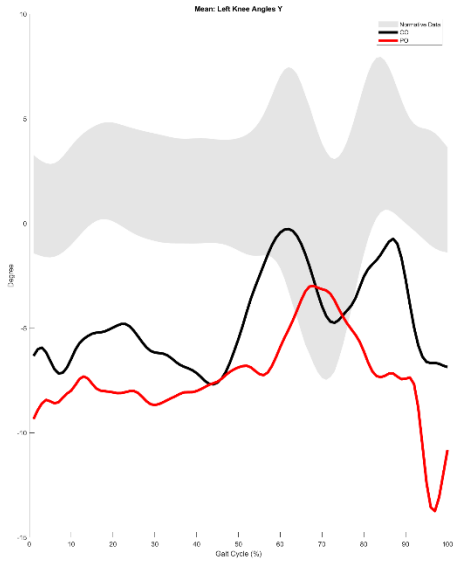

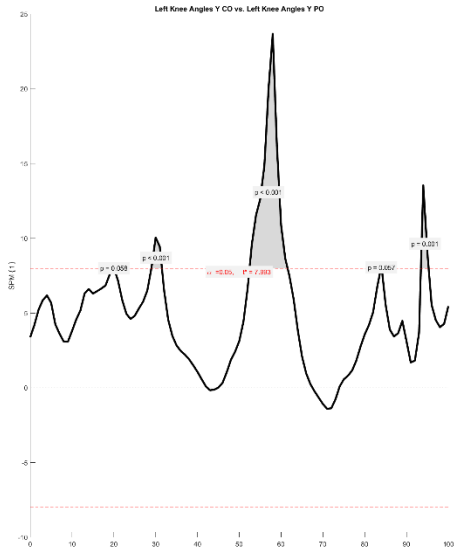

Left Knee Angles Z

0.0-89.6%, 93.8-100.0%

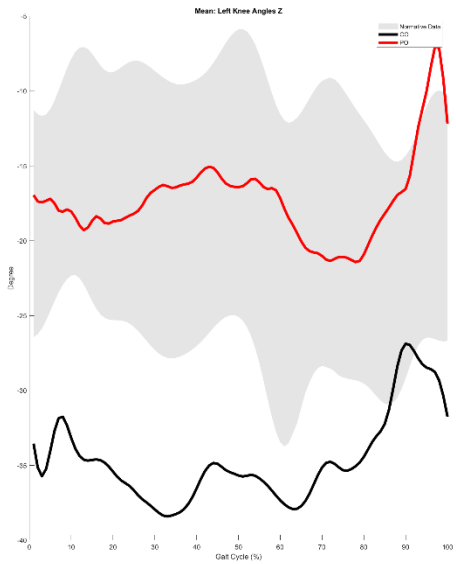

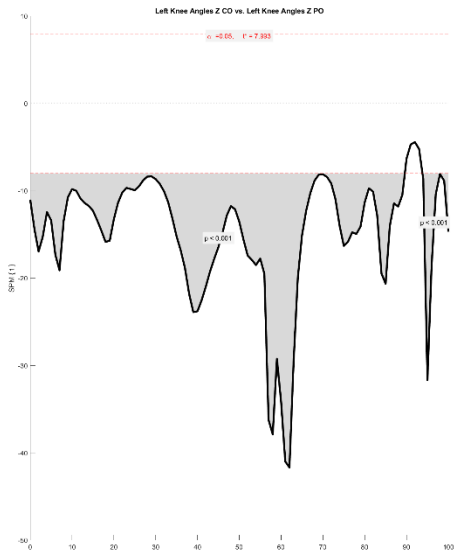

Right Ankle Angles X

5.8-73.6%, 85.7-86.7%, 99.2-100.0%

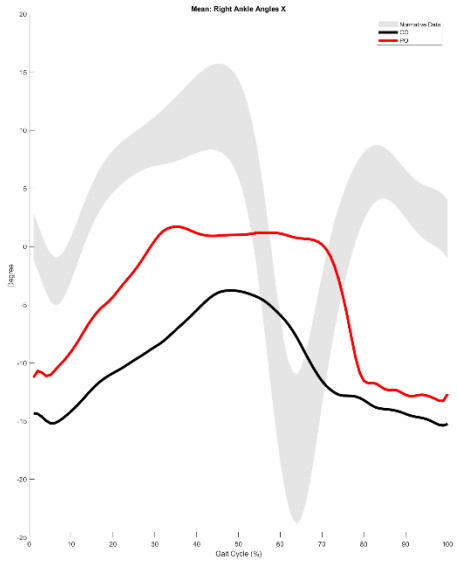

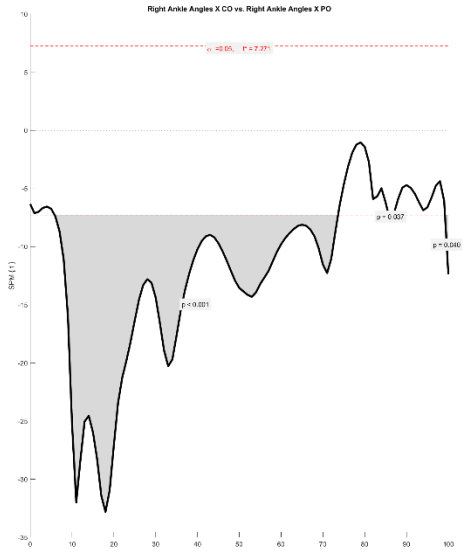

Right Ankle Angles Y

8.9-29.1%, 31.2-44.5%, 72.0-77.6%

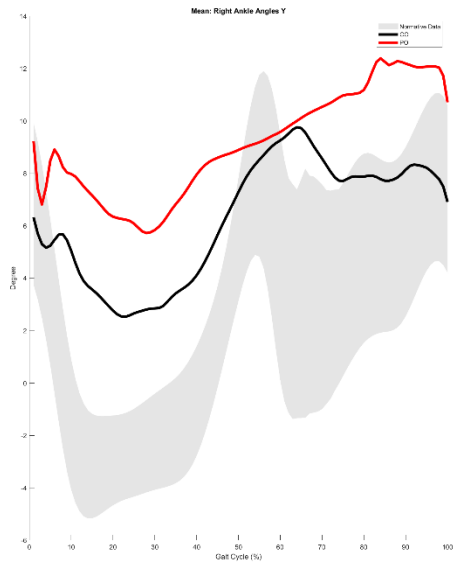

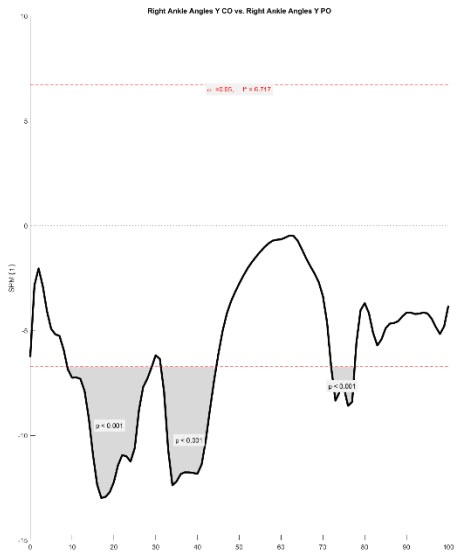

Left Ankle Angles X

13.2-16.9%, 18.2-25.2%, 48.8-62.7%, 80.6-82.6%

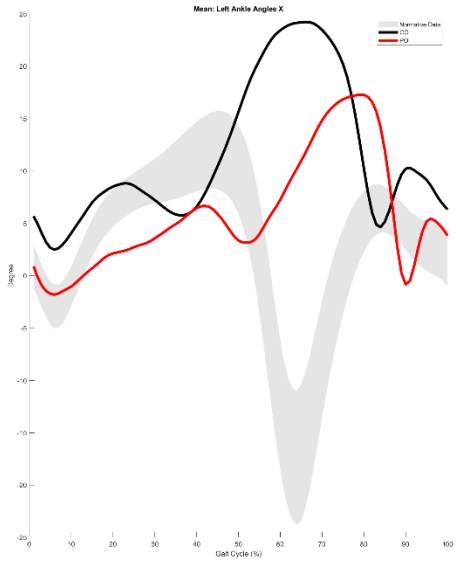

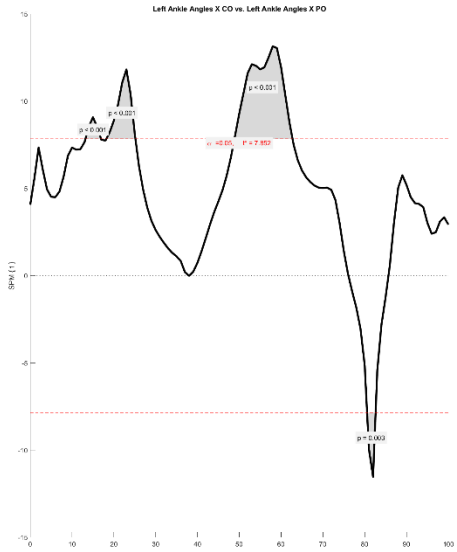

Left Ankle Angles Y

0.0-0.8%, 11.9-86.8%, 89.5-97.9%

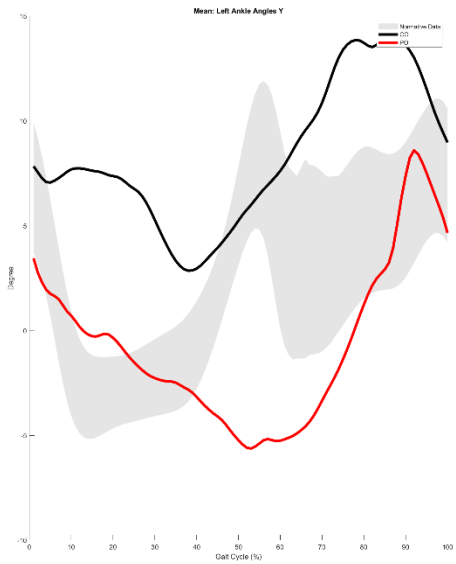

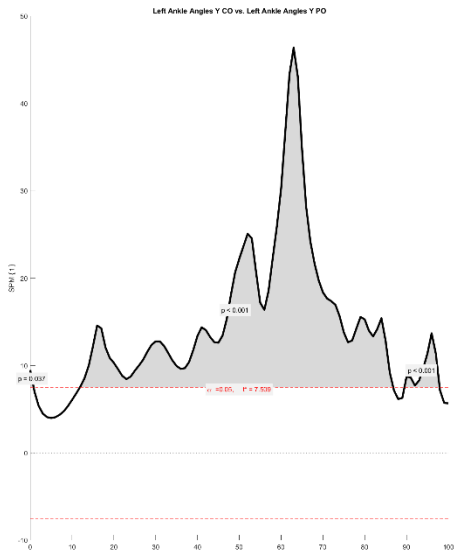

Right Foot Pitch Angles X

0.0-2.5%, 68.1-73.8%

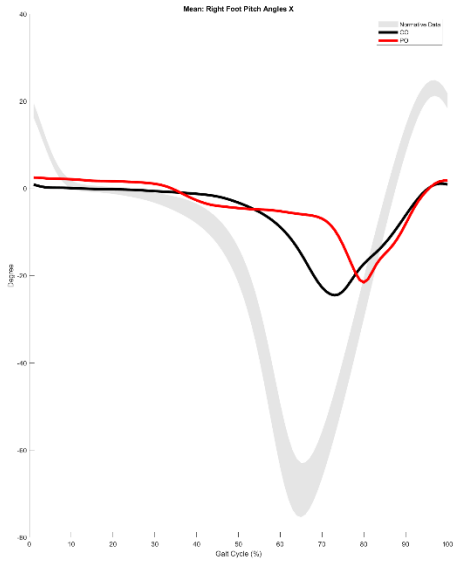

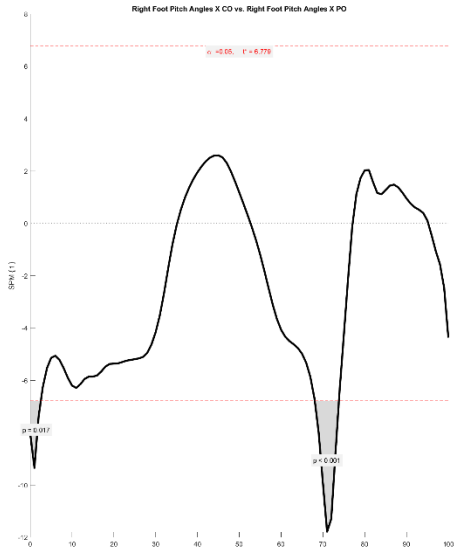

Left Foot Pitch Angles X

0.9-69.9%, 80.5-81.9%, 87.8-91.4%, 99.3-100.0%

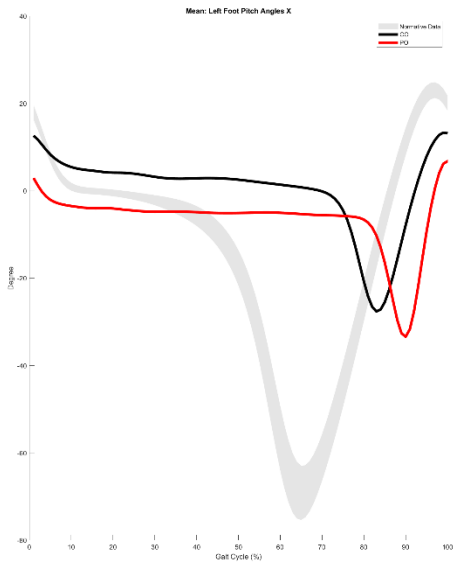

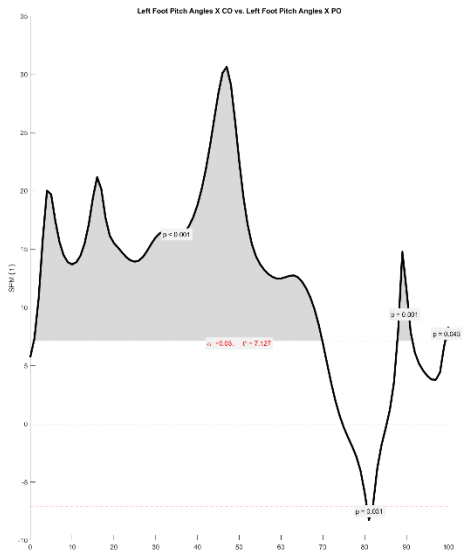

Right Foot Progression Z

81.3-86.0%

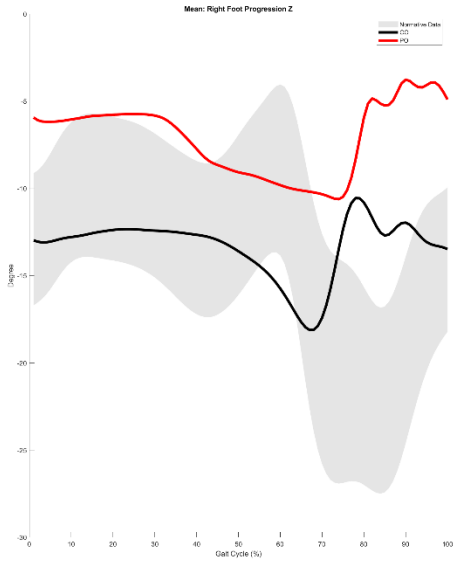

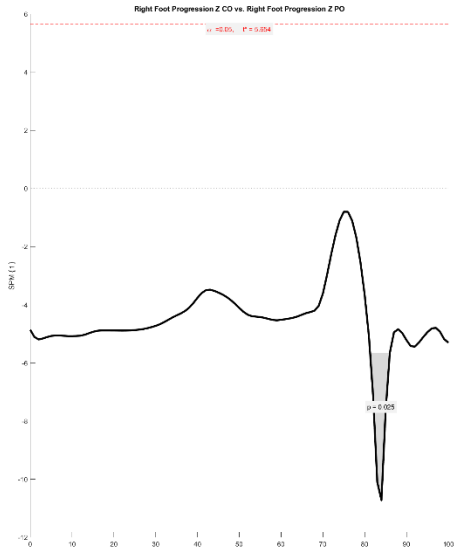

Left Foot Progression Z

2.4-75.9%, 80.5-81.7%

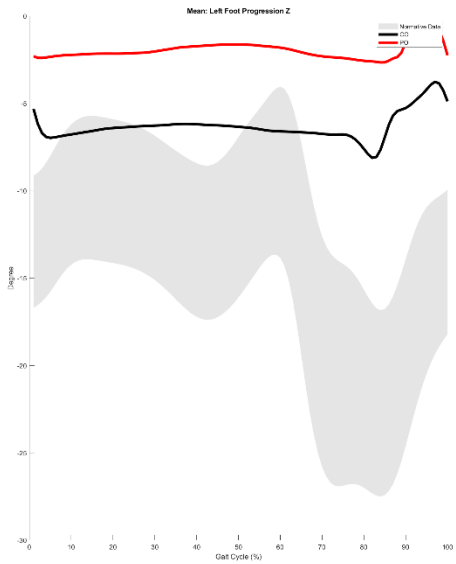

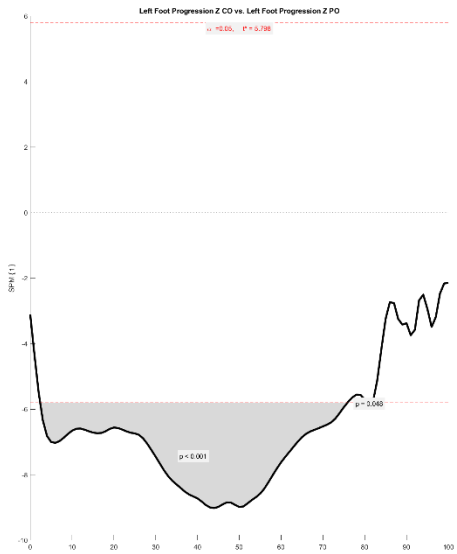

Right Hip Moment X

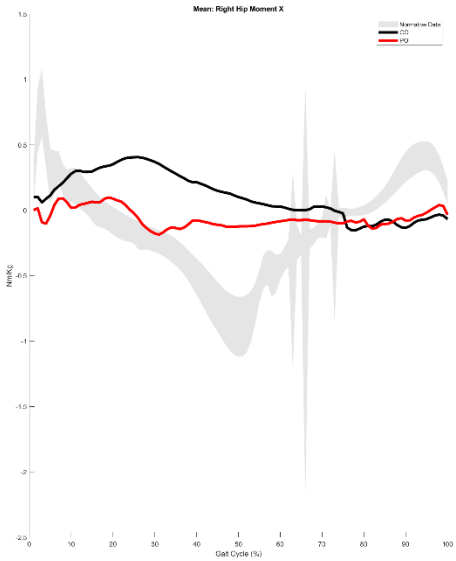

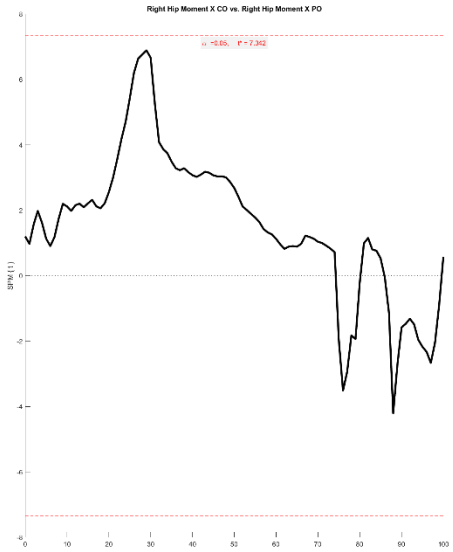

Right Hip Moment Y

67.4-72.9%

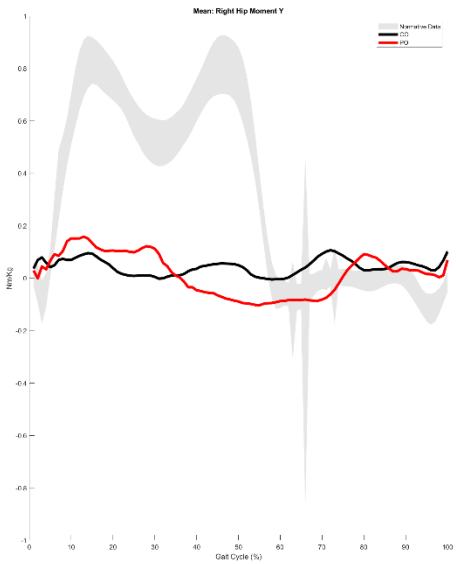

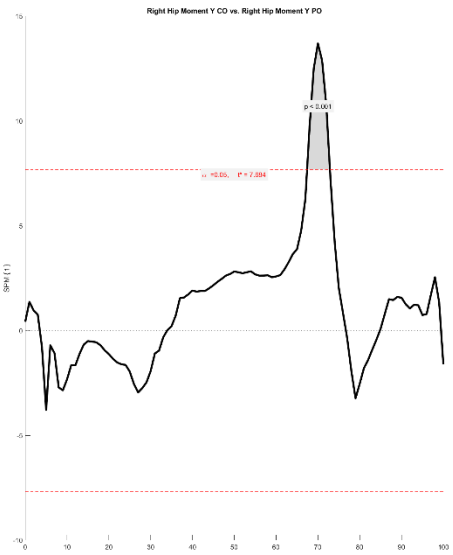

Left Hip Moment X

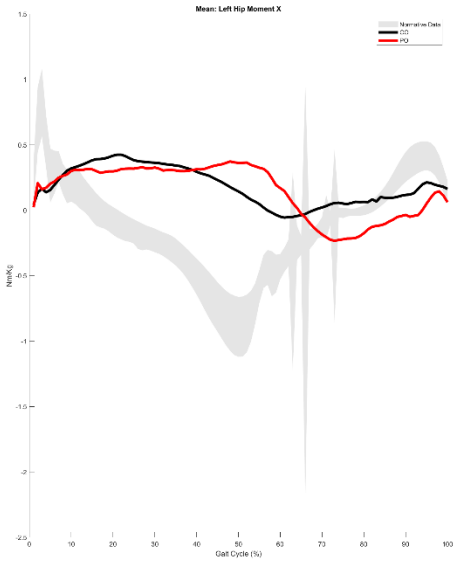

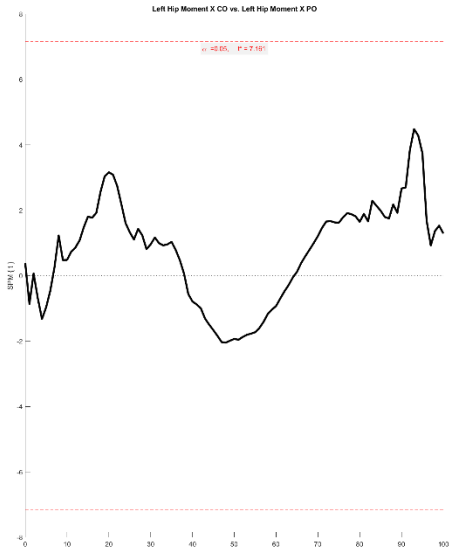

Left Hip Moment Y

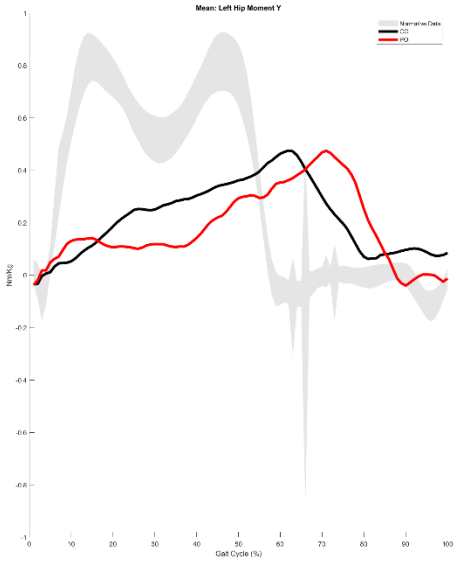

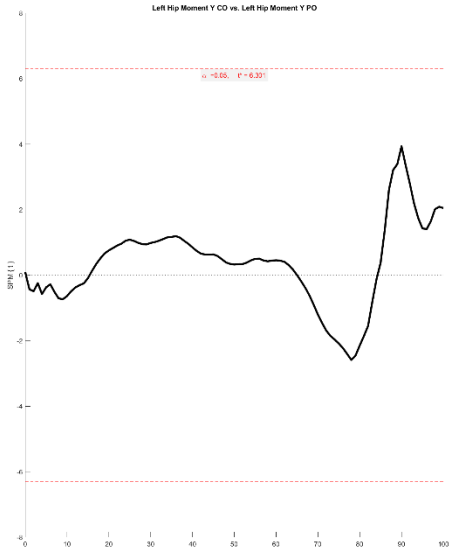

Right Knee Moment X

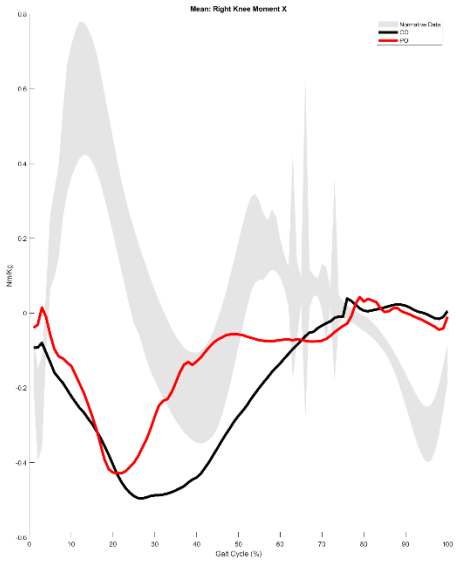

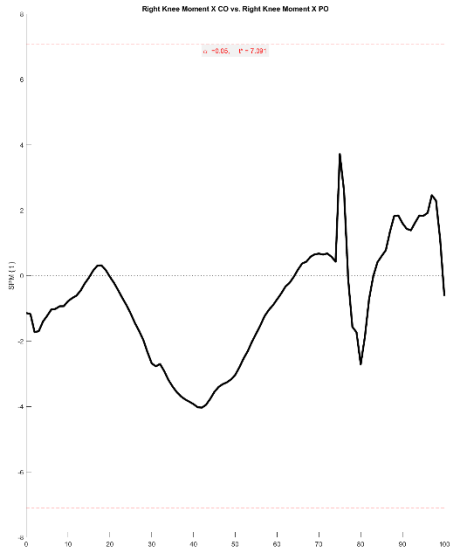

Right Knee Moment Y

66.2-73.1%

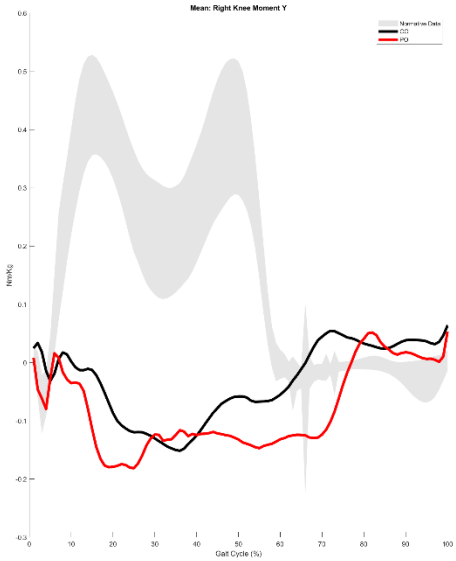

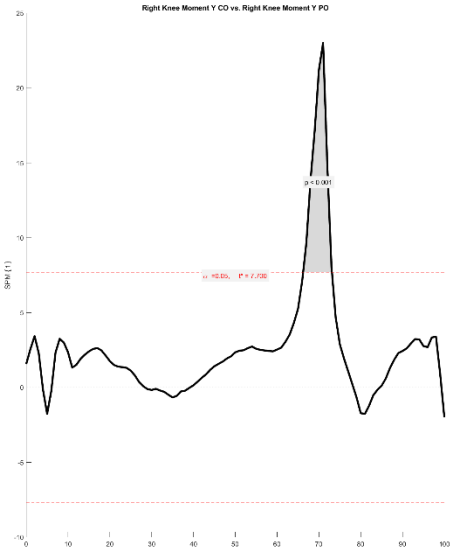

Left Knee Moment X

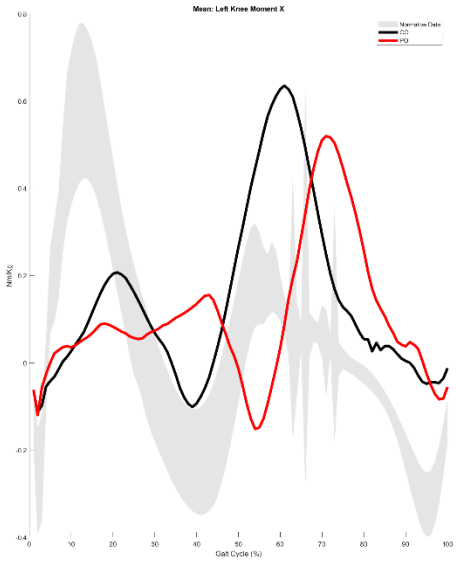

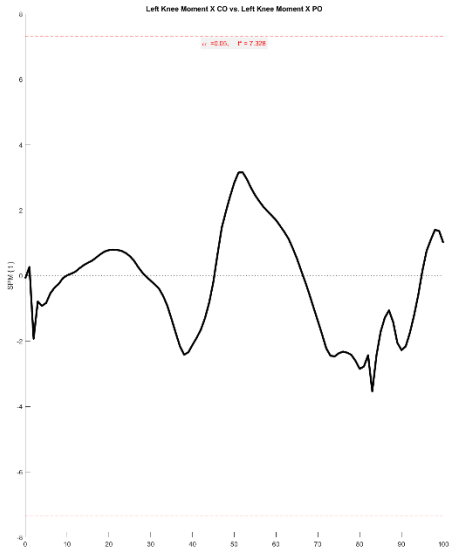

Left Knee Moment Y

83.4-87.5%

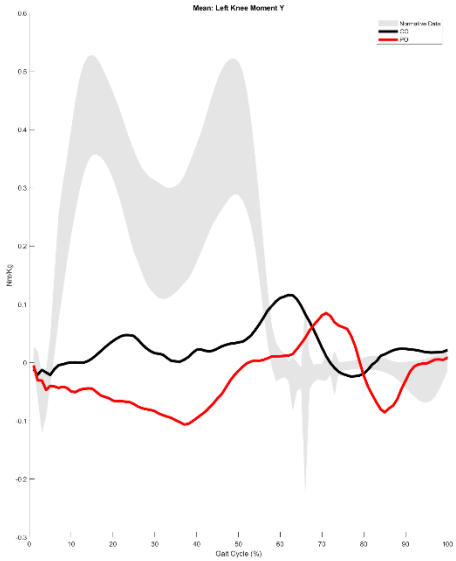

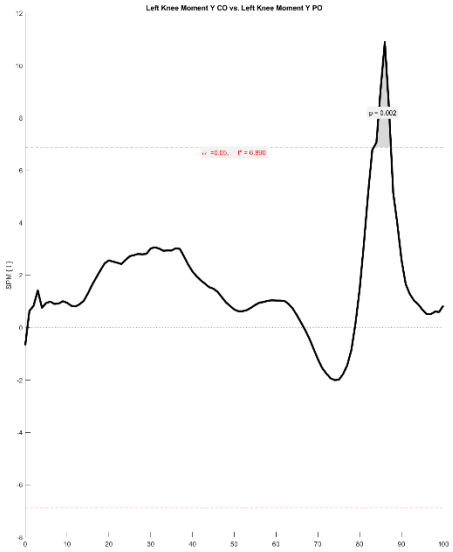

Right Ankle Moment X

67.8-70.4%

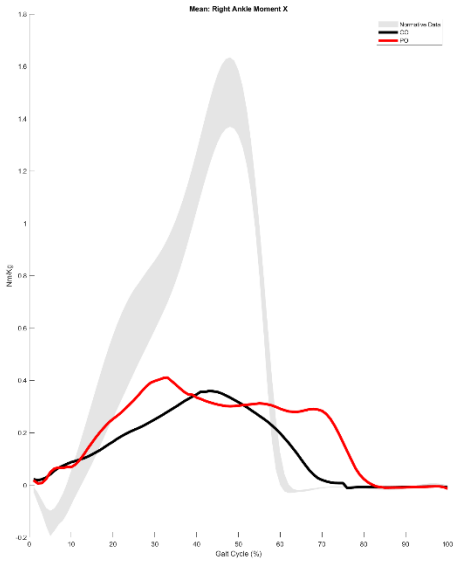

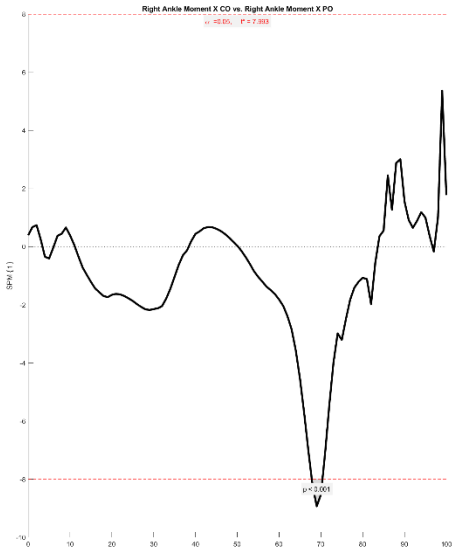

Right Ankle Moment Y

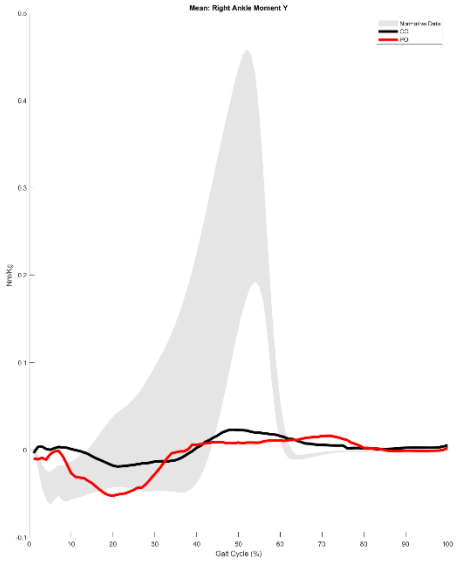

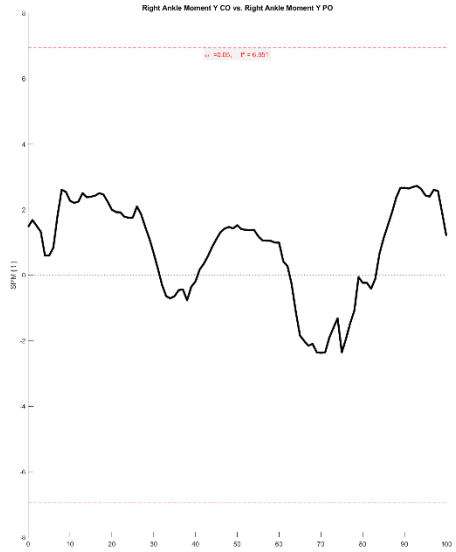

Left Ankle Moment X

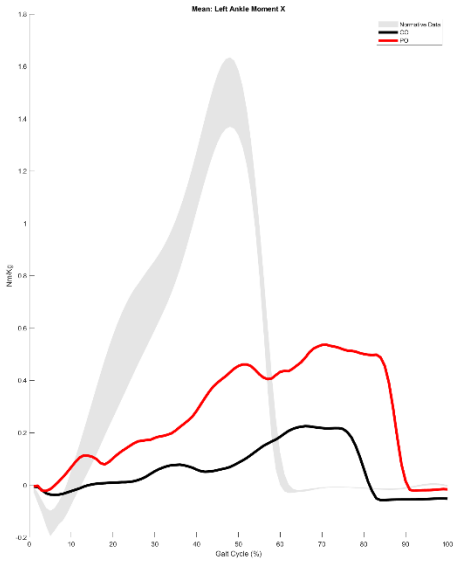

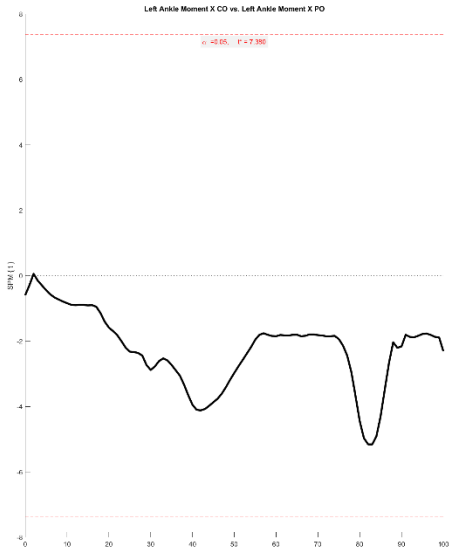

Left Ankle Moment Y

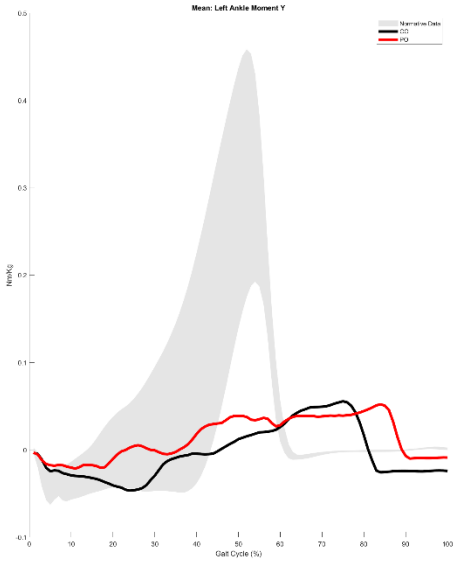

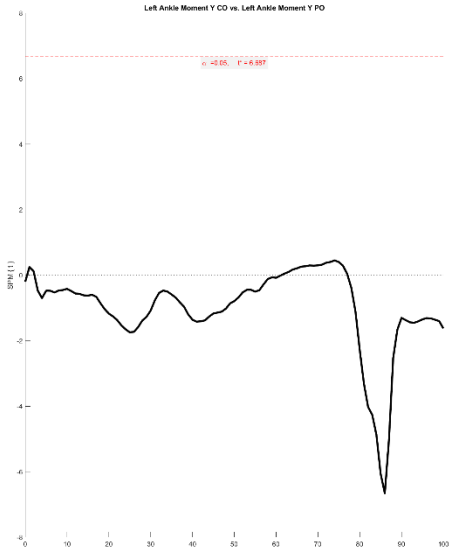

PO

Step Length

REP	Left	Right	IS (50%)	IS (0%)
1	0.18847	0.34753	64.8377	59.3507
2	0.17991	0.32037	64.0381	56.1526
3	0.16919	0.3153	65.0787	60.315
4	0.16705	0.2889	63.3622	53.4488
5	0.16074	0.27091	62.7615	51.046
6	0.15934	0.25077	61.147	44.588
Mean	0.170783	0.2989633	63.5375	54.1502
SD	0.010363	0.0323901	1.33316	5.33264

CO

Step Length

REP	Left	Right	IS (50%)	IS (0%)
1	0.24672	0.33783	57.7932	31.1727
2	0.2434	0.33282	57.7592	31.0368
3	0.23154	0.31685	57.7782	31.1129
4	0.22585	0.30573	57.5135	30.0538
5	0.22385	0.30188	57.4211	29.6844
6	0.20896	0.29475	58.5158	34.0633
Mean	0.2300533	0.3149767	57.7968	31.1873
SD	0.0126438	0.0158656	0.35123	1.40493

PO

Swing Time

REP	Left	Right	IS (50%)	IS (0%)
1	0.375	0.65833	63.7096	54.8382
2	0.35	0.61667	63.7932	55.1729
3	0.35	0.59167	62.832	51.328
4	0.34167	0.575	62.727	50.9082
5	0.33333	0.54167	61.9051	47.6206
6	0.33333	0.5	60.0002	40.001
Média	0.347222	0.5805567	62.4945	49.9781
DP	0.014165	0.0508409	1.2845	5.13802

CO

Swing Time

REP	Left	Right	IS (50%)	IS (0%)
1	0.45833	0.65833	58.9553	35.8211
2	0.41667	0.65	60.9373	43.7492
3	0.39167	0.625	61.4752	45.9008
4	0.35833	0.61667	63.2482	52.9928
5	0.35	0.59167	62.832	51.328
6	0.34167	0.55833	62.0367	48.1467
Mean	0.3861117	0.6166667	61.5808	46.3231
SD	0.0412939	0.0340206	1.40666	5.62663

PO

Stance Time

REP	Left	Right	IS (50%)	IS (0%)
1	2.69167	2.425	47.3941	10.4236
2	2.5	2.14167	46.1401	15.4397
3	2.40833	2.075	46.2826	14.8698
4	2.375	2.05	46.3277	14.6893
5	2.375	1.99167	45.6107	17.5571
6	2.36667	1.99167	45.6979	17.2084
Mean	2.452778	2.1125017	46.2422	15.0313
SD	0.116038	0.1488956	0.58328	2.33311

CO

Stance Time

REP	Left	Right	IS (50%)	IS (0%)
1	1.73333	1.475	45.9741	16.1037
2	1.71667	1.33333	43.7157	25.137
3	1.66667	1.31667	44.1341	23.4636
4	1.6	1.26667	44.1861	23.2556
5	1.575	1.225	43.75	25
6	1.55833	1.21667	43.844	24.6241
Mean	1.6416667	1.3055567	44.2673	22.9307
SD	0.0680421	0.0870903	0.78405	3.13622

	Left	Right
Step Length PO	0.17	0.30
Step Length CO	0.23	0.31
Swing Time PO	0.35	0.58
Swing Time CO	0.39	0.62
Stance Time PO	2.45	2.11
Stance Time CO	1.64	1.31

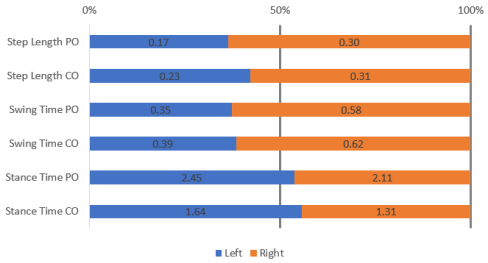

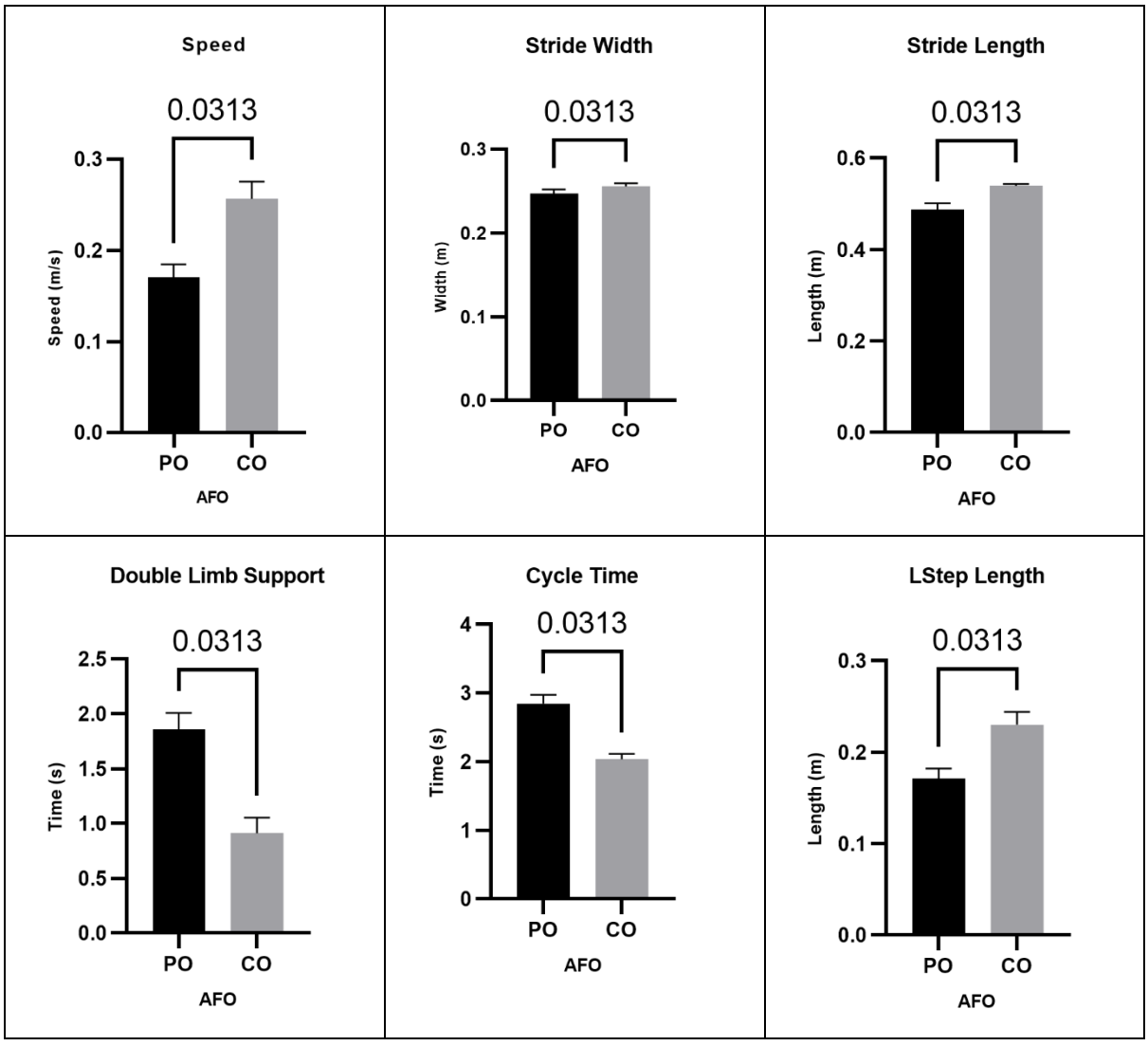

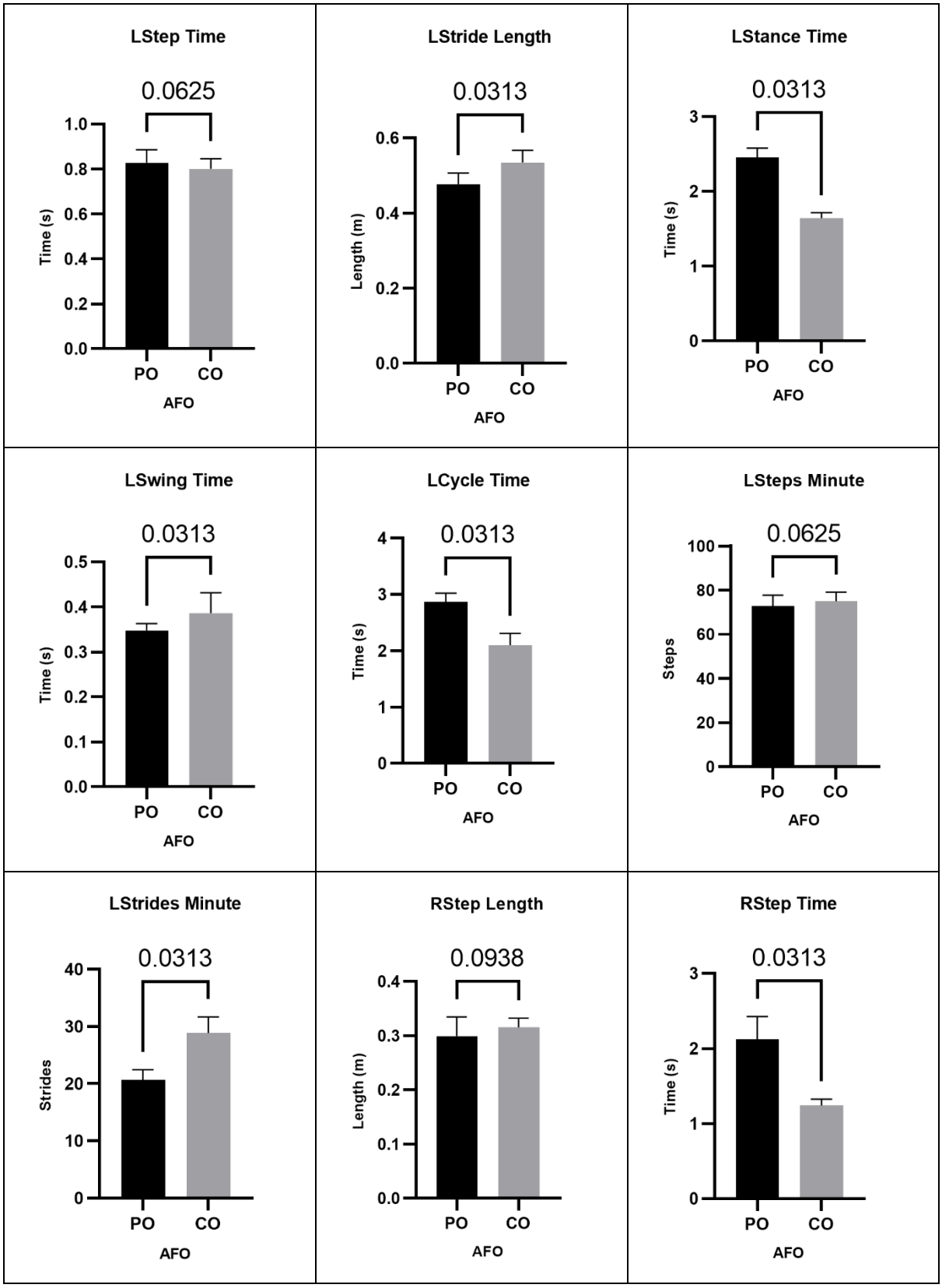
LStep Time
0.0625
Time (s)
1.0
0.8
0.6
0.4
0.2
0.0
PO
CO
AFO
LStride Length
0.0313
Length (m)
0.6
0.4
0.2
0.0
PO
CO
AFO
LStance Time
0.0313
Time (s)
3
2
1
0
PO
CO
AFO
LSwing Time
0.0313
Time (s)
0.5
0.4
0.3
0.2
0.1
0.0
PO
CO
AFO
LCycle Time
0.0313
Time (s)
4
3
2
1
0
PO
CO
AFO
LSteps Minute
0.0625
Steps
100
80
60
40
20
0
PO
CO
AFO
LStrides Minute
0.0313
Strides
40
30
20
10
0
PO
CO
AFO
RStep Length
0.0938
Length (m)
0.4
0.3
0.2
0.1
0.0
PO
CO
AFO
RStep Time
0.0313
Time (s)
3
2
1
0
PO
CO
AFO

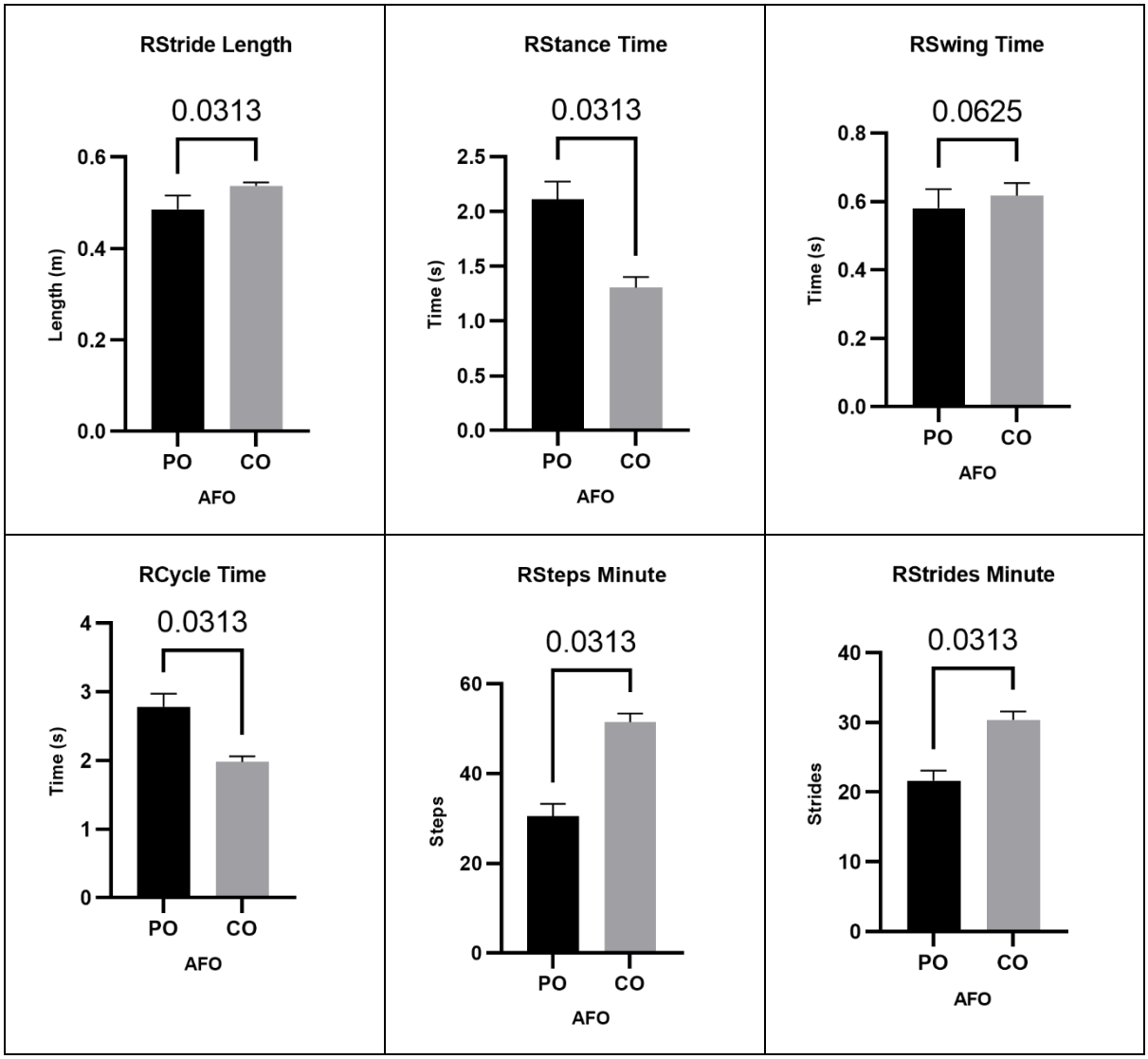
RStride Length
0.0313
Length (m)
0.6
0.4
0.2
0.0
PO
CO
AFO
RStance Time
0.0313
Time (s)
2.5
2.0
1.5
1.0
0.5
0.0
PO
CO
AFO
RSwing Time
0.0625
Time (s)
0.8
0.6
0.4
0.2
0.0
PO
CO
AFO
RCycle Time
0.0313
Time (s)
4
3
2
1
0
PO
CO
AFO
RSteps Minute
0.0313
Steps
60
40
20
0
PO
CO
AFO
RStrides Minute
0.0313
Strides
40
30
20
10
0
PO
CO
AFO

PATIENT 6

Right Pelvic Angles X

18.0-20.5%, 76.7-83.5%, 86.3-87.1%

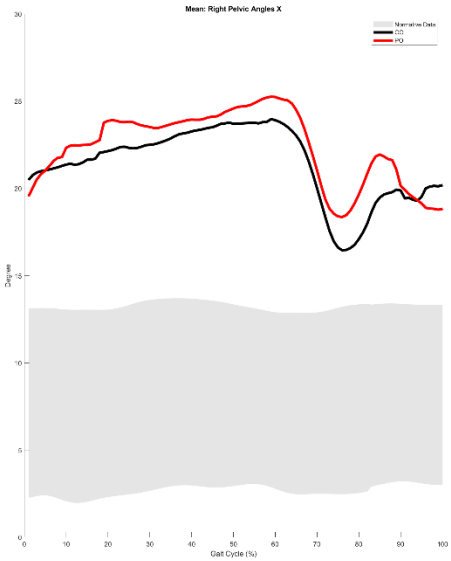

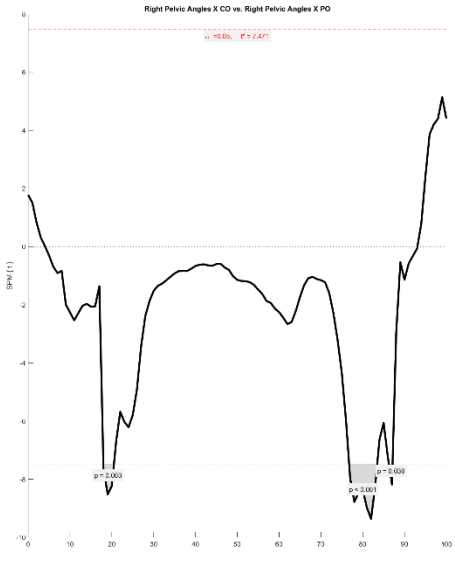

Right Pelvic Angles Y

2.5-32.9%, 56.5-87.7%

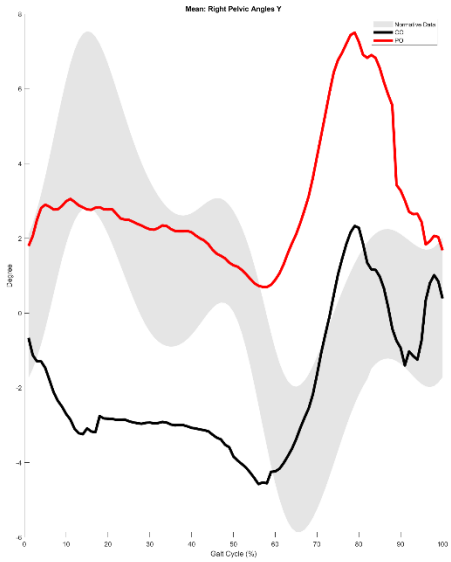

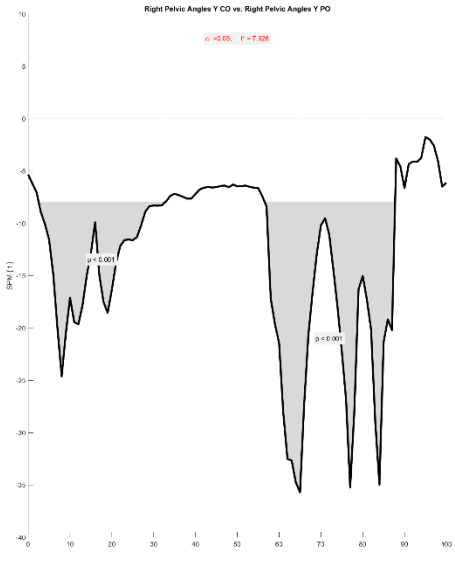

Right Pelvic Angles Z

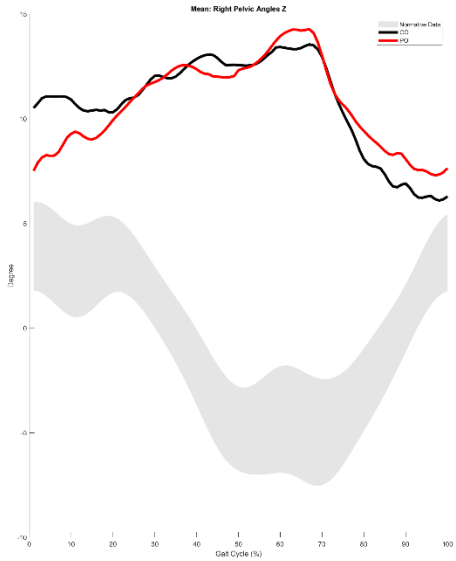

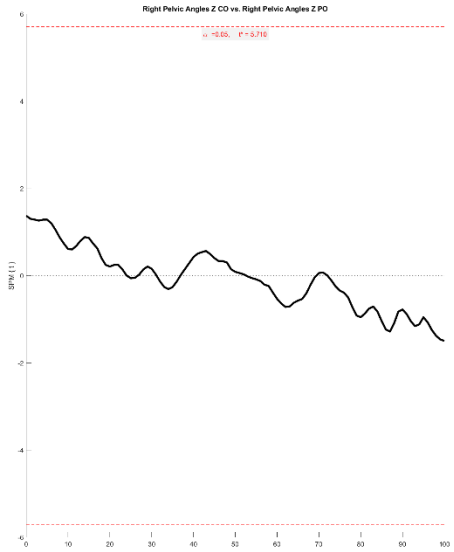

Left Pelvic Angles X

5.0-9.3%

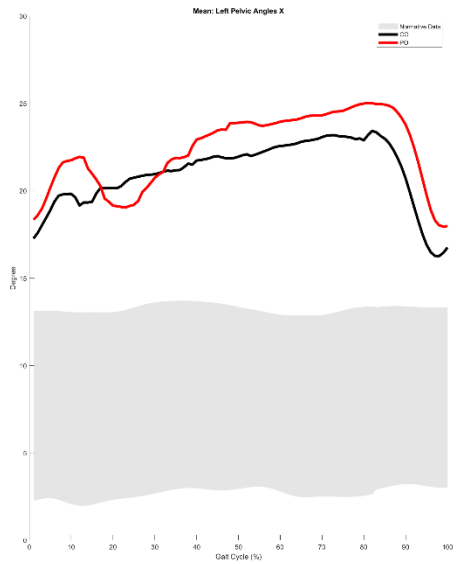

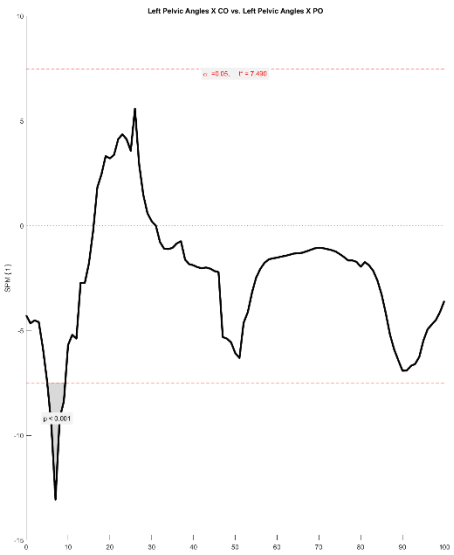

Left Pelvic Angles Y

0.0-12.4%, 28.1-100.0%

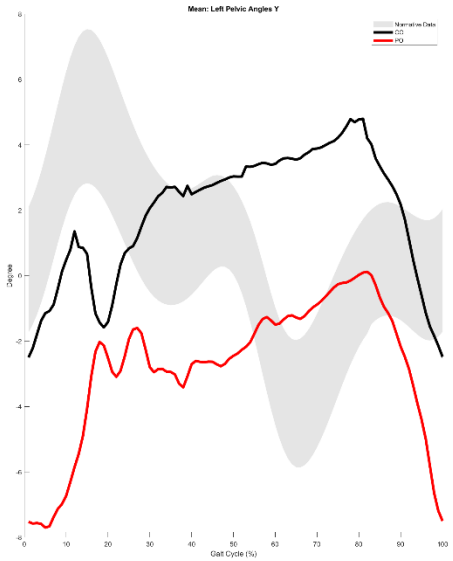

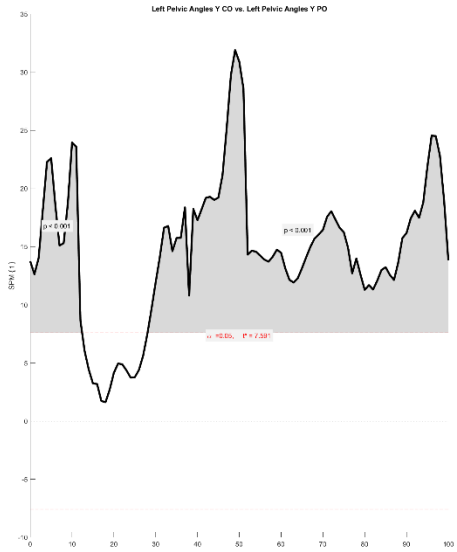

Left Pelvic Angles Z

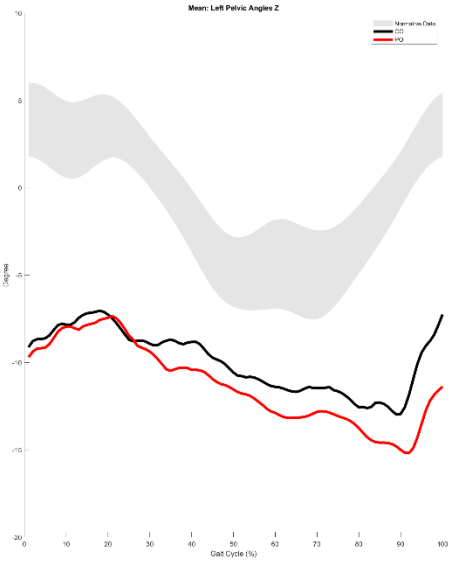

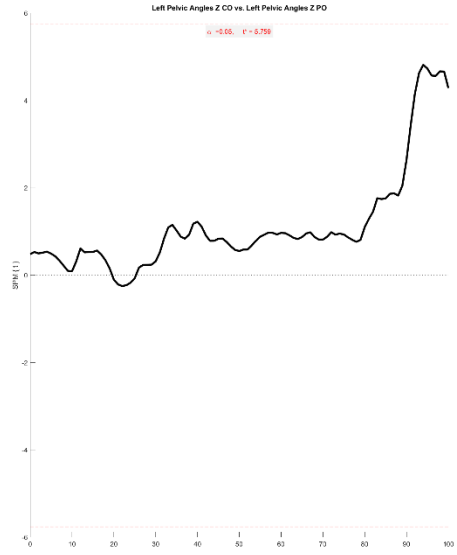

Right Hip Angles X

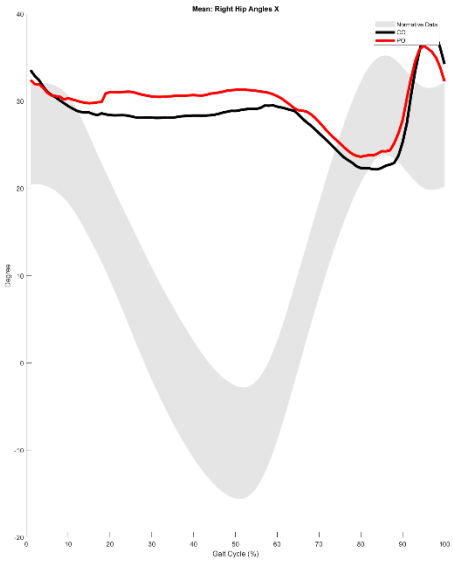

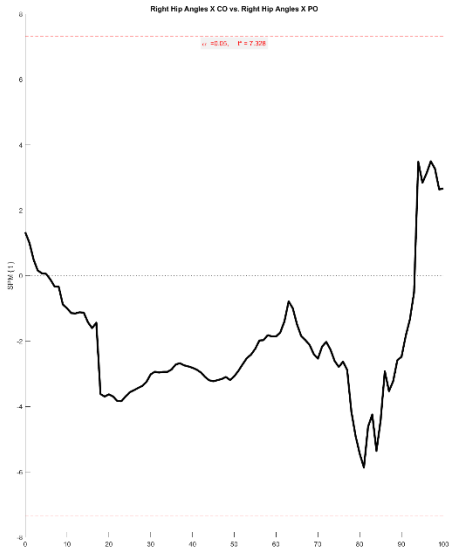

Right Hip Angles Y

9.5-15.2%, 16.6-18.9%, 29.9-30.1%, 71.4-85.8%

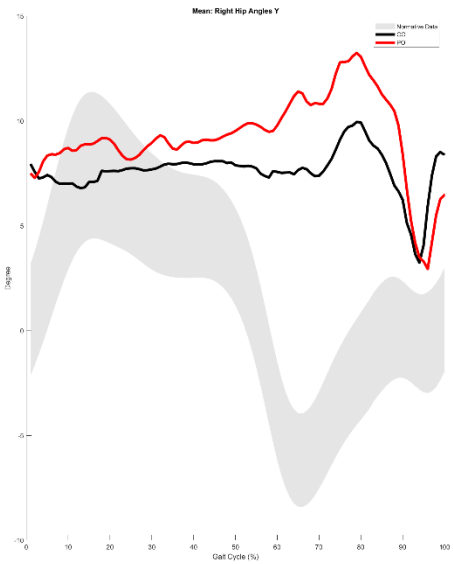

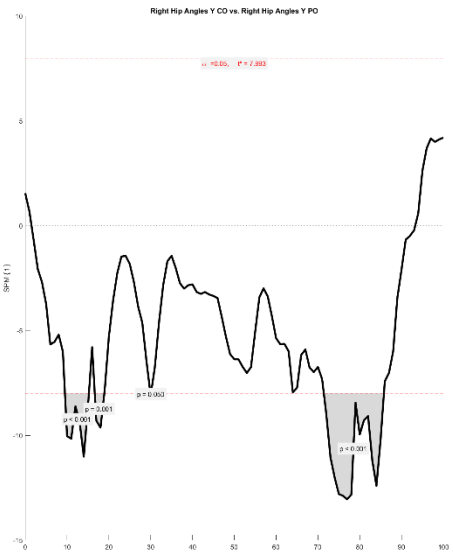

Right Hip Angles Z

39.4-42.6%, 47.7-48.2%, 68.5-70.9%, 72.3-81.6%, 86.8-89.2%, 96.7-97.3%

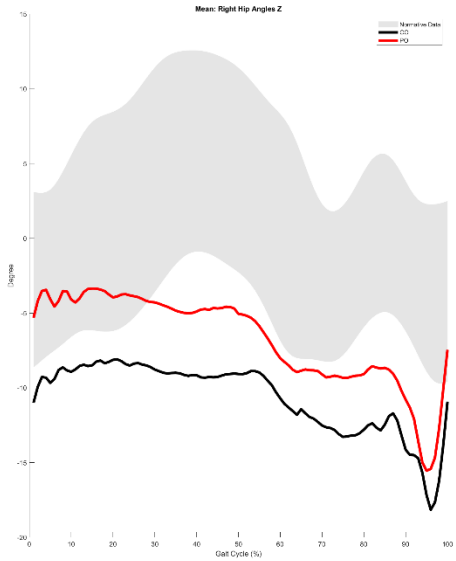

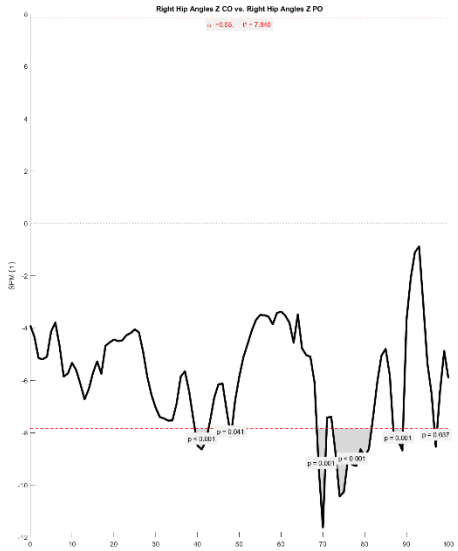

Left Hip Angles X

3.7-7.1%

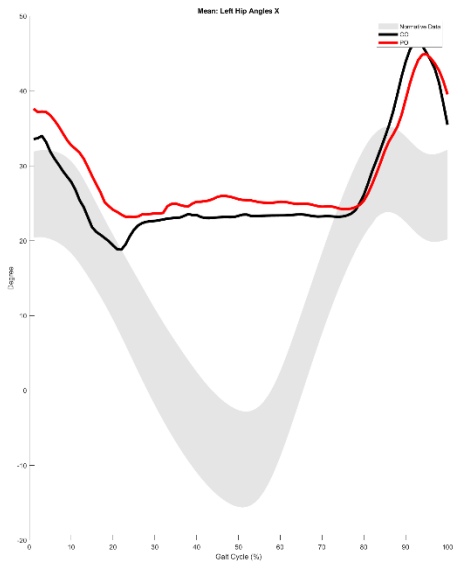

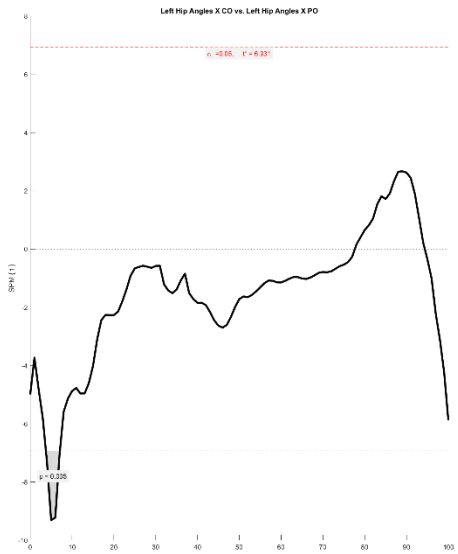

Left Hip Angles Y

0.0-12.8%, 15.2-16.8%, 38.3-97.4%, 99.4-100.0%

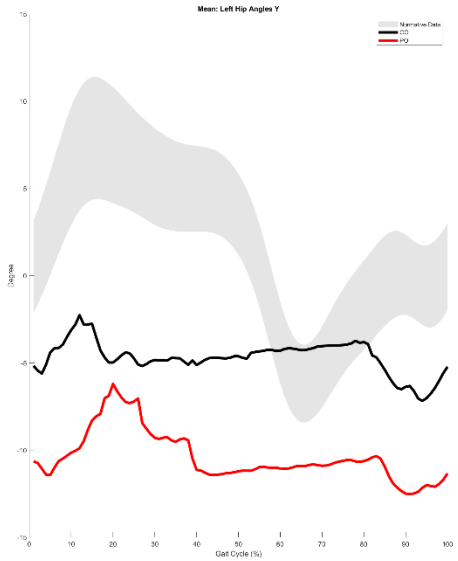

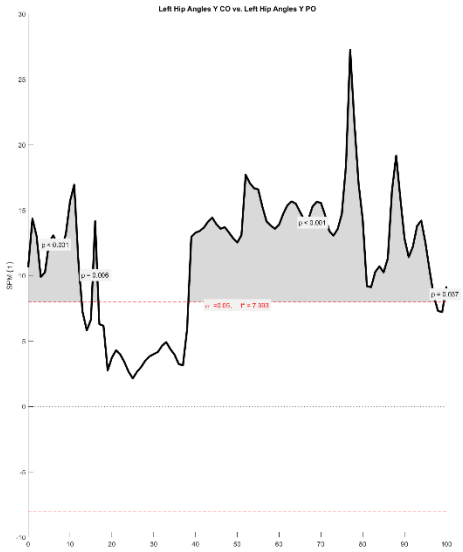

Left Hip Angles Z

3.9-4.1%, 17.0-17.1%, 51.2-53.7%

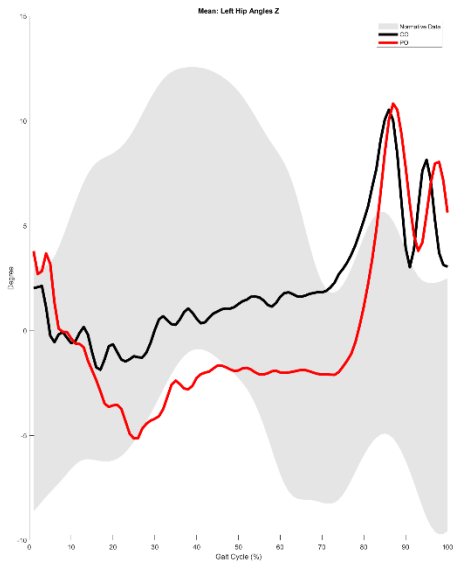

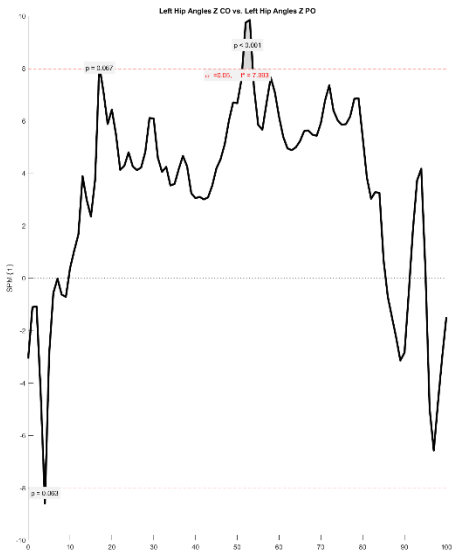

Right Knee Angles X

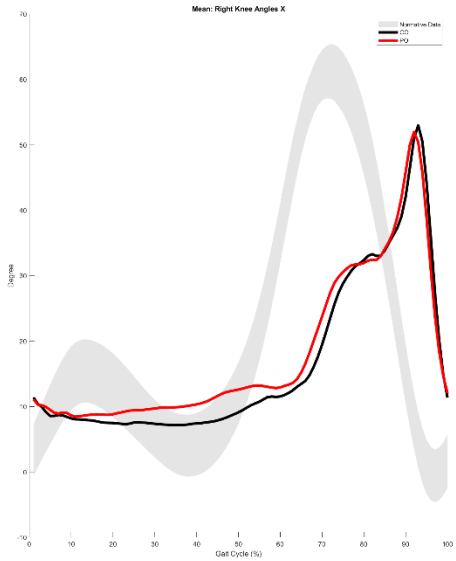

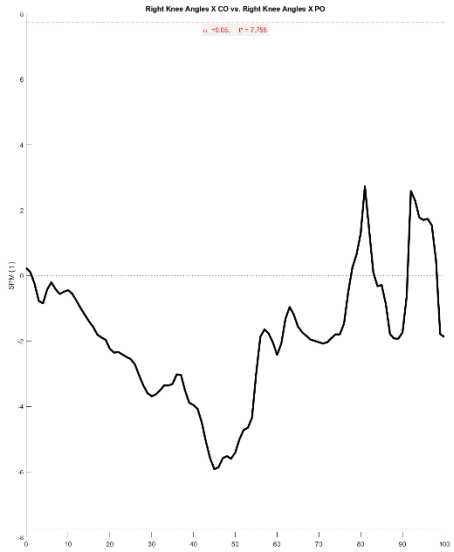

Right Knee Angles Y

0.0-4.4%, 8.5-11.5%, 14.1-60.7%, 95.3-100.0%

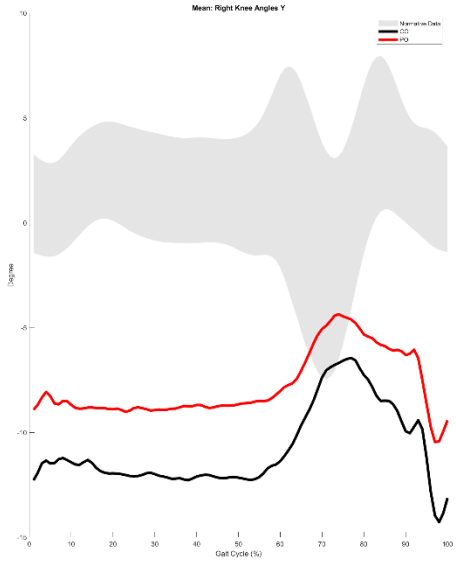

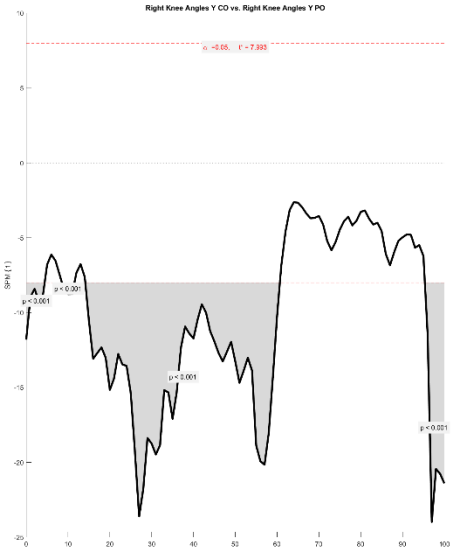

Right Knee Angles Z

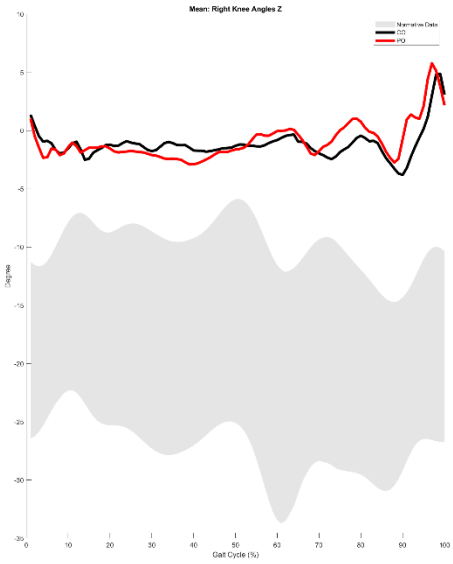

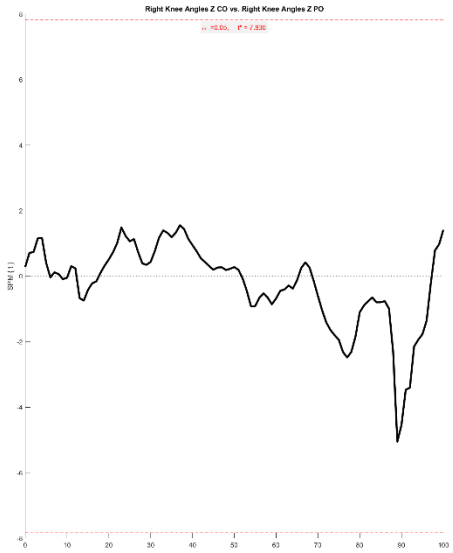

Left Knee Angles X

85.0-86.1%

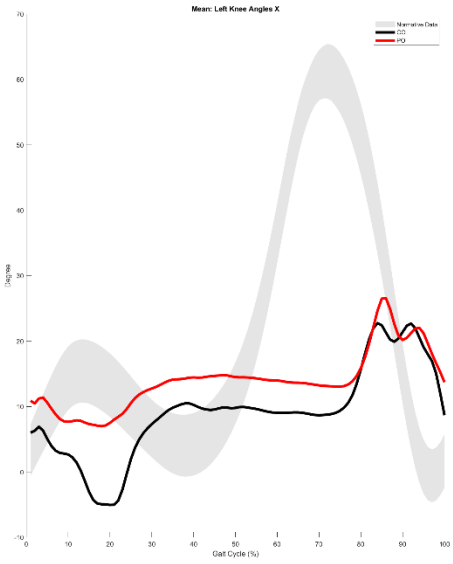

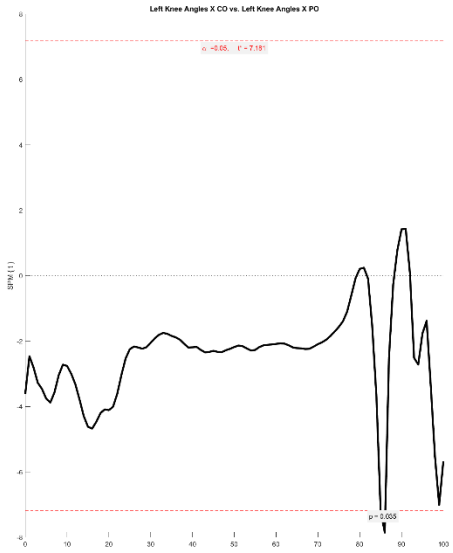

Left Knee Angles Y

16.8-18.7%, 84.4-85.5%

Left Knee Angles Z

0.0-4.8%, 6.1-23.4%, 25.2-32.8%, 37.1-58.7%, 60.5-64.2%, 65.1-79.4%, 82.4-86.0%, 87.9-91.8%, 93.5-100.0%

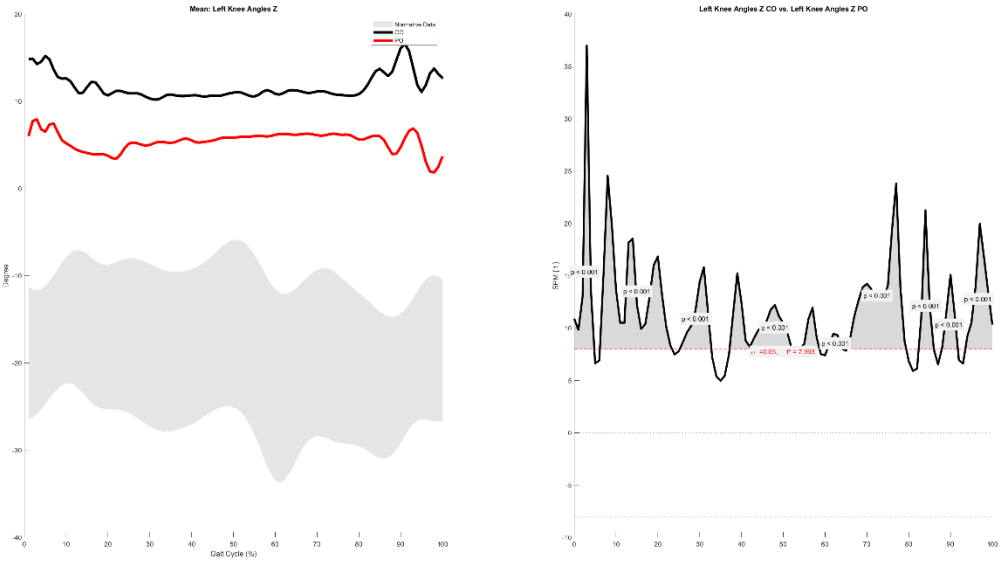

Right Ankle Angles X

0.7-64.0%, 70.2-86.0%, 94.4-100.0%

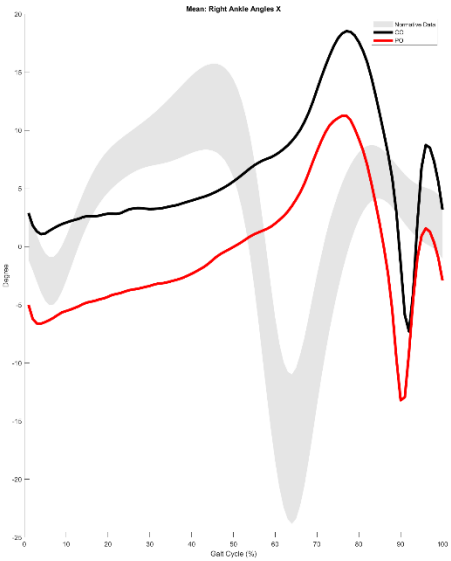

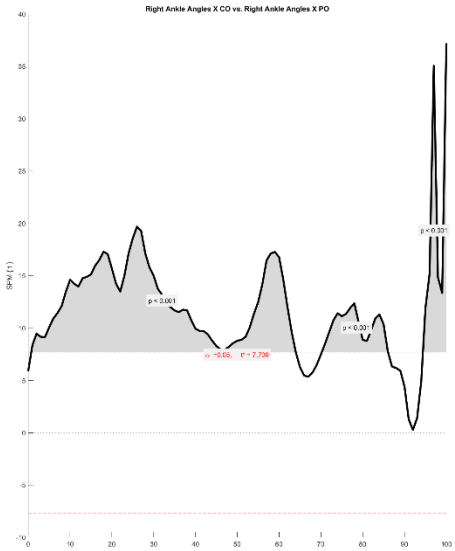

Right Ankle Angles Y

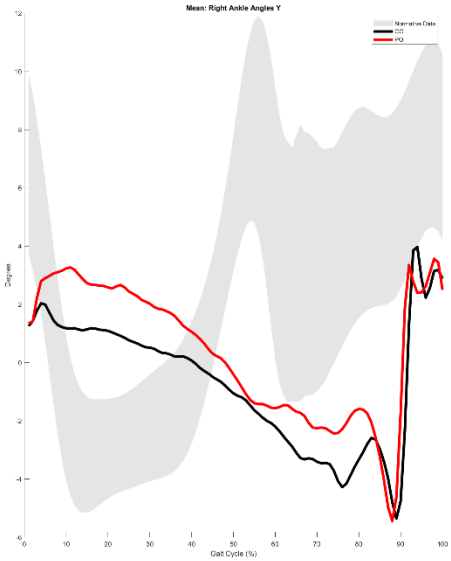

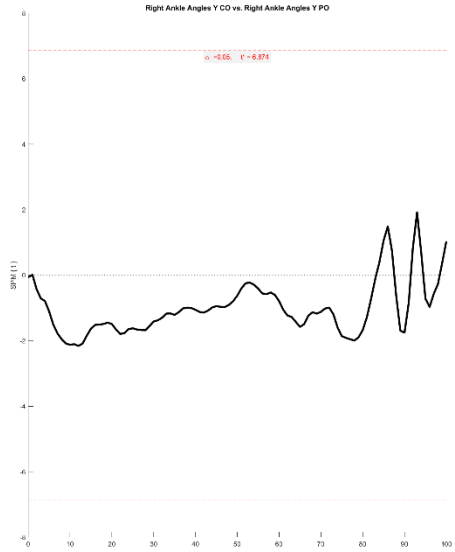

Left Ankle Angles X

85.1-86.6%, 89.2-93.8%

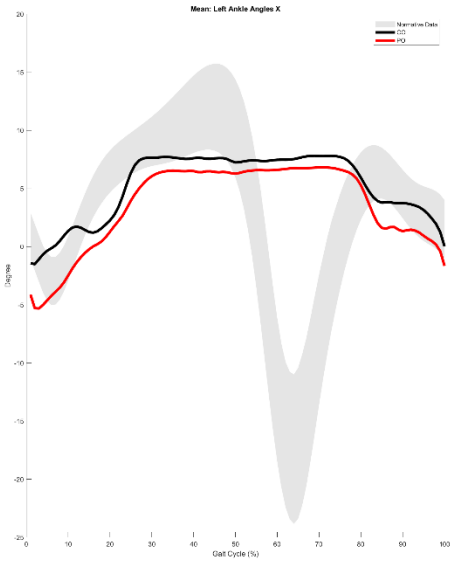

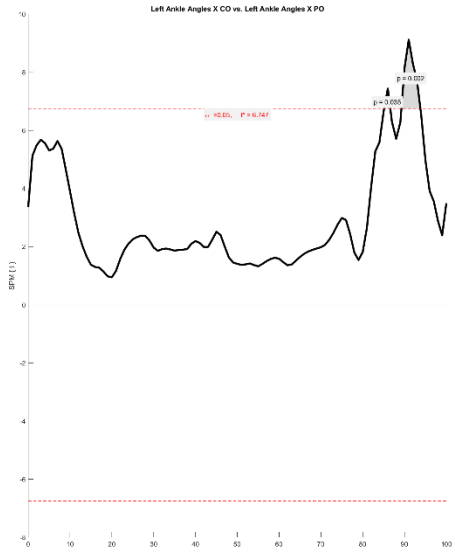

Left Ankle Angles Y

0.0-17.6%, 19.3-22.7%, 31.3-100.0%

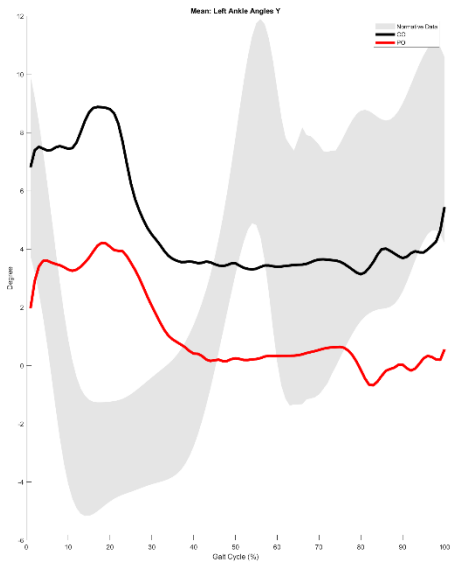

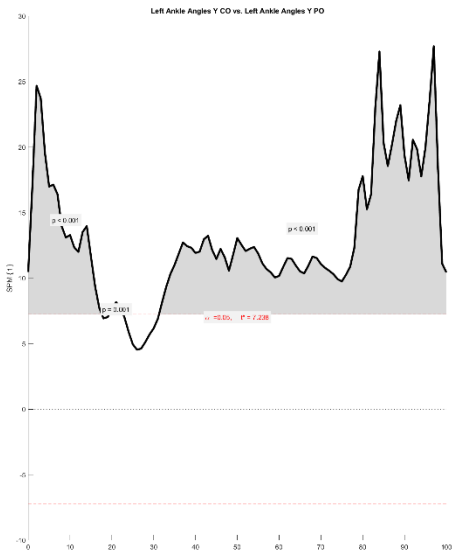

Right Foot Pitch Angles X

0.4-85.4%, 100.0-100.0%

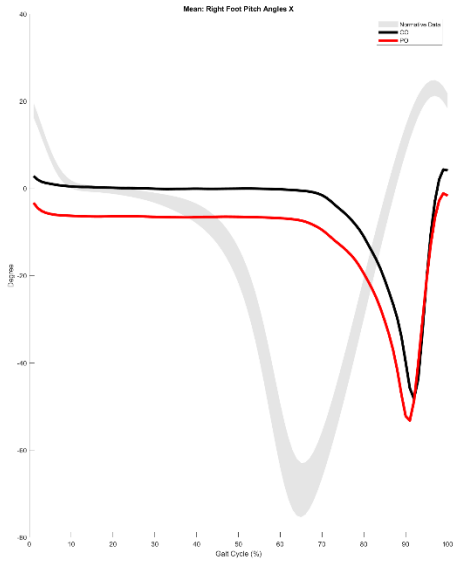

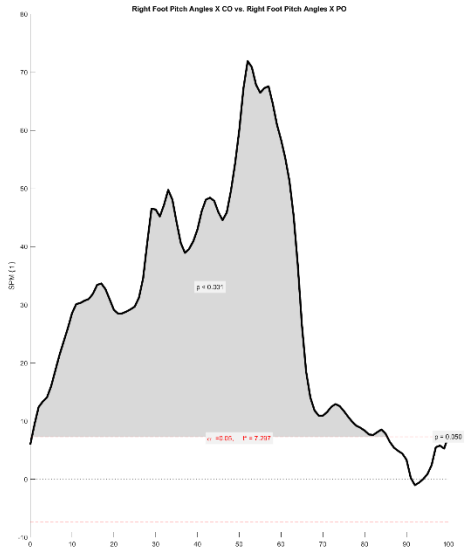

Left Foot Pitch Angles X

0.0-26.9%, 83.0-83.1%, 85.2-94.9%, 99.8-100.0%

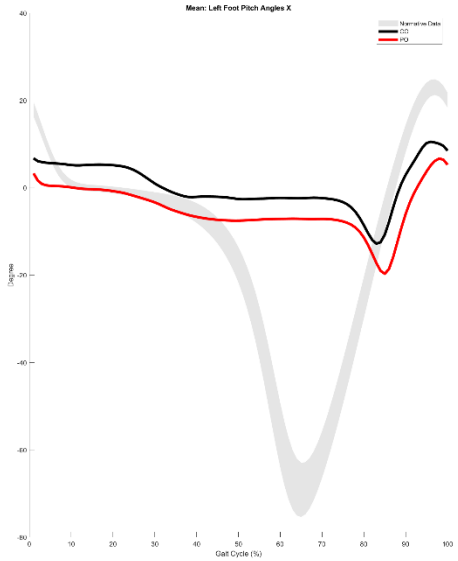

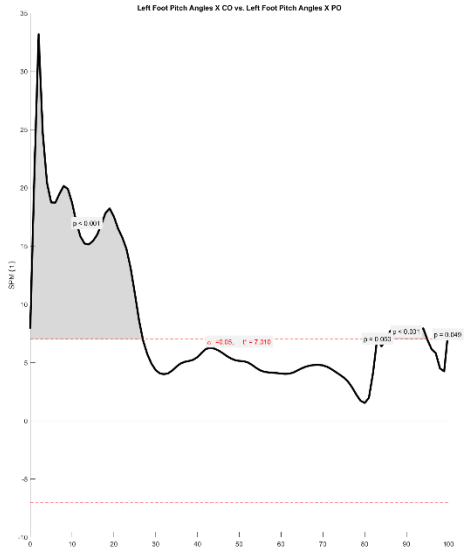

Right Foot Progression Z

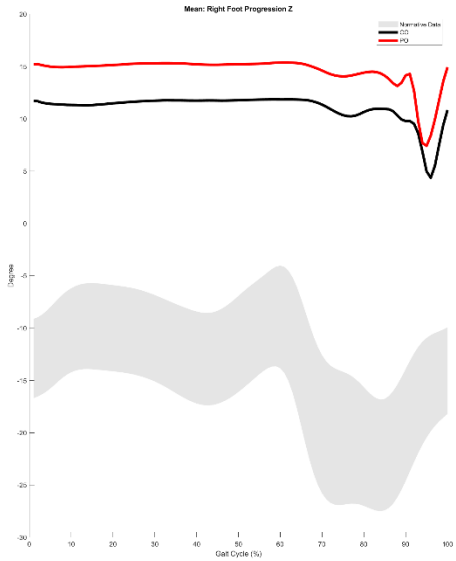

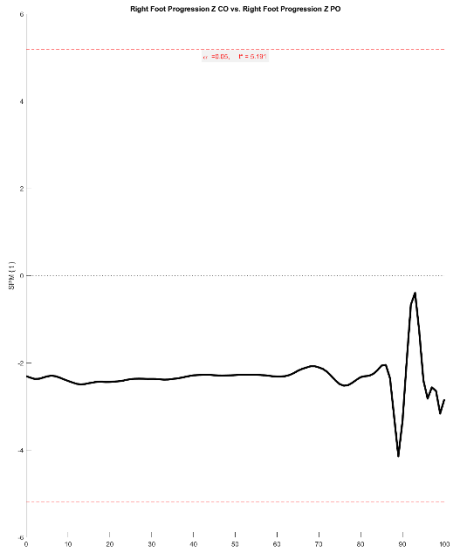

Left Foot Progression Z

84.0-84.0%, 91.3-96.5%

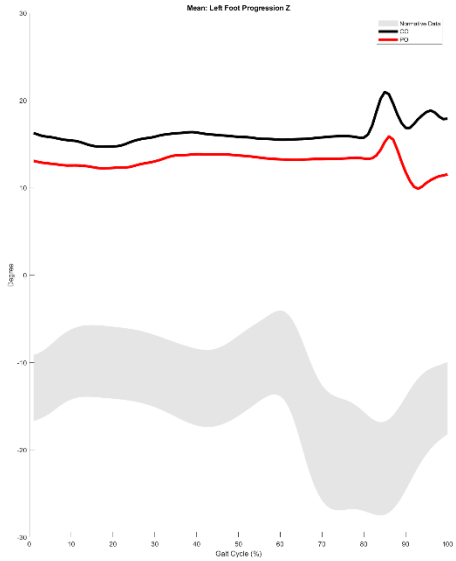

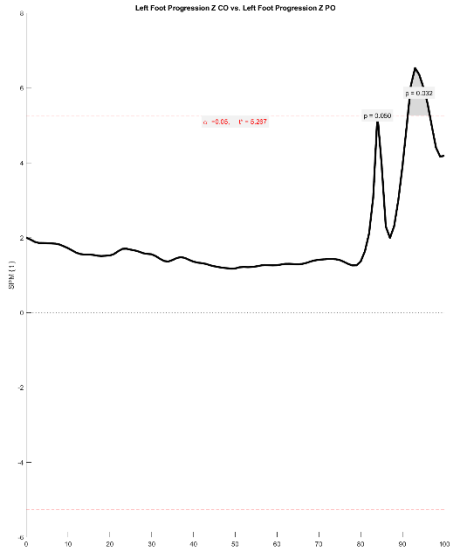

PO

Step Length

REP	Left	Right	IS (50%)	IS (0%)
1	0.30924	0.14224	31.5053	73.9789
2	0.30822	0.14224	31.5766	73.6936
3	0.30767	0.14073	31.3849	74.4603
4	0.30307	0.14011	31.6147	73.5412
5	0.30234	0.13905	31.5028	73.989
6	0.30197	0.13702	31.2126	75.1498
Mean	0.305418	0.1402317	31.4661	74.1355
SD	0.003011	0.0018276	0.13419	0.53677

CO

Step Length

REP	Left	Right	IS (50%)	IS (0%)
1	0.31161	0.13966	30.9482	76.2071
2	0.30958	0.13217	29.9196	80.3214
3	0.30818	0.12881	29.4766	82.0934
4	0.30728	0.12871	29.5213	81.9147
5	0.30353	0.12712	29.5182	81.9273
6	0.30185	0.12147	28.6946	85.2216
Mean	0.307005	0.1296567	29.6798	81.2809
SD	0.0033651	0.0054993	0.67448	2.69791

PO

Swing Time

REP	Left	Right	IS (50%)	IS (0%)
1	0.74167	0.5	40.2683	38.9266
2	0.74167	0.5	40.2683	38.9266
3	0.71667	0.49167	40.6897	37.2412
4	0.70833	0.48333	40.5594	37.7624
5	0.70833	0.48333	40.5594	37.7624
6	0.70833	0.475	40.141	39.4362
Mean	0.720833	0.4888883	40.4144	38.3426
SD	0.015026	0.0092137	0.19802	0.79208

CO

Swing Time

REP	Left	Right	IS (50%)	IS (0%)
1	0.80833	0.50833	38.6075	45.5699
2	0.79167	0.50833	39.1023	43.5908
3	0.78333	0.50833	39.3548	42.5809
4	0.775	0.49167	38.816	44.7362
5	0.775	0.49167	38.816	44.7362
6	0.75833	0.48333	38.9261	44.2955
Mean	0.7819433	0.49861	38.9371	44.2516
SD	0.0155284	0.0101097	0.23799	0.95197

PO

Stance Time

REP	Left	Right	IS (50%)	IS (0%)
1	3.15	3.425	52.0913	8.36502
2	3.14167	3.41667	52.0966	8.38627
3	3.13333	3.39167	51.9796	7.91847
4	3.125	3.39167	52.0461	8.18424
5	3.11667	3.375	51.9897	7.95881
6	3	3.35833	52.8178	11.2712
Mean	3.111112	3.3930567	52.1702	8.68067
SD	0.050842	0.0227808	0.29307	1.17229

CO

Stance Time

REP	Left	Right	IS (50%)	IS (0%)
1	3.21667	3.46667	51.8703	7.48129
2	3.2	3.44167	51.8193	7.27739
3	3.15	3.43333	52.1519	8.6075
4	3.13333	3.375	51.8566	7.42648
5	3.125	3.375	51.9231	7.69231
6	3.11667	3.35833	51.8661	7.4644
Mean	3.156945	3.4083333	51.9146	7.65823
SD	0.0380116	0.0405419	0.11039	0.44157

	Left	Right
Step Length PO	0.31	0.14
Step Length CO	0.31	0.13
Swing Time PO	0.72	0.49
Swing Time CO	0.78	0.50
Stance Time PO	3.11	3.39
Stance Time CO	3.16	3.41

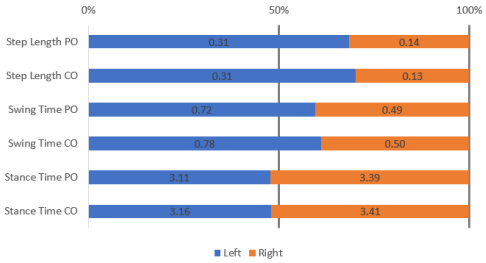

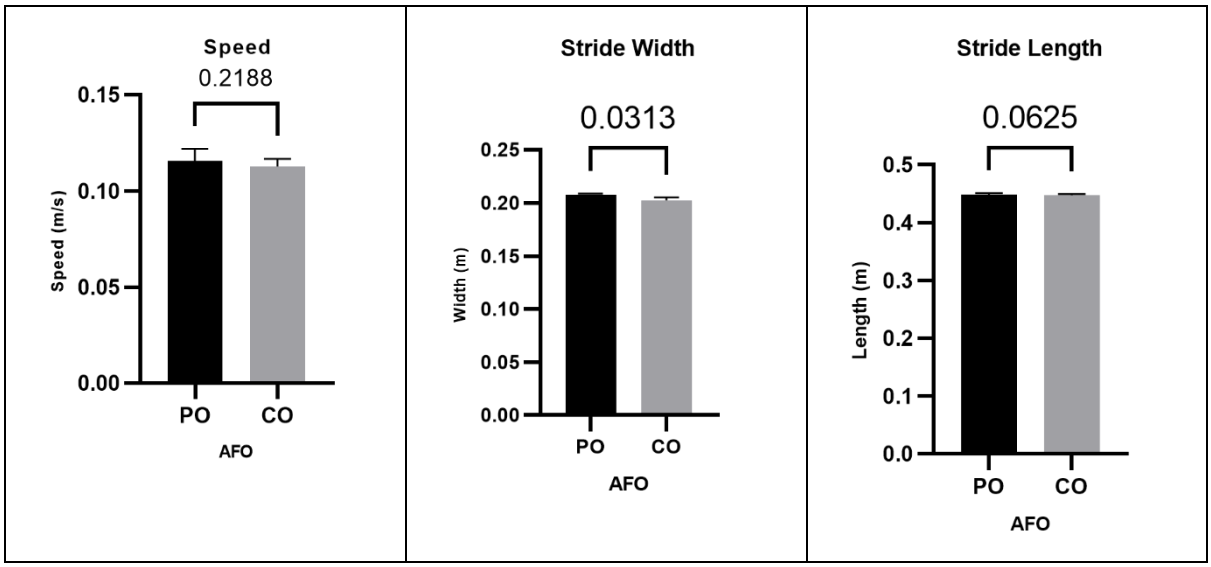

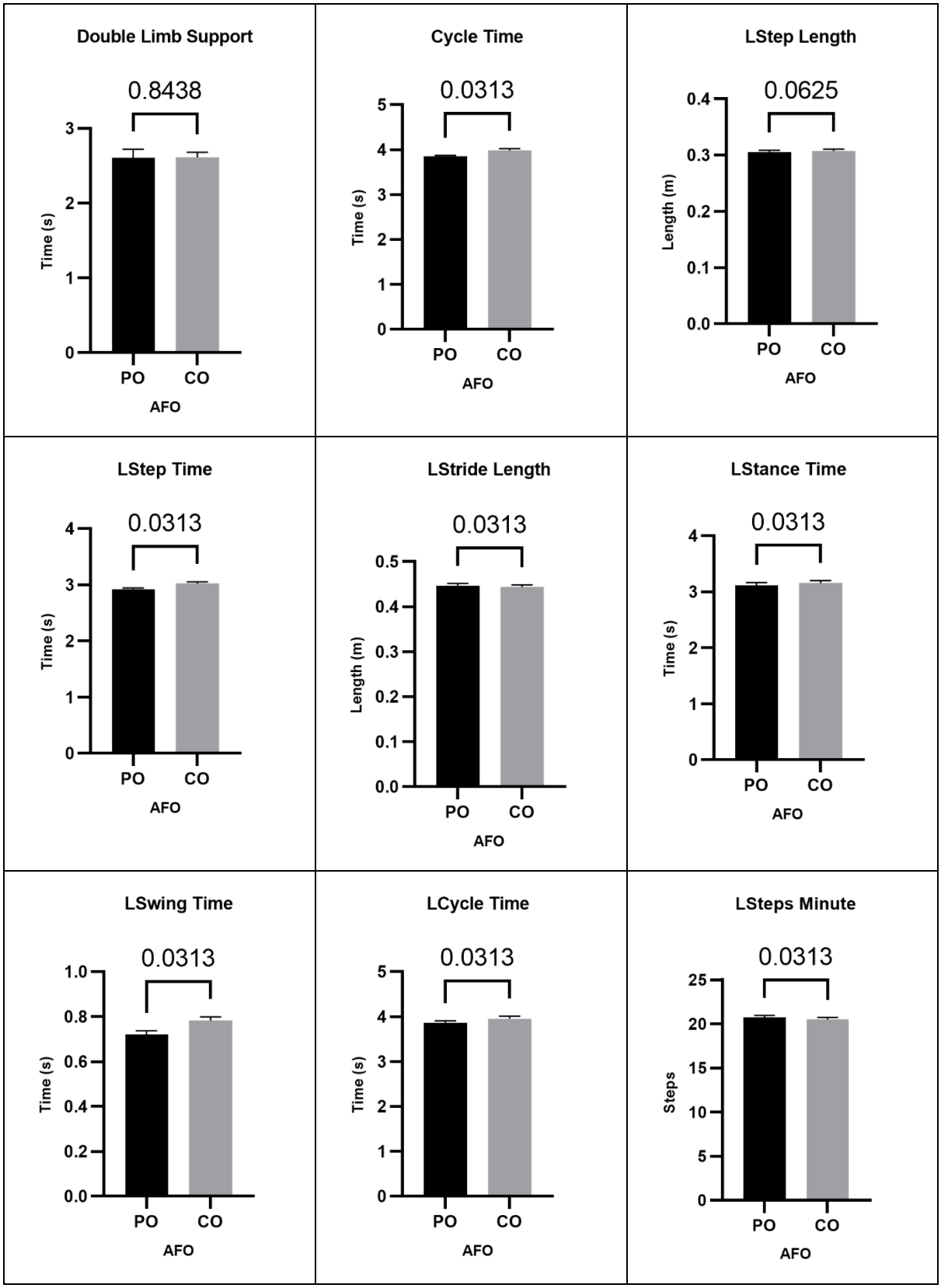
Double Limb Support
0.8438
Time (s)
PO
CO
AFO
Cycle Time
0.0313
Time (s)
PO
CO
AFO
LStep Length
0.0625
Length (m)
PO
CO
AFO
LStep Time
0.0313
Time (s)
PO
CO
AFO
LStride Length
0.0313
Length (m)
PO
CO
AFO
LStance Time
0.0313
Time (s)
PO
CO
AFO
LSwing Time
0.0313
Time (s)
PO
CO
AFO
LCycle Time
0.0313
Time (s)
PO
CO
AFO
LSteps Minute
0.0313
Steps
PO
CO
AFO

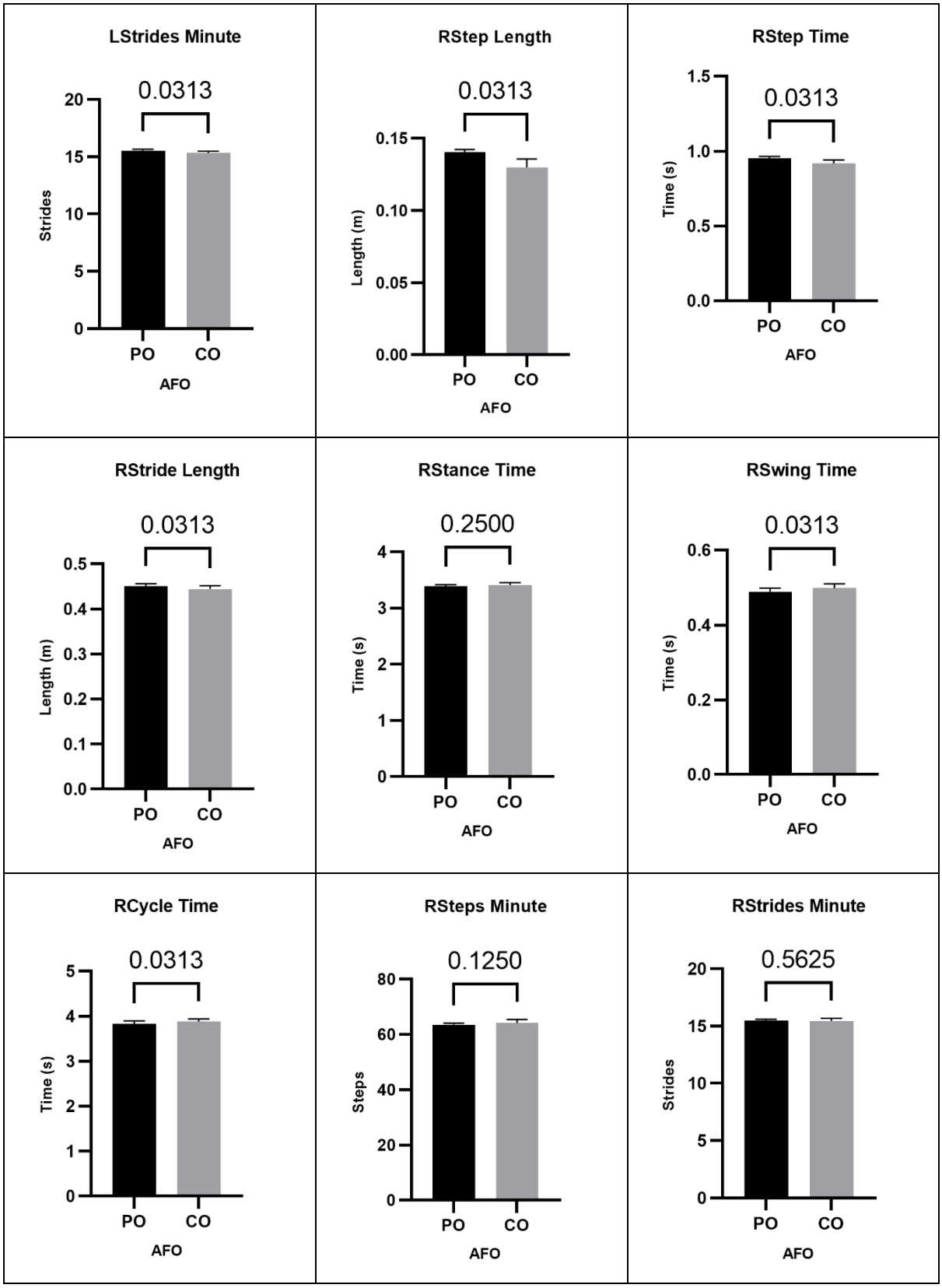
LStrides Minute
0.0313
Strides
20
15
10
5
0
PO
CO
AFO
RStep Length
0.0313
Length (m)
0.15
0.10
0.05
0.00
PO
CO
AFO
RStep Time
0.0313
Time (s)
1.5
1.0
0.5
0.0
PO
CO
AFO
RStride Length
0.0313
Length (m)
0.5
0.4
0.3
0.2
0.1
0.0
PO
CO
AFO
RStance Time
0.2500
Time (s)
4
3
2
1
0
PO
CO
AFO
RSwing Time
0.0313
Time (s)
0.6
0.4
0.2
0.0
PO
CO
AFO
RCycle Time
0.0313
Time (s)
5
4
3
2
1
0
PO
CO
AFO
RSteps Minute
0.1250
Steps
80
60
40
20
0
PO
CO
AFO
RStrides Minute
0.5625
Strides
20
15
10
5
0
PO
CO
AFO

PATIENT 7

Right Pelvic Angles X

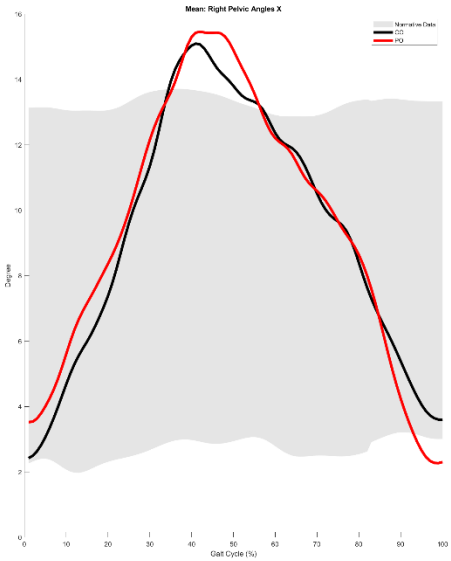

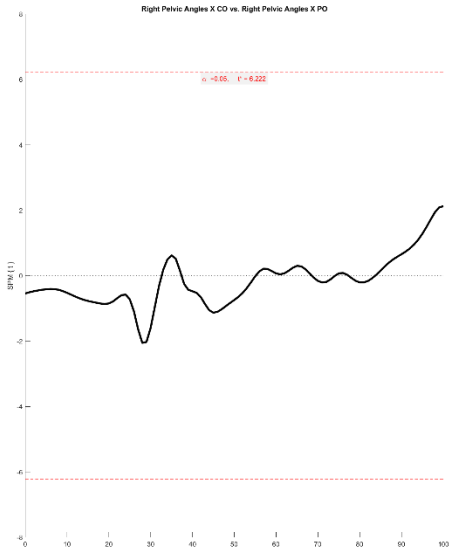

Right Pelvic Angles Y

91.3-96.4%

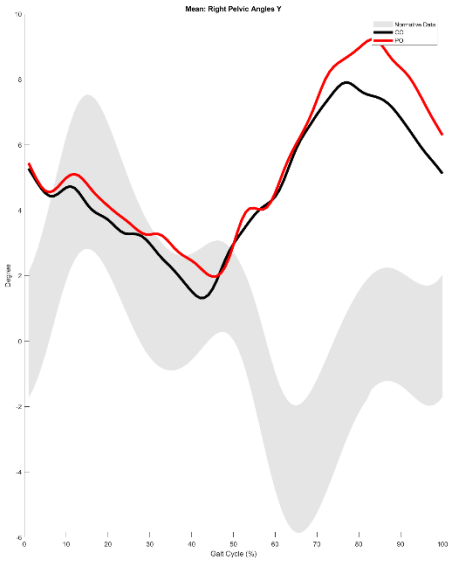

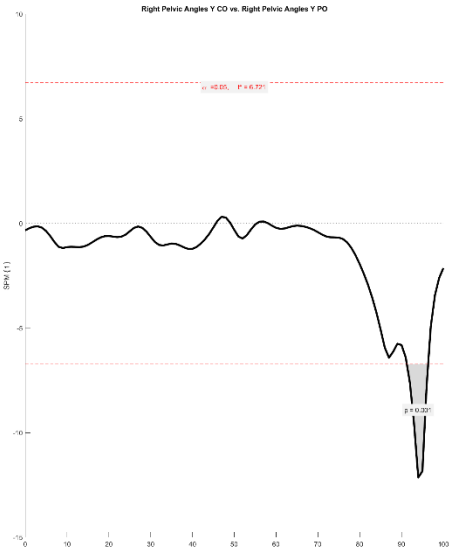

Right Pelvic Angles Z

37.8-42.8%

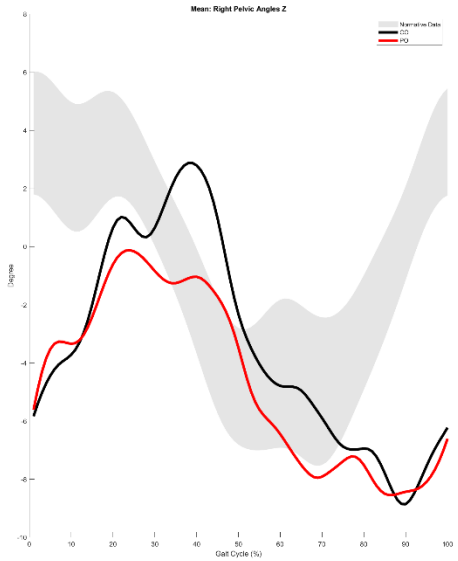

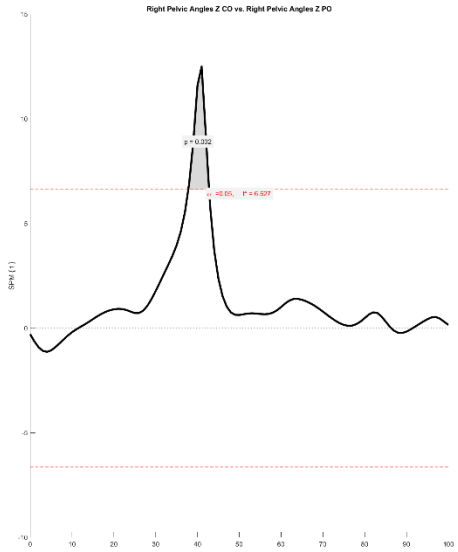

Left Pelvic Angles X

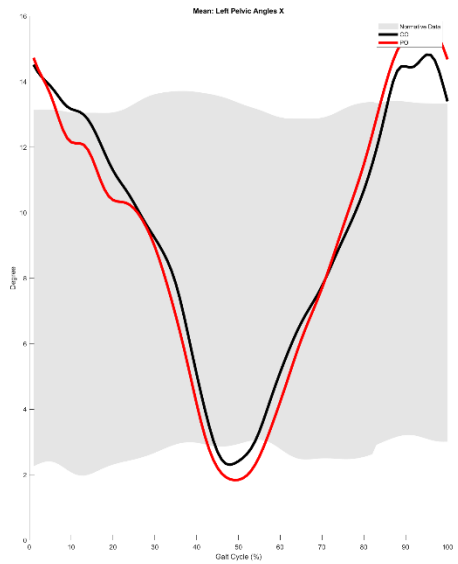

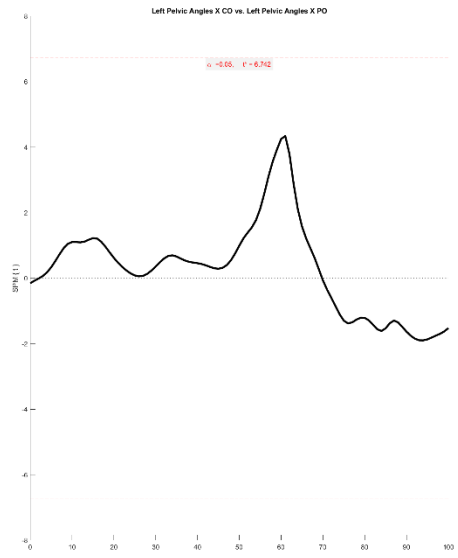

Left Pelvic Angles Y

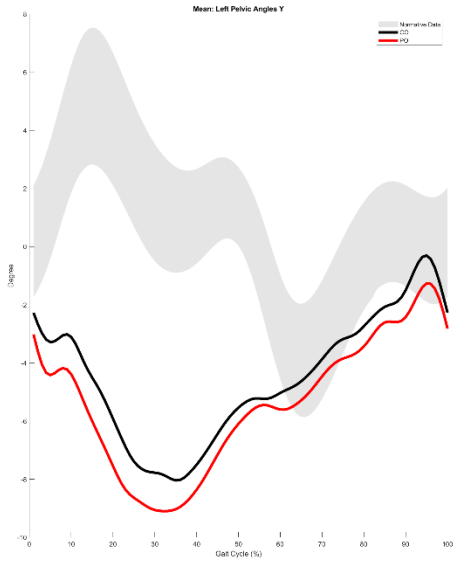

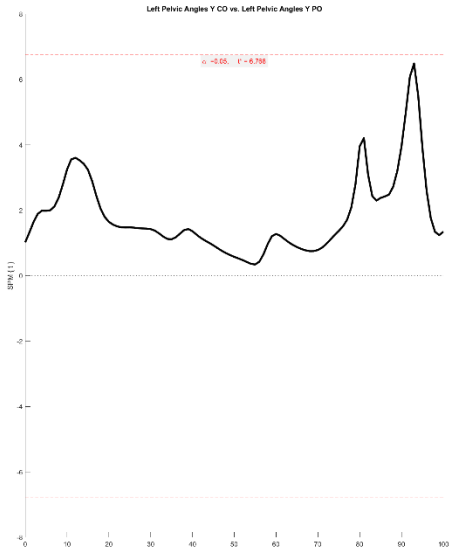

Left Pelvic Angles Z

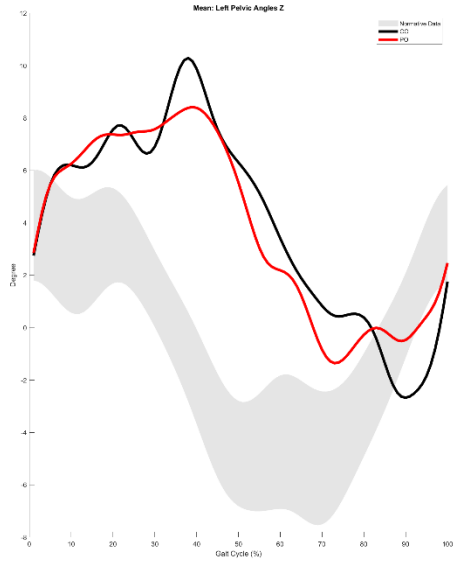

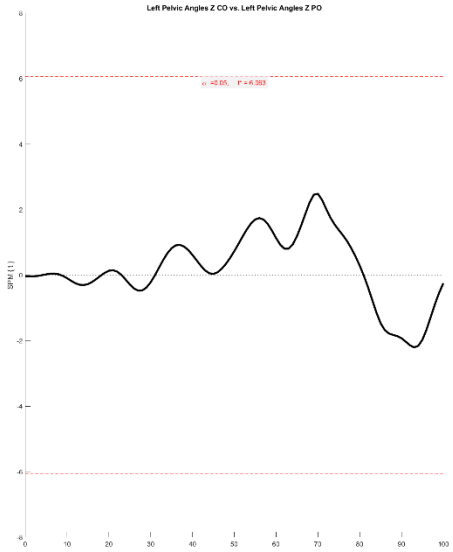

Right Hip Angles X

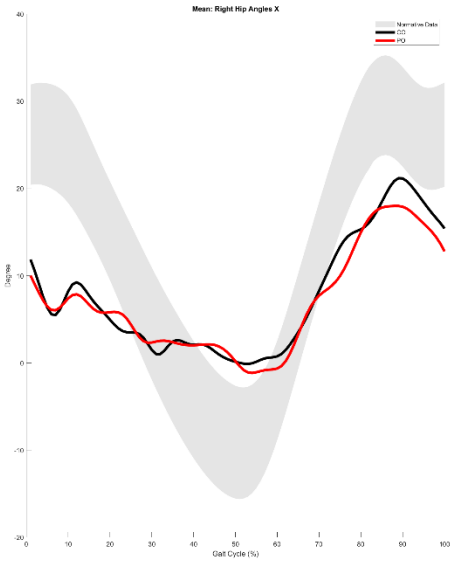

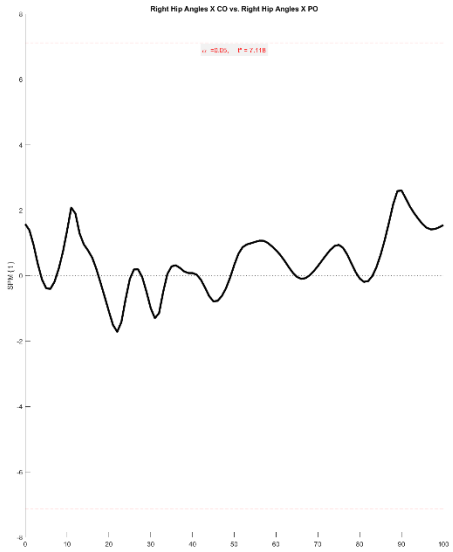

Right Hip Angles Y

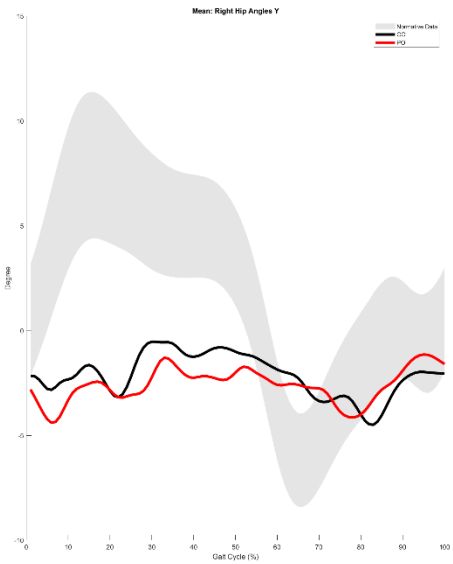

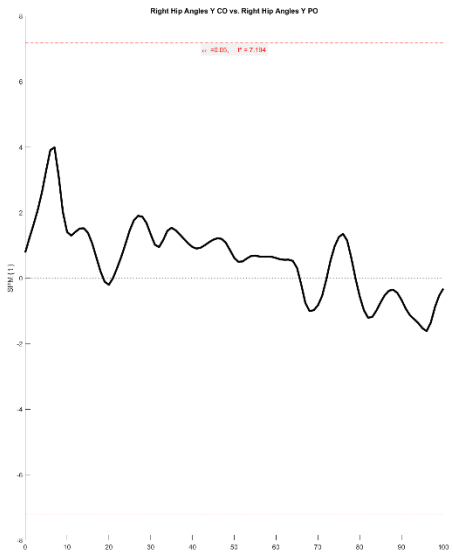

Right Hip Angles Z

6.2-9.3%, 98.8-100.0%

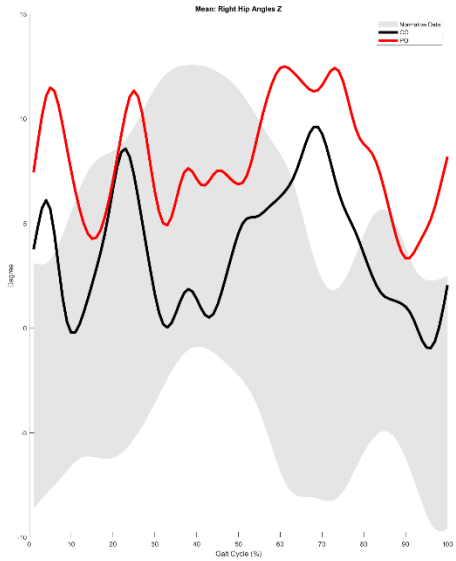

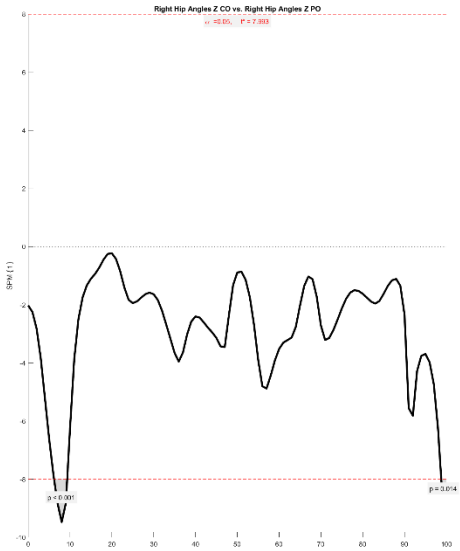

Left Hip Angles X

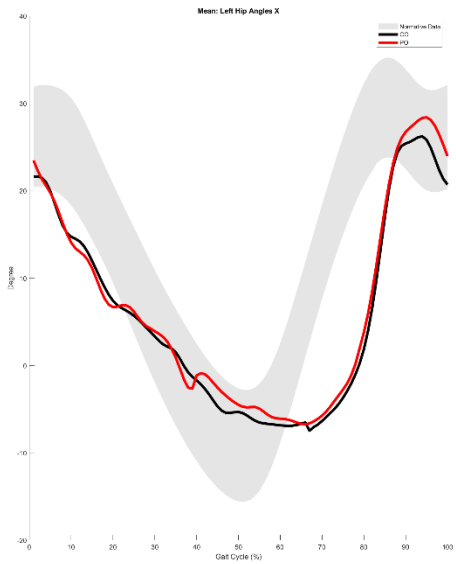

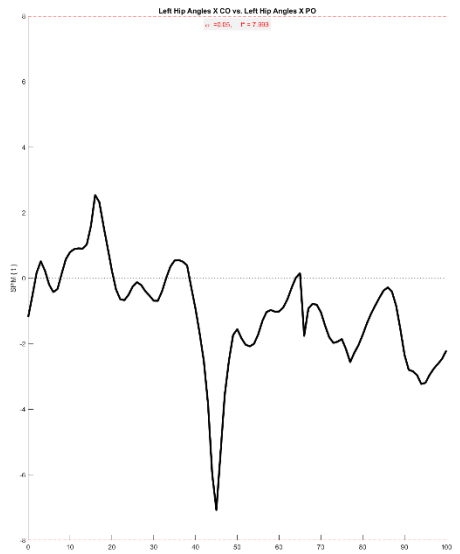

Left Hip Angles Y

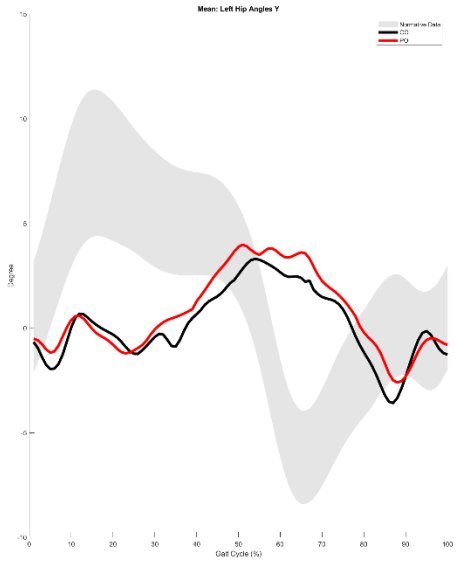

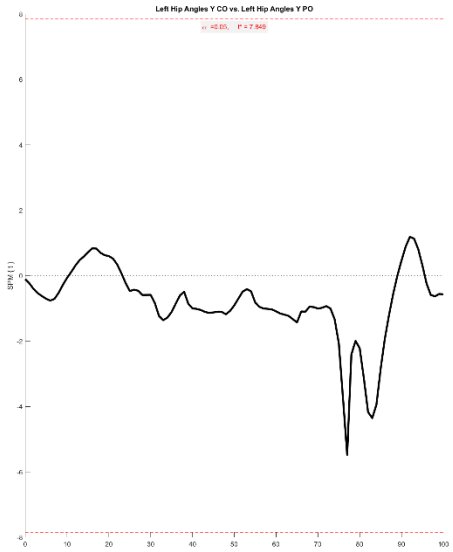

Left Hip Angles Z

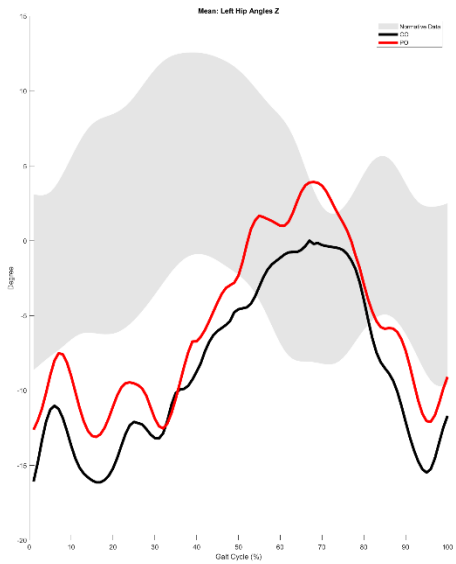

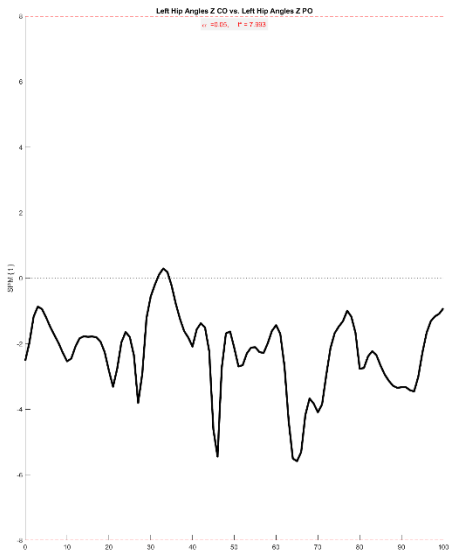

Right Knee Angles X

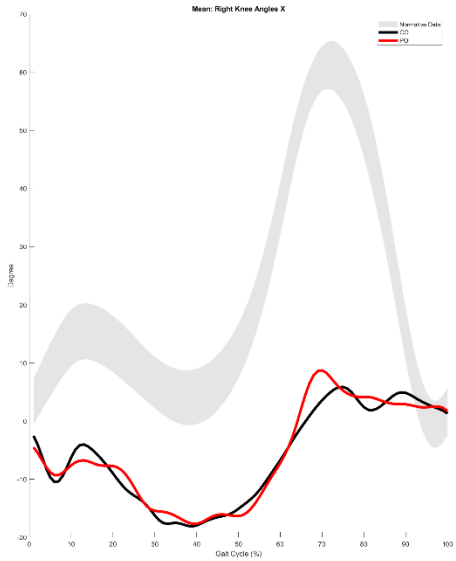

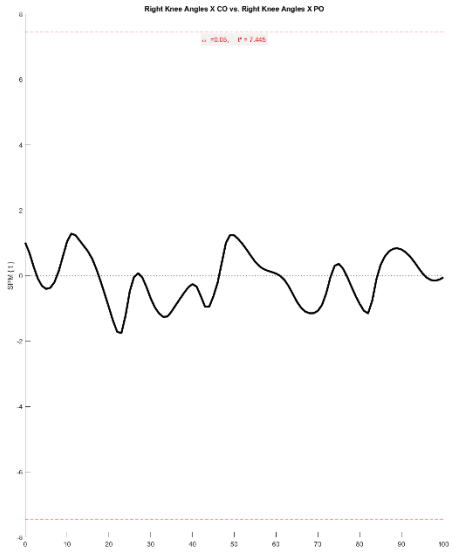

Right Knee Angles Y

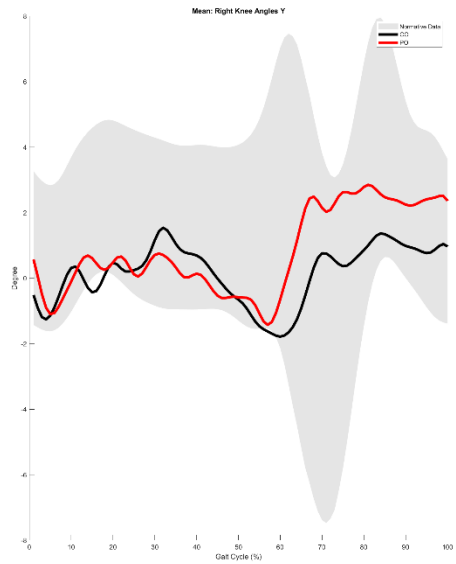

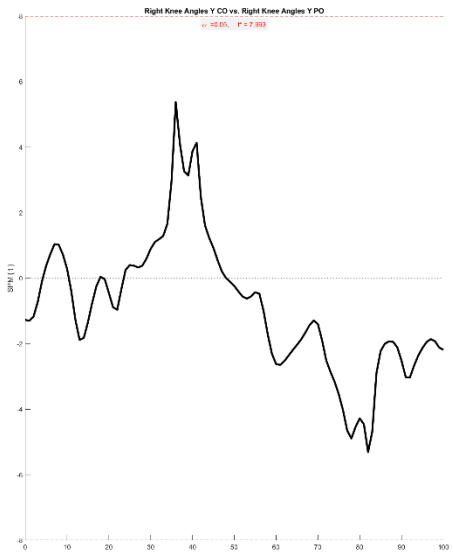

Right Knee Angles Z

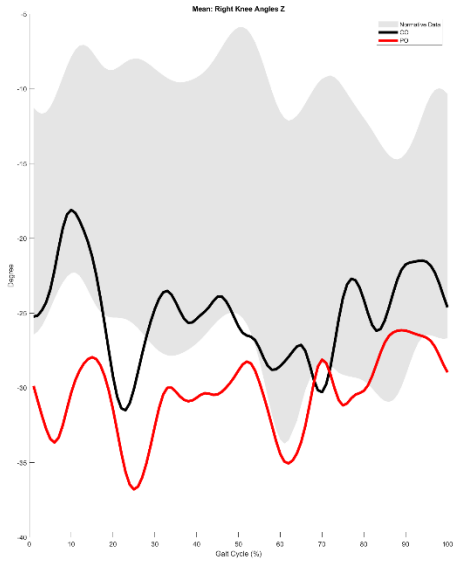

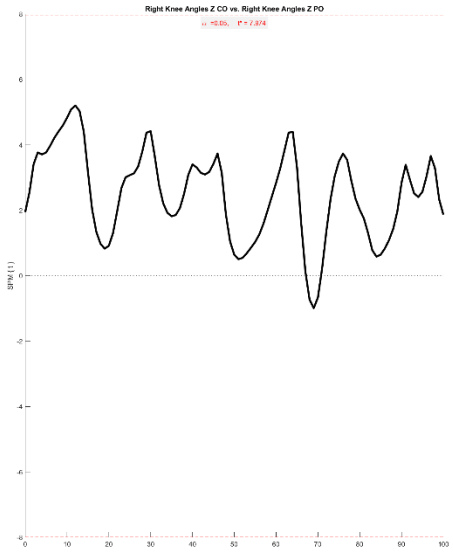

Left Knee Angles X

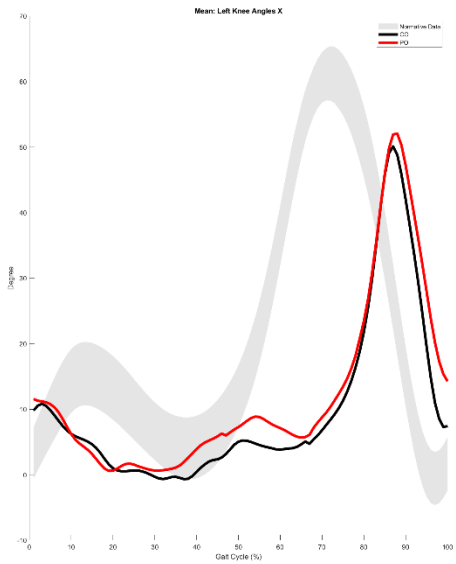

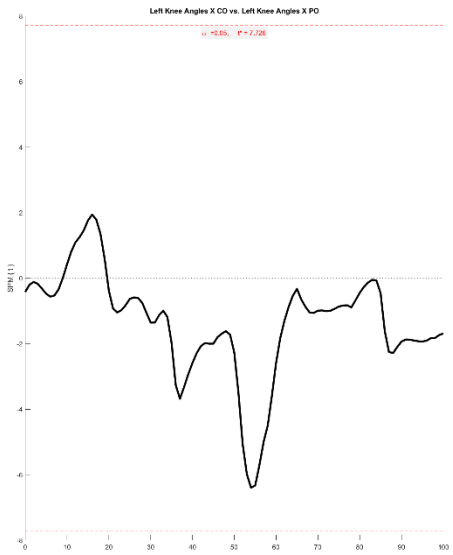

Left Knee Angles Y

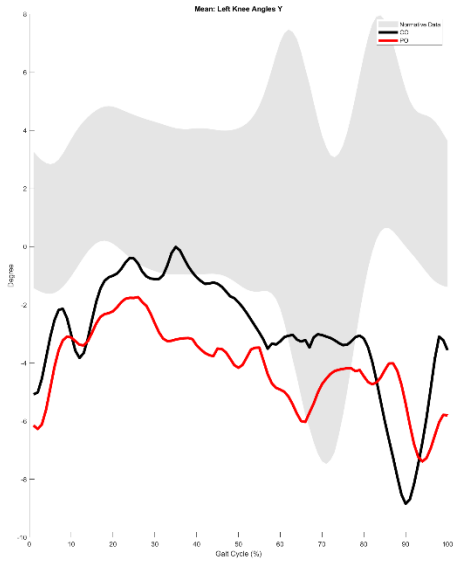

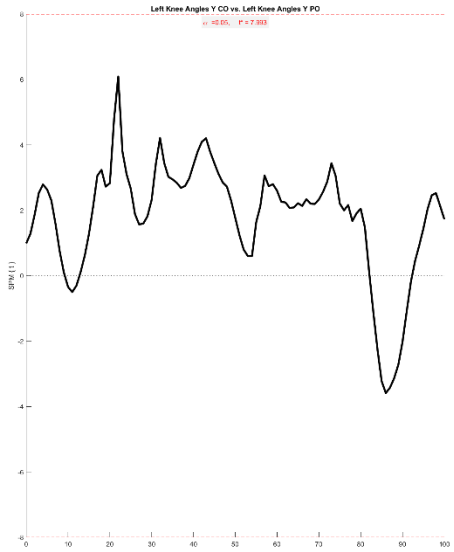

Left Knee Angles Z

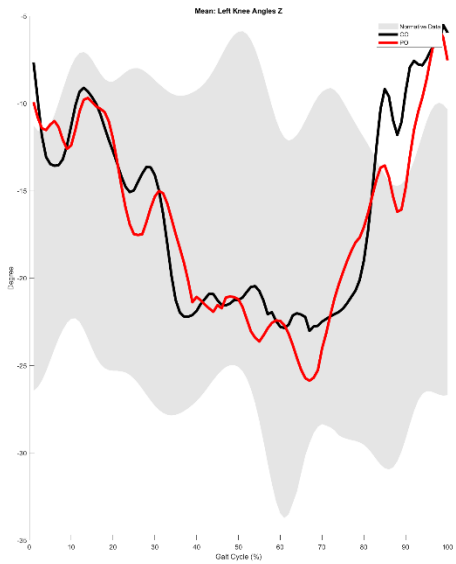

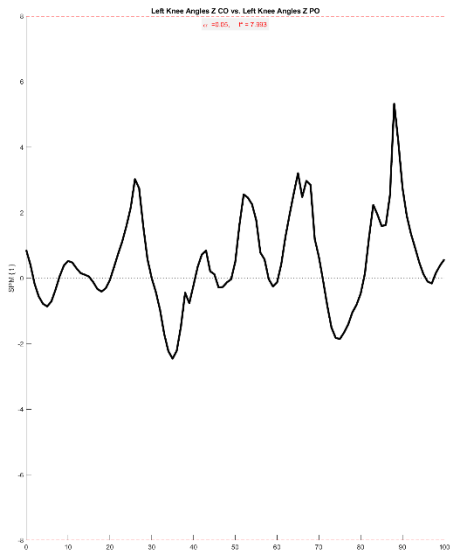

Right Ankle Angles X

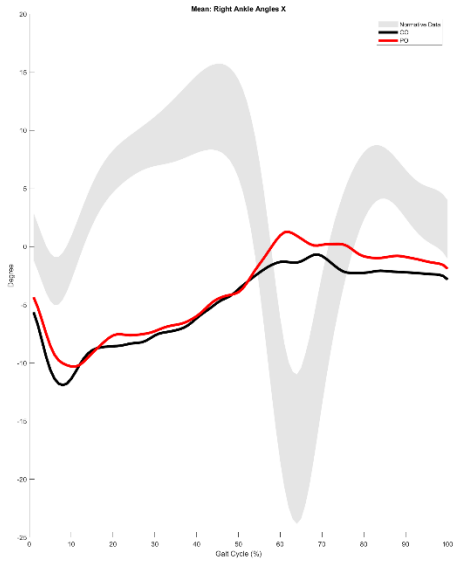

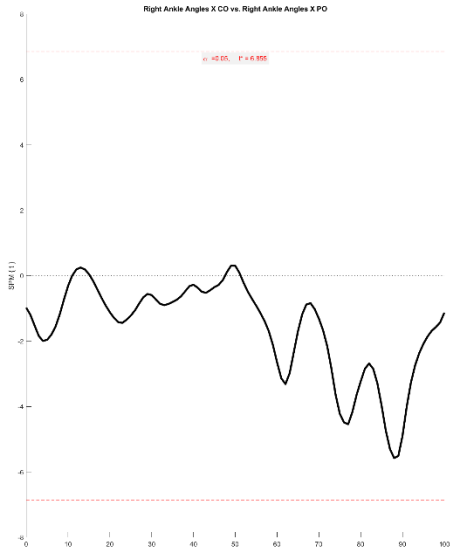

Right Ankle Angles Y

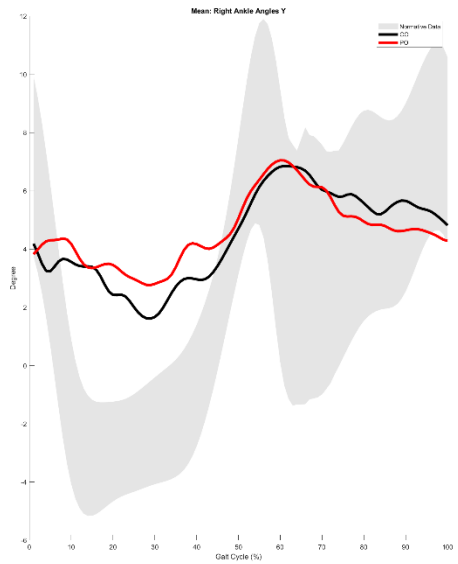

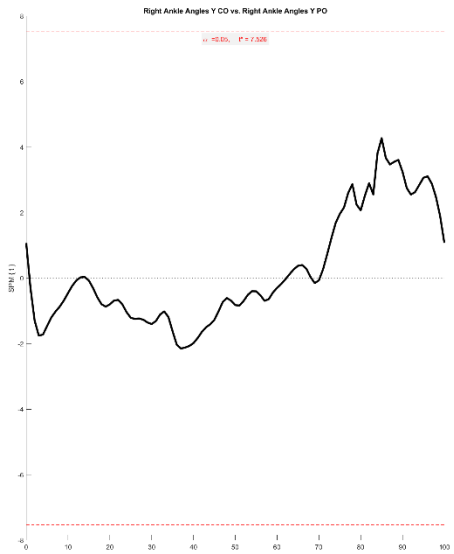

Left Ankle Angles X

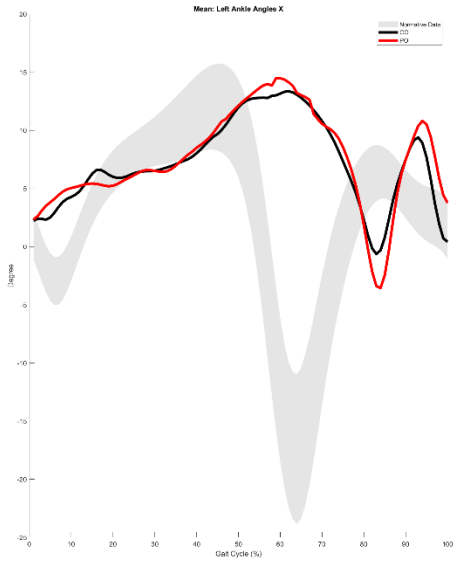

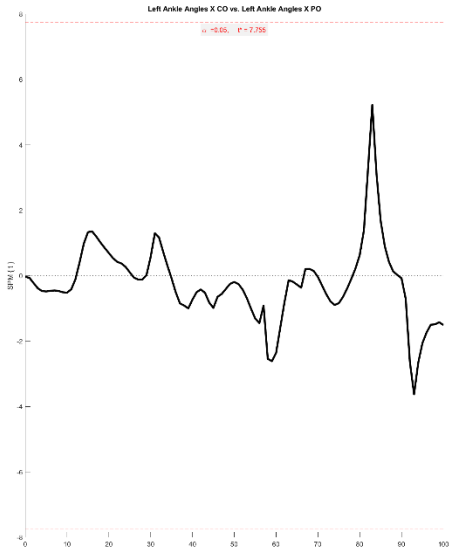

Left Ankle Angles Y

72.7-73.4%

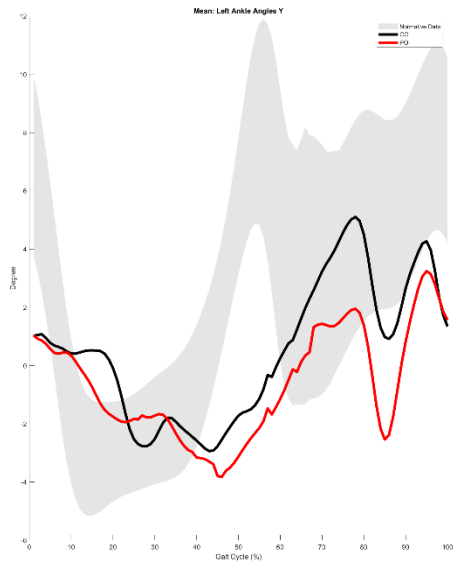

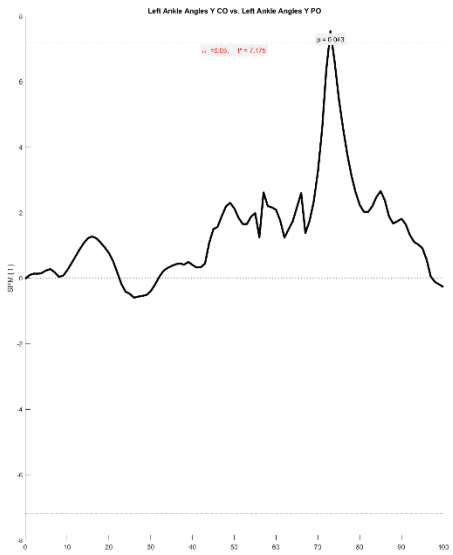

Right Foot Pitch Angles X

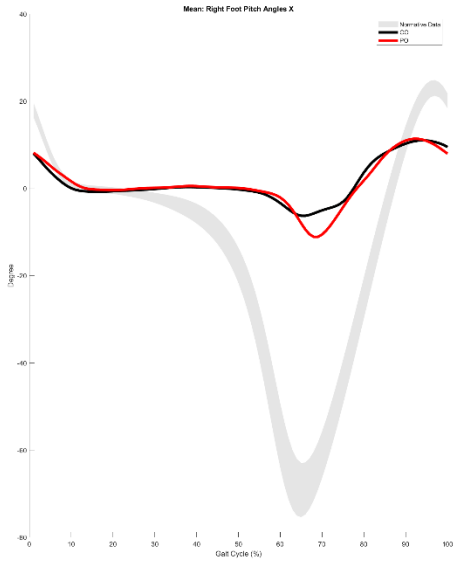

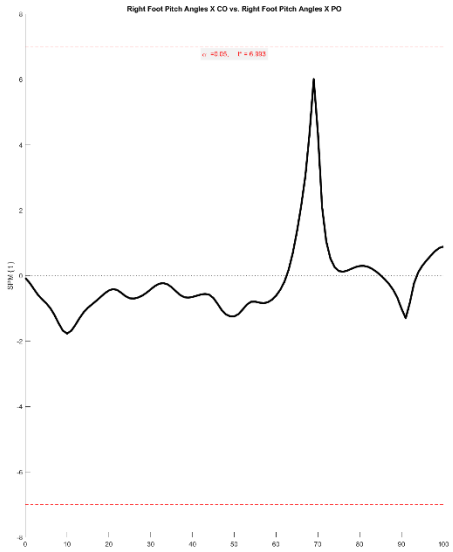

Left Foot Pitch Angles X

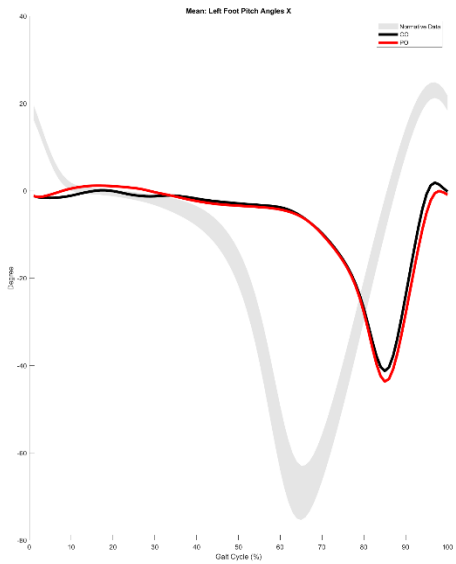

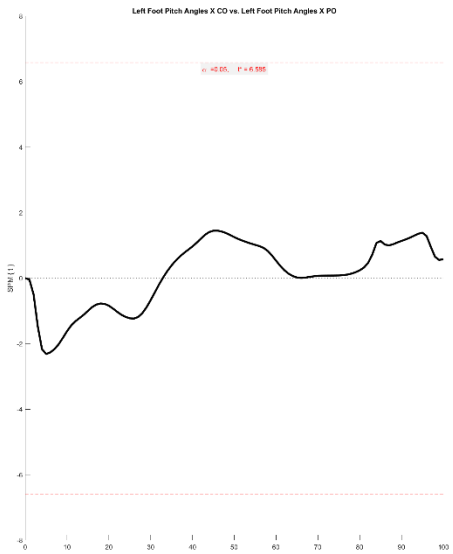

Right Foot Progression Z

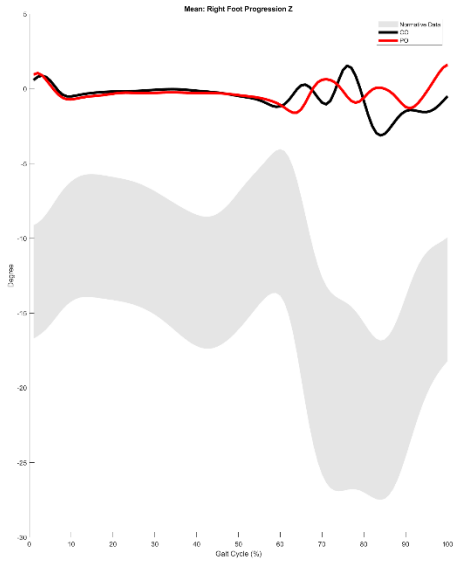

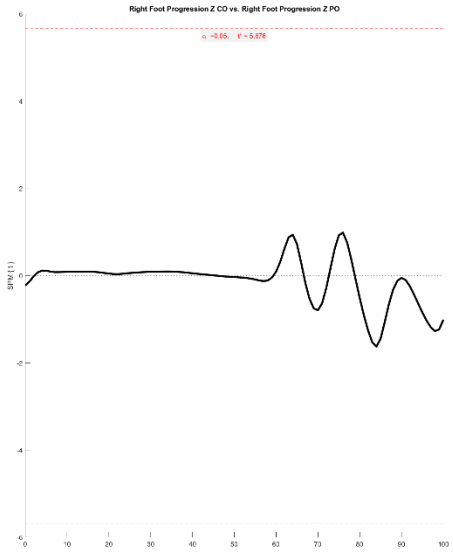

Left Foot Progression Z

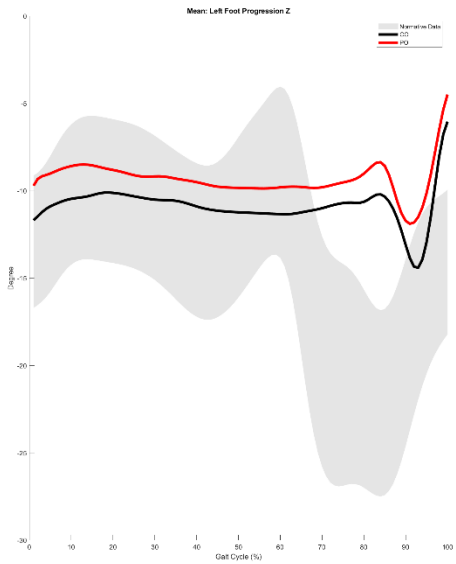

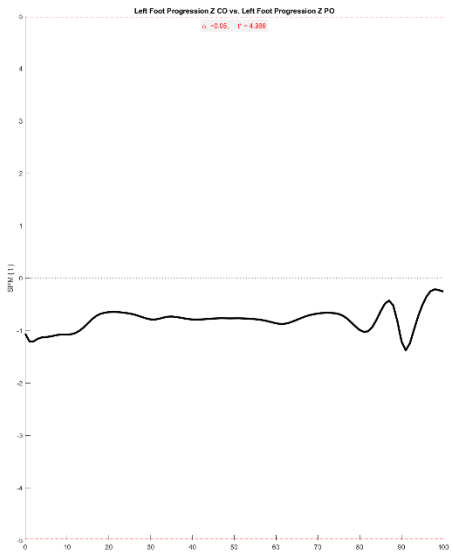

Right Hip Moment X

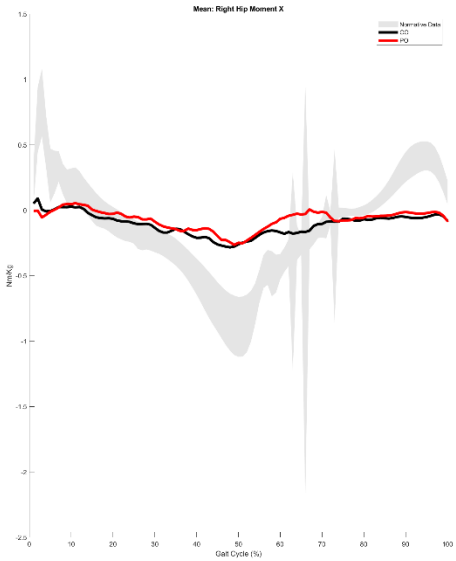

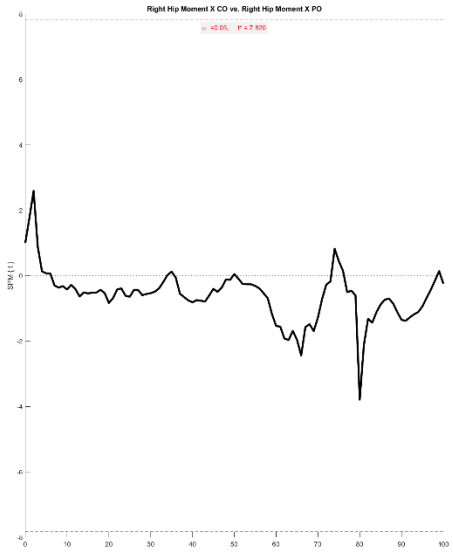

Right Hip Moment Y

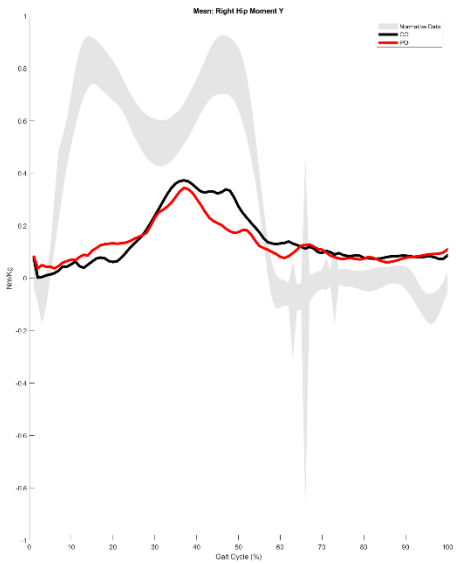

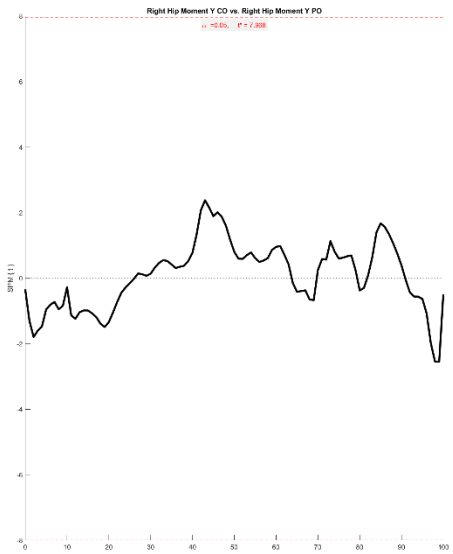

Left Hip Moment X

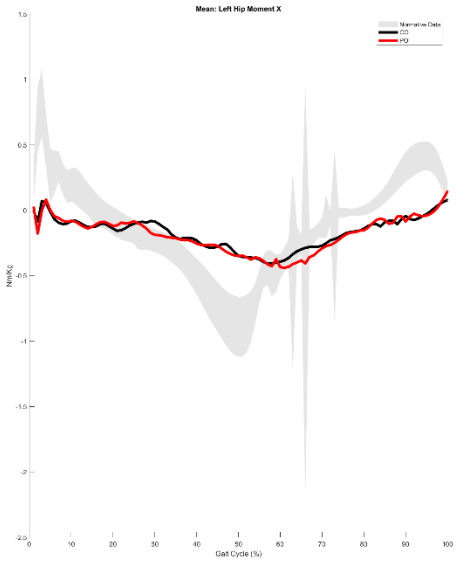

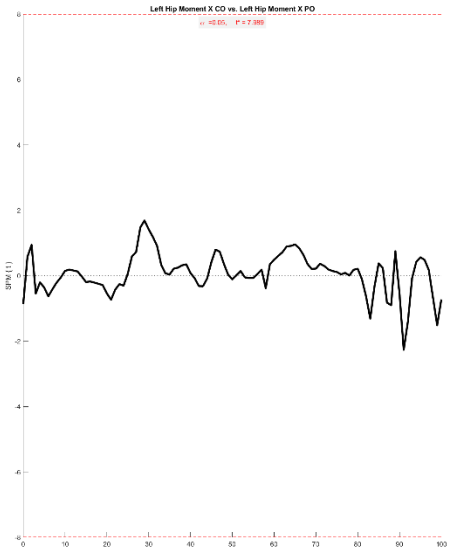

Left Hip Moment Y

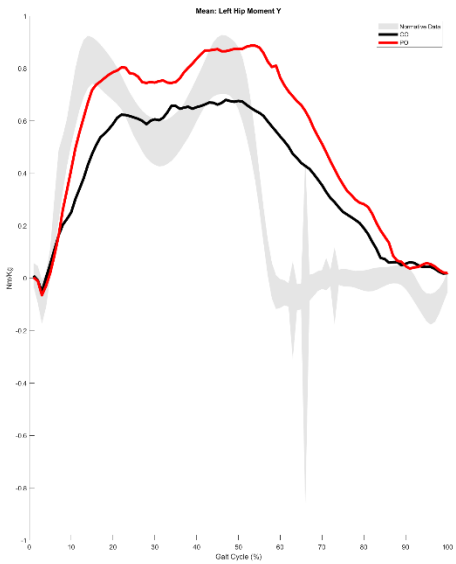

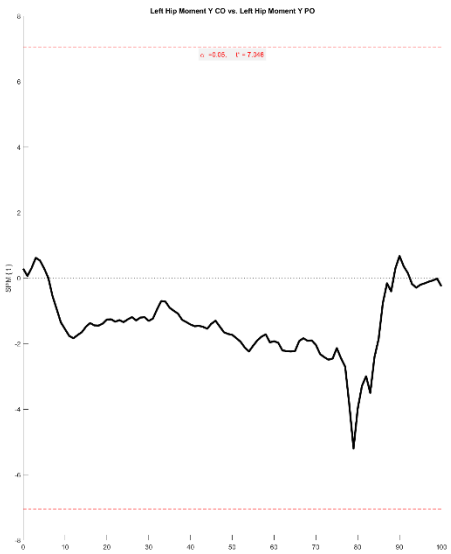

Right Knee Moment X

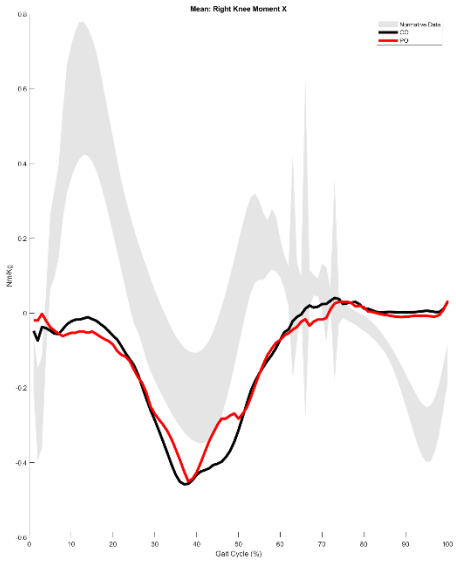

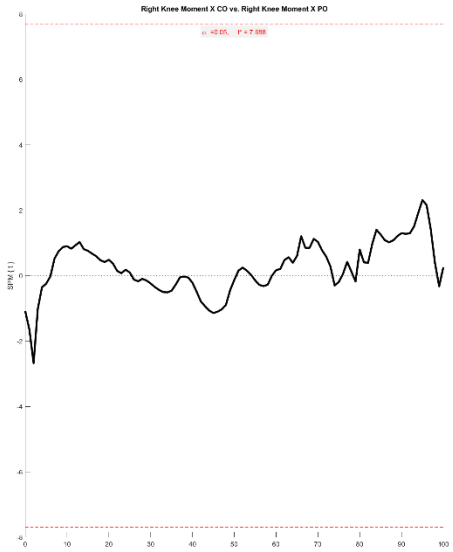

Right Knee Moment Y

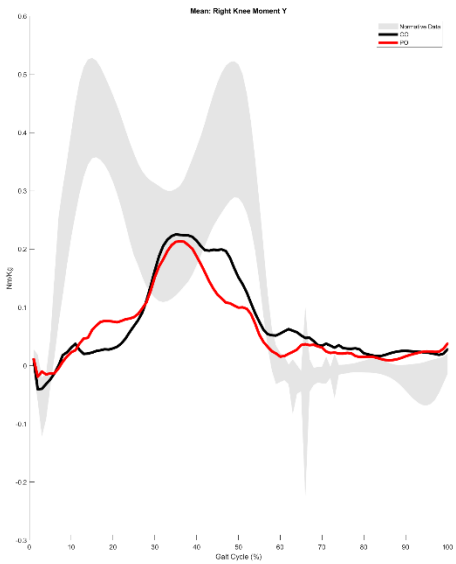

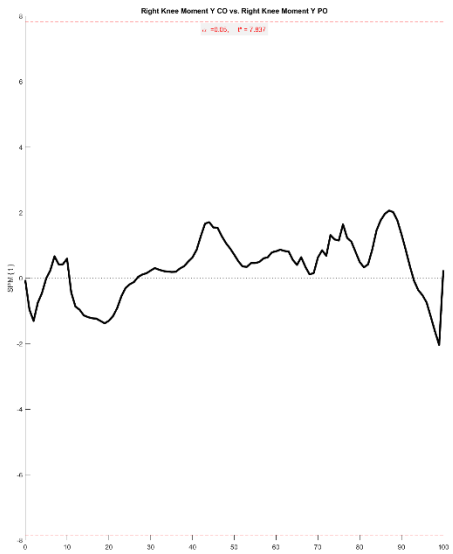

Left Knee Moment X

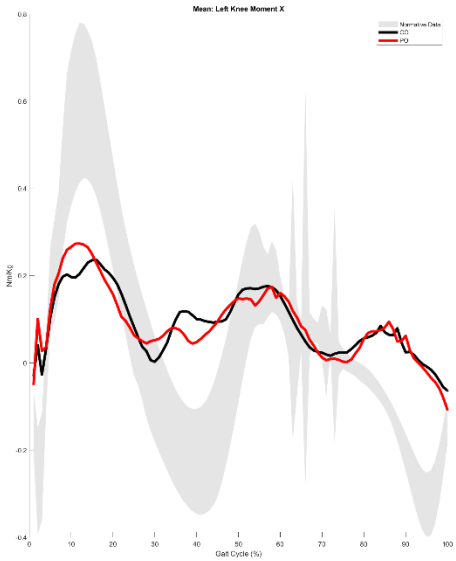

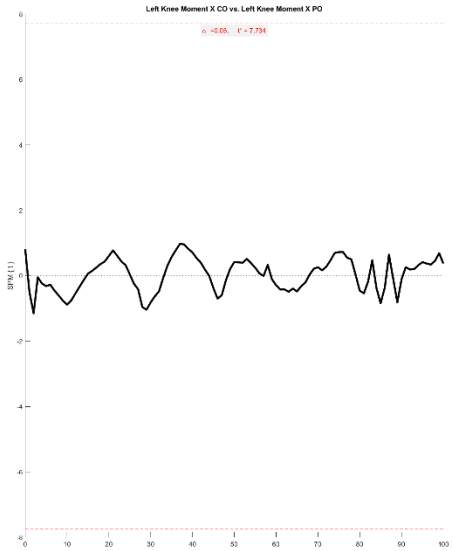

Left Knee Moment Y

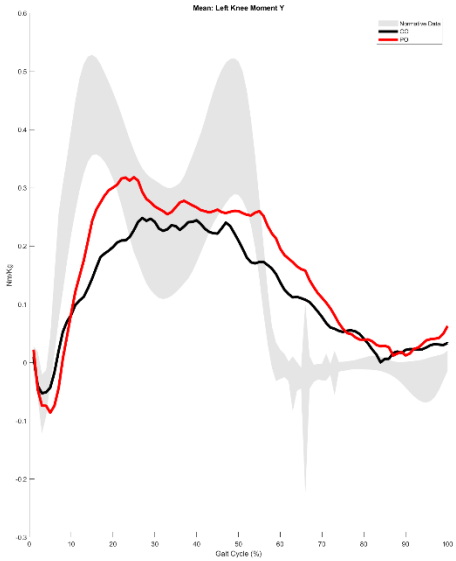

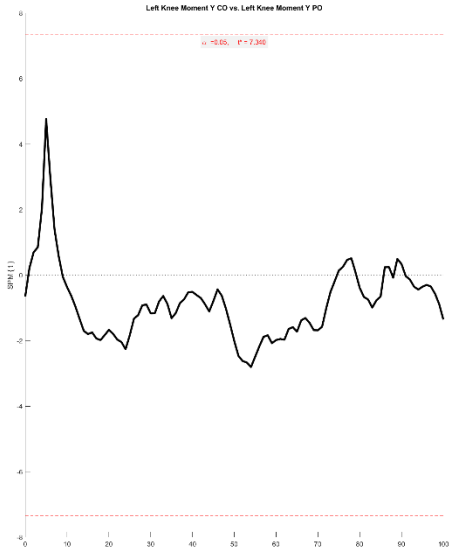

Right Ankle Moment X

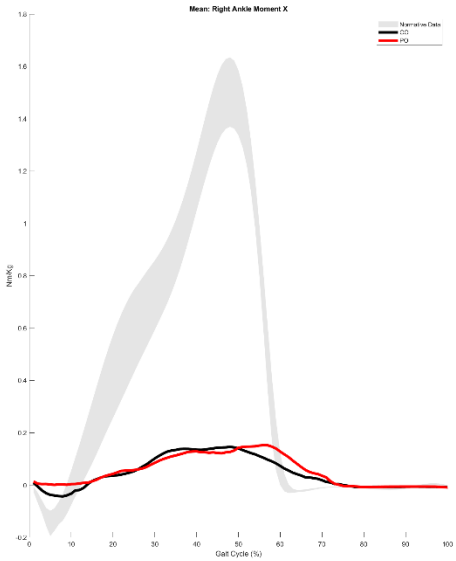

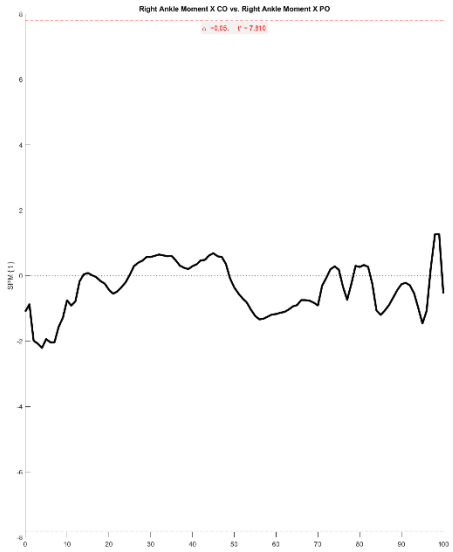

Right Ankle Moment Y

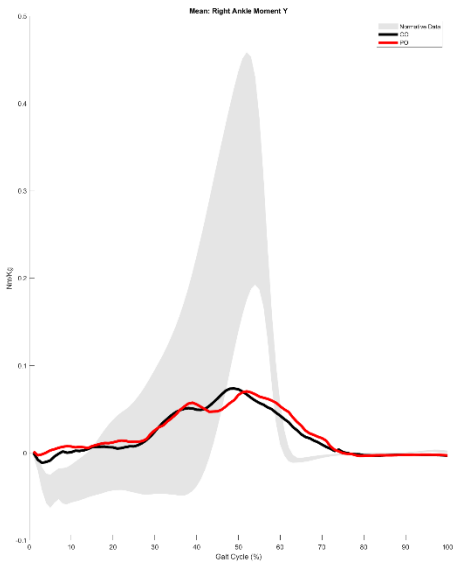

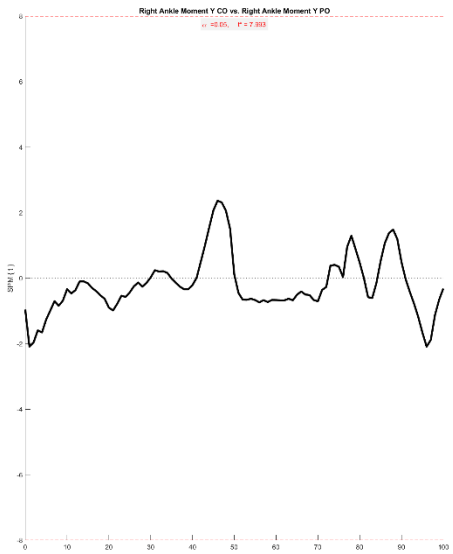

Left Ankle Moment X

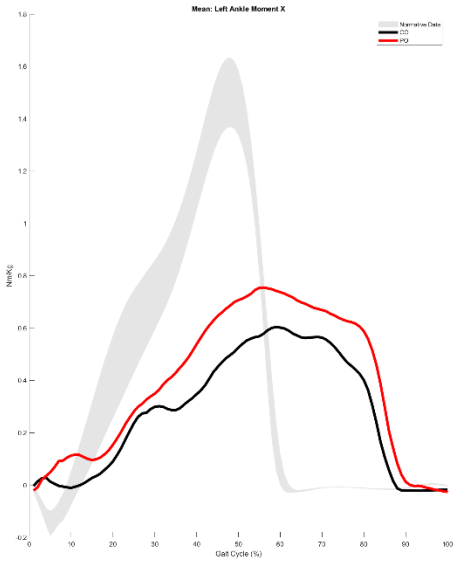

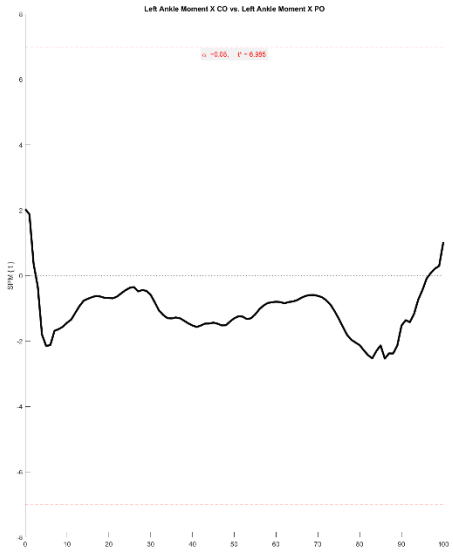

Left Ankle Moment Y

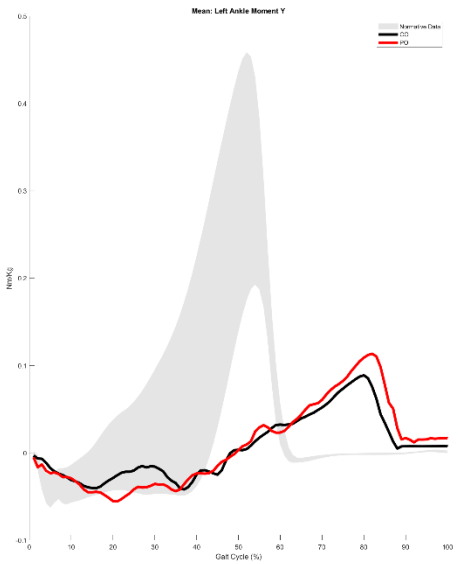

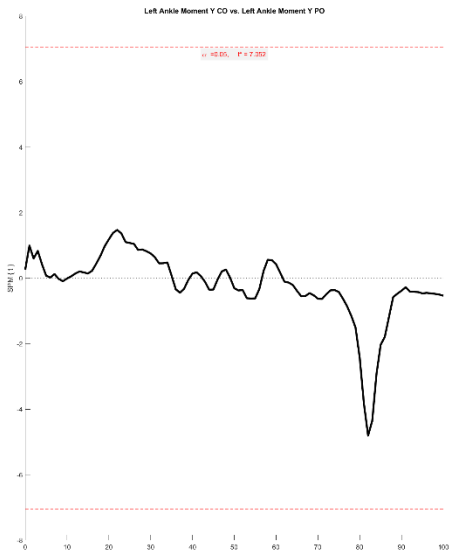

PO

Step Length

REP	Left	Right	IS (50%)	IS (0%)
1	0.1822	0.27826	60.4309	41.7235
2	0.17713	0.25078	58.6058	34.4231
3	0.1692	0.15833	48.3406	6.63756
4	0.164	0.24624	60.0234	40.0936
5	0.16291	0.28311	63.4747	53.8989
6	0.15525	0.24592	61.3007	45.2028
Mean	0.168448	0.2437733	58.696	36.9966
SD	0.009034	0.0410225	4.85858	14.7945

CO

Step Length

REP	Left	Right	IS (50%)	IS (0%)
1	0.19932	0.26812	57.3592	29.4369
2	0.1726	0.26696	60.7335	42.9338
3	0.1704	0.26271	60.6566	42.6266
4	0.16999	0.26143	60.5976	42.3902
5	0.16979	0.25882	60.3859	41.5436
6	0.16814	0.25613	60.3696	41.4783
Mean	0.17504	0.2623617	60.0171	40.0683
SD	0.0109368	0.0042164	1.19608	4.78432

PO

Swing Time

REP	Left	Right	IS (50%)	IS (0%)
1	0.38333	0.74167	65.9262	63.7049
2	0.38333	0.73333	65.6717	62.6869
3	0.35833	0.71667	66.667	66.6679
4	0.35	0.70833	66.929	67.7161
5	0.34167	0.69167	66.9354	67.7415
6	0.325	0.65833	66.949	67.7962
Mean	0.356943	0.7083333	66.5131	66.0523
SD	0.021199	0.0276395	0.51919	2.07676

CO

Swing Time

REP	Left	Right	IS (50%)	IS (0%)
1	0.43333	0.79167	64.6261	58.5045
2	0.425	0.775	64.5833	58.3333
3	0.41667	0.75	64.2855	57.1421
4	0.40833	0.73333	64.2337	56.9346
5	0.4	0.725	64.4444	57.7778
6	0.375	0.71667	65.649	62.5958
Mean	0.4097217	0.7486117	64.637	58.548
SD	0.0188905	0.0269679	0.4744	1.89761

PO

Stance Time

REP	Left	Right	IS (50%)	IS (0%)
1	1.875	1.53333	44.9877	20.0491
2	1.86667	1.525	44.9631	20.1476
3	1.86667	1.51667	44.8276	20.6896
4	1.85833	1.5	44.6651	21.3398
5	1.85	1.48333	44.4999	22.0002
6	1.84167	1.475	44.4723	22.1107
Mean	1.859723	1.505555	44.736	21.0562
SD	0.011197	0.0213367	0.20559	0.82237

CO

Stance Time

REP	Left	Right	IS (50%)	IS (0%)
1	1.94167	1.65	45.9396	16.2415
2	1.93333	1.65	46.0466	15.8138
3	1.925	1.64167	46.0281	15.8876
4	1.925	1.55	44.6043	21.5827
5	1.90833	1.54167	44.6861	21.2557
6	1.89167	1.54167	44.9029	20.3883
Mean	1.9208333	1.595835	45.3679	18.5283
SD	0.0164919	0.0515381	0.64387	2.57549

	Left	Right
Step Length PO	0.17	0.24
Step Length CO	0.18	0.26
Swing Time PO	0.36	0.71
Swing Time CO	0.41	0.75
Stance Time PO	1.86	1.51
Stance Time CO	1.92	1.60

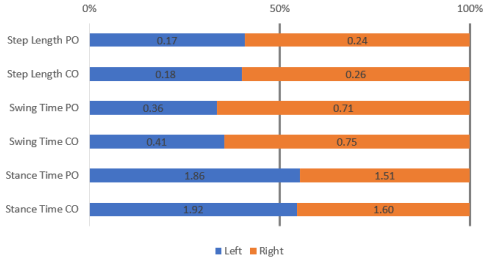

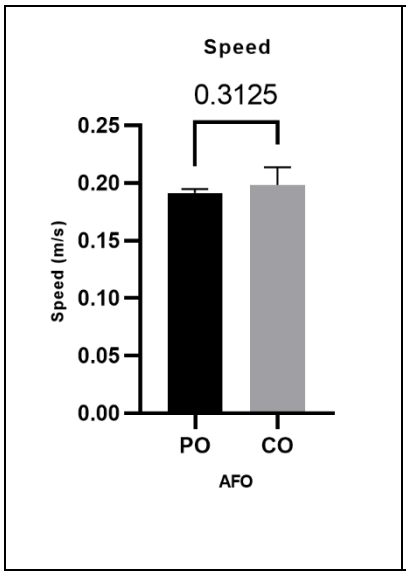

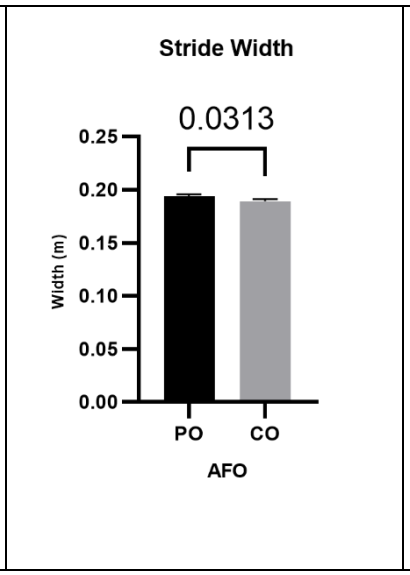

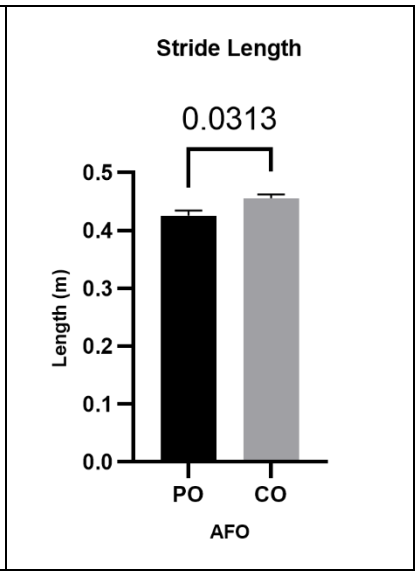

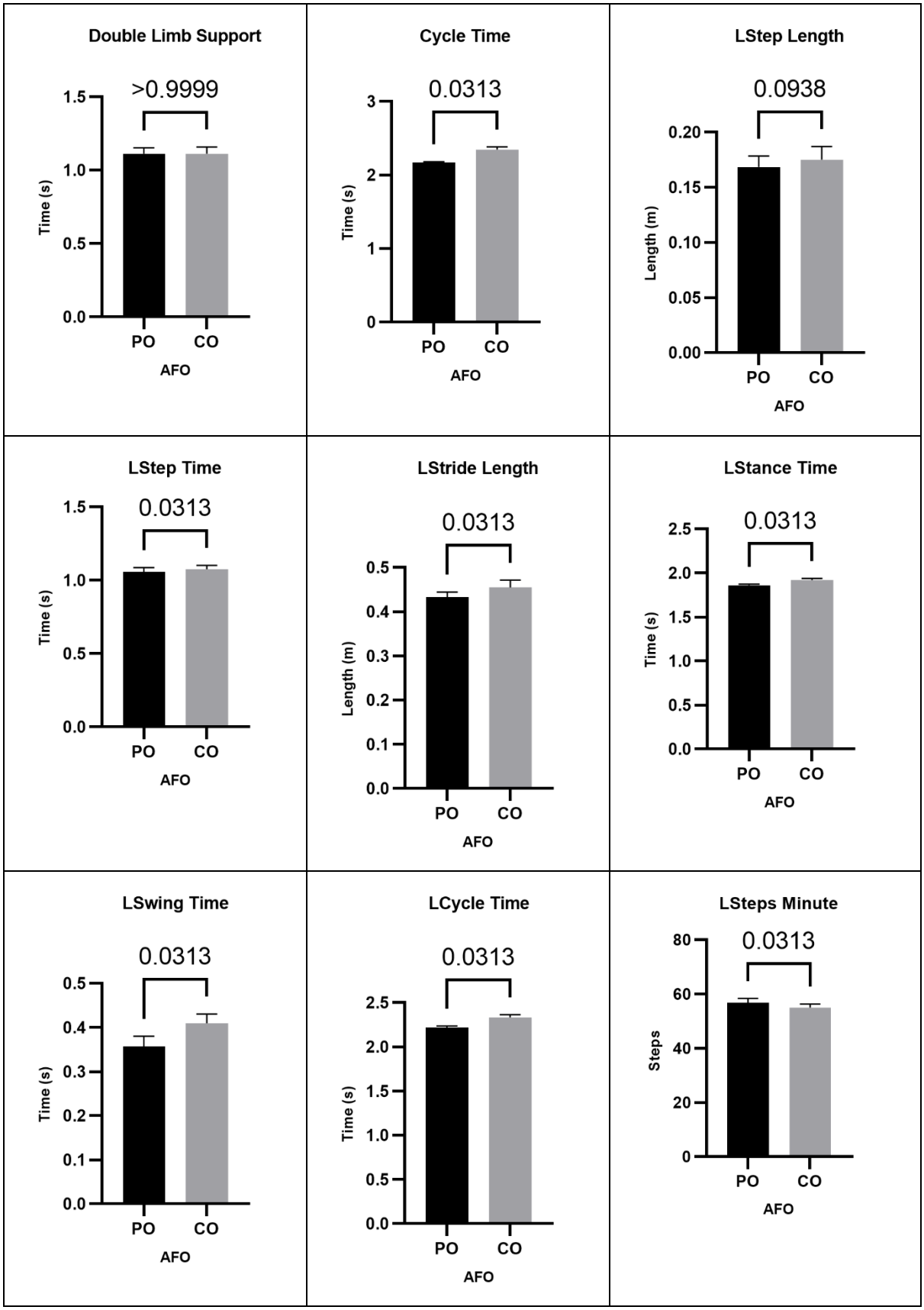
Double Limb Support
>0.9999
Time (s)
1.5
1.0
0.5
0.0
PO
CO
AFO
Cycle Time
0.0313
Time (s)
3
2
1
0
PO
CO
AFO
LStep Length
0.0938
Length (m)
0.20
0.15
0.10
0.05
0.00
PO
CO
AFO
LStep Time
0.0313
Time (s)
1.5
1.0
0.5
0.0
PO
CO
AFO
LStride Length
0.0313
Length (m)
0.5
0.4
0.3
0.2
0.1
0.0
PO
CO
AFO
LStance Time
0.0313
Time (s)
2.5
2.0
1.5
1.0
0.5
0.0
PO
CO
AFO
LSwing Time
0.0313
Time (s)
0.5
0.4
0.3
0.2
0.1
0.0
PO
CO
AFO
LCycle Time
0.0313
Time (s)
2.5
2.0
1.5
1.0
0.5
0.0
PO
CO
AFO
LSteps Minute
0.0313
Steps
80
60
40
20
0
PO
CO
AFO

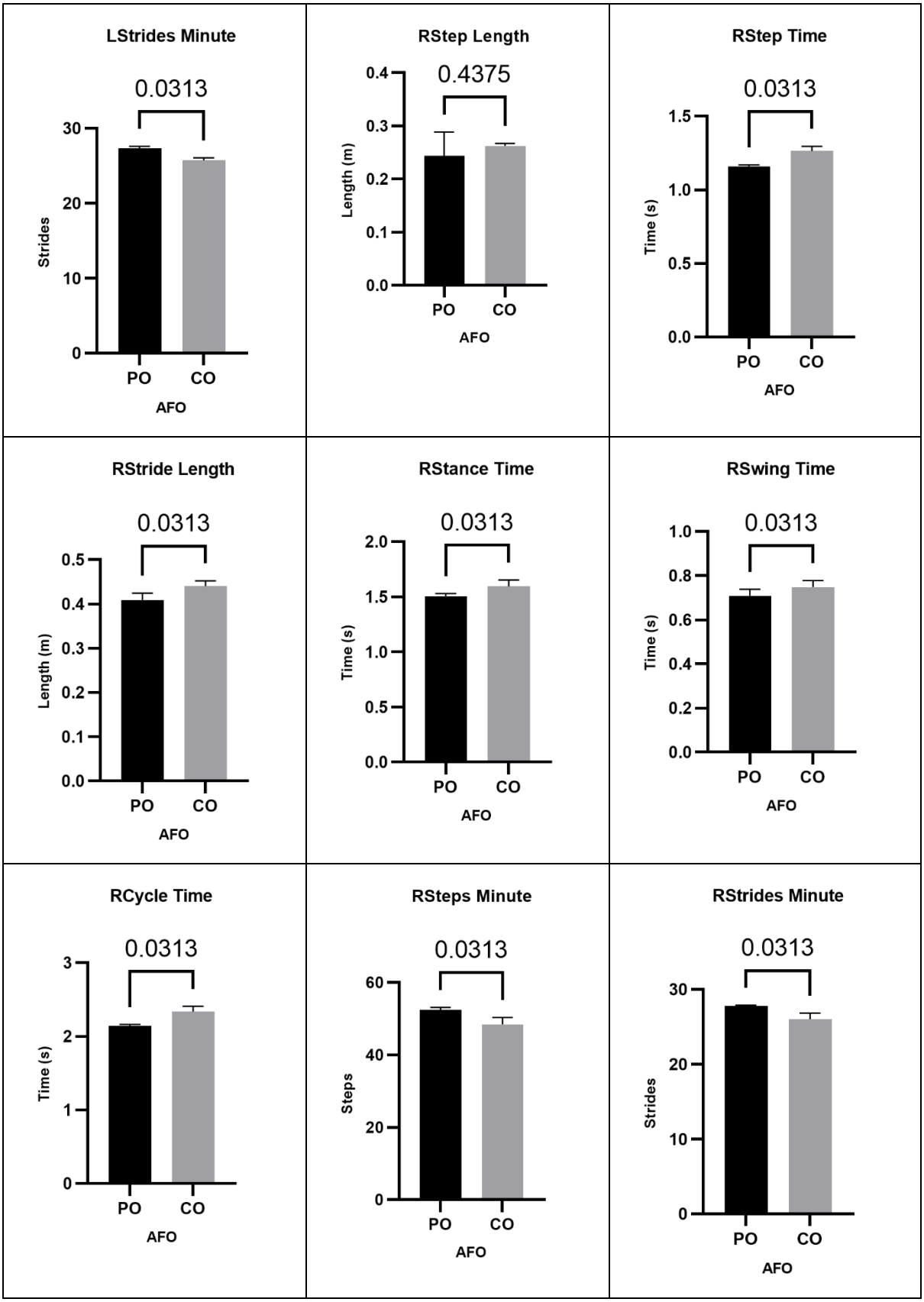
LStrides Minute
0.0313
Strides
30
20
10
0
PO
CO
AFO
RStep Length
0.4375
Length (m)
0.4
0.3
0.2
0.1
0.0
PO
CO
AFO
RStep Time
0.0313
Time (s)
1.5
1.0
0.5
0.0
PO
CO
AFO
RStride Length
0.0313
Length (m)
0.5
0.4
0.3
0.2
0.1
0.0
PO
CO
AFO
RStance Time
0.0313
Time (s)
2.0
1.5
1.0
0.5
0.0
PO
CO
AFO
RSwing Time
0.0313
Time (s)
1.0
0.8
0.6
0.4
0.2
0.0
PO
CO
AFO
RCycle Time
0.0313
Time (s)
3
2
1
0
PO
CO
AFO
RSteps Minute
0.0313
Steps
60
40
20
0
PO
CO
AFO
RStrides Minute
0.0313
Strides
30
20
10
0
PO
CO
AFO

PATIENT 8

Right Pelvic Angles X

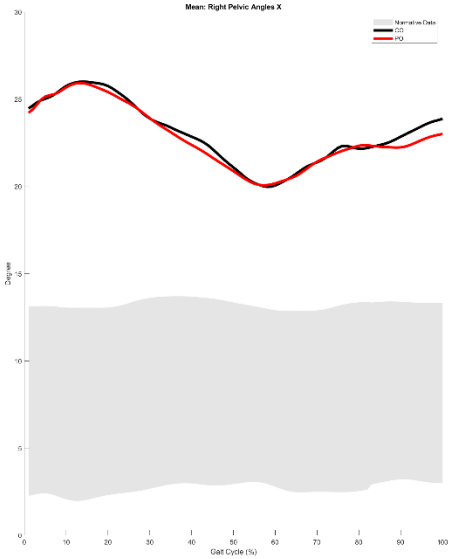

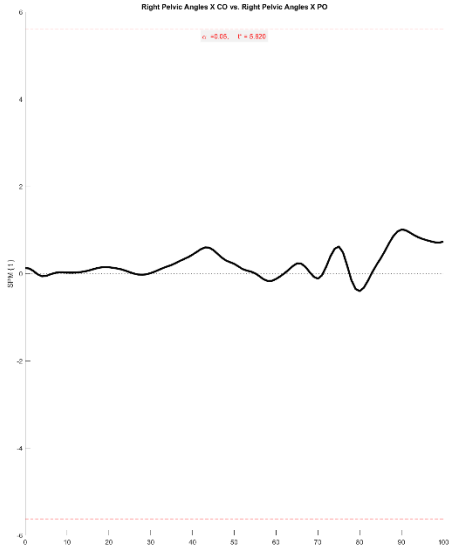

Right Pelvic Angles Y

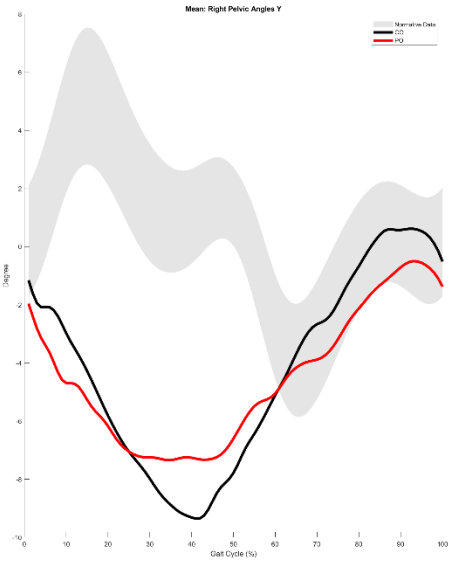

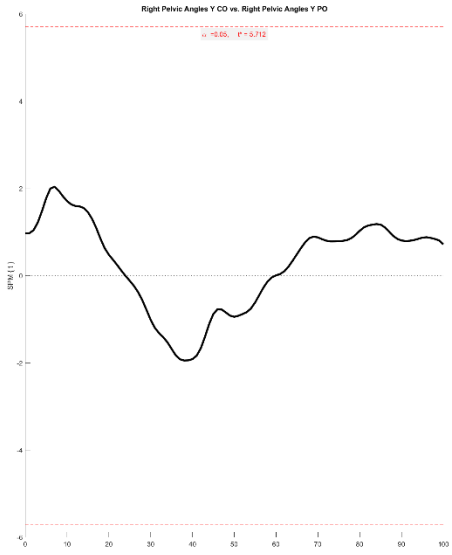

Right Pelvic Angles Z

0.0-5.1%

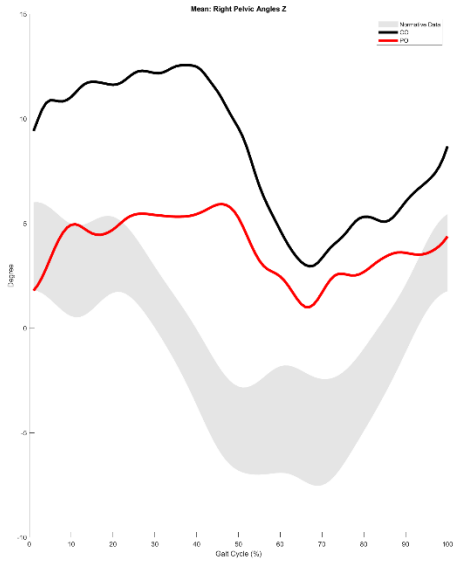

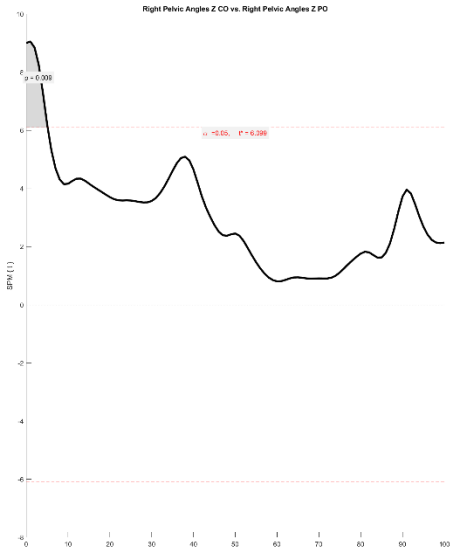

Left Pelvic Angles X

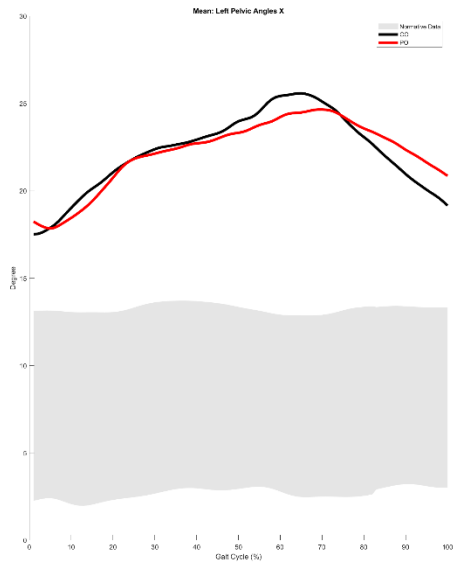

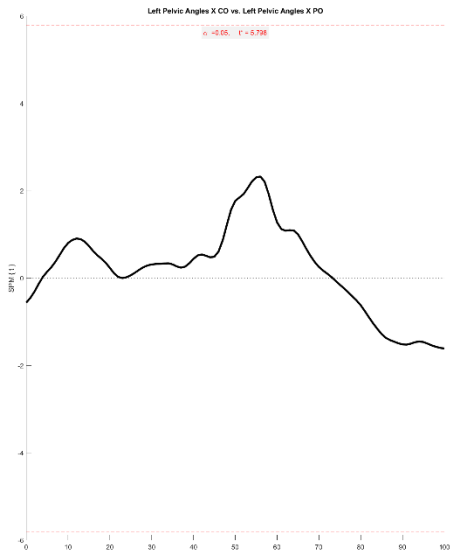

Left Pelvic Angles Y

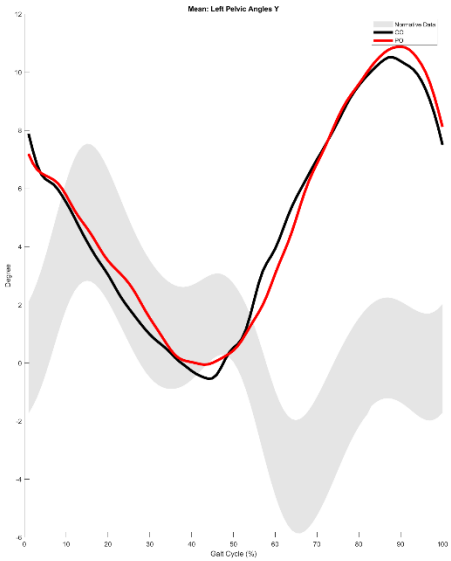

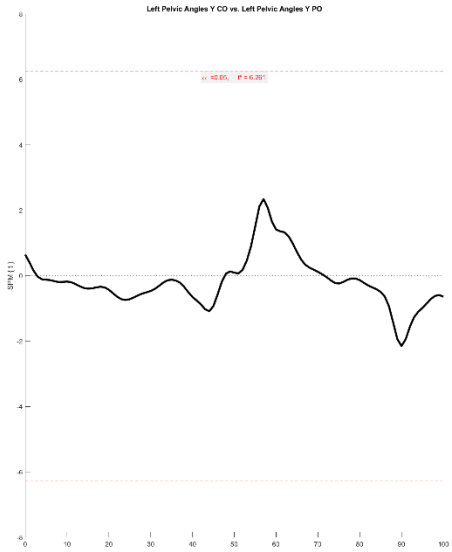

Left Pelvic Angles Z

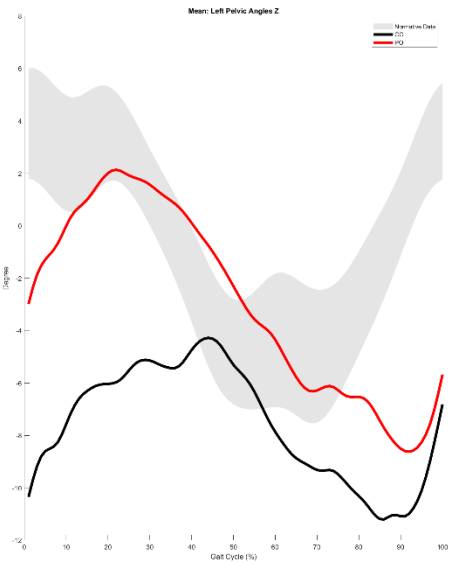

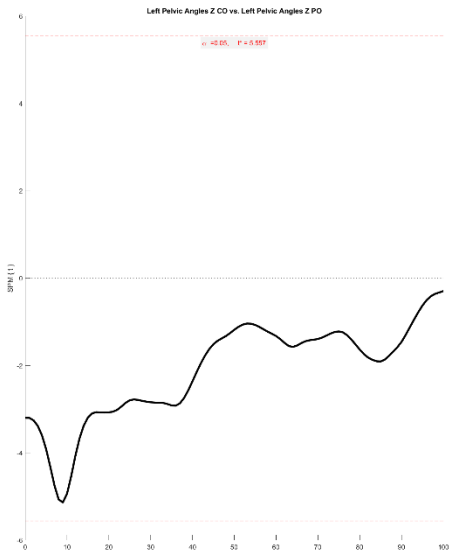

Right Hip Angles X

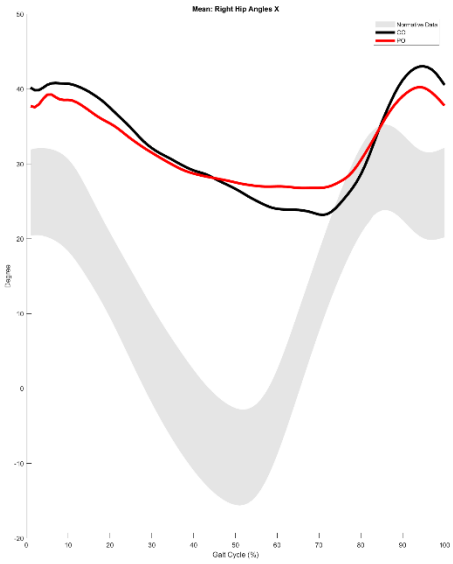

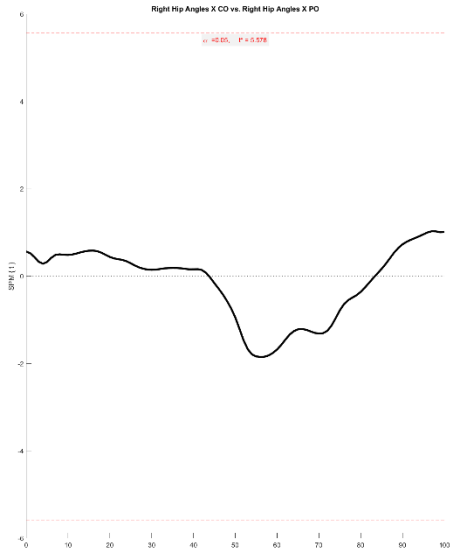

Right Hip Angles Y

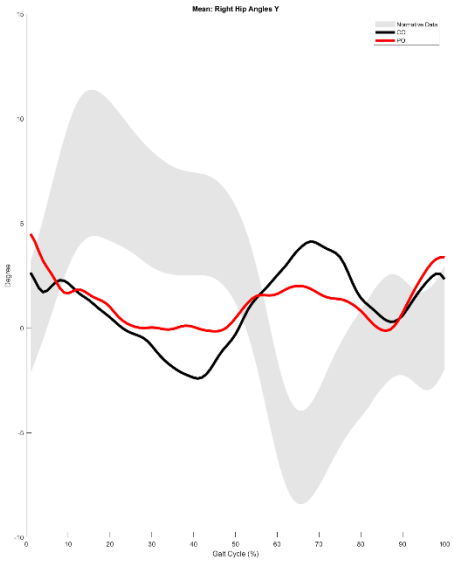

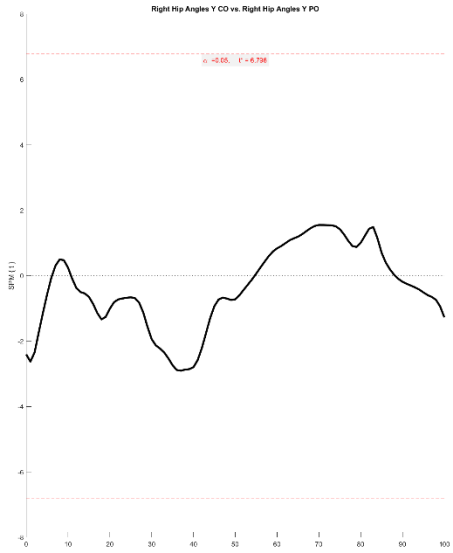

Right Hip Angles Z

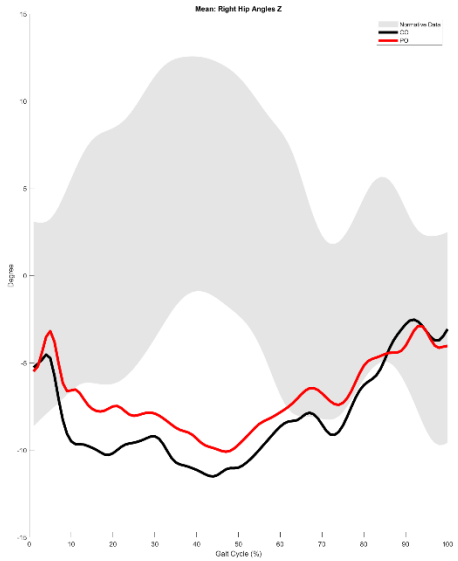

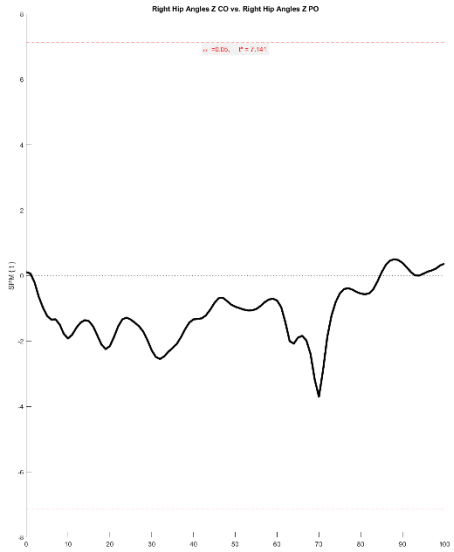

Left Hip Angles X

76.5-91.8%

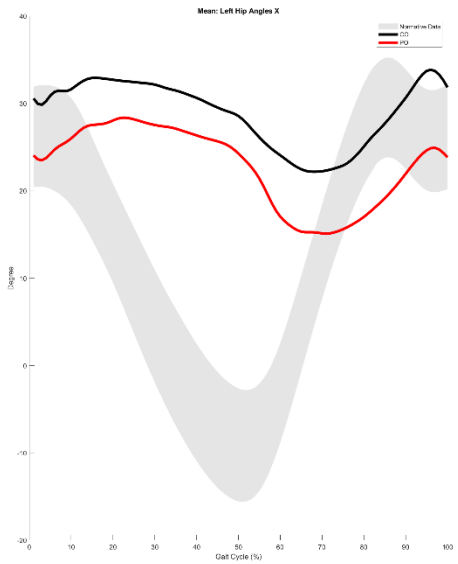

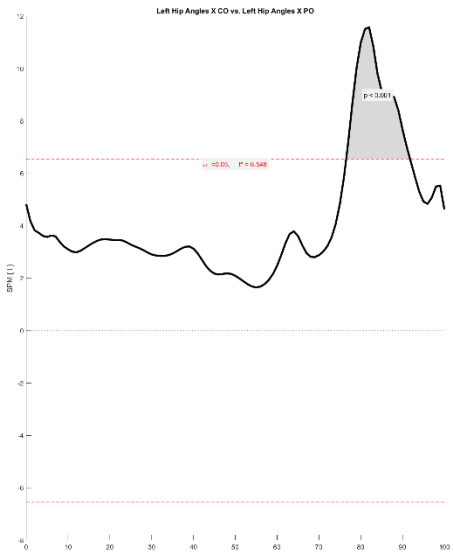

Left Hip Angles Y

99.9-100.0%

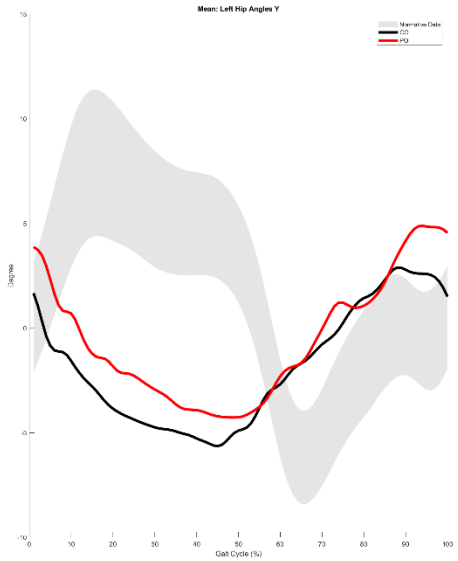

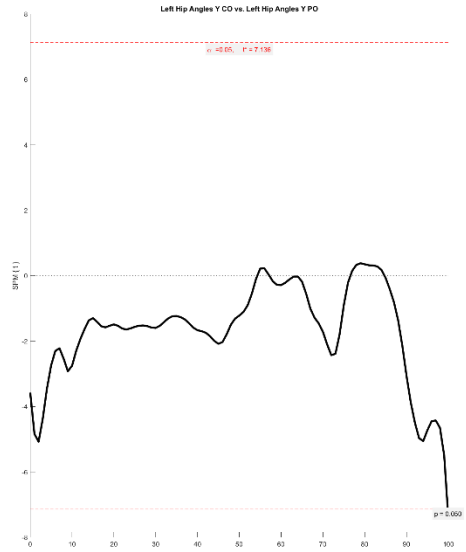

Left Hip Angles Z

0.0-4.7%, 32.4-56.2%, 94.9-98.7%

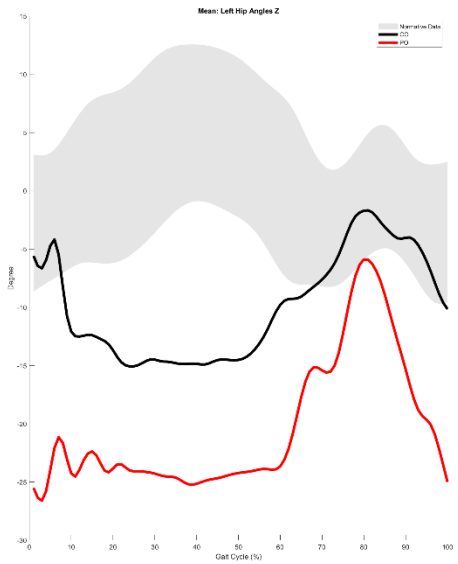

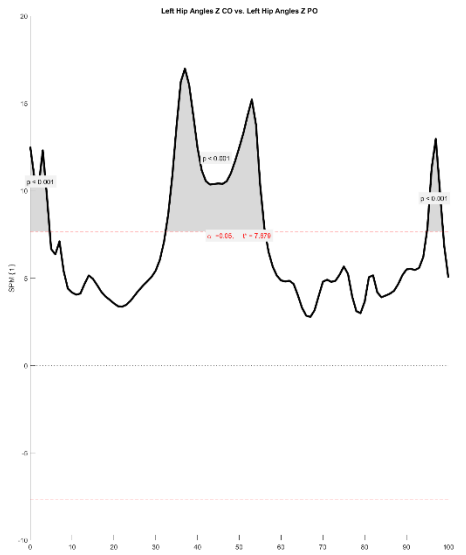

Right Knee Angles X

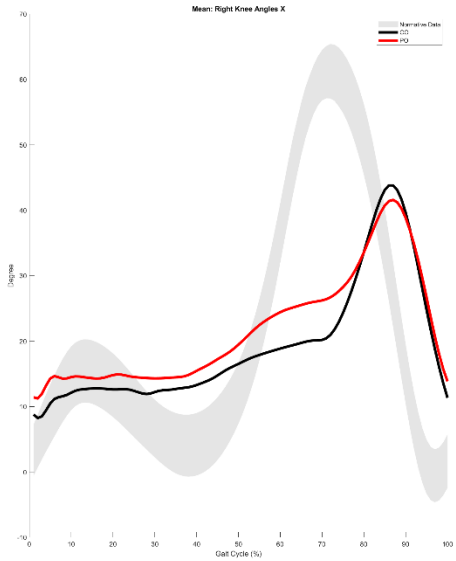

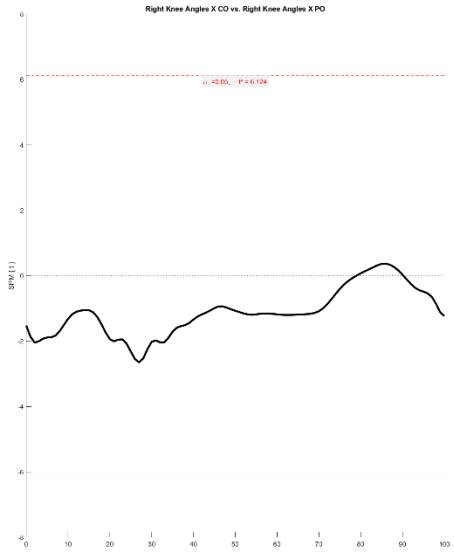

Right Knee Angles Y

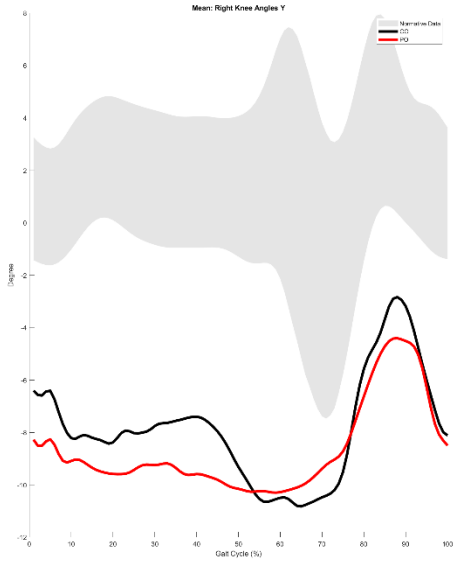

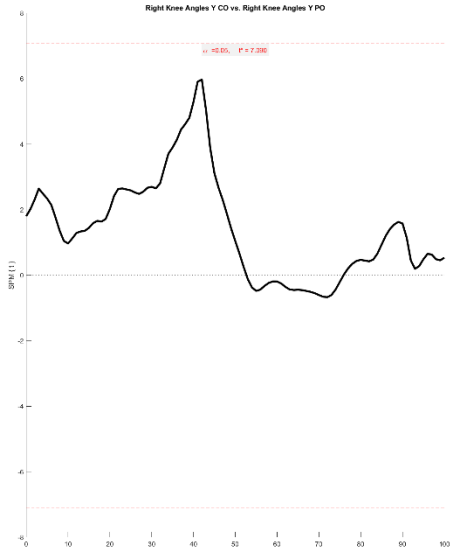

Right Knee Angles Z

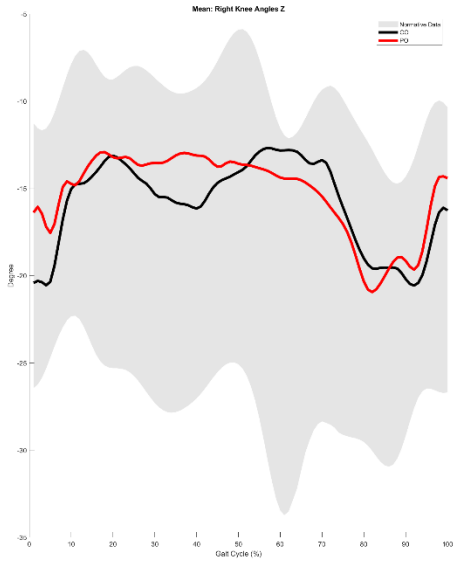

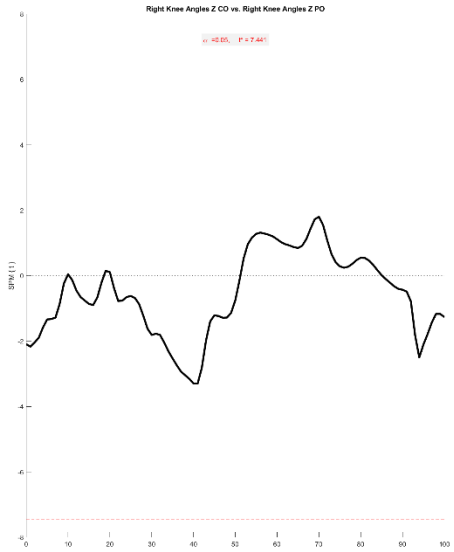

Left Knee Angles X

26.5-28.3%, 38.5-43.7%

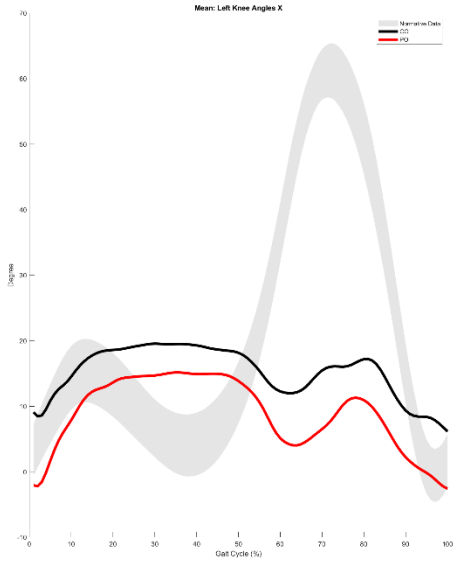

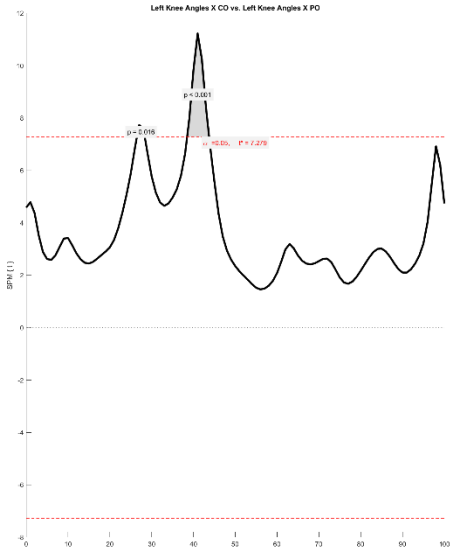

Left Knee Angles Y

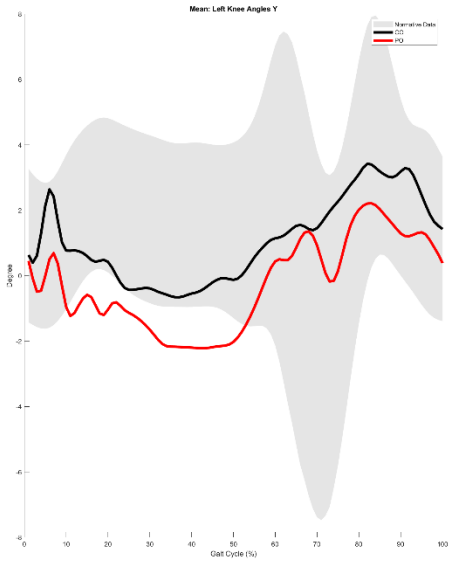

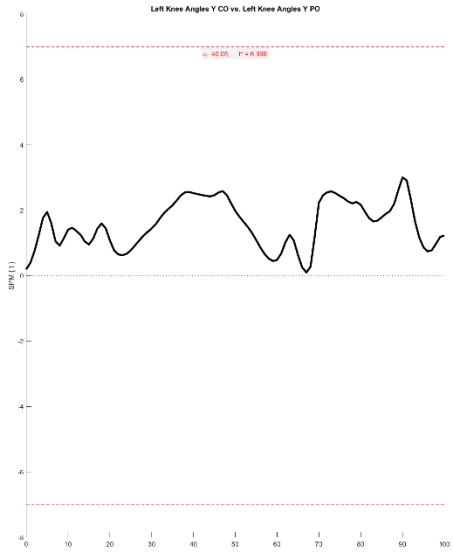

Left Knee Angles Z

88.7-99.7%

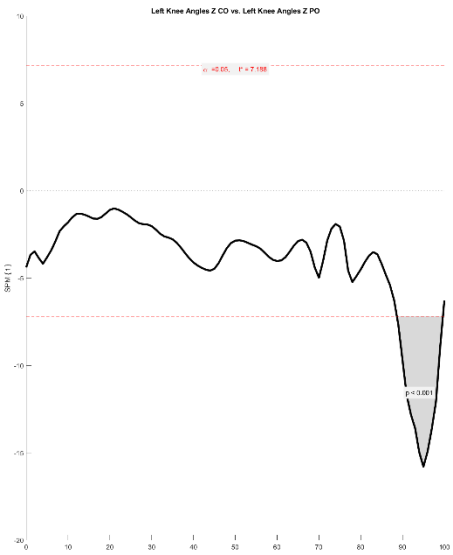

Right Ankle Angles X

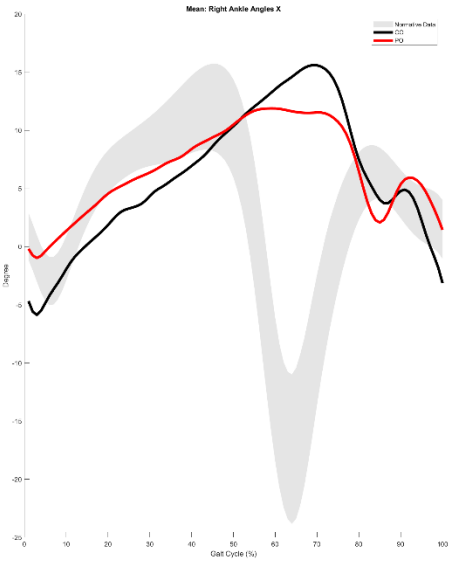

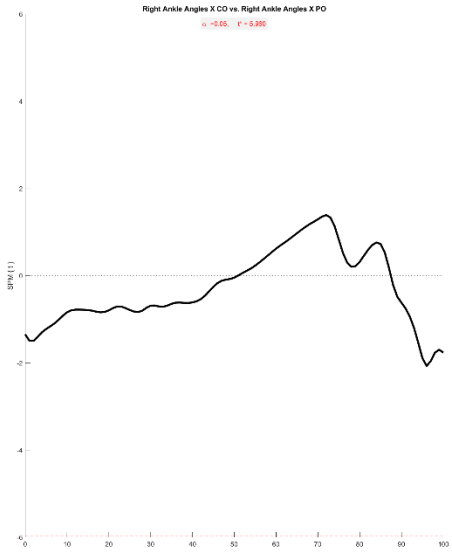

Right Ankle Angles Y

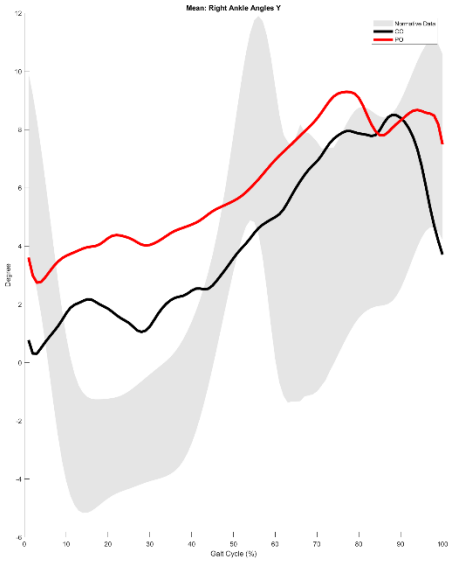

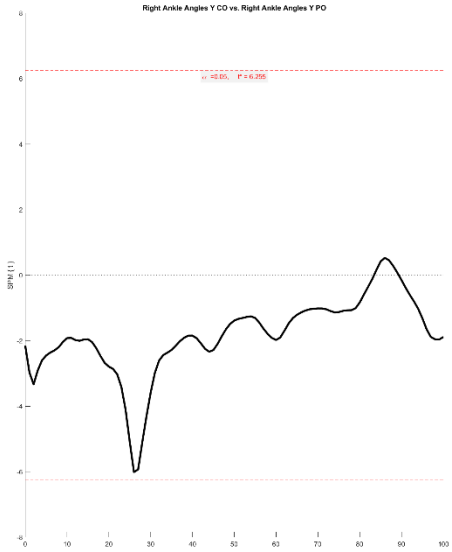

Left Ankle Angles X

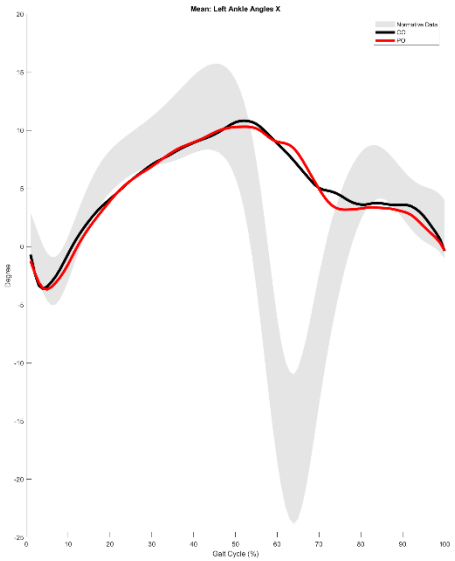

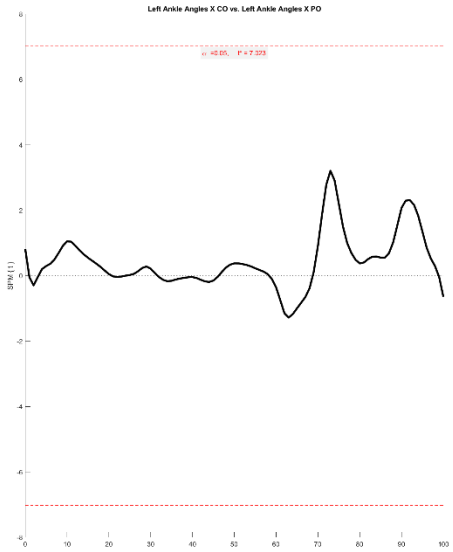

Left Ankle Angles Y

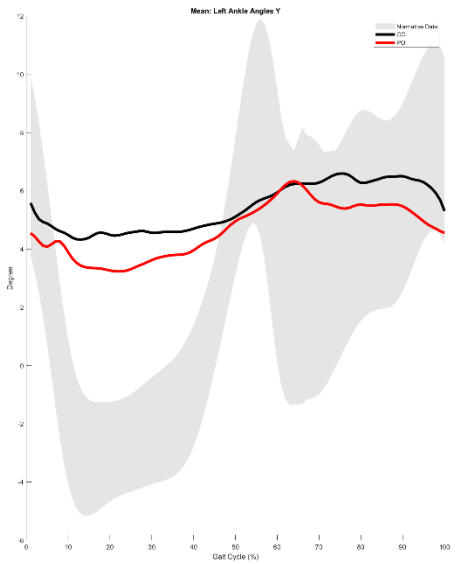

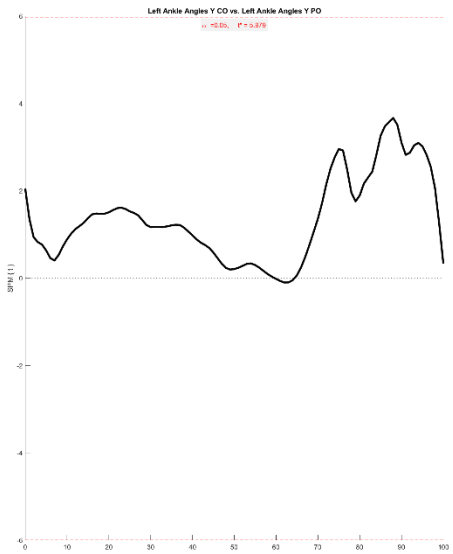

Right Foot Pitch Angles X

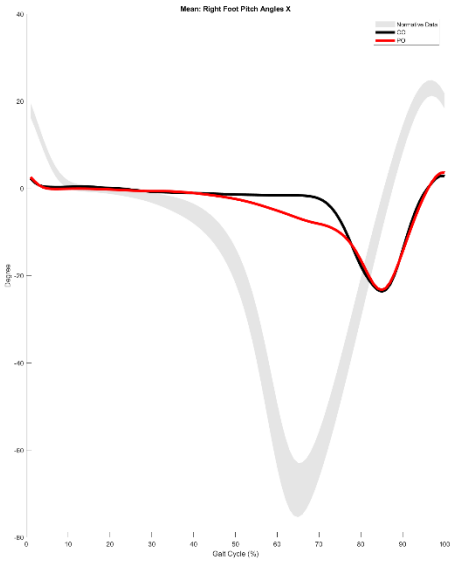

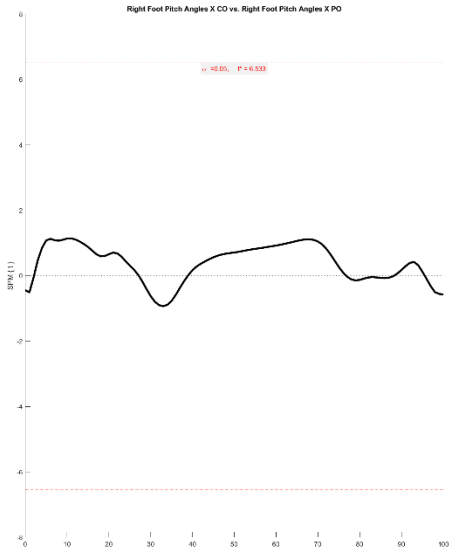

Left Foot Pitch Angles X

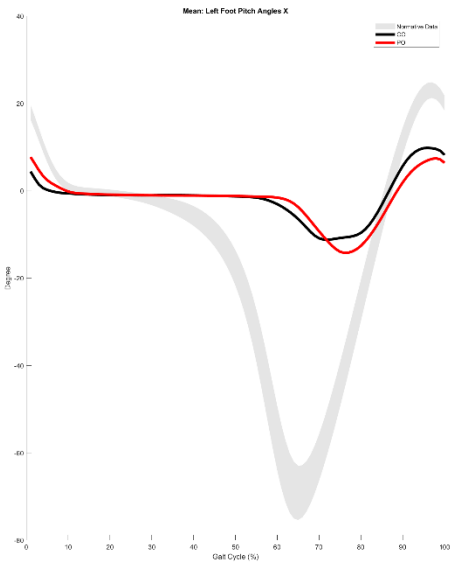

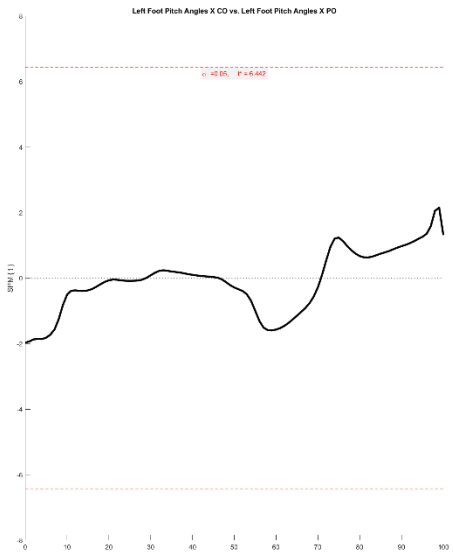

Right Foot Progression Z

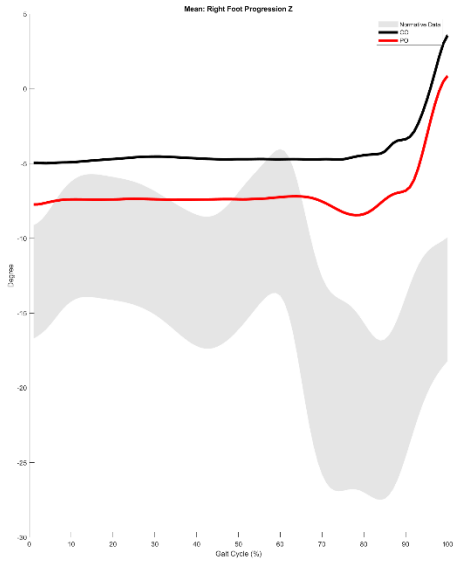

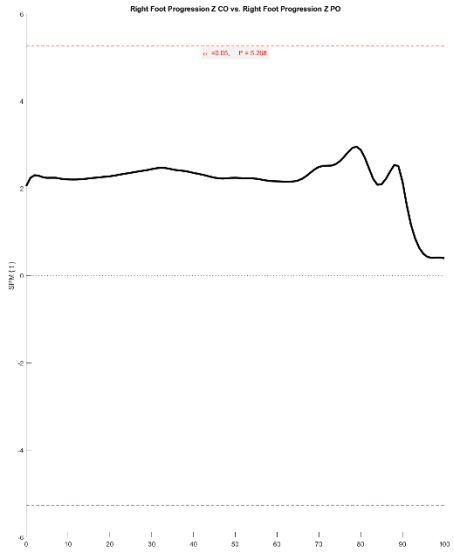

Left Foot Progression Z

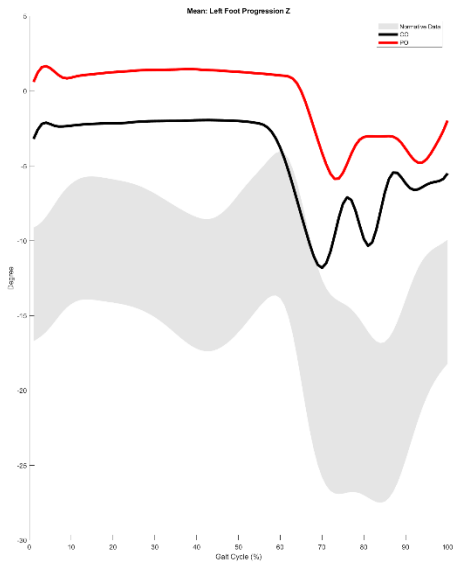

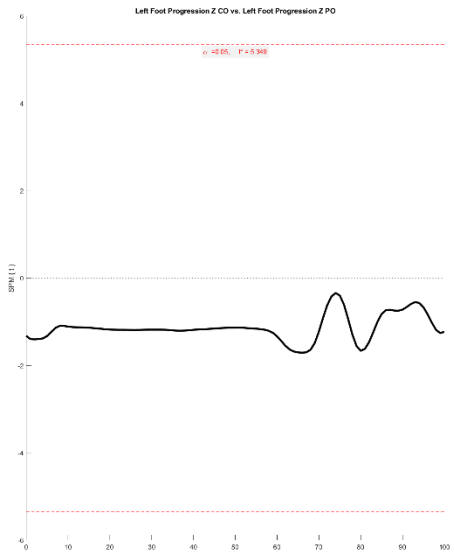

Right Hip Moment X

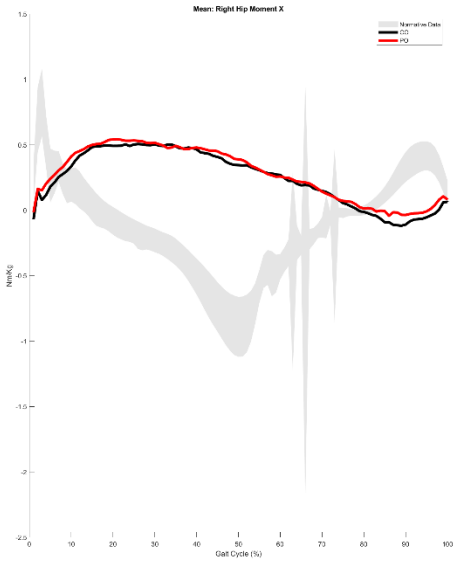

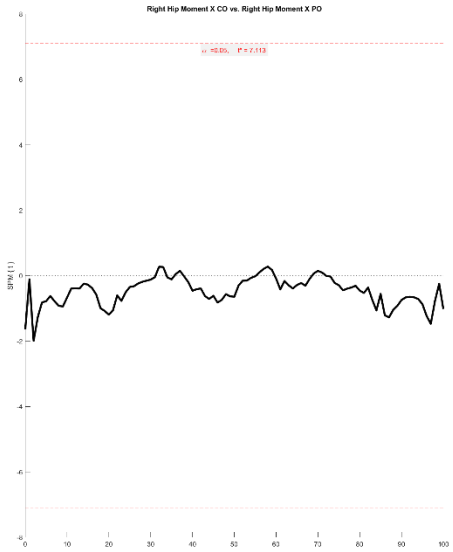

Right Hip Moment Y

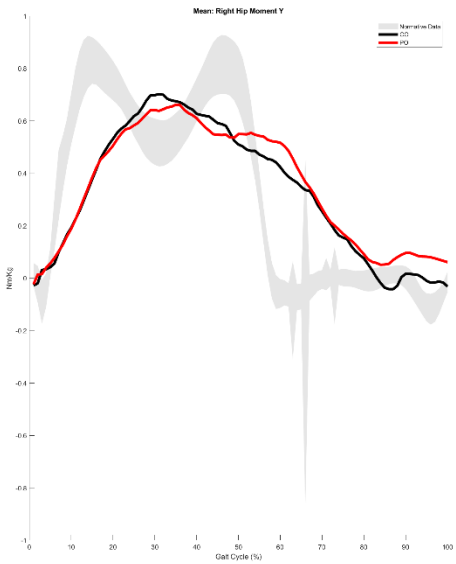

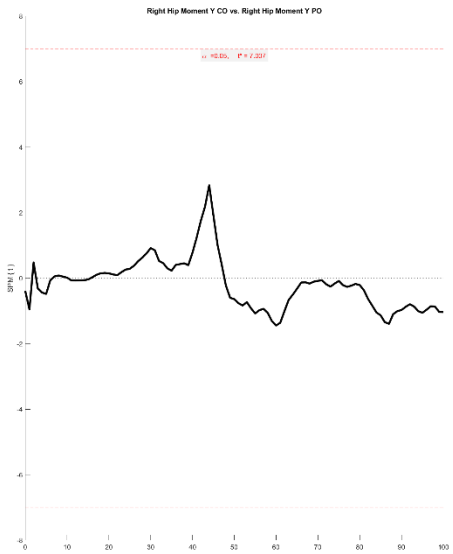

Left Hip Moment X

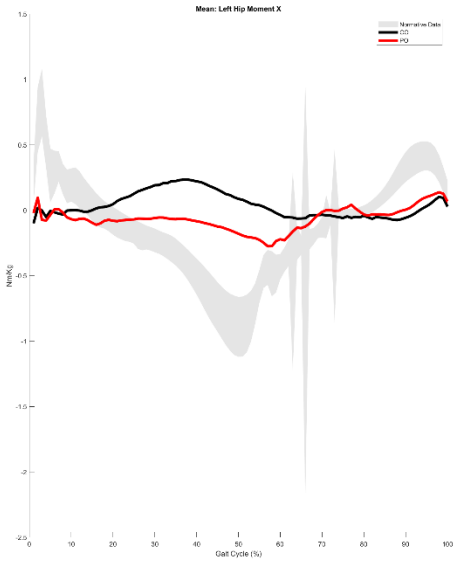

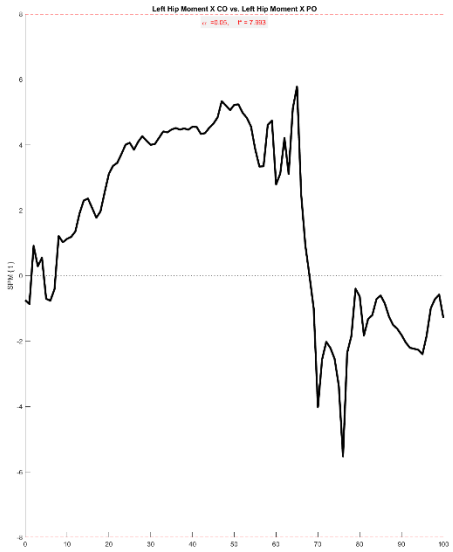

Left Hip Moment Y

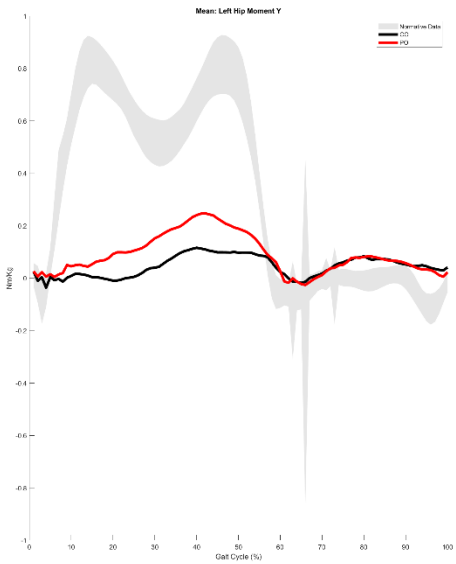

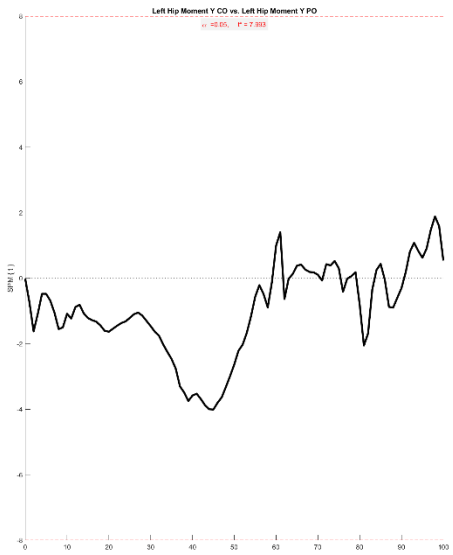

Right Knee Moment X

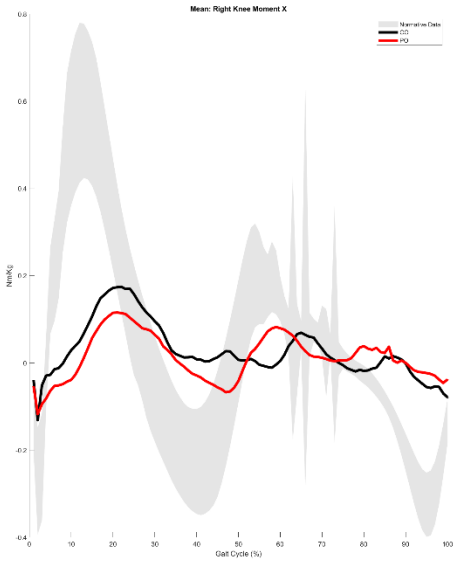

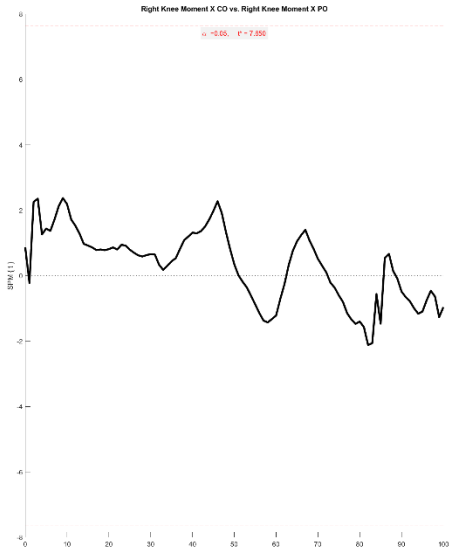

Right Knee Moment Y

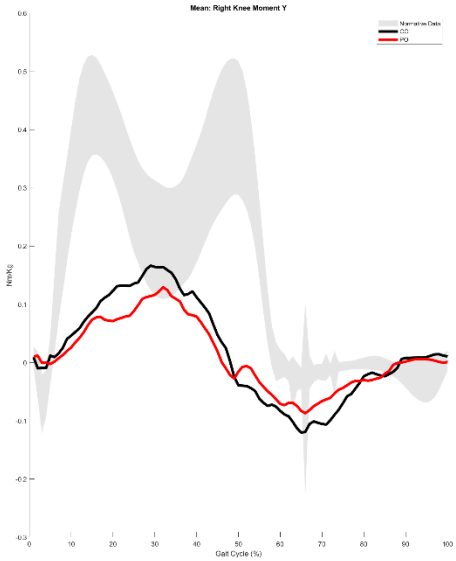

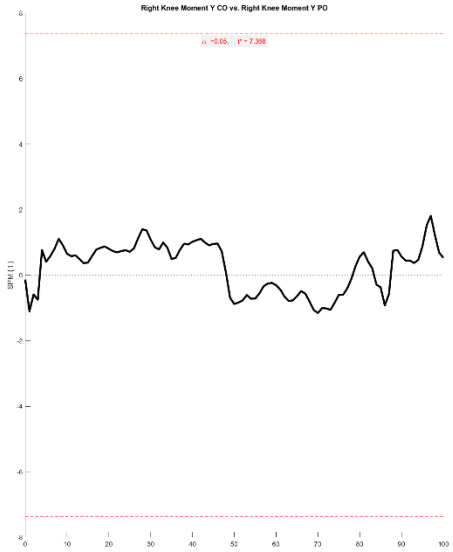

Left Knee Moment X

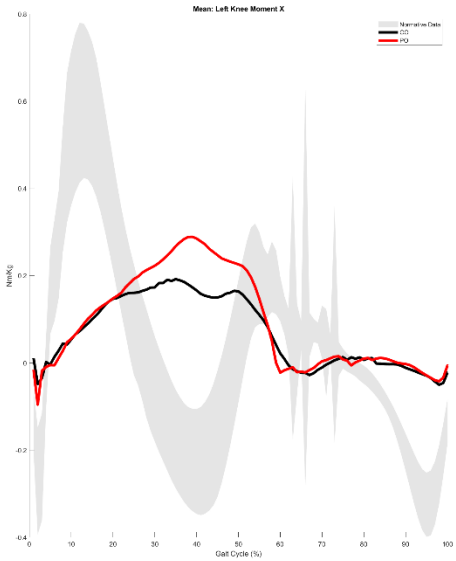

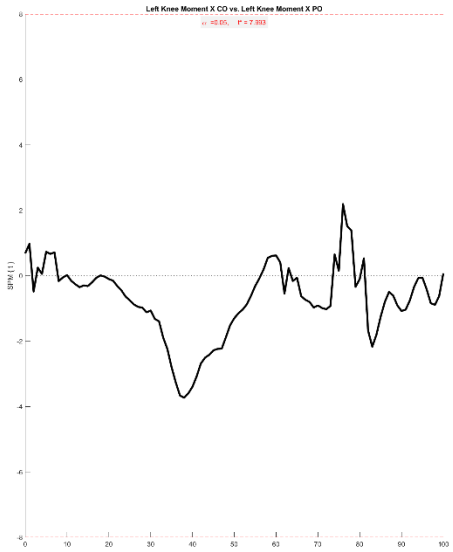

Left Knee Moment Y

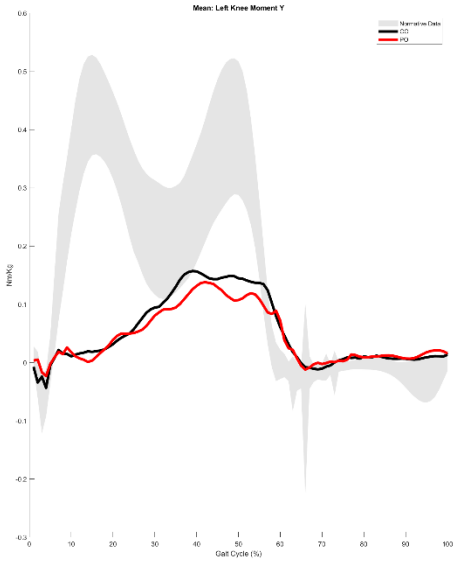

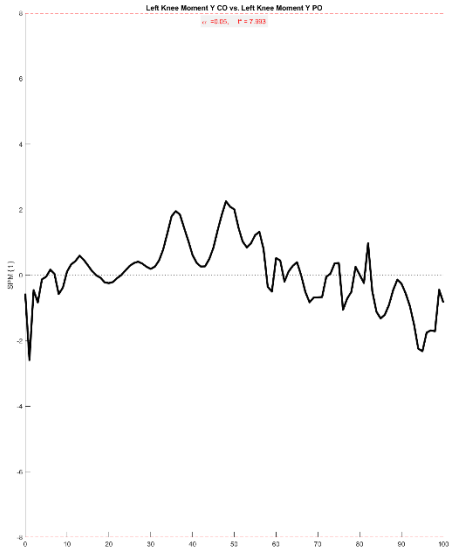

Right Ankle Moment X

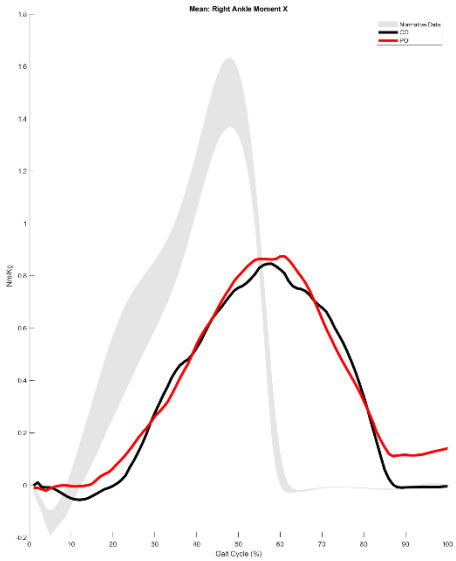

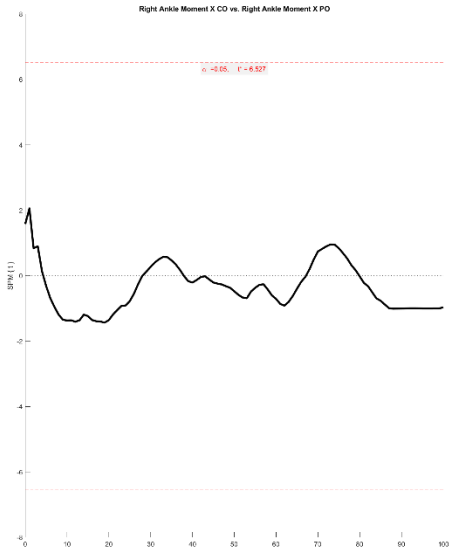

Right Ankle Moment Y

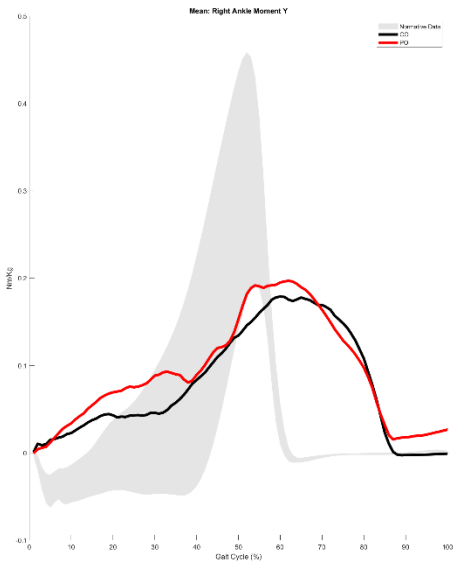

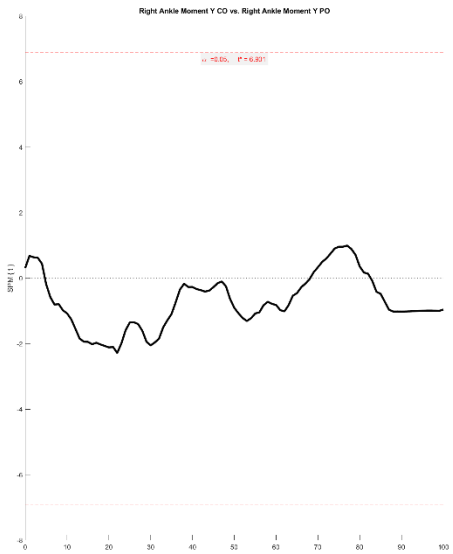

Left Ankle Moment X

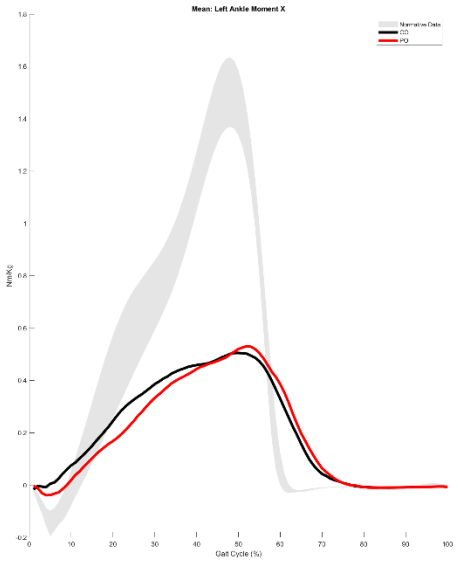

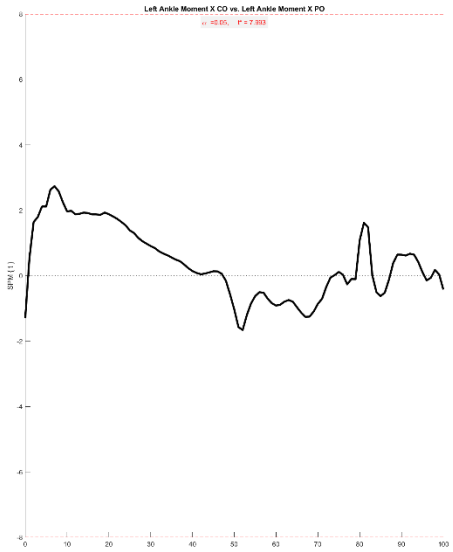

Left Ankle Moment Y

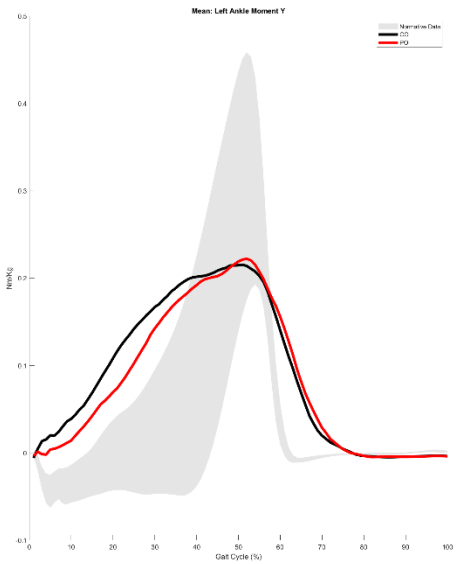

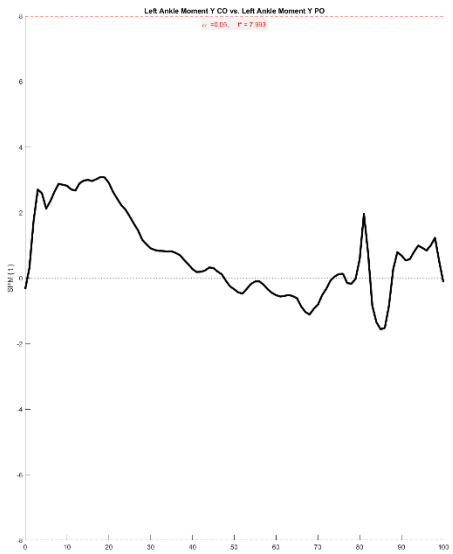

PO

Step Length

REP	Left	Right	IS (50%)	IS (0%)
1	0.26721	0.29505	52.4757	9.90289
2	0.25223	0.29217	53.6683	14.673
3	0.23018	0.28885	55.6519	22.6076
4	0.18555	0.28591	60.6435	42.5741
5	0.17779	0.28085	61.2354	44.9416
6	0.17102	0.28027	62.1042	48.4168
Mean	0.213997	0.2871833	57.6298	30.5193
SD	0.037688	0.0054628	3.83566	15.3426

CO

Step Length

REP	Left	Right	IS (50%)	IS (0%)
1	0.28193	0.28996	50.7021	2.80823
2	0.2463	0.26926	52.2267	8.90682
3	0.24596	0.26257	51.6331	6.53255
4	0.23858	0.25671	51.8302	7.32096
5	0.2211	0.24321	52.381	9.52381
6	0.21141	0.23212	52.3347	9.33871
Mean	0.24088	0.2589717	51.8513	7.40518
SD	0.0223804	0.0185006	0.58079	2.32316

PO

Swing Time

REP	Left	Right	IS (50%)	IS (0%)
1	0.79167	0.56667	41.7178	33.1287
2	0.73333	0.55833	43.2258	27.0969
3	0.71667	0.54167	43.0464	27.8144
4	0.68333	0.54167	44.218	23.1282
5	0.68333	0.525	43.4484	26.2064
6	0.64167	0.50833	44.2026	23.1896
Mean	0.708333	0.5402783	43.3098	26.7607
SD	0.047141	0.0194952	0.84181	3.36724

CO

Swing Time

REP	Left	Right	IS (50%)	IS (0%)
1	0.84167	0.525	38.4145	46.3418
2	0.84167	0.525	38.4145	46.3418
3	0.80833	0.50833	38.6075	45.5699
4	0.74167	0.49167	39.8649	40.5403
5	0.70833	0.48333	40.5594	37.7624
6	0.68333	0.475	41.0073	35.9708
Mean	0.7708333	0.5013883	39.478	42.0878
SD	0.0630551	0.019494	1.05495	4.21979

PO

Stance Time

REP	Left	Right	IS (50%)	IS (0%)
1	2.2	2.25833	50.6542	2.61667
2	2.19167	2.25833	50.749	2.99596
3	2.125	2.23333	51.2428	4.97117
4	2.09167	2.16667	50.8806	3.5225
5	2.075	2.00833	49.1836	3.26547
6	2.01667	1.975	49.478	2.08785
Mean	2.116668	2.1499983	50.3647	3.24327
SD	0.064549	0.1164674	0.75826	0.89934

CO

Stance Time

REP	Left	Right	IS (50%)	IS (0%)
1	2.075	2.16667	51.0806	4.32235
2	2.04167	2.05833	50.2032	0.81268
3	1.975	2.05	50.9317	3.72671
4	1.9	2.01667	51.4894	5.95761
5	1.88333	1.94167	50.7626	3.05046
6	1.85833	1.85	49.8877	0.44926
Mean	1.955555	2.01389	50.7259	3.05318
SD	0.0814622	0.0989141	0.5367	1.92788

	Left	Right
Step Length PO	0.21	0.29
Step Length CO	0.24	0.26
Swing Time PO	0.71	0.54
Swing Time CO	0.77	0.50
Stance Time PO	2.12	2.15
Stance Time CO	1.96	2.01

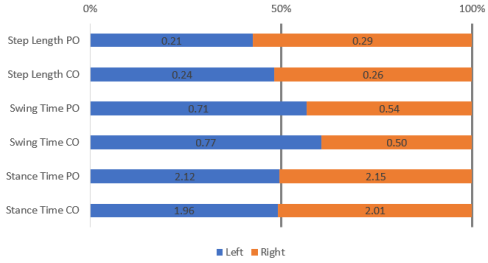

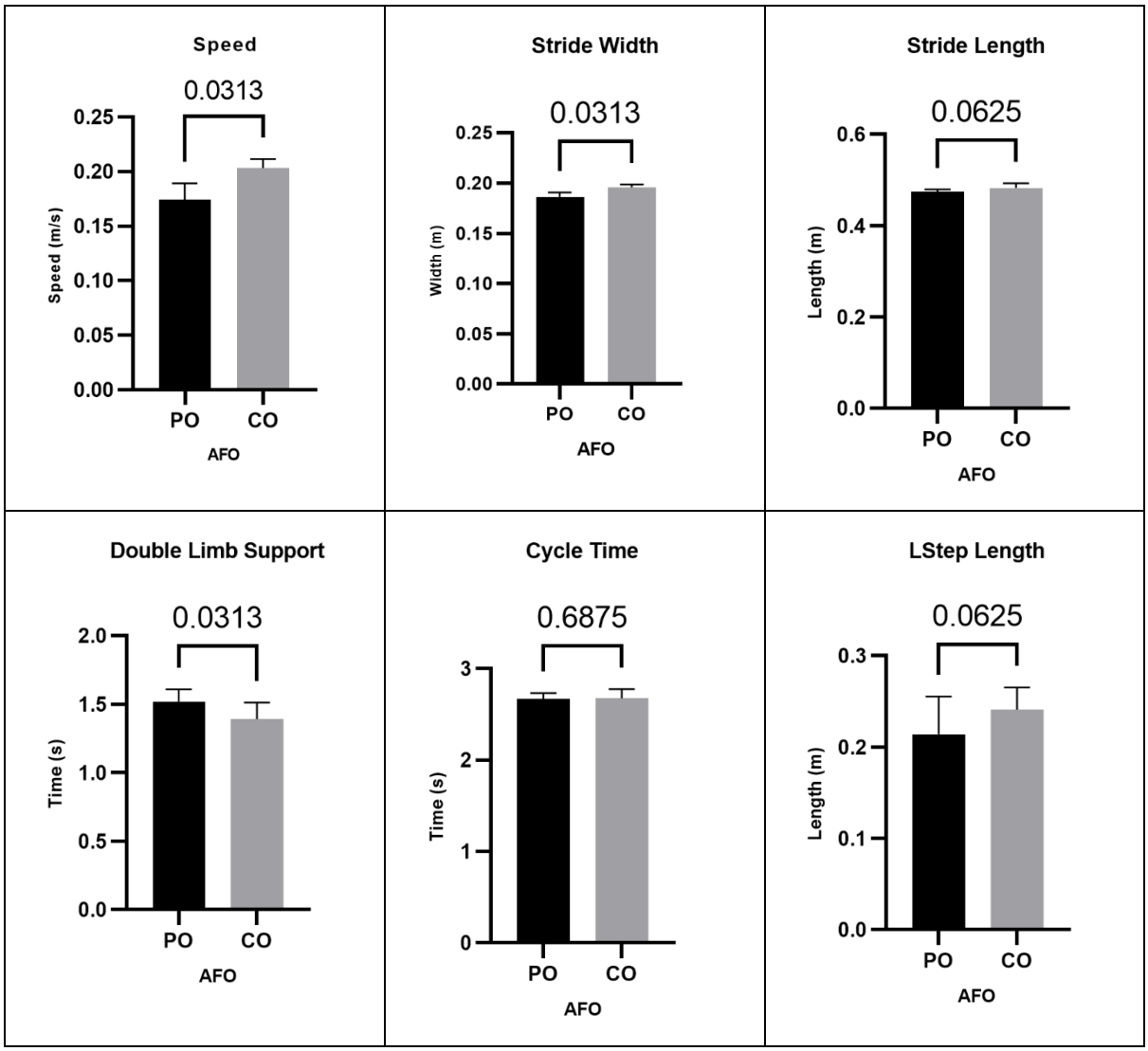

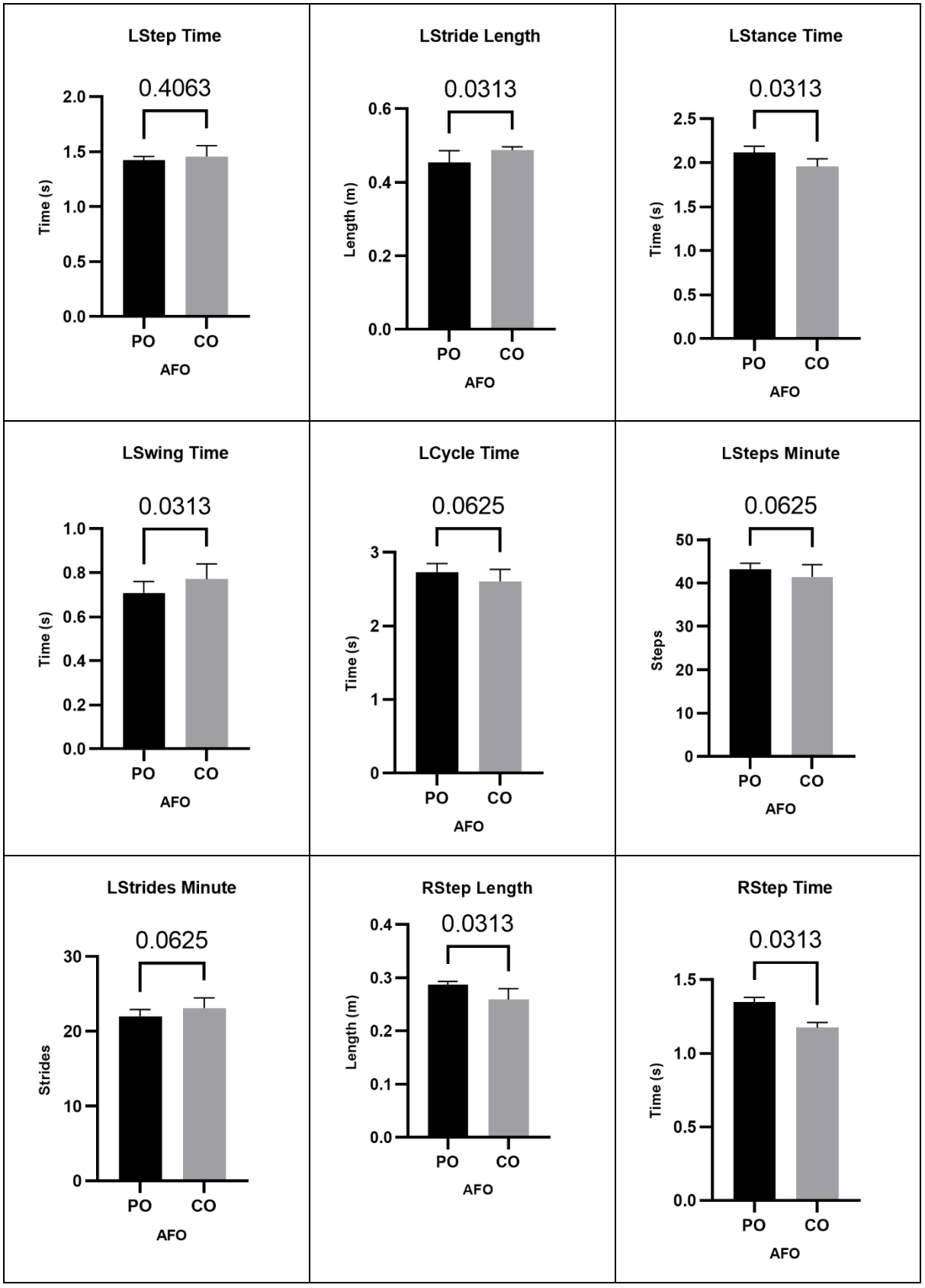
LStep Time
0.4063
Time (s)
2.0
1.5
1.0
0.5
0.0
PO
CO
AFO
LStride Length
0.0313
Length (m)
0.6
0.4
0.2
0.0
PO
CO
AFO
LStance Time
0.0313
Time (s)
2.5
2.0
1.5
1.0
0.5
0.0
PO
CO
AFO
LSwing Time
0.0313
Time (s)
1.0
0.8
0.6
0.4
0.2
0.0
PO
CO
AFO
LCycle Time
0.0625
Time (s)
3
2
1
0
PO
CO
AFO
LSteps Minute
0.0625
Steps
50
40
30
20
10
0
PO
CO
AFO
LStrides Minute
0.0625
Strides
30
20
10
0
PO
CO
AFO
RStep Length
0.0313
Length (m)
0.4
0.3
0.2
0.1
0.0
PO
CO
AFO
RStep Time
0.0313
Time (s)
1.5
1.0
0.5
0.0
PO
CO
AFO

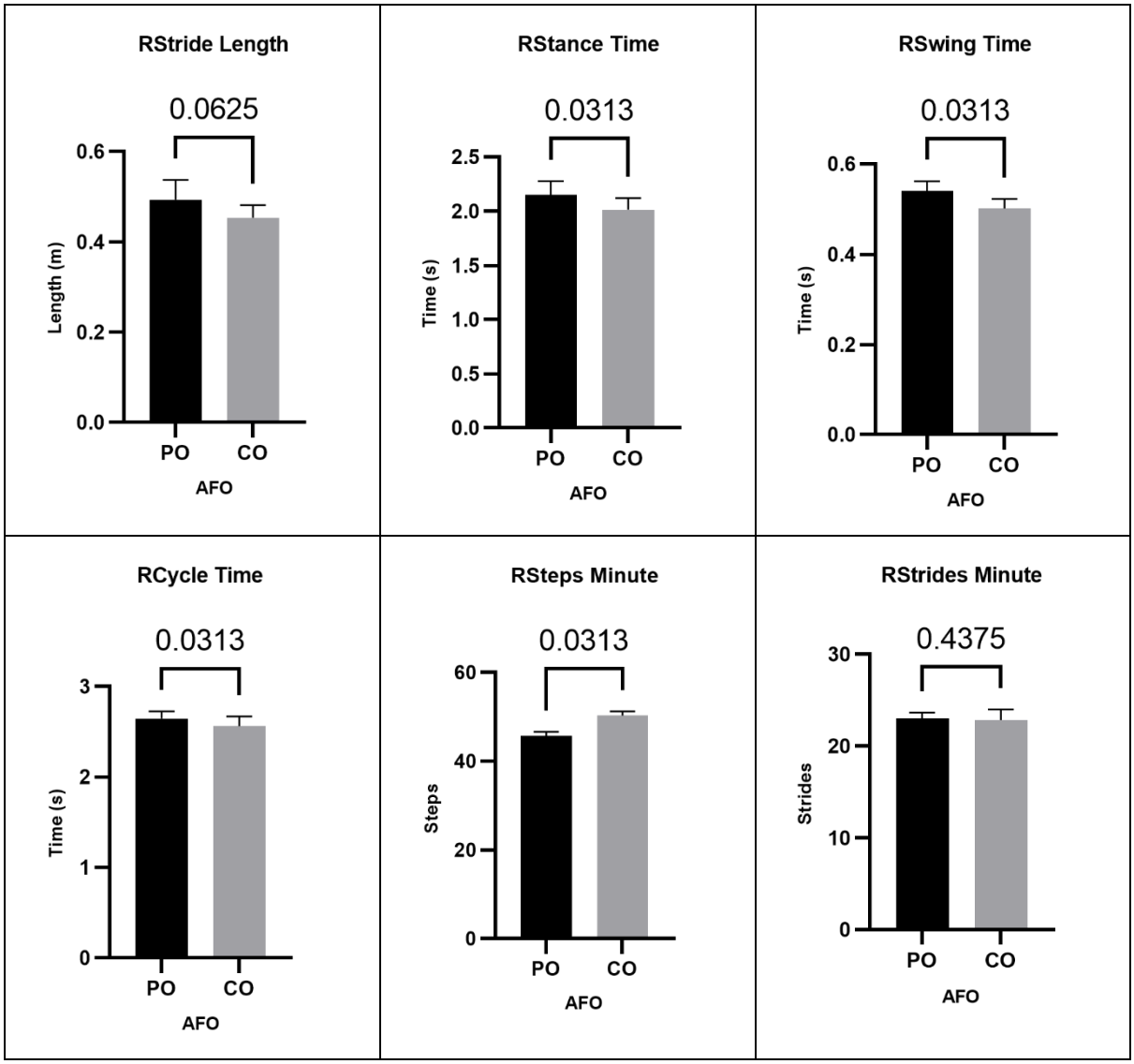
RStride Length
0.0625
Length (m)
0.6
0.4
0.2
0.0
PO
CO
AFO
RStance Time
0.0313
Time (s)
2.5
2.0
1.5
1.0
0.5
0.0
PO
CO
AFO
RSwing Time
0.0313
Time (s)
0.6
0.4
0.2
0.0
PO
CO
AFO
RCycle Time
0.0313
Time (s)
3
2
1
0
PO
CO
AFO
RSteps Minute
0.0313
Steps
60
40
20
0
PO
CO
AFO
RStrides Minute
0.4375
Strides
30
20
10
0
PO
CO
AFO

PATIENT 9

Right Pelvic Angles X

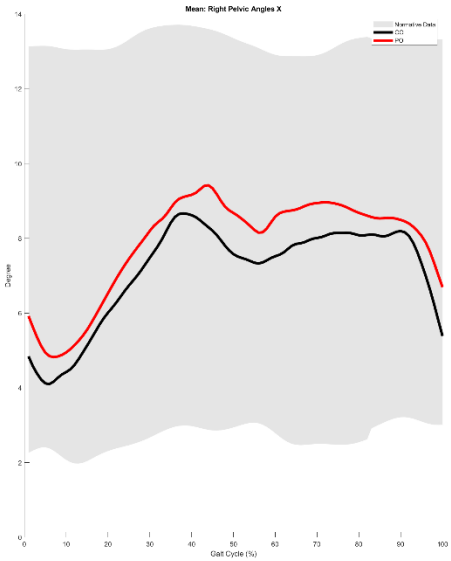

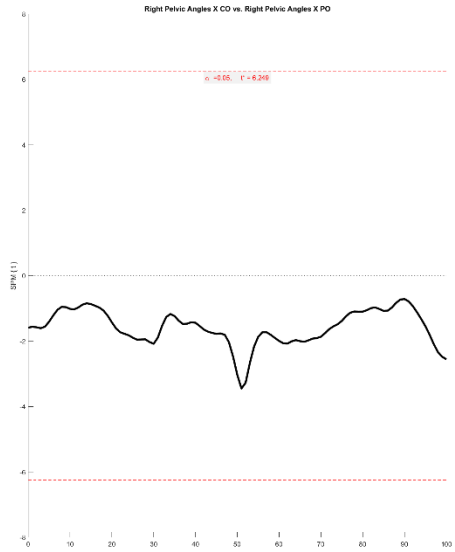

Right Pelvic Angles Y

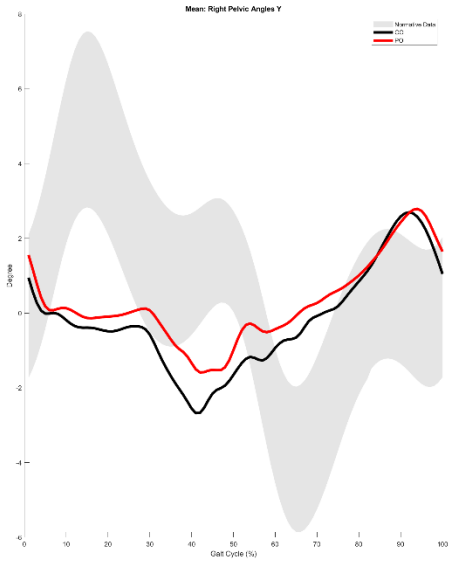

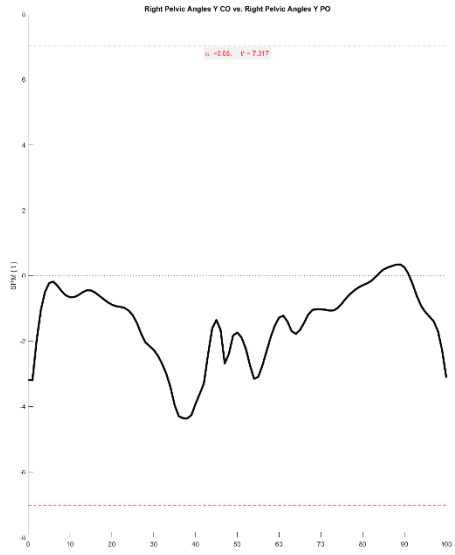

Right Pelvic Angles Z

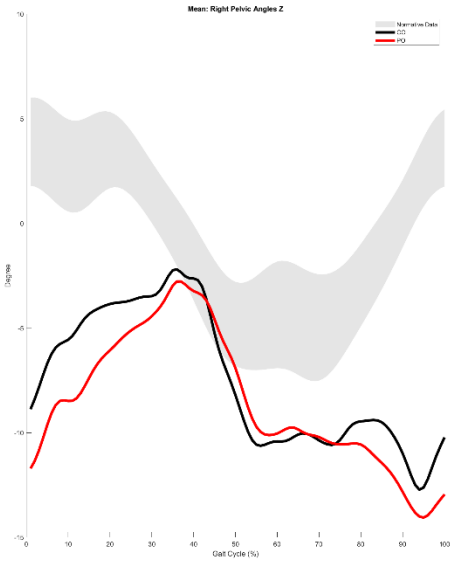

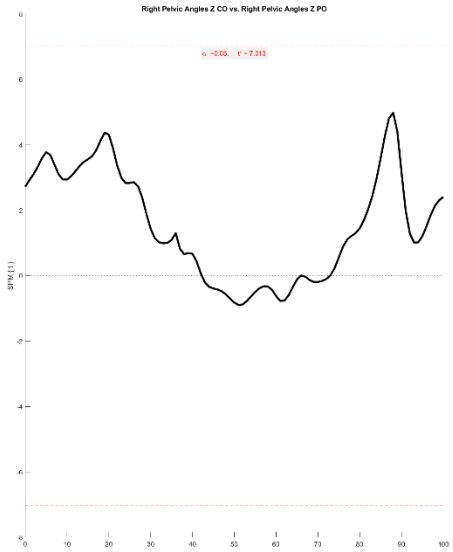

Left Pelvic Angles X

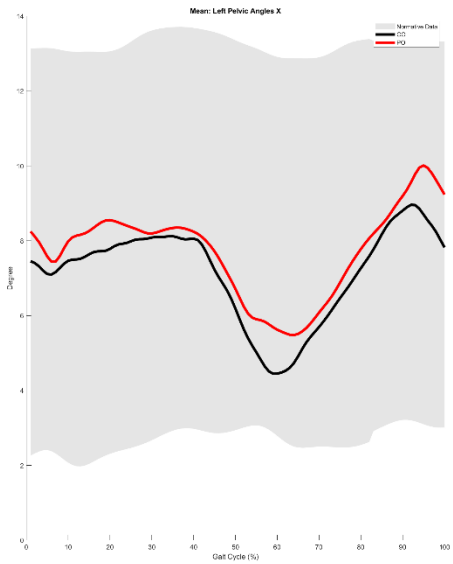

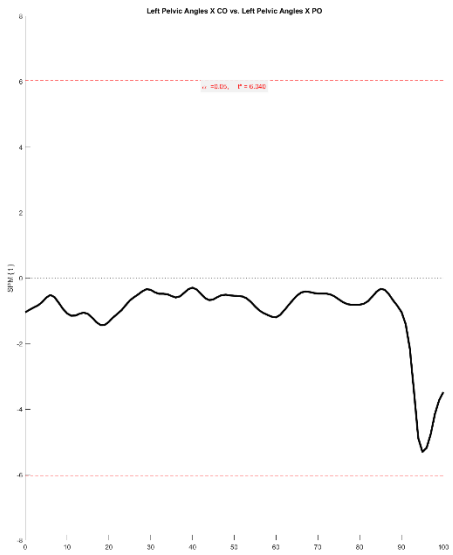

Left Pelvic Angles Y

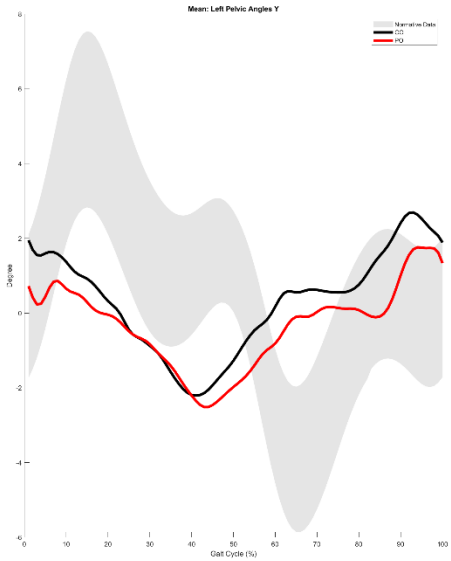

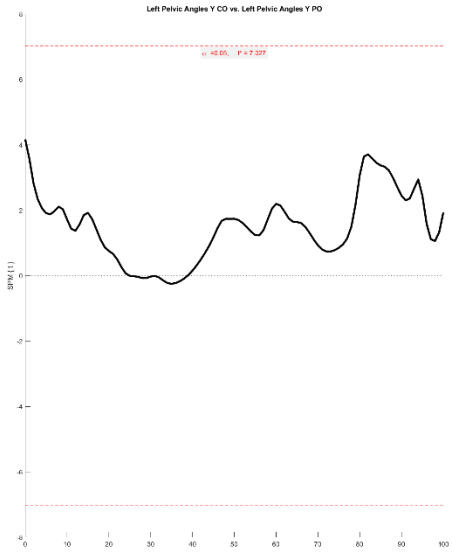

Left Pelvic Angles Z

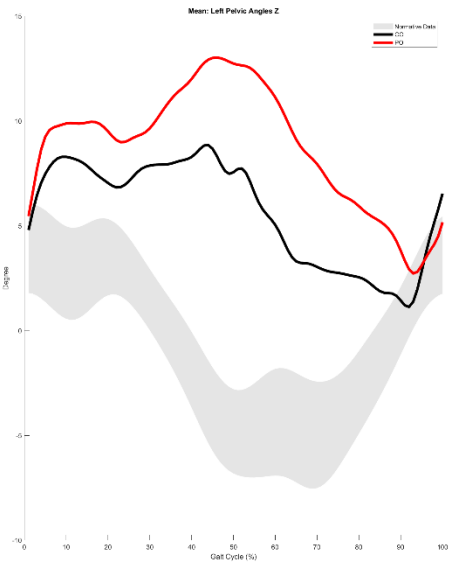

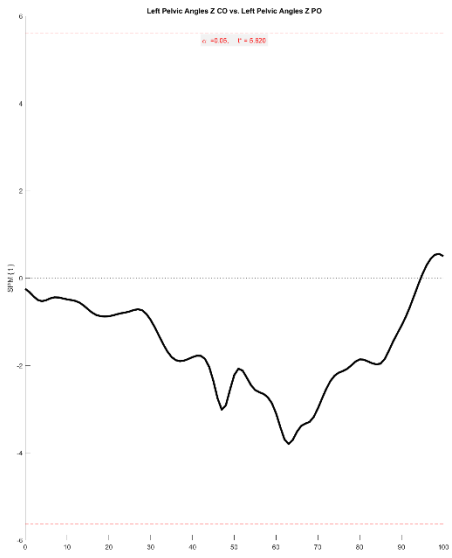

Right Hip Angles X

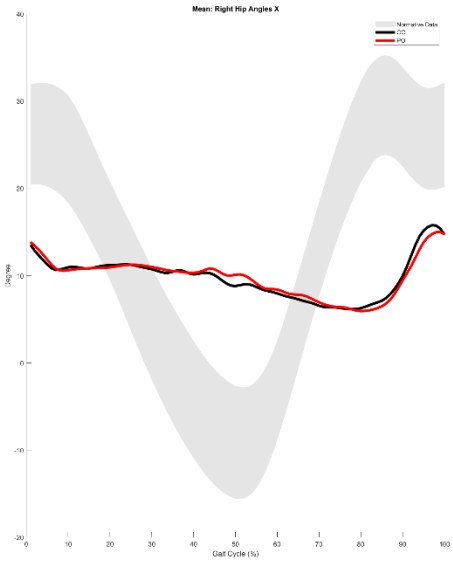

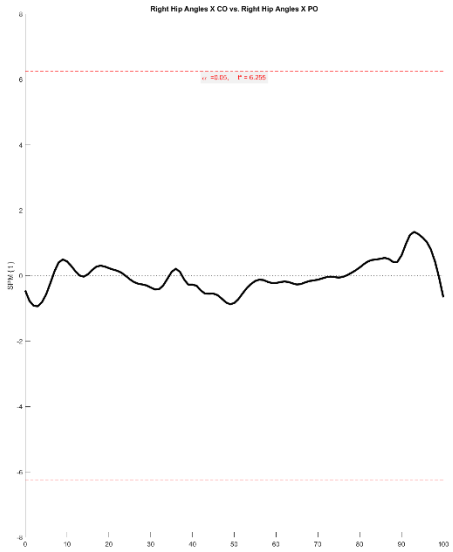

Right Hip Angles Y

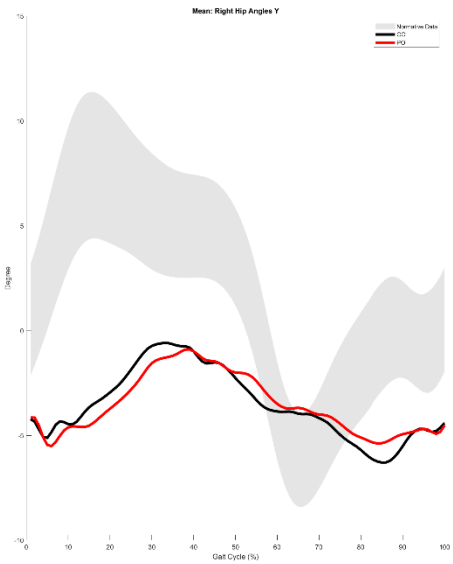

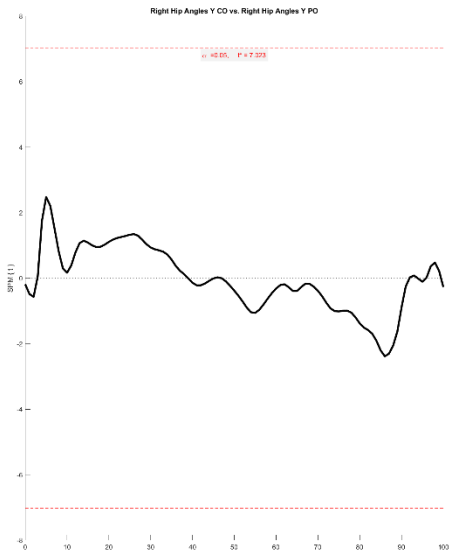

Right Hip Angles Z

88.8-89.2%

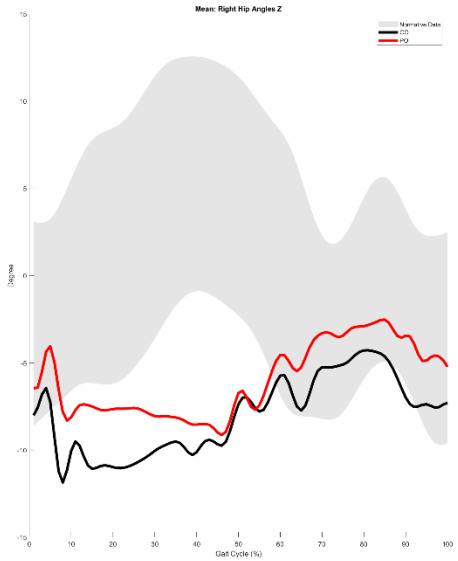

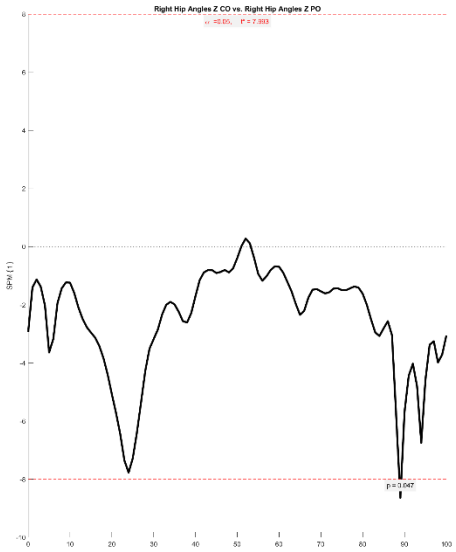

Left Hip Angles X

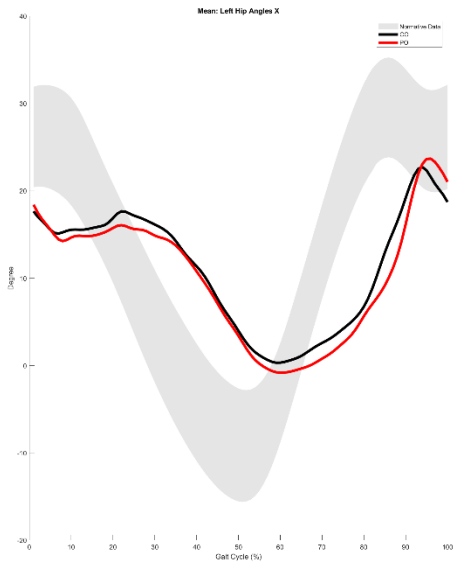

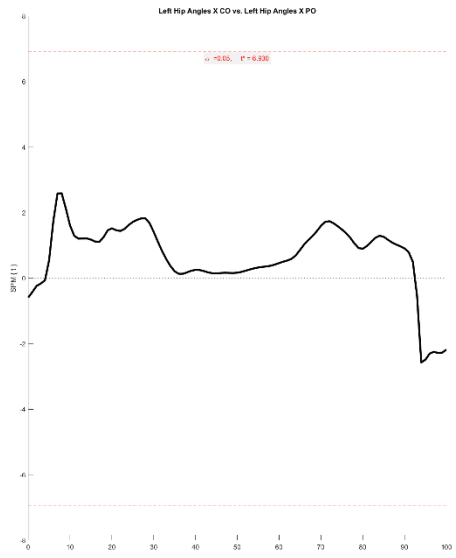

Left Hip Angles Y

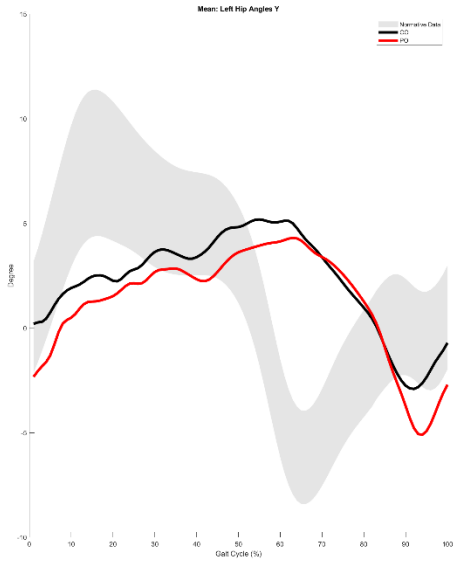

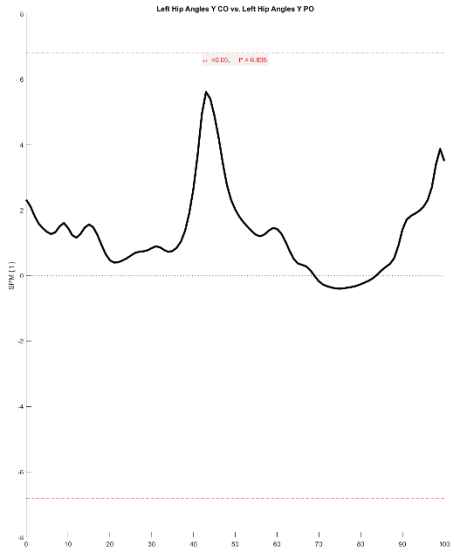

Left Hip Angles Z

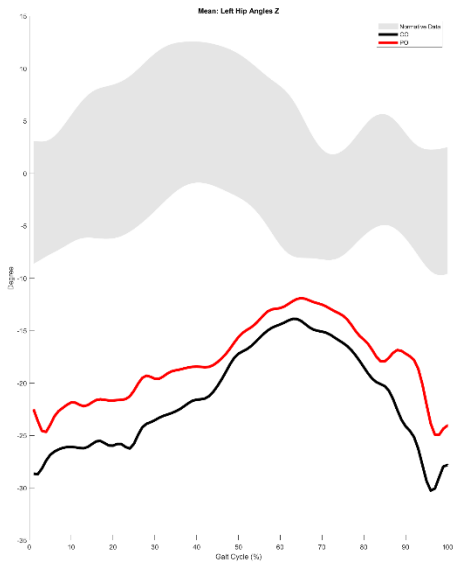

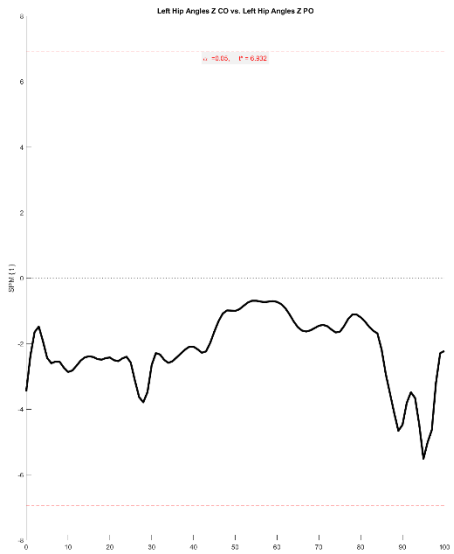

Right Knee Angles X

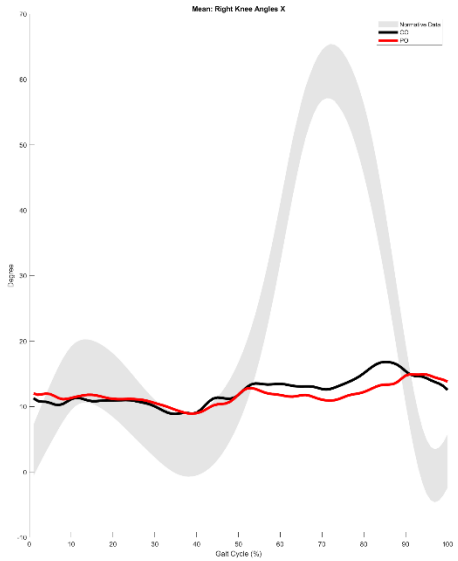

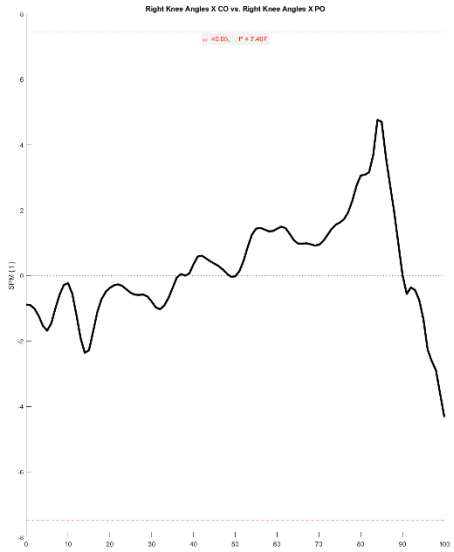

Right Knee Angles Y

36.0-38.1%

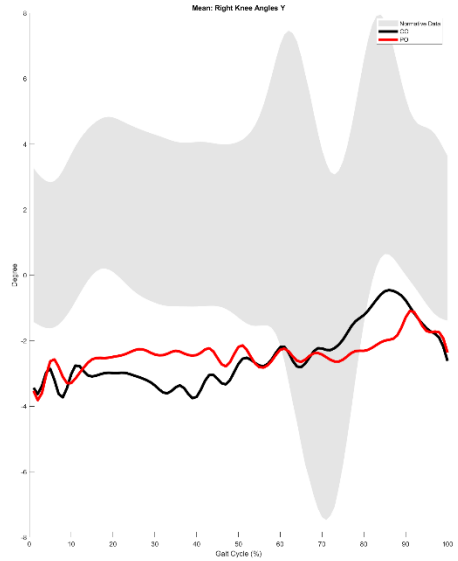

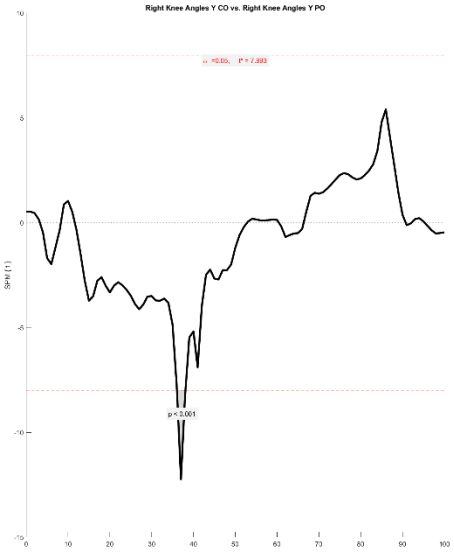

Right Knee Angles Z

0.0-1.6%, 4.6-7.4%, 13.5-16.3%, 20.1-32.4%, 61.3-63.4%, 88.8-92.9%, 93.2-97.3%

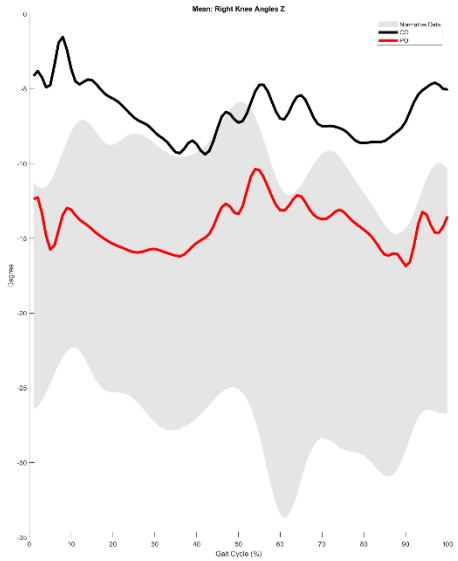

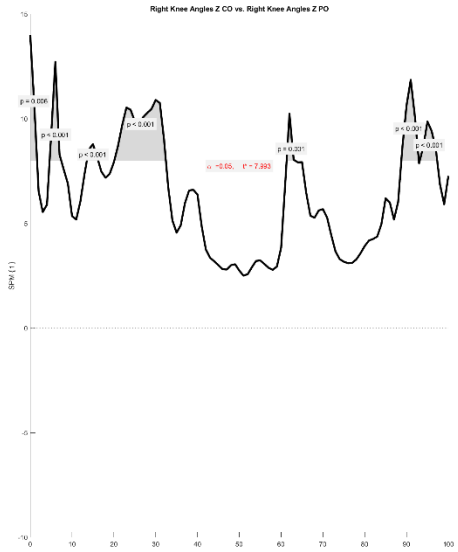

Left Knee Angles X

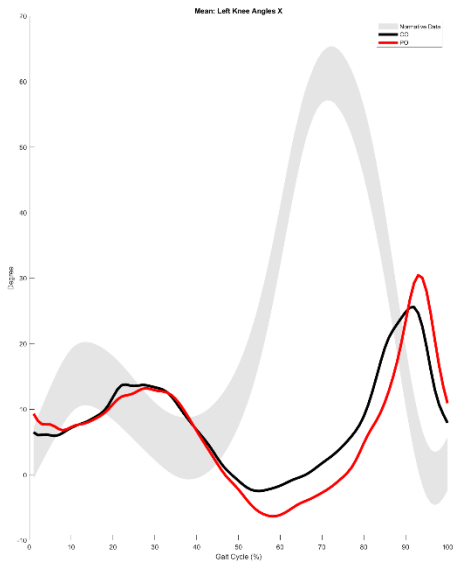

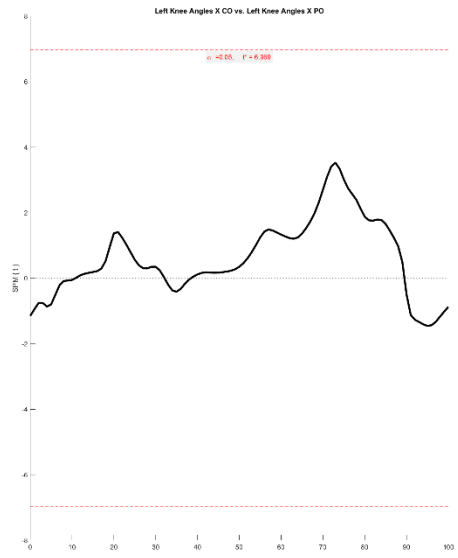

Left Knee Angles Y

68.8-75.4%, 82.6-85.0%

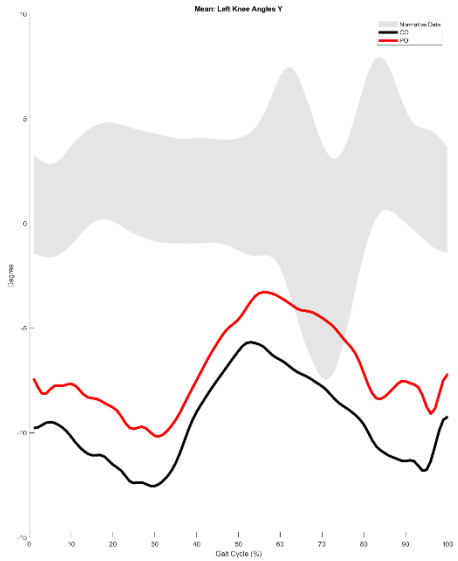

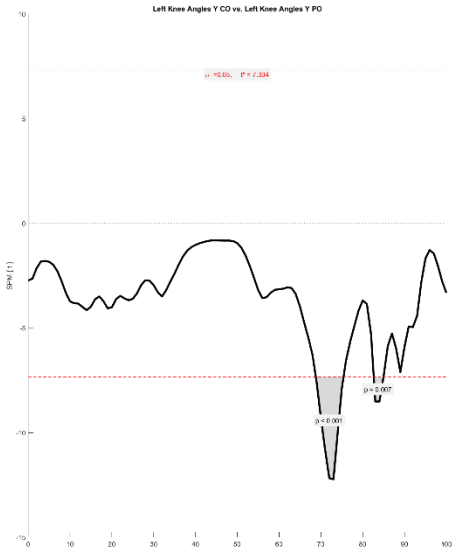

Left Knee Angles Z

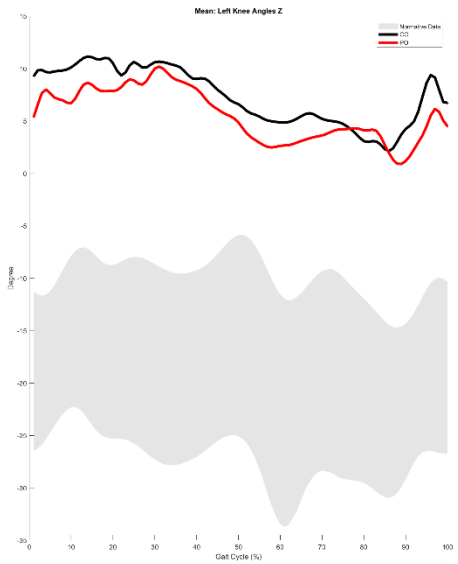

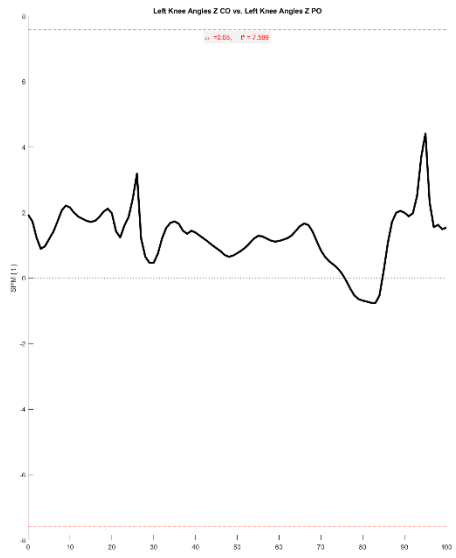

Right Ankle Angles X

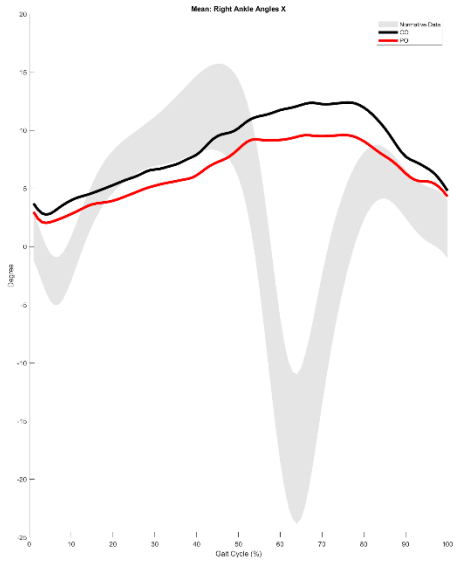

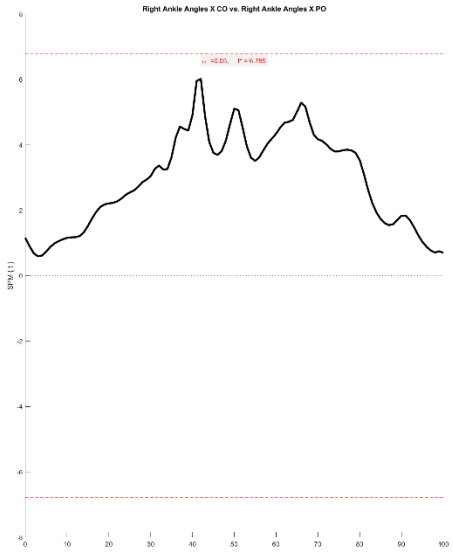

Right Ankle Angles Y

83.1-84.4%

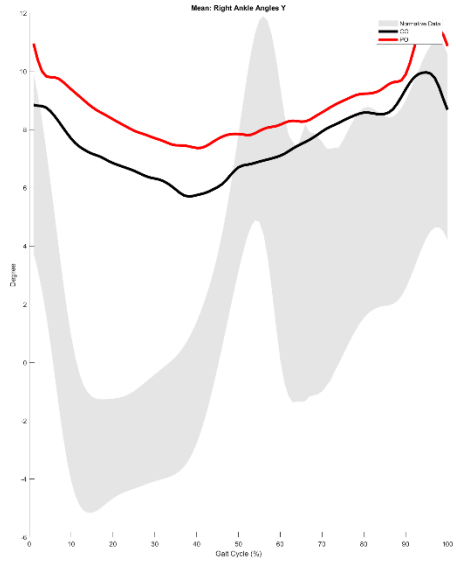

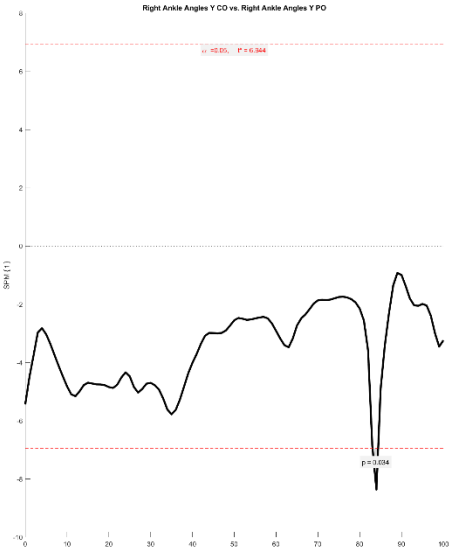

Left Ankle Angles X

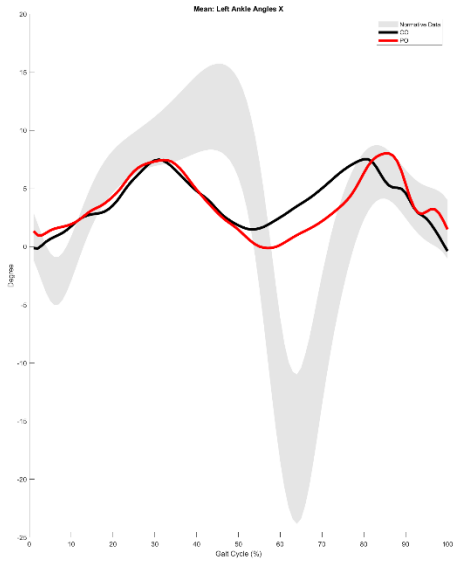

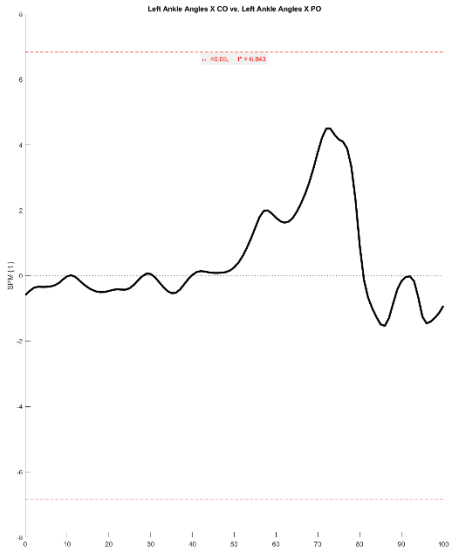

Left Ankle Angles Y

59.5-65.2%

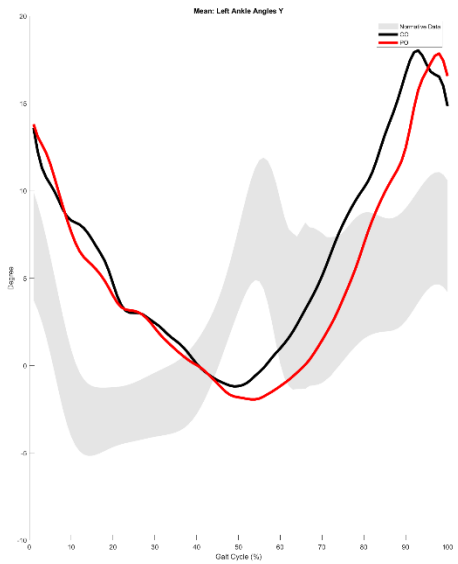

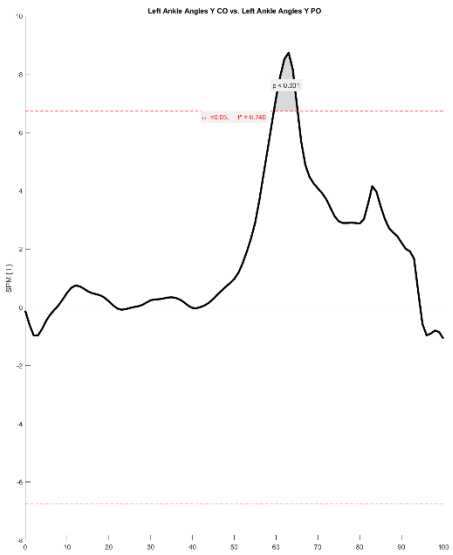

Right Foot Pitch Angles X

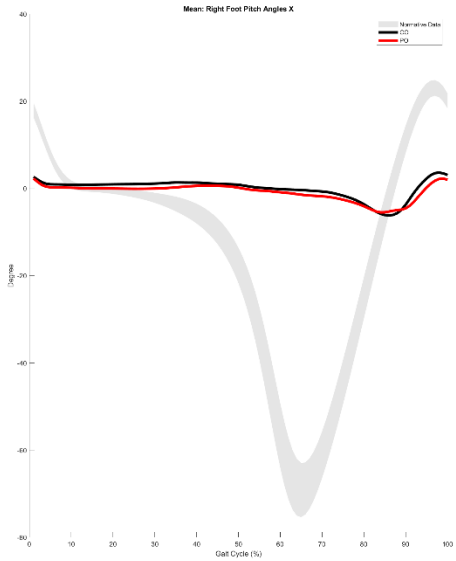

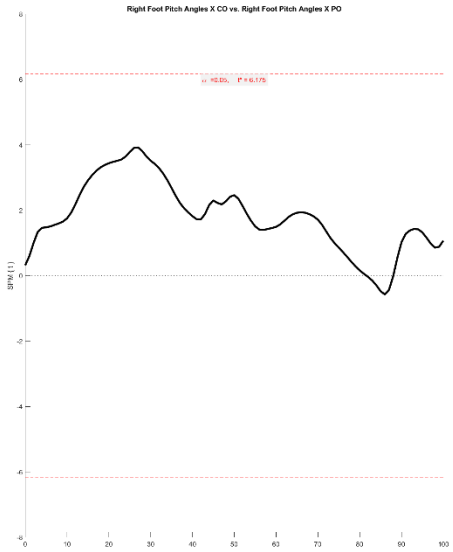

Left Foot Pitch Angles X

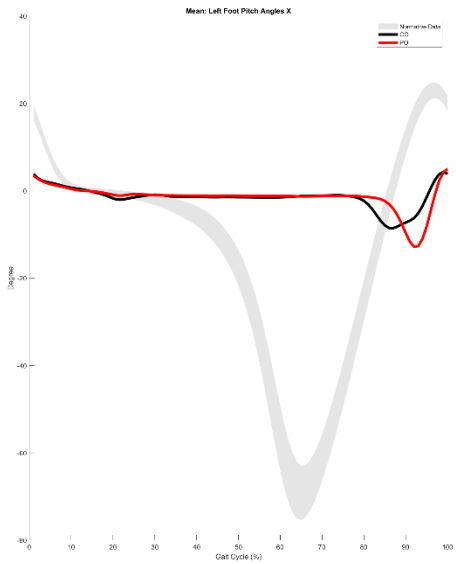

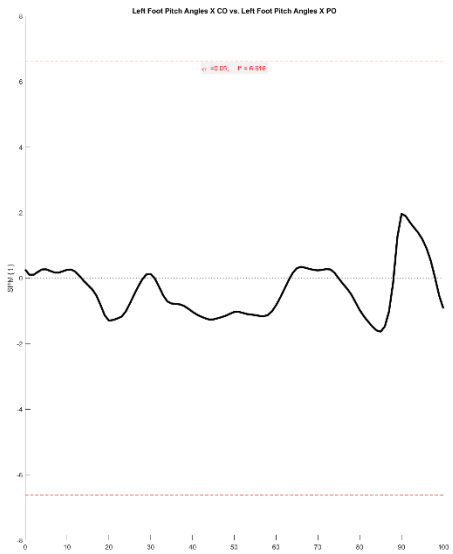

Right Foot Progression Z

17.4-24.7%, 50.2-53.8%, 54.2-62.6%

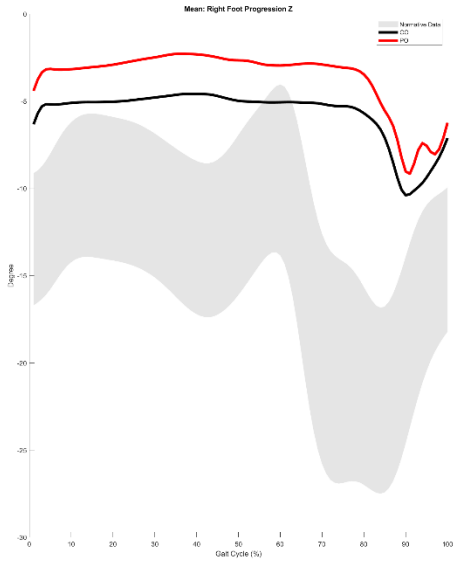

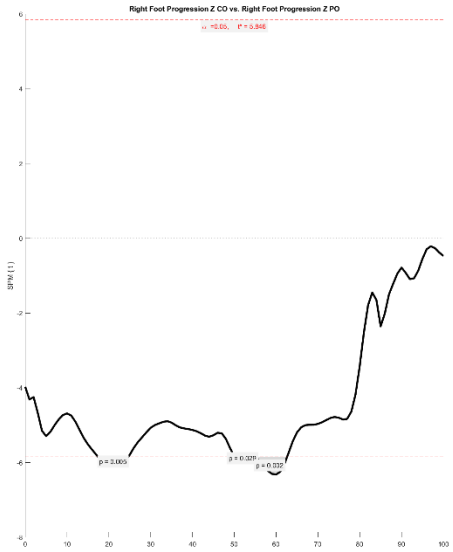

Left Foot Progression Z

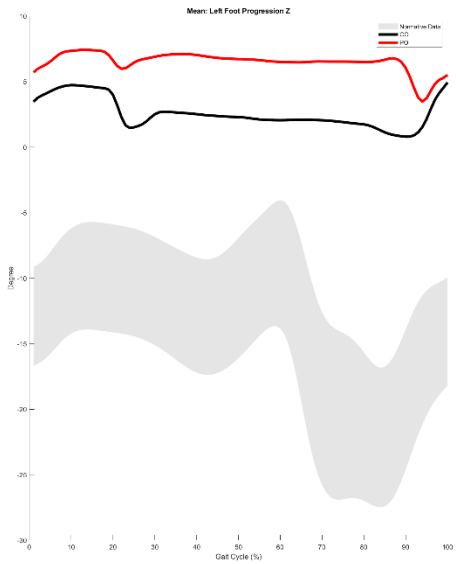

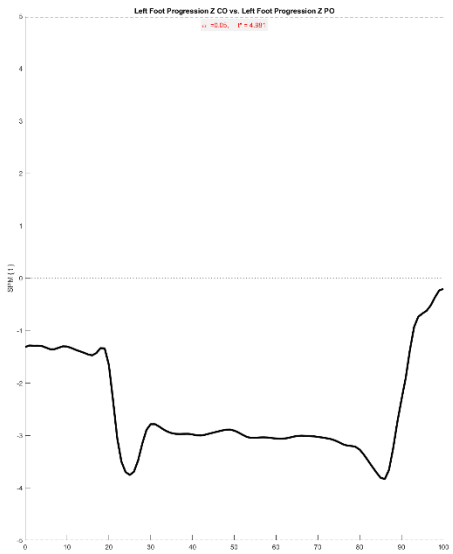

Right Hip Moment X

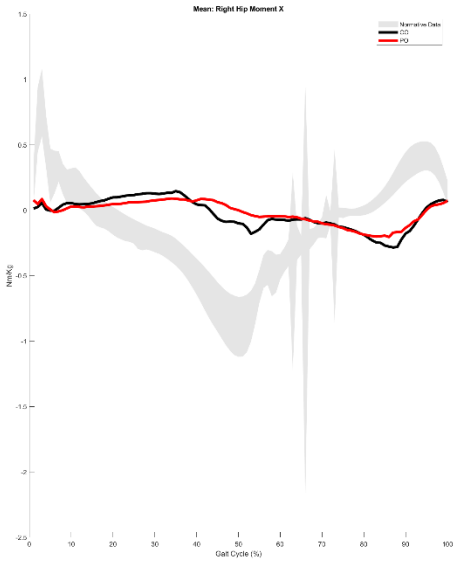

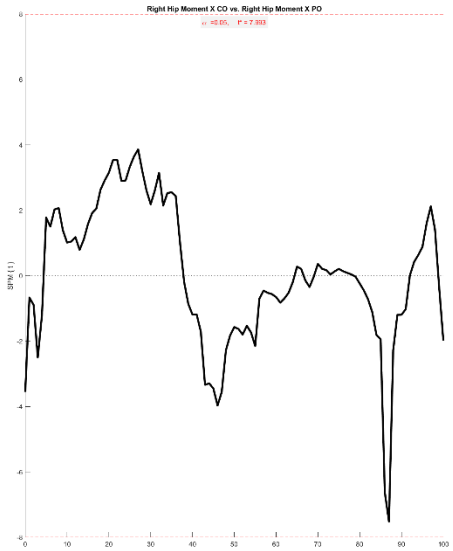

Right Hip Moment Y

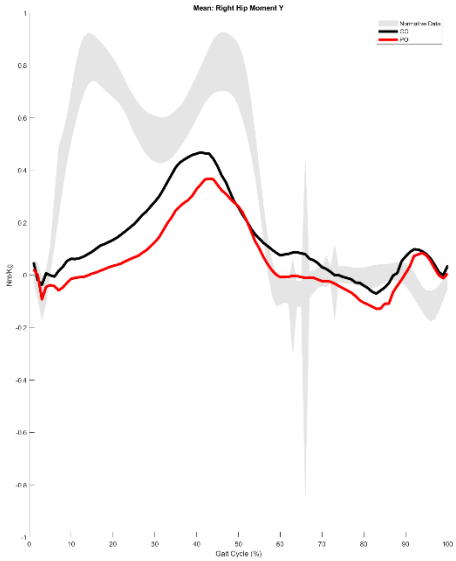

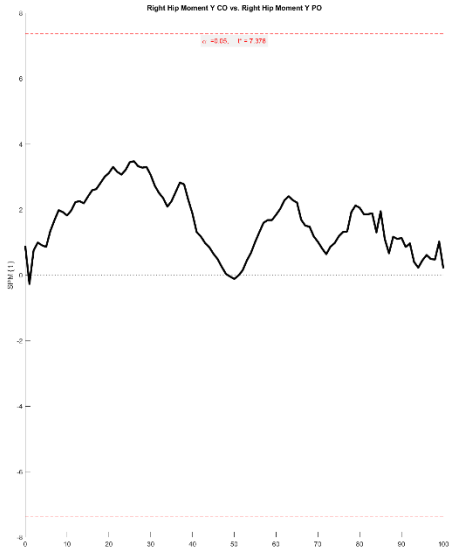

Left Hip Moment X

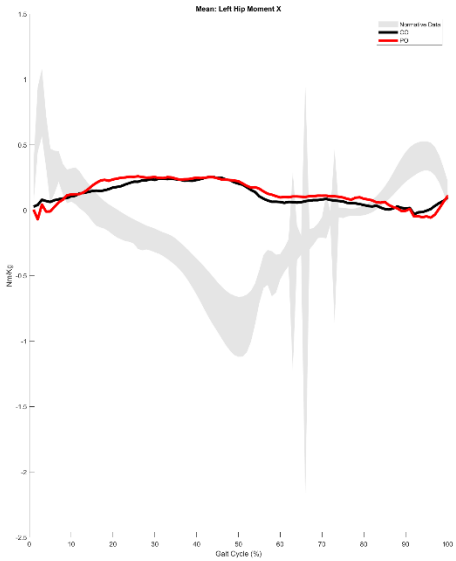

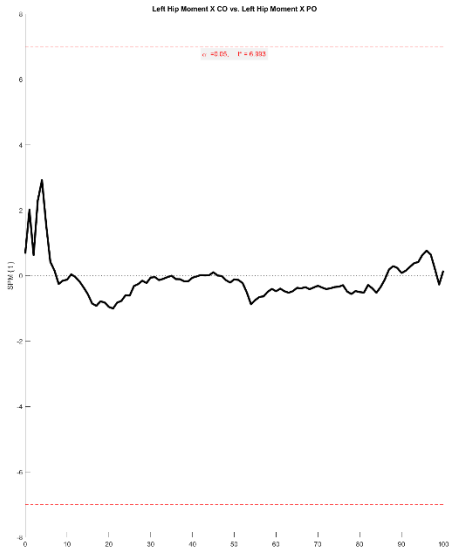

Left Hip Moment Y

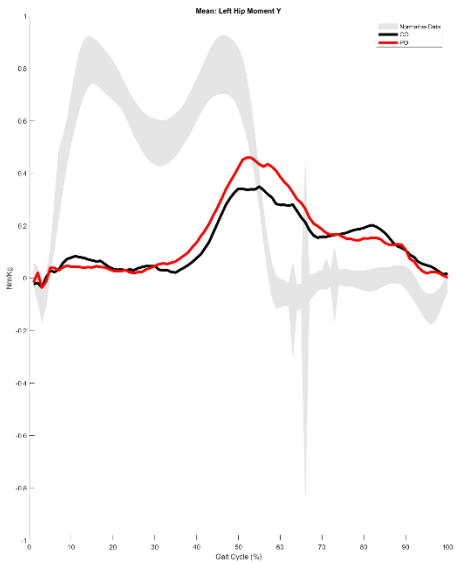

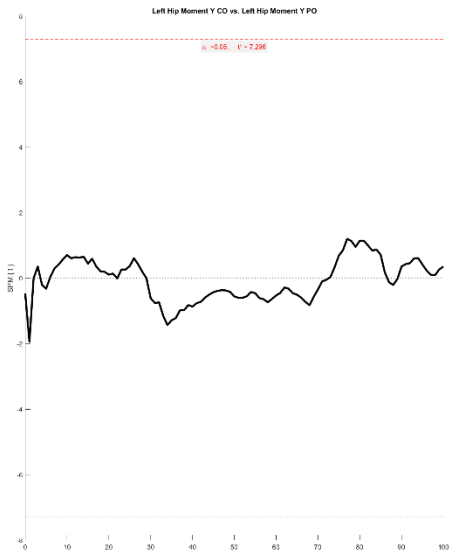

Right Knee Moment X

42.7-44.4%

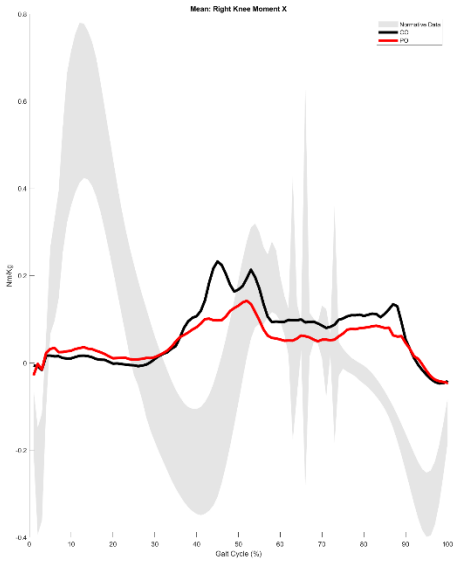

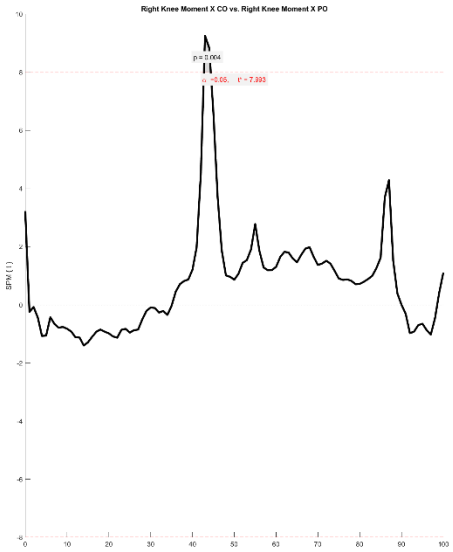

Right Knee Moment Y

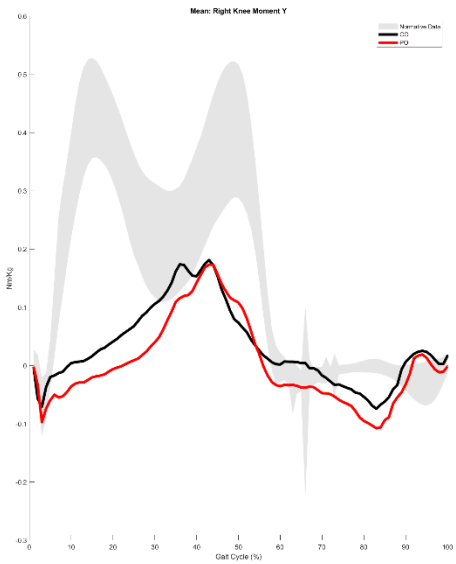

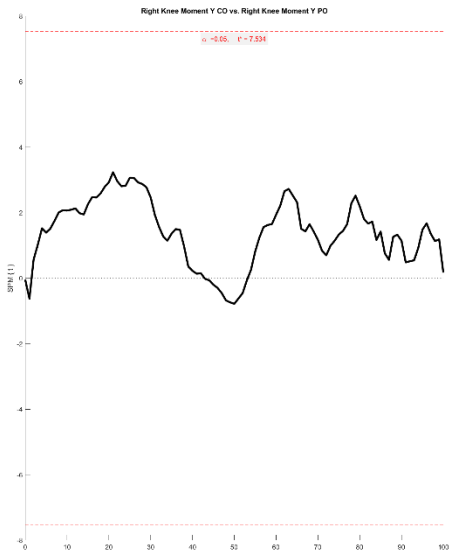

Left Knee Moment X

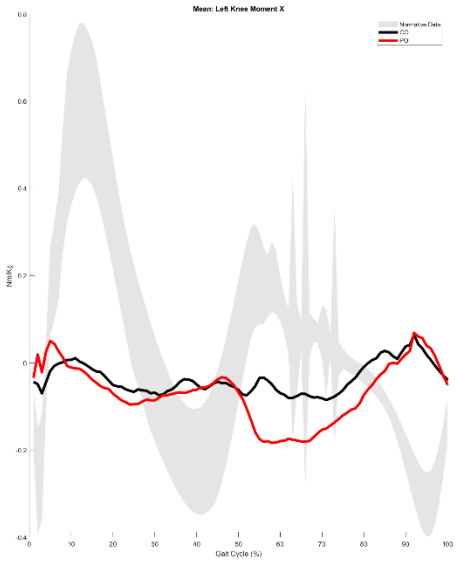

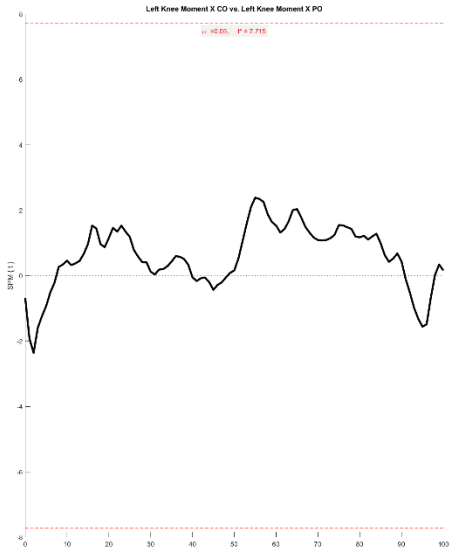

Left Knee Moment Y

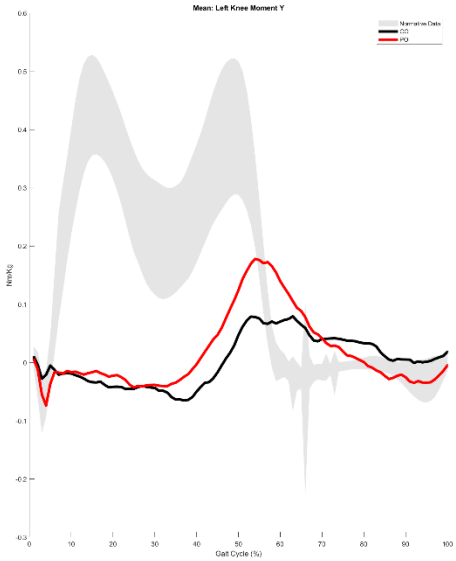

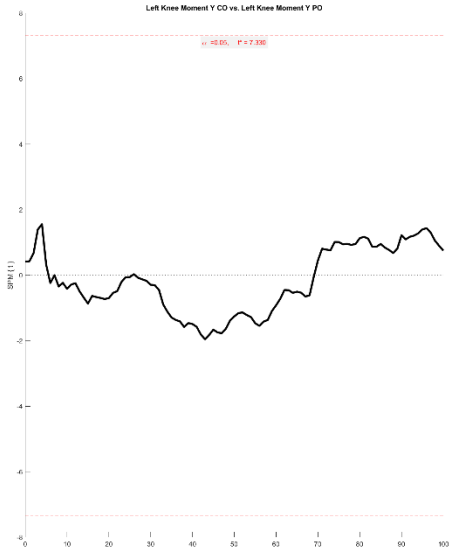

Right Ankle Moment X

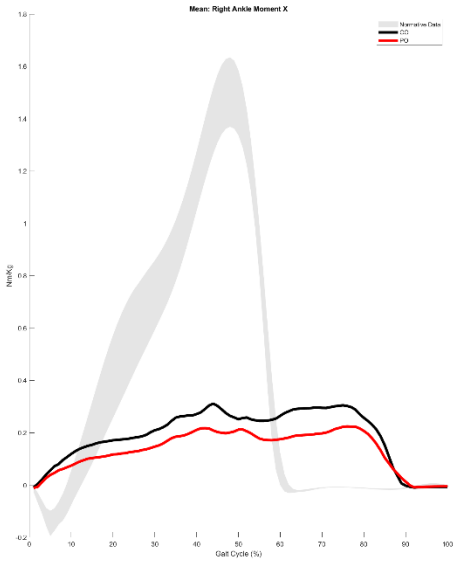

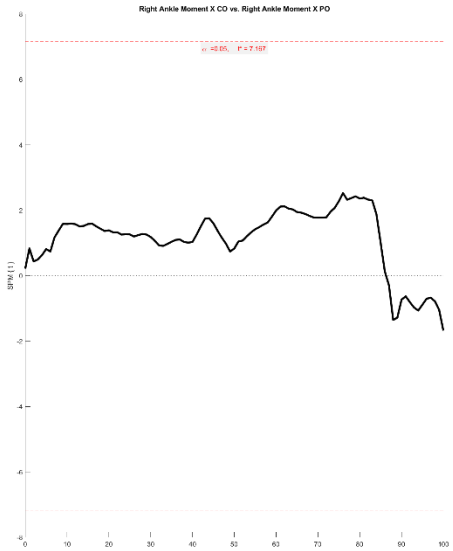

Right Ankle Moment Y

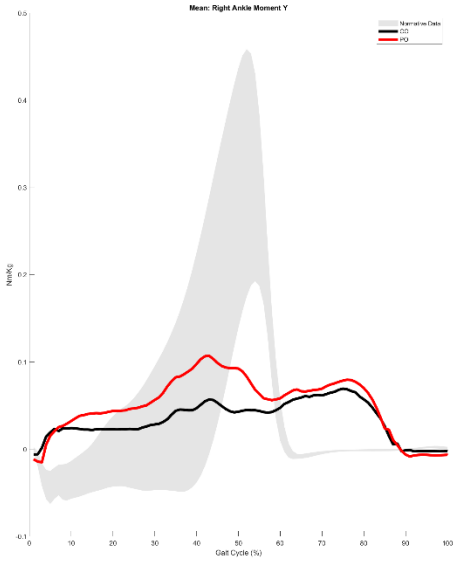

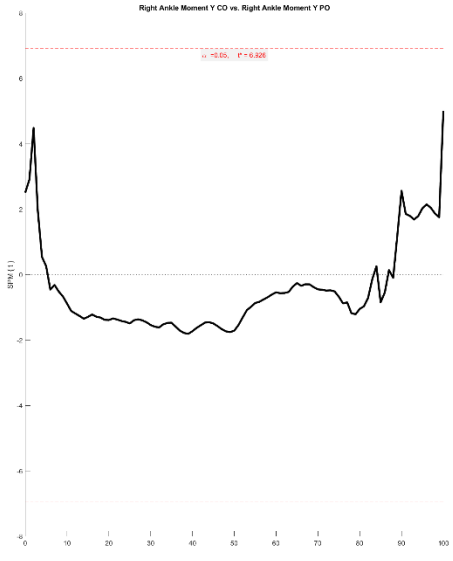

Left Ankle Moment X

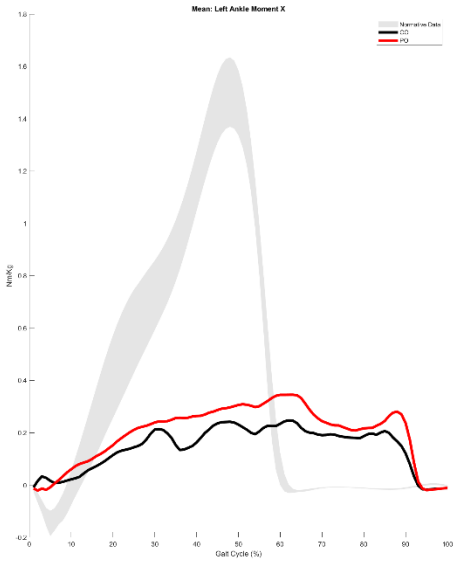

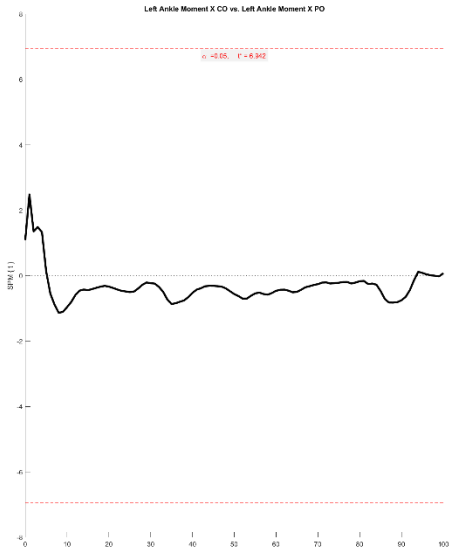

Left Ankle Moment Y

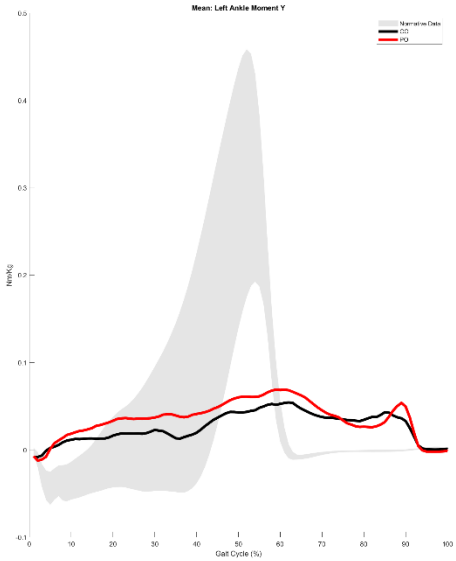

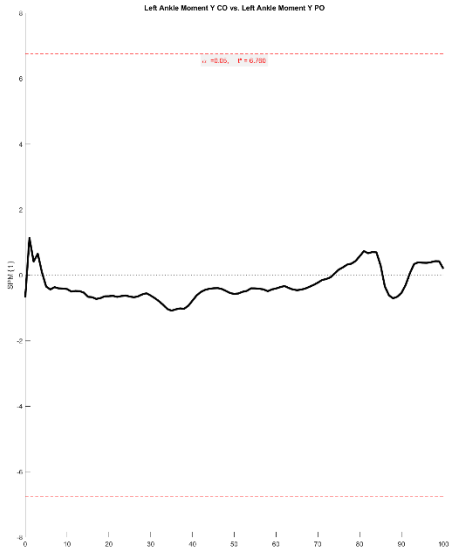

PO

Step Length

REP	Left	Right	IS (50%)	IS (0%)
1	0.18145	0.08184	31.0836	75.6656
2	0.17752	0.0733	29.2241	83.1034
3	0.17685	0.06363	26.4596	94.1617
4	0.17291	0.06209	26.4213	94.3149
5	0.1728	0.04869	21.9829	112.068
6	0.16956	0.03742	18.079	127.684
Mean	0.175182	0.0611617	25.5418	97.833
SD	0.003873	0.0147258	4.36359	17.4543

CO

Step Length

REP	Left	Right	IS (50%)	IS (0%)
1	0.18166	0.09898	35.2694	58.9225
2	0.17715	0.09773	35.5537	57.7852
3	0.16746	0.08638	34.0293	63.8828
4	0.16686	0.08542	33.8592	64.5632
5	0.16399	0.0524	24.2155	103.138
6	0.16196	0.05006	23.611	105.556
Mean	0.1698467	0.078495	31.0897	75.6413
SD	0.0071182	0.0199551	5.11361	20.4544

PO

Swing Time

REP	Left	Right	IS (50%)	IS (0%)
1	0.28333	0.475	62.6376	50.5506
2	0.26667	0.46667	63.6362	54.545
3	0.26667	0.45833	63.2179	52.8717
4	0.26667	0.45	62.7904	51.1616
5	0.25833	0.4	60.7598	43.0392
6	0.25833	0.36667	58.6672	34.6688
Mean	0.266667	0.4361117	61.9515	47.8061
SD	0.008333	0.0392828	1.72354	6.89416

CO

Swing Time

REP	Left	Right	IS (50%)	IS (0%)
1	0.35	0.5	58.8235	35.2941
2	0.33333	0.48333	59.1837	36.735
3	0.325	0.475	59.375	37.5
4	0.31667	0.45	58.6954	34.7816
5	0.30833	0.44167	58.8893	35.5573
6	0.3	0.40833	57.6469	30.5874
Mean	0.3222217	0.4597217	58.769	35.0759
SD	0.0164335	0.0302065	0.55096	2.20383

PO

Stance Time

REP	Left	Right	IS (50%)	IS (0%)
1	2.54167	2.425	48.8255	4.69812
2	2.51667	2.41667	48.9865	4.05405
3	2.45833	2.375	49.138	3.44814
4	2.4	2.35833	49.5621	1.75145
5	2.325	2.3	49.7297	1.08108
6	2.25833	2.18333	49.1557	3.37712
Mean	2.416667	2.343055	49.2329	3.06833
SD	0.100924	0.0824154	0.31542	1.26166

CO

Stance Time

REP	Left	Right	IS (50%)	IS (0%)
1	2.66667	2.55	48.8818	4.47297
2	2.43333	2.425	49.9143	0.34292
3	2.375	2.34167	49.6467	1.41329
4	2.225	2.325	51.0989	4.3956
5	2.225	2.26667	50.4639	1.85543
6	2.20833	2.19167	49.8107	0.75727
Mean	2.355555	2.3500017	49.9694	2.20625
SD	0.16278	0.1142597	0.68746	1.64594

	Left	Right
Step Length PO	0.18	0.06
Step Length CO	0.17	0.08
Swing Time PO	0.27	0.44
Swing Time CO	0.32	0.46
Stance Time PO	2.42	2.34
Stance Time CO	2.36	2.35

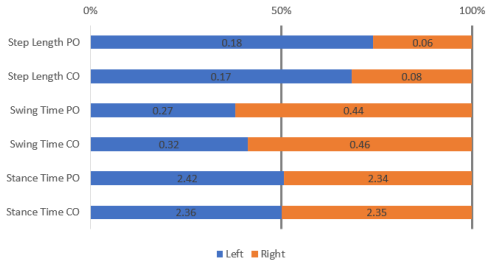

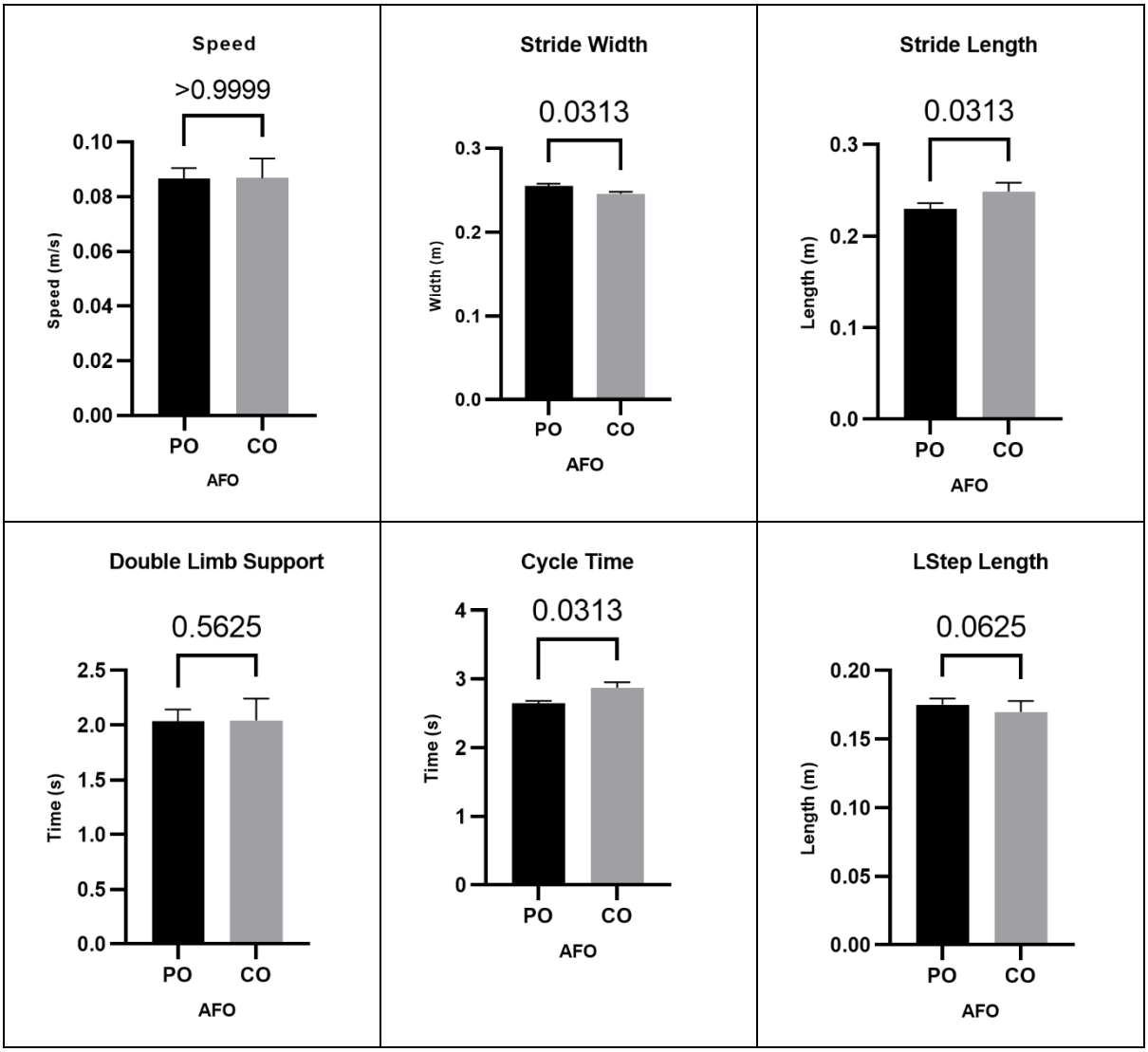

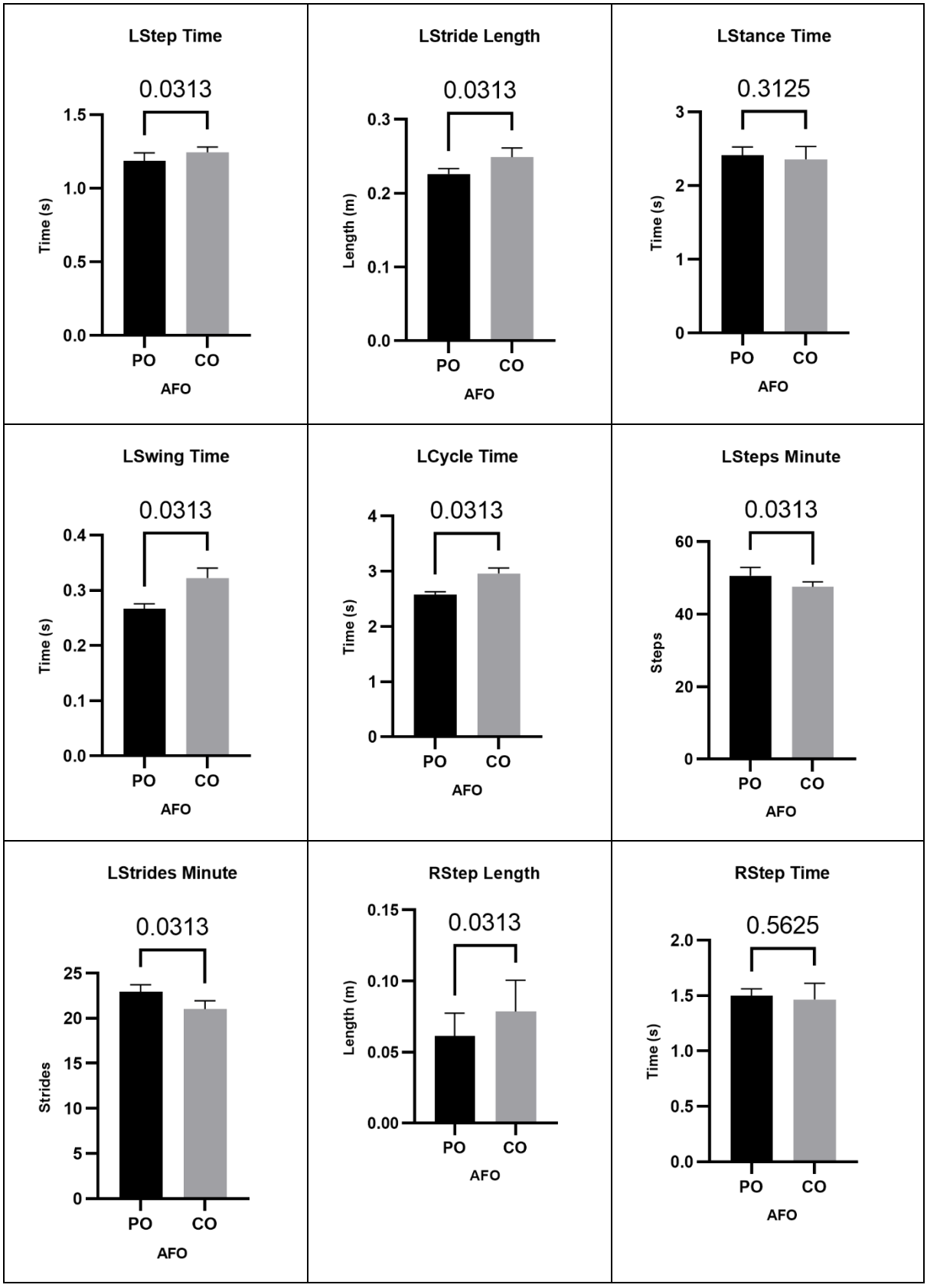
LStep Time
0.0313
Time (s)
1.5
1.0
0.5
0.0
PO
CO
AFO
LStride Length
0.0313
Length (m)
0.3
0.2
0.1
0.0
PO
CO
AFO
LStance Time
0.3125
Time (s)
3
2
1
0
PO
CO
AFO
LSwing Time
0.0313
Time (s)
0.4
0.3
0.2
0.1
0.0
PO
CO
AFO
LCycle Time
0.0313
Time (s)
4
3
2
1
0
PO
CO
AFO
LSteps Minute
0.0313
Steps
60
40
20
0
PO
CO
AFO
LStrides Minute
0.0313
Strides
25
20
15
10
5
0
PO
CO
AFO
RStep Length
0.0313
Length (m)
0.15
0.10
0.05
0.00
PO
CO
AFO
RStep Time
0.5625
Time (s)
2.0
1.5
1.0
0.5
0.0
PO
CO
AFO

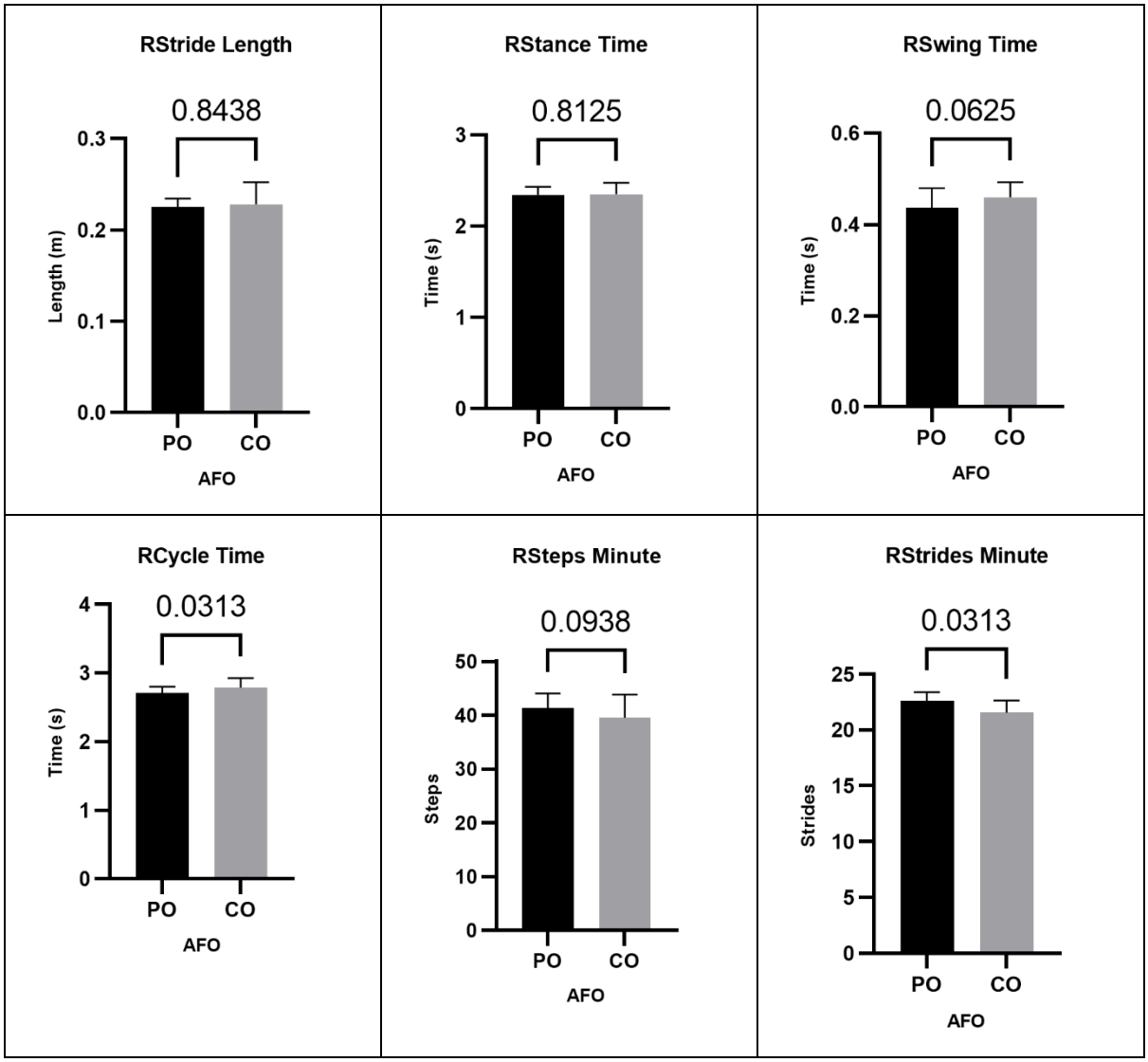
RStride Length
0.8438
Length (m)
0.3
0.2
0.1
0.0
PO
CO
AFO
RStance Time
0.8125
Time (s)
3
2
1
0
PO
CO
AFO
RSwing Time
0.0625
Time (s)
0.6
0.4
0.2
0.0
PO
CO
AFO
RCycle Time
0.0313
Time (s)
4
3
2
1
0
PO
CO
AFO
RSteps Minute
0.0938
Steps
50
40
30
20
10
0
PO
CO
AFO
RStrides Minute
0.0313
Strides
25
20
15
10
5
0
PO
CO
AFO

PATIENT 10

Right Pelvic Angles X

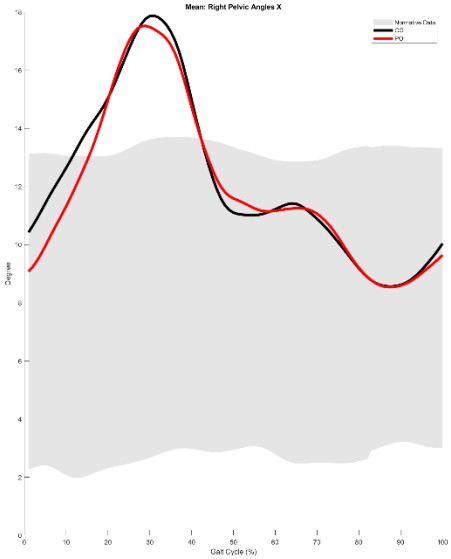

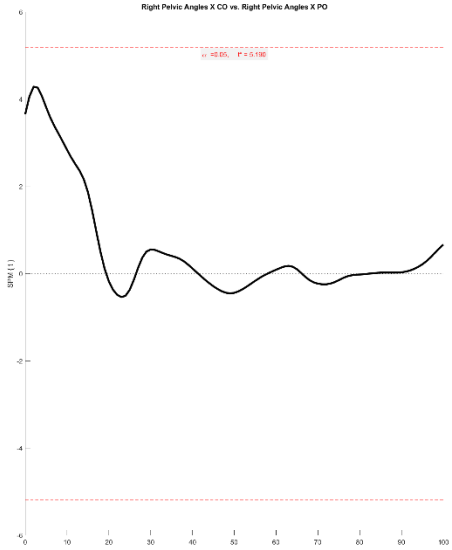

Right Pelvic Angles Y

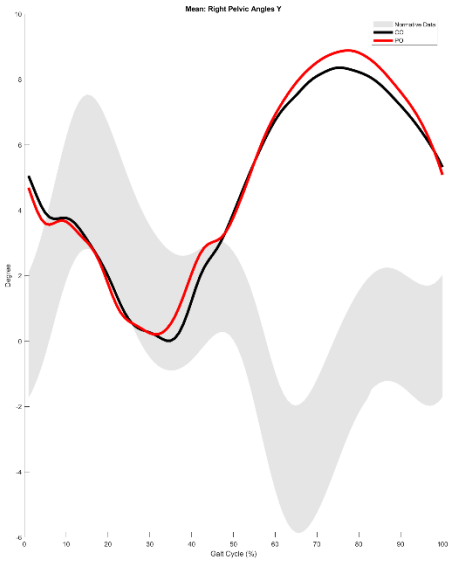

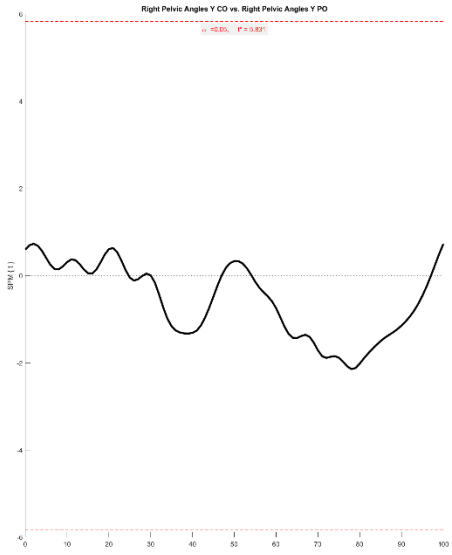

Right Pelvic Angles Z

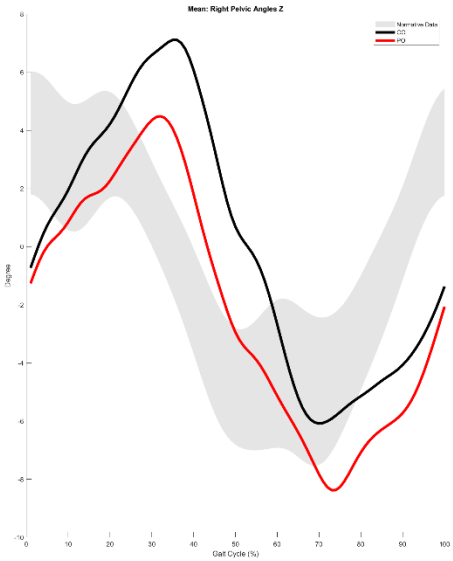

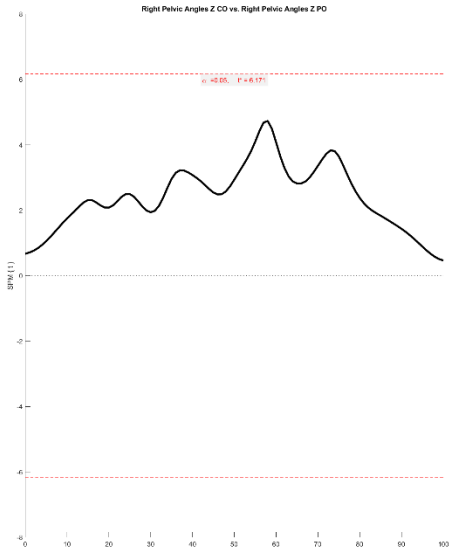

Left Pelvic Angles X

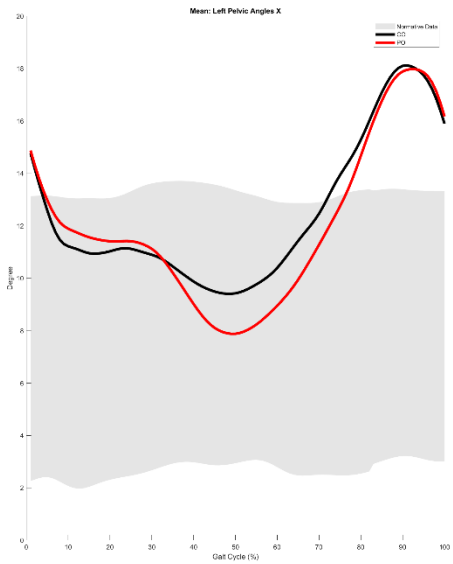

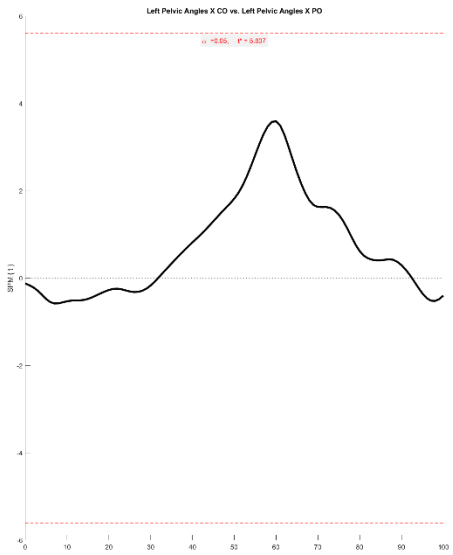

Left Pelvic Angles Y

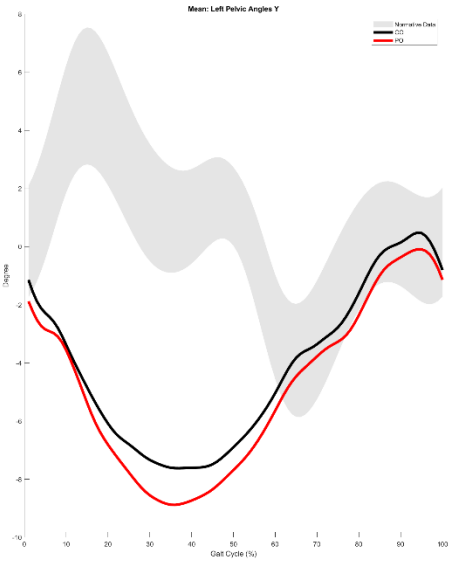

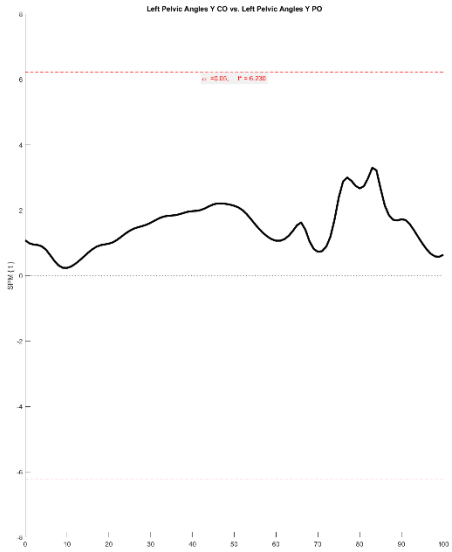

Left Pelvic Angles Z

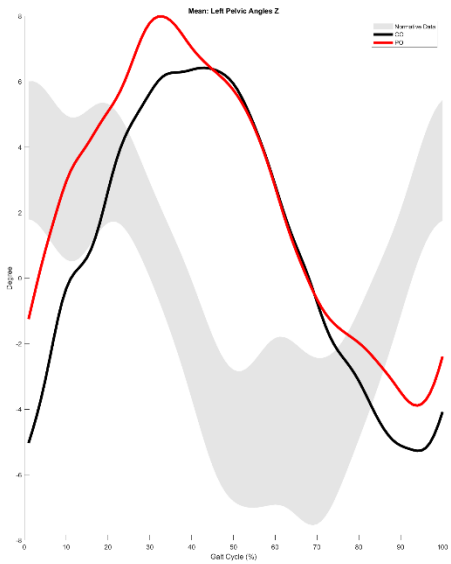

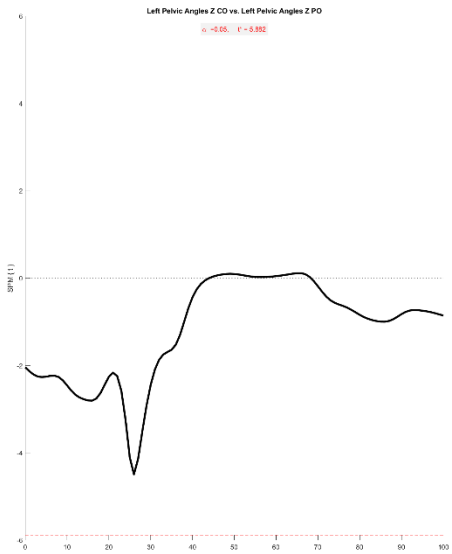

Right Hip Angles X

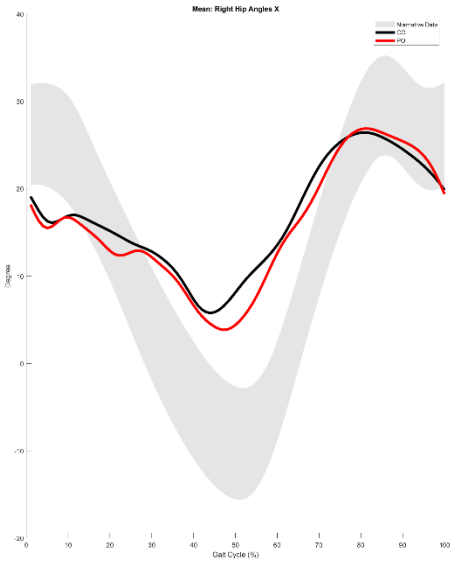

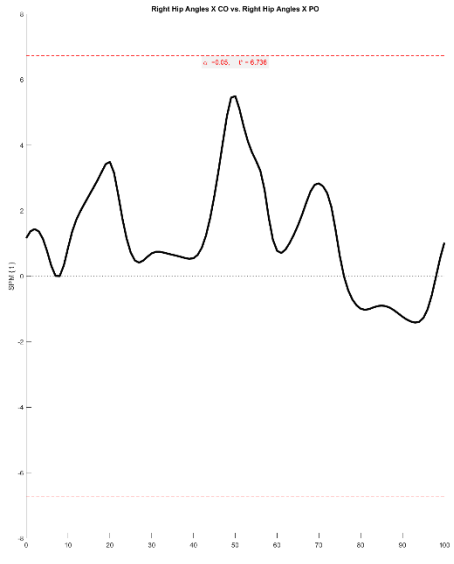

Right Hip Angles Y

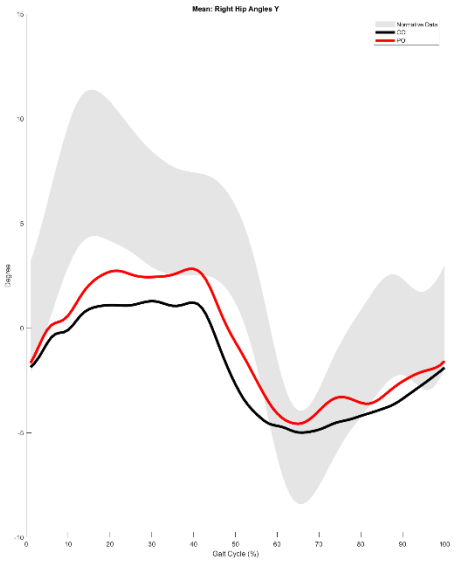

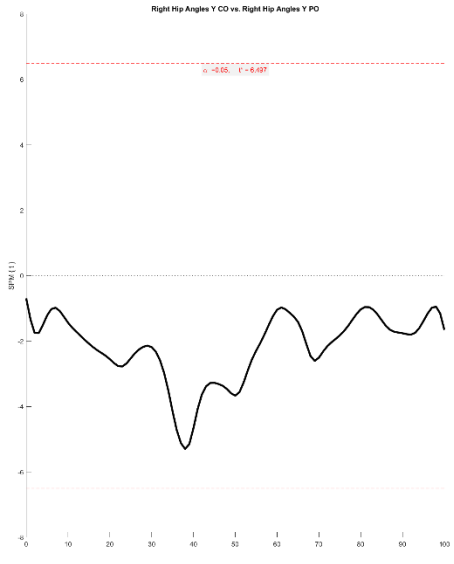

Right Hip Angles Z

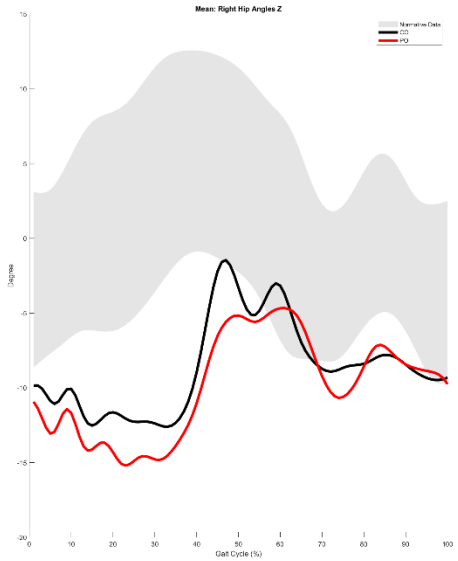

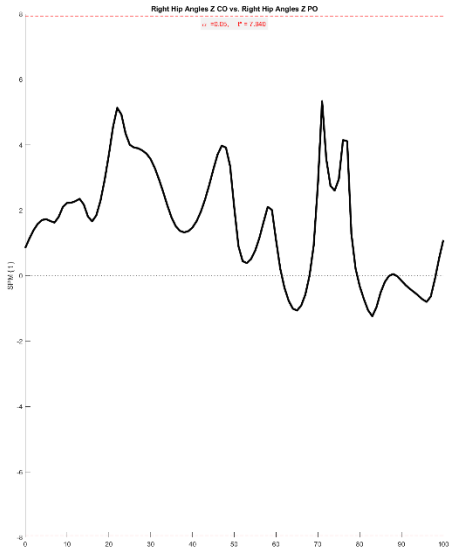

Left Hip Angles X

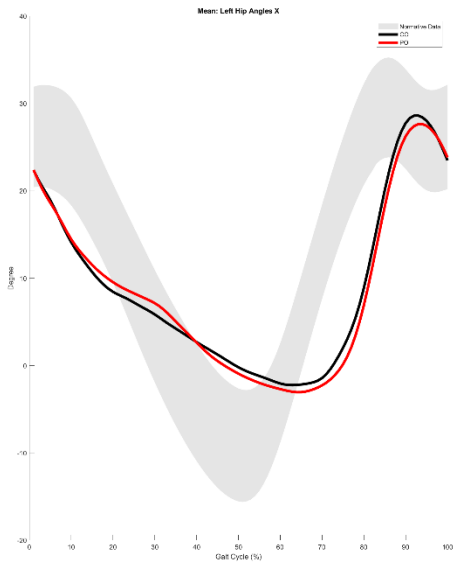

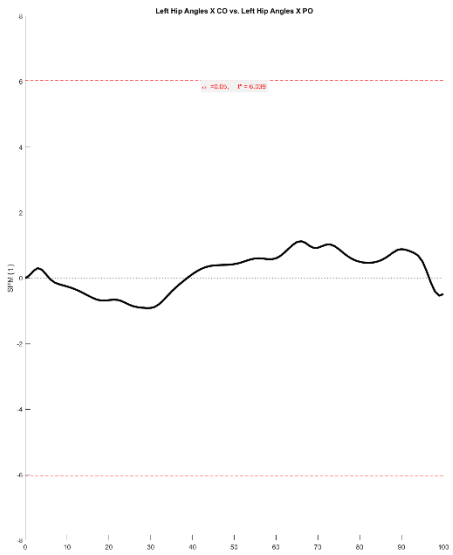

Left Hip Angles Y

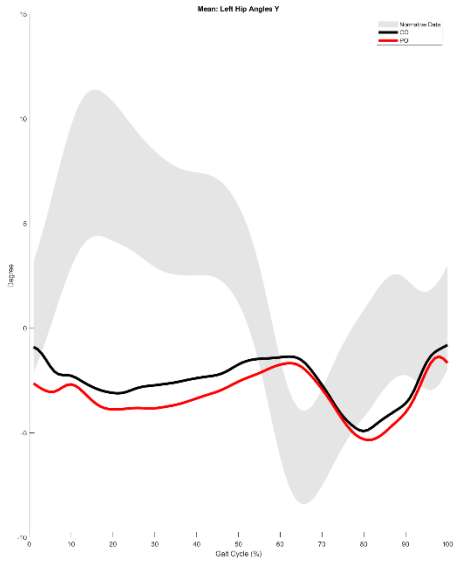

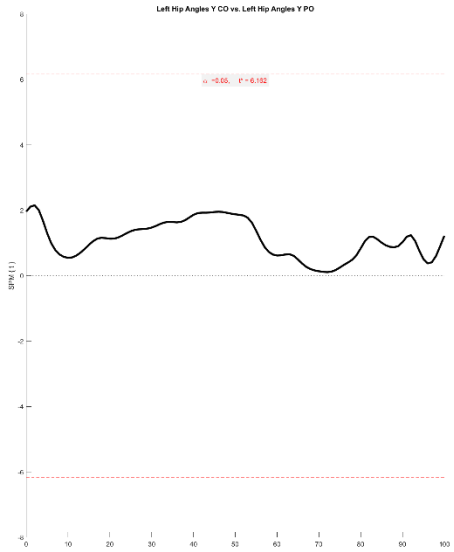

Left Hip Angles Z

88.2-90.5%

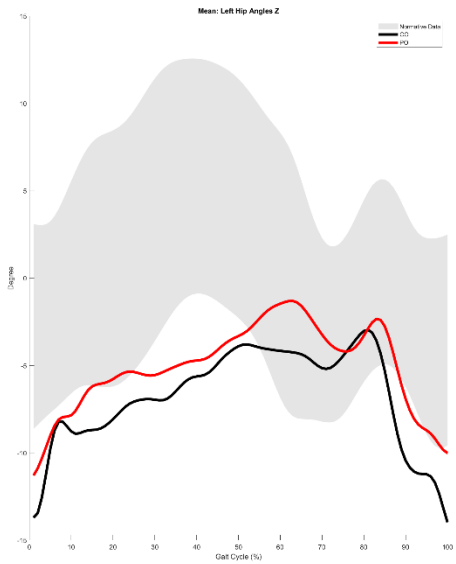

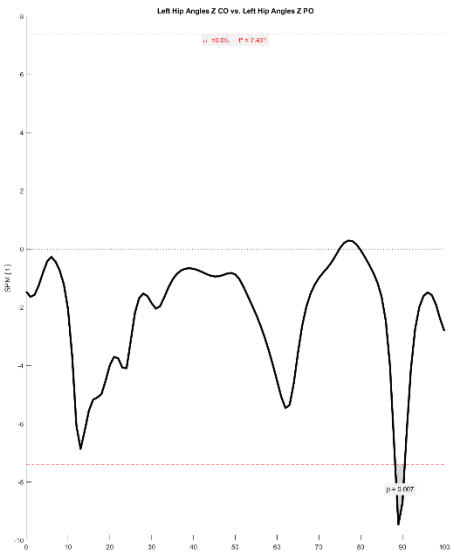

Right Knee Angles X

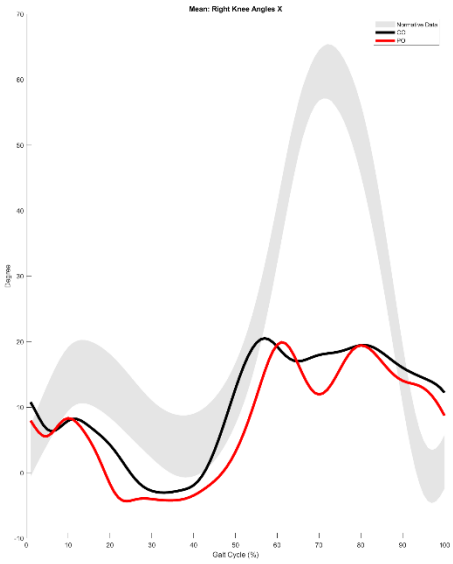

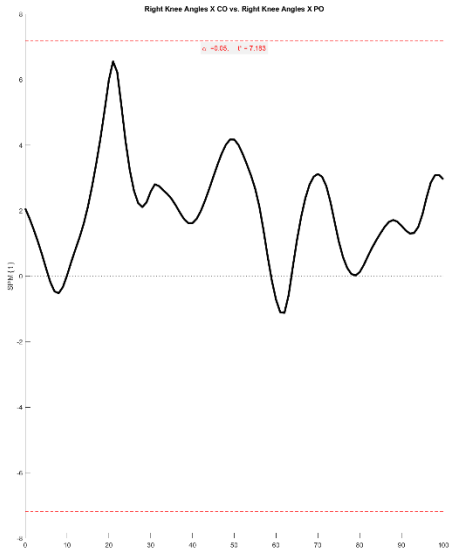

Right Knee Angles Y

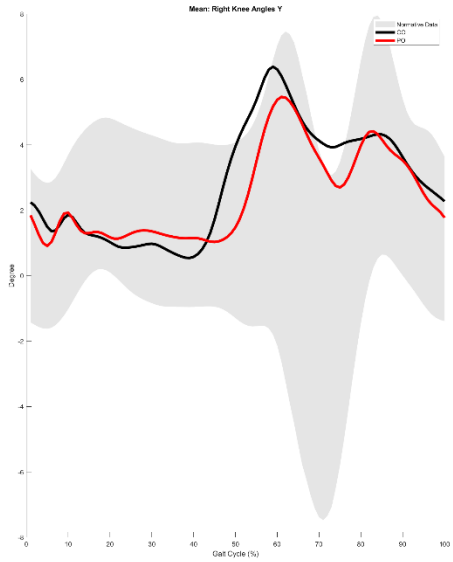

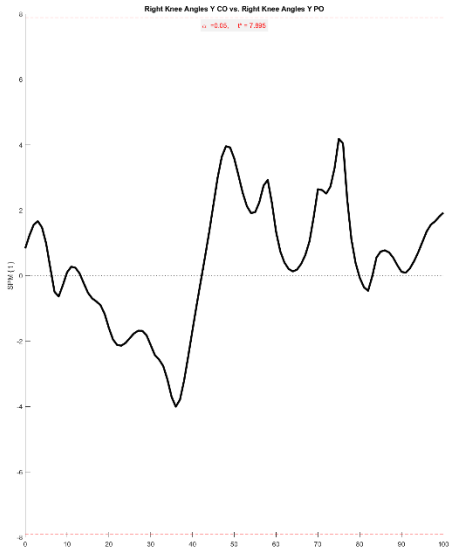

Right Knee Angles Z

85.1-89.0%

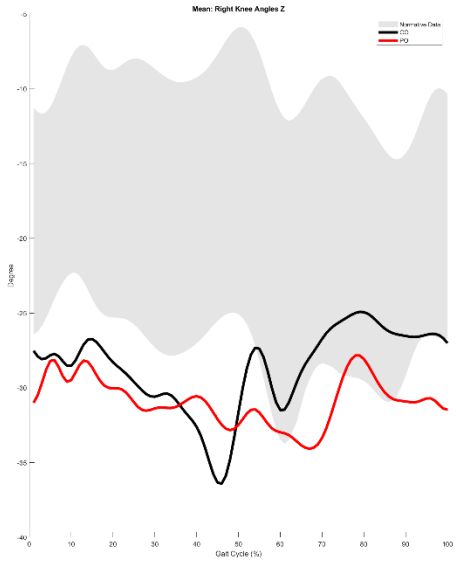

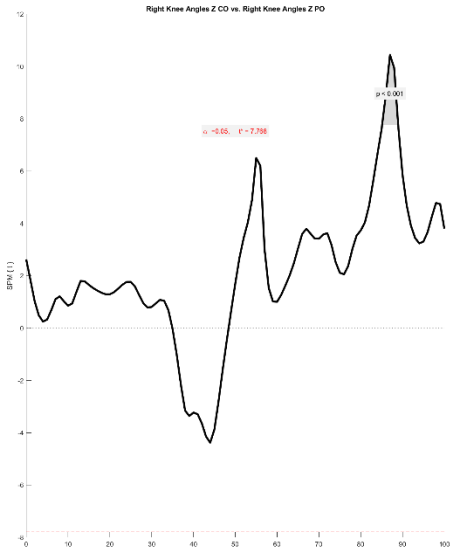

Left Knee Angles X

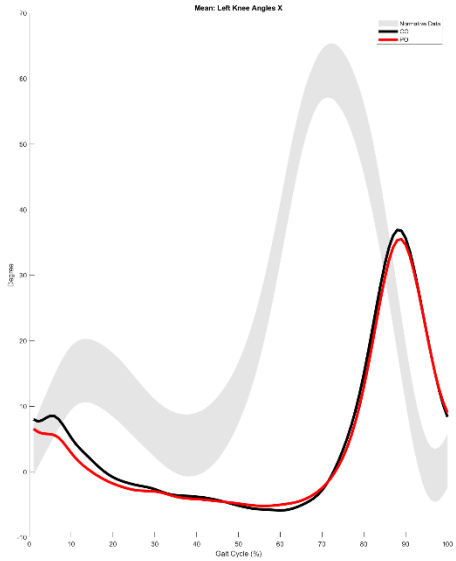

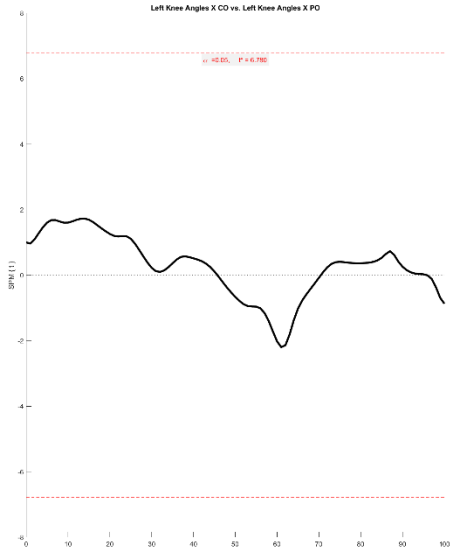

Left Knee Angles Y

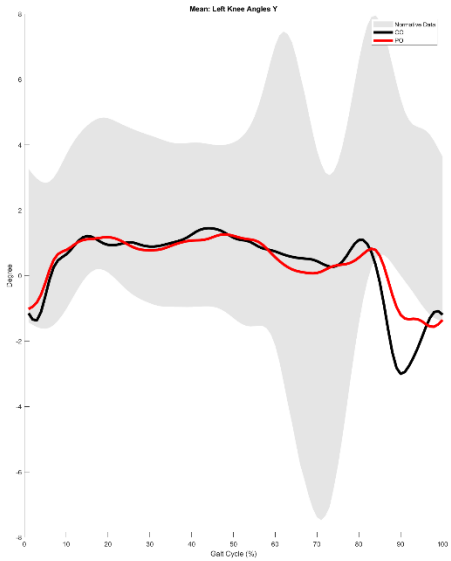

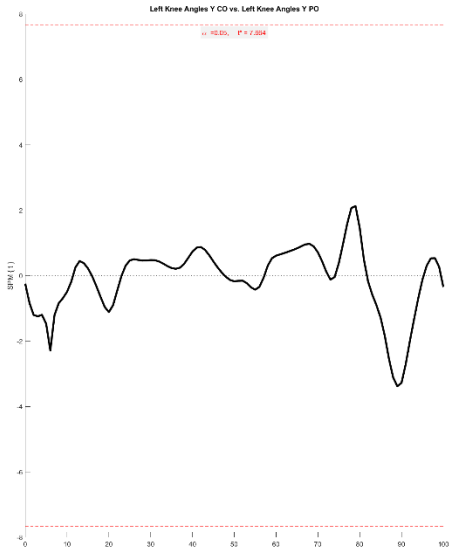

Left Knee Angles Z

63.5-64.6%

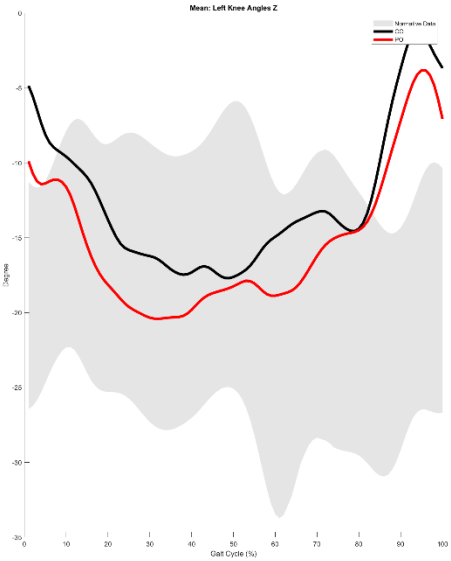

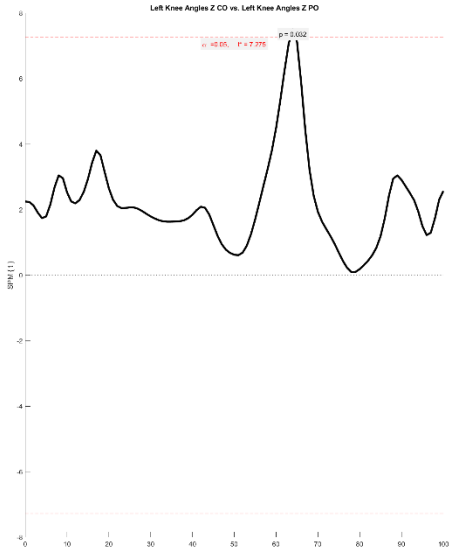

Right Ankle Angles X

0.0-100.0%

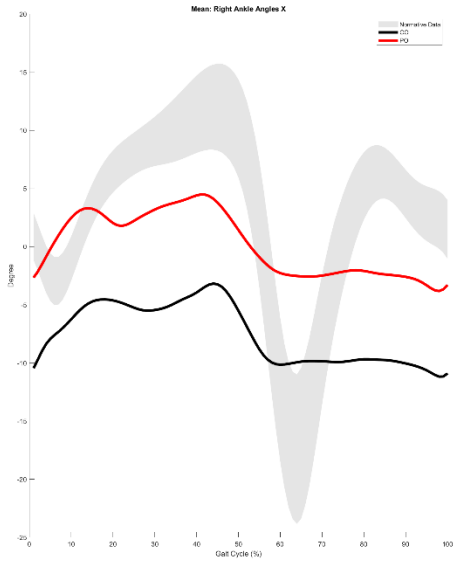

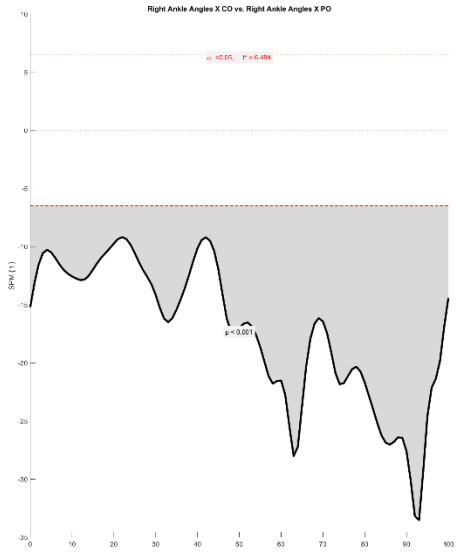

Right Ankle Angles Y

0.0-4.8%, 9.6-10.5%, 52.3-100.0%

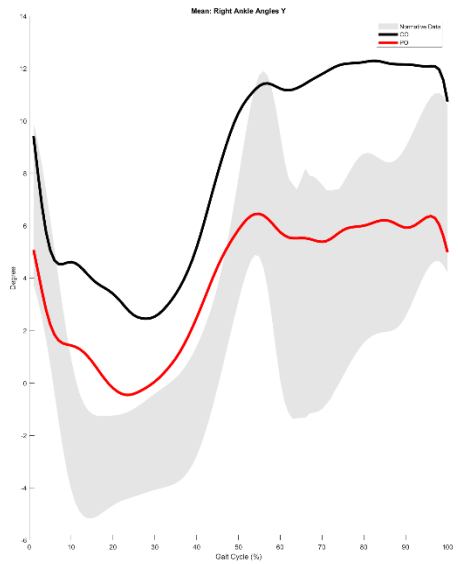

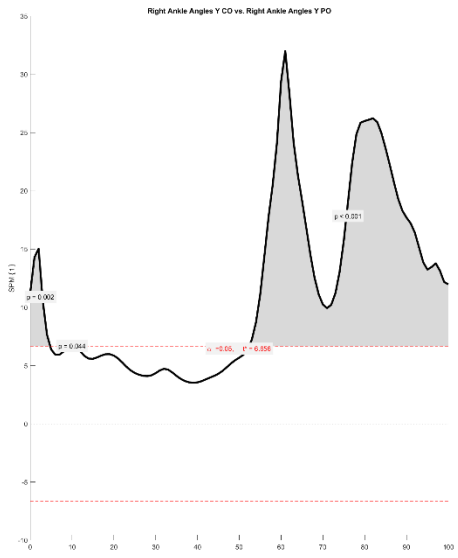

Left Ankle Angles X

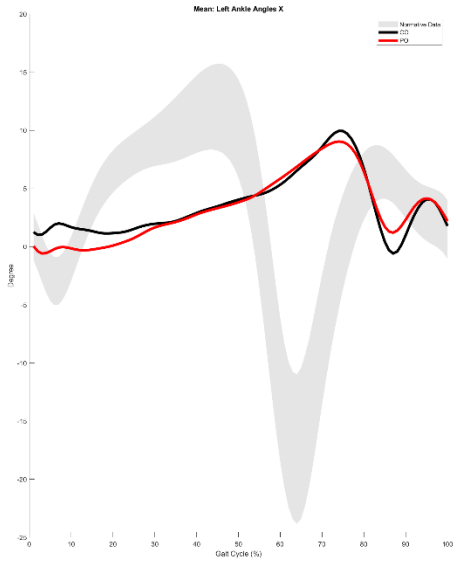

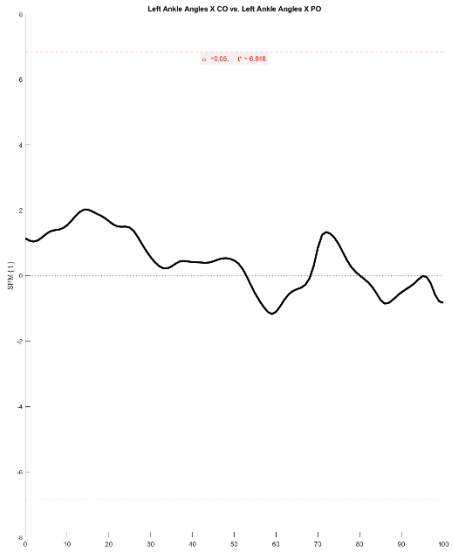

Left Ankle Angles Y

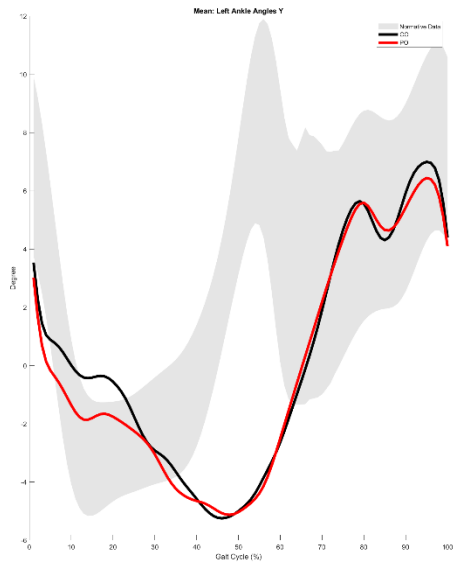

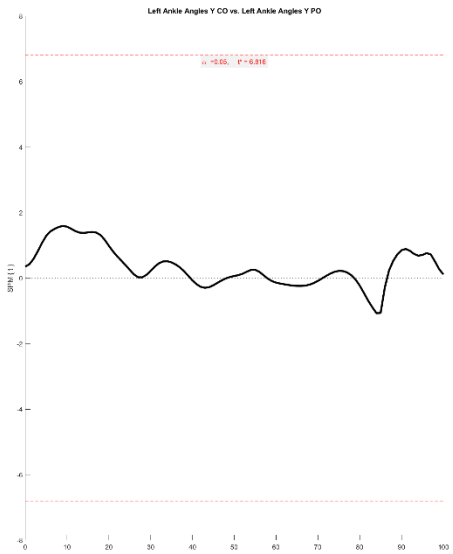

Right Foot Pitch Angles X

0.0-45.5%, 98.4-100.0%

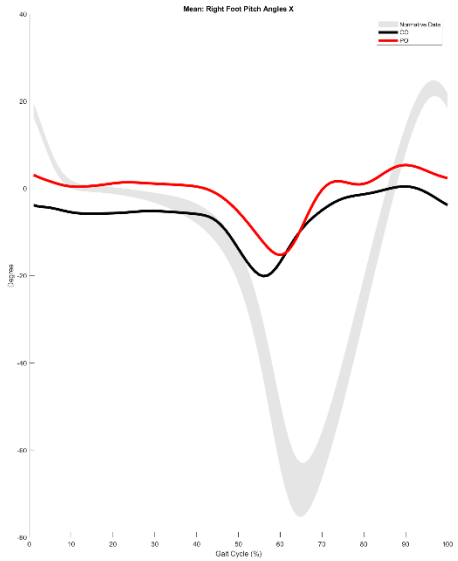

Left Foot Pitch Angles X

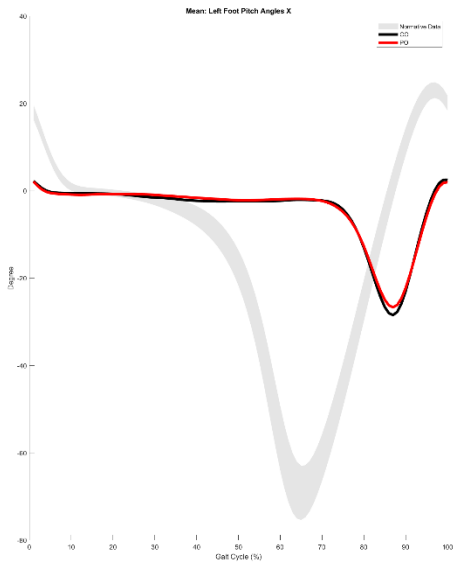

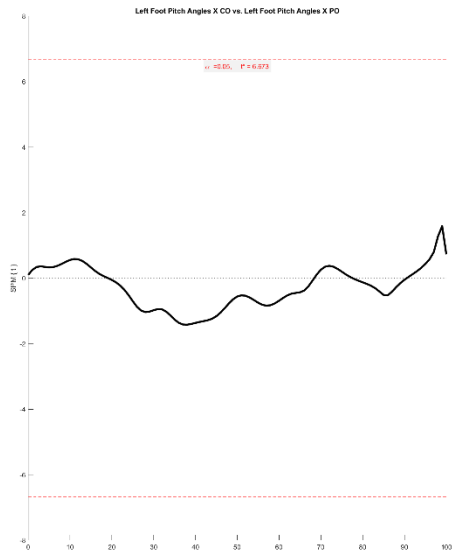

Right Foot Progression Z

50.2-55.3%

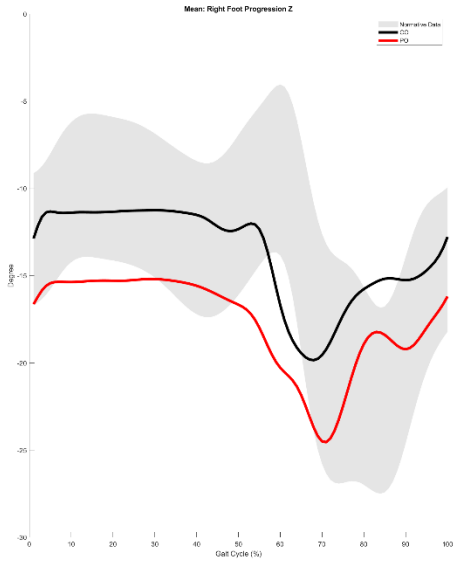

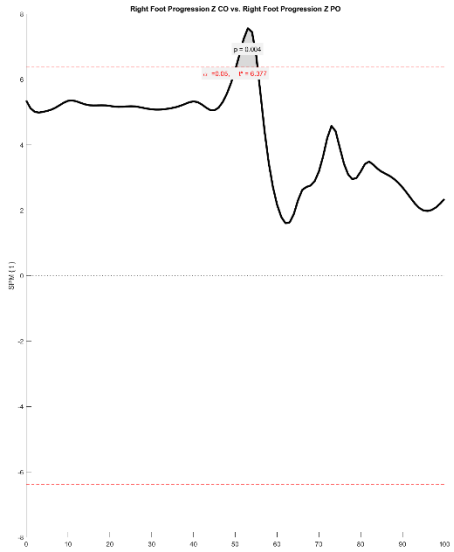

Left Foot Progression Z

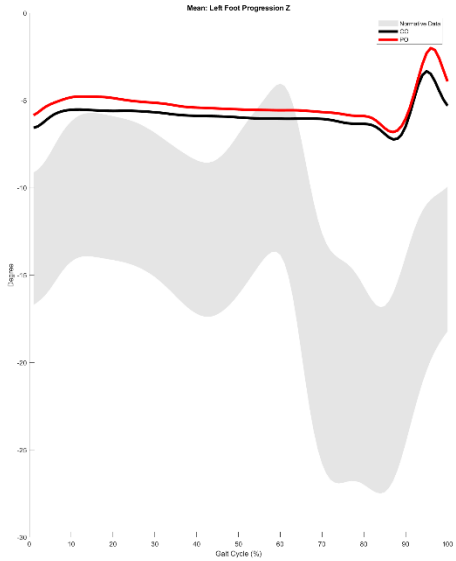

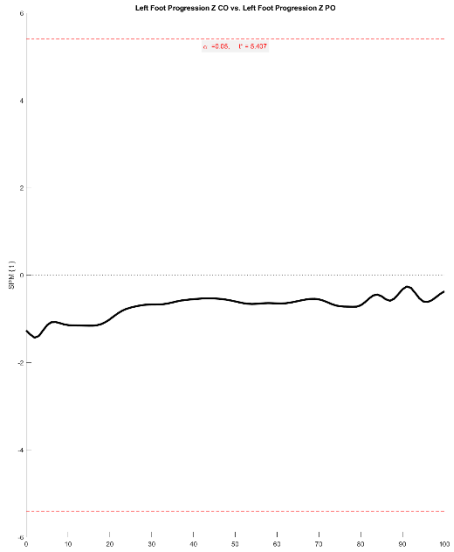

Right Hip Moment X

53.3-54.5%

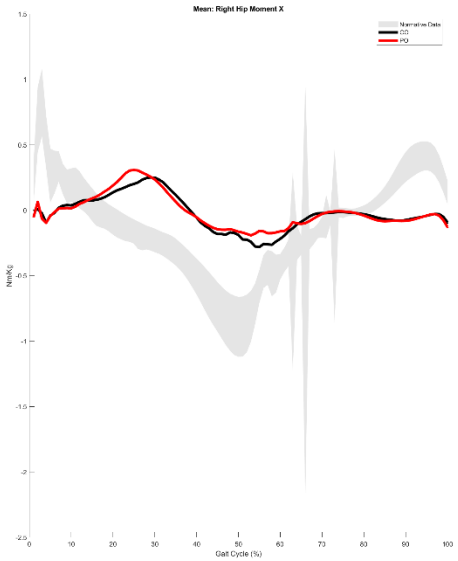

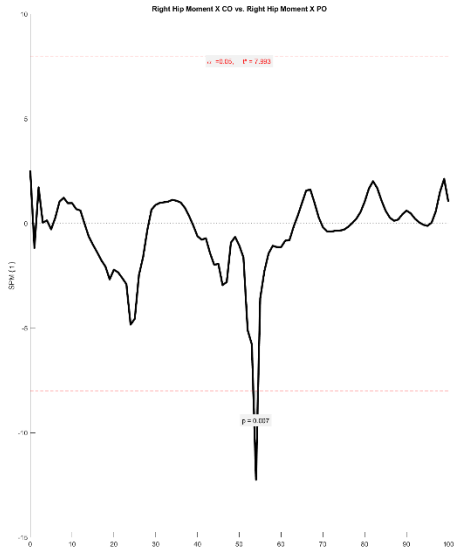

Right Hip Moment Y

37.4-39.7%

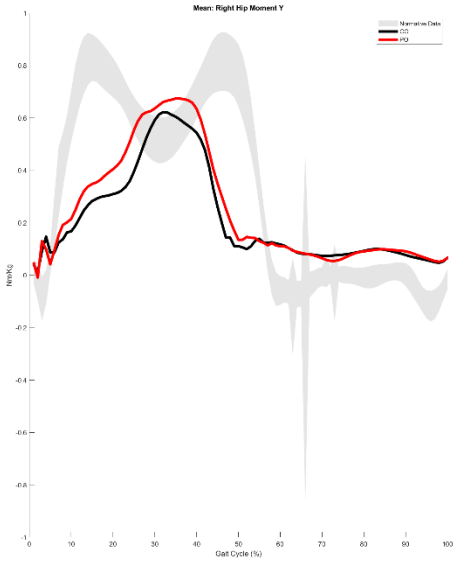

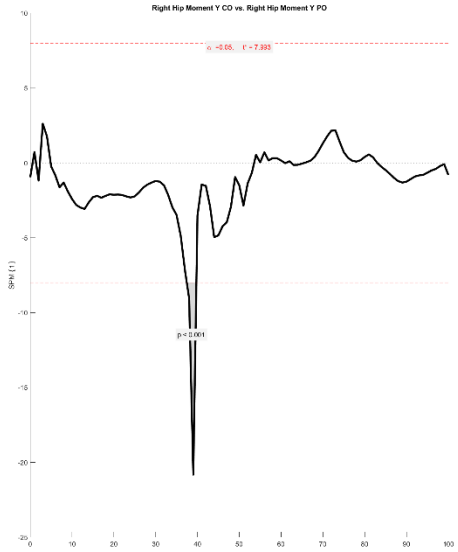

Left Hip Moment X

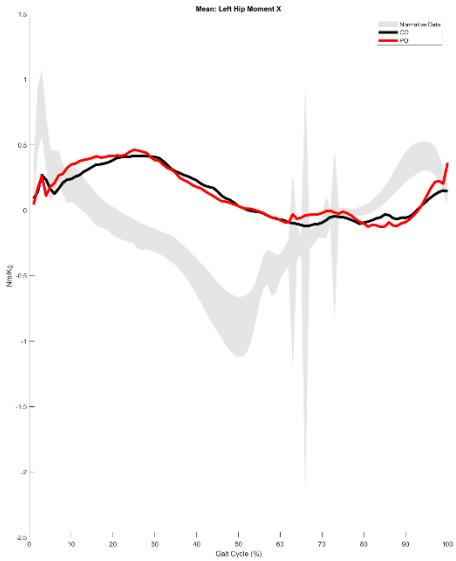

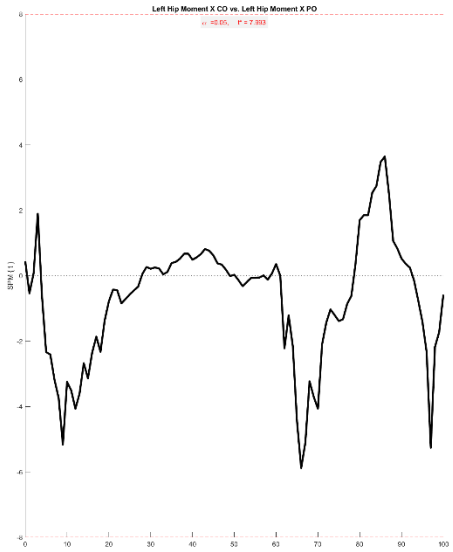

Left Hip Moment Y

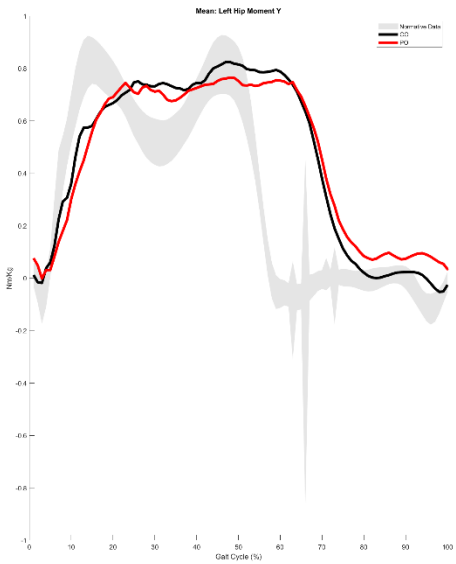

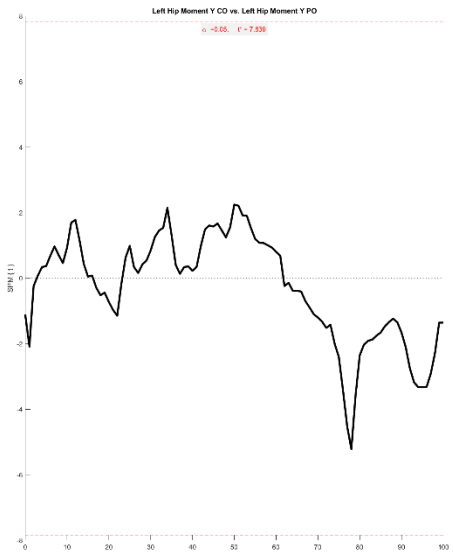

Right Knee Moment X

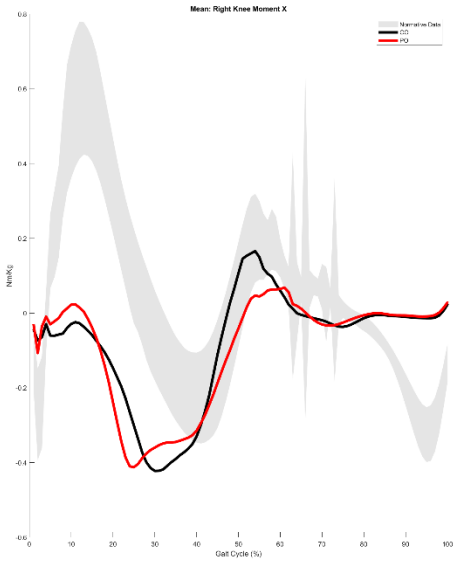

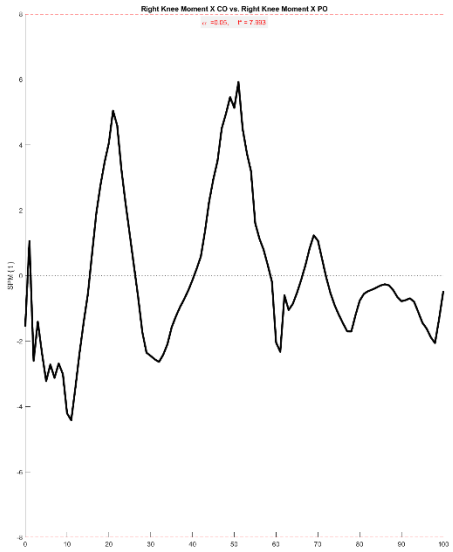

Right Knee Moment Y

42.5-44.0%

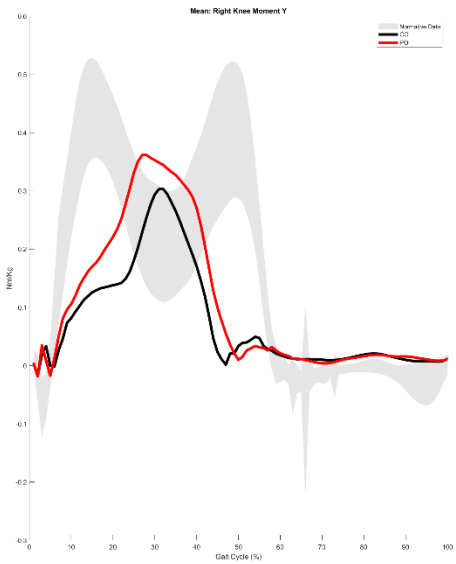

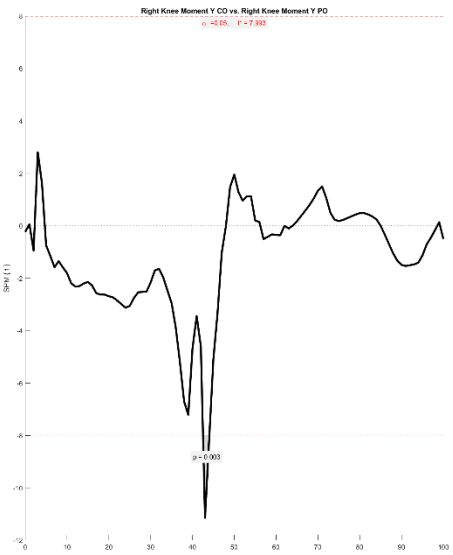

Left Knee Moment X

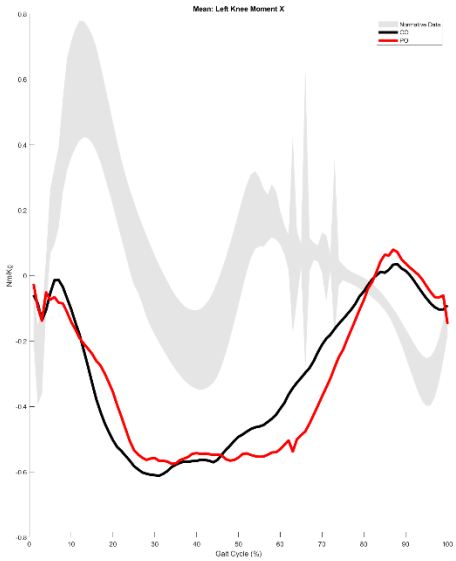

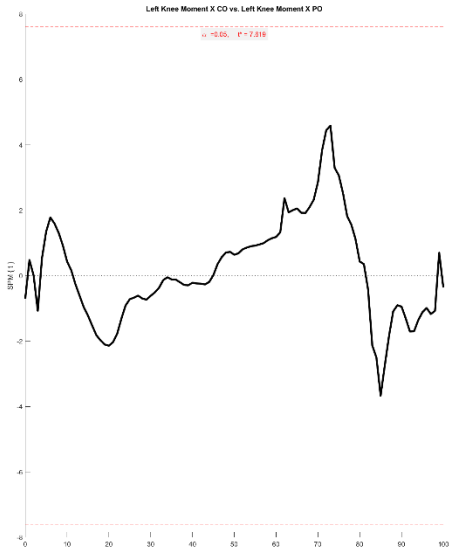

Left Knee Moment Y

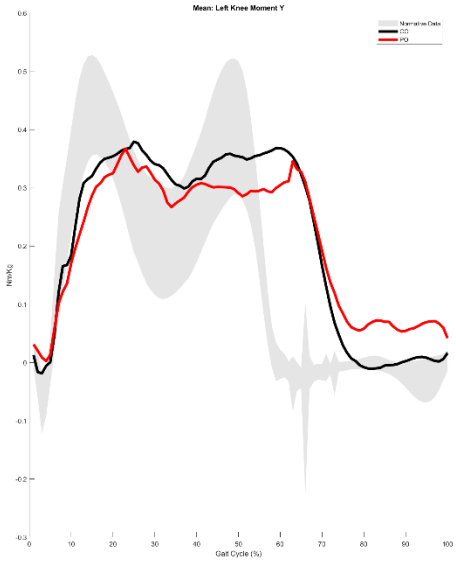

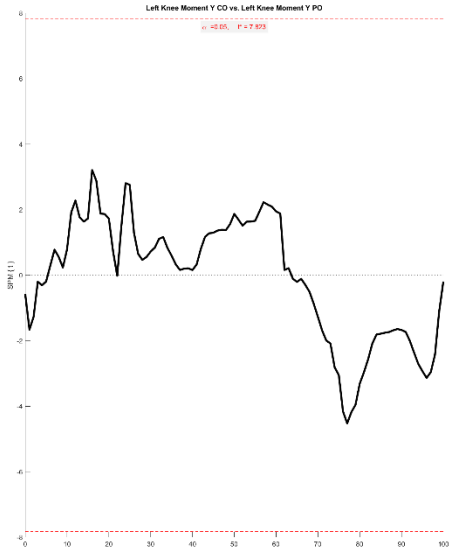

Right Ankle Moment X

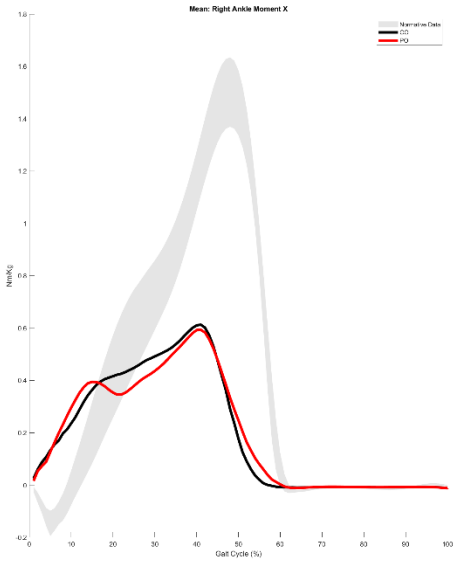

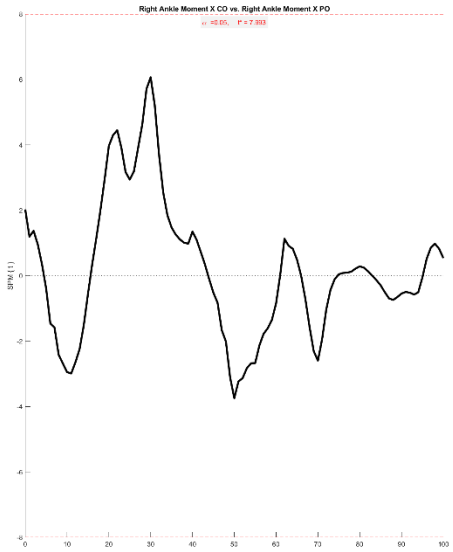

Right Ankle Moment Y

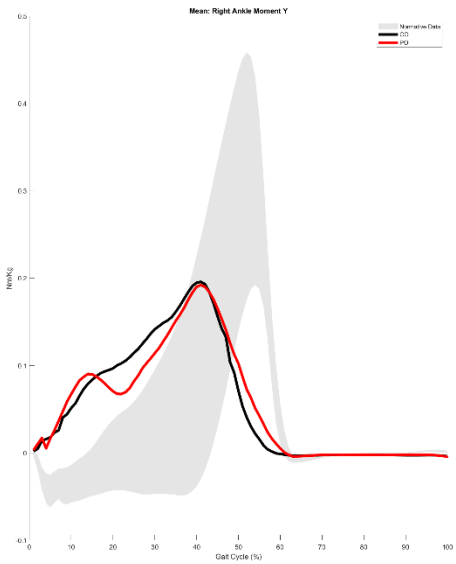

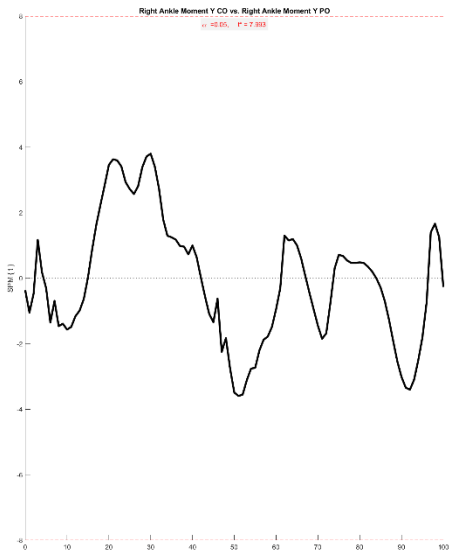

Left Ankle Moment X

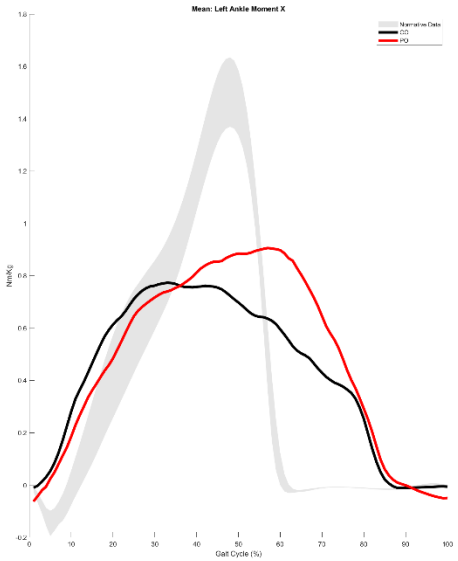

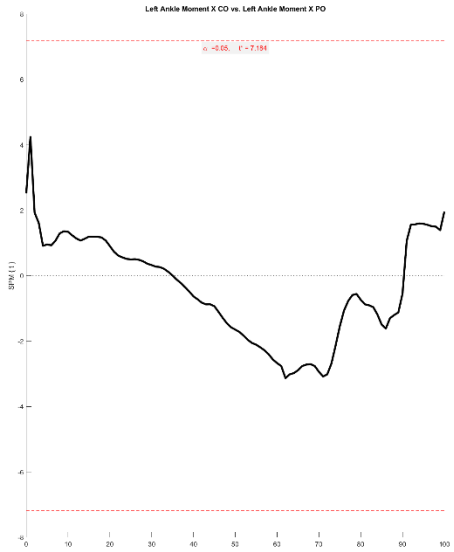

Left Ankle Moment Y

48.9-57.3%, 78.7-80.0%

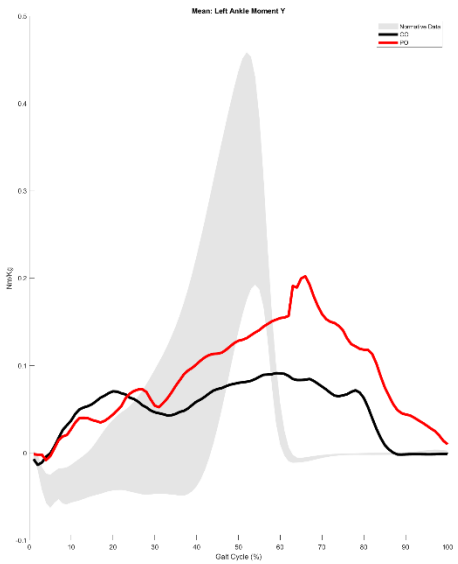

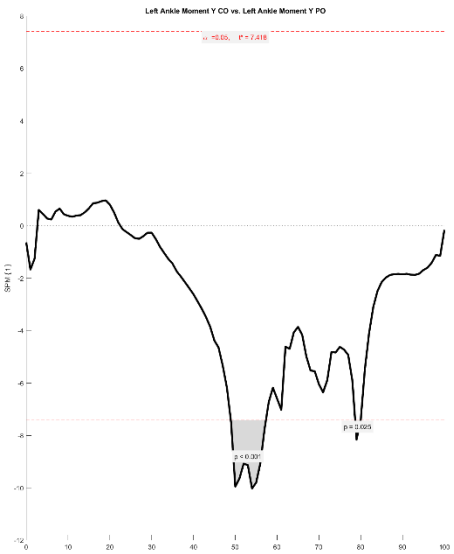

PO

Step Length

REP	Left	Right	IS (50%)	IS (0%)
1	0.17826	0.26035	59.358	37.4319
2	0.16521	0.25231	60.4306	41.7226
3	0.15121	0.24639	61.9693	47.8773
4	0.14167	0.23688	62.5756	50.3025
5	0.1276	0.23382	64.6948	58.7793
6	0.1267	0.23217	64.6947	58.7789
Mean	0.148442	0.2436533	62.2872	49.1487
SD	0.018845	0.0102928	1.99183	7.96731

CO

Step Length

REP	Left	Right	IS (50%)	IS (0%)
1	0.14637	0.22391	60.4705	41.8818
2	0.14198	0.22171	60.9613	43.845
3	0.13894	0.21979	61.2689	45.0757
4	0.13591	0.21889	61.6939	46.7756
5	0.13412	0.21784	61.8934	47.5736
6	0.13228	0.21411	61.8118	47.2473
Mean	0.1382667	0.219375	61.35	45.3998
SD	0.0048044	0.0030687	0.5096	2.03839

	Left	Right
Step Length PO	0.15	0.24
Step Length CO	0.14	0.22
Swing Time PO	0.33	0.82
Swing Time CO	0.32	0.79
Stance Time PO	1.62	1.04
Stance Time CO	1.54	1.06

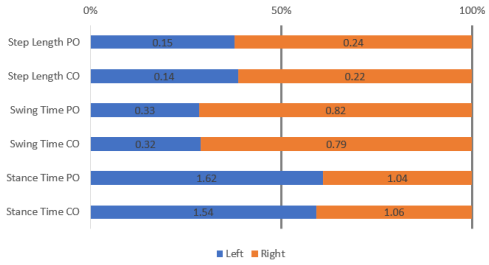

PO

Swing Time

REP	Left	Right	IS (50%)	IS (0%)
1	0.33333	0.85833	72.0281	88.1124
2	0.33333	0.83333	71.4287	85.7148
3	0.325	0.81667	71.5329	86.1317
4	0.325	0.80833	71.3234	85.2938
5	0.325	0.79167	70.8956	83.5824
6	0.31667	0.78333	71.2118	84.8473
Média	0.326388	0.8152767	71.4034	85.6137
DP	0.005724	0.0251912	0.34366	1.37464

CO

Swing Time

REP	Left	Right	IS (50%)	IS (0%)
1	0.34167	0.85	71.3285	85.3139
2	0.33333	0.84167	71.6315	86.526
3	0.325	0.78333	70.6766	82.7064
4	0.31667	0.78333	71.2118	84.8473
5	0.30833	0.775	71.5387	86.1547
6	0.30833	0.725	70.1615	80.6461
Mean	0.3222217	0.793055	71.0914	84.3657
SD	0.012424	0.0423335	0.51627	2.06507

PO

Stance Time

REP	Left	Right	IS (50%)	IS (0%)
1	1.74167	1.1	38.7096	45.1615
2	1.64167	1.04167	38.8199	44.7204
3	1.61667	1.04167	39.185	43.2601
4	1.6	1.03333	39.2404	43.0383
5	1.55833	1.00833	39.2857	42.8573
6	1.54167	1	39.3442	42.6232
Mean	1.616668	1.0375	39.0975	43.6101
SD	0.065264	0.0321858	0.24216	0.96866

CO

Stance Time

REP	Left	Right	IS (50%)	IS (0%)
1	1.6	1.09167	40.5573	37.7706
2	1.59167	1.08333	40.4983	38.0067
3	1.56667	1.05833	40.3173	38.7307
4	1.53333	1.05	40.6452	37.4191
5	1.5	1.05	41.1765	35.2941
6	1.43333	1.03333	41.8919	32.4325
Mean	1.5375	1.06111	40.8478	36.609
SD	0.0576867	0.0202236	0.53651	2.14603

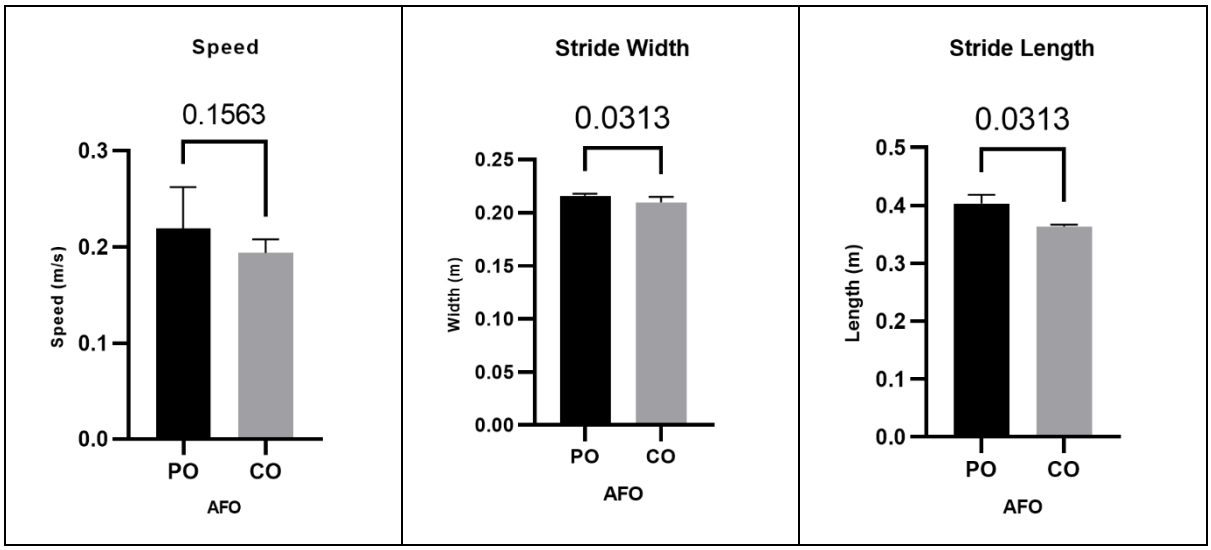

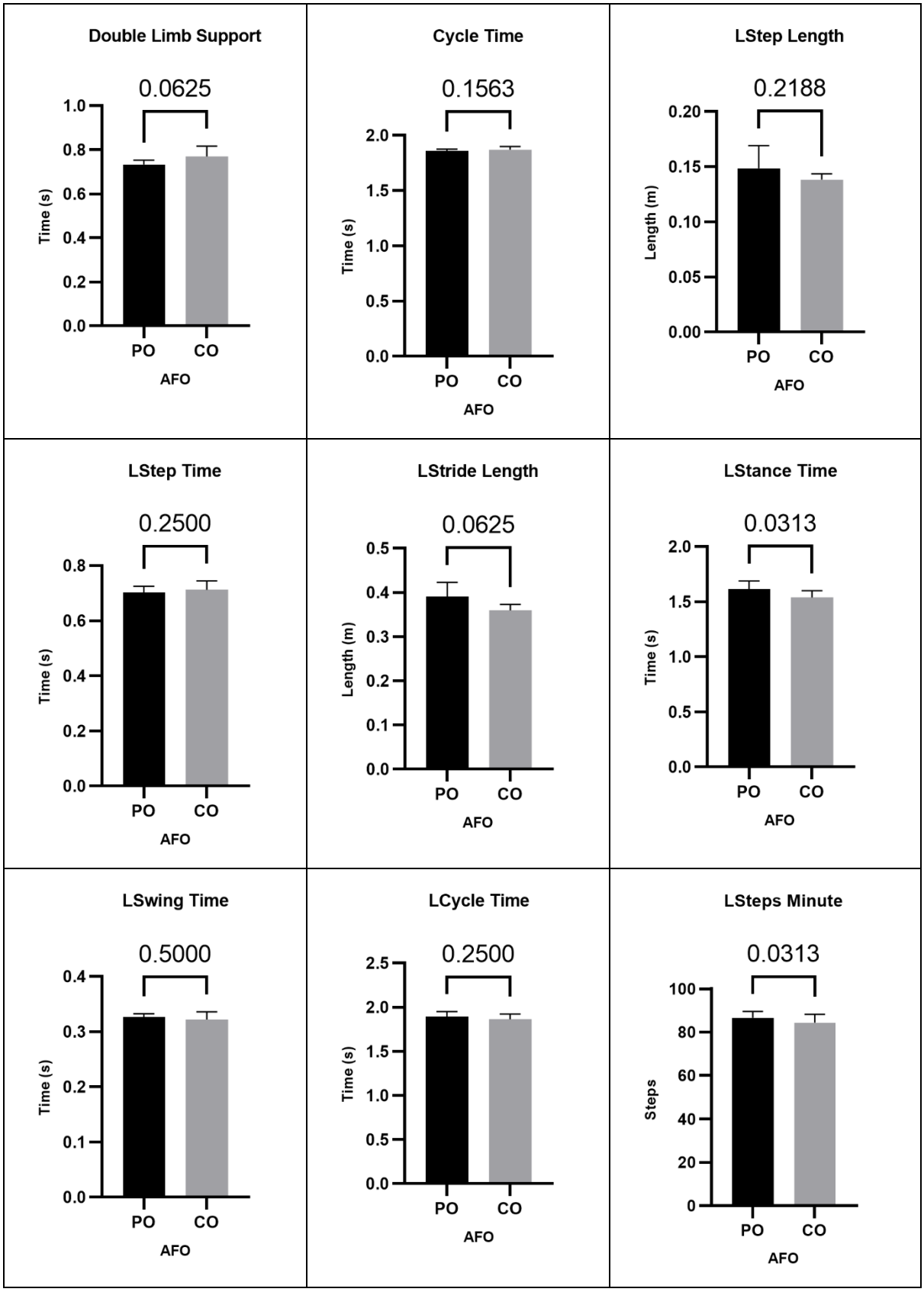
Double Limb Support
0.0625
Time (s)
1.0
0.8
0.6
0.4
0.2
0.0
PO
CO
AFO
Cycle Time
0.1563
Time (s)
2.0
1.5
1.0
0.5
0.0
PO
CO
AFO
LStep Length
0.2188
Length (m)
0.20
0.15
0.10
0.05
0.00
PO
CO
AFO
LStep Time
0.2500
Time (s)
0.8
0.6
0.4
0.2
0.0
PO
CO
AFO
LStride Length
0.0625
Length (m)
0.5
0.4
0.3
0.2
0.1
0.0
PO
CO
AFO
LStance Time
0.0313
Time (s)
2.0
1.5
1.0
0.5
0.0
PO
CO
AFO
LSwing Time
0.5000
Time (s)
0.4
0.3
0.2
0.1
0.0
PO
CO
AFO
LCycle Time
0.2500
Time (s)
2.5
2.0
1.5
1.0
0.5
0.0
PO
CO
AFO
LSteps Minute
0.0313
Steps
100
80
60
40
20
0
PO
CO
AFO

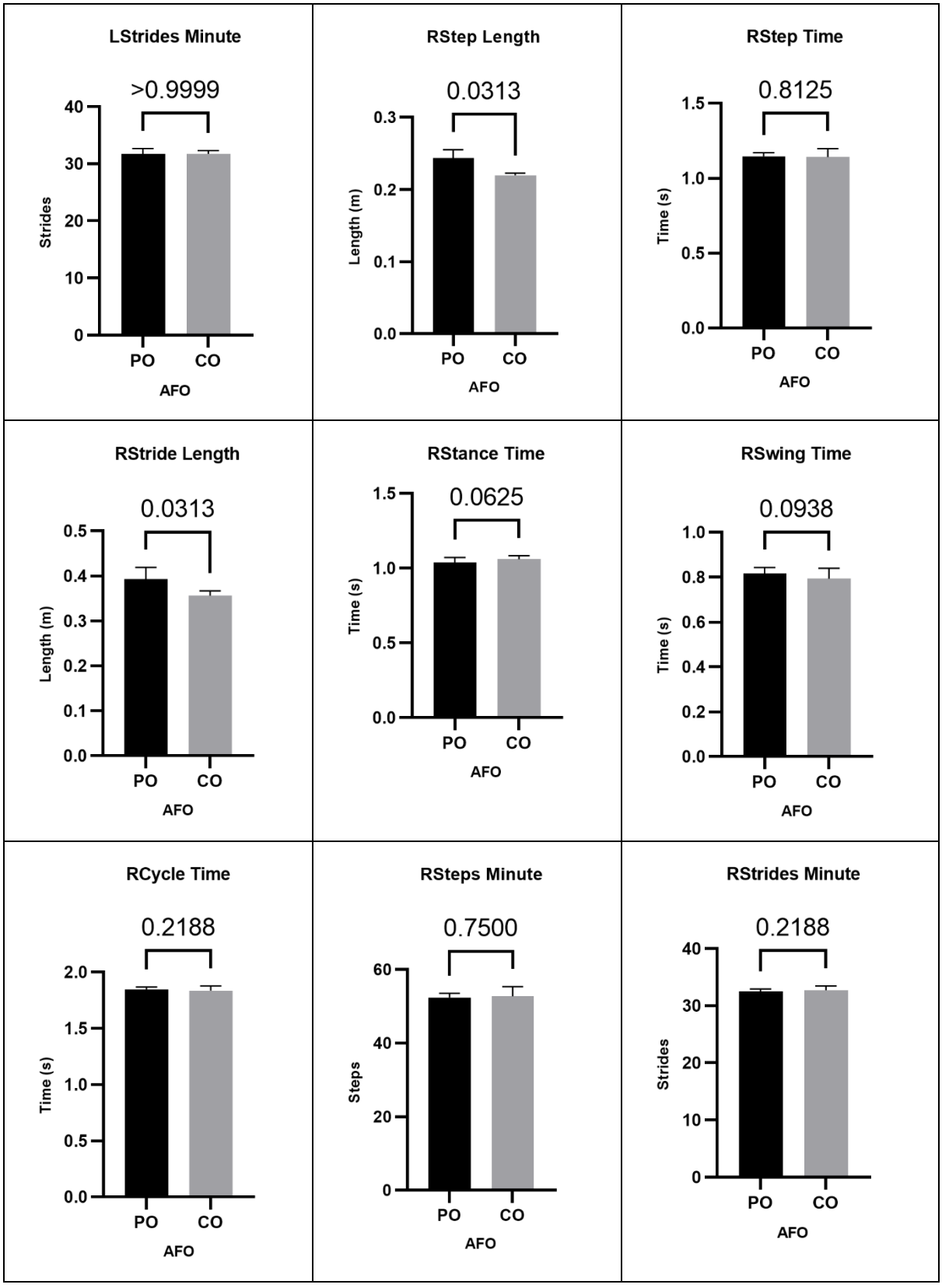
LStrides Minute
>0.9999
Strides
40
30
20
10
0
PO
CO
AFO
RStep Length
0.0313
Length (m)
0.3
0.2
0.1
0.0
PO
CO
AFO
RStep Time
0.8125
Time (s)
1.5
1.0
0.5
0.0
PO
CO
AFO
RStride Length
0.0313
Length (m)
0.5
0.4
0.3
0.2
0.1
0.0
PO
CO
AFO
RStance Time
0.0625
Time (s)
1.5
1.0
0.5
0.0
PO
CO
AFO
RSwing Time
0.0938
Time (s)
1.0
0.8
0.6
0.4
0.2
0.0
PO
CO
AFO
RCycle Time
0.2188
Time (s)
2.0
1.5
1.0
0.5
0.0
PO
CO
AFO
RSteps Minute
0.7500
Steps
60
40
20
0
PO
CO
AFO
RStrides Minute
0.2188
Strides
40
30
20
10
0
PO
CO
AFO

GLOBAL

Unaffected Limb Pelvic Angles X

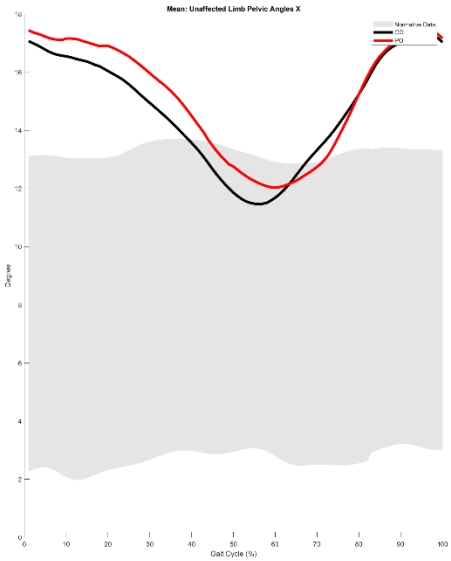

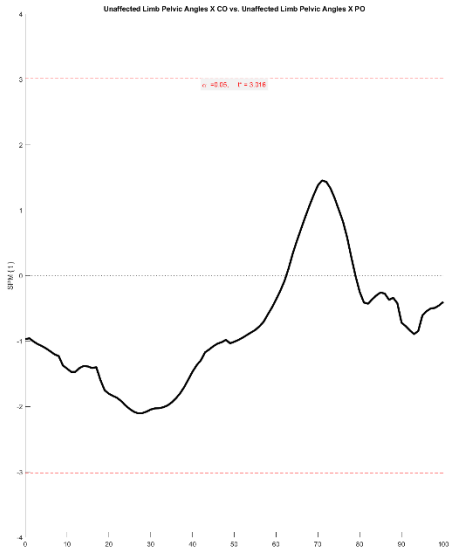

Unaffected Limb Pelvic Angles Y

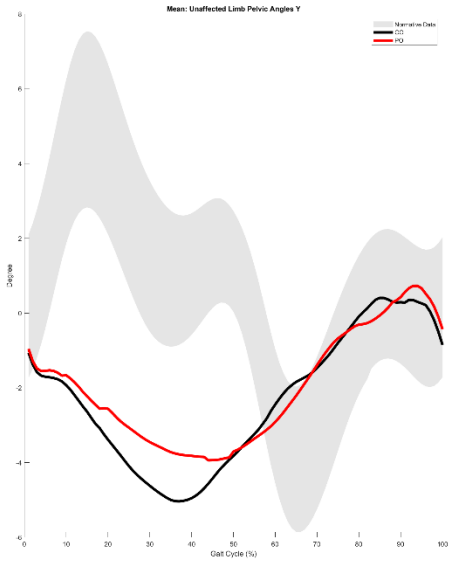

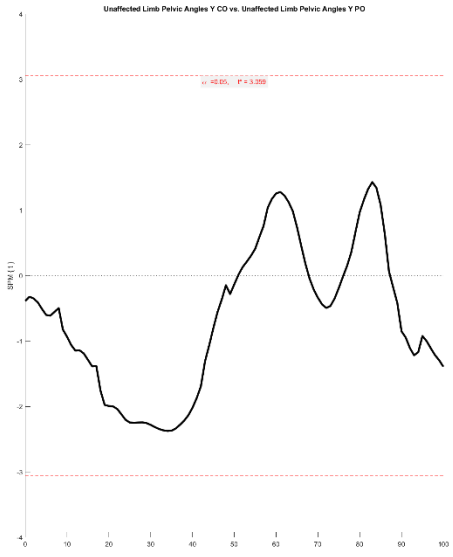

Unaffected Limb Pelvic Angles Z

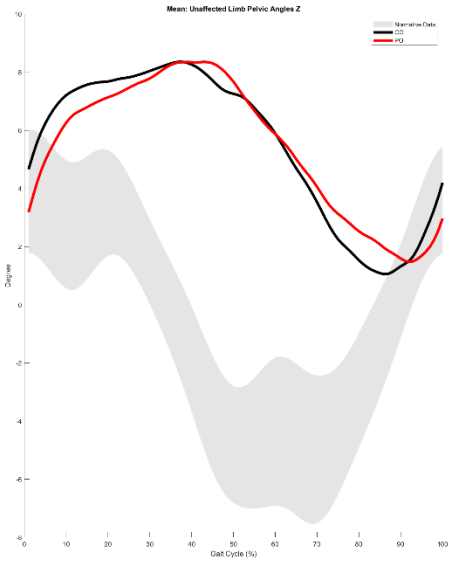

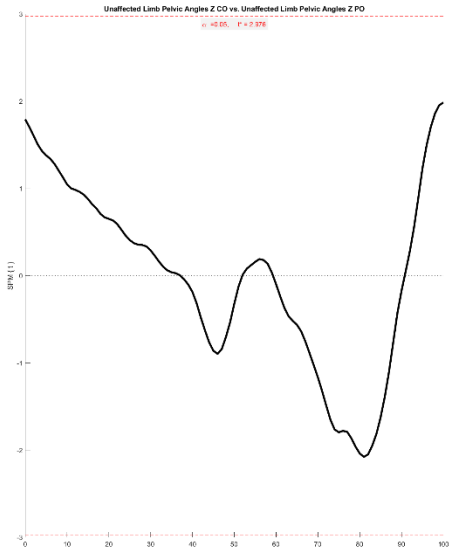

Affected Limb Pelvic Angles X

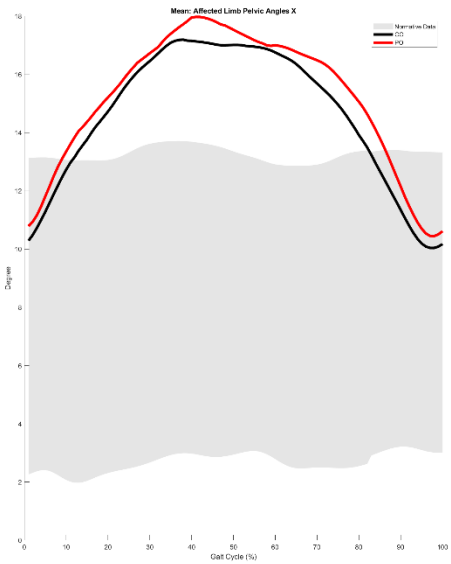

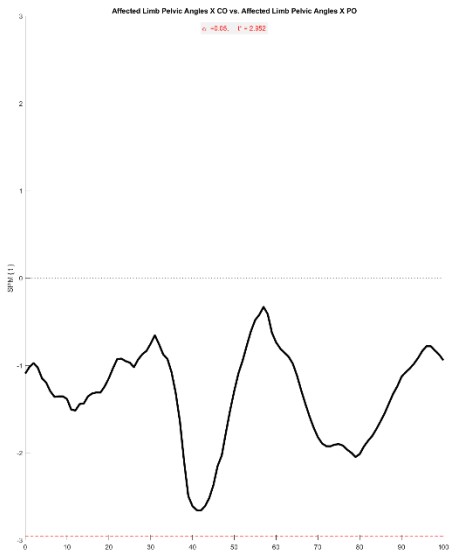

Affected Limb Pelvic Angles Y

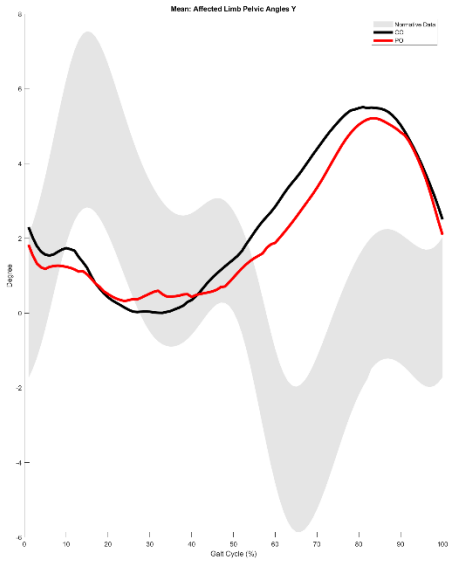

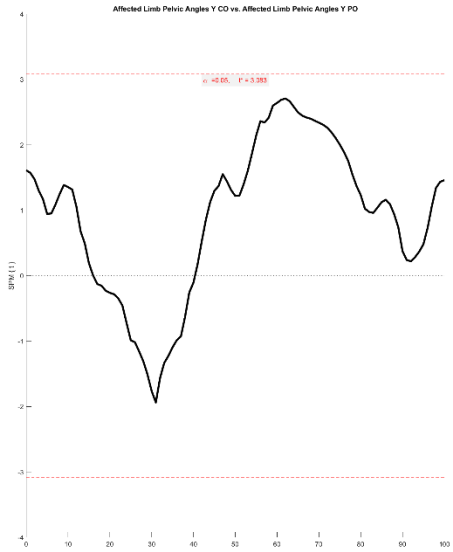

Affected Limb Pelvic Angles Z

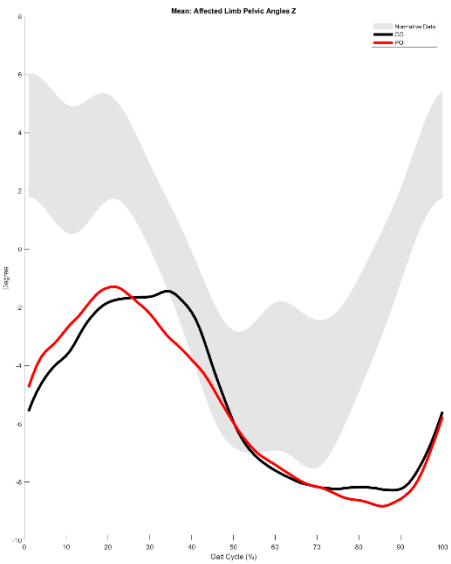

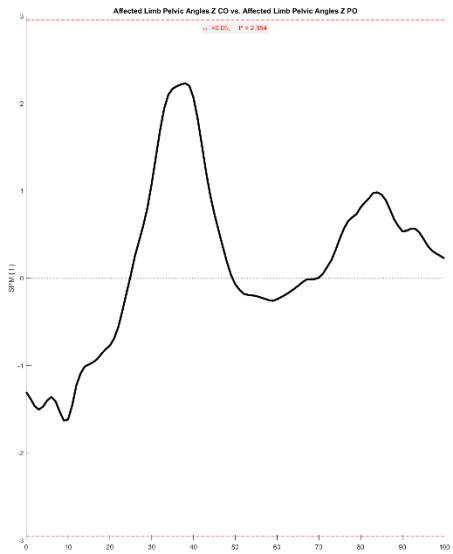

Unaffected Limb Hip Angles X

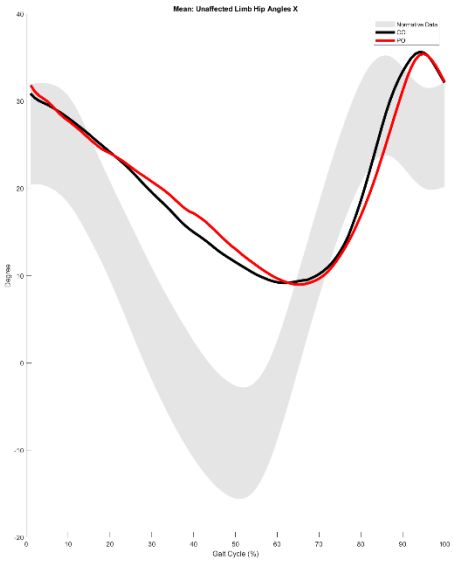

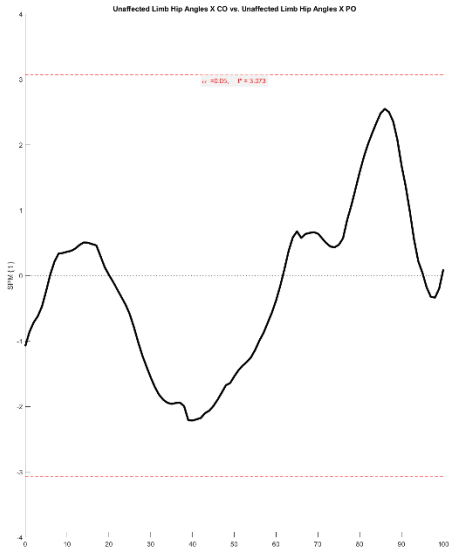

Unaffected Limb Hip Angles Y

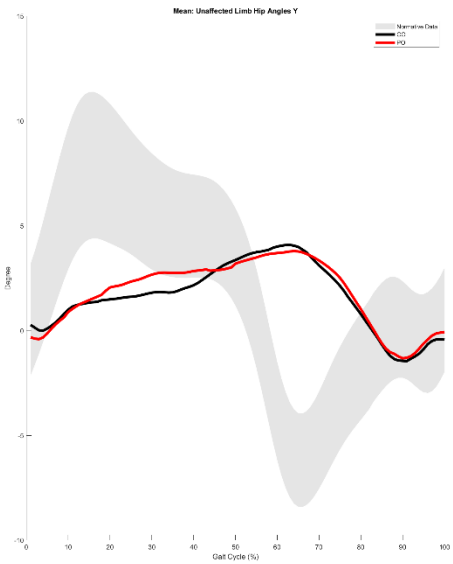

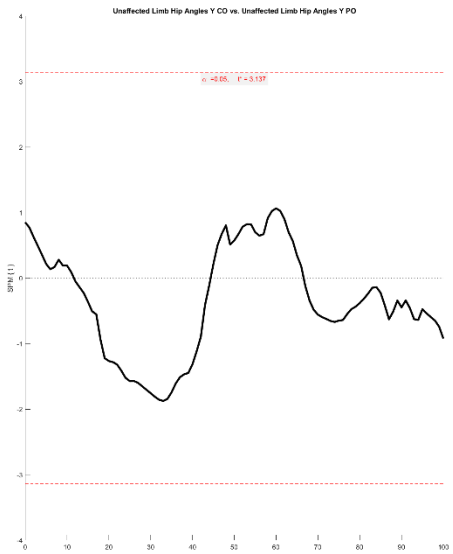

Unaffected Limb Hip Angles Z

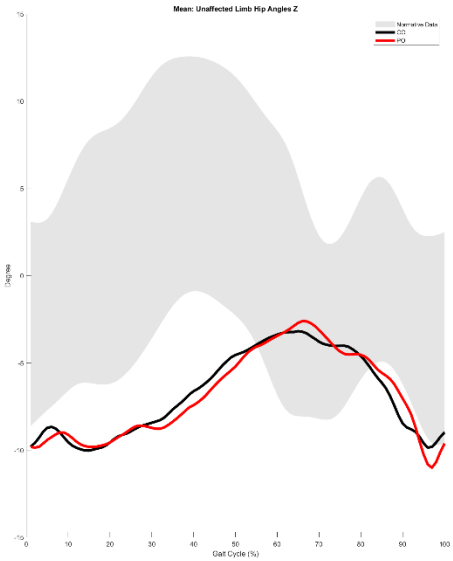

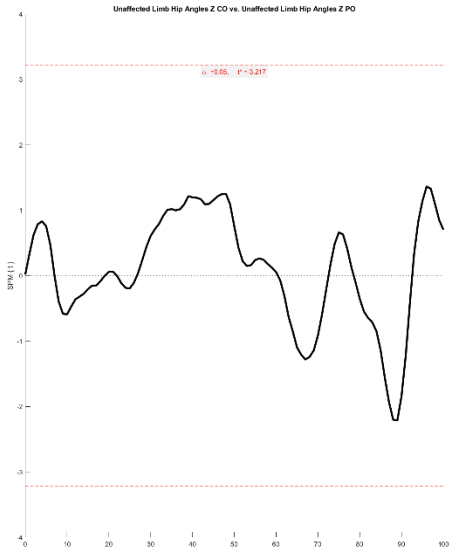

Affected Limb Hip Angles X

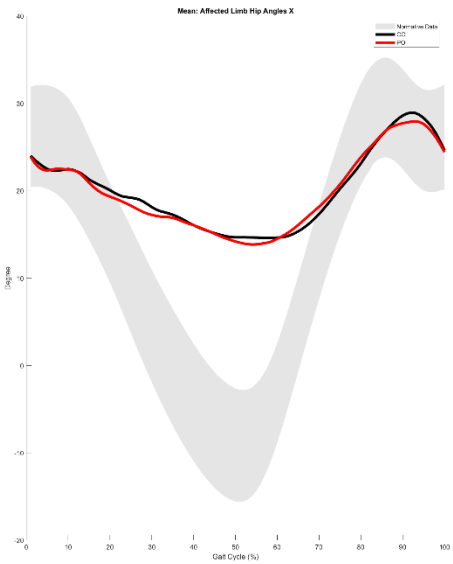

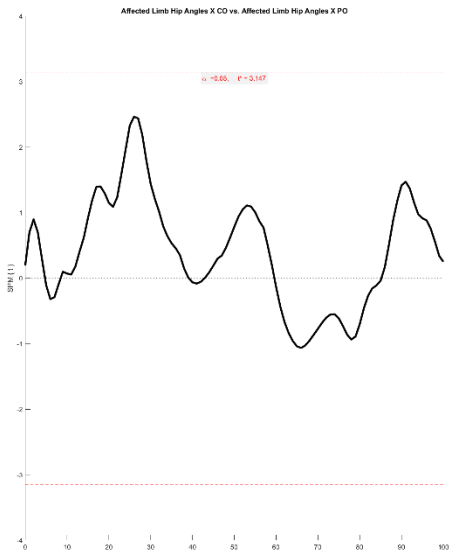

Affected Limb Hip Angles Y

59.7-70.2%

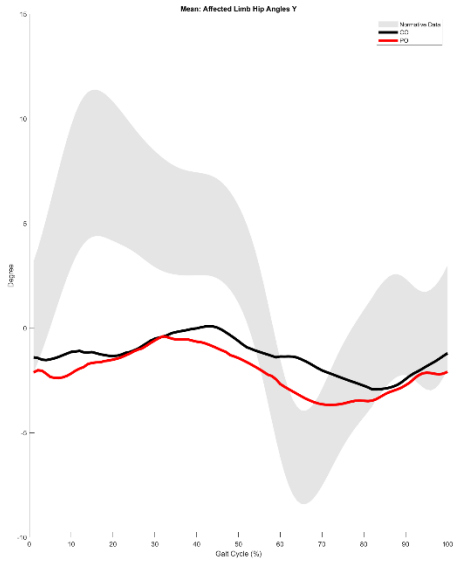

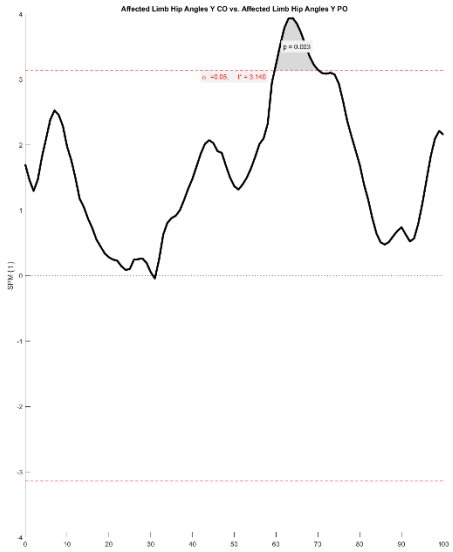

Affected Limb Hip Angles Z

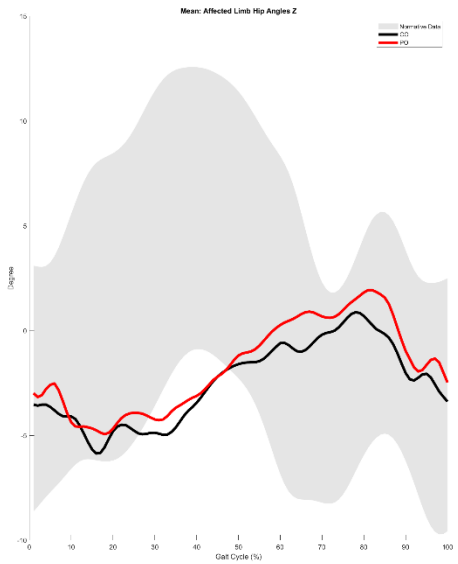

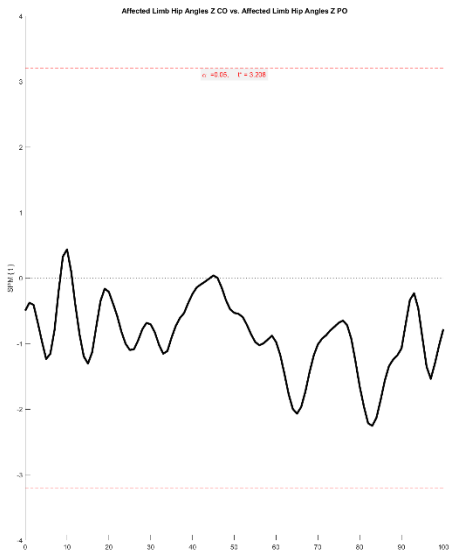

Unaffected Limb Knee Angles X

98.9-100.0%

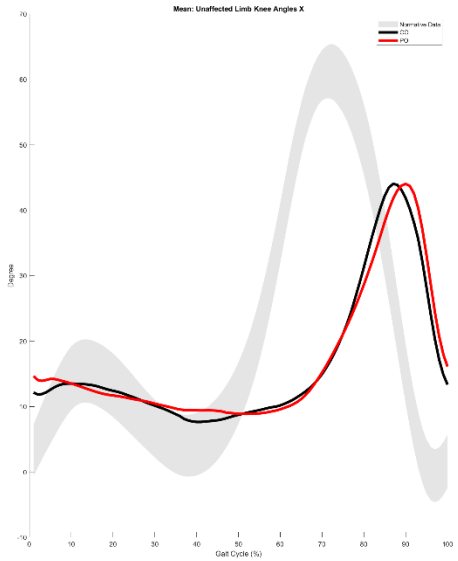

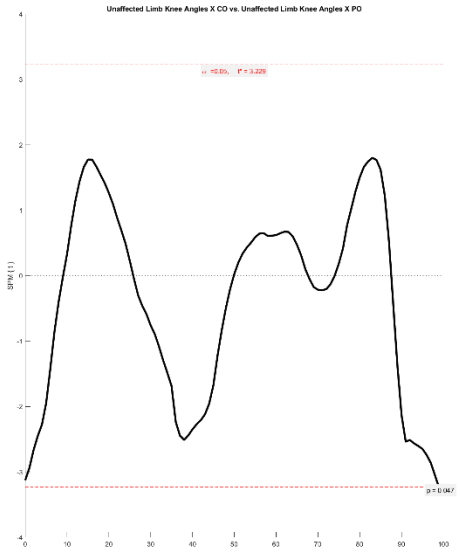

Unaffected Limb Knee Angles Y

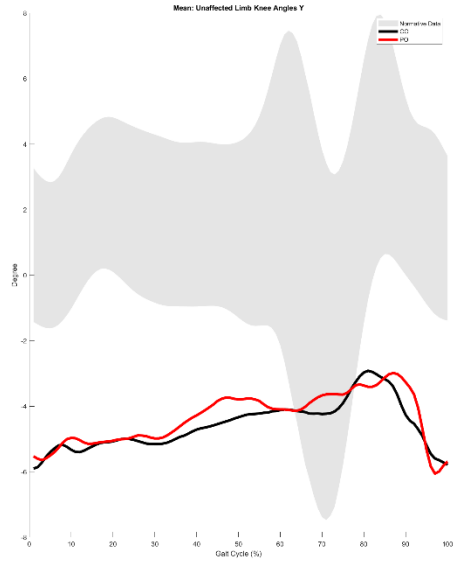

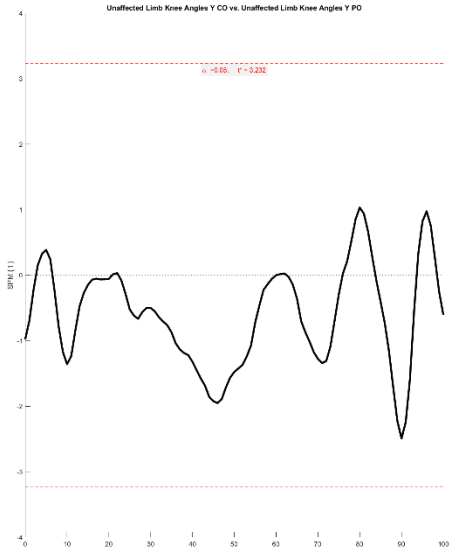

Unaffected Limb Knee Angles Z

95.0-97.6%

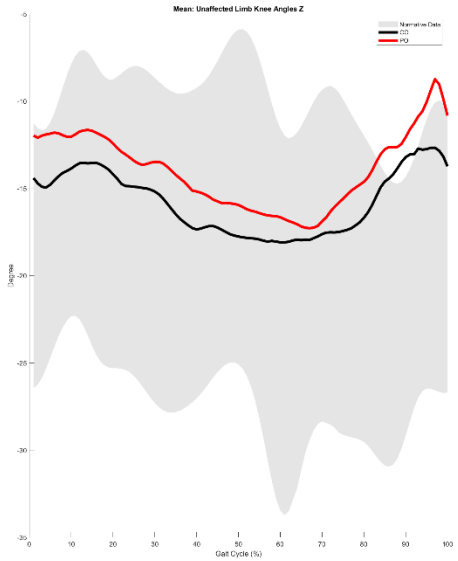

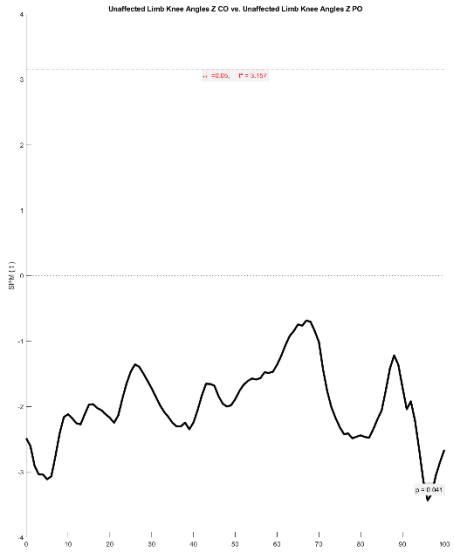

Affected Limb Knee Angles X

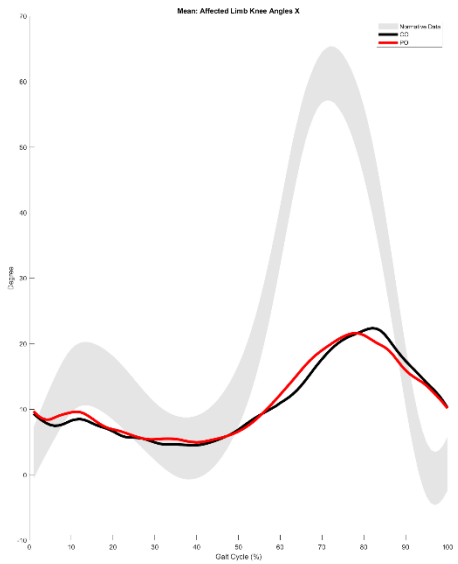

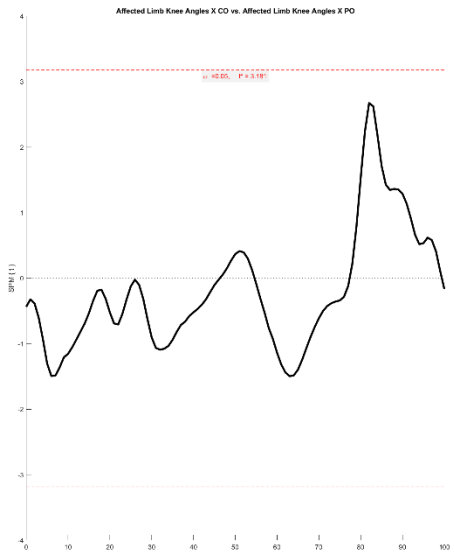

Affected Limb Knee Angles Y

0.0-0.7%, 4.0-7.2%, 61.8-67.3%

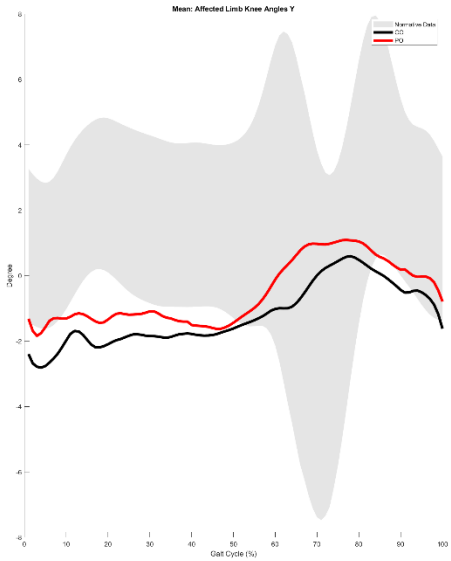

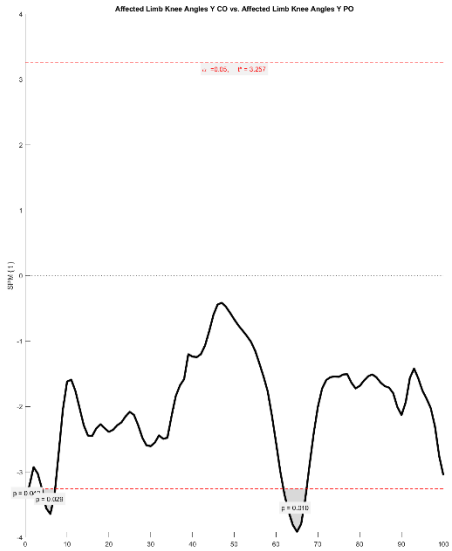

Affected Limb Knee Angles Z

3.2-7.4%, 11.3-18.5%, 74.8-98.2%

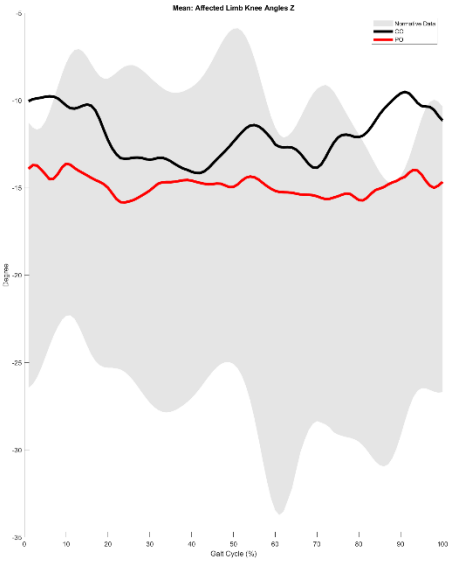

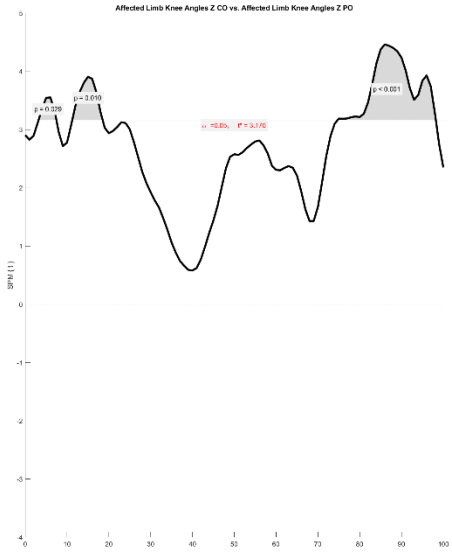

Unaffected Limb Ankle Angles X

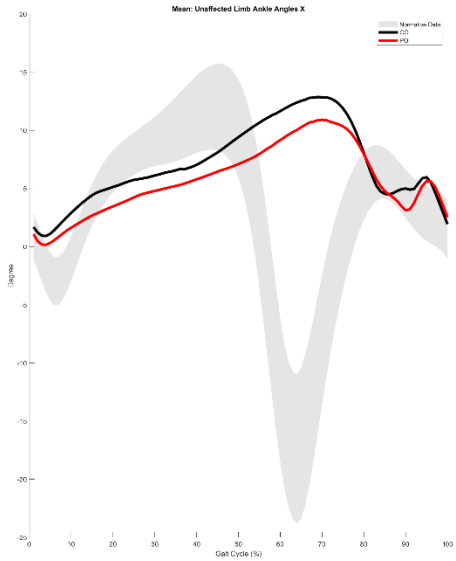

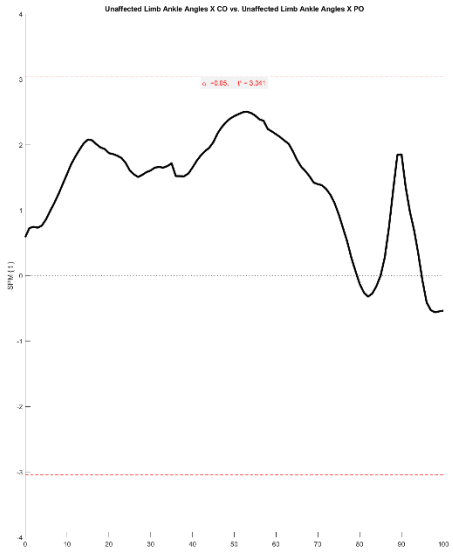

Unaffected Limb Ankle Angles Y

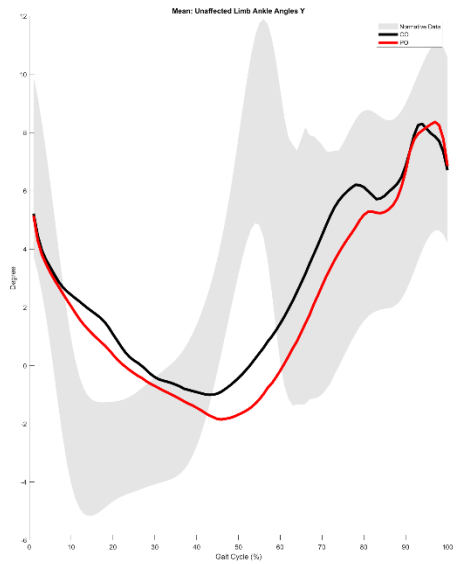

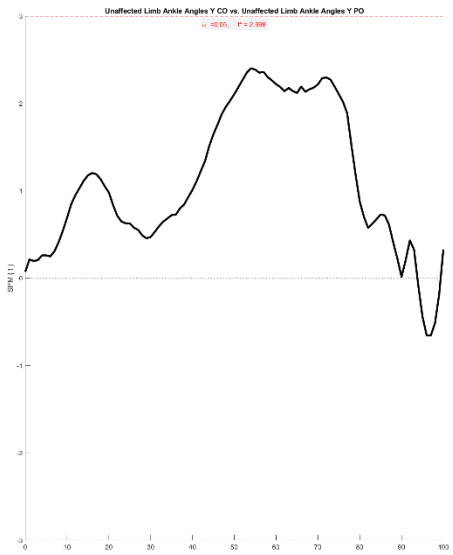

Affected Limb Ankle Angles X

17.9-35.1%, 54.8-63.7%

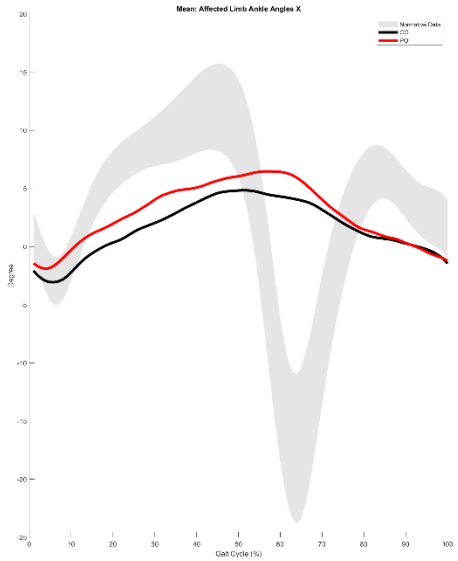

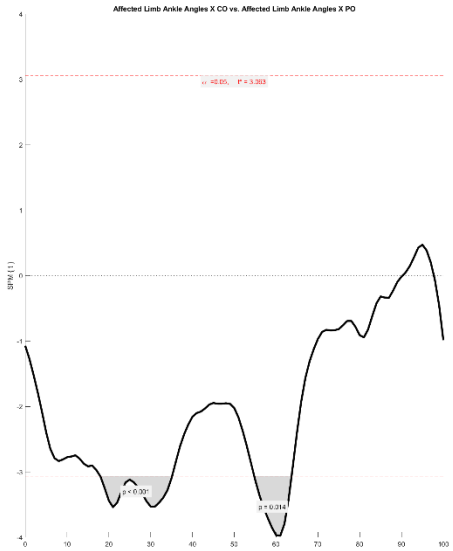

Affected Limb Ankle Angles Y

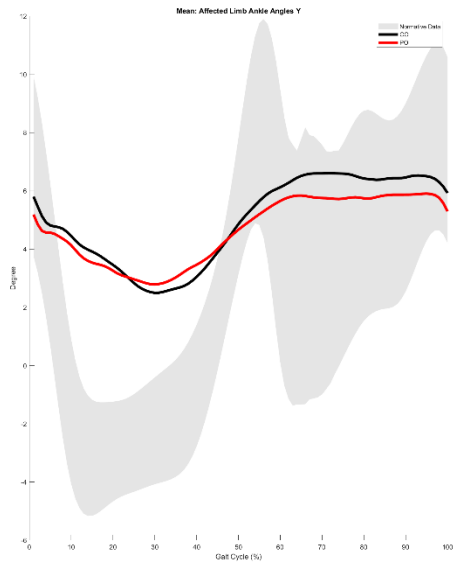

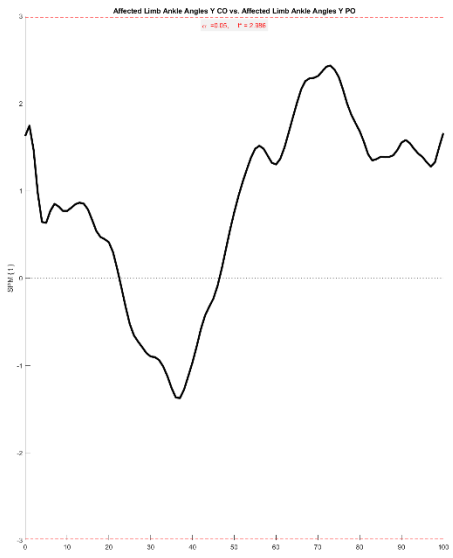

Unaffected Limb Foot Pitch X

88.8-97.5%

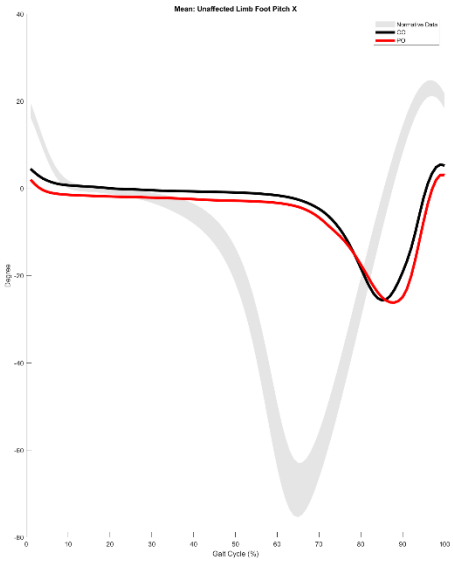

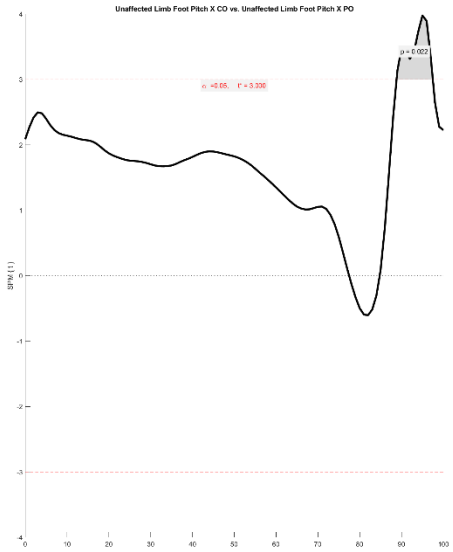

Affected Limb Foot Pitch X

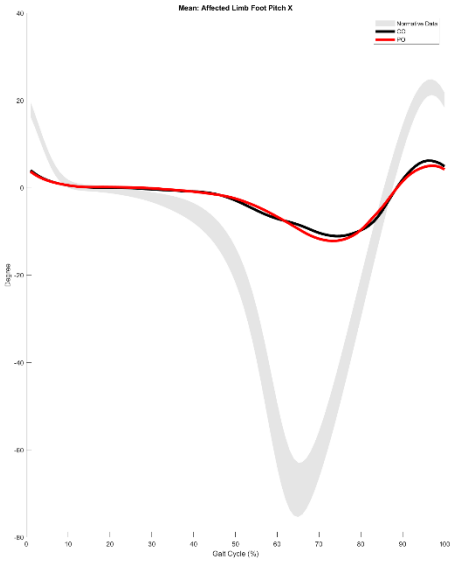

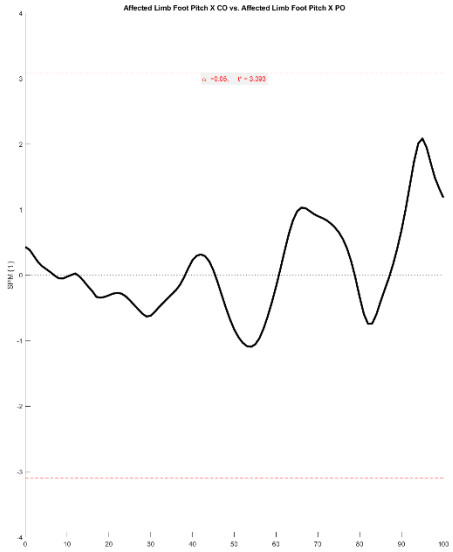

Unaffected Limb Foot Progression Z

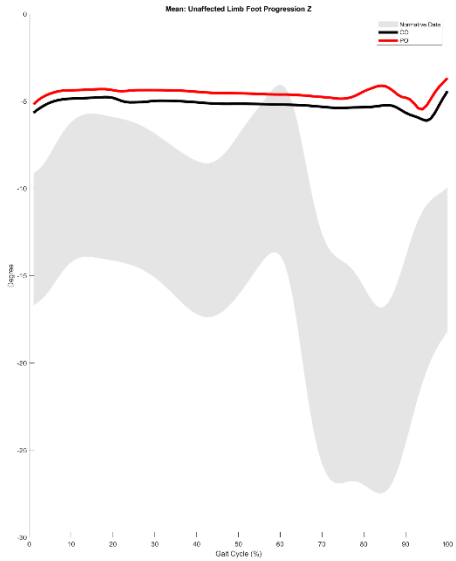

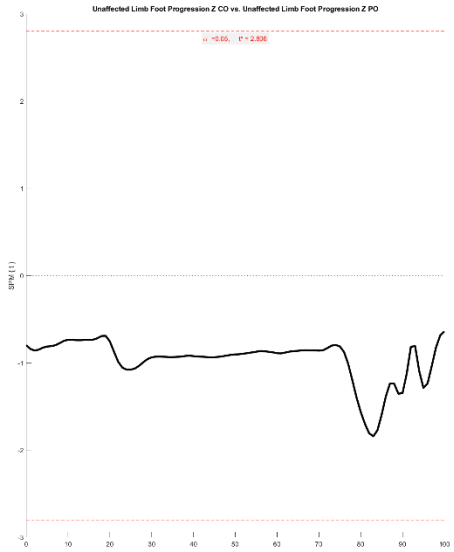

Affected Limb Foot Progression Z

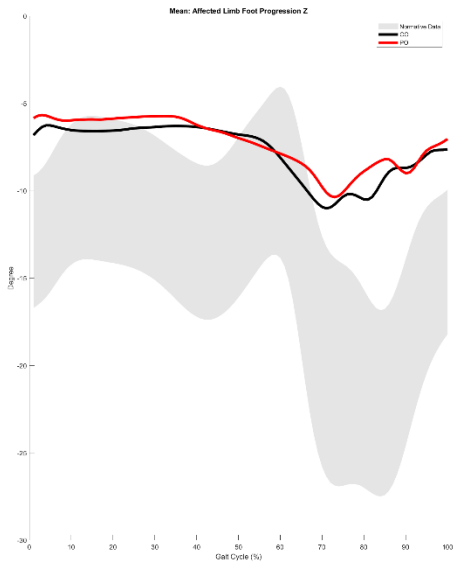

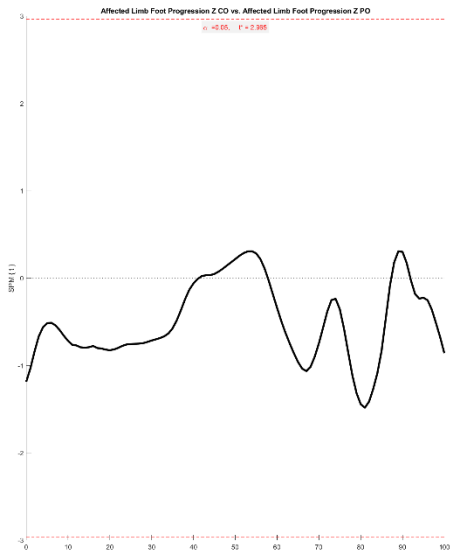

Unaffected Limb Hip Moment X

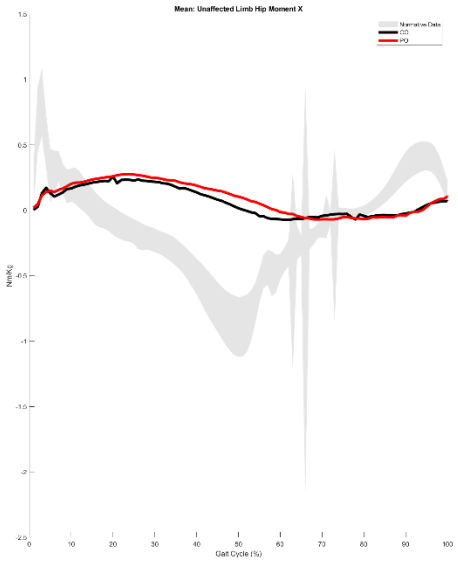

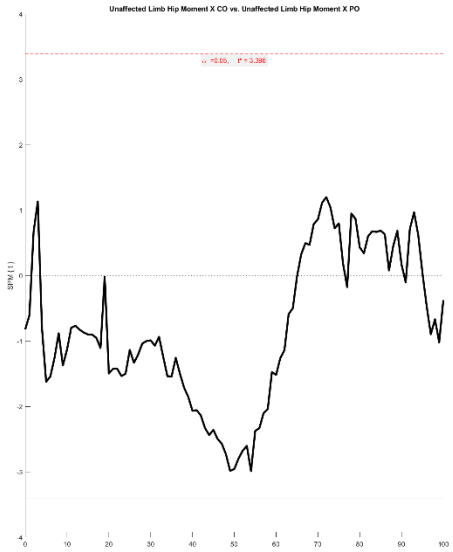

Unaffected Limb Hip Moment Y

80.7-81.1%

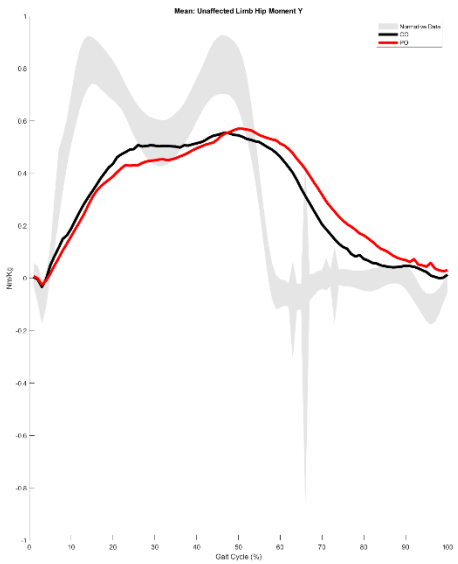

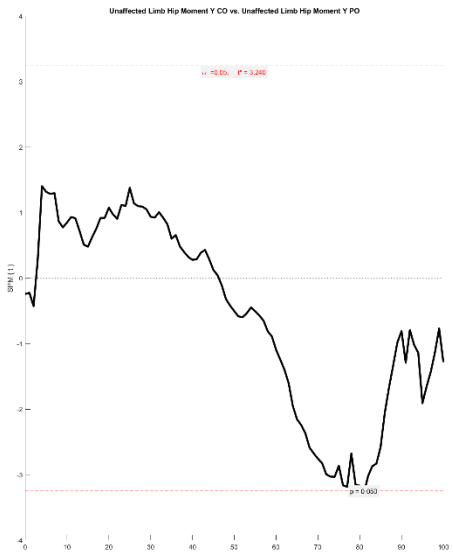

Affected Limb Hip Moment X

26.8-35.9%

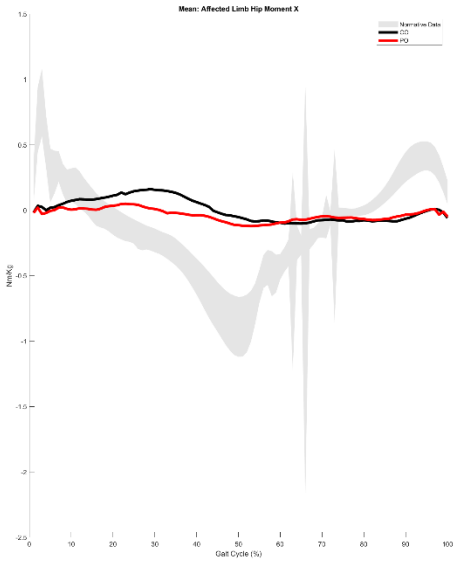

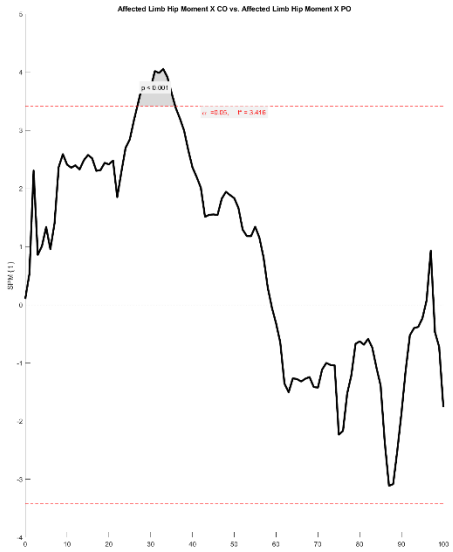

Affected Limb Hip Moment Y

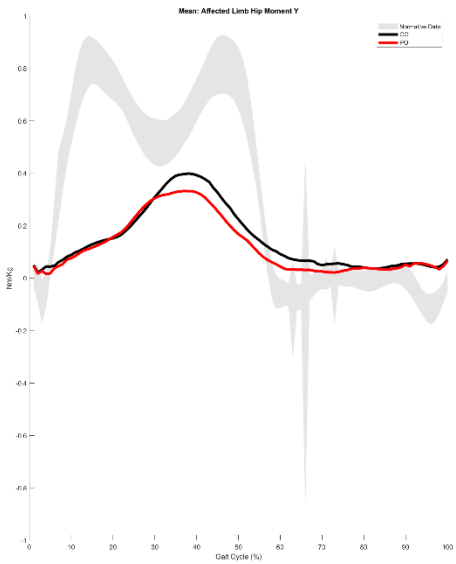

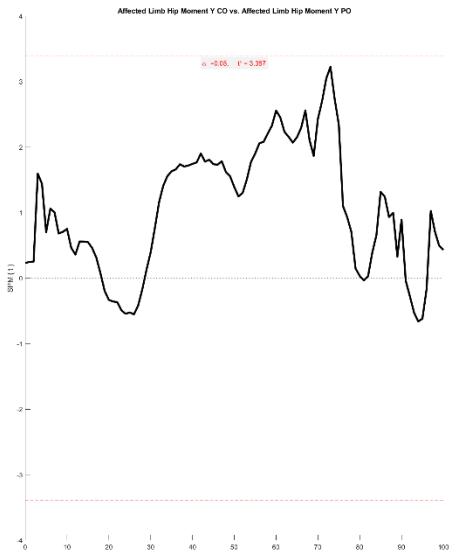

Unaffected Limb Knee Moment X

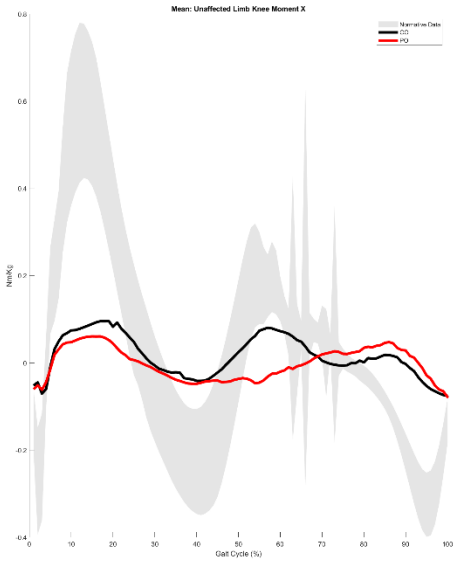

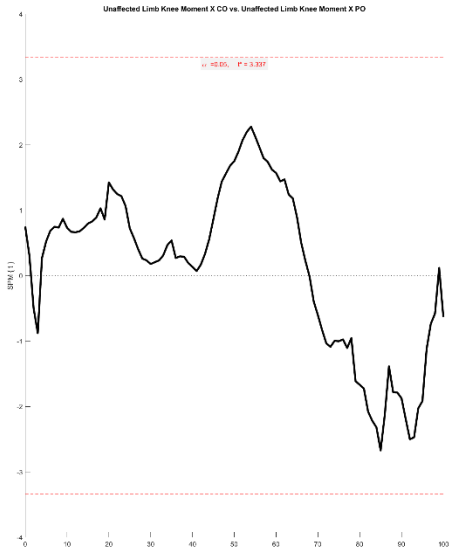

Unaffected Limb Knee Moment Y

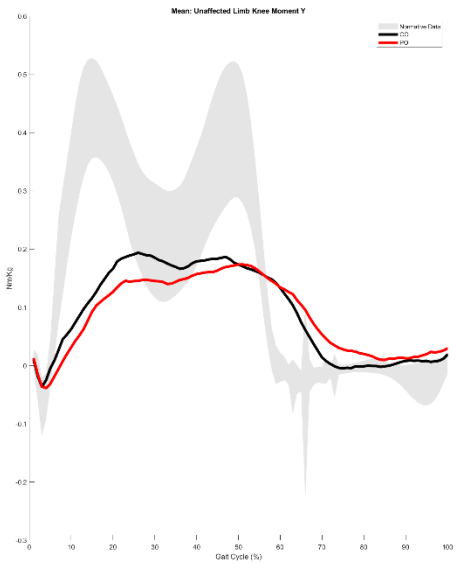

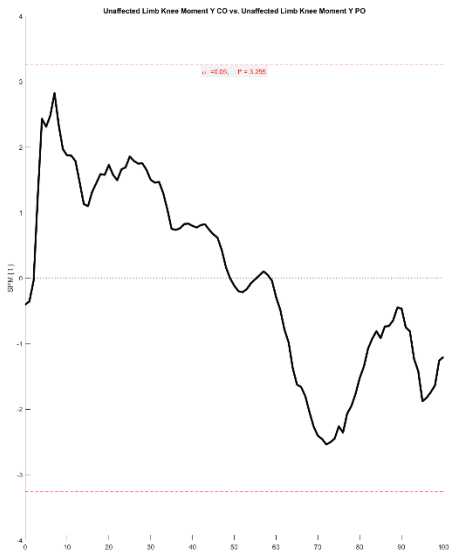

Affected Limb Knee Moment X

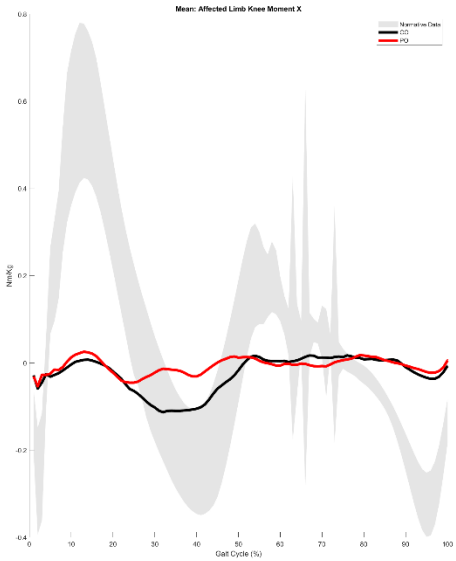

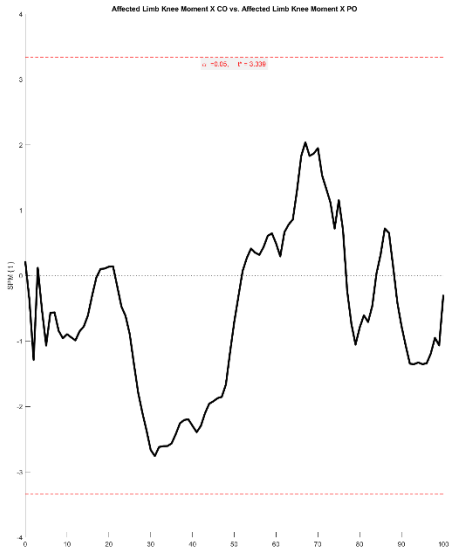

Affected Limb Knee Moment Y

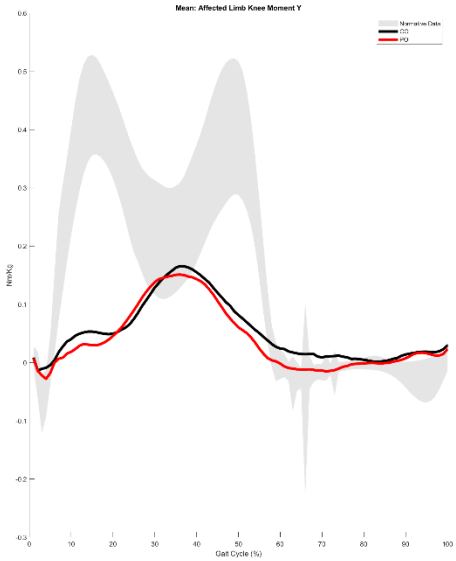

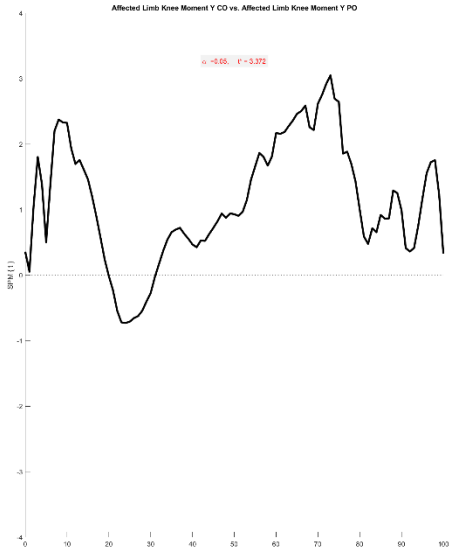

Unaffected Limb Ankle Moment X

51.7-52.6%, 80.0-87.0%

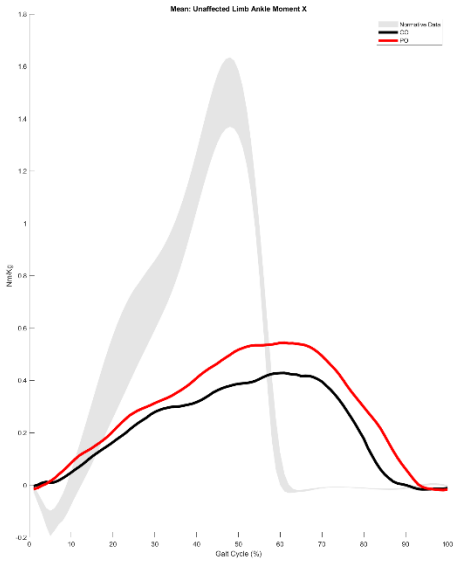

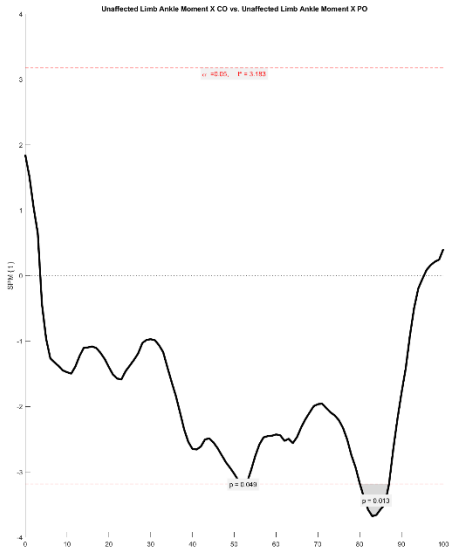

Unaffected Limb Ankle Moment Y

33.4-39.6%, 48.8-54.2%, 80.4-86.9%

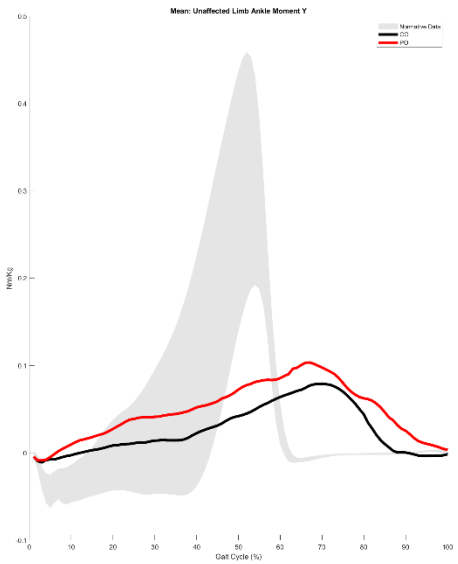

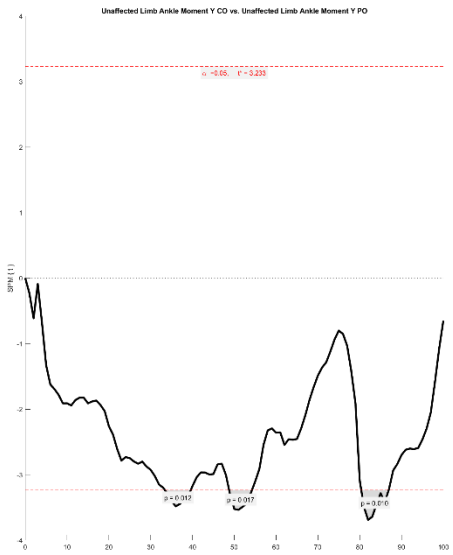

Affected Limb Ankle Moment X

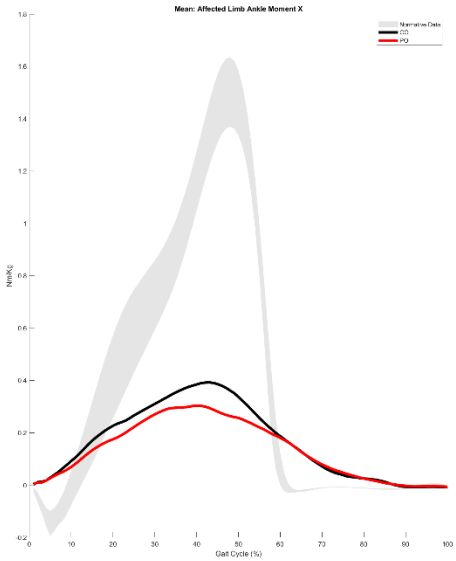

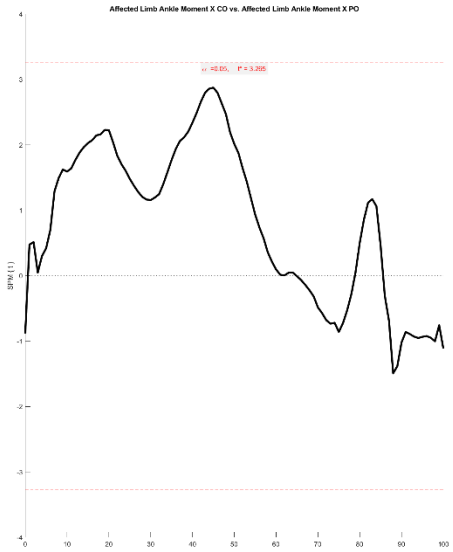

Affected Limb Ankle Moment Y

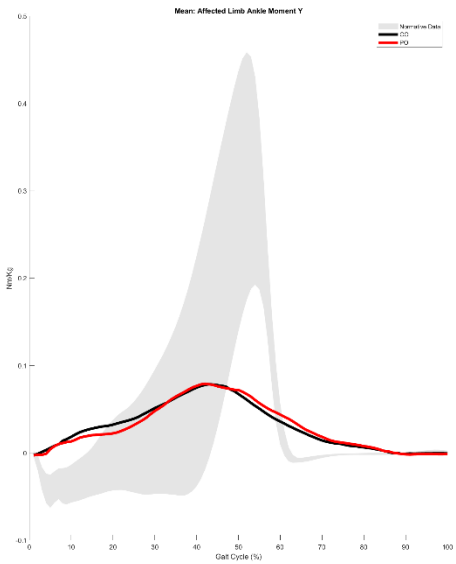

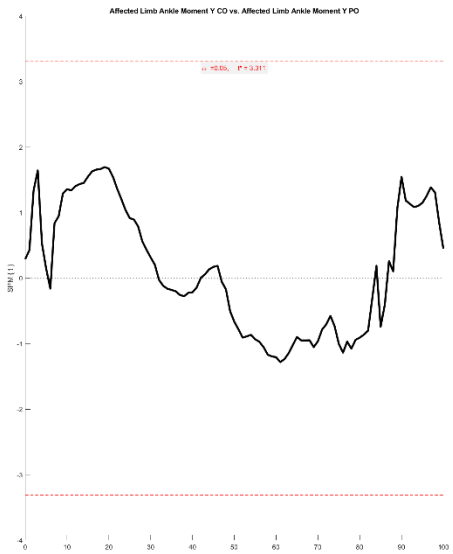

			PO					CO			
	REP	Affected	Step Length Unaffected	IS (50%)	IS (0%)		REP	Affected	Step Length Unaffected	IS (50%)	IS (0%)
1	1	0.21238	0.32345	39.6357054	41.4571786	1	1	0.26541	0.39947	39.9185	40.3261
	2	0.21046	0.31968	39.6989474	41.2042102		2	0.26442	0.39387	40.1677	39.3292
	3	0.19398	0.30221	39.0938955	43.6244181		3	0.22154	0.38621	36.4525	54.19
	4	0.19287	0.29782	39.3058754	42.7764984		4	0.20939	0.38284	35.3562	58.5752
	5	0.189	0.29558	39.0028478	43.9886087		5	0.20912	0.37691	35.6842	57.2633
	6	0.18186	0.22925	44.2363358	23.0546569		6	0.18943	0.34139	35.6863	57.2548
2	7	0.24646	0.13351	64.8630155	59.452062	2	7	0.25432	0.15423	62.2494	48.9977
	8	0.24257	0.13183	64.7889957	59.1559829		8	0.25105	0.15345	62.0643	48.2571
	9	0.24148	0.13149	64.7451538	58.9806151		9	0.24825	0.15276	61.9062	47.6247
	10	0.23987	0.11642	67.3243706	69.2974824		10	0.24802	0.14221	63.5574	54.2296
	11	0.23577	0.11545	67.1288651	68.5154604		11	0.24611	0.13707	64.2283	56.9132
	12	0.23556	0.11106	67.9591483	71.8365934		12	0.24355	0.13062	65.0907	60.3629
3	13	0.28932	0.19744	59.437916	37.7516641	3	13	0.26634	0.16644	61.5417	46.1666
	14	0.28903	0.18466	61.0166987	44.0667947		14	0.2659	0.16046	62.3651	49.4605
	15	0.27429	0.17494	61.05781	44.2312401		15	0.2654	0.15718	62.8047	51.2187
	16	0.27411	0.17328	61.2686917	45.074767		16	0.25428	0.15158	62.6521	50.6086
	17	0.26715	0.17309	60.6828094	42.7312375		17	0.24922	0.14209	63.6886	54.7545
	18	0.26611	0.16854	61.2239733	44.8958932		18	0.24889	0.13765	64.3892	57.5568
4	19	0.32046	0.23779	57.4043887	29.6175549	4	19	0.34624	0.26941	56.2397	24.959
	20	0.31248	0.2305	57.549081	30.196324		20	0.33083	0.23522	58.4454	33.7815
	21	0.30987	0.223	58.1511438	32.6045752		21	0.31671	0.22539	58.4228	33.6912
	22	0.30089	0.22129	57.6218928	30.4875713		22	0.31518	0.19457	61.8303	47.3212
	23	0.29314	0.20541	58.7985157	35.1940628		23	0.30185	0.18601	61.8723	47.489
	24	0.28858	0.2022	58.8002771	35.2011084		24	0.27418	0.17858	60.5575	42.2299
5	25	0.34753	0.18847	64.8376866	59.3507463	5	25	0.33783	0.24672	57.7932	31.1727
	26	0.32037	0.17991	64.0381386	56.1525546		26	0.33282	0.2434	57.7592	31.0368
	27	0.3153	0.16919	65.0787426	60.3149704		27	0.31685	0.23154	57.7782	31.1129
	28	0.2889	0.16705	63.3622108	53.4488431		28	0.30573	0.22585	57.5135	30.0538
	29	0.27091	0.16074	62.7614966	51.0459863		29	0.30188	0.22385	57.4211	29.6844
	30	0.25077	0.15934	61.1470093	44.5880374		30	0.29475	0.20896	58.5158	34.0633
6	31	0.30924	0.14224	68.4947284	73.9789138	6	31	0.31161	0.13966	69.0518	76.2071
	32	0.30822	0.14224	68.4233894	73.6935577		32	0.30958	0.13217	70.0804	80.3214
	33	0.30767	0.14073	68.6150758	74.4603033		33	0.30818	0.12881	70.5234	82.0934
	34	0.30307	0.14011	68.3853062	73.5412248		34	0.30728	0.12871	70.4787	81.9147
	35	0.30234	0.13905	68.4972473	73.9889893		35	0.30353	0.12712	70.4818	81.9273
	36	0.30197	0.13702	68.7874439	75.1497756		36	0.30185	0.12147	71.3054	85.2216
7	37	0.27826	0.1822	60.4308735	41.7234939	7	37	0.26812	0.19932	[illegible]	[illegible]
	38	0.25078	0.17713	58.6057816	34.4231264		38	0.26696	0.1726	[illegible]	[illegible]
	39	0.15833	0.1692	48.34061	6.63755992		39	0.26271	0.1704	60.6566	42.6266
	40	0.24624	0.164	60.0234009	40.0936037		40	0.26143	0.16999	60.5976	42.3902
	41	0.28311	0.16291	63.4747321	53.8989283		41	0.25882	0.16979	60.3859	41.5436
	42	0.24592	0.15525	61.3006955	45.2027819		42	0.25613	0.16814	60.3696	41.4783
8	43	0.26721	0.29505	47.524277	9.9028919	8	43	0.28193	0.28996	49.2979	2.80823
	44	0.25223	0.29217	46.3317414	14.6730345		44	0.2463	0.26926	47.7733	8.90682
	45	0.23018	0.28885	44.3481109	22.6075564		45	0.24596	0.26257	48.3669	6.53255
	46	0.18555	0.28591	39.3564671	42.5741314		46	0.23858	0.25671	48.1698	7.32096
	47	0.17779	0.28085	38.7646084	44.9415664		47	0.2211	0.24321	47.619	9.52381
	48	0.17102	0.28027	37.8958098	48.4167608		48	0.21141	0.23212	47.6653	9.33871
9	49	0.08184	0.18145	31.083596	75.6656159	9	49	0.09898	0.18166	35.2694	58.9225
	50	0.0733	0.17752	29.2241448	83.1034208		50	0.09773	0.17715	35.5537	57.7852
	51	0.06363	0.17685	26.4595808	94.1616766		51	0.08638	0.16746	34.0293	63.8828
	52	0.06209	0.17291	26.4212766	94.3148936		52	0.08542	0.16686	33.8592	64.5632
	53	0.04869	0.1728	21.9829338	112.068265		53	0.0524	0.16399	24.2155	103.138
	54	0.03742	0.16956	18.0790415	127.683834		54	0.05006	0.16196	23.611	105.556
10	55	0.26035	0.17826	59.3579718	37.4318871	10	55	0.22391	0.14637	60.4705	41.8818
	56	0.25231	0.16521	60.4306381	41.7225522		56	0.22171	0.14198	60.9613	43.845
	57	0.24639	0.15121	61.9693159	47.8772636		57	0.21979	0.13894	61.2689	45.0757
	58	0.23688	0.14167	62.5756175	50.30247		58	0.21889	0.13591	61.6939	46.7756
	59	0.23382	0.1276	64.6948149	58.7792596		59	0.21784	0.13412	61.8934	47.5736
	60	0.23217	0.1267	64.6947363	58.778945		60	0.21411	0.13228	61.8118	47.2473
	Mean	0.24	0.19	54.61	52.20		Mean	0.25	0.20	55.16	47.47
	SD	0.07	0.06	13.43	22.41		SD	0.07	0.07	11.97	21.54

		PO Swing Time						CO Swing Time			
	REP	Left	Right	IS (50%)	IS (0%)		REP	Left	Right	IS (50%)	IS (0%)
1	1	0.91	0.49	65	60	1	1	0.86	0.54	61.4286	45.7143
	2	0.91	0.45	66.9117647	67.6470588		2	0.79	0.47	62.6984	50.7937
	3	0.83	0.39	68.0327869	72.1311475		3	0.77	0.44	63.6364	54.5455
	4	0.8	0.36	68.9655172	75.862069		4	0.74	0.43	63.2479	52.9915
	5	0.77	0.32	70.6422018	82.5688073		5	0.62	0.36	63.2653	53.0612
	6	0.75	0.31	70.754717	83.0188679		6	0.55	0.33	62.5	50
2	7	0.47	0.35	57.3170732	29.2682927	2	7	0.47	0.32	59.4937	37.9747
	8	0.46	0.34	57.5	30		8	0.47	0.31	60.2564	41.0256
	9	0.45	0.33	57.6923077	30.7692308		9	0.45	0.3	60	40
	10	0.43	0.33	56.5789474	26.3157895		10	0.45	0.28	61.6438	46.5753
	11	0.43	0.32	57.3333333	29.3333333		11	0.42	0.28	60	40
	12	0.42	0.3	58.3333333	33.3333333		12	0.42	0.28	60	40
3	13	0.48	0.37	56.4705882	25.8823529	3	13	0.44	0.38	53.6585	14.6341
	14	0.41	0.36	53.2467532	12.987013		14	0.38	0.34	52.7778	11.1111
	15	0.41	0.36	53.2467532	12.987013		15	0.38	0.33	53.5211	14.0845
	16	0.4	0.35	53.3333333	13.3333333		16	0.38	0.3	55.8824	23.5294
	17	0.39	0.34	53.4246575	13.6986301		17	0.38	0.29	56.7164	26.8657
	18	0.37	0.3	55.2238806	20.8955224		18	0.33	0.29	53.2258	12.9032
4	19	0.95	0.55833	62.9835646	51.9342584	4	19	0.61667	0.96667	38.9474	44.2103
	20	0.94167	0.54166	63.4835134	53.9340538		20	0.58333	0.94167	38.2511	46.9954
	21	0.93333	0.525	63.9999177	55.9996709		21	0.54167	0.86667	38.4616	46.1536
	22	0.91667	0.48333	65.4764286	61.9057143		22	0.525	0.86667	37.7245	49.1022
	23	0.90833	0.48333	65.2695342	61.0781369		23	0.50834	0.85833	37.1955	51.2179
	24	0.88333	0.46667	65.4318519	61.7274074		24	0.50833	0.83334	37.8879	48.4486
5	25	0.65833	0.375	63.7095604	54.8382414	5	25	0.45833	0.65833	41.0447	35.8211
	26	0.61667	0.35	63.7932283	55.1729132		26	0.41667	0.65	39.0627	43.7492
	27	0.59167	0.35	62.83199	51.3279599		27	0.39167	0.625	38.5248	45.9008
	28	0.575	0.34167	62.7270446	50.9081785		28	0.35833	0.61667	36.7518	52.9928
	29	0.54167	0.33333	61.9051429	47.6205714		29	0.35	0.59167	37.168	51.328
	30	0.5	0.33333	60.00024	40.00096		30	0.34167	0.55833	37.9633	48.1467
6	31	0.74167	0.5	59.7316517	38.9266069	6	31	0.80833	0.50833	61.3925	45.5699
	32	0.74167	0.5	59.7316517	38.9266069		32	0.79167	0.50833	60.8977	43.5908
	33	0.71667	0.49167	59.3102935	37.2411738		33	0.78333	0.50833	60.6452	42.5809
	34	0.70833	0.48333	59.4406123	37.762449		34	0.775	0.49167	61.184	44.7362
	35	0.70833	0.48333	59.4406123	37.762449		35	0.775	0.49167	61.184	44.7362
	36	0.70833	0.475	59.8590419	39.4361674		36	0.75833	0.48333	61.0739	44.2955
7	37	0.74167	0.38333	65.9262222	63.7048889	7	37	0.43333	0.79167	35.3739	58.5045
	38	0.73333	0.38333	65.6717354	62.6869414		38	0.425	0.775	35.4167	58.3333
	39	0.71667	0.35833	66.6669767	66.667907		39	0.41667	0.75	35.7145	57.1421
	40	0.70833	0.35	66.9290297	67.7161188		40	0.40833	0.73333	35.7663	56.9346
	41	0.69167	0.34167	66.9353746	67.7414984		41	0.4	0.725	35.5556	57.7778
	42	0.65833	0.325	66.9490405	67.796162		42	0.375	0.71667	34.351	62.5958
8	43	0.79167	0.56667	58.2821679	33.1286718	8	43	0.84167	0.525	61.5855	46.3418
	44	0.73333	0.55833	56.7742285	27.096914		44	0.84167	0.525	61.5855	46.3418
	45	0.71667	0.54167	56.9536055	27.8144222		45	0.80833	0.50833	61.3925	45.5699
	46	0.68333	0.54167	55.7820408	23.1281633		46	0.74167	0.49167	60.1351	40.5403
	47	0.68333	0.525	56.5516043	26.2064171		47	0.70833	0.48333	59.4406	37.7624
	48	0.50833	0.64167	44.2026087	23.1895652		48	0.68333	0.475	58.9927	35.9708
9	49	0.475	0.28333	62.637638	50.5505519	9	49	0.35	0.5	41.1765	35.2941
	50	0.46667	0.26667	63.6362397	54.5449587		50	0.33333	0.48333	40.8163	36.735
	51	0.45833	0.26667	63.217931	52.8717241		51	0.325	0.475	40.625	37.5
	52	0.45	0.26667	62.7904056	51.1616225		52	0.31667	0.45	41.3046	34.7816
	53	0.4	0.25833	60.7598013	43.0392053		53	0.30833	0.44167	41.1107	35.5573
	54	0.36667	0.25833	58.6672	34.6688		54	0.3	0.40833	42.3531	30.5874
10	55	0.85833	0.33333	72.0280953	88.112381	10	55	0.34167	0.85	28.6715	85.3139
	56	0.83333	0.33333	71.4286939	85.7147755		56	0.33333	0.84167	28.3685	86.526
	57	0.81667	0.325	71.5329298	86.1317193		57	0.325	0.78333	29.3234	82.7064
	58	0.80833	0.325	71.3234451	85.2937803		58	0.31667	0.78333	28.7882	84.8473
	59	0.79167	0.325	70.8956093	83.5824371		59	0.30833	0.775	28.4613	86.1547
	60	0.78333	0.31667	71.2118182	84.8472727		60	0.30833	0.725	29.8385	80.6461
	Mean	0.66	0.39	62.11	49.23		Mean	0.51	0.56	48.09	46.76
	SD	0.18	0.09	5.75	21.30		SD	0.18	0.19	12.26	16.63

	Affected Limb	SD	Unaffected Limb	SD
Step Length PO	0.24	0.07	0.19	0.06
Step Length CO	0.25	0.07	0.20	0.07
Swing Time PO	0.66	0.18	0.39	0.09
Swing Time CO	0.51	0.18	0.56	0.19
Stance Time PO	1.97	0.64	1.89	0.71
Stance Time CO	1.79	0.60	1.81	0.69

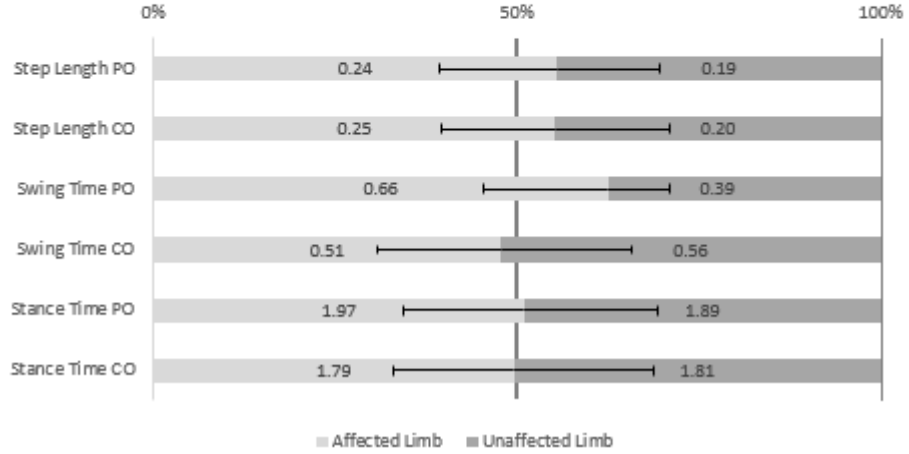

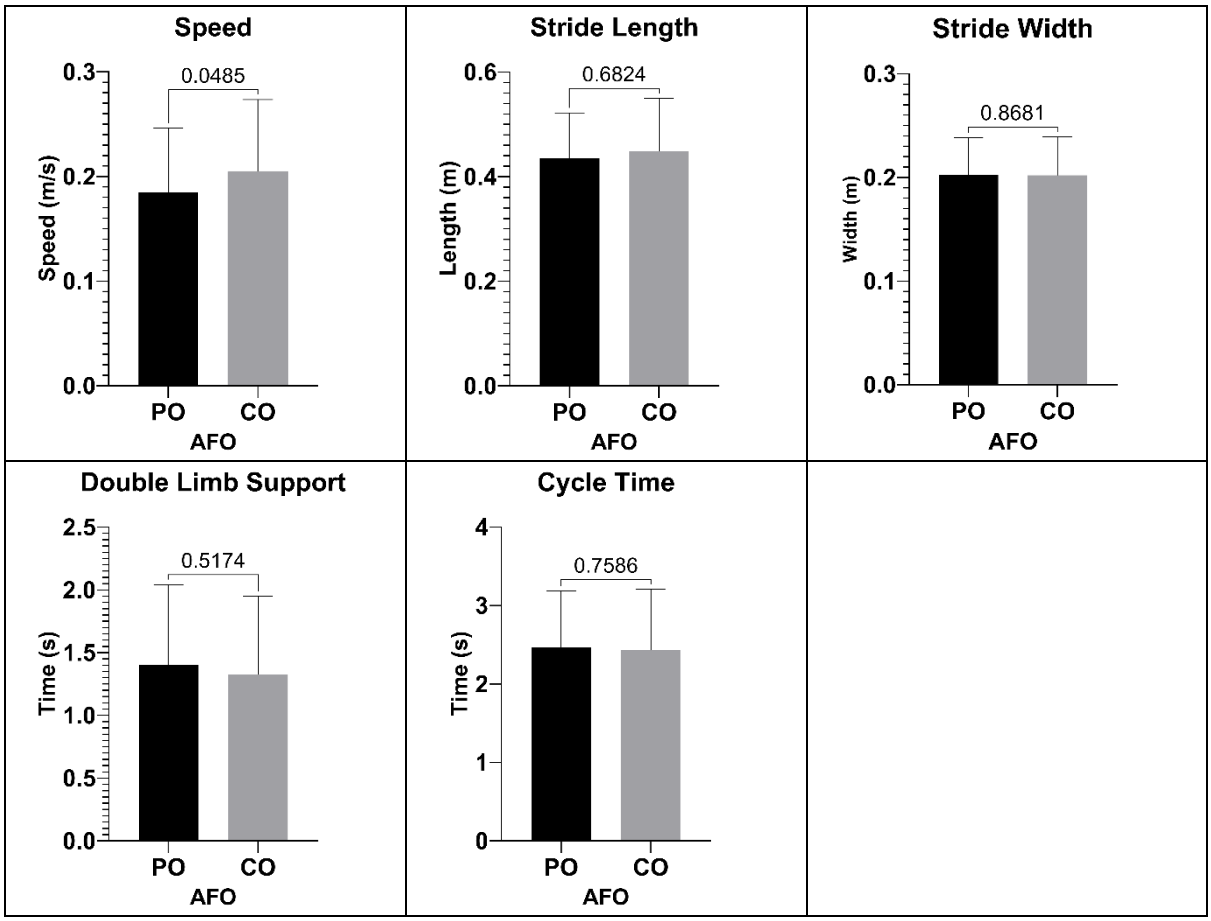

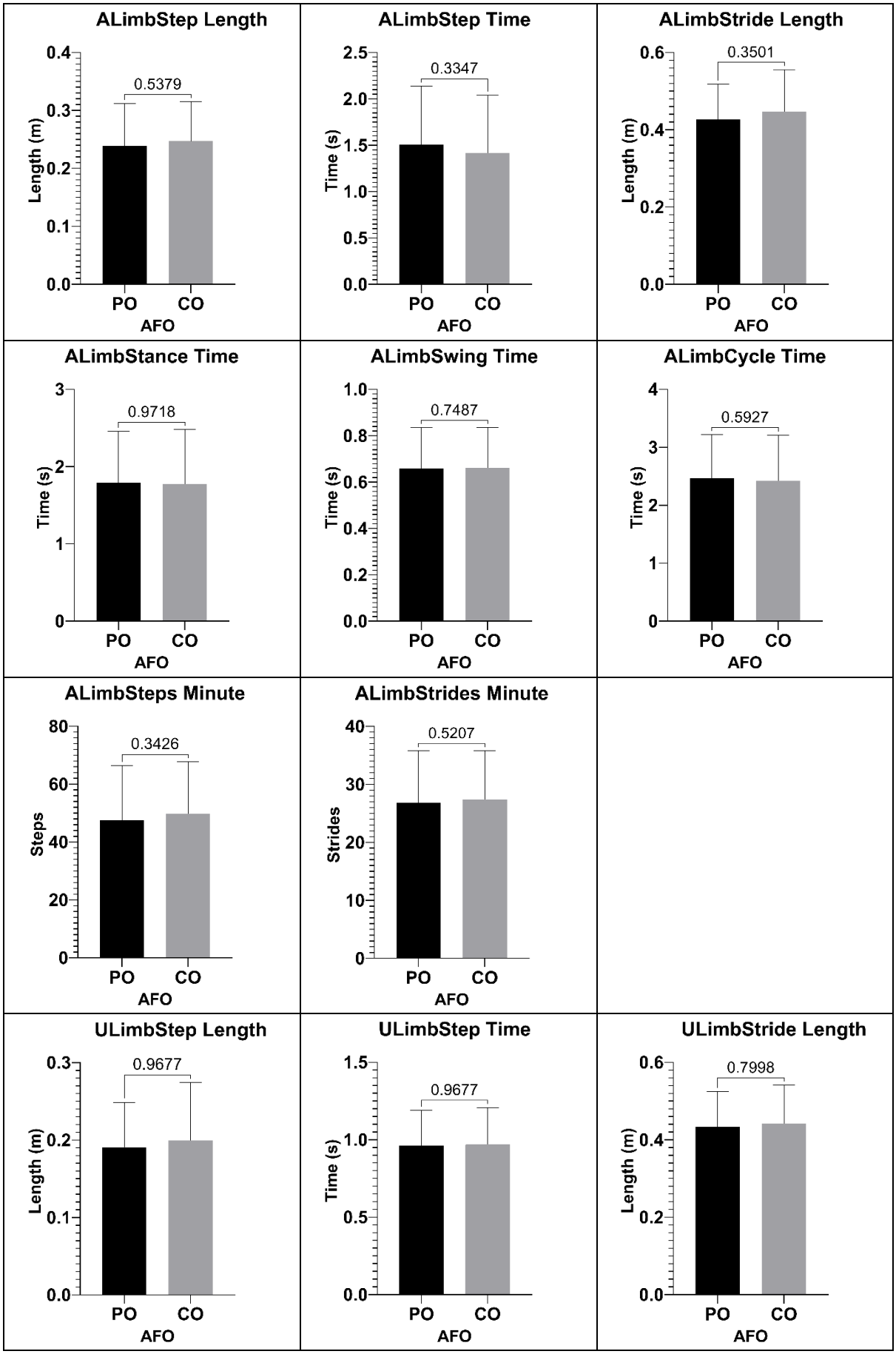
ALimbStep Length
Length (m)
0.4
0.3
0.2
0.1
0.0
0.5379
PO
CO
AFO
ALimbStep Time
Time (s)
2.5
2.0
1.5
1.0
0.5
0.0
0.3347
PO
CO
AFO
ALimbStride Length
Length (m)
0.6
0.4
0.2
0.0
0.3501
PO
CO
AFO
ALimbStance Time
Time (s)
3
2
1
0
0.9718
PO
CO
AFO
ALimbSwing Time
Time (s)
1.0
0.8
0.6
0.4
0.2
0.0
0.7487
PO
CO
AFO
ALimbCycle Time
Time (s)
4
3
2
1
0
0.5927
PO
CO
AFO
ALimbSteps Minute
Steps
80
60
40
20
0
0.3426
PO
CO
AFO
ALimbStrides Minute
Strides
40
30
20
10
0
0.5207
PO
CO
AFO
ULimbStep Length
Length (m)
0.3
0.2
0.1
0.0
0.9677
PO
CO
AFO
ULimbStep Time
Time (s)
1.5
1.0
0.5
0.0
0.9677
PO
CO
AFO
ULimbStride Length
Length (m)
0.6
0.4
0.2
0.0
0.7998
PO
CO
AFO

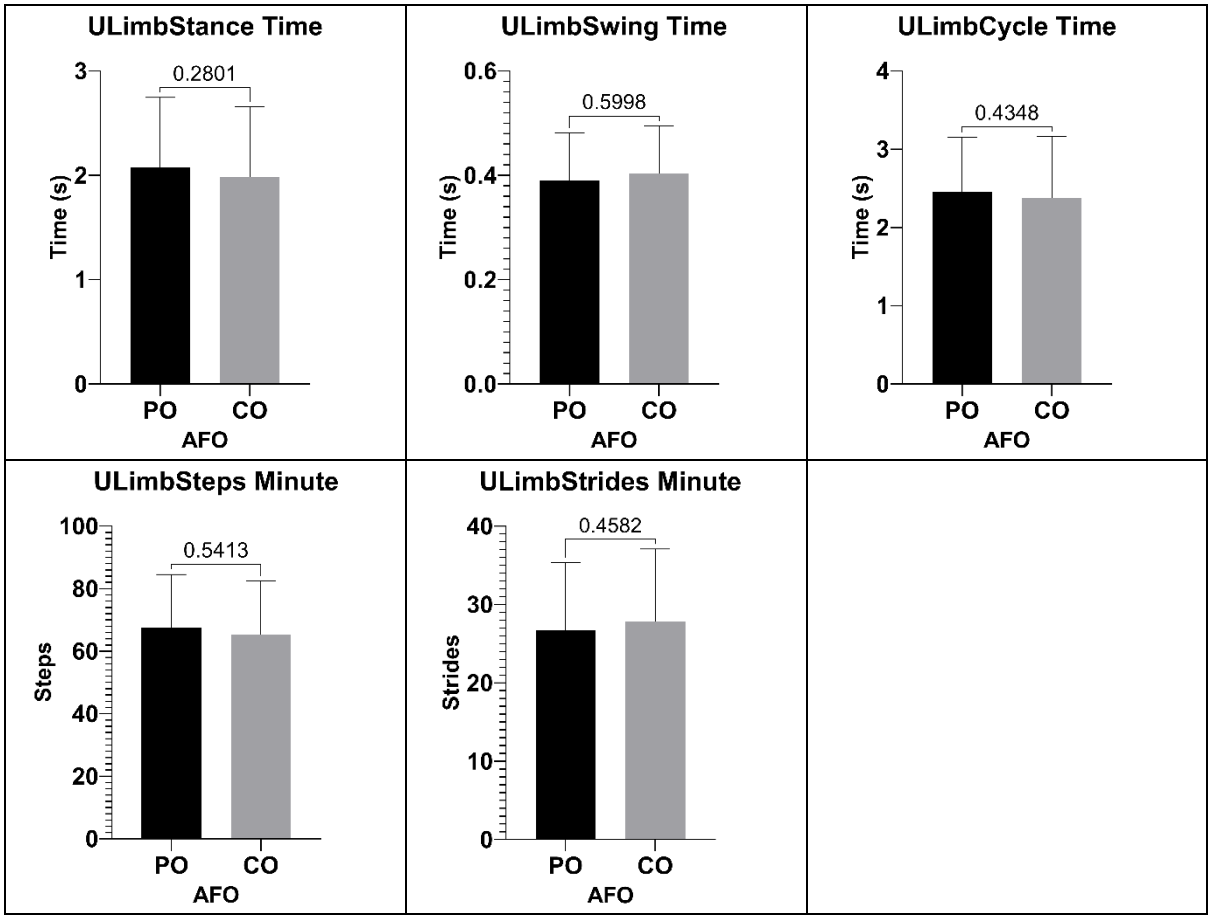
ULimbStance Time
0.2801
Time (s)
3
2
1
0
PO
CO
AFO
ULimbSwing Time
0.5998
Time (s)
0.6
0.4
0.2
0.0
PO
CO
AFO
ULimbCycle Time
0.4348
Time (s)
4
3
2
1
0
PO
CO
AFO
ULimbSteps Minute
0.5413
Steps
100
80
60
40
20
0
PO
CO
AFO
ULimbStrides Minute
0.4582
Strides
40
30
20
10
0
PO
CO
AFO

Compression Tests

ASA

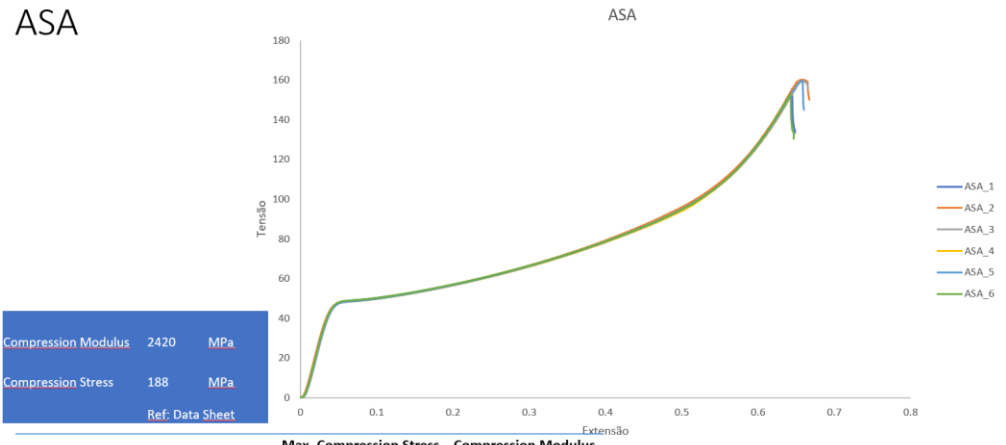

Compression Modulus	2420 MPa
Compression Stress	188 MPa
	Ref: Data Sheet

	Amostra	Max Load (N)	Max. Compression Stress (MPa)	Compression Modulus (Mpa)
ASA	1	19110	153,095	1485,5
	2	20000	160,224	1501,8
	3	19840	159,448	1467,6
	4	19810	158,201	**1447,3**
	5	19940	159,744	**1474,3**
	6	19060	153,1795	**1508,1**
	Média	**19626,667**	**157,316**	**1480,767**

		XZ Orientation[1]	ZX Orientation[1]
Compression Properties: ASTM D695			
Yield Strength	MPa	75.4 (3.8)	188 (28)
	psi	10900 (540)	27200 (4100)
Modulus	GPa	2.05 (0.060)	2.42 (0.26)
	ksi	297 (8.7)	351 (38)

Nylon 12

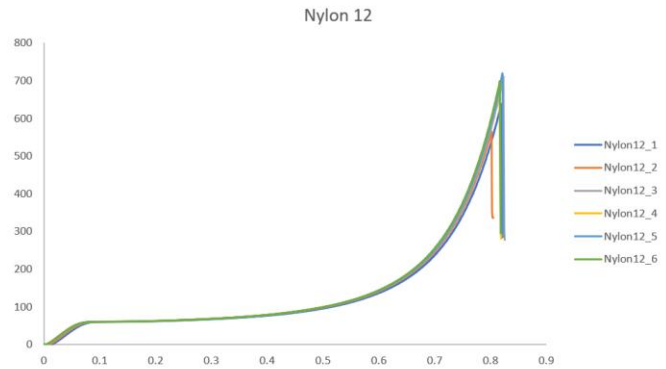

	Amostra	Max Load (N)	Max. Compression Stress (MPa)	Compression Modulus (Mpa)
Nylon 12	1	80650	637,986	1083,2
	2	70870	565,0653	1093,4
	3	88780	711,239	1072,8
	4	85910	686,068	1092,9
	5	90370	719,4052	1095,1
	6	87250	698,98138	1094,7
	Média	83971,667	669,791	1088,683

Compression Modulus	1070 - 6800	MPa
Compression Stress	6 – 167	MPa
	Ref: MatWeb	

PC

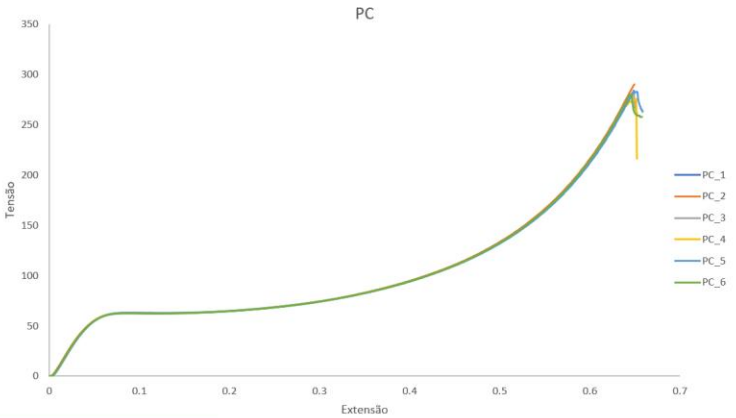

Compression Modulus		MPa
Compression Yield Strenght	18 – 86	MPa
Ref: MatWeb		

	Amostra	Max Load (N)	Max. Compression Stress (MPa)	Compression Modulus (Mpa)
PC	1	35730	286,2419	1455,2
	2	36230	290,247511	1454,1
	3	58640	284,2892288	1452,5
	4	34390	275,5068149	1460,3
	5	35350	283,6473	1453,4
	6	34990	280,3136	1459,8
	Média	**39221,667**	**283,374**	**1455,883**

		XZ Orientation[1]	ZX Orientation[1]
Compression Properties: ASTM D695			
Yield Strength	MPa	245 (10)	290 (20)
	psi	35410 (1930)	42055 (2795)
Modulus	GPa	1.95 (0.05)	2.11 (0.09)
	ksi	280 (10)	305 (15)

PC-ABS

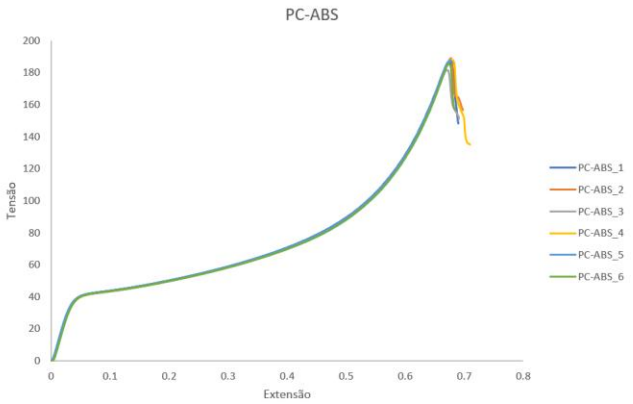

	Amostra	Max Load (N)	Max. Compression Stress (MPa)	Compression Modulus (Mpa)
PC-ABS	1	23270	186,718	1287,2
	2	23640	189,086	1302,7
	3	22810	181,583	1299,9
	4	23510	188,046	1287,7
	5	23450	187,566	1297,8
	6	23330	185,429	1289,2
	Média	23335	186,40	1294,083

Compression Modulus		MPa
Compression Stress		MPa
Ref: MatWeb		Ref: MakeItForm

PETG

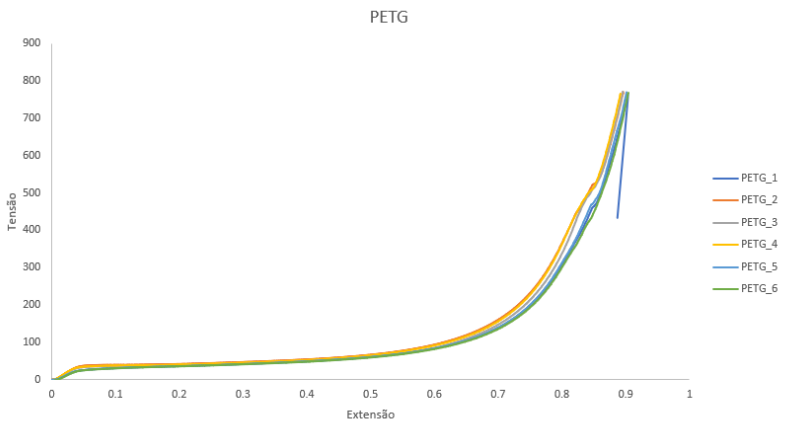

	Amostra	Max Load (N)	Max. Compression Stress (MPa)	Compression Modulus (Mpa)
	1	95770	763,5996	819,43
	2	96640	770,5363239	1148,9
PETG	3	97470	771,0420527	1039,5
	4	96290	765,3218605	1081,9
	5	97470	769,8283	820,54
	6	97020	767,4823017	850,05
	Média	96776,667	767,968	960,053

Compression Modulus	2010 - 2110	MPa
Compression Stress		MPa
Ref: https://dielectricmfg.com/knowledge-base/petg/		

PLA

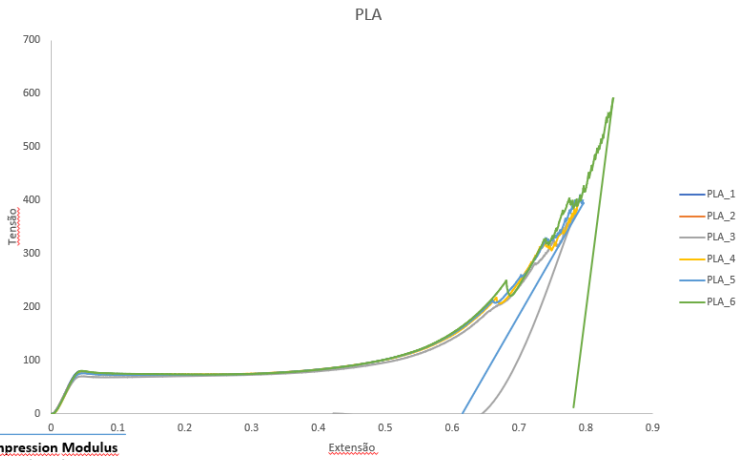

	Amostra	Max Load (N)	Max. Compression Stress (MPa)	Compression Modulus (Mpa)
	1	10050	79,376	2583,9
	2	9740	76,565	2451,1
PLA	3	37480	300,738	2317,5
	4	27650	217,355	2537,1
	5	27090	213,623	2402
	6	75940	592,300	2587,4
	Média	31325	246,659	2479,833

Compression Modulus	MPa
Compression Stress	MPa
Ref: MatWeb	Ref: MakeItForm

TPU

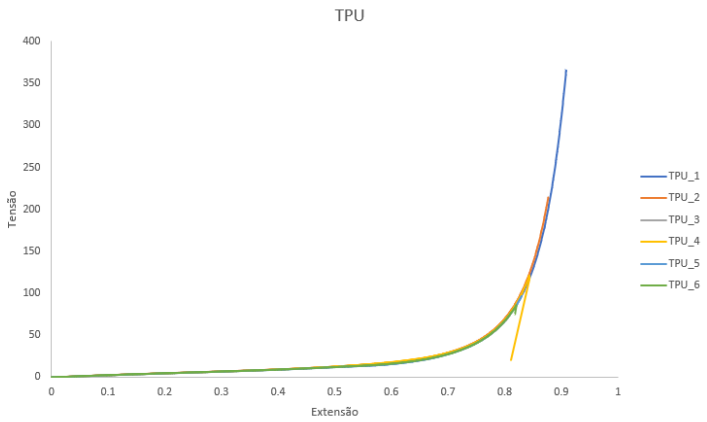

	Amostra	Max Load (N)	Max. Compression Stress (MPa)	Compression Modulus (Mpa)
TPU	1	45190	365,4982	1039,6
	2	26500	214,3329	1113,3
	3	8823	71,24712	348,67
	4	14900	121,2836	1144,5
	5	12050	96,68883	1066,5
	6	10600	85,86994	926,62
	Média	21848	176,734679	1058,104

Compression Modulus	16.9	MPa
Compression Stress	2.6	MPa
Ref: MatWeb	Ref: data sheet	

ULTEM 1010

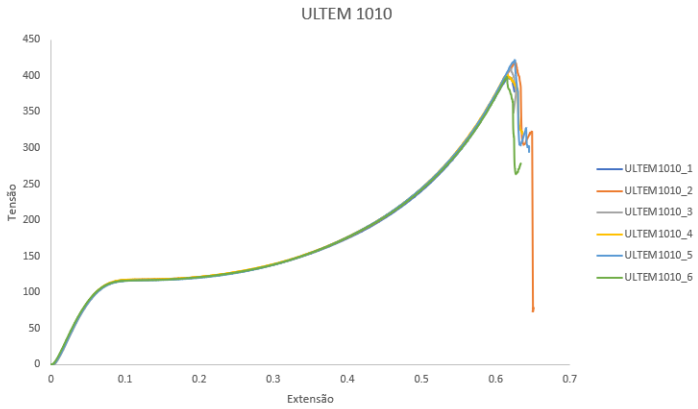

	Amostra	Max Load (N)	Max. Compression Stress (MPa)	Compression Modulus (Mpa)
ULTEM 1010	1	50490	398,148	2098,2
	2	52790	417,598	2123,9
	3	51740	409,938	2117,3
	4	50540	401,063	2140,3
	5	53220	421,664	2120
	6	50360	398,376	2110,5
	Média	51523,333	407,798	2118,367

Compression Modulus	3230	MPa
Compression Stress	438	MPa
Ref: Ficha Técnica		

ULTEM 9085

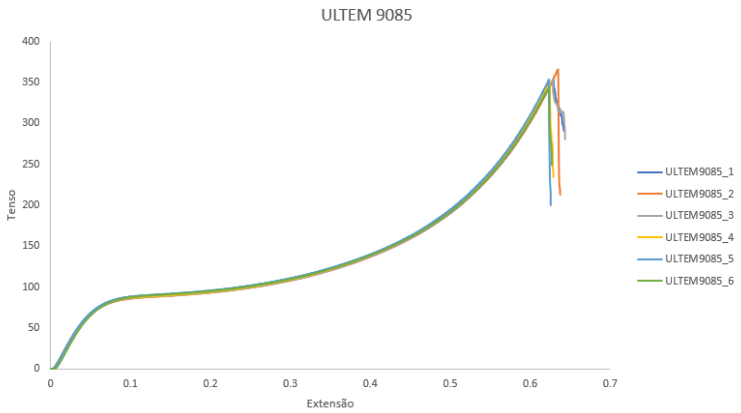

	Amostra	Max Load (N)	Max. Compression Stress (MPa)	Compression Modulus (Mpa)
ULTEM 9085	1	43850	352,970702	1736,6
	2	45510	365,7512	1741,8
	3	44130	352,9763	1733,3
	4	43530	350,9526	1744,3
	5	43810	353,2100409	1767,4
	6	42670	343,4723	1760,3
	Média	43916,667	353,222	1747,283

Compression Modulus	2280	MPa
Compression Stress	340	MPa
Ref: Ficha técnica		

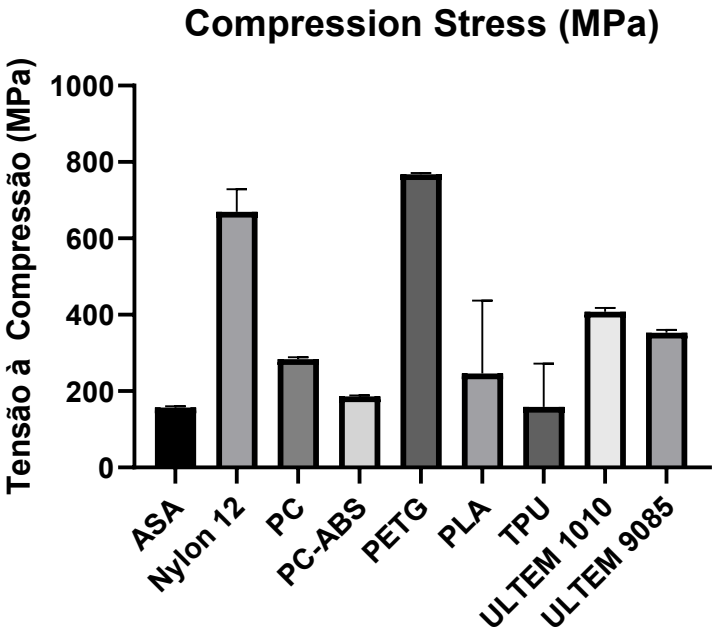

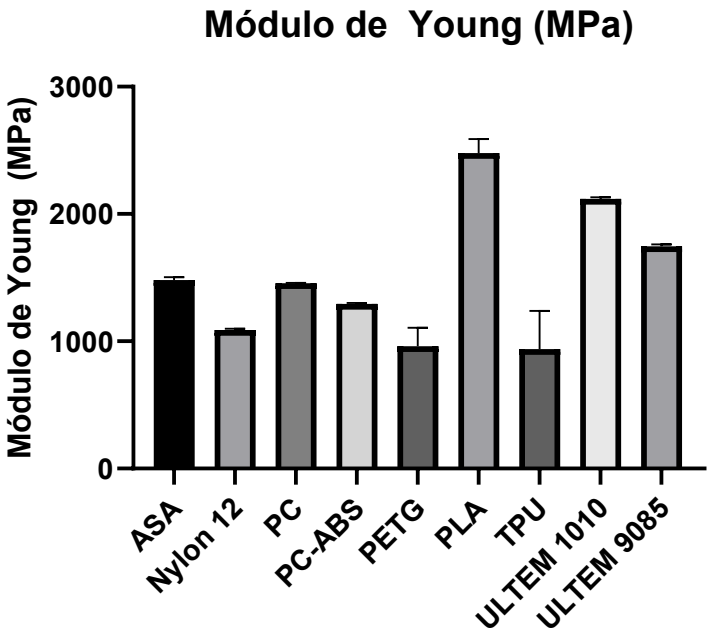
Módulo de Young (MPa)
Módulo de Young (MPa)
3000
2000
1000
0
ASA
Nylon 12
PC
PC-ABS
PETG
PLA
TPU
ULTEM 1010
ULTEM 9085

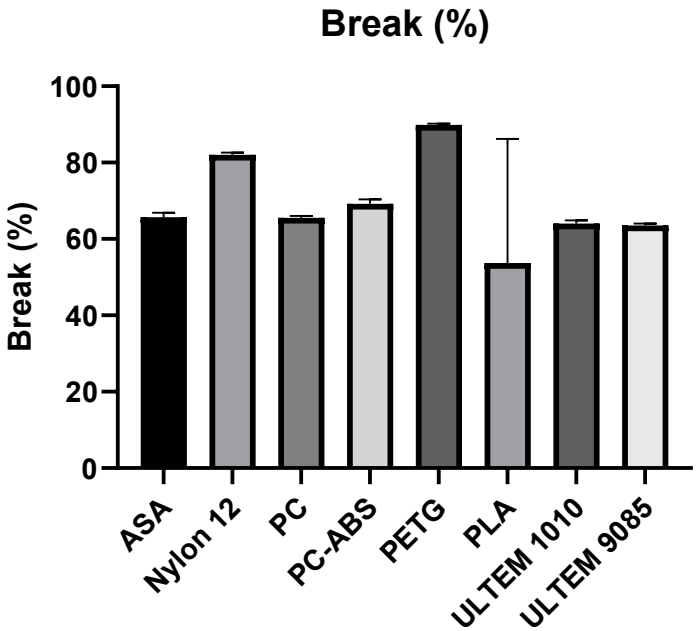
Break (%)
Break (%)
100
80
60
40
20
0
ASA
Nylon 12
PC
PC-ABS
PETG
PLA
ULTEM 1010
ULTEM 9085

Material	Resistência à Compressão (MPa)	Módulo de Young (MPa)	Break (%)
ABS	158.1 ± 2.919	1475 ± 20.31	65.80 ± 1.304
Nylon12	690.7 ± 32.07	1088 ± 9.657	82.20 ± 0.4472
PC	283,2 ± 5.627	1457 ± 3.255	65.60 ± 0.5477
PC-ABS	187.4 ± 1.381	1293 ± 6.951	69.20 ± 1.304
PETG	768.8 ± 2.394	988.2 ± 145.3	89.80 ± 0.4472
PLA	280,7 ± 191.4	2486 ± 120.3	62.00 ± 28.39
TPU	176.7 ± 117.0	1058 ± 83.98	
ULTEM 1010	405.0 ± 8.506	2118 ± 15.66	64.00 ± 1.000
ULTEM 9085	355.2 ± 5.984	1745 ± 13.41	63.60 ± 0.5477

Flexural Tests

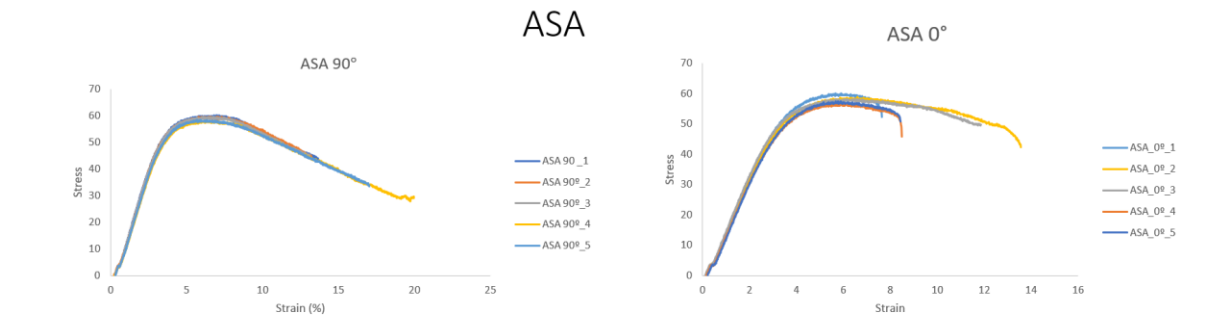

	Amostra	Max Load (N)	Max. Flexural Stress (MPa)	Flexural Modulus (Mpa)
ABS (100% Vertical - 90°)	1	95,0	60,103	1965,182
	2	94,5	59,557	1924,884
	3	94,5	59,794	1935,504
	4	95,51	57,942	1839,434
	5	95,01	58,524	1875,910
	Média	101,1275	58,505	1837,064

Mean Flex.Modulus	1908,183	MPa	Mean Flex. Stress	59,18	MPa
Dev. Padrao	44,81566	MPa	Dev. Padrao	0,816459	MPa
Desvio padrão %	2,348604	%	Desvio padrão %	1,379519	%
Int. conf 95_%	39,28194	MPa	Int. conf 95_%	0,715645	MPa
Mean max load	94,91	N			
Dev. Padrao	0,374166	N			
Desvio padrão %	0,394232	%			
Int. conf 95_%	0,327965	N			

Flexural Modulus	1720-1930	2600	MPa
Flexural Stress	36-60	55	MPa
Ref: MatWeb		Ref: MakeItForm	

	Amostra	Max Load (N)	Max. Flexural Stress (MPa)	Flexural Modulus (Mpa)
ABS (100% Horizontal - 0°)	1	100,5	59,943	1921,942
	2	103	58,811	1817,621
	3	101,5	57,913	1795,296
	4	97,5	56,472	1787,440
	5	99,5	57,353	1813,396
	Média	101,1275	58,505	1837,064

Mean Flex.Modulus	1837,06	MPa	Mean Flex. Stress	58,51	MPa
Dev. Padrao	49,71681	MPa	Dev. Padrao	0,979729	MPa
Desvio padrão %	2,706319	%	Desvio padrão %	2,057496	%
Int. conf 95_%	43,57791	MPa	Int. conf 95_%	1,047773	MPa
			Mean max load	101,13	N
			Dev. Padrao	1,289872	N
			Desvio padrão %	1,27549	%
			Int. conf 95_%	1,130602	N

Nylon 12

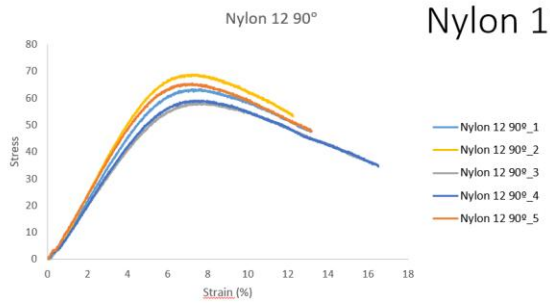

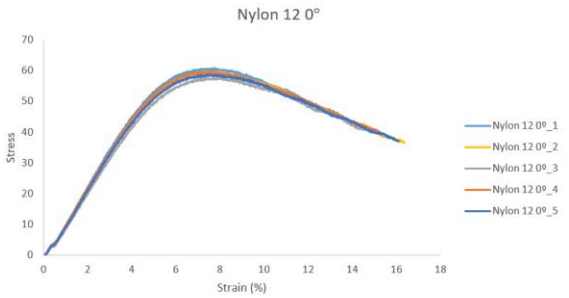

	Amostra	Max. Load (N)	Max. Flexural Stress (MPa)	Flexural Modulus (Mpa)
Nylon 12 (100% Vertical - 90°)	1	105,5	63,255	1260,505
	2	106	68,795	1372,534
	3	106,5	68,438	1098,404
	4	104,5	59,008	1165,137
	5	106	65,482	1307,399
	Média	105,5	64,135	1276,394

Mean Flex.Modulus	1276,394	MPa	Mean Flex. Stress	64,14	MPa
Dev. Padrao	75,55592	MPa	Dev. Padrao	3,556107	MPa
Desvio padrão %	5,919484	%	Desvio padrão %	5,544719	%
Int. conf 95_%	66,22647	MPa	Int. conf 95_%	3,117008	MPa

Mean max load	105,50	N
Dev. Padrao	0,612372	N
Desvio padrão %	0,580448	%
Int. conf 95_%	0,536758	N

Flexural Modulus	190-9500	MPa
Flexural Stress	5,45-900	MPa
Ref: MatWeb		

	Amostra	Max. Load (N)	Max. Flexural Stress (MPa)	Flexural Modulus (Mpa)
Nylon 12 (100% Horizontal - 0°)	1	104,5	60,938	1248,160
	2	105,5	59,685	1176,711
	3	104,5	57,693	1147,263
	4	104,5	59,804	1203,935
	5	104,5	58,784	1204,125
	Média	104,75	59,80281905	1208,233

Mean Flex.Modulus	1208,233	MPa	Mean Flex. Stress	59,80	MPa
Dev. Padrao	33,45743	MPa	Dev. Padrao	1,086554	MPa
Desvio padrão %	2,769121	%	Desvio padrão %	1,816895	%
Int. conf 95_%	29,32619	MPa	Int. conf 95_%	0,952389	MPa

Mean max load	104,70	N
Dev. Padrao	0,4	N
Desvio padrão %	0,382044	%
Int. conf 95_%	0,350609	N

PC

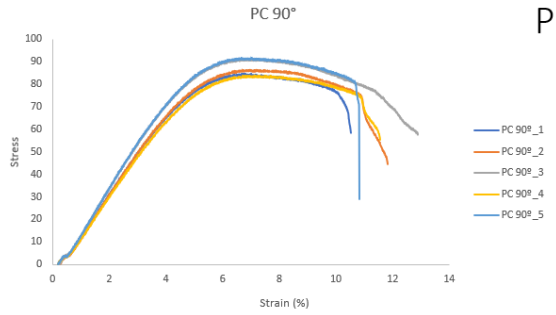

- **Necessário fazer mais um teste de PC Horizontal devido à amostra nº5**

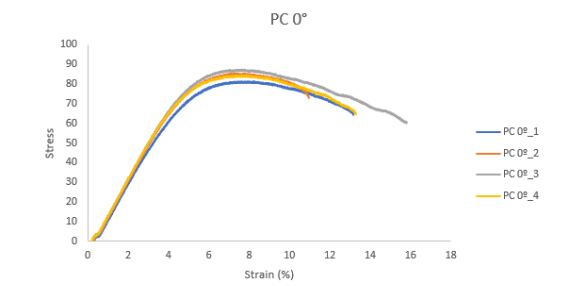

	Amostra	Max. Load (N)	Max. Flexural Stress (MPa)	Flexural Modulus (Mpa)
PC (100% Vertical - 90°)	1	143,5	84,452	1880,876
	2	146,5	86,395	1943,806
	3	147	91,338	2104,811
	4	145,5	83,876	1865,229
	5	146	91,547	2081,640
	Média	146,25	88,289	1996,639

Mean Flex.Modulus	1996,639	MPa	Mean Flex. Stress	88,289	MPa
Dev. Padrao	101,766	MPa	Dev. Padrao	3,277405	MPa
Desvio padrão %	5,096864	%	Desvio padrão %	3,712134	%
Int. conf 95_%	89,20017	MPa	Int. conf 95_%	2,872719	MPa

Mean max load	146,250	mm
Dev. Padrao	1,208305	MPa
Desvio padrão %	0,826191	%
Int. conf 95_%	1,059106	MPa

Flexural Modulus	1960-3100	2300-10000	MPa
Flexural Stress	72-103	92-160	MPa
Ref: MatWeb		Ref: MakeItForm	

	Amostra	Max. Load (N)	Max. Flexural Stress (MPa)	Flexural Modulus (Mpa)
PC (100% Horizontal - 0°)	1	145	81,309	1850,986
	2	151,5	85,185	1892,945
	3	157	87,063	1907,416
	4	150	84,199	1861,512
	5	125	69,160	1884,008
	Média	150,875	84,439	1858,970

Mean Flex.Modulus	1858,970	MPa	Mean Flex. Stress	84,44	MPa
Dev. Padrao	21,37679	MPa	Dev. Padrao	2,08	MPa
Desvio padrão %	1,149926	%	Desvio padrão %	2,462649	%
Int. conf 95_%	18,73724	MPa	Int. conf 95_%	1,822674	MPa

Mean max load	150,88	mm
Dev. Padrao	4,28	MPa
Desvio padrão %	2,835118	%
Int. conf 95_%	3,749312	MPa

PC-ABS

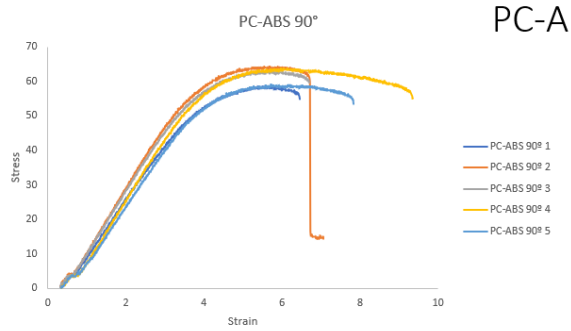

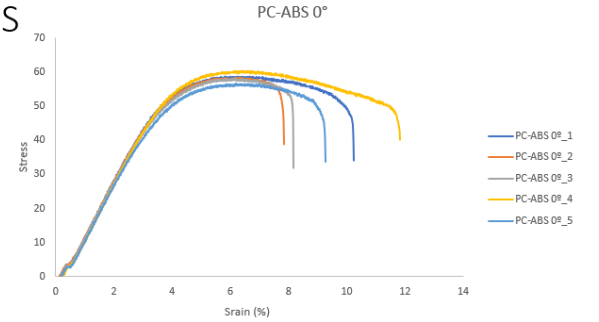

	Amostra	Max. Load (N)	Max. Flexural Stress (MPa)	Flexural Modulus (MPa)
PC-ABS (100% Vertical - 90°)	1	103,5	58,694	1694,435
	2	105,5	64,235	1884,769
	3	106	63,031	1805,911
	4	107	63,899	1807,732
	5	104	59,172	1662,967
	Média	**105,5**	**63,031**	**1812,130**

Mean Flex Modulus	1790,345	MPa
Dev. Padrao	80,13372	MPa
Desvio padrão %	4,475882	%
Int. conf 95_%	70,23902	MPa

Mean Flex. Stress	62,584	MPa
Dev. Padrao	2,018208	MPa
Desvio padrão %	3,22479	%
Int. conf 95_%	1,769005	MPa

Mean max load	105,625	mm
Dev. Padrao	1,28841	MPa
Desvio padrão %	1,219796	%
Int. conf 95_%	1,12932	MPa

Flexural Modulus	1680 (ZX)	1900 (XZ)	MPa
Flexural Stress		45	MPa
Ref: MatWeb			

	Amostra	Max. Load (N)	Max. Flexural Stress (MPa)	Flexural Modulus (MPa)
PC-ABS (100% Horizontal - 0°)	1	106,5	58,442	1632,495
	2	106,5	58,245	1627,119
	3	107	58,341	1618,986
	4	108	60,281	1637,559
	5	106	56,666	1581,157
	Média	**107**	**58,395**	**1645,929**

Mean Flex.Modulus	1629,040	MPa
Dev. Padrao	6,879018	MPa
Desvio padrão %	0,422274	%
Int. conf 95_%	6,029614	MPa

Mean Flex. Stress	58,827	MPa
Dev. Padrao	0,841988	MPa
Desvio padrão %	1,431291	%
Int. conf 95_%	0,738021	MPa

Mean max load	107,000	mm
Dev. Padrao	0,612372	MPa
Desvio padrão %	0,572311	%
Int. conf 95_%	0,536758	MPa

PETG

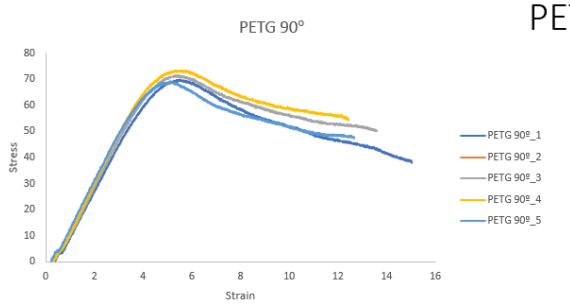

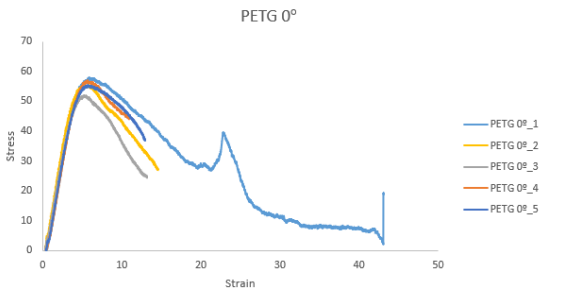

	Amostra	Max. Load (N)	Max. Flexural Stress (MPa)	Flexural Modulus (MPa)
PETG (100% Vertical - 90°)	1	116	69,783	1774,135
	2	118	70,077	1911,613
	3	121,5	71,378	1859,678
	4	118	73,438	1950,567
	5	114	69,054	1858,436
	Média	117,875	70,987	1895,074

Mean Flex.Modulus	1895,074	MPa
Dev. Padrao	38,56239	MPa
Desvio padrão %	2,034876	%
Int. conf 95_%	33,8008	MPa

Mean Flex. Stress	70,987	MPa
Dev. Padrao	1,637	MPa
Desvio padrão %	2,306716	%
Int. conf 95_%	1,43527	MPa

Mean max load	117,875	mm
Dev. Padrao	46,59387	MPa
Desvio padrão %	39,5282	%
Int. conf 95_%	40,84057	MPa

Flexural Modulus	1170-2760	2100	MPa
Flexural Stress	39,2-88,9	77	MPa
Ref: MatWeb		Ref: MakeItForm	

	Amostra	Max. Load (N)	Max. Flexural Stress (MPa)	Flexural Modulus (MPa)
PETG (100% Horizontal - 0°)	1	100,5	57,892	1575,465
	2	86	55,454	1623,473
	3	84,5	51,953	1511,923
	4	90,5	56,953	1543,399
	5	93,5	55,558	1551,081
	Média	92,628	56,464	1573,355

Mean Flex.Modulus	1573,355	MPa
Dev. Padrao	31,26403	MPa
Desvio padrão %	1,987094	%
Int. conf 95_%	27,40363	MPa

Mean Flex. Stress	56,464	MPa
Dev. Padrao	1,015	MPa
Desvio padrão %	1,797161	%
Int. conf 95_%	0,889457	MPa

Mean max load	92,628	mm
Dev. Padrao	36,54853	MPa
Desvio padrão %	39,45754	%
Int. conf 95_%	32,03561	MPa

PLA

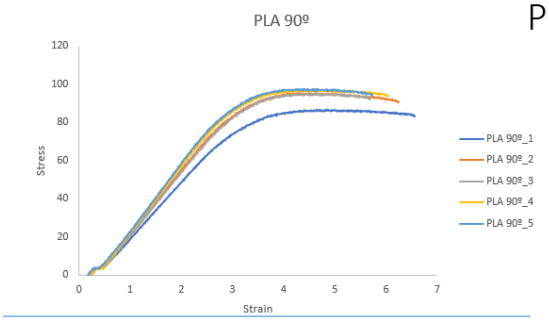

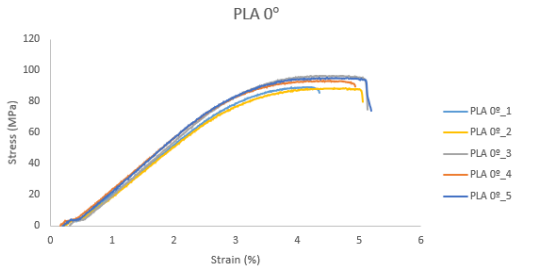

	Amostra	Max. Load (N)	Max. Flexural Stress (MPa)	Flexural Modulus
PLA (100% Vertical - 90°)	1	162	86,629	2998,896
	2	164,5	95,412	3419,204
	3	163,5	94,832	3316,004
	4	163,5	96,904	3499,264
	5	162,5	97,360	3524,515
	Média	163,50	96,13	3439,75

Mean Flex.Modulus	3439,747	MPa
Dev. Padrao	81,33608	MPa
Desvio padrão %	2,364595	%
Int. conf 95_%	71,29291	MPa

Mean Flex. Stress	96,127	MPa
Dev. Padrao	1,038	MPa
Desvio padrão %	1,080049	%
Int. conf 95_%	0,910021	MPa

Mean max load	163,500	mm
Dev. Padrao	65,40306	MPa
Desvio padrão %	40,00187	%
Int. conf 95_%	57,32725	MPa

Flexural Modulus	178-13800	4000	MPa
Flexural Stress	0,170-159	80	MPa
Ref: MatWeb		Ref: MakeItForm	

	Amostra	Max. Load (N)	Max. Flexural Stress (MPa)	Flexural Modulus (MPa)
PLA (100% Horizontal - 0°)	1	156,00	89,067	3121,156
	2	155,5	88,907	3186,871
	3	157,5	96,266	3475,981
	4	158	93,184	3313,039
	5	156,5	95,287	3445,126
	Média	156,875	93,411	3355,254

Mean Flex.Modulus	3355,254	MPa
Dev. Padrao	114,877	MPa
Desvio padrão %	3,423795	%
Int. conf 95_%	100,6923	MPa

Mean Flex. Stress	93,411	MPa
Dev. Padrao	2,829	MPa
Desvio padrão %	3,028201	%
Int. conf 95_%	2,479392	MPa

Mean max load	156,875	mm
Dev. Padrao	0,960143	MPa
Desvio padrão %	0,612043	%
Int. conf 95_%	0,841587	MPa

TPU

- Load cell too high, no sensitivity for this material
- **Results inconclusive!**

	Amostra	Pico Máximo (N)	Max. Flexural Stress (MPa)	Flexural Modulus
TPU (100% Vertical - 90°)	1	4,5	2,830	
	2	5,5	3,463	
	3	5,5	3,523	
	4	5	3,189	
	5	4,5	2,865	
		5,125	3,260	

	Amostra	Pico Máximo (N)	Max. Flexural Stress (MPa)	Flexural Modulus
TPU(100% Horizontal - 0°)	1	4,5	2,709	
	2	4	2,384	
	3	3	1,840	
	4	3,5	2,100	
	5	4	2,370	
		4,000	2,391	

Flexural Modulus	25,6 (XY)	36,9 (XZ) - vertical	MPa
Flexural Stress	1,8 (XY)	2,4 (XZ) - vertical	MPa
Ref: FDM TPU 92ª - Stratasys			

ULTEM 1010

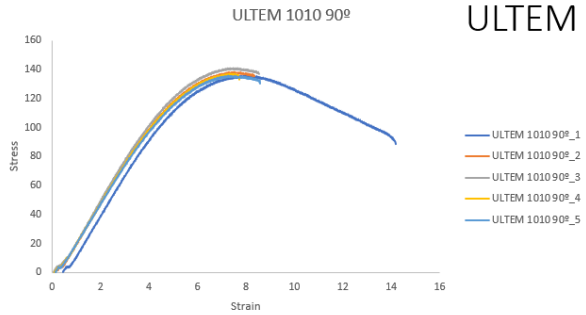

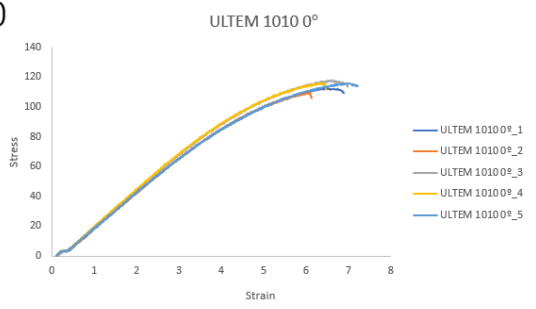

	Amostra	Max. Load (N)	Max. Flexural Stress (MPa)	Flexural Modulus (MPa)
ULTEM 1010 (100% Vertical - 90°)	1	217,5	135,422	2808,389
	2	223,5	138,182	2821,469
	3	226	141,005	2920,950
	4	222,5	136,914	2806,491
	5	222	135,407	2753,356
	Média	223,500	137,877	2825,567

Mean Flex.Modulus	2825,567	MPa
Dev. Padrao	60,60741	MPa
Desvio padrão %	2,144965	%
Int. conf 95_%	53,12376	MPa

Mean max load	223,500	mm
Dev. Padrao	89,41063	MPa
Desvio padrão %	40,00475	%
Int. conf 95_%	78,37043	MPa

Mean Flex. Stress	137,877	MPa
Dev. Padrao	2,056	MPa
Desvio padrão %	1,491052	%
Int. conf 95_%	1,801972	MPa

Flexural Modulus	2.64 (ZX)	2.91 (XZ) - vertical	MPa
Flexural Stress	77 (ZX)	144 (XZ) - vertical	MPa

Ref:
- https://info.stratasysdirect.com/rs/626-SBR-192/images/Data%20Sheet%20-%20%20EN%20ULTEM%201010.pdf
- https://www.rnd-tech.com/media/fdm-pdfs/spec-sheets/ultem1010materialspecsheeten1014.pdf

	Amostra	Max. Load (N)	Max. Flexural Stress (MPa)	Flexural Modulus (MPa)
ULTEM 1010 (100% Horizontal - 0°)	1	193	112,523	2452,317
	2	191	109,111	2387,341
	3	200	117,411	2489,934
	4	198	115,439	2518,804
	5	202	115,745	2390,588
	Média	198,25	115,28	2462,91

Mean Flex.Modulus	2462,911	MPa
Dev. Padrao	47,95081	MPa
Desvio padrão %	1,946916	%
Int. conf 95_%	42,02996	MPa

Mean Flex. Stress	115,280	MPa
Dev. Padrao	1,759	MPa
Desvio padrão %	1,526237	%
Int. conf 95_%	1,54219	MPa

Mean max load	198,250	mm
Dev. Padrao	79,35641	MPa
Desvio padrão %	40,02845	%
Int. conf 95_%	69,55768	MPa

Flexural Modulus	2910 (XZ)	MPa
Flexural Stress	130 (XZ)	MPa

Ref: MatWeb

ULTEM 9085

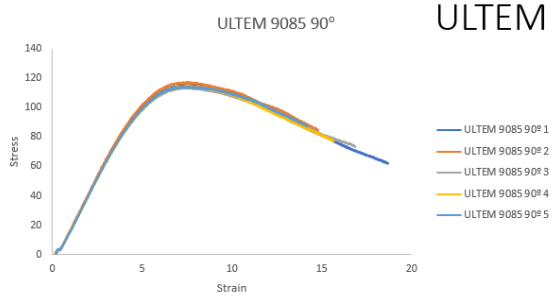

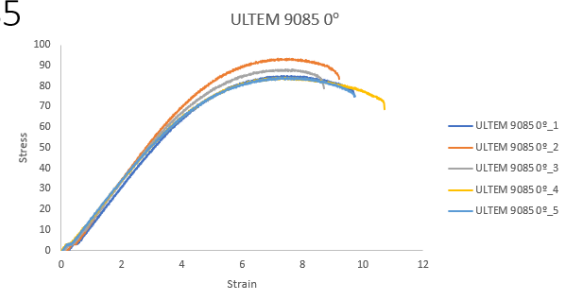

	Amostra	Max. Load (N)	Max. Flexural Stress (MPa)	Flexural Modulus (MPa)
ULTEM 9085 (100% Vertical - 90°)	1	186	115,451	2379,499
	2	186	117,356	2429,619
	3	184	113,625	2394,764
	4	185,5	115,023	2361,212
	5	183	114,141	2396,448
	Média	185,38	115,143	2400,083

Mean Flex. Modulus	2400,083	MPa
Dev. Padrao	18,28648	MPa
Desvio padrão %	0,76191	%
Int. conf 95_%	16,02851	MPa

Mean max load	184,750	mm
Dev. Padrao	1,299038	MPa
Desvio padrão %	0,703133	%
Int. conf 95_%	1,138636	MPa

Mean Flex. Stress	115,143	MPa
Dev. Padrao	1,440	MPa
Desvio padrão %	1,251017	%
Int. conf 95_%	1,262599	MPa

Flexural Modulus	2620 (XZ)	MPa
Flexural Stress	100 (XZ)	MPa

Ref: MatWeb

Flexural Modulus	2.62 (ZX)	2.27 (XZ) - vertical	MPa
Flexural Stress	90 (ZX)	130 (XZ) - vertical	MPa

Ref:
- https://www.stratasys.com/materials/search/ultem9085

	Amostra	Max. Load (N)	Max. Flexural Stress (MPa)	Flexural Modulus (MPa)
ULTEM 9085 (100% Horizontal - 0°)	1	148	84,764	1878,670
	2	162,5	92,974	2036,562
	3	152	88,141	1942,193
	4	14	84,021	1818,302
	5	145,5	83,648	1837,870
	Média	**146**	**84,764**	**1870,835**

Mean Flex. Modulus	1881,620	MPa
Dev. Padrao	73,13057	MPa
Desvio padrão %	3,886576	%
Int. conf 95_%	64,10059	MPa

Mean Flex. Stress	86,710	MPa
Dev. Padrao	3,512	MPa
Desvio padrão %	4,050448	%
Int. conf 95_%	3,078456	MPa

Mean max load	150,800	mm
Dev. Padrao	56,49164	MPa
Desvio padrão %	37,4613	%
Int. conf 95_%	49,5162	MPa

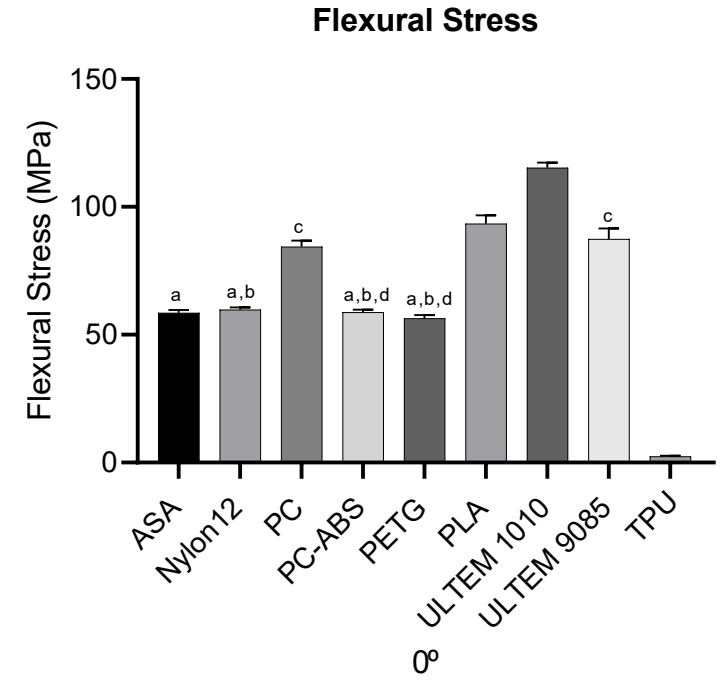
Flexural Stress
Flexural Stress (MPa)
150
100
50
0
a
a,b
c
a,b,d
a,b,d
c
ASA
Nylon12
PC
PC-ABS
PETG
PLA
ULTEM 1010
ULTEM 9085
TPU
0º

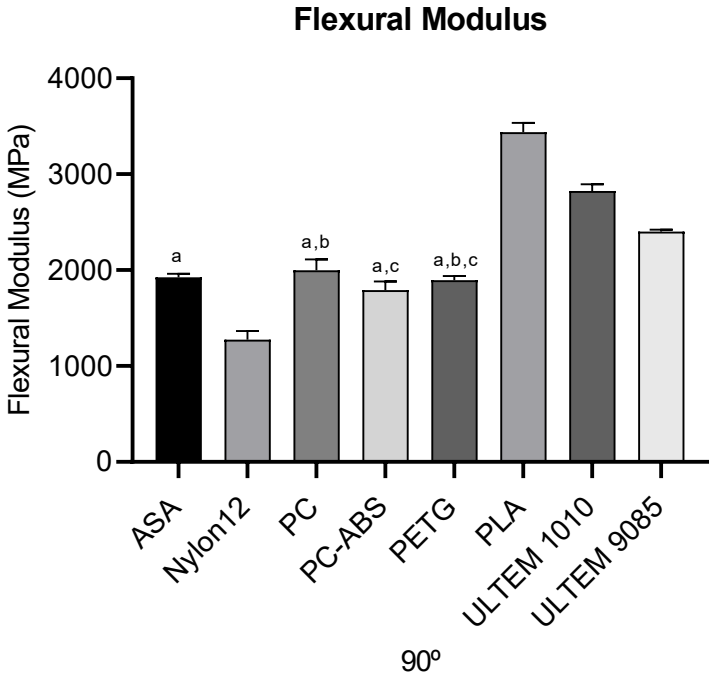
Flexural Modulus
Flexural Modulus (MPa)
4000
3000
2000
1000
0
a
a,b
a,c
a,b,c
ASA
Nylon12
PC
PC-ABS
PETG
PLA
ULTEM 1010
ULTEM 9085
90º

Material	Módulo à Flexão(MPa)	Resistência à Flexão (MPa)
ABS Horizontal	1826	56,5
ABS Vertical	1885	59,6
Nylon12 Horizontal	1181	59,7
Nylon 12 Vertical	1236	63,3
PC Horizontal	1864	84,2
PC Vertical	1943	86,4
PC-ABS Horizontal	1646	56,7
PC-ABS Vertical	1767	63,0
PETG Horizontal	1555	55,6
PETG Vertical	1866	71,4
PLA Horizontal	3314	93,2
PLA Vertical	3343	94,8
ULTEM 1010 Horizontal	2428	112,5
ULTEM 1010 Vertical	2816	138,2
ULTEM 9085 Horizontal	1882	84,8
ULTEM 9085 Vertical	2388	114,1

Tensile Tests

ABS

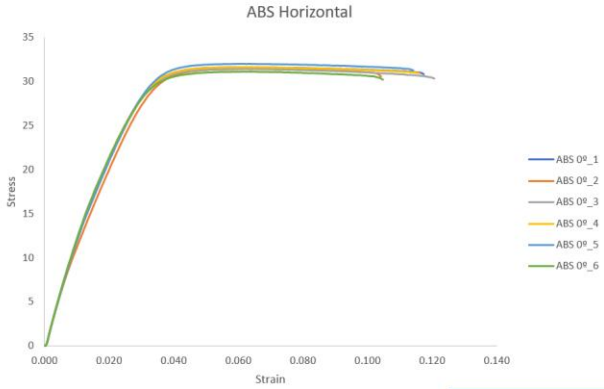

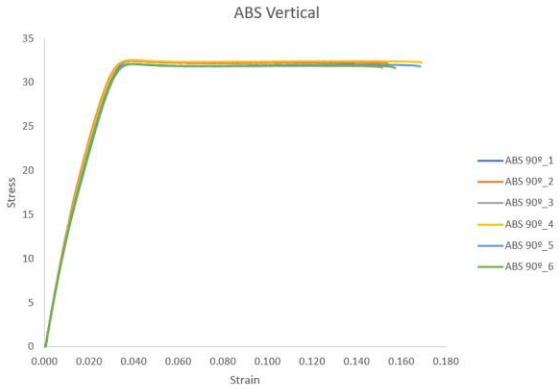

Tensile Modulus	2600	MPa
Tensile Stress	55	MPa
Tensile Strength, Yield	34-40	MPa

Ref: MatWeb Ref: MakeItForm

TPU

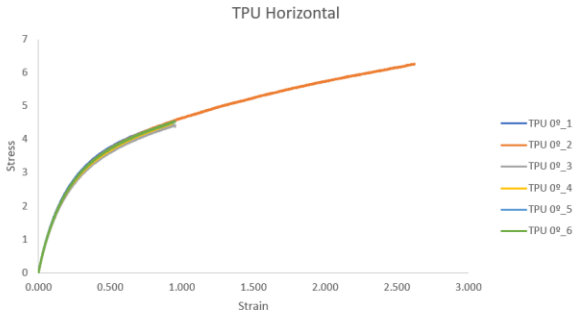

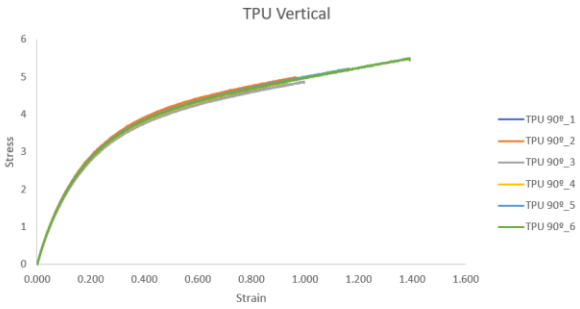

Tensile Modulus		MPa
Tensile Stress		MPa
Tensile Strength, Yield		MPa

Ref: MatWeb Ref: MakeItForm

PC

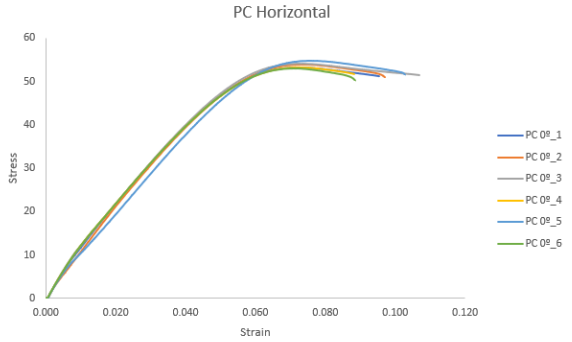

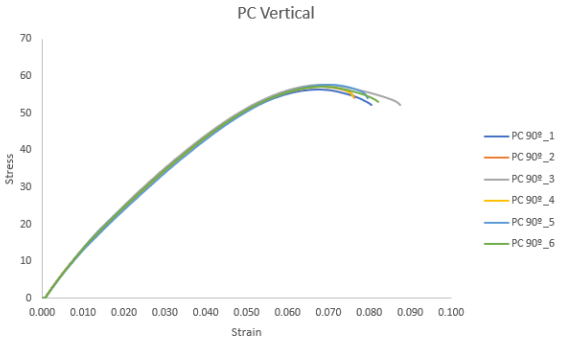

Tensile Modulus		2300-10000	MPa
Tensile Stress	28-75	66-160	MPa
Tensile Strength, Yield	39-70		MPa
	Ref: MatWeb	Ref: MakeItForm	

PC-ABS

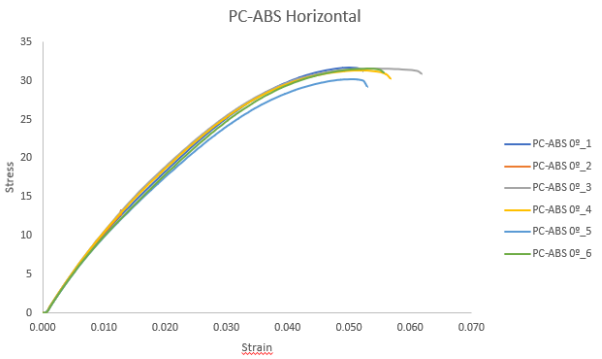

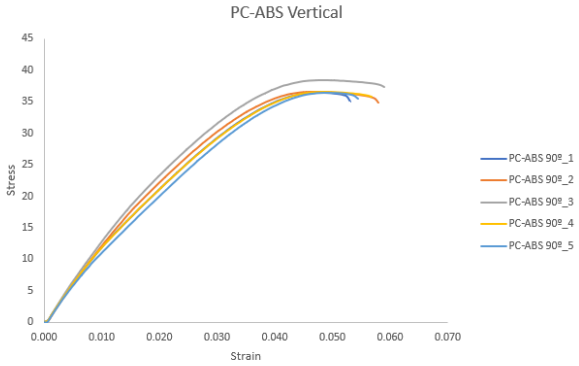

Tensile Modulus			MPa
Tensile Stress			MPa
Tensile Strength, Yield			MPa
	Ref: MatWeb	Ref: MakeItForm	

ULTEM 9085

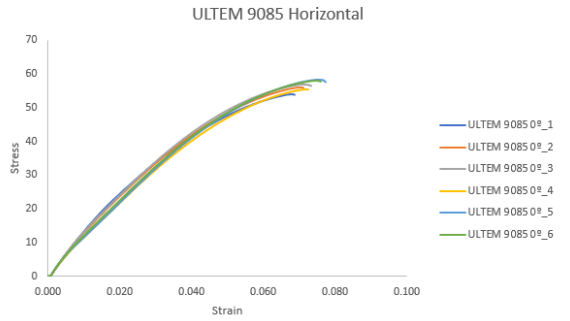

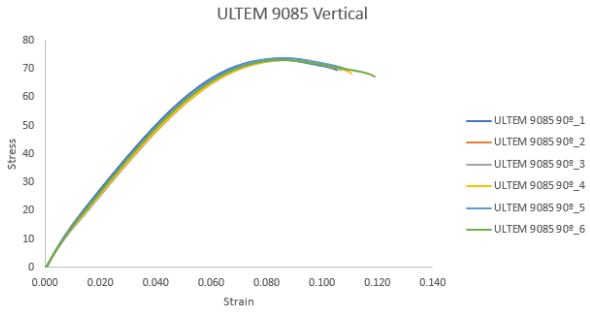

Tensile Modulus		MPa
Tensile Stress	58 (ZX) 77 (XZ)	MPa
Tensile Strength, Yield		MPa
	Ref: MatWeb	Ref: MakeItForm

ULTEM 1010

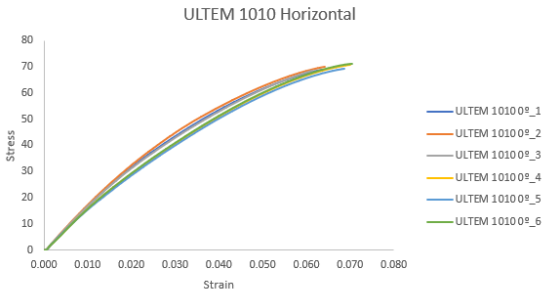

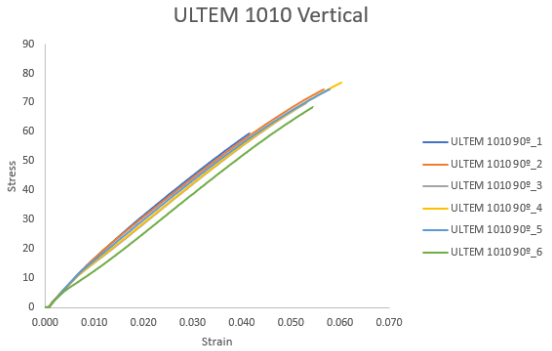

Tensile Modulus		MPa
Tensile Stress		MPa
Tensile Strength, Yield		MPa
	Ref: MatWeb	Ref: MakeItForm

Nylon 12

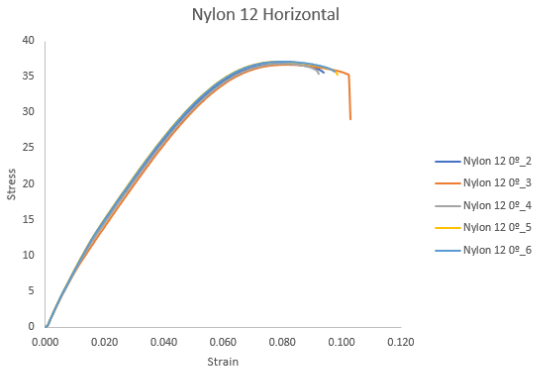

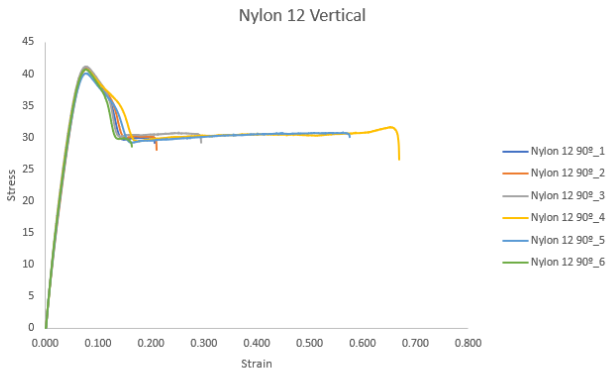

Tensile Modulus	MPa
Tensile Stress	MPa
Tensile Strength, Yield	MPa

Ref: MatWeb Ref: MakeItForm

PLA

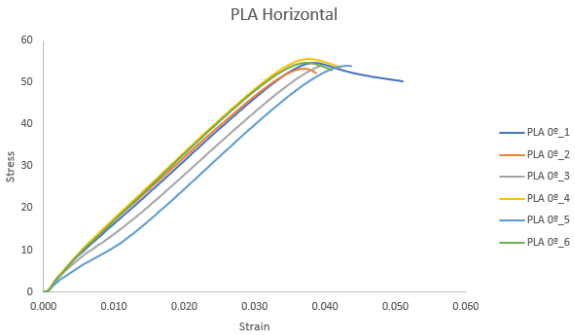

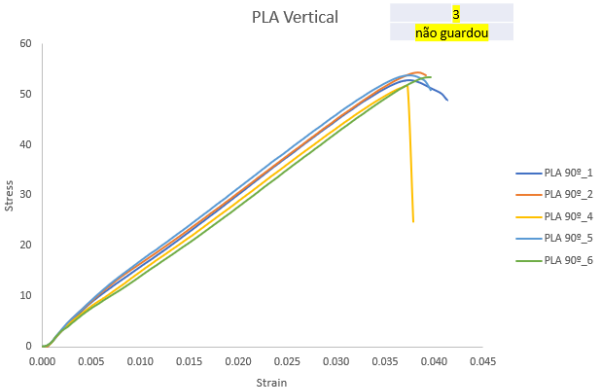

Tensile Modulus	MPa
Tensile Stress	MPa
Tensile Strength, Yield	MPa

Ref: MatWeb Ref: MakeItForm

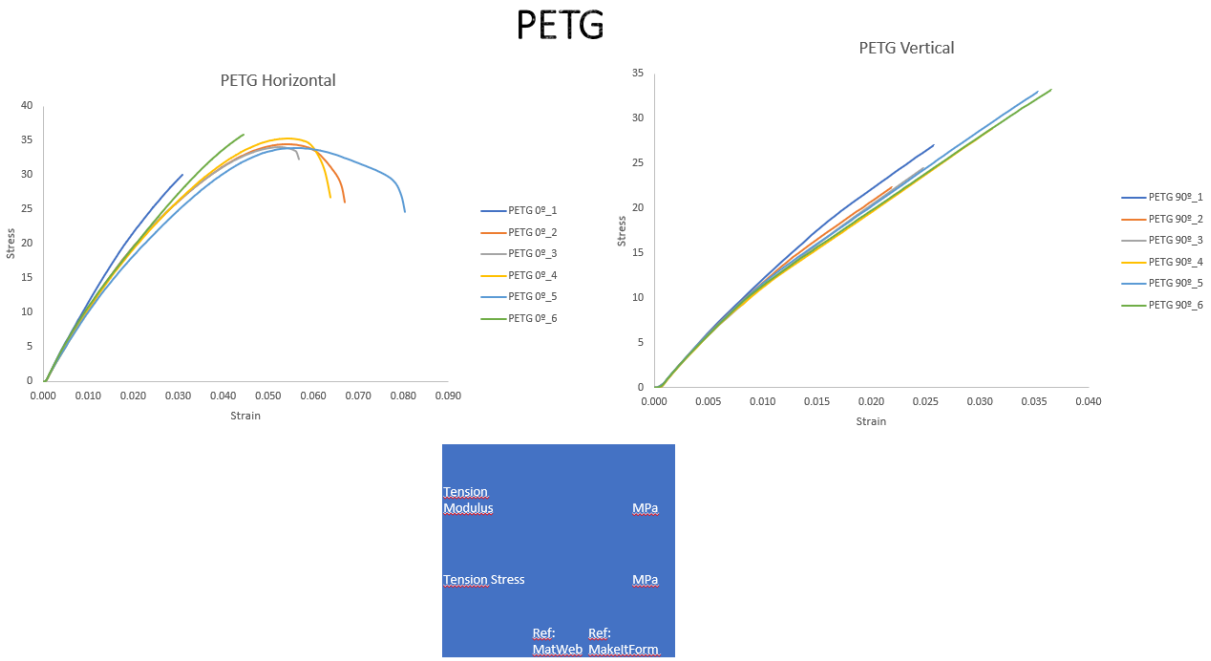
PETG
PETG Horizontal
Stress
Strain
PETG 0º_1
PETG 0º_2
PETG 0º_3
PETG 0º_4
PETG 0º_5
PETG 0º_6
PETG Vertical
Stress
Strain
PETG 90º_1
PETG 90º_2
PETG 90º_3
PETG 90º_4
PETG 90º_5
PETG 90º_6
Tension Modulus
MPa
Tension Stress
MPa
Ref: MatWeb
Ref: MakeItForm

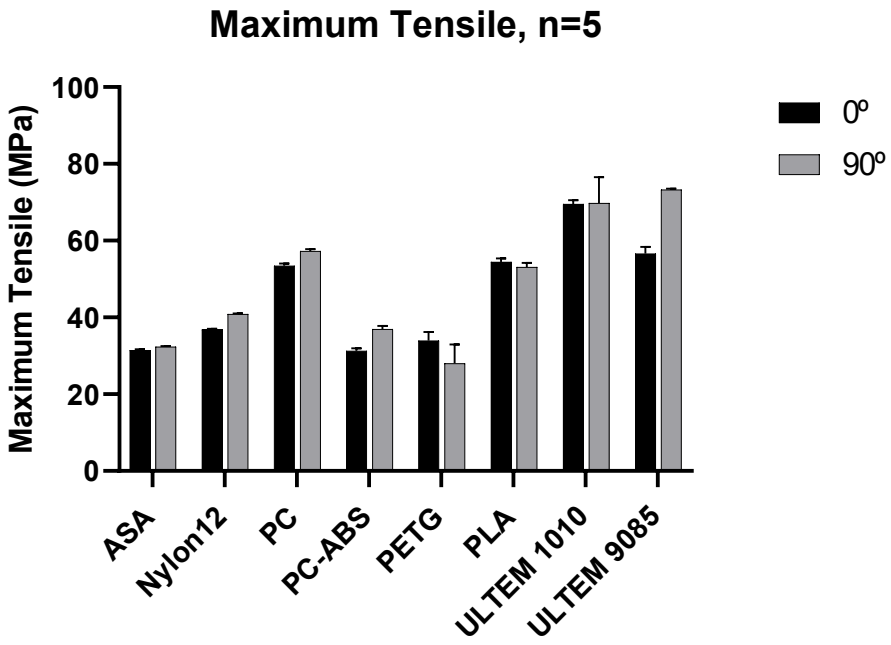
Maximum Tensile, n=5
Maximum Tensile (MPa)
0º
90º
ASA
Nylon12
PC
PC-ABS
PETG
PLA
ULTEM 1010
ULTEM 9085

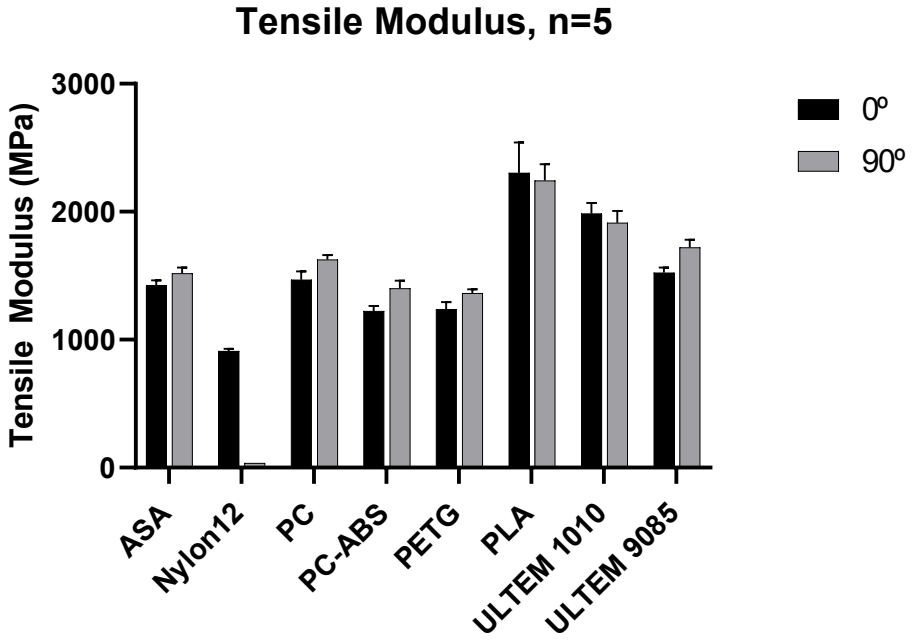
Tensile Modulus, n=5
Tensile Modulus (MPa)
3000
2000
1000
0
0º
90º
ASA
Nylon12
PC
PC-ABS
PETG
PLA
ULTEM 1010
ULTEM 9085

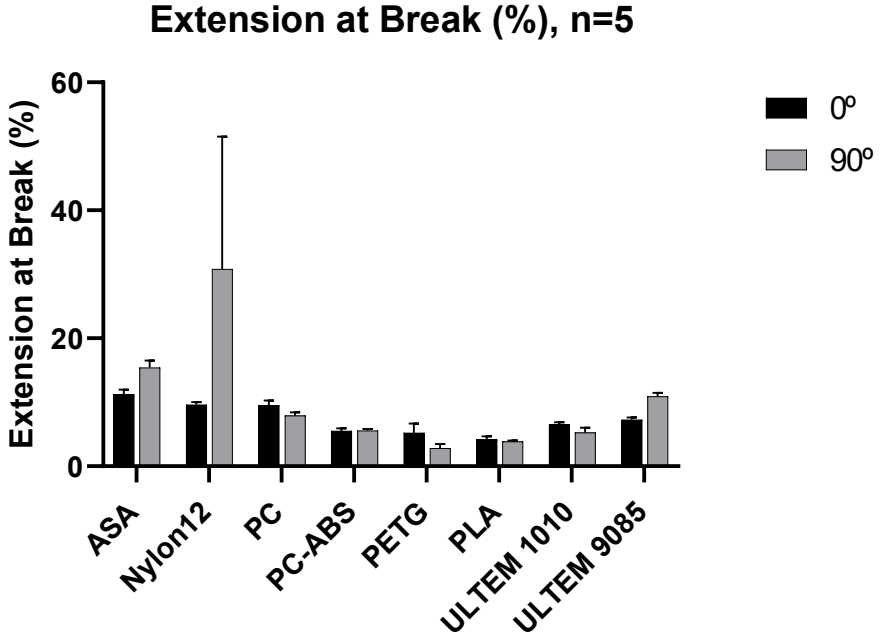
Extension at Break (%), n=5
Extension at Break (%)
60
40
20
0
0º
90º
ASA
Nylon12
PC
PC-ABS
PETG
PLA
ULTEM 1010
ULTEM 9085

Material	Orientação de Impressão	
	Horizontal (0°)	Vertical (90°)
ASA	31,473 ± 0.224[a]	32,3484 ±0.220[a,b]
Nylon 12	36,8856 ± 0.196[b,c]	40,866 ± 0.215[c,d]
PC	53,4924 ± 0.516[e]	57,2626 ± 0.517[e,f]
PC-ABS	31,292 ± 0.637[a,b,g]	36,9278 ± 0.876[b,c,d,h]
PETG	33,9414 ± 2.255[a,b,c,g,h]	28,0054 ± 4.967[a,b,g]
PLA	54,4544 ± 0.930[e,f,i]	53,1134 ± 1.097[e,f,i,j]
ULTEM 1010	69,5086 ± 0.999[l]	69,8332 ± 6.744[l,m]
ULTEM 9085	56,6332 ± 1.718[e,f,i,j]	73,3234 ± 0.229[l,m]
TPU	4,8136 ± 0.646[n]	5,0946 ± 0.271[n]

Material	Orientação de Impressão	
	Horizontal (0°)	Vertical (90°)
ASA	1426,1 ± 38.714[a]	1519,22 ± 44.171[a,b]
Nylon 12	911,402 ± 17.436	988,5966 ± 22,532[c]
PC	1469,32 ± 64.296[a,b,d]	1627,28 ± 34.973[b,d,e]
PC-ABS	1224,04 ± 39.276[f]	1402,26 ± 58.991[a,b,d,f,g]
PETG	1239,88 ± 53.280[f,g,h]	1363,28 ± 30.262[a,b,d,f,g,h,i]
PLA	2303,94 ± 237.073[j]	2243,86 ± 126.398[j]
ULTEM 1010	1985,6 ± 84.069[k]	1913,5 ± 93.386[k]
ULTEM 9085	1522,82 ± 41.036[a,b,d,e,g,i]	1722,16 ± 59.410[e]
TPU	20,008 ± 0.942[c,l]	24,2536 ± 0.604[c,l]

Material	Orientação de Impressão	
	Horizontal (0°)	Vertical (90°)
ASA	1426,1 ± 38.714[a]	1519,22 ± 44.171[a,b]
Nylon 12	911,402 ± 17.436	988,5966 ± 22,532[c]
PC	1469,32 ± 64.296[a,b,d]	1627,28 ± 34.973[b,d,e]
PC-ABS	1224,04 ± 39.276[f]	1402,26 ± 58.991[a,b,d,f,g]
PETG	1239,88 ± 53.280[f,g,h]	1363,28 ± 30.262[a,b,d,f,g,h,i]
PLA	2303,94 ± 237.073[j]	2243,86 ± 126.398[j]
ULTEM 1010	1985,6 ± 84.069[k]	1913,5 ± 93.386[k]
ULTEM 9085	1522,82 ± 41.036[a,b,d,e,g,i]	1722,16 ± 59.410[e]
TPU	20,008 ± 0.942[c,l]	24,2536 ± 0.604[c,l]